CARBOXYLATIVE METHODOLOGIES VIA PHOTOREDOX CATALYSIS

Julien Lyonnet

UNIVERSITAT ROVIRA i VIRGILI

Carboxylative Methodologies via Photoredox Catalysis

Julien Lyonnet

DOCTORAL THESIS
2024

Carboxylative Methodologies via Photoredox Catalysis

Julien Lyonnet

DOCTORAL THESIS

Supervised by Prof. Rubén Martín Romo

Institut Català d'Investigació Química (ICIQ)
Universitat Rovira i Virgili (URV)
Department of Analytical Chemistry & Organic Chemistry

Tarragona, 2024

UNIVERSITAT ROVIRA i VIRGILI

ICIQ Institute of Chemical Research of Catalonia

Prof. Rubén Martín Romo, Group Leader at the Institute of Chemical Research of Catalonia (ICIQ) and Research Professor of the Catalan Institution for Research and Advanced Studies (ICREA),

STATES that the present study, entitled "Carboxylative Methodologies via Photoredox Catalysis", presented by Julien Lyonnet for the award of the degree of Doctor, has been carried out under his supervision at the Institute of Chemical Research of Catalonia (ICIQ).

Tarragona, June 2024

Doctoral Thesis Supervisor

Ruben Martin Romo - DNI 38129823D (TCAT)

Firmado digitalmente por Ruben Martin Romo - DNI 38129823D (TCAT)
Fecha: 2024.06.21 12:42:32 +02'00'

Prof. Rubén Martín Romo

« Le seul véritable voyage, le seul bain de Jouvence, ce ne serait pas d'aller vers de nouveaux paysages, mais d'avoir d'autres yeux, de voir l'univers avec les yeux d'un autre, de cent autres, de voir les cent univers que chacun d'eux voit. »

- Marcel Proust, dans *La Prisonnière*

Acknowledgements

Before thanking anyone else, I would like to deeply thank my supervisor **Prof. Ruben Martin** for taking me on this journey with him. You have been a fantastic boss and mentor over those past four years. For the group meeting discussions, your advice and suggestions when meeting in your office, but also for the social times outside the lab. I have learned so much by being part of this group, and also met so many people from all across the world. Thank you for everything.

I would also like to thank the members of the committee, **Dr. Arkaitz Correa**, **Dr. Manuel Nappi** and **Dr. Ana Belén Cuenca González** for accepting to evaluate my work.

During my work at ICIQ, I had the chance to work in collaboration with great scientists from other institutions who should be acknowledged. **Bjørn Carvalho**, **Prof. Kathrin Hopmann** and **Dr. Per-Ola Norrby**. In addition, I would like to thank two people who have greeted me in their labs for short stays. **Dr. Charles Elmore** and **Prof. Troels Skrydstrup**, you both are brilliant scientists, it has been fantastic to have interacted with you over those years.

David Sádaba, I don't think the lab would stand a week without you around, thanks for being there and being so efficient at what you do, and for helping we with the UPLC, your work is really appreciated.

I have had the chance to be part of an ITN funding named **CO2PERATE**, in which I have made great friends. To **Gabriel**, **Ha**, **Yunfei**, **Bjørn, Georgia**, **Doriane**, **Sahil**, **Stephanie**, **Mahika**, **Kim**, **Weiheng**, **Jiali** and **Pierre**, thanks for all the good times all across Europe, it was amazing to meet all of you, to discuss nice science and simply to have fun together. Our meetings were definitely amongst the best memories I will have of my PhD! I am sure we will meet again in the future, in the meantime I wish you all the best.

To the **past and present Martinis**, thank you for all for the time spent inside and outside the lab, I had a great time with you all. Starting with the PhD alumni: **Bradley**, babe, you probably were the first friend I made in the group when COVID was still around, preventing us to do anything. Thanks for socializing with me online at the time and for staying a great friend since then, I have learned so much from you, and I admire your messiness <3. **Craig**, you are a true inspiration, it was amazing to spend time with you in two different groups, I'm convinced that you'll go very far! Thanks for the good

times in Aarhus. **Laura**, it has been fun to learn to climb with you. Thanks for your energy to do group activities and for the dinners at your place. **Carlota**, it has been a pleasure to meet you, I wish you all the best for your future. **Dmitry**, my travel buddy, I will never forget the struggles we had when trying to go to Aarhus starting at 4:30 and arriving at 23:30. I hope everything goes well for you. **Fei**, what an energy you have, it was really fun going to Koyo with the group and order a lot of n°54, I hope everything is going well for you. **Xinyang** and **Wenjun**, you got me anxious when I arrived in lab 2.12 and saw you doing a thousand columns every day! Joke apart, thanks for all the interesting discussions we had.

Chris, thanks for being one of my first social contacts I had arriving in Tarragona, the world situation was not fun, but we managed. You are such a clever chemist, I hope everything is going well for you. **Jessica**, thank you for the energy you brought in the beginning of my journey, it was great to meet you. **Hongfei**, the man, the legend. I hope we can meet again someday, thanks for the great times and for showing me around the lab in the beginning. **Yaya**, thank you for helping me with my first project. **Ciro**, man I don't even know what to write. From you supervising me in Geneva when I was a Bachelor student, to sharing a lab as *actual* colleagues in ICIQ, most of my knowledge comes from you. Also, thanks for the countless drinks we shared in twins, I am sure we will meet a lot of times more. **Robert**, it's been so nice to get to know you, thank you for the dinners with your family, I wish you all the best and I hope to meet again someday. **Riccardo**, you made me run my very first 10k race, I don't think I could have done it without your motivation! Thanks for the good vibes, I hope we meet again in the future. **Matt**, the beach-volley king, thanks for your energy, I'll never forget nights out! I hope Barcelona treats you well. **Jake**, thanks for your help and for working with me, you are an inspiration. All the best to you and your family. **Roman**, my G, you are such a legend. Thanks for all the good times, the banter and the fabulous discussions we had. You are a gem of a human, I hope life treats you well! **Santosh**, it has been great sharing the lab with you, I hope you are doing well. **Franz**, thanks for all the discussions, for the social times, and for sharing part of a trip in Japan. I will never forget our okonomiyaki in Hiroshima, I'm sure we will meet again in the future.

To the current workforce of the group: **Julita**, I could write a whole page for you, I cannot imagine doing this PhD without you around. I will never forget our gossips, our *rare* intelligent discussions, our nights out, and of course the times you had to come with me to the hospital because I can't handle a syringe properly. Thank you for being there when I had my lows, you are a true friend. No need to say that we will meet many more times in the future. **Adrian**, keep on partying boy, I love your energy, never change that. **Filip**,

you are a great scientist, I am convinced that everything will go well for you. In the meantime, keep on going! It's been great to share time in the group with you. **Joan**, it has been a pleasure to meet you, you are such a kind person, I wish you all the best for the PhD! **Wei**, you are someone who loves learning, it is so nice to see. I am happy I could try to help you the way others have helped me. I hope to come to Shanghai one day. **Hui**, **Hao** and **Yubiao**, you all are amazing people, I wish you all the best for your future. **Shuai**, **Zuoyu**, **Ricardo**, **Huilin**, **Eva** and **Julian**, you are the future of this group, try to make the atmosphere as good as it can be, and enjoy! I hope your journey through science will be a great one.

Álvaro, hombre, it's been really nice to share a lab and projects with you! You are a hardworking man; I am sure this will lead you far. All the best. **Anna**, thanks for being there for the last part of my time here, it is so nice to spend time with you and go to monobloc together. I hope that you won't have to do 8 postdocs before your next step ;). **Dani**, it's been great to have you in Tarragona after meeting in Uppsala! Thanks for all the times running and the good vibes in general, I hope you will become the biker you dream of being! **Jesús** and **Tomás**, it has been a pleasure to get to know you, I hope everything will go well for you. **Zhong**, **Liangliang** and **Hui-Qing**, it has been great to share the lab with you, I wish you the best for your future.

Papa, **Maman**, merci énormément pour tout le soutien que vous m'avez apporté au cours de ces longues années. Cela a été long, mais ça en aura voulu la peine je l'espère. Je ne pourrai jamais assez vous remercier pour tout ce que vous m'avez apporté, depuis toujours.

Troligtvis den viktigaste personen, **Patricia**, sötis, det har inte varit lätt att vara borta i fyra år, tack för ditt tålamod. Tack för ditt ovillkorliga stöd genom avståndet. Jag är så glad att vi äntligen kan börja ett liv tillsammans! Tack för allt, jag älskar dig.

Preface

The present thesis has been performed at the Institute for Chemical Research of Catalonia (ICIQ) under the supervision of Professor Rubén Martin. This thesis is arranged in five chapters: a general introduction, three research chapters, and a final chapter that concludes the thesis.

Chapter 1, "Introduction". The main themes and concepts approached during this thesis will be introduced and described. The concept of carbon dioxide reduction and its behavior with transition metals will be discussed as well as its use in photoredox catalysis.

Chapter 2, "Photocatalytic Multicomponent Radical Coupling for the Direct Incorporation of Labelled Carbon Dioxide", describes the development of a radical coupling involving 4 or 5 molecules depending on the starting material class. Iterative radical couplings ending with addition of carbon dioxide allows for the rapid synthesis of complex compounds bearing a labelled carbon atom such as ^{13}C. The reaction involves only a photocatalyst with blue light irradiation to be functional.

Chapter 3, "Kinetically-Controlled Ni-Catalyzed Direct Carboxylation of Unactivated Secondary Alkyl Bromides", narrates the maturation of a long-lasting endeavor. The carboxylation of unactivated secondary alkyl bromides with carbon dioxide. The methodology involves mild dual photoredox and nickel catalysis in order to obtain the target acids with excellent selectivity. Preliminary mechanistic studies are disclosed, showing the important free radical intermediates and the reactivity of a nickel(I) species.

Chapter 4, "Redox-Neutral Ni-Catalyzed Direct Carboxylation of Unactivated Secondary Alkyl Bromides", showcases the elaboration of an improved direct carboxylation of secondary bromides, following what is described in Chapter 3. The method makes use of formate salts instead of carbon dioxide gas as carboxylating agent. The involvement of formate allows for a redox neutral process, which makes use of the CO_2 radical anion as reactive intermediate.

Chapter 5, "General Conclusions". The chapter summarizes the work described in the thesis.

Abbreviations

BDE: Bond dissociation energy
BHE: β-hydride elimination
bpy: Bipyridine
conPET: Consecutive photo-induced electron transfer
CRA: CO_2 radical anion
DFT: Density functional theory
DMA: Dimethylacetamide
DME: 1,2-dimethoxyethane
DMF: Dimethylformamide
DMSO: Dimethylsulfoxide
dtbbpy: 4,4'-di-tert-butylbipyridine
ETMS: Ethyl trimethyl silane
EtOAc: Ethyl acetate
FLPs: Frustrated Lewis pairs
GSA: Gravimetric specific activity
HAT: Hydrogen atom transfer
HEH: Hantzsch ester
HOMO: Highest occupied molecular orbital
LUMO: Lowest unoccupied molecular orbital
MCR: Multicomponent reaction
MO: Molecular orbital
NMP: N-methyl-2-pyrrolidone
RCY: Radiochemical yield
RPC: Radical polar crossover
SA: Specific activity
SET: Single electron transfer
TBAB: Tetrabutyl ammonium bromide
TBADT: Tetra-n-butylammonium decatungstate
THF: Tetrahydrofuran
TMS: Trimethylsilane
XEC: Cross-electrophile coupling

Abstract

Over the last 15 years, both photoredox and carboxylation chemistries have witnessed a substantial involvement from the community, leading to a plethora of new methodologies and concepts to be developed.[1] The association of both fields, namely photoredox carboxylation reactions, consists of the current state-of-the-art when it comes to making carboxylic acids from simpler starting materials.

In accordance with the Martin group's research interests within the carboxylation arena, the work presented herein focuses on the merging of photoredox chemistry and catalytic systems for the carboxylation of organic molecules. More specifically, the work showcased consists of the development of a multicomponent coupling with $^{13}CO_2$ (Chapter 2), the design of a direct reductive carboxylation of *unactivated* secondary alkyl bromides (Chapter 3) and the elaboration of a redox neutral methodology for the direct carboxylation of *unactivated* secondary alkyl bromides using formate salts (Chapter 4).

Given that carboxylation methodologies aiming at giving labeled compound has received only little attention, we ought to develop a protocol that would allow for the incorporation of labeled CO_2 while installing a complex molecular scaffold, all in one step. This first study, described in Chapter 2, shows the coupling of a sulfinate salt with an alkene, an acrylate and CO_2 under photocatalytic conditions to yield complex labeled compounds. The general structure of the products can be altered depending on the class of alkene used in the reaction, giving rise to a broader range of possibilities. A preliminary mechanistic study reveals the reversibility of radical intermediates to be at the source of such selectivity.

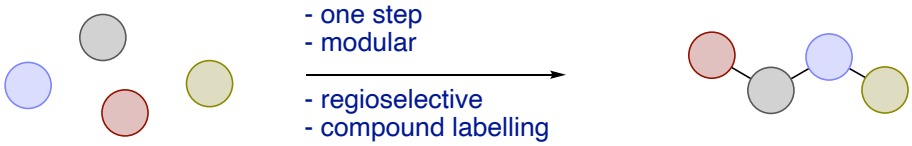

Figure i: Multicomponent photocatalytic carboxylative reaction.

[1] (a) Chan, A. Y.; Perry, I. B.; Bissonnette, N. B.; Buksh, B. F.; Edwards, G. A.; Frye, L. I.; Garry, O. L.; Lavagnino, M. N.; Li, B. X.; Liang, Y.; Mao, E.; Millet, A.; Oakley, J. V.; Reed, N. L.; Sakai, H. A.; Seath, C. P.; MacMillan, D. W. C. Metallaphotoredox: The Merger of Photoredox and Transition Metal Catalysis. *Chem. Rev.* **2022**, *122*, 1485–1542. (b) Tortajada, A.; Juliá-Hernández, F.; Börjesson, M.; Moragas, T.; Martin, R. Transition-Metal-Catalyzed Carboxylation Reactions with Carbon Dioxide. *Angew. Chem. Int. Ed.* **2018**, *57*, 15948–15982.

Aiming at synthesizing carboxylic acids from available starting materials and given the central role of alkyl halides in transition metal catalysis,[2] we elaborated a protocol granting secondary carboxylic acids from their related *unactivated* bromides. Such reaction was developed with the aim of avoiding known chain-walking processes from nickel catalysts, which was achieved by increase of single electron transfer rates along with ligand design. The mild reaction conditions are reflected within the scope of the reaction. A mechanistic investigation has been done which shows the generation of free alkyl radicals along with the importance of Ni(I) intermediates (Chapter 3).

Following the same lines, an improved system was developed allowing for the use of formic acid salts instead of CO_2 gas as a C1 source for carboxylation. This achievement was possible through redox neutral conditions generating the CO_2 radical anion, a powerful reductant, granting access to the desired products. The reaction could be performed in the context of radiolabeling, granting access to 14C-labeled molecules, useful when it comes to ADME studies within pharmaceutical development. The use of formate salts as carboxylating agent also makes a step forward toward the possible implementation of carboxylation chemistry in industrial settings, which is typically not used by companies albeit the elegant advances done by the community.[3]

Figure ii: Photoredox carboxlation of alkyl bromides with formate

[2] Kwiatkowski, M. R.; Alexanian, E. J. Transition-Metal (Pd, Ni, Mn)-Catalyzed C–C Bond Constructions Involving Unactivated Alkyl Halides and Fundamental Synthetic Building Blocks. *Acc. Chem. Res.* **2019**, *52*, 1134–1144.

[3] Davies, J.; Lyonnet, J. R.; Zimin, D. P.; Martin, R. The Road to Industrialization of Fine Chemical Carboxylation Reactions. *Chem* **2021**, *7*, 2927–2942.

Chapter 1. General Introduction

1.1. Carbon Dioxide

Carbon dioxide is one of the main gases in our atmosphere, present at about 420 ppm. It is fairly well understood and proven that this gas is one of the major responsible for the global warming observed since a few decades. While it is not a gas that is desired in excess amount in our atmosphere, its implementation in chemistry as a synthetic block is rather appealing. Indeed, while a considerable amount of people believes that using CO_2 directly as a C1 building block could allow for reducing its amount in the atmosphere, this is not the case in synthetic chemistry, since purification of the gas and general production cost is still a net positive emitting process. Though, the interest lies on another aspect, less well understood. When synthesizing molecules, an organic chemist is usually interested in adding carbons to a structure, through different strategies, using a synthetic catalogue as old as about 200 years, and still counting. Any molecule used for the purpose of adding carbons, has an industrial production energy cost, leading to a certain amount of carbon dioxide emissions. As previously mentioned, although CO_2 production would emit more equivalents of itself compared to the amount put in a container, the corresponding production-related emission is still considerably lower than for any other carbon synthon in organic chemistry, thanks to its inherent availability and ease of production. Thus, building molecules from CO_2 is highly desirable in order for our modern society to *reduce* its carbon dioxide emissions, and potentially manufacturing costs too. Currently, an already high amount of CO_2 is used to industrially manufacture feedstock chemicals, which holds promises for the future, although there still is ample room for more implementation.[1,2]

Before diving into the rich field of carboxylation chemistry, a systematic description of the molecule of interest will be given to understand its reactivity and the challenges associated with the development of processes utilizing carbon dioxide.

1.1.1. Electronics and orbitals

Being part of the $D_{\infty h}$ point group, CO_2 is a linear molecule in its ground state. The two double C-O bonds give net partial charges over each atom. Because of the linearity and the opposed direction of the two dipoles, the molecule is non-polar. This character, together with the molecular orbitals (see Figure 1.1) involved in most of the reactivity of this gas, explain its behavior. The HOMO showcases most electron density at the oxygens atoms, giving a slight Lewis basic character. The LUMO being mostly located on the carbon atom, reveals an electrophilic behavior which is exploited in the majority of

the carboxylation chemistry, most easily demonstrated by the straightforward carboxylation of Grignard and organolithium reagents using a simple atmosphere of carbon dioxide or dry ice.[3]

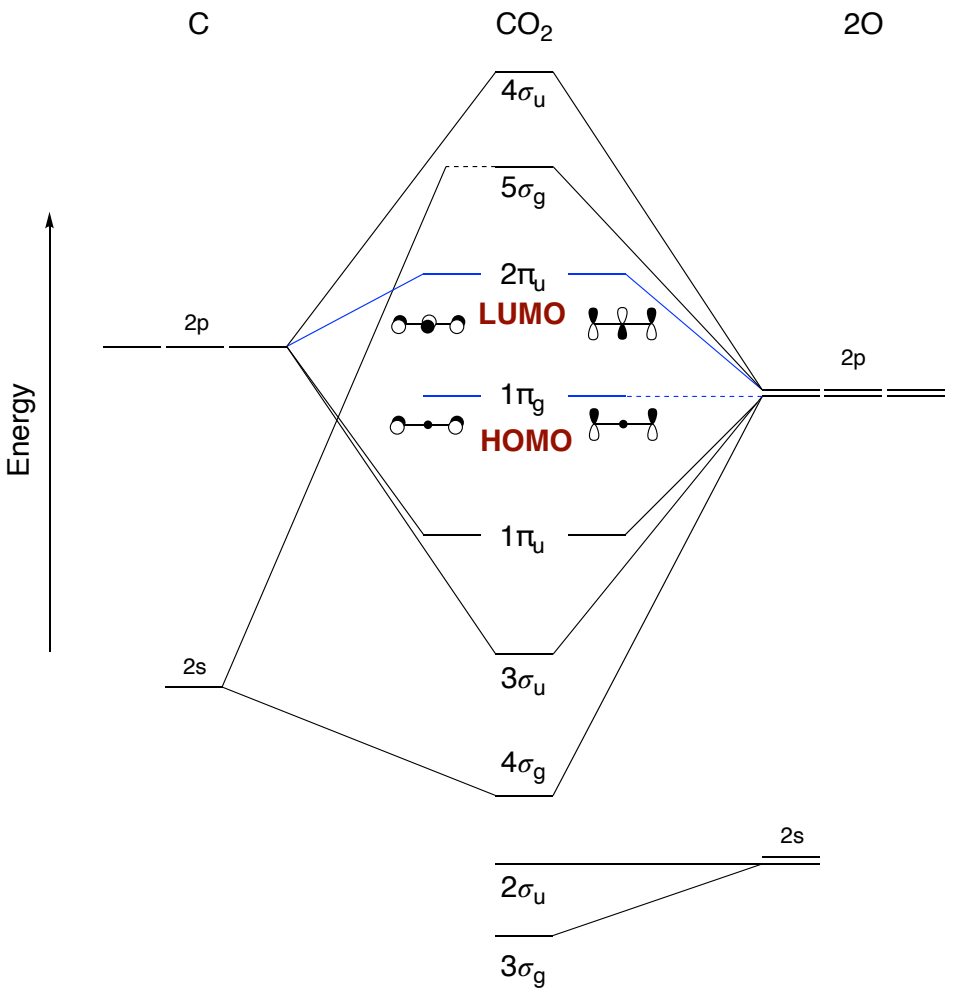

Figure 1.1 : MO diagram of the carbon dioxide molecule.

The Walsh diagram associated with CO_2 (Figure 1.2)[4–6] shows the relative, and qualitative, evolution of the energy levels of each orbital depending on the angle of the molecule, from linearity (180°) to highly bent (90°). By bending the molecule, the energy levels will inevitably change based on favored/unfavored molecular orbital interactions. Bending the molecule changes the point group and therefore splits the degenerate energy levels, as observed for $1\pi_u$, $1\pi_g$ and $2\pi_u$. This splitting is due to the fact that the orbitals become non-equivalent. While $1\pi_u$ and $1\pi_g$ are mildly affected by bending, $2\pi_u$

is more affected, especially in the case of the $6a_1$ normal mode.[5] This drastic stabilizing effect of the $2\pi_u$, the LUMO, transposes into a bending of the molecule in case of population of this orbital, calculated to be 138°.[7] This phenomenon has been observed in many different fields of chemistry, for example when a Lewis base interacts with CO_2 or when the molecule is directly reduced to the corresponding radical anion.[8–11] This observation is also translated, to a broader sense, into the geometry of carboxylic acids, esters, and other related carbonyl compounds, commonly referred to as the sp^2 configuration. The necessary geometric rearrangement of the carbon dioxide molecule, when reduced with one electron, is reflected by an elevated amount of energy required. The reduction potential for the $CO_2/CO_2^{\bullet-}$ couple is equal to -1.90 V vs NHE.[12] While the radical anion is used (directly or indirectly) in CO_2 reduction chemistry attempting to make bulk products derived from this gas,[13–16] organic chemistry has also seen use of it in the recent years as a carboxylating source or reducing agent.[17]

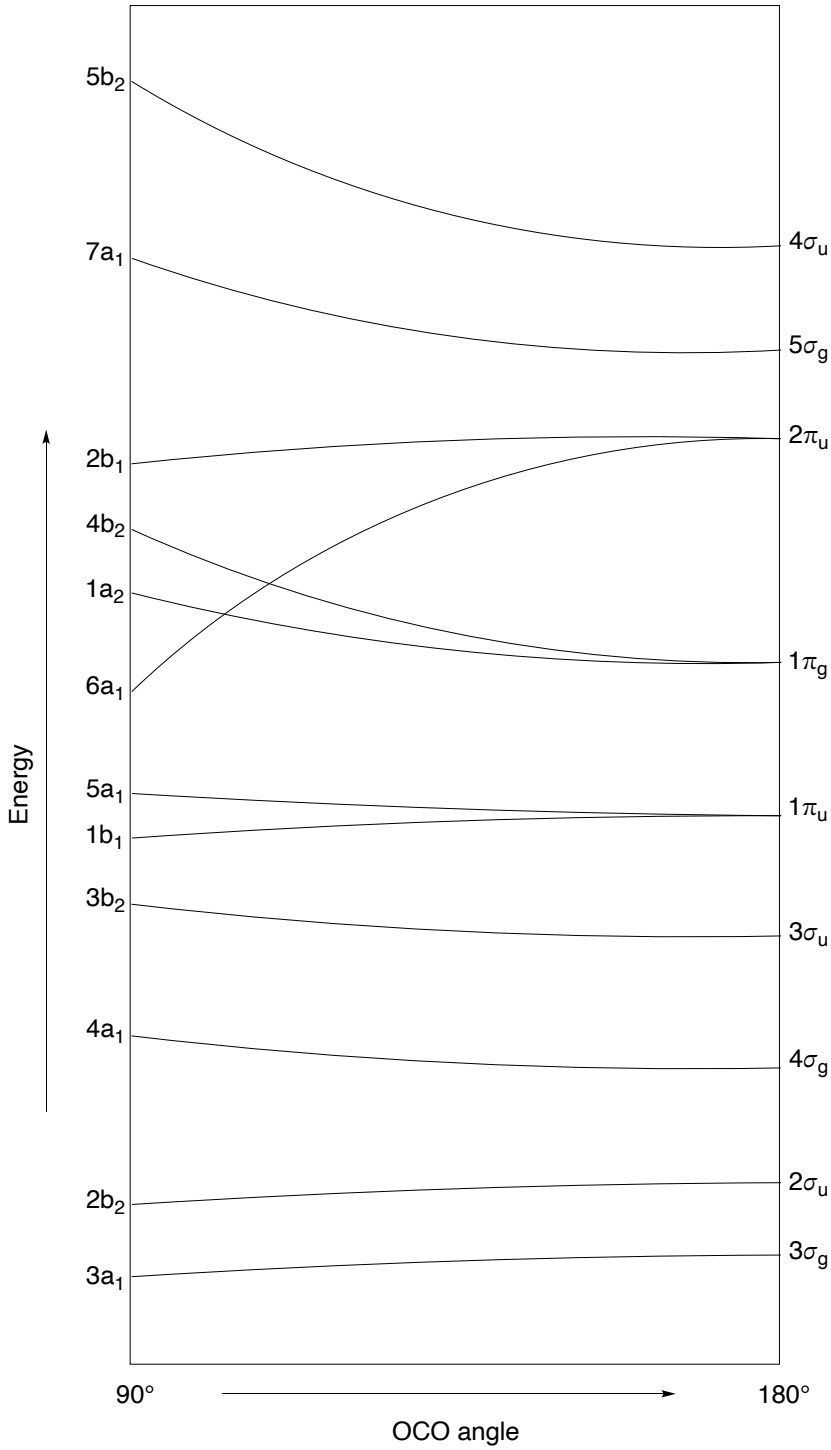

Figure 1.2: Qualitative Walsh diagram of the CO2 molecule.

1.1.2. Binding modes and reactivity

As was discussed in the previous section, carbon dioxide shows an electrophilic character at the carbon atom and some basicity at the oxygen atoms. All its reactivity is therefore rather straight forward when interacting with nucleophiles (Figure 2, left), while its coordination to metals can imply a variety of binding modes (Figure 2, middle). In the case of nucleophilic attack at the carbon atom, the previously described bending of the CO_2 molecule leads to a sp^2 carbon as a carboxylate species, creating a negative charge at the oxygens. This chemistry is historically used with Grignard or organolithium reagent, but modern methods were developed involving a variety of strategies to access carbon-based nucleophiles. More will be discussed on this topic within the following section. The various binding modes of carbon dioxide are directed based on Lewis acidity/basicity but few other parameters such as nuclei radius, electronegativity, vacant coordination site number or geometry amongst others can have an influence. This makes the binding mode of CO_2 difficult to anticipate. It is worth mentioning that some metals might only coordinatively interact with CO_2 when reaching a certain oxidation state, which may require reduction of the metal center. The different binding modes (for monometallic interactions) are the following, as depicted on Figure 1.3, η^1-C, η^1-O and η^2-(C, O).[18–21] As the most representative complex for the work described in this thesis, Aresta's complex shows a Ni η^2-(C, O) coordination of CO_2. Other binding modes involving more than one metal center are also known but will not be discussed in this thesis.

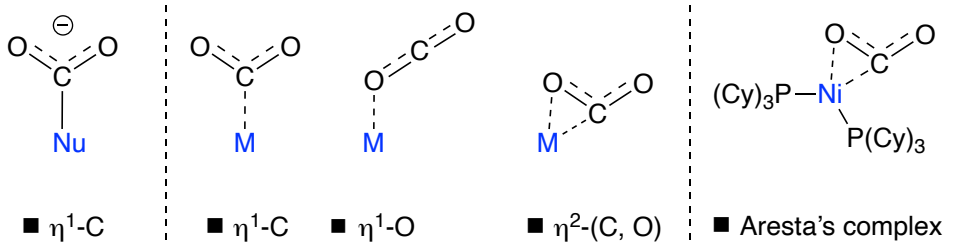

Figure 1.3: Binding modes of carbon dioxide.

It is perhaps important to note that all these binding modes have been characterized at the solid state, suitable for X-Ray diffraction analysis. In solution, these complexes and any metal complex mixed with CO_2, may be amenable to some equilibria for which CO_2 can decoordinate and might also involve other binding modes to be present in lesser amount, including non-described bimetallic modes. We consider Ni to bind with the described η^2-(C, O) mode in the Aresta's complex, but in solution, the other modes

cannot be excluded. The potential shift from η^2 to η^1 should in theory allow for the creation of a new vacant coordination site, which leads to compatibility with reactivity in catalysis. While coordination of CO_2 to a metal might potentially happen to virtually any metal with free coordination sites in solution through Lewis acid/basic interactions, it is generally observed that low oxidation states are typically required to trigger reactivity in CO_2 coupling catalysis. This could be attributed to two factors: 1) the more Lewis basic character of the metal, activating CO_2 in a more pronounced manner and 2) the increase of nucleophilicity of any carbon-based ligand meant to react with carbon dioxide. In the specific case of nickel carboxylation chemistry, more precisely for alkyl carboxylation, Ni(I) has been shown by different studies to be necessary for a carboxylation event to happen.[22–26]

1.2. Carboxylation Reactions

Carboxylation reactions have been widely explored, tracing back to when Victor Grignard first tested his eponymous reagents with carbon dioxide up until nowadays, where ever-more elaborated reactions for the incorporation of CO_2 are being developed. The incorporation of carbon dioxide into organic molecules can be performed using metal catalysis and as a metal-free approach. It is important to stress that some reactions involve metal catalysts for the reaction, but do not involve the metal itself for the carboxylation step. Such reactions will be classified herein as metal-free carboxylation. More recently showcased methodologies involving photoredox chemistry will be discussed separately, as more concepts, introduced in the following section, are involved in those cases. As was introduced before, the vast majority of the carboxylation chemistry happens by nucleophilic activation at the carbon atom. Although it has been shown that for frustrated Lewis pairs (FLPs) catalysis in the context of CO_2 activation, the reactivity relies mostly on the electrophilic counterpart of the pair, namely, the Lewis acid.[27]

1.2.1. Stoichiometric reactions

Historically, direct carboxylation of organic molecules from carbon dioxide has been demonstrated with particularly strong nucleophiles, such as Grignard reagents and organolithium compounds (Figure 1.4).[28]

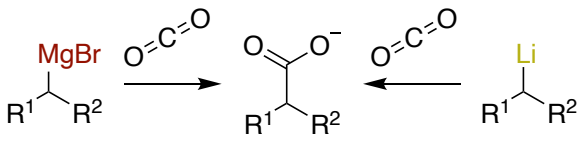

Figure 1.4: Stoichiometric direct carboxylation chemistry.

As an extension and follow-up of these examples, carboxylation of typical nucleophiles encountered in classical organic chemistry has been shown. The first example has been demonstrated by Bottaccio *et al.* in 1966, in which activated methylene groups, α-carbonyl carbons, could be carboxylated by deprotonation, forming the enolate intermediate (Scheme 1.1, a).[29] Many other similar reactions have then been reported.[30–33]

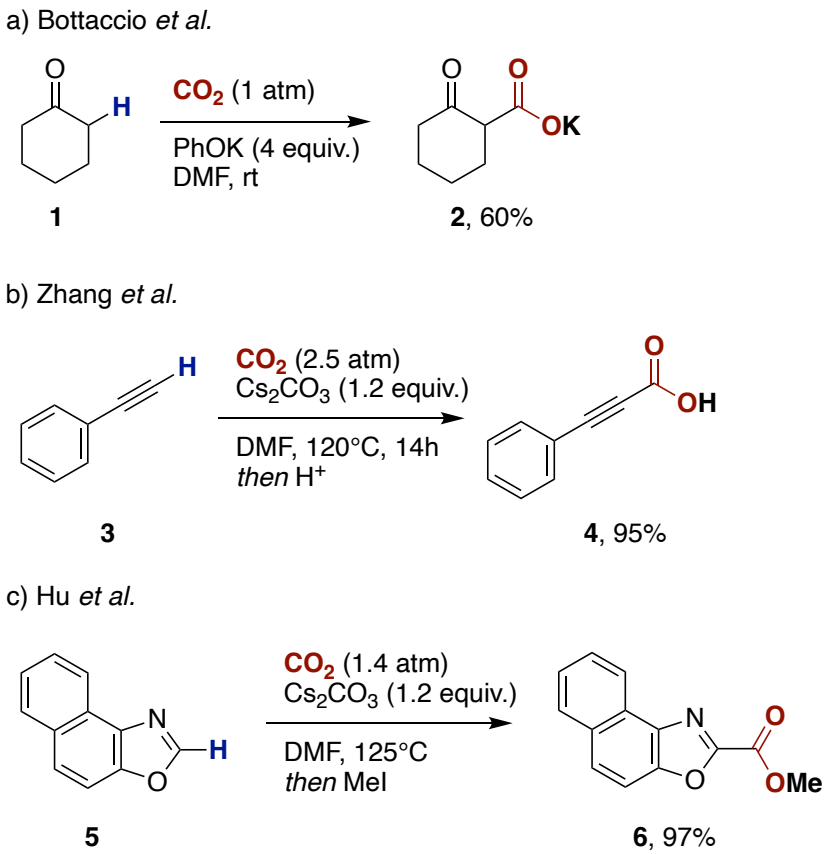

Scheme 1.1: Stoichiometric reactions of carbon-based nucleophiles.

Another reaction that was rapidly developed is the synthesis of propiolic acids from the corresponding terminal alkynes, as alkynes have a relatively acidic proton. Early

findings and general approach used either Cu or Ag to catalytically coordinate the π-cloud of the triple bond in order to acidify further the terminal C-H bond.[34,35] Though, a direct, catalyst free, carboxylation has been reported in 2011 by Zhang, for which Cs_2CO_3 proved to be sufficient in DMF at 120°C (Scheme 1.1, b).[36] Zhang's conditions were inspired from a procedure reported the preceding year by Hu, which allowed for the carboxylation of acidic C-H bond containing heterocycles (Scheme 1.1, c).[37] All three of these examples showcase perfectly that nucleophilic carbons are typically well reacting with carbon dioxide. Nevertheless, the need to access carboxylic acids from varied functional groups and the necessity for milder conditions pushed chemists to develop transition metal (TM) catalyzed processes that would allow for carboxylation chemistry from carbon dioxide.

1.2.2. Organometallic catalysis

The field of catalytic carboxylation reaction by means of TM catalysis has shown a lot of attention over the last decade. While stoichiometric reactions were rather well established, it is not before 1997 that the community was granted with the first report consisting of a catalytic system based on a TM (Scheme 1.2, a). The reaction, showcased by Nicholas *et al.*, catalyzed the carboxylation of allylic stannanes using $Pd(PPh_3)_4$ as catalyst in THF at 70°C. A subsequent milestone in the field was reported by Iwasawa in 2006, when the group managed to catalytically carboxylate aryl derivatives for the first time. The group made use of Rh(I) as catalyst together with dppp as ligand (Scheme 1.2, b).[38]

Until this time, all reported procedures involved redox neutral conditions, and thus the need for a nucleophilic starting material to be coupled with CO_2. In order to be able to couple the most typical functional groups in TM catalysis, halides, reductive conditions were yet to be investigated. It is in 2009 that Martin & coworkers solved this puzzle, using a Pd catalyst along with a phosphine ligand, to carboxylate aryl bromides (Scheme 1.2, c).[39] Et_2Zn was the reductant of choice in this case. Although the conditions were not particularly mild given the reactive organozinc used and the high CO_2 pressure (10 atm), this reaction set the stage for improvement and further development of the newly born field of reductive catalytic carboxylation chemistry. Countless reactions have been disclosed to this day involving a range of amenable substrates for TM catalysis, including but not limited to nucleophiles (organoboron, stannanes, organozinc), alkenes, alkynes and electrophiles such as (pseudo)halides to cite a few.[40,41]

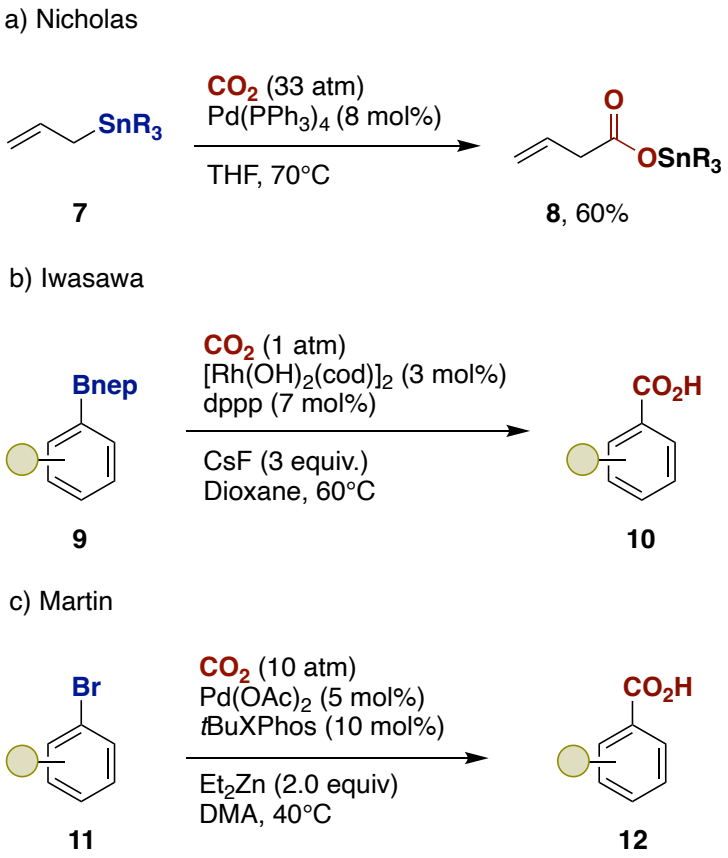

Scheme 1.2: First key reports on transition metal catalyzed carboxylation.

When mentioning step-economical chemistry and related atom-economical principle, the most desired transformation that can be realized is the functionalization of C-H bonds, alleviating the need for functional group installations. While acidic C-H bonds can simply be deprotonated for further nucleophilic functionalization, as shown in Scheme 1.1, the functionalization of non-activated bonds, such as on a phenyl ring, happen to be much more difficult to perform. An elegant solution, within the carboxylation chemistry, to this challenge has been brought to light by the group of Iwasawa in 2011 using a Rh catalyst which is guided by a pyridine directing group towards the ortho C-H bond (Scheme 1.3).[42] The driving force of the reaction is the production of methane from a methyl aluminum derivative that efficiently reduces the oxidative addition complex Rh(III) back to Rh(I), becoming the active carboxylating species. The proposed mechanism is initiated by the ligand exchange of the Rh(I) chloride precatalyst to methyl-Rh species **15**. This low valent Rh intermediate is then able to insert into a C-H bond, guided by the pyridine substituent, giving Rh(III) **16**. A reductive elimination then happens by extruding methane, leaving the aryl-Rh(I) **17** as active carboxylating species.

Rh-carboxylate **18** closes the catalytic cycle through a transmetallation with the methyl-aluminum in solution. The crude carboxylic acid obtained from **19** is methylated using $TMSCHN_2$ in order to isolate the methyl ester. This methodology, stepping into the difficult field of C-H functionalization, has unfortunately received virtually no echo, and therefore remains a challenge to be undertaken for the development of improved systems.

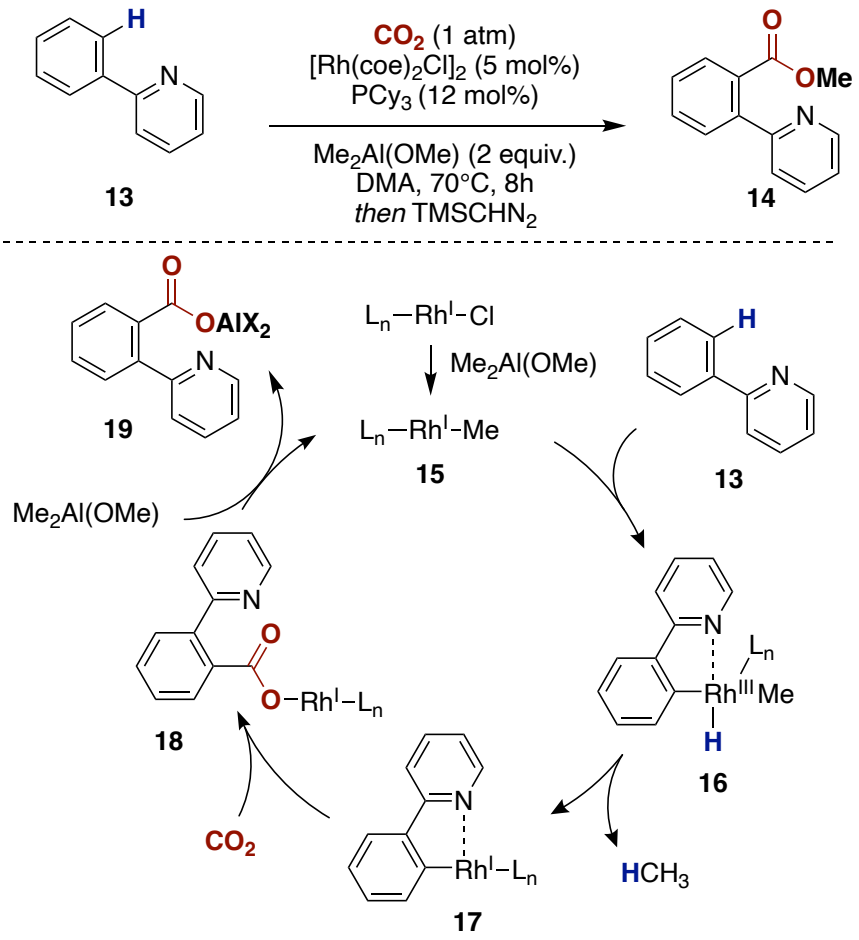

Scheme 1.3: Iwasawa's methodology for the sp2 C-H carboxylation.

Considerable attention has been given instead to the reductive carboxylation of (pseudo) halide compounds, given their availability. As previously introduced, the first report from Martin consisted in a Pd catalyzed process, but looking through the literature, one can rapidly observe that Ni is at the center stage of the field. A methodology reported by Tsuji *et al.* in 2012 represented the cornerstone in the shift

towards this metal (Scheme 1.4). Indeed, the group reported the direct carboxylation of aryl and vinyl chlorides, being even more available than bromides, using a Ni(II) precatalyst bearing triphenylphosphines as ligands under one atmosphere of CO_2. The work also demonstrated the first appearance of Mn as a sacrificial reductant for Ni, being still nowadays one of the most used reductants within the field.

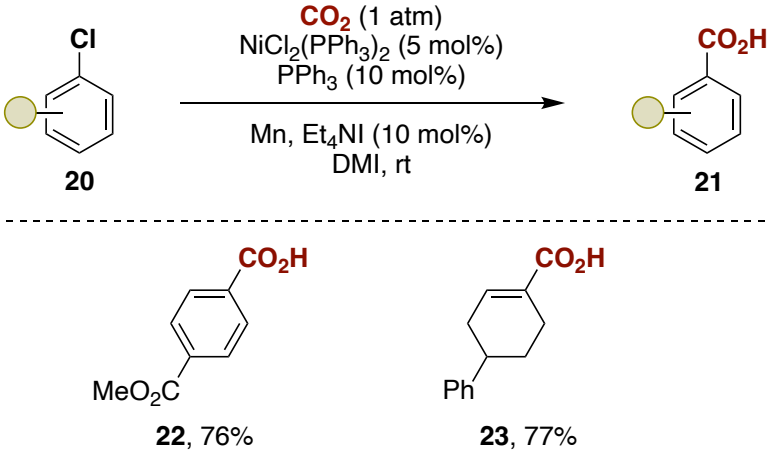

Scheme 1.4: Tsuji's Ni reductive carboxylation of aryl and vinyl chlorides.

Ever since, the field has only grown more, and new challenges needed to be overcome. While all these reactions, along with all the reactions that haven't been mentioned, are of high interest, the emergence of photochemistry opened new doors for chemists to develop even more carboxylation methods to reach milder conditions along with broader scopes.

1.3. Photochemistry

Energy is at the center stage of chemistry, whether it is fundamentally, in its thermodynamics, or at the societal level, where we, humans, look every day for a better energy-efficient infrastructures. All chemical reactions have an activation barrier, corresponding to the minimum amount of energy required for it to occur, noted E_a. A thermal reaction proceeds when the temperature of the reaction medium is giving at least the minimum required amount of energy to the molecules involved. If the activation barrier is high, heating is necessary, and conversely, if the reaction barrier is very low, cooling may be applied to slow the reaction down. While thermal reactions represent the vast majority of chemistry, early findings of reactions triggered by the presence of

light have been described. The first observation of light interaction in organic chemistry was reported as early as in 1834 by Tromsdorff.[43,44]

1.3.1. Fundamentals

For a photochemical reaction to happen, a photon is being absorbed by a molecule (depicted as A on the following figures). The absorption leads to the excitation of the electronic state of the molecule, to an electronic configuration higher in energy than the initial state, in most of the cases, the ground state. Electronic states of atoms and molecules are leveled at specific energies, as described by quantum physics. The energy interval between two energy levels is typically written as ΔE. For a photon to be absorbed by a molecule and therefore for excitation to happen, the energy of the photon must match with ΔE. The energy of a photon can be simply calculated based on its wavelength according to Eq. 1. In this equation, *h* corresponds to the Planck's constant, *c* to the speed of light and λ to the wavelength of the photon.

$$E = \frac{hc}{\lambda} \quad \text{Eq. 1}$$

After being excited, a molecule has a higher energy level, which is exactly what is being exploited by the photochemist in order to establish reactivity. Once at the excited state, it is typical that the following activation barrier (E_a'), for a chemical reaction, falls in the range of room-temperature energy activation. Therefore, the reaction proceeds (usually) without the need for heat and a light source serves as sole energy input. The excitation of a molecule and the activation barrier change is depicted in Figure 1.5.

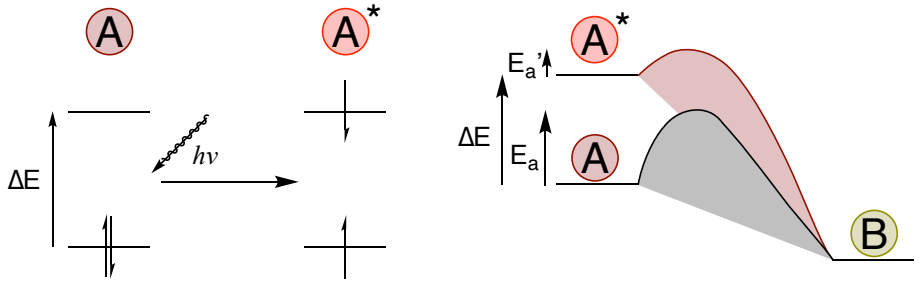

Figure 1.5: Photon absorption and molecule excitation with light.

Once excited, a molecule has essentially four different reactivity profiles available, of which not all molecules are susceptible to. First, an excited molecule can engage in a monomolecular reactivity, transforming only with exposure to light, or a bimolecular

reaction with another reagent, leading in both cases to a different molecule B (Figure 1.6, a). This is most famously the case for the biosynthesis of Vitamin D_3.[45] The three other possible events are bimolecular processes, called quenching events. One of them (Figure 1.6, b) is an energy transfer quench. An energy transfer consists of the bimolecular interaction of the excited molecule (A*) and a second molecule called a quencher (Q). Upon return to the ground state, molecule A will bring the quencher to its excited state (Q*). The two last possible events are called oxidative quench (Figure 1.6, c) and reductive quench (Figure 1.6, d). Those processes involve a SET between A* and Q. In the case of a reductive quench, the quencher accepts in its LUMO the excited electron from A*, giving rise to the radical cation of A and radical anion of Q. For the oxidative quench, Q gives one of its electrons of the HOMO to the lowest SOMO of A*, leading to the radical anion of A and radical cation of Q.

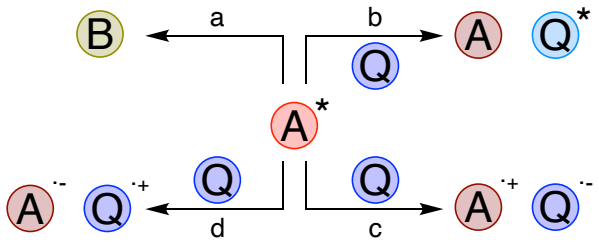

Figure 1.6: Non radiative excited state reactivity.

In modern photochemistry, molecule A is called a photosensitizer or photocatalyst (PC), which under specific light irradiation drives the reaction towards the products by formation of key intermediates, often radical intermediates when oxidative and/or reductive quenches are involved.

1.3.2. Redox of photochemistry

Since any reaction has to respect electronic neutrality, not becoming electrically charged over time, a PC performing a reductive quench must give its gained electron to another molecule, called acceptor, in order to come back to its original state. The opposite goes in the case of an oxidative quench, by interaction with a donor molecule. All the redox potentials of the ground state and the excited state can be measured, giving the chemist a good idea of the use of a particular photocatalyst against another, as can be exemplified in Figure 1.7 for 4-CzIPN.[46]

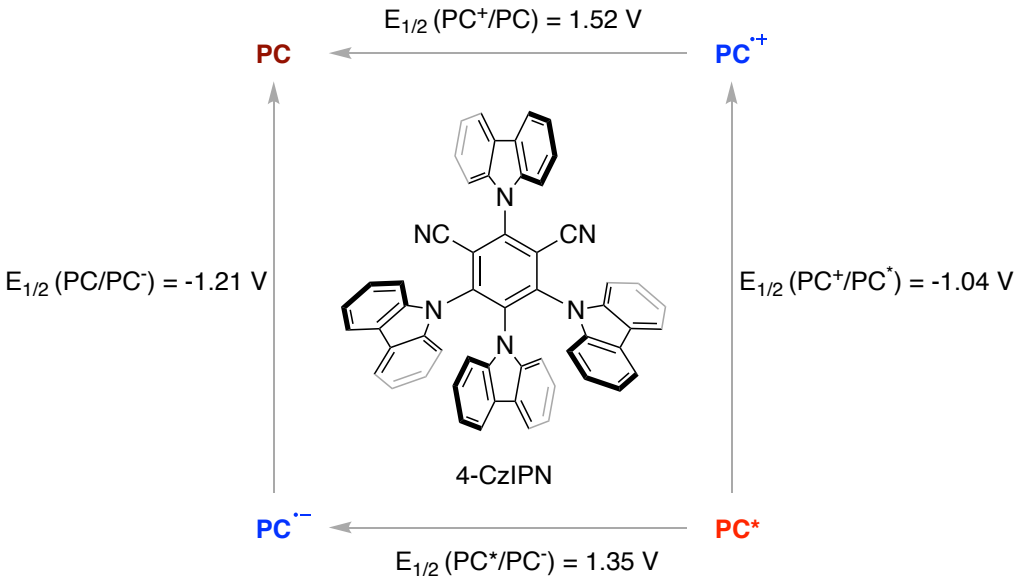

Figure 1.7: Redox potentials associated to 4-CzIPN. Potentials given against SCE.

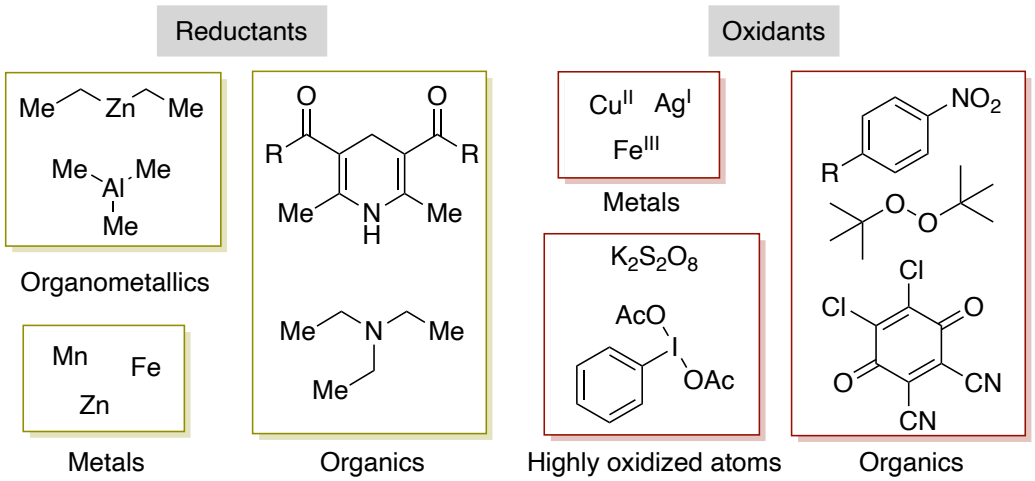

Figure 1.8: Examples of sacrificial reductants and oxidants.

In order to reach electronic neutrality, a typical reaction involves a species that gets oxidized and another that gets reduced. This allows for the coexistence of (minimum) two independent SET events within the same catalytic cycle. Thus, the attractive feature that makes photoredox chemistry of interest, is the formation of open shell, typically radical, species. This allows for new disconnections to be established when designing a synthesis. Photoredox reactions, like thermal reactions, can also be net oxidative or reductive, when two nucleophiles or electrophiles need to be coupled. In such cases, a sacrificial oxidant or reductant must be used, see Figure 1.8 for some examples. The use of such sacrificial compounds allows for the utilization of only one of the two redox processes, when of interest, in a synthetically productive manner. The undesired SET will thus be compensated by the sacrificial reagent.

Illustrating a redox neutral reaction, Hou, Li & coworkers have recently shown the carboxylation of terminal alkenes in a redox neutral fashion, using cheap formate salts as a C1 synthon.[47] As shown on Scheme 1.5 and according to the authors, the reaction starts with the photoexcitation of the PC, Eosin B or Ir[(ppy)$_2$(dtbbpy)]PF$_6$, followed by a reductive quench from the formate salt **25** to give an oxygen based radical **25'** and the reduced form of the PC. The newly formed radical is then able to undergo a hydrogen atom transfer (HAT) with another equivalent of **25** thanks to the high bond dissociation energy (BDE) of the O-H bond of formic acid (111.5 kcal/mol), yielding formic acid **25-H** and the CO_2 radical anion (CRA). In the next step, the CRA does a radical addition into the alkene starting material **24**, giving a carbon radical species, which in this work corresponds either to a benzylic site or an α-carbonyl carbon. The generated radicals are then reduced to the corresponding anions with the reduced PC to complete the catalytic

cycle, and final protonation of the anion, likely from the generated formic acid **25-H**, yields the product of the reaction.

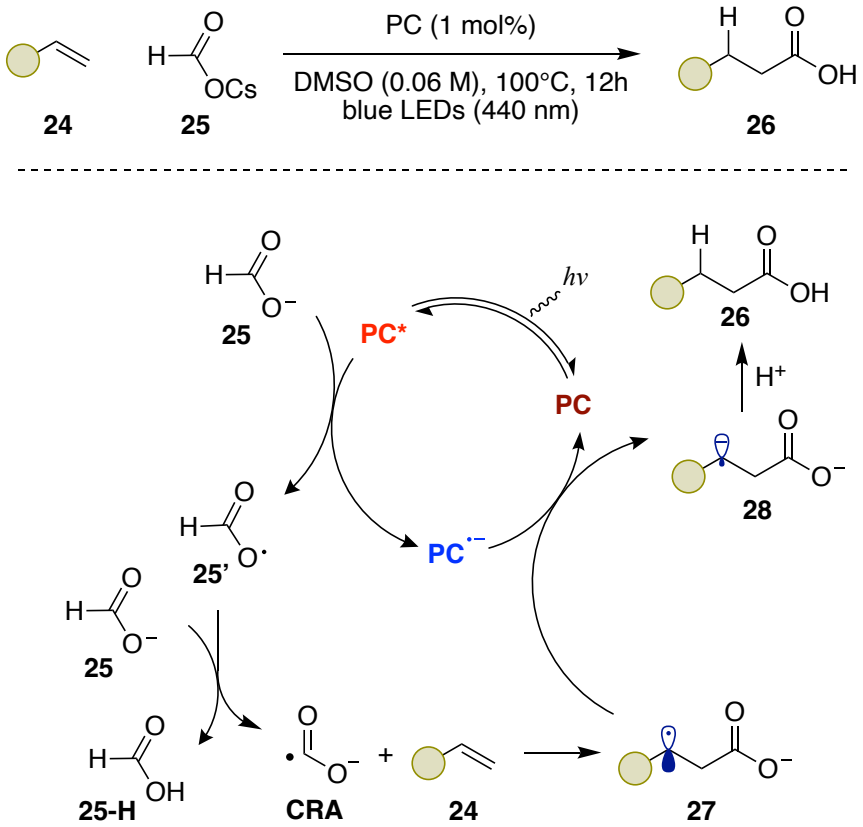

Scheme 1.5: Application of a redox neutral photoredox reaction in carboxylation chemistry.

1.3.3. Reductive photoredox chemistry

When it comes to reductive photoredox chemistry, many different types of compounds can be used for the purpose of giving the extra electrons needed. One of the historically most used classes of reducing molecules is amines, trialkyl amines in particular.[48] Illustrating such methodology, Yu has recently published an elegant way to make carboxylic acids from terminal alkenes too. Unlike Hou and Li as previously shown in Scheme 1.5 and others using formate salts,[49–51] Yu's group has managed to use CO_2 directly to access the CRA species as carboxylating intermediate.[52] This methodology, depicted in Scheme 1.6, also represented at the time the first example of hydrocarboxylation of unactivated alkenes using the CRA. The authors managed to

develop this reaction by using fac-Ir(ppy)$_3$ as PC, DIPEA as sacrificial reductant with tBuOK and TBAC in NMP under blue light irradiation.

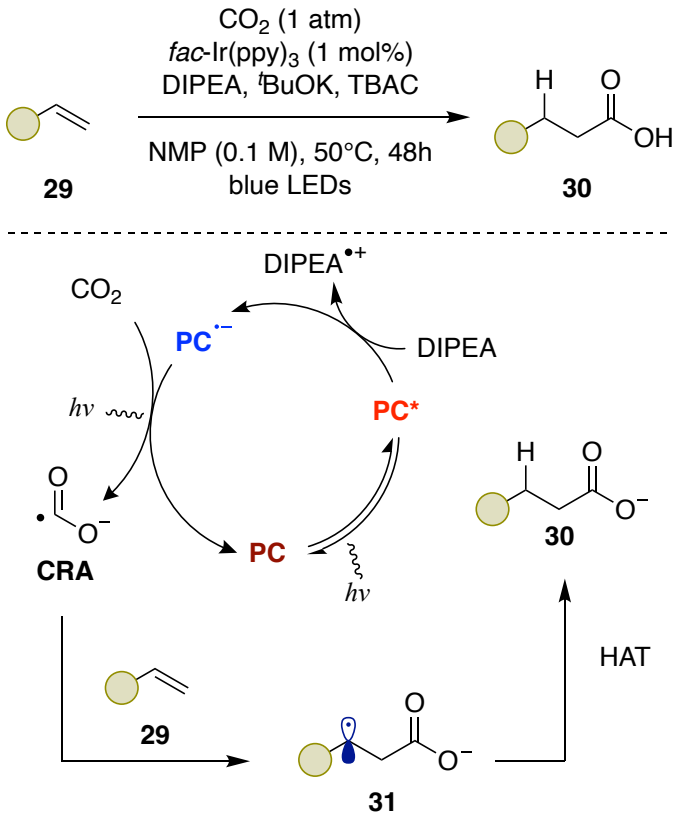

Scheme 1.6: Reductive photoredox manifold for the hydrocarboxylation of alkenes.

The reaction is initiated by the photoactivation of the photocatalyst, which can be reduced after reductive quenching from DIPEA. The authors mention the need for what they call "consecutive photo-induced electron transfer (conPET)", which corresponds to another photon absorption of the PC after the initial photoinduced SET, but before giving away the electron it gained from quenching. Such an activated species is able to reach very low reduction potentials and hence reduce CO_2 to the CRA.[53,54] This conPET generates the CRA, which can add into the alkene **29**, giving radical intermediate **31**. Final HAT from the solvent or DIPEA yields the final carboxylic acid product **30** after acid quenching of the reaction mixture.

1.3.4. Metallaphotoredox

Unsurprisingly, chemists, understanding the benefits of photochemistry, quickly tried to develop methods that would constitute a double catalytic system. A traditional TM catalyst would be present in order to couple intermediates to form products of interest, and a photocatalyst to mediate the electron transfers inside the reaction vessel. The earliest report on a modern dual photoredox-transition metal catalyzed reaction was done in 2007 by the group of Osawa (Scheme 1.7).[55]

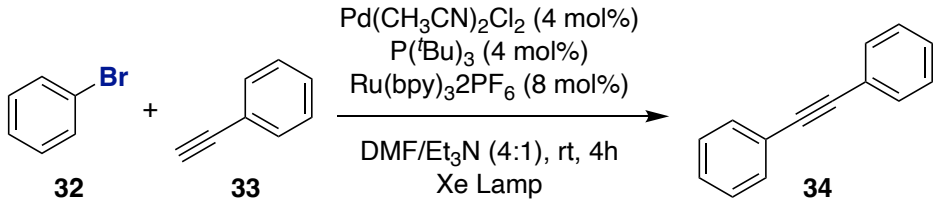

Scheme 1.7: Osawa's metallaphotoredox Sonogashira coupling.

This photoredox mediated Sonogashira coupling offered for the first time a dual catalytic system. The presence of the photocatalyst $Ru(bpy)_32PF_6$ alleviated the need for a typical copper co-catalyst, traditionally used for Sonogashira couplings. Although this report consisted in itself as a breakthrough for the, back then, practically inexistent field, it took several years for the community to understand the implications and advantages of such a powerful catalytic pairing. The use of Pd as a metal proved compatible, but its well-known appreciation for even oxidation states hampers its systematic use in routine metallaphotoredox chemistry, although many reports have been disclosed.[56]

Metals that are able to access successive even and odd oxidation states are inherently more suited for systematic metallaphotoredox methodology development. Such TM mainly lies on the first row, and comprise Co, Ni and Cu as key players. Focusing on Ni particularly, this metal has proved to become a “go-to” catalyst for the combination of halide electrophiles and radical precursors thanks to its ease of accommodation with photoredox chemistry, along with about a decade of experience from the community at the time of writing. The seminal work attributed to nickel metallaphotoredox chemistry comes from the groups of MacMillan and Doyle who, in 2014, reported the coupling of amino acids with aryl bromides (Scheme 1.8).[57] The reaction proceeded by decarboxylation of the amino acid to generate an α-amino radical.

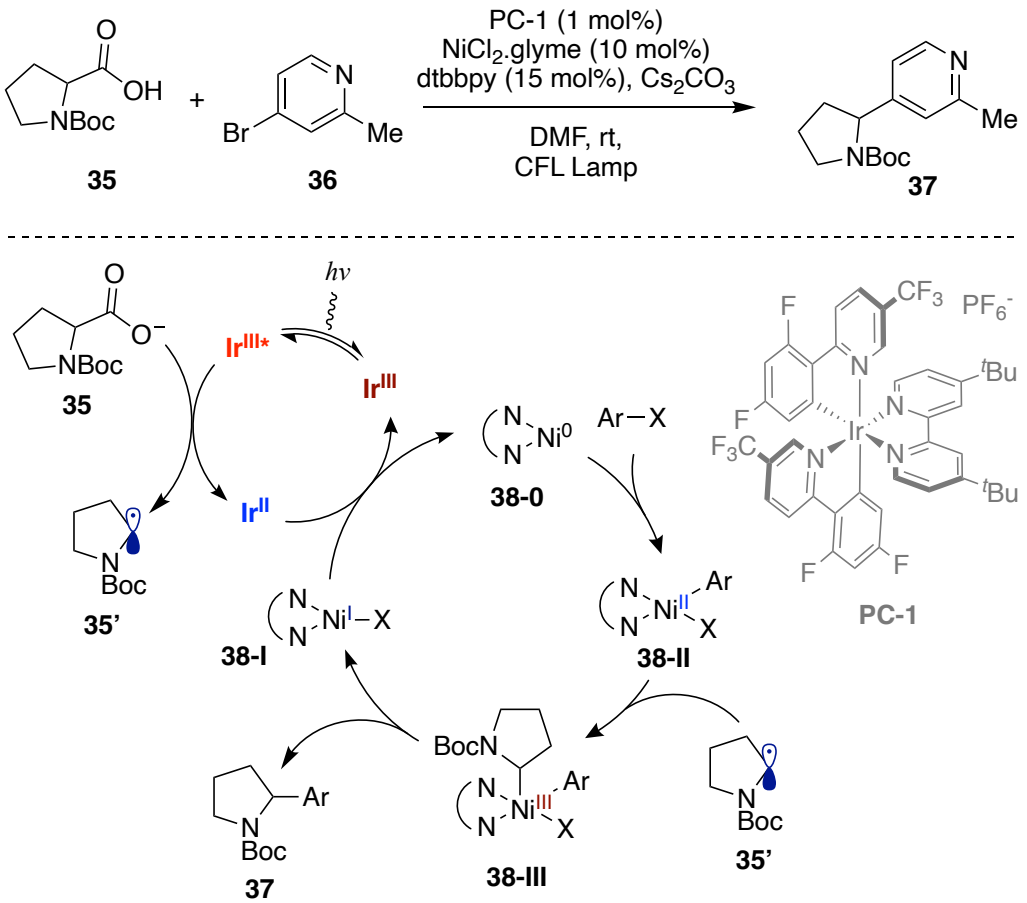

Scheme 1.8: Doyle and MacMillan's seminal work on Ni metallaphotoredox.

The reaction starts with the reduction of the Ni(II) precatalyst to the active Ni(0) species, mediated by the PC. In order to get reduced, the PC, once photoactivated, oxidizes the amino acid, which after a loss of CO_2, yields free radical **35'**. The authors mention that $E_{1/2}$ (Ir^{III}/Ir^{II}) = -1.37 V vs SCE while the two-electron reduction $E_{1/2}$ (Ni^{II}/Ni^{0}) = -1.2 V vs SCE. According to these redox potentials, the reduced PC should be able to reduce Ni all the way down to the d^{10} complex Ni(0) **38-0**. Following classical organometallic catalysis, the low valent complex **38-0** can easily undergo oxidative addition into an aryl halide present in solution, yielding the Ni(II) intermediate **38-II**. Previously generated radical **35'** adds to the complex, generating a high valent Ni(III) complex **38-III**. The higher oxidation state of this complex favors the reductive elimination step, giving the product and Ni(I) complex **38-I**. One electron reduction of this complex back to Ni(0) **38-0** closes the catalytic cycle.

While metallaphotoredox and photochemistry in general became their own fields of study,[56] the carboxylation arena has also benefited from light mediated chemistry.[58–62]

1.3.5. Photoredox carboxylation

The first disclosure of the combination of photochemistry and carboxylation was reported in 2017 by Iwasawa & coworkers with use of dual photoredox and rhodium catalysis (Scheme 1.9).[63] The work showcased the hydrocarboxylation of alkenes using trialkyl amines as sacrificial reductant, giving mild conditions. The product gave only one carboxylic acid isomer on the benzylic site, with no observable amounts of linear product. The main side product being the reduction of the double bond which could be avoided by addition of Cs_2CO_3 to the mixture.

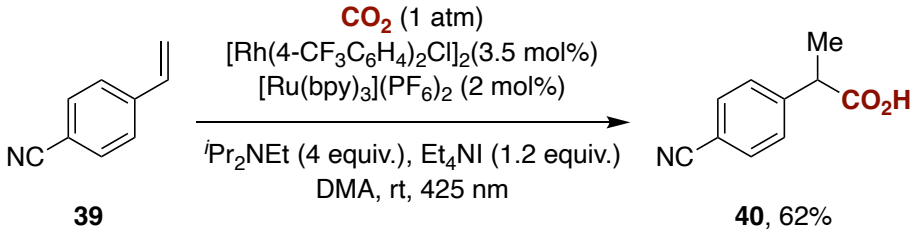

Scheme 1.9: Iwasawa's photoredox hydrocarboxylation of styrenes.

Radical-polar crossover (RPC) reactions have come to life thanks to photoredox systems. The principle relies on the generation of a radical, typically on an activated site such as a benzylic position, that would easily be reduced via SET to the corresponding anion. This anion, following historical reports on carboxylation, reacts with CO_2 to give the corresponding carboxylate. Thus, two different approaches have been taken by chemists. In the first one, the most direct, a HAT process is used to homolytically remove a hydrogen atom on a benzylic site to give the radical, followed by RPC, giving the desired product. The second approach, giving rise to a lot of possible variations, consists in generating a radical from various sources, which can itself participate in an addition into , generally, a styrene. The intermediate after addition is not different than in the case of a HAT strategy which once again allows easy RPC followed by carboxylation. In 2019, the groups of König[64] and Murakami[65] independently reported a C-H benzylic carboxylation method (Scheme 1.10). Both protocols generated the same benzylic radical intermediate using HAT technologies, albeit from different approaches. While for Murakami the radical was then recombined with Ni for what resembles a type of classical Ni metallaphotoredox system, König opted for a RPC strategy, requiring less reagents and less energy intensive light for the same outcome. A silane was used as a HAT catalyst

in this case. The advantage of Murakami's method was that it could be translated to non-activated sp^3 carbons, granting carboxylation of aliphatic solvents.

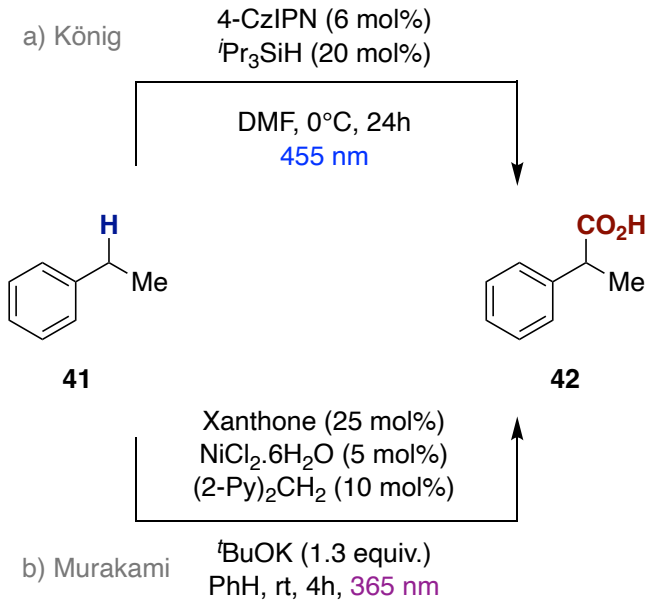

Scheme 1.10: König and Murakami's conditions for the C-H benzylic carboxylation.

The second approach for the carboxylation of benzylic sites using RPC has been first reported by Martin & coworkers with their seminal work from 2017 (Scheme 1.11).[66] Carbon-centered radicals were added to a styrene, leaving a benzylic radical that could be easily reduced to its corresponding anion, giving a carboxylate in the presence of carbon dioxide. Martin made use of Langlois reagent as a CF_3 radical source for reaction development, but other carbon radical precursors were amenable to the same reactivity. Different sulfinates, oxalates and trifluoroborates were therefore showcased.

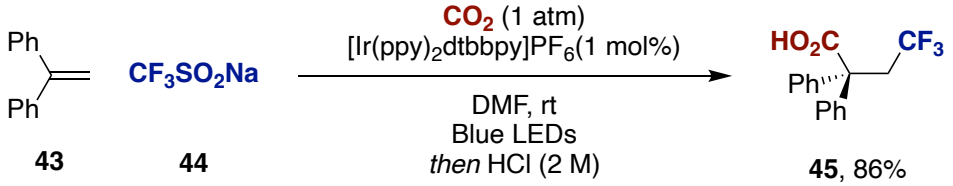

Scheme 1.11: Martin's seminal work on radical polar crossover carboxylation.

More recently, hydrocarboxylation of alkenes has been shown using photochemistry without using a CO_2 atmosphere for the reaction, but rather a reduction product of carbon dioxide, formate salts. Being already reduced compared to carbon dioxide, a reaction involving a formate salt as a C1 synthon with an electrophile becomes redox

neutral and avoids the use of a sacrificial reductant, while also offering a monophasic system, easier to handle than typical carbon dioxide atmosphere. This also brings the advantage of bringing the C1 source down to near stoichiometric amounts, since the formate salts can be weighed on a bench. The Wickens group was the first to photochemically report such a process in 2021, where activated alkenes could be hydrocarboxylated using a PC and a thiol HAT catalyst (Scheme 1.12).[50] The key reactive intermediate in the reaction was the CRA, which was not formed by direct reduction, but rather by HAT on the sole hydrogen atom of the formate anion. The CRA can then add directly into the alkene, leaving a carbon radical that can perform the final HAT step, recovering the hydrogen leading to the product. The authors performed deuterium experiments to show that the hydrogen atom added on the benzylic site does come from the formate salt and not from DMSO, although water traces in the solvent could also be a source of hydrogen. This method was later expanded by the same team to *unactivated* alkenes using a very similar strategy only that no PC was necessary.[51] Indeed, after doing some studies, the group found that the thiol HAT catalyst was directly activated by the light source. Yu & coworkers also reported a methodology for the hydrocarboxylation of alkenes by intermediate of the CRA, although in this case, the radical anion was generated by direct reduction, as shown earlier in Scheme 1.6.

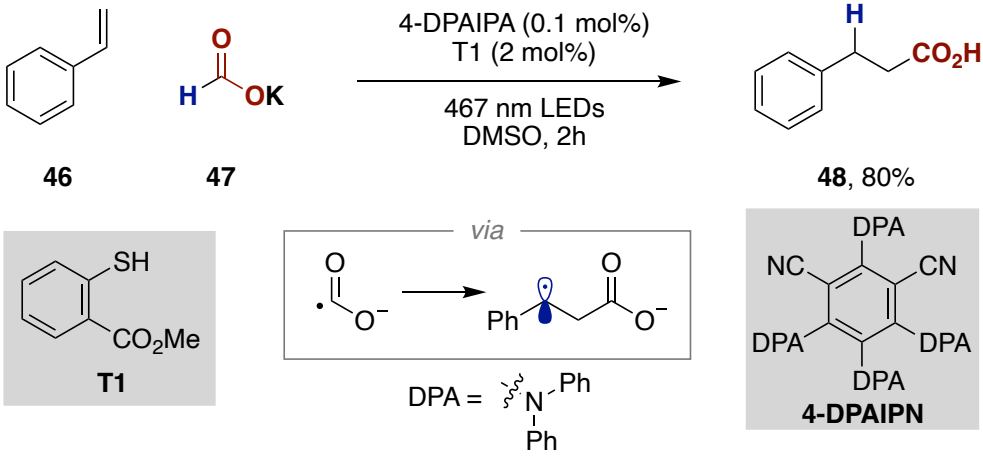

Scheme 1.12: Wickens' photochemical hydrocarboxylation.

1.4. Nickel Catalysis

Nickel is the element number 28, sitting on the 10th column and 4th row of the periodic table. The metal has been discovered in 1751 by the Swedish chemist von Cronstedt. Its first use in catalysis has been reported in 1954 by Kharasch, noticing that a catalytic amount of $NiCl_2$ gave a homocoupling of Grignard reagents.[67] Transition metal catalysis as a field has mostly benefited by the use of lower-row transition metals such as palladium, ruthenium, rhodium, or iridium. Indeed, Nobel prizes have been given for the development of rhodium, ruthenium, and palladium catalyzed reaction.[68–70] The field of nickel catalysis has shown great expansion over the past few decades thanks to the low price of the metal compared to lower transition metals and due to its similarities, but also differences, in reactivity with palladium. The surge of metallaphotoredox chemistry, as discussed above, put nickel as a mainstream catalyst for such reactions. Although similar on some aspects to palladium thanks to the same valence composition, both metals naturally show differences in their intrinsic properties. Nickel is a smaller atom, less electronegative and accesses all oxidation states from 0 to IV, while palladium favorizes even oxidation states.[71] These differences allow nickel to engage more easily with one electron chemistry. Indeed, it is able to perform oxidative addition in a two or one electron fashion, but also doing it from Ni(0) or Ni(I), which can affect the reactivity further. While this makes it seem like nickel is superior to palladium, in reality it only makes its implementation into catalytic methodologies more difficult to tame due to the plethora of possible side-paths it offers. This is the reason why the community focused for decades mostly on palladium and other metals, thanks to their milder and more predictable reactivities, and why nickel only saw a recent emergence in catalysis thanks to the advances made.

1.4.1. Nickel cross-coupling reactivity

Because of its smaller size and being more reducing compared to Pd, Ni is able to perform oxidative additions with more ease.[72] To exemplify this, as shown in Scheme 1.13, it has been calculated that for the oxidative addition into chlorobenzene, the N-heterocyclic carbene (NHC) complex of Pd requires 23.7 kcal/mol while the related Ni complex only needs 0.8 kcal/mol.[73] This difference is further observed by the studies and then development of strong C-X bond insertion reactions using Ni.

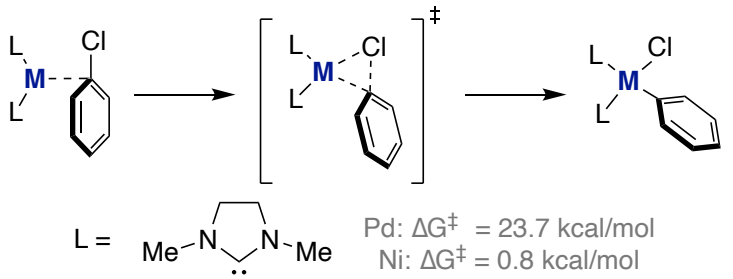

Scheme 1.13: Comparison of the oxidative addition barriers between Ni and Pd.

One of the most striking examples of strong C-X bond functionalization using Ni is the insertion into C-O bonds. Many C-O electrophiles have been used with other transition metals such as palladium, the oxygen counterpart typically represented a rather activated group, such as aryl sulfonates. Nickel, in its case, is able to undergo reactivity with bonds that were typically considered difficult to react, such as aryl methyl ethers.[74,75] A methodology from Dankwardt & coworkers nicely showcases the early findings of the field (Scheme 1.14).[76] The incorporation of methoxy groups as electrophiles for cross-coupling reactions is of great interest as phenols are more available and overall cheaper than their halogenated counterparts. Their utilization within catalysis would therefore point towards greener catalysis as it represents a more sustainable source of electrophiles. While Dankwardt reported a Kumada-type coupling from aryl methyl ethers, the further development of the field led to more types of couplings such as Suzuki,[77–79] Buchwald-Hartwig[80,81] or Hiyama-type.[74,82,83]

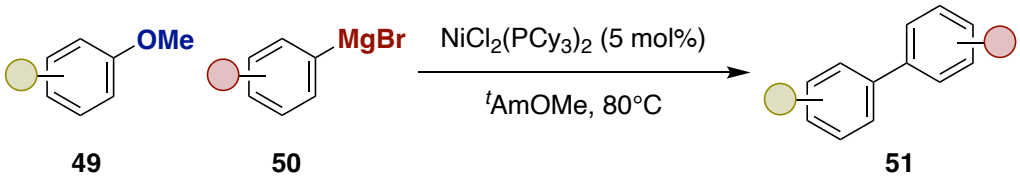

Scheme 1.14: Dankwardt's catalytic C-OMe functionalization.

1.4.2. Cross-electrophile coupling

A key feature that made nickel an appealing metal to work with is its ability to engage in cross electrophile couplings (XEC).[84–88] The appeal for such a reaction comes from the fact that a) some electrophiles might be more available than a nucleophilic derivative b) it might be more step-economical not to transform an electrophile into a nucleophile before coupling c) some electrophiles are not easily transformed into a nucleophile by nature, such as CO_2. The process is reminiscent for what was described within the

photoredox context but can also be set in a thermally controlled setting. The fact that nickel is able to undergo SET processes allows for the generation of carbon based radical from diverse precursors, which will further react further down with an aryl/alkyl-Ni species by radical capture giving a highly oxidized nickel that can easily reductively eliminate a product.[89] The three main classes of couplings are the sp^2-sp^2, sp^2-sp^3 and sp^3-sp^3 couplings, to which nickel finds use.[90] In the context of this thesis, CO_2 is the electrophile that is mainly depicted, nonetheless, plenty of various electrophiles are also known to react with the metal. The biggest challenge when it comes to cross-electrophile coupling is to avoid so-called "homocoupling" when dealing with two different electrophiles. Therefore, the fact that nickel can engage in either one or two electron processes enables a discrimination between both electrophiles for good cross-selectivity. The mechanism involved for most of the reductive cross-coupling is similar to the mechanism involved in the case of photoredox although slightly different. Nickel is first reduced down to Ni(0), which allows for a classical oxidative addition towards a Ni(II) species. Then, a radical, generated from a precursors and Ni(I) adds to the oxidative addition complex to generate the Ni(III) intermediate that easily undergoes reductive elimination to form the Ni(I) species typically involved in a SET radical generation. This leaves a Ni(II) compound that can be reduced down to Ni(0), closing the catalytic cycle. An outline is depicted in Figure 1.9.

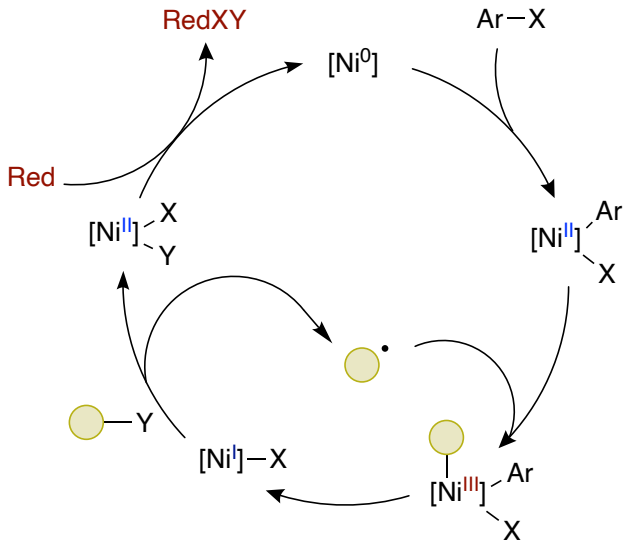

Figure 1.9: General mechanism of a Ni cross-electrophile coupling.

A recent study by Hazari *et al.* shows how the development of 6,6'-disubstituted bipyridines as ligands have helped the field, making competent catalysts.[91] The

introduction of such substituents has for effect to disturb the geometry, and thus the spin-state, of the Ni(II) halide complex from a square planar for non-substituted bipyridines to a distorted tetrahedral geometry when substituted (Figure 1.10). The consequences are in the redox potentials, essentially dissociating further apart the Ni(II)/Ni(I) and Ni(I)/Ni(0) couples, making some reductants unable to reach Ni(0), which can be a desired feature or not, but also stabilizing Ni(I) species when bulky substituents are used. The presence of substituents was also detrimental for the radical capture from Ni(II) intermediates and can therefore be inimical to XEC reactions. The ligand design for a reaction should therefore be well-thought according to a reaction's specific mechanism and cannot follow simple trends based on steric bulk for example. Citing the authors: "different ligand design strategies compared to those that have been successful for precious metal systems will need to be applied because of the tendency of Ni complexes to adopt multiple spin states."

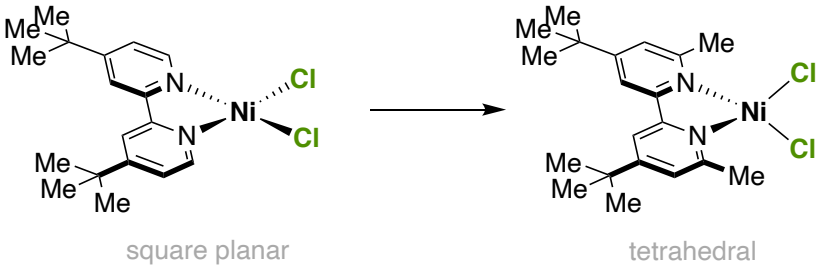

Figure 1.10: Geometry change depending on the presence of substituents.

1.4.3. Remote C-H functionalization

Chain-walking is described as the ability for a metal to "walk" along an alkyl chain. The process starts from a metal-alkyl complex and consists of iterative β-hydride elimination (BHE) followed by 1,2-insertion steps until the metal finds a position that is thermodynamically favored, before further elementary steps occur (Figure 1.11, top). This type of reaction is known for various metals and is not a specific feature of nickel.[92–94] Nonetheless, nickel has found profound use in remote functionalization of alkyl-containing molecules and is currently a field still under active investigation.[95,96] The interest for nickel in such transformation started in 2013 when Ong *et al.* reported a remote hydroarylation of allylbenzenes with a NHC as ligand (Figure 1.11, bottom).[97] The report showcased the arylation selectively at the benzylic position, with only minor isomers produced as linear products. The following year, the Hartwig group showed an improved system that was not restricted to allylbenzenes but could use of different octene isomers, again using a nickel-NHC system.[98]

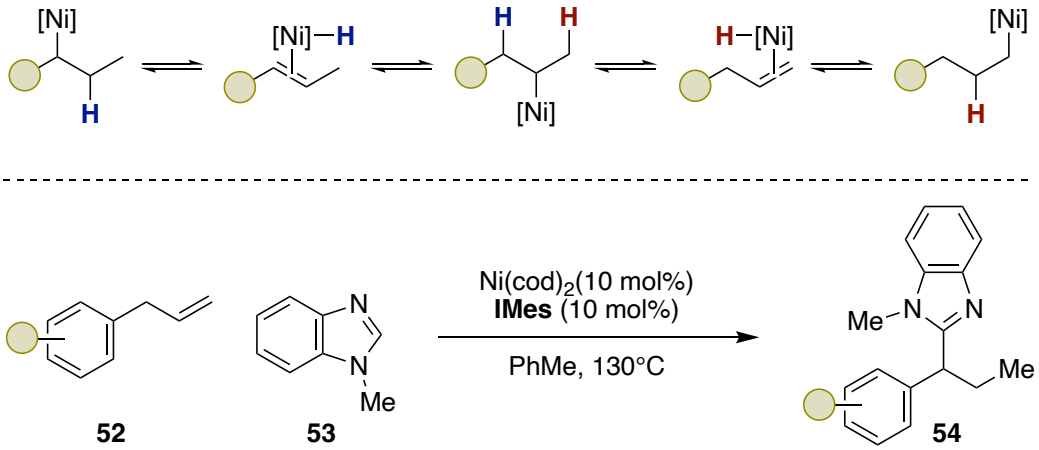

Figure 1.11: Rationalization of the chain walking process and Ong's Ni catalyzed report.

The current state of the art when it comes to catalytic systems involving a Ni based chain-walking reaction bears NN ligands. These NN ligands are, in most cases, bipyridine or phenanthroline derivatives, although many examples have been shown to be using pyOx or BiOx ligands amongst others.[95,96] The first appearance of a reaction making use of a NN ligand, more specifically 6,6'-bipyridine, was disclosed by the group of Zhu in 2017 (Scheme 1.15).[99] This reaction was also a hydroarylation of alkenes but using aryl iodides as electrophile and performing at room temperature. Consequently, the changing of ligand class allowed for the conditions to become milder while conserving an excellent selectivity and broad scope. The reaction was selective towards benzylic functionalization, with very little amounts of linear products observed.

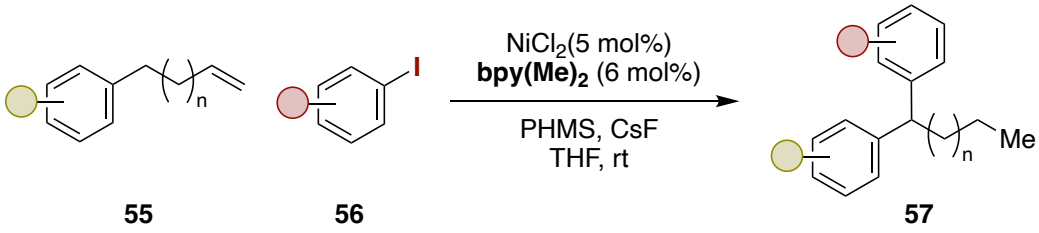

Scheme 1.15: Zhu's hydroarylation with Ni-bipyridine system. PHMS = polymethylhydrosiloxane.

Zhu, later the same year, improved this report by allowing for the coupling of alkyl bromides with aryl bromides, using the same ligand and with manganese as sacrificial reductant (Scheme 1.16).[100] The group made use of propyl bromide as an additive in order to generate a Ni-hydride species from BHE *in situ* for the catalyst to re-engage with potential alkene side-products in case of metal-alkene dissociation over the chain-walking process.

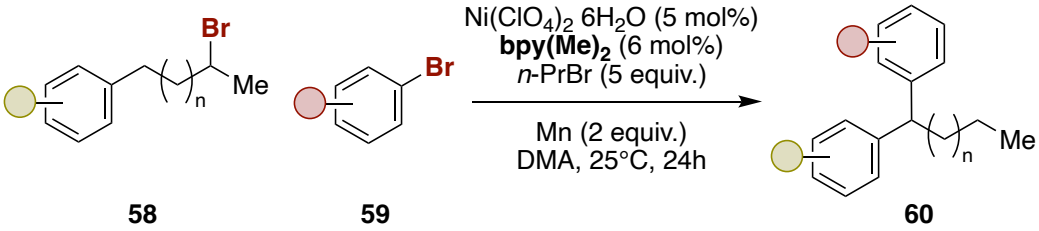

Scheme 1.16: Zhu's chain-walking XEC reaction.

To summarize, many different ways have been developed in order to use carbon dioxide as a C1 synthon. The use of nickel in the chemistry is rather central, especially when it comes to reductive coupling technologies. Moreover, the emergence of photoredox catalysis presented and still is an opportunity that is able to bring new answers to current challenges faced by chemists towards this endeavor.

1.5. References

(1) *Carbon Dioxide Recovery and Utilization*; Aresta, M., Ed.; Springer Netherlands: Dordrecht, **2003**. https://doi.org/10.1007/978-94-017-0245-4.

(2) Von Der Assen, N.; Voll, P.; Peters, M.; Bardow, A. Life Cycle Assessment of CO_2 Capture and Utilization: A Tutorial Review. *Chem. Soc. Rev.* **2014**, *43*, 7982–7994. https://doi.org/10.1039/C3CS60373C.

(3) Grignard, V. *Victor Grignard – Nobel Lecture.* NobelPrize.org. https://www.nobelprize.org/prizes/chemistry/1912/grignard/lecture/.

(4) *Carbon Dioxide and Organometallics*; Lu, X.-B., Ed.; Topics in Organometallic Chemistry; Springer International Publishing: Cham, **2016**; Vol. 53. https://doi.org/10.1007/978-3-319-22078-9.

(5) Dodson, L. G.; Thompson, M. C.; Weber, J. M. Characterization of Intermediate Oxidation States in CO_2 Activation. *Annu. Rev. Phys. Chem.* **2018**, *69*, 231–252. https://doi.org/10.1146/annurev-physchem-050317-021122.

(6) Walsh, A. D. The Electronic Orbitals, Shapes, and Spectra of Polyatomic Molecules. Part II. Non-Hydride AB2 and BAC Molecules. *J. Chem. Soc.* **1953**, 2266. https://doi.org/10.1039/jr9530002266.

(7) Sommerfeld, T.; Meyer, H.-D.; Cederbaum, L. S. Potential Energy Surface of the CO_2 Anion. *Phys. Chem. Chem. Phys.* **2004**, *6*, 42. https://doi.org/10.1039/b312005h.

(8) Schröder, D.; Schalley, C. A.; Harvey, J. N.; Schwarz, H. On the Formation of the Carbon Dioxide Anion Radical $CO_2^{\cdot -}$ in the Gas Phase. *Int. J. Mass Spectrom.* **1999**, *185–187*, 25–35. https://doi.org/10.1016/S1387-3806(98)14042-3.

(9) Stephan, D. W.; Erker, G. Frustrated Lewis Pair Chemistry of Carbon, Nitrogen and Sulfur Oxides. *Chem. Sci.* **2014**, *5*, 2625–2641. https://doi.org/10.1039/C4SC00395K.

(10) Ye, J.; Kalvet, I.; Schoenebeck, F.; Rovis, T. Direct α-Alkylation of Primary Aliphatic Amines Enabled by CO2 and Electrostatics. *Nat. Chem.* **2018**, *10*, 1037–1041. https://doi.org/10.1038/s41557-018-0085-9.

(11) Agarwala, H.; Chen, X.; Lyonnet, J. R.; Johnson, B. A.; Ahlquist, M.; Ott, S. Alternating Metal-Ligand Coordination Improves Electrocatalytic CO_2 Reduction by a Mononuclear Ru Catalyst. *Angew. Chem. Int. Ed.* **2023**, *62*, e202218728. https://doi.org/10.1002/anie.202218728.

(12) Benson, E. E.; Kubiak, C. P.; Sathrum, A. J.; Smieja, J. M. Electrocatalytic and Homogeneous Approaches to Conversion of CO_2 to Liquid Fuels. *Chem. Soc. Rev.* **2009**, *38*, 89–99. https://doi.org/10.1039/B804323J.

(13) Kumar, B.; Llorente, M.; Froehlich, J.; Dang, T.; Sathrum, A.; Kubiak, C. P. Photochemical and Photoelectrochemical Reduction of CO_2. *Annu. Rev. Phys. Chem.* **2012**, *63*, 541–569. https://doi.org/10.1146/annurev-physchem-032511-143759.

(14) Tamaki, Y.; Ishitani, O. Supramolecular Photocatalysts for the Reduction of CO_2. *ACS Catal.* **2017**, *7*, 3394–3409. https://doi.org/10.1021/acscatal.7b00440.

(15) He, J.; Johnson, N. J. J.; Huang, A.; Berlinguette, C. P. Electrocatalytic Alloys for CO_2 Reduction. *ChemSusChem* **2018**, *11*, 48–57. https://doi.org/10.1002/cssc.201701825.

(16) Nam, D.-H.; De Luna, P.; Rosas-Hernández, A.; Thevenon, A.; Li, F.; Agapie, T.; Peters, J. C.; Shekhah, O.; Eddaoudi, M.; Sargent, E. H. Molecular Enhancement of Heterogeneous CO_2 Reduction. *Nat. Mater.* **2020**, *19*, 266–276. https://doi.org/10.1038/s41563-020-0610-2.

(17) Majhi, J.; Molander, G. A. Recent Discovery, Development, and Synthetic Applications of Formic Acid Salts in Photochemistry. *Angew. Chem. Int. Ed.* **2023**, e202311853. https://doi.org/10.1002/anie.202311853.

(18) Aresta, M.; Nobile, C. F.; Albano, V. G.; Forni, E.; Manassero, M. New Nickel–Carbon Dioxide Complex: Synthesis, Properties, and Crystallographic Characterization of (Carbon Dioxide)-Bis(Tricyclohexylphosphine)Nickel. *J. Chem. Soc. Chem. Commun* **1975**, *1*, 636–637. https://doi.org/10.1039/C39750000636.

(19) Calabrese, J. C.; Herskovitz, T.; Kinney, J. B. Carbon Dioxide Coordination Chemistry. 5. The Preparation and Structure of the Rhodium Complex Rh(Eta 1-CO_2)(Cl)(Diars)$_2$. *J. Am. Chem. Soc.* **1983**, *105*, 5914–5915. https://doi.org/10.1021/ja00356a033.

(20) Gibson, D. H. Carbon Dioxide Coordination Chemistry: Metal Complexes and Surface-Bound Species. What Relationships? *Coord. Chem. Rev.* **1999**, *185–186*, 335–355. https://doi.org/10.1016/S0010-8545(99)00021-1.

(21) Castro-Rodriguez, I. A Linear, O-Coordinated 1-CO_2 Bound to Uranium. *Science* **2004**, *305*, 1757–1759. https://doi.org/10.1126/science.1102602.

(22) Sayyed, F. B.; Tsuji, Y.; Sakaki, S. The Crucial Role of a Ni(i) Intermediate in Ni-Catalyzed Carboxylation of Aryl Chloride with CO_2: A Theoretical Study. *Chem. Commun.* **2013**, *49*, 10715. https://doi.org/10.1039/c3cc45836a.

(23) Sayyed, F. B.; Sakaki, S. The Crucial Roles of $MgCl_2$ as a Non-Innocent Additive in the Ni-Catalyzed Carboxylation of Benzyl Halide with CO_2. *Chem. Commun.* **2014**, *50*, 13026–13029. https://doi.org/10.1039/C4CC04962D.

(24) Diccianni, J. B.; Hu, C. T.; Diao, T. Insertion of CO_2 Mediated by a (Xantphos)Ni^{I} – Alkyl Species. *Angew. Chem. Int. Ed.* **2019**, *58*, 13865–13868. https://doi.org/10.1002/anie.201906005.

(25) Somerville, R. J.; Odena, C.; Obst, M. F.; Hazari, N.; Hopmann, K. H.; Martin, R. Ni(I)–Alkyl Complexes Bearing Phenanthroline Ligands: Experimental Evidence for CO_2 Insertion at Ni(I) Centers. *J. Am. Chem. Soc.* **2020**, *142*, 10936–10941. https://doi.org/10.1021/jacs.0c04695.

(26) Zhang, B.; Yang, S.; Li, D.; Hao, M.; Chen, B.-Z.; Li, Z. Insights into the Regioselective Hydrocarboxylation of Styrenes with CO_2 Controlled by the Ligand of Nickel Catalysts. *ACS Sustain. Chem. Eng.* **2021**, *9*, 4091–4101. https://doi.org/10.1021/acssuschemeng.0c08845.

(27) Liu, L.; Lukose, B.; Ensing, B. A Free Energy Landscape of CO_2 Capture by Frustrated Lewis Pairs. *ACS Catal.* **2018**, *8*, 3376–3381. https://doi.org/10.1021/acscatal.7b04072.

(28) Hussey, A. S. The Carbonation of Grignard Reagent Solutions. *J. Am. Chem. Soc.* **1951**, *73*, 1364–1365. https://doi.org/10.1021/ja01147a517.

(29) Bottaccio, G.; Chiusoli, G. P. A New Method for Carboxylating Active Methylene Groups with Carbon Dioxide. *Chem. Commun. Lond.* **1966**, 17, 618a. https://doi.org/10.1039/c1966000618a.

(30) Haruki, E.; Arakawa, M.; Matsumura, N.; Otsuji, Y.; Imoto, E. Carboxylation of Active Methylene Compounds Using the Reagent of 1,8-Diazabicyclo(5.4.0)-7-Undecene and Carbon Dioxide. *Chem. Lett.* **1974**, *3*, 427–428. https://doi.org/10.1246/cl.1974.427.

(31) Sakurai, H.; Shirahata, A.; Hosomi, A. α-Carboxylation Reaction of Carbonyl Compounds with Bromomagnesium Ureide-Carbon Dioxide Adducts. *Tetrahedron Lett.* **1980**, *21*, 1967–1970. https://doi.org/10.1016/S0040-4039(00)93659-1.

(32) Mori, H.; Satake, Y. Carboxylation of Cyclohexanone with Carbon Dioxide and Potassium Phenoxide. Dependence of the Reaction upon the Amount of Carbon Dioxide Complexed with Potassium Phenoxide. *Chem. Pharm. Bull. (Tokyo)* **1985**, *33*, 3469–3472. https://doi.org/10.1248/cpb.33.3469.

(33) Flowers, B. J.; Gautreau-Service, R.; Jessop, P. G. β-Hydroxycarboxylic Acids from Simple Ketones by Carboxylation and Asymmetric Hydrogenation. *Adv. Synth. Catal.* **2008**, *350*, 2947–2958. https://doi.org/10.1002/adsc.200800516.

(34) Fukue, Y.; Oi, S.; Inoue, Y. Direct Synthesis of Alkyl 2-Alkynoates from Alk-1-Ynes, CO_2, and Bromoalkanes Catalysed by Copper(I) or Silver(I) Salt. *J. Chem. Soc. Chem. Commun.* **1994**, 18, 2091. https://doi.org/10.1039/c39940002091.

(35) Zhang, X.; Zhang, W.-Z.; Ren, X.; Zhang, L.-L.; Lu, X.-B. Ligand-Free Ag(I)-Catalyzed Carboxylation of Terminal Alkynes with CO_2. *Org. Lett.* **2011**, *13*, 2402–2405. https://doi.org/10.1021/ol200638z.

(36) Dingyi, Y.; Yugen, Z. The Direct Carboxylation of Terminal Alkynes with Carbon Dioxide. *Green Chem.* **2011**, *13*, 1275. https://doi.org/10.1039/c0gc00819b.

(37) Vechorkin, O.; Hirt, N.; Hu, X. Carbon Dioxide as the C1 Source for Direct C–H Functionalization of Aromatic Heterocycles. *Org. Lett.* **2010**, *12*, 3567–3569. https://doi.org/10.1021/ol101450u.

(38) Ukai, K.; Aoki, M.; Takaya, J.; Iwasawa, N. Rhodium(I)-Catalyzed Carboxylation of Aryl- and Alkenylboronic Esters with CO_2. *J. Am. Chem. Soc.* **2006**, *128*, 8706–8707. https://doi.org/10.1021/ja061232m.

(39) Correa, A.; Martín, R. Palladium-Catalyzed Direct Carboxylation of Aryl Bromides with Carbon Dioxide. *J. Am. Chem. Soc.* **2009**, *131*, 15974–15975. https://doi.org/10.1021/ja905264a.

(40) Liu, A.-H.; Gao, J.; He, L.-N. Catalytic Activation and Conversion of Carbon Dioxide into Fuels/Value-Added Chemicals Through C-C Bond Formation. In *New and Future Developments in Catalysis*; Elsevier, **2013**; 81–147. https://doi.org/10.1016/B978-0-444-53882-6.00005-X.

(41) Tortajada, A.; Juliá-Hernández, F.; Börjesson, M.; Moragas, T.; Martin, R. Transition-Metal-Catalyzed Carboxylation Reactions with Carbon Dioxide. *Angew. Chem. Int. Ed.* **2018**, *57*, 15948–15982. https://doi.org/10.1002/anie.201803186.

(42) Mizuno, H.; Takaya, J.; Iwasawa, N. Rhodium(I)-Catalyzed Direct Carboxylation of Arenes with CO_2 via Chelation-Assisted C–H Bond Activation. *J. Am. Chem. Soc.* **2011**, *133*, 1251–1253. https://doi.org/10.1021/ja109097z.

(43) Trommsdorff, H. Ueber Santonin. *Ann. Pharm.* **1834**, *11*, 190–207. https://doi.org/10.1002/jlac.18340110207.

(44) Roth, H. D. The Beginnings of Organic Photochemistry. *Angew. Chem. Int. Ed. Engl.* **1989**, *28*, 1193–1207. https://doi.org/10.1002/anie.198911931.

(45) Holick, M. F. Photosynthesis of Vitamin D in the Skin: Effect of Environmental and Life-Style Variables. *Fed. Proc.* **1987**, *46*, 1876–1882.

(46) Shang, T.-Y.; Lu, L.-H.; Cao, Z.; Liu, Y.; He, W.-M.; Yu, B. Recent Advances of 1,2,3,5-Tetrakis(Carbazol-9-Yl)-4,6-Dicyanobenzene (4CzIPN) in Photocatalytic Transformations. *Chem. Commun.* **2019**, *55*, 5408–5419. https://doi.org/10.1039/C9CC01047E.

(47) Huang, Y.; Hou, J.; Zhan, L.-W.; Zhang, Q.; Tang, W.-Y.; Li, B.-D. Photoredox Activation of Formate Salts: Hydrocarboxylation of Alkenes via Carboxyl Group Transfer. *ACS Catal.* **2021**, *11*, 15004–15012. https://doi.org/10.1021/acscatal.1c04684.

(48) Ho, T.; Chow, Y. L. Photochemistry of Amines and Amino Compounds. In *PATAI'S Chemistry of Functional Groups*; Patai, S., Ed.; Wiley, **1996**; 683–745. https://doi.org/10.1002/047085720X.ch15.

(49) Seo, H.; Liu, A.; Jamison, T. F. Direct β-Selective Hydrocarboxylation of Styrenes with CO_2 Enabled by Continuous Flow Photoredox Catalysis. *J. Am. Chem. Soc.* **2017**, *139*, 13969–13972. https://doi.org/10.1021/jacs.7b05942.

(50) Alektiar, S. N.; Wickens, Z. K. Photoinduced Hydrocarboxylation via Thiol-Catalyzed Delivery of Formate Across Activated Alkenes. *J. Am. Chem. Soc.* **2021**, *143*, 13022–13028. https://doi.org/10.1021/jacs.1c07562.

(51) Alektiar, S. N.; Han, J.; Dang, Y.; Rubel, C. Z.; Wickens, Z. K. Radical Hydrocarboxylation of Unactivated Alkenes via Photocatalytic Formate Activation. *J. Am. Chem. Soc.* **2023**, *145*, 10991–10997. https://doi.org/10.1021/jacs.3c03671.

(52) Song, L.; Wang, W.; Yue, J.-P.; Jiang, Y.-X.; Wei, M.-K.; Zhang, H.-P.; Yan, S.-S.; Liao, L.-L.; Yu, D.-G. Visible-Light Photocatalytic Di- and Hydro-Carboxylation of Unactivated Alkenes with CO_2. *Nat. Catal.* **2022**, *5*, 832–838. https://doi.org/10.1038/s41929-022-00841-z.

(53) Ghosh, I.; Ghosh, T.; Bardagi, J. I.; König, B. Reduction of Aryl Halides by Consecutive Visible Light-Induced Electron Transfer Processes. *Science* **2014**, *346*, 725–728. https://doi.org/10.1126/science.1258232.

(54) Cowper, N. G. W.; Chernowsky, C. P.; Williams, O. P.; Wickens, Z. K. Potent Reductants via Electron-Primed Photoredox Catalysis: Unlocking Aryl Chlorides for Radical Coupling. *J. Am. Chem. Soc.* **2020**, *142*, 2093–2099. https://doi.org/10.1021/jacs.9b12328.

(55) Osawa, M.; Nagai, H.; Akita, M. Photo-Activation of Pd-Catalyzed Sonogashira Coupling Using a Ru/Bipyridine Complex as Energy Transfer Agent. *Dalton Trans.* **2007**, 8, 827. https://doi.org/10.1039/b618007h.

(56) Chan, A. Y.; Perry, I. B.; Bissonnette, N. B.; Buksh, B. F.; Edwards, G. A.; Frye, L. I.; Garry, O. L.; Lavagnino, M. N.; Li, B. X.; Liang, Y.; Mao, E.; Millet, A.; Oakley, J. V.; Reed, N. L.; Sakai, H. A.; Seath, C. P.; MacMillan, D. W. C. Metallaphotoredox: The Merger of Photoredox and Transition Metal Catalysis. *Chem. Rev.* **2022**, *122*, 1485–1542. https://doi.org/10.1021/acs.chemrev.1c00383.

(57) Zuo, Z.; Ahneman, D. T.; Chu, L.; Terrett, J. A.; Doyle, A. G.; MacMillan, D. W. C. Merging Photoredox with Nickel Catalysis: Coupling of α-Carboxyl Sp^3 -Carbons with Aryl Halides. *Science* **2014**, *345*, 437–440. https://doi.org/10.1126/science.1255525.

(58) Hou, J.; Li, J.; Wu, J. Recent Development of Light-Mediated Carboxylation Using CO_2 as the Feedstock. *Asian J. Org. Chem.* **2018**, *7*, 1439–1447. https://doi.org/10.1002/ajoc.201800226.

(59) Yeung, C. S. Photoredox Catalysis as a Strategy for CO_2 Incorporation: Direct Access to Carboxylic Acids from a Renewable Feedstock. *Angew. Chem. Int. Ed.* **2019**, *58*, 5492–5502. https://doi.org/10.1002/anie.201806285.

(60) Zhang, Z.; Ye, J.-H.; Ju, T.; Liao, L.-L.; Huang, H.; Gui, Y.-Y.; Zhou, W.-J.; Yu, D.-G. Visible-Light-Driven Catalytic Reductive Carboxylation with CO_2. *ACS Catal.* **2020**, 10, 10871–10885. https://doi.org/10.1021/acscatal.0c03127.

(61) Zhang, G.; Cheng, Y.; Beller, M.; Chen, F. Direct Carboxylation with Carbon Dioxide via Cooperative Photoredox and Transition-Metal Dual Catalysis. *Adv. Synth. Catal.* **2021**, *363*, 1583–1596. https://doi.org/10.1002/adsc.202001280.

(62) Davies, J.; Lyonnet, J. R.; Zimin, D. P.; Martin, R. The Road to Industrialization of Fine Chemical Carboxylation Reactions. *Chem* **2021**, *7*, 2927–2942. https://doi.org/10.1016/j.chempr.2021.10.016.

(63) Murata, K.; Numasawa, N.; Shimomaki, K.; Takaya, J.; Iwasawa, N. Construction of a Visible Light-Driven Hydrocarboxylation Cycle of Alkenes by the Combined Use of Rh(I) and Photoredox Catalysts. *Chem. Commun.* **2017**, *53*, 3098–3101. https://doi.org/10.1039/C7CC00678K.

(64) Meng, Q.-Y.; Schirmer, T. E.; Berger, A. L.; Donabauer, K.; König, B. Photocarboxylation of Benzylic C–H Bonds. *J. Am. Chem. Soc.* **2019**, *141*, 11393–11397. https://doi.org/10.1021/jacs.9b05360.

(65) Ishida, N.; Masuda, Y.; Imamura, Y.; Yamazaki, K.; Murakami, M. Carboxylation of Benzylic and Aliphatic C–H Bonds with CO_2 Induced by Light/Ketone/Nickel. *J. Am. Chem. Soc.* **2019**, *141*, 19611–19615. https://doi.org/10.1021/jacs.9b12529.

(66) Yatham, V. R.; Shen, Y.; Martin, R. Catalytic Intermolecular Dicarbofunctionalization of Styrenes with CO_2 and Radical Precursors. *Angew. Chem. Int. Ed.* **2017**, *56*, 10915–10919. https://doi.org/10.1002/anie.201706263.

(67) Kharasch, M. S.; Reinmuth, O. *Grignard Reactions of Nonmetallic Substances*; Chemistry series; Prentice-Hall, **1954**.

(68) *The Nobel Prize in Chemistry 2001*. NobelPrize.org. https://www.nobelprize.org/prizes/chemistry/2001/summary/.

(69) *The Nobel Prize in Chemistry 2005*. NobelPrize.org. https://www.nobelprize.org/prizes/chemistry/2005/summary/.

(70) *The Nobel Prize in Chemistry 2010*. NobelPrize.org. https://www.nobelprize.org/prizes/chemistry/2010/summary/.

(71) Diccianni, J.; Lin, Q.; Diao, T. Mechanisms of Nickel-Catalyzed Coupling Reactions and Applications in Alkene Functionalization. *Acc. Chem. Res.* **2020**, *53*, 906–919. https://doi.org/10.1021/acs.accounts.0c00032.

(72) Chernyshev, V. M.; Ananikov, V. P. Nickel and Palladium Catalysis: Stronger Demand than Ever. *ACS Catal.* **2022**, *12*, 1180–1200. https://doi.org/10.1021/acscatal.1c04705.

(73) Menezes Da Silva, V. H.; Braga, A. A. C.; Cundari, T. R. N-Heterocyclic Carbene Based Nickel and Palladium Complexes: A DFT Comparison of the Mizoroki–Heck Catalytic Cycles. *Organometallics* **2016**, *35*, 3170–3181. https://doi.org/10.1021/acs.organomet.6b00532.

(74) Álvarez-Bercedo, P.; Martin, R. Ni-Catalyzed Reduction of Inert C–O Bonds: A New Strategy for Using Aryl Ethers as Easily Removable Directing Groups. *J. Am. Chem. Soc.* **2010**, *132*, 17352–17353. https://doi.org/10.1021/ja106943q.

(75) Cornella, J.; Gómez-Bengoa, E.; Martin, R. Combined Experimental and Theoretical Study on the Reductive Cleavage of Inert C–O Bonds with Silanes: Ruling out a Classical Ni(0)/Ni(II) Catalytic Couple and Evidence for Ni(I) Intermediates. *J. Am. Chem. Soc.* **2013**, *135*, 1997–2009. https://doi.org/10.1021/ja311940s.

(76) Dankwardt, J. W. Nickel-Catalyzed Cross-Coupling of Aryl Grignard Reagents with Aromatic Alkyl Ethers: An Efficient Synthesis of Unsymmetrical Biaryls. *Angew. Chem. Int. Ed.* **2004**, *43*, 2428–2432. https://doi.org/10.1002/anie.200453765.

(77) Tobisu, M.; Yasutome, A.; Kinuta, H.; Nakamura, K.; Chatani, N. 1,3-Dicyclohexylimidazol-2-Ylidene as a Superior Ligand for the Nickel-Catalyzed Cross-Couplings of Aryl and Benzyl Methyl Ethers with Organoboron Reagents. *Org. Lett.* **2014**, *16*, 5572–5575. https://doi.org/10.1021/ol502583h.

(78) Nakamura, K.; Tobisu, M.; Chatani, N. Nickel-Catalyzed Formal Homocoupling of Methoxyarenes for the Synthesis of Symmetrical Biaryls via C–O Bond Cleavage. *Org. Lett.* **2015**, *17*, 6142–6145. https://doi.org/10.1021/acs.orglett.5b03151.

(79) Guo, L.; Liu, X.; Baumann, C.; Rueping, M. Nickel-Catalyzed Alkoxy–Alkyl Interconversion with Alkylborane Reagents through C–O Bond Activation of Aryl and Enol Ethers. *Angew. Chem. Int. Ed.* **2016**, *55*, 15415–15419. https://doi.org/10.1002/anie.201607646.

(80) Tobisu, M.; Shimasaki, T.; Chatani, N. Ni^0-Catalyzed Direct Amination of Anisoles Involving the Cleavage of Carbon–Oxygen Bonds. *Chem. Lett.* **2009**, *38*, 710–711. https://doi.org/10.1246/cl.2009.710.

(81) Tobisu, M.; Yasutome, A.; Yamakawa, K.; Shimasaki, T.; Chatani, N. Ni(0)/NHC-Catalyzed Amination of N-Heteroaryl Methyl Ethers through the Cleavage of Carbon–oxygen Bonds. *Tetrahedron* **2012**, *68*, 5157–5161. https://doi.org/10.1016/j.tet.2012.04.005.

(82) Tobisu, M.; Yamakawa, K.; Shimasaki, T.; Chatani, N. Nickel-Catalyzed Reductive Cleavage of Aryl–Oxygen Bonds in Alkoxy- and Pivaloxyarenes Using Hydrosilanes as a Mild Reducing Agent. *Chem. Commun.* **2011**, *47*, 2946. https://doi.org/10.1039/c0cc05169a.

(83) Zarate, C.; Nakajima, M.; Martin, R. A Mild and Ligand-Free Ni-Catalyzed Silylation via C–OMe Cleavage. *J. Am. Chem. Soc.* **2017**, *139*, 1191–1197. https://doi.org/10.1021/jacs.6b10998.

(84) Everson, D. A.; Weix, D. J. Cross-Electrophile Coupling: Principles of Reactivity and Selectivity. *J. Org. Chem.* **2014**, *79*, 4793–4798. https://doi.org/10.1021/jo500507s.

(85) Gu, J.; Wang, X.; Xue, W.; Gong, H. Nickel-Catalyzed Reductive Coupling of Alkyl Halides with Other Electrophiles: Concept and Mechanistic Considerations. *Org. Chem. Front.* **2015**, *2*, 1411–1421. https://doi.org/10.1039/C5QO00224A.

(86) Weix, D. J. Methods and Mechanisms for Cross-Electrophile Coupling of Csp^2 Halides with Alkyl Electrophiles. *Acc. Chem. Res.* **2015**, *48*, 1767–1775. https://doi.org/10.1021/acs.accounts.5b00057.

(87) Poremba, K. E.; Dibrell, S. E.; Reisman, S. E. Nickel-Catalyzed Enantioselective Reductive Cross-Coupling Reactions. *ACS Catal.* **2020**, *10*, 8237–8246. https://doi.org/10.1021/acscatal.0c01842.

(88) Charboneau, D. J.; Hazari, N.; Huang, H.; Uehling, M. R.; Zultanski, S. L. Homogeneous Organic Electron Donors in Nickel-Catalyzed Reductive Transformations. *J. Org. Chem.* **2022**, *87*, 7589–7609. https://doi.org/10.1021/acs.joc.2c00462.

(89) Lin, Q.; Spielvogel, E. H.; Diao, T. Carbon-Centered Radical Capture at Nickel(II) Complexes: Spectroscopic Evidence, Rates, and Selectivity. *Chem* **2023**, *9*, 1295–1308. https://doi.org/10.1016/j.chempr.2023.02.010.

(90) Yi, L.; Ji, T.; Chen, K.-Q.; Chen, X.-Y.; Rueping, M. Nickel-Catalyzed Reductive Cross-Couplings: New Opportunities for Carbon–Carbon Bond Formations through Photochemistry and Electrochemistry. *CCS Chem.* **2022**, *4*, 9–30. https://doi.org/10.31635/ccschem.021.202101196.

(91) Huang, H.; Alvarez-Hernandez, J. L.; Hazari, N.; Mercado, B. Q.; Uehling, M. R. Effect of 6,6′-Substituents on Bipyridine-Ligated Ni Catalysts for Cross-Electrophile Coupling. *ACS Catal.* **2024**, 6897–6914. https://doi.org/10.1021/acscatal.4c00827.

(92) Vasseur, A.; Bruffaerts, J.; Marek, I. Remote Functionalization through Alkene Isomerization. *Nat. Chem.* **2016**, *8*, 209–219. https://doi.org/10.1038/nchem.2445.

(93) Fiorito, D.; Scaringi, S.; Mazet, C. Transition Metal-Catalyzed Alkene Isomerization as an Enabling Technology in Tandem, Sequential and Domino Processes. *Chem. Soc. Rev.* **2021**, *50*, 1391–1406. https://doi.org/10.1039/D0CS00449A.

(94) Scaringi, S.; Mazet, C. Transition Metal-Catalyzed (Remote) Deconjugative Isomerization of α,β-Unsaturated Carbonyls. *Tetrahedron Lett.* **2022**, *96*, 153756. https://doi.org/10.1016/j.tetlet.2022.153756.

(95) Janssen-Müller, D.; Sahoo, B.; Sun, S.; Martin, R. Tackling Remote Sp^3 C–H Functionalization via Ni-Catalyzed "Chain-walking" Reactions. *Isr. J. Chem.* **2020**, *60*, 195–206. https://doi.org/10.1002/ijch.201900072.

(96) Wang, Y.; He, Y.; Zhu, S. NiH-Catalyzed Functionalization of Remote and Proximal Olefins: New Reactions and Innovative Strategies. *Acc. Chem. Res.* **2022**, *55*, 3519–3536. https://doi.org/10.1021/acs.accounts.2c00628.

(97) Lee, W.-C.; Wang, C.-H.; Lin, Y.-H.; Shih, W.-C.; Ong, T.-G. Tandem Isomerization and C–H Activation: Regioselective Hydroheteroarylation of Allylarenes. *Org. Lett.* **2013**, *15*, 5358–5361. https://doi.org/10.1021/ol402644y.

(98) Bair, J. S.; Schramm, Y.; Sergeev, A. G.; Clot, E.; Eisenstein, O.; Hartwig, J. F. Linear-Selective Hydroarylation of Unactivated Terminal and Internal Olefins with Trifluoromethyl-Substituted Arenes. *J. Am. Chem. Soc.* **2014**, *136*, 13098–13101. https://doi.org/10.1021/ja505579f.

(99) He, Y.; Cai, Y.; Zhu, S. Mild and Regioselective Benzylic C–H Functionalization: Ni-Catalyzed Reductive Arylation of Remote and Proximal Olefins. *J. Am. Chem. Soc.* **2017**, *139*, 1061–1064. https://doi.org/10.1021/jacs.6b11962.

(100) Chen, F.; Chen, K.; Zhang, Y.; He, Y.; Wang, Y.-M.; Zhu, S. Remote Migratory Cross-Electrophile Coupling and Olefin Hydroarylation Reactions Enabled by in Situ Generation of NiH. *J. Am. Chem. Soc.* **2017**, *139*, 13929–13935. https://doi.org/10.1021/jacs.7b08064.

CHAPTER 2. Photocatalytic Multicomponent Radical Coupling for the Direct Incorporation of Labelled Carbon Dioxide

Project done in collaboration with: Dr. Álvaro Velasco-Rubio, Dr. Roman Abrams, Dr. Kim Mühlfenzl, Xuemeng Chen, Ha Phan, Dr. Alessandro Cerveri, Dr. José Tiago M. Correia. The results presented are a combination from the contribution of all people listed above.

2.1. Introduction

2.1.1. Carbon labelling

Carbon, as an atom, can exist as a plurality of various stable isotopes. The three natural isotopes are ^{12}C, ^{13}C and ^{14}C, while ^{11}C can be made artificially. ^{12}C is the most abundant isotope with 98.93% followed by ^{13}C with an abundance of 1.07%. Both these isotopes are stable and do not show any radioactive decomposition. On the other hand, the third natural isotope of the element, present only in trace amounts, is ^{14}C, which shows radioactivity decomposing with a half-life of 5730 years (Figure 2.1). The decomposition turns a neutron to a proton through β-decay, giving ^{14}N.[1] It is generated in the high atmosphere of the earth from nitrogen after interacting with a thermal-neutron, expelling a proton during the process.

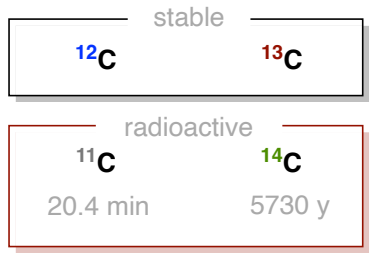

Figure 2.1: Main isotopes of the carbon element.

While it may seem to someone learning organic chemistry that using various isotopes of carbon is irrelevant, their use in synthesis is in fact a necessity when it comes to drug development in pharmaceutical companies and medical research. Although labelling organic compounds can be performed with a plethora of elements (carbon, hydrogen, nitrogen, iodine, etc.), the present chapter will focus only on carbon isotopomers labelling. Labelled compounds are used during the ADME studies (Administration, Distribution, Metabolism, Excretion). Introducing stable isotopes such as ^{13}C allows for a heavier compound ensuring that it will have a separate yet defined mass on spectrometric measurement. Therefore, the compound can be retrieved after excretion from the body, allowing the researchers to follow the path taken from the drug. On the other hand, radioisotopes such as ^{14}C grant researchers with an easier detection of the molecules given the very low background natural radioactivity, giving the possibility for low amount detections. This, in turn, allows for the investigation of the metabolites derived from the parent drug. Radioactivity being independent from the structure of the

labelled molecule, quantification of the drug, or its metabolites, can be done without use of an external reference.[2]

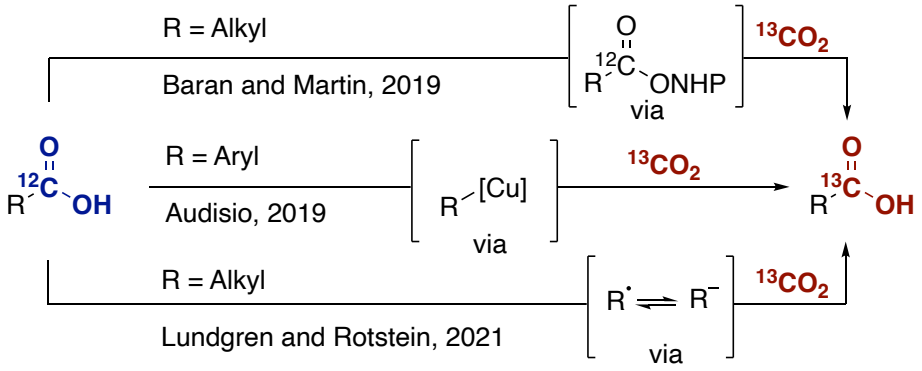

Figure 2.2: CDC approach for molecular labelling.

When it comes to synthesizing labelled molecules, the cost of production increases dramatically given that pure isotopomers other than ^{12}C must be artificially produced. This, in turn, incites the radiochemist to incorporate the labelled atom as late as possible in the route. This might require changes from the route developed by the medicinal or process chemists. Additionally, the starting materials used for labelling are typically very simple for production reasons, and can be $^{13}CO_2$, ^{13}CN, or $Ba^{13}CO_3$ (amongst others and including their ^{14}C counterparts).[3–5] Carbon dioxide is therefore very attractive as a labelling source when it comes to isotope implementation. Also, the need for late-stage isotope incorporation is greatly appreciated and led to the development of plenty of methodologies to do so.[5] Given the price related to the synthesis of such compounds, robust methods are preferred, such as the historical carboxylation of a Grignard from CO_2 gas.[5] More recently, several groups have come up with new ways of introducing a carbon isotope from CO_2 in a late-stage fashion as a catalytic decarboxylating-carboxylation (CDC) strategy. As the name suggests, the purpose of these technologies consists of decarboxylating a carboxylic acid present in the molecule, typically giving an organic radical, which can be captured or reduced for further reaction with labelled CO_2 present in the reaction medium (Figure 2.2). In 2019, both the groups of Baran and Martin independently reported a CDC reaction using nickel with activated NHP esters.[6,7] In the case of Baran, the reaction required a stoichiometric equivalent of nickel while Martin's report made use of 10 mol%. The same year, Audisio & coworkers independently reported a CDC reaction using copper as a catalyst, starting from the cesium salt of the carboxylic acids of interest.[8] This method proved to be quite straight-forward and did not necessitate the use of many reagents. In 2021, Lundgren and Rotstein disclosed an elegant procedure allowing for a fast, dynamic carbon isotope exchange technology.[9] The protocol made use of cesium carbonate to deprotonate the

carboxylic acids *in situ* and 4-CzIPN as photocatalyst (PC). Oxidation of the acid by the PC extruded CO_2, leaving an organic radical which could be reduced by the PC through radical polar crossover (RPC) to give the anionic species, nucleophilic enough to attack CO_2 from the reaction medium. Since they used an atmosphere of labelled carbon dioxide, the product will be statistically labelled with the desired isotope. Although this method is very direct and easy to make use of, it was limited to activated positions such as benzylic or α-carbonyl.

While many carboxylation reactions have been reported in the context of labelling from aryl halides or aryl boron materials,[5] in practice, such compounds are typically made from the corresponding acid by means of decarboxylative functionalization. This is due to the fact that radiochemists, most of the time, get their intermediates through other departments within the company such as process chemists. Therefore, they cannot access desired halides or organoboron, for route design reasons, without making those themselves. Given the structurally complex nature of pharmaceutically relevant molecules, the development of methodologies offering labelling while *building* molecular complexity is highly desirable. One way to gain access to structurally complex scaffolds in a minimal number of synthetic steps is the use of so-called "multicomponent reactions".

2.1.2. Multicomponent reactions

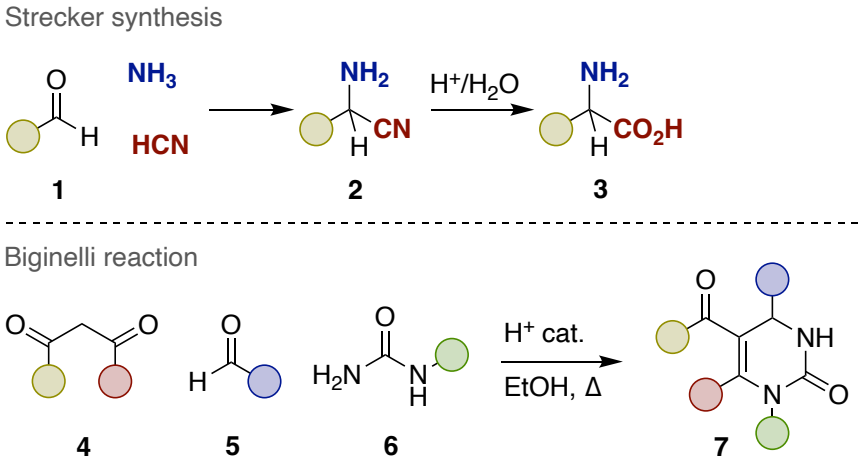

Scheme 2. 1: Two examples of MCRs developed in the 1800s.

In organic chemistry, a multicomponent reaction (MCR) is a reaction consisting of at least three different compounds giving a sole product made out of most of the atoms from the starting materials. Such reaction has been known for almost as long as organic chemistry has existed, and thus includes textbook organic chemistry examples such as

the Strecker synthesis or the Biginelli reaction (see Scheme 2.1). While during the 1800s chemists developing MCRs did not do so in order to achieve step-economy but rather by the simple desired to make new types of compounds, chemists of our age are interested in reactions that will yield complex structures in a minimum number of steps, ideally one, and making use of readily available starting materials. A perhaps more recent example of a MCR is the A^3-coupling, developed by the group of Li in the early 2000s (Scheme 2.2).[10] The name of this reaction comes from its starting materials: an alkyne, an amine and an aldehyde. Mixed together with a transition metal catalyst, the reaction yields propargylic amines in good to excellent yields. The reaction is inspired from the Mannich reaction, generating an iminium species *in situ*, to which a metal-acetylide will add, giving the propargylic product. The most used metals for this reaction are metals known for their affinity with alkynes such as Ru, Cu, Ag or Au.[11]

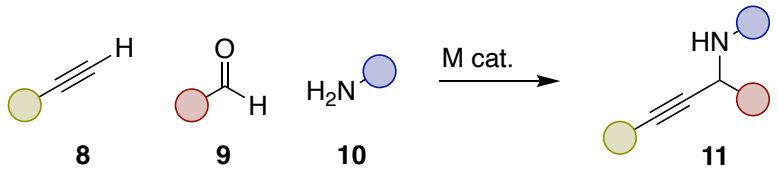

Scheme 2.2: Li's A^3-coupling reaction.

Photochemistry, being intimately linked to open-shell radical intermediates, offered the ability for chemists to come up with new ways of combining molecules, aiming at creating new multicomponent technologies. One of the key aspects in this endeavor is the concept of polarity-match within radical chemistry. This concept, generally speaking, classifies radicals as being electron-poor or electron-rich. In other words, electrophilic or nucleophilic. The matching of the SOMO energy levels between two radicals or a radical and a radical-trap might dictate reactivity, and anticipation of the radical behaviors can therefore be drawn.[12] This concept is rather well exemplified with a work from Gansäuer.[13] In their report, the group showed that cyclopropyl carbinyl radicals undergo ring opening extremely fast ($k = 9 \times 10^8$ s^{-1}) and much slower reversed ring closure ($k \approx 3 \times 10^4$ s^{-1}). By designing a specific material in which the cyclopropyl-containing radical would be electron-poor, being alpha to an ester, the radical could be reduced by SET to the anion, which would not be the case for the ring-opened product, being too electron-rich to be reduced. This demonstrates indirectly the fact that radicals can have different electronic properties and involves more synthetic concepts. The fact that radicals can be electrophilic or nucleophilic is reminiscent to conventional electrophiles and nucleophiles. An electron-poor radical will interact faster with an electron-rich acceptor and *vice versa*. This phenomenon can be exploited to guide reactivity in a sequential, well controlled manner, for the obtention of specific structures as output. Glorius & coworkers have recently disclosed a few methodologies relying on

iterative radical polarity-match additions giving rise to multicomponent coupling reactions.[14–16] An example from the group's report from 2022 is shown in Scheme 2.3. The reaction starts with the photoexcitation of thioxanthone which is quenched by starting material **12** through an energy transfer. Once itself at the excited state, the compound undergoes a homolytic cleavage at the N-O bond, giving a nitrogen (**16**) and an oxygen-centered (**17**) radical. According to the authors, the oxygen-centered radical **17**, an electrophilic radical, adds into alkene **14**, yielding electron-rich radical **18** which will itself react with **13** following a well-known Giese addition.[17] The intermediate product of the Giese addition is the electron-poor radical **19**, being on the α-position of the electron-withdrawing group. This electrophilic radical can finally react with the ambiphilic nitrogen-centered radical **16**, giving final product **15**.

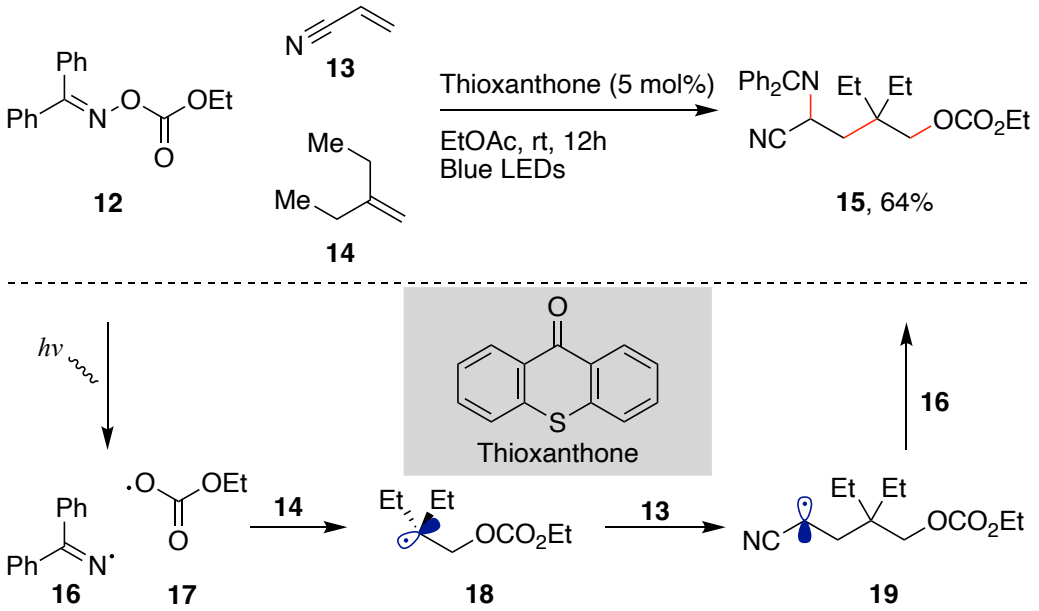

Scheme 2.3: Glorius' radical multicomponent reaction.

Taking in account the fact that complex structures can be generated with multicomponent reaction, notably with high chemoselectivity using radical chemistry, we envisioned to develop a methodology allowing for both the buildup of a complex molecular scaffold and implementing labelled CO_2 at once. This would potentially alleviate the need for a CDC reaction when attempting to add labelled carbons to the structure.

2.2. General aim of the project

The field of molecular labelling has only received little attention for the past couple of decades, still, elegant procedures have been reported allowing for the incorporation of labelled carbon dioxide gas. On the other hand, photochemistry has been subject to a skyrocketing expansion over the past two decades. Noticing both of these trends, we decided to come up with a protocol that would grant elaborated structure while incorporating labelled carbon dioxide at once.

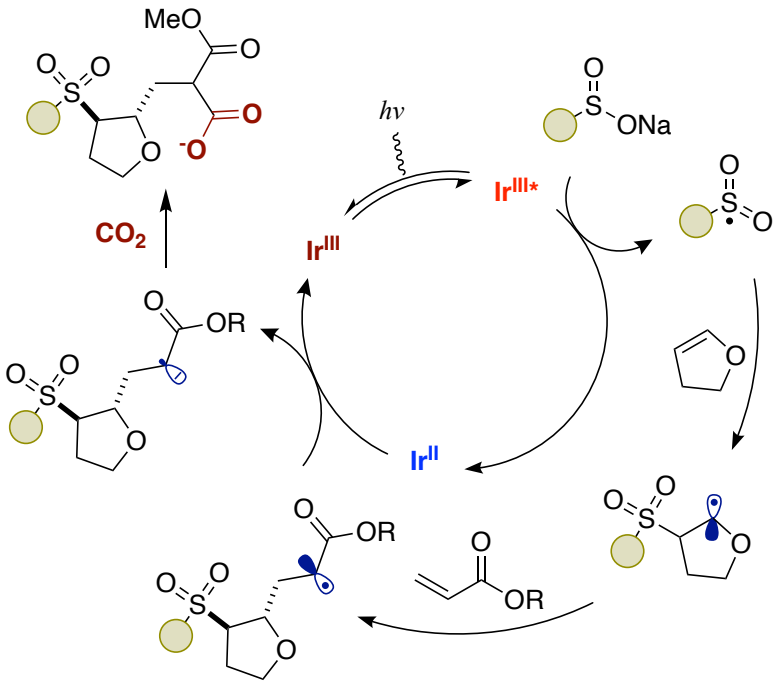

Scheme 2.4: Project overview, with proposed mechanism.

We therefore anticipated that oxidizing a sulfinate salt, known to give electrophilic sulfonyl radicals, would allow for an addition into an electron-rich alkene, which would be able to add itself into an electron-poor alkene such as an acrylate in a Giese addition fashion. The final acrylic radical could undergo RPC to give an enolate, nucleophilic enough to generate a malonate moiety from labelled CO_2. Additionally, we anticipated that the carbonyl group of the acrylate could be removed by careful installment of a reactive substituent on its esterified moiety, making a decarboxylation feasible only to leave the desired labelled carbonyl coming from CO_2.

2.3. Reaction Optimization

In order to start the reaction discovery process, sodium benzene sulfinate **20a**, methyl acrylate **21-Me**, and dihydrofuran (DHF) **22a** were mixed in DMA with a PC at 10°C under CO_2 atmosphere. The product of the first round of investigation was the desired product **24**. The reaction proved to be working using a few different photocatalysts, although (Ir[df(CF_3)ppy]$_2$(dtbbpy))PF_6 gave the best results with 54% NMR yield (Table 2.1, entries 1-4). A change in solvent, testing DMF (entry 5) and DMSO (entry 6) was not improving the yield while changing the stoichiometry of the reaction to make the sulfinate salt **20a** the limiting reagent improved the yield to 65% (entry 7). Finally, increasing the concentration to 0.2 M (entry 8) pushed the yield further up to 73%.

Table 2.1: Reaction discovery.

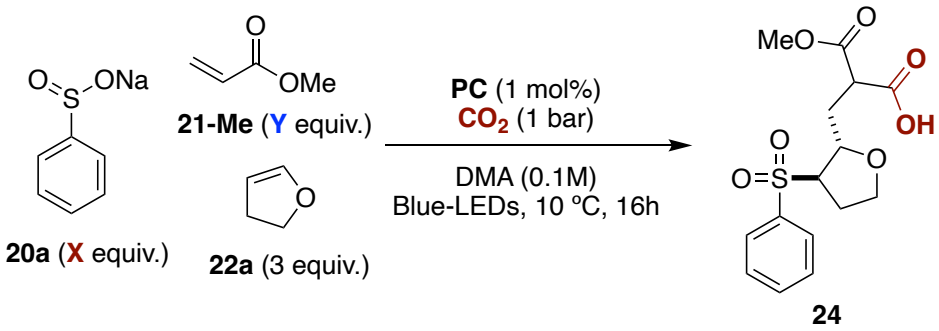

entry	PC	X	Y	yield (%)
1	$Ru(bpy)_3(PF_6)_2$	1.2	1.0	49
2	4-CzIPN	1.2	1.0	50
3	(Ir[df(CF_3)ppy]$_2$(dtbbpy))PF_6	1.2	1.0	54
4	(Ir[df(CF_3)ppy]$_2$(bpy))PF_6	1.2	1.0	31
5	(Ir[df(CF_3)ppy]$_2$(dtbbpy))PF_6	1.2	1.0	50[a]
6	(Ir[df(CF_3)ppy]$_2$(dtbbpy))PF_6	1.2	1.0	43[b]
7	(Ir[df(CF_3)ppy]$_2$(dtbbpy))PF_6	1.0	1.5	65
8	(Ir[df(CF_3)ppy]$_2$(dtbbpy))PF_6	1.0	1.5	73[c]

Reaction conditions: on the basis of 0.20 mmol, **20a** (x equiv.), **21-Me** (y equiv.), **22a** (3 equiv., 0.60 mmol), PC (1%), DMA (0.1 M), 10°C, CO_2 (1 bar), 451 nm LEDs,16h. NMR yield using CH_2Br_2 as internal standard. [a]DMF as solvent. [b]DMSO used as solvent at 20°C. [c]DMA (0.2 M).

Next, as introduced in the general aim of the project, we wanted to modify the acrylate moiety with a substituent on the esterified side for us to be able to decarboxylate the final product. After seeing a procedure giving what we were after, we decided to functionalize the acrylate with an ethyl trimethylsilane group (ETMS).[18] After simple addition of a fluoride source, TBAF more precisely, TMSF could be removed along with ethylene gas, leaving a malonic carboxylate behind. With the help of heat, the carboxylate could be extruded by CO_2 removal, granting us with only the desired carboxylate. The deprotection was first tested on compound **25**, derived from the modified acrylate to which CO_2 was not added. Other fluoride sources were tried, without success (Table 2.2).

Table 2.2: ETMS group deprotection screening.

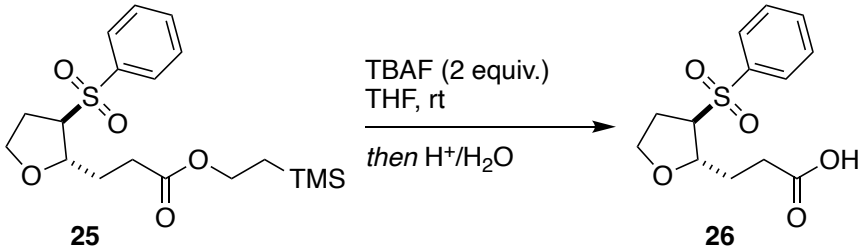

entry	deviation from conditions	yield (%)
1	none	99
2	CsF (2 equiv.)	n.r.
3	KF (2 equiv.)	n.r.
4	HF.Py (2 equiv.)	decomp.

At first, we tried to develop a reaction that would consist of a three-step sequence in a one pot manner, making the reaction as straight forward as possible, as depicted on Scheme 2.5. While we could obtain product **23a'** in good 69% yield, a few parameters made us reconsider this approach. The first observation was that two side products could be generated at the end of the sequence. The main side-product, **23a-1**, was formed after the final decarboxylation, and is a simple methylation of the formed enolate with unreacted methyl iodide. This side-product could be obtained in various amounts, and sometimes in greater quantities than the desired product when the reaction was tested on different starting materials. The second side-product, **23a-2**, observed only in small amounts, is the product of TMS removal, but protonated at the ethyl group. It is still unclear to this date how the side-product is formed exactly since the TMSF and ethylene removal should be a concerted process. In any case, since the one-pot procedure gave us irregularity problems along with decreased yields when trying the scope of the reaction, we decided to modify this procedure to a more reliable one even after many attempts of making the one-pot reaction doable.

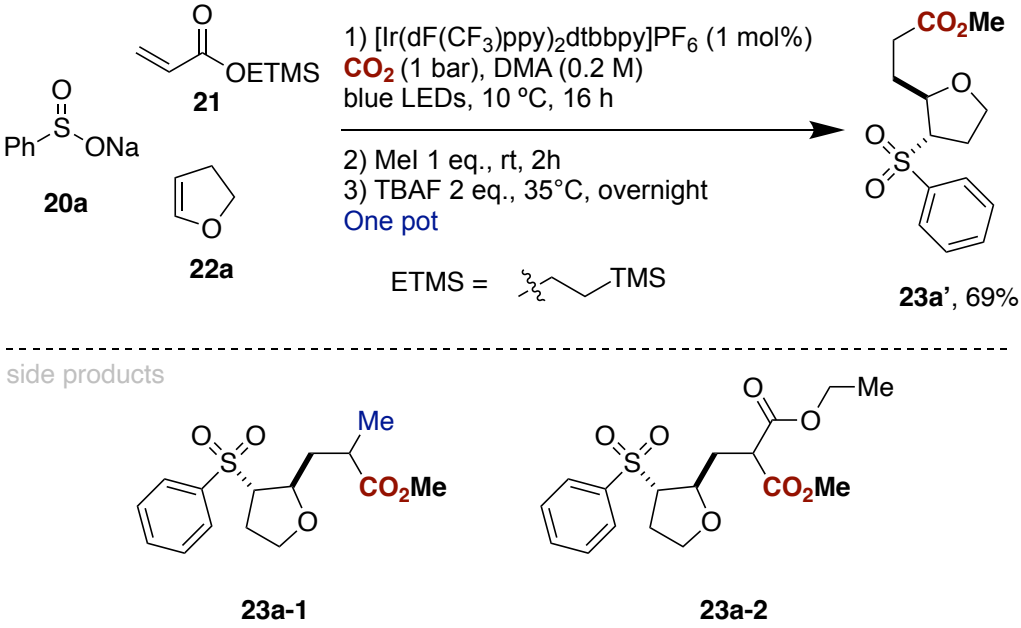

Scheme 2.5: One-pot protocol.

After a few attempts, a very simple modification granted us with a reliable procedure. The effective change was a solvent swap after methylation, using THF as solvent for the TBAF addition. Thus, the reaction was worked-up after methylation and the crude, without purification, submitted to deprotection/decarboxylation. The step itself was also modified, in the one-pot sequence, blue light irradiation was shone since the PC was still in solution, believing that it would help decarboxylate the product by SET oxidation of the carboxylate. Now that the procedure removed most of the PC by work-up, decarboxylation was triggered purely by a thermal process, and hence heated at 45°C. After finally having a reliable procedure yielding 65% of product, we ought to try it using $^{13}CO_2$, since this was the whole purpose of having a decarboxylative manifold. Unfortunately, we could only obtain 37% of desired product at first. Luckily, we quickly understood that the problem came from the CO_2 pressure used for the reaction. The C-12 reactions were performed at 1 bar above atmospheric pressure, and the ^{13}C carbon dioxide bottles we had only given a low pressure. While we could not know the used pressure, lacking manometers, we could get a qualitative understanding when opening the flasks after reaction. When changing the bottle to a new one with higher pressure (still unknown but above atmospheric pressure), the yields could be raised to a satisfying 51% (Scheme 2.6).

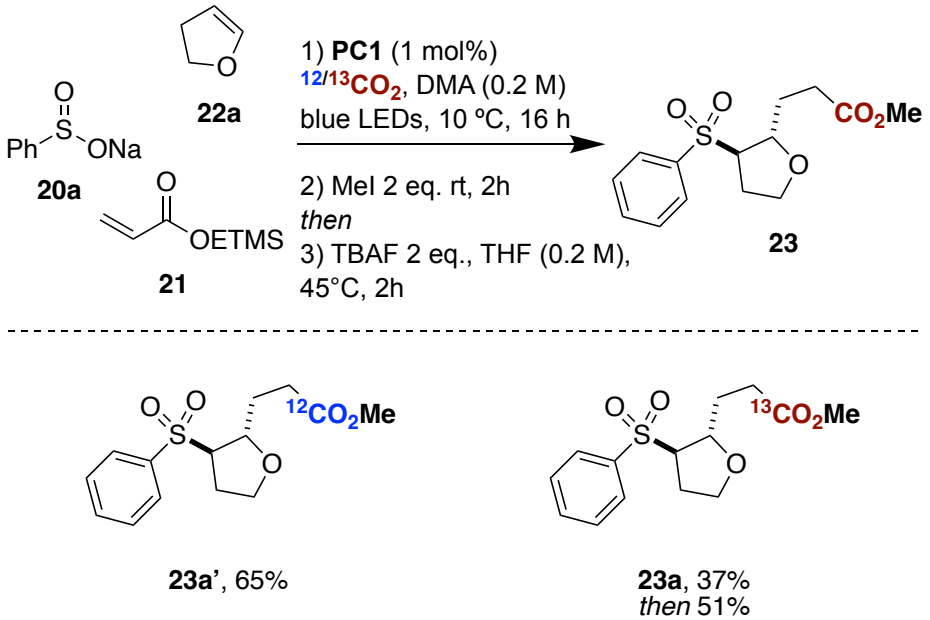

Scheme 2.6:Final sequence developed with first labelling experiments.

Final optimization of the protocol with $^{12}CO_2$, the sulfinate salt was replaced with sodium 4-fluorobenzene sulfinate for NMR purposes. The results were the following (Table 2.3). The reaction, with intermediate work-up after methylation, gave product **27** in 68% NMR yield using our new standard conditions. While DMSO (at 20°C) gave the same result (entry 2), other solvents were detrimental to the reaction outcome (entries 2-5). Decreasing the concentration reduced the yield too (entry 6), as was the case when decreasing the stoichiometry of **22a** (7). Other PCs gave good but lower yields at around 50% (entries 8 and 9), while heating the reaction to 25°C proved to be detrimental (entry 10). Control experiments with no PC or light showed the necessity of these two for the reaction to happen at all (entries 11 and 12).

Table 2.3: Final optimization and control experiments.

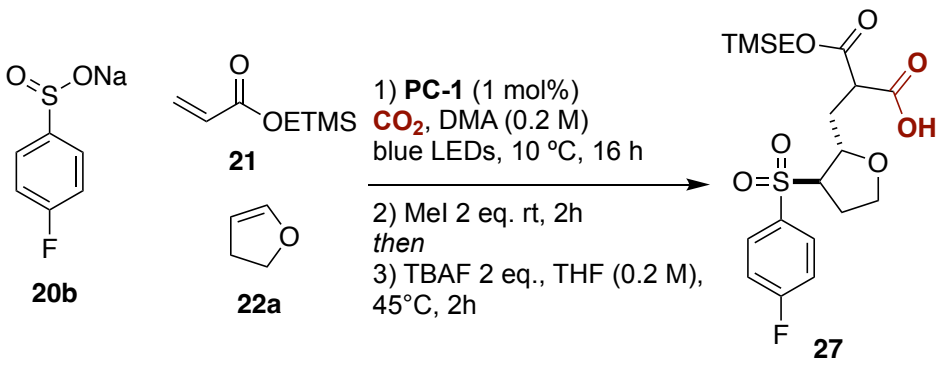

entry	deviation standard conditions	yield (%)
1	none	68
2	using DMSO instead of DMA	68
3	using NMP instead of DMA	58
4	using MeCN instead of DMA	15
5	using THF instead of DMA	<5
6	in DMA (0.1 M)	52
7	using 1 eq. of **22a** instead of 3 eq.	33
8	4-CzIPN 2 mol% as PC	50
9	$Ru(bpy)_3(PF_6)_2$ 2 mol% as PC	51
10	at 25°C	39
11	no photocatalyst	0
12	no light	0

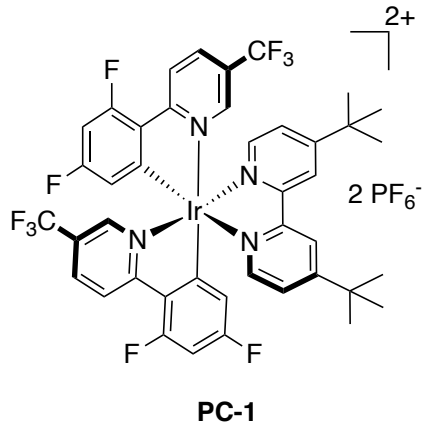

PC-1

Reaction conditions: **20b** (0.20 mmol), **21** (1.5 equiv., 0.30 mmol), **22a** (3 equiv., 0.60 mmol), PC (1%), DMA (0.2 M), 10°C, CO_2 (1 bar), 451 nm LEDs,16h. NMR yield using CH_2Br_2 as internal standard. [a]DMF as solvent. [b]DMSO used as solvent at 20°C. [c]DMA (0.2 M).

2.4. Substrate scope

2.4.1. Four-component coupling

With optimized conditions in hand, we decided to move on with the scope of the reaction, by evaluating various sulfinate salts and alkenes. It is worth noting that while the yields seem moderate at first sight, those encompass a total of four new bonds and the breaking of one. If all the bond making or breaking process happen with an efficiency of 90%, the final yield would be about 60%. The sulfinate salts scope (Figure 2.3) showed good functional group compatibility with electron-poor and electron-rich sulfinate salts, although electron-rich ones proved to be better tolerated. Halogens (**23b**, **23e**, **23h**), extended π-systems (**23g**) and pyridine derivative (**23c**) worked in good yields. The best results were obtained when unsubstituted (**23a**), 4-methoxy- (**23f**) and 4-methylbenzene (**23d**) sulfinates were used, showing the preference for a more electron rich sulfur atom.

In the case of the alkene scope (Figure 2.4), a satisfying variety was compatible with the conditions. While DHF **22a** was used as model substrate, we were delighted to see that related nitrogen-based Cbz-protected dihydropyrrole **22i** gave good 51% yield. Vinyl amides **22k** and **22m** gave 47 and 45% yield, respectively. Non-cyclic substrates such as **22j** and **22l** proved to react well, though product **23j** being the lowest yield observed for the scope. **23n**, a phenyl substituted DHF was obtained in 40% with no mixture of diastereoisomers, only a pair of enantiomers were found, with the sulfone being on the same side as the phenyl ring. We rationalize this observation in a similar way as the endo selectivity for Diels-Alders reaction, in which the π-clouds of the two reactants overlap, easing a same side approach of the radical to the olefin. The always-trans configuration between the sulfone and the alkyl substituent for five-membered rings will be discussed after the scope of the reaction. Finally, **22o** gave four-membered ring compound **23o** as product, which we could obtain an X-ray structure of. **22o** is a 1,1-disubstituted olefin, interestingly, a different product was obtained when subjecting other olefins of this class. While we were expecting the typical four-component coupling product pattern, a heavier compound with two additions of acrylates was serendipitously obtained, which we therefore named a pseudo-five-component coupling. After slight modification of the reaction conditions of the newly discovered reaction, we continued with a scope of 1,1-disubstituted olefins. The reason why **23o** was obtained as a four-component product will be explained when discussing the mechanism, although, minor amount of pseudo-five-component coupling product could still be observed in that particular case.

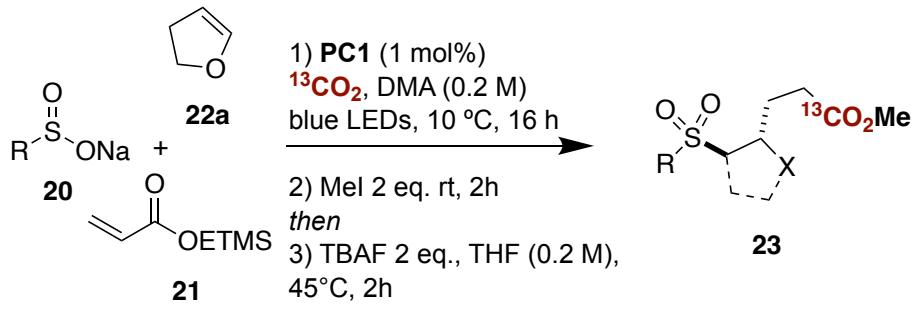

■ Sulfinate salts:

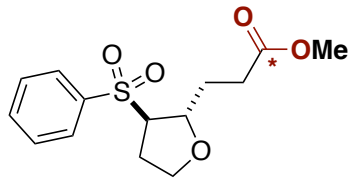

23a, 51%

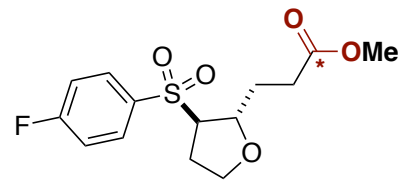

23b, 50%

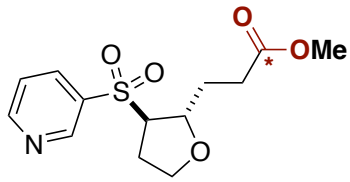

23c, 49%

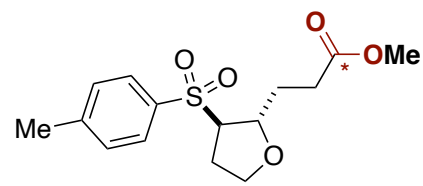

23d, 60%

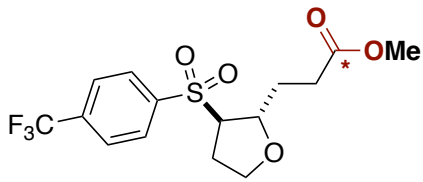

23e, 44%

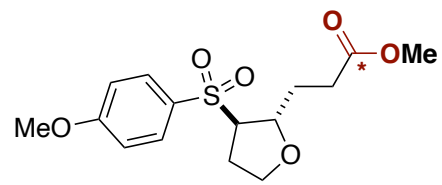

23f, 56%

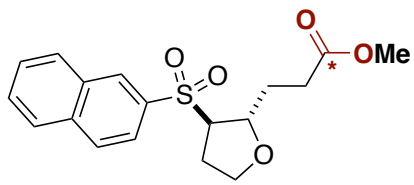

23g, 36%

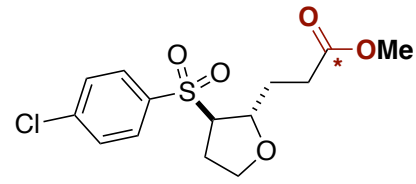

23h, 50%

Figure 2.3: Sulfinate salt scope of the reaction.

Reaction conditions: **20** (0.20 mmol), **21** (1.5 equiv., 0.30 mmol), **22a** (3 equiv., 0.60 mmol), PC-1 (1%), DMA (0.2 M), 10°C, $^{13}CO_2$ (1 bar), 451 nm LEDs,16h. Isolated yields, average of two independent runs.

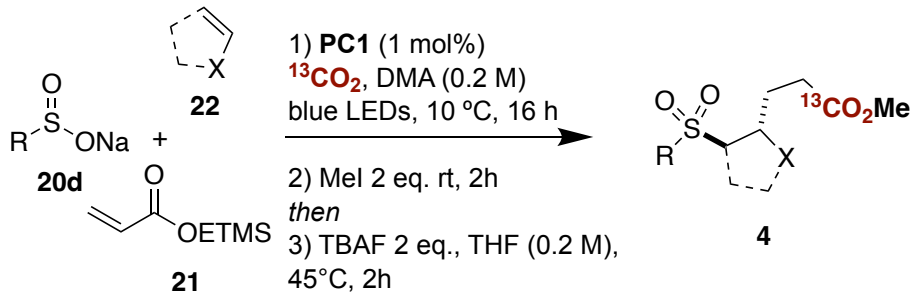

■ Electron rich alkene:

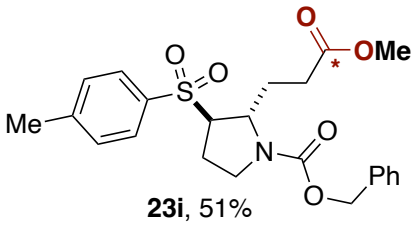

23i, 51%

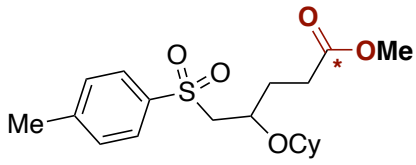

23j, 31%

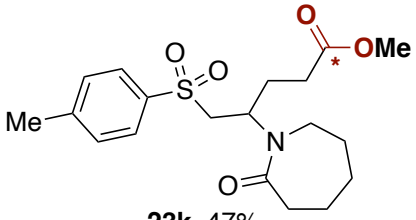

23k, 47%

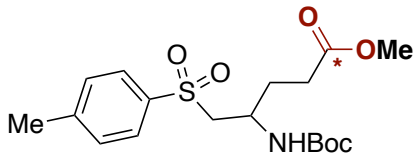

23l, 44%

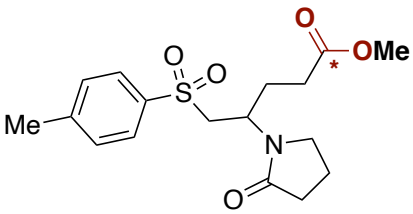

23m, 45%

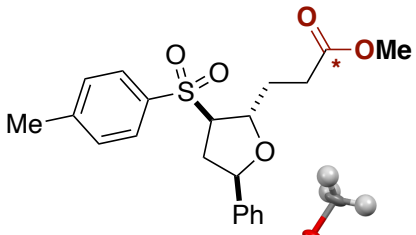

23n, 40%

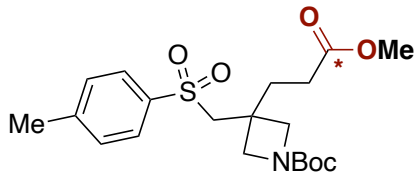

23o, 43%

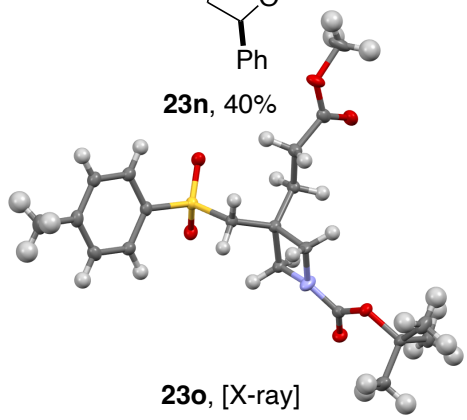

23o, [X-ray]

Figure 2.4: Alkene scope of the reaction.

2.4.2. Pseudo-five-component coupling

The pseudo-five-component reaction was modified compared to the four-component coupling. Here, DMSO was used as solvent, and thus a temperature of 20°C was preferred for the reaction to proceed. The reaction proceeds this time by an addition of the sulfonyl radical into acrylate **21** at first, followed by the addition of the electron-poor radical into the 1,1-disubstituted olefin, which then follows the normal reactivity. Addition into acrylate **21** followed by RPC for a nucleophilic attack on carbon dioxide gives the product. Because of the lower overall yielding process, the full sequence was not performed on such products and isolation was done after methylation. In this case electron-poor sulfinates gave better yields. The reaction scope is given in Figure 2.5. **28a** was obtained in 63% yield while **28e** in 35%. Non-substituted sulfinate (**28c**), 4-fluoro- (**28b**) and 4-methylbenezene (**28d**) sulfinates were obtained in 55, 64 and 56% yield, respectively. In the case of alkenes, 6-membered ring nitrogen containing **22f'** yielded **28f** in 41%. **28g** was interesting, showing that the reaction was not limited to cyclic molecules. Although the scope was done after the methylation step, we wanted to demonstrate that deprotection followed by decarboxylation are still feasible. When subjecting the protected products to the initial conditions with TBAF at 45°C, deprotection and decarboxylation happened as expected but no deprotection could be observed for the internal ester. The temperature was therefore raised to 70°C, allowing a full sequence from **20d** and **22a'**, yielding **28j** in 31% yield (Scheme 2.7). The attractive feature with the obtained structure is the plethora of synthetic modifications offered to the chemist. Having a sulfone, an acid, and an ester at once.

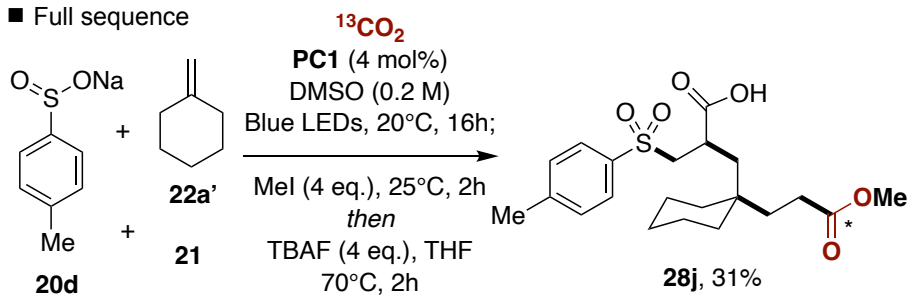

Scheme 2.7: Full sequence on the pseudo-five-component coupling.

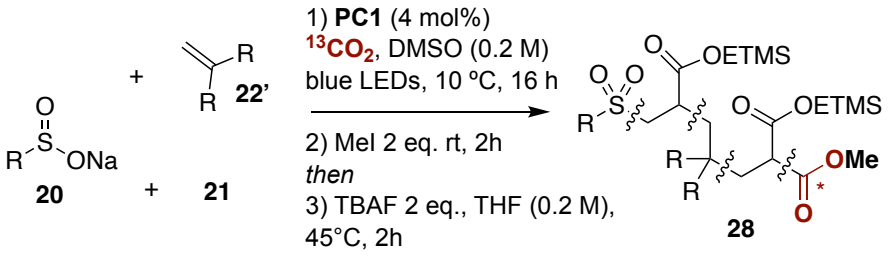

■ Sulfinate salts:

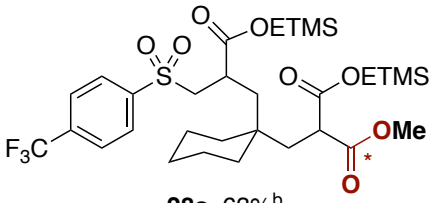

28a, 63%[b]
dr = 1.4:1

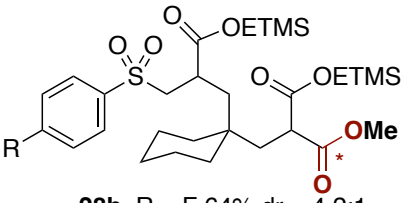

28b, R = F 64% dr = 4.2:1
28c, R = H 55% dr = 6.3:1

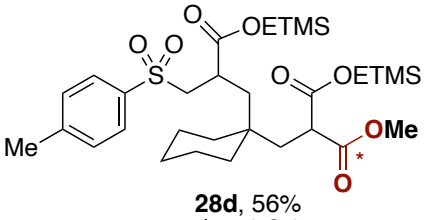

28d, 56%
dr = 1.6:1

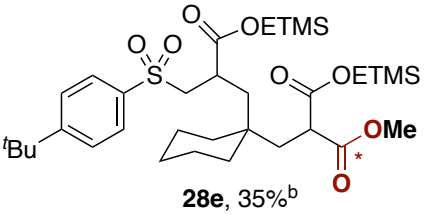

28e, 35%[b]
dr = 1.6:1

■ Alkenes

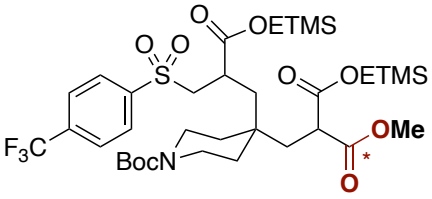

28f, 41%[c]
dr = 1:1

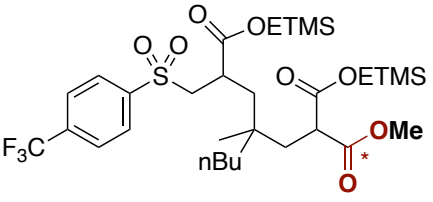

28g, 36%[c]
dr = 1:1.4:1:1.2

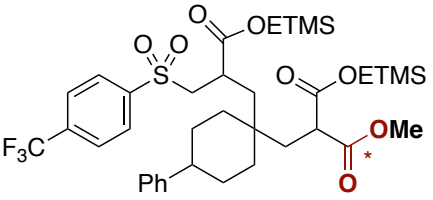

28h, 50%[c]
dr = 6.7:5.1:1:1

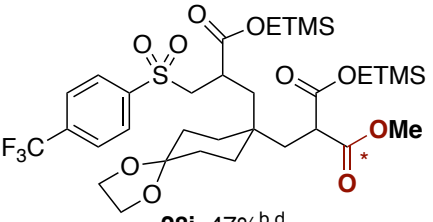

28i, 47%[b,d]
dr = 2.3:1.6:1

Figure 2.5: Scope of the pseudo-five-component reaction.

2.5. Mechanism

2.5.1. Investigation

After exploring the scope of the reaction, we decided to understand the reason behind the *trans*-configuration of the five-membered rings, in addition to why six-membered rings showed no products when tried. Very simple DFT calculations have been done in order to have some hints. When computing the structure and orbitals of radical **29**, we obtained what is depicted in Figure 2.6, top. As we can see in red, the main part of the SOMO orbital is placed *trans* to the sulfone group, favoring a Giese addition with such stereoselectivity. We assume that the steric bulk coming from the sulfone on the locked structure of a ring prohibits addition in a *syn* fashion. Performing the same DFT calculation on the related six-membered ring radical **30** showed that the SOMO was mostly placed *syn* to the sulfone group, ultimately preventing further reactivity, which is what we experimentally observe. While these results tend towards our observations, the results cannot be taken for granted given our lack of expertise in DFT calculations, and the possible involvement of various other parameters.

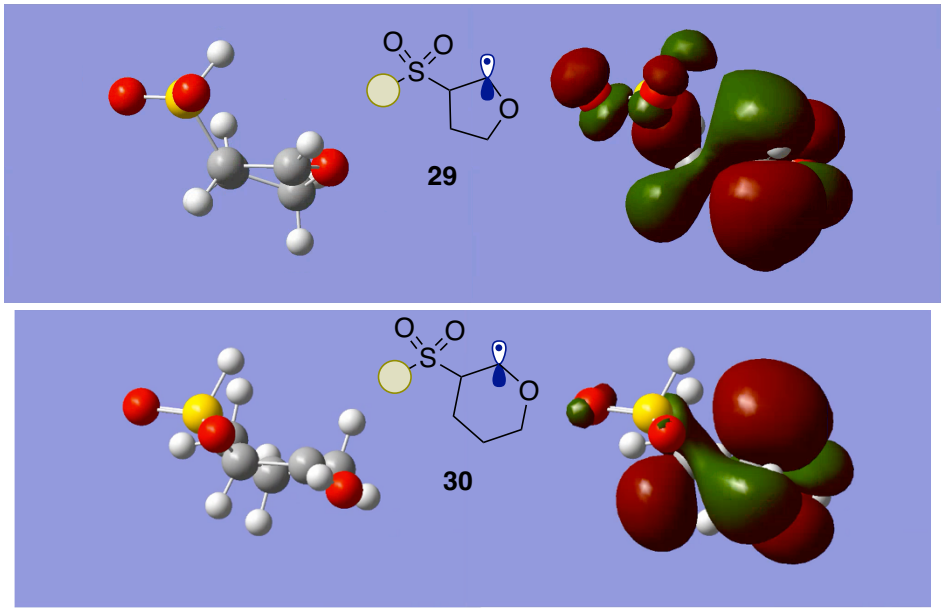

Figure 2.6: DFT structure optimization and related SOMO.

We continued towards the understanding of the reactivity of this process, more specifically, trying to decipher the selectivity observed for the pseudo-five-component

coupling. Why would a polarity-mismatch such as sulfonyl radical doing a Giese addition into the acrylate would be more favored than addition into the olefin? To answer this question, we designed a simple experiment, meant to be a radical kinetic trap for the sulfonyl radical. Since any addition of the sulfonyl radical into a 1,1-disubstituted olefin will inevitably lead to a tertiary radical, we wondered if this was the cause for different selectivity, given that reports are known describing this process as easily reversible. By using a specific 1,1-disubstituted alkene that would open upon radical addition from the sulfonyl radical, generating a primary or secondary radical instead, we could probe for whether the sulfonyl radical adds into 1,1-disubstituted alkenes at all, or if this process is in fact not feasible, leading directly to the addition into the acrylate. The alkene of choice for this radical trap was β-pinene **29**.

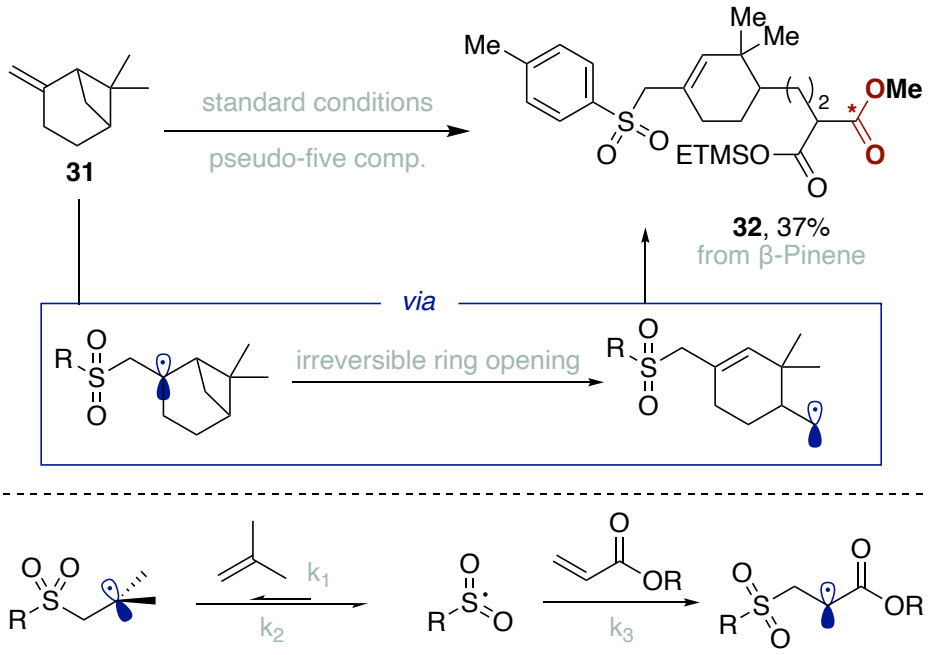

Scheme 2.8: Radical trap experiment.

The product obtained from the reaction of **31** with **20d** and **21** gave the four-component coupling scaffold in 37% yield after methylation, compound **32** (Scheme 2.8). The result suggests two separate information allowing us to understand what happens in a flask when performing a pseudo-five-component coupling reaction. Firstly, this tells that addition of the sulfonyl radical into 1,1-disubstituted olefins is a feasible process and therefore happens in solution. The second information, which is indirect from the observation made, is relating to the kinetics of the additions and therefore the selectivity. As previously mentioned, β-sulfonyl radicals are known to undergo sulfonyl radical elimination, the typical rate being estimated at $1x10^7$ s^{-1}.[19] While this might also

happen when secondary or primary radicals are generated from various alkene materials in our reaction, the stability of the tertiary radical in this case, in addition to a bulkier radical, might make the subsequent Giese addition unfavorable, and thus slower than the rate of sulfonyl radical elimination. Those rates are represented on Scheme 2.8, bottom, as k_1 and k_2 respectively. While the addition of sulfonyl radicals directly into acrylates should be disfavored due to polarity mismatch, the reaction is likely still a feasible process, albeit in a relatively slow manner. Our rational is therefore that k_2 becomes so high compared to k_1 that the tertiary radical is virtually inexistent in solution at any given time. Simultaneously, while addition of the sulfonyl radical into the acrylate is disfavored and likely slow, its addition would generate an electron-poor radical that can itself react with the alkene to give another tertiary radical. This intermediate, not being a β-sulfonyl radical, cannot eliminate any group and is forced to undergo the expected sequence with another acrylate giving the final product. Coming back to β-pinene as starting material, once the addition of the sulfonyl radical into the olefin happens, a radical ring-opening reaction takes place, giving a primary radical intermediate that cannot react backwards to the tertiary radical. The more reactive primary radical then follows the expected sequence giving **32** as product. By showing the four-component type of product with β-pinene, we can demonstrate that sulfonyl radicals and 1,1-disubstituted alkenes are in fact reacting and that the selectivity comes from the reversible nature of the process when the tertiary radical is stable at the β-sulfonyl position. We propose the mechanism depicted in Figure 2.7.

2.5.2. Mechanistic proposal

The reaction starts with the activation of the iridium PC with light, which can then undergo reductive quench with sulfinate **20**. The sulfonyl radical **31**, as discussed, can add into alkene **22a'** to generate the tertiary radical **34'**, but its reversible reaction being favored gives back sulfonyl radical **33**. This intermediate can instead perform a Giese addition into **21**, itself also theoretically reversible, giving intermediate **34**. Once reacting with alkene **22a'**, the generation of intermediate **35** is what drives the reaction forward being irreversible, through the Le Châtelier principle. From this point on, the reaction resembles the four-component one, performing a Giese addition followed by RPC and nucleophilic attack to CO_2. While most compounds reacted in this way, this was not the case when submitting **22o**, giving the four-component product **23o** as major product. The pseudo-five-component product could be observed in minor amounts and therefore indicates that both mechanisms are coexisting in this case. We rationalize the major formation of **23o** by the fact that the four-membered ring bearing the tertiary

makes it less sterically bulky, and thus probably more prone to undergo Giese addition with acrylate **21**. Additionally, the lone pair of nitrogen being parallel with the p-orbital of the radical might prevent radical elimination by overlap, forming an extended molecular orbital.

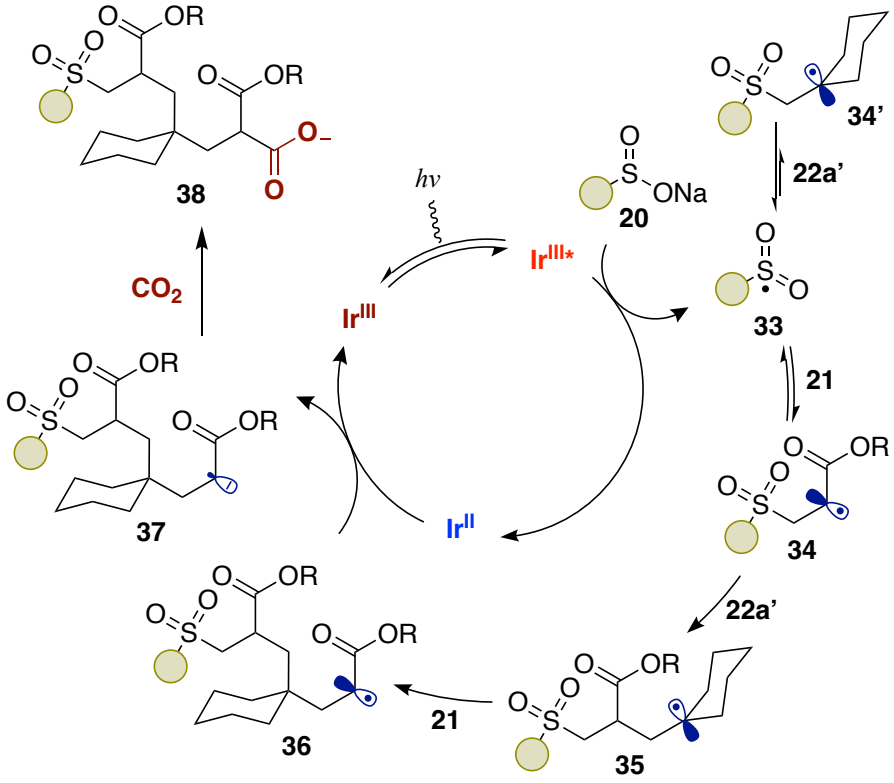

Figure 2.7: Proposed mechanism for the pseudo-five-component coupling.

2.6. Conclusions

A new methodology allowing for the synthesis of molecularly complex scaffolds from simple starting materials while labelling the compounds with carbon dioxide has been described. The reaction is done through a three step sequence requiring only one final purification. The deprotection/decarboxylation allows for the incorporation of only one carboxylate, coming from carbon dioxide. This also allows for a formal coupling of ethylene gas and CO_2 instead of an acrylate. The reaction can yield two different types of products depending on the class of alkene used in the reaction. A radical trap experiment has been done to show the intricacies involved in the selectivity of the reaction. This method therefore grants the synthetic chemist with a rapid access to the backbones described herein, aiding isotope chemists and potentially medicinal chemists to rapidly generate compounds of this type.

2.7. Experimental details

2.7.1. Multicomponent carboxylative coupling

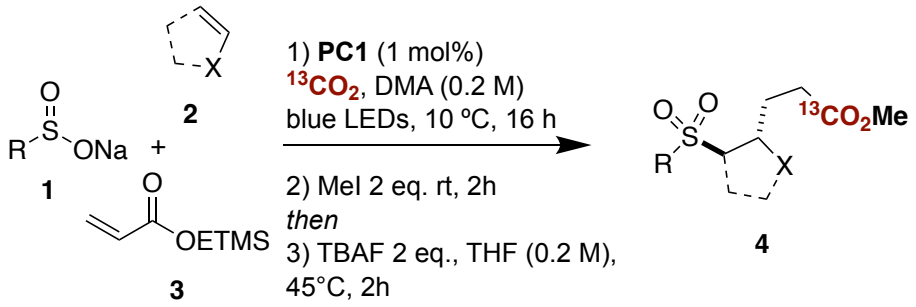

General Procedure 1 for <u>four-component</u> coupling (GP1):

An oven-dried Schlenk tube containing a magnetic stir bar was charged with the sulfinic acid sodium salt (1.0 equiv., 0.20 mmol), and **PC-1** (1 mol%, 2.0 µmol, 2.2 mg). The Schlenk tube was then connected to a vacuum line where it was evacuated and backfilled with argon at least three times. DMA (1 mL, 0.2 M), the acrylate **3** (1.5 equiv., 0.30 mmol, 54 µL) and the alkene (3.0 equiv., 0.60 mmol) were added under positive argon flow. Once all the components were added, the Schlenk tube was put in liquid N_2 to freeze the solvent. *(Caution! Note that the Schlenk tube was not dipped too much to avoid solidification of argon on the walls.*) Once the mixture was solid, high vacuum was applied for 30 seconds, followed by $^{13}CO_2$ injection (while the exact pressure could not be determined, a "hiss" sound when opening a Schlenk tube indicates that pressure is higher than atmospheric pressure). The tube was then sealed and placed in a temperature controlled photoreactor with water/IPA cooling at 10 ºC. Once thawed, the reaction mixture was stirred for 16 h in the presence of continuous irradiation with blue light (451 nm, 2 W LED). The reaction was then quenched with 2 equiv. of MeI (25 µL, 0.40 mmol) to methylate the labelled carboxylate, and the tube sealed again and stirred at 25°C for 2h. After this, the solution was diluted with EtOAc and washed 3 times with water. The organic phase was dried over $MgSO_4$, filtered and solvents removed under reduced pressure. The crude was dissolved in 1 mL of THF to which was added 2 equiv. of TBAF (400 µL, 1 M solution in THF), the dark solution was then stirred at 45°C for 2h (Note: the vial has to be open, or a needle is put in a septum). Finally, a 1 M aqueous HCl solution was used to quench the reaction. The solution was diluted with EtOAc and washed 3 times with water and the combined organic phases were dried over $MgSO_4$, filtered and solvents removed under reduced pressure. Flash column chromatography was performed to yield the pure products.

General Procedure 2 for <u>pseudo-five-component</u> coupling (GP2):

An oven-dried Schlenk tube containing a magnetic stir bar was charged with the sulfinic acid sodium salt (2.0 equiv., 0.40 mmol), and **PC-1** (4 mol%, 8.0 µmol, 8.8 mg). The Schlenk tube was then connected to a vacuum line where it was evacuated and backfilled with argon at least three times. DMSO (1 mL, 0.2 M), the acrylate **21** (2.0 equiv., 0.40 mmol, 72 µL) and the alkene **22'** (3.0 equiv., 0.60 mmol) were added under positive argon flow. Once all the components were added, the Schlenk tube was put in liquid N_2 to freeze the solvent. *(Caution! Note that the Schlenk tube was not dipped too much to avoid solidification of argon on the walls.)* Once the mixture was solid, high vacuum was applied for 30 seconds, followed by $^{13}CO_2$ injection (while the exact pressure could not be determined, the "hiss" sound when opening a Schlenk tube indicates pressure slightly higher than atmospheric pressure). The tube was then sealed and placed in a temperature controlled photoreactor with water cooling at 20 ºC. Once thawed, the reaction mixture was stirred for 16 h in the presence of continuous irradiation with blue light (451 nm, 2 W LED). The reaction was then quenched with a saturated aqueous solution of NH_4Cl. The mixture was then diluted with EtOAc and washed 3 times with water. The organic phase was dried over $MgSO_4$, filtered and solvents removed under reduced pressure. The crude was purified by quick flash column chromatography to yield the slightly impure acid product (usually containing photocatalyst impurity). The compound was then solubilized in 1 mL of Et_2O/MeOH (2:1) and cooled to 0°C. $TMSCHN_2$ (2 equiv., 0.40 mmol) was added dropwise, and the reaction was stirred at the same temperature for 1h after which the volatiles were removed under reduced pressure. The crude was purified using flash column chromatography to yield the pure methylated product.

General Procedure 3 for <u>pseudo-five-component</u> coupling (GP3):

An oven-dried Schlenk tube containing a magnetic stir bar was charged with the sulfinic acid sodium salt (2.0 equiv., 0.40 mmol), and **PC-1** (4 mol%, 8.0 µmol, 8.8 mg). The Schlenk tube was then connected to a vacuum line where it was evacuated and backfilled

with argon at least three times. DMSO (1 mL, 0.2 M), the acrylate **21** (2.0 equiv., 0.40 mmol, 72 µL) and the alkene **22'** (3.0 equiv., 0.60 mmol) were added under positive argon flow. Once all the components were added, the Schlenk tube was put in liquid N_2 to freeze the solvent. *(Caution! Note that the Schlenk tube was not dipped too much to avoid solidification of argon on the walls.)* Once the mixture was solid, high vacuum was applied for 30 seconds, followed by $^{13}CO_2$ injection (while the exact pressure could not be determined, the "hiss" sound when opening a Schlenk tube indicates pressure slightly higher than atmospheric pressure). The tube was then sealed and placed in a temperature controlled photoreactor with water cooling at 20 ºC. Once thawed, the reaction mixture was stirred for 16 h in the presence of continuous irradiation with blue light (451 nm, 2 W LED). The reaction was then quenched with 3 equiv. of MeI (37 µL, 0.60 mmol), and the tube sealed again and stirred at 25°C for 2h. After this, the solution was diluted with EtOAc and washed 3 times with water. The organic phase was dried over $MgSO_4$, filtered and solvents removed under reduced pressure. The crude was purified by flash column chromatography to yield the product.

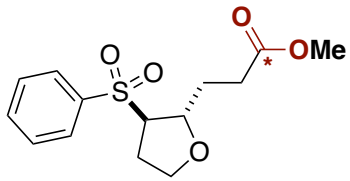

Methyl 3-((2S*,3R*)-3-(phenylsulfonyl)tetrahydrofuran-2-yl)propanoate-1-^{13}C (23a). Following **GP1**, sodium benzenesulfinate **20a** (32.8 mg, 0.20 mmol) 2,3-dihydrofuran **22a** (45.4 µL, 0.60 mmol) and 2-(trimethylsilyl)ethyl acrylate (54 µL, 0.30 mmol) afforded the product after flash column chromatography on silica gel (n-hexane/EtOAc 2:1) as a white solid (on average: 30.2 mg, 51% yield). **^{1}H NMR (500 MHz, $CDCl_3$):** δ (ppm) = 7.95 – 7.87 (m, 2H), 7.71 – 7.64 (m, 1H), 7.64 – 7.55 (m, 2H), 4.27 (ddd, J = 8.5, 6.0, 4.3 Hz, 1H), 3.87 (ddd, J = 8.7, 7.4, 4.3 Hz, 1H), 3.75 (td, J = 8.4, 6.9 Hz, 1H), 3.64 (d, J = 3.9 Hz, 3H), 3.38 (ddd, J = 9.8, 6.0, 4.8 Hz, 1H), 2.48 – 2.30 (m, 3H), 2.13 (ddt, J = 13.4, 9.8, 7.8 Hz, 1H), 1.86 – 1.70 (m, 2H); **^{13}C NMR (126 MHz, $CDCl_3$)** δ (ppm) = 173.43, 138.34, 134.20, 129.58, 128.72, 77.97 (d, J = 3.9 Hz), 68.36, 67.33, 51.77 (d, J = 2.7 Hz), 30.39 (d, J = 58.3 Hz), 30.24 (d, J = 1.4 Hz), 28.75. **IR (neat, cm^{-1}):** 2870, 1688, 1441, 1358, 1303, 1144, 1107, 1083, 1023, 961, 934, 891, 752, 718, 588, 548; **HRMS** calcd. for ($C_{13}H_{18}NaO_5S^{13}C$) $[M+Na]^+$: 322.0801 found 322.0804. **MP** = 50°C.

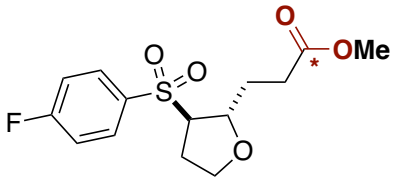

Methyl 3-((2S*,3R*)-3-((4-fluorophenyl)sulfonyl)tetrahydrofuran-2-yl)propanoate-1-^{13}C (23b). Following **GP1**, sodium 4-fluorobenzenesulfinate **20b** (36.4 mg, 0.20 mmol) 2,3-dihydrofuran **22a** (45.4 µL, 0.60 mmol) and 2-(trimethylsilyl)ethyl acrylate (54 µL, 0.30 mmol) afforded the product after flash column chromatography on silica gel (pentane/EtOAc 2:1) as a white solid (on average: 31.9 mg, 50% yield). **^{1}H NMR (500 MHz, $CDCl_3$):** δ (ppm) = 7.97 – 7.89 (m, 2H), 7.30 – 7.22 (m, 2H), 4.27 (ddd, J = 8.7, 6.0, 4.2 Hz, 1H), 3.87 (ddd, J = 8.7, 7.4, 4.4 Hz, 1H), 3.75 (td, J = 8.4, 7.0 Hz, 1H), 3.65 (d, J = 3.9 Hz, 3H), 3.37 (ddd, J = 9.8, 6.0, 4.9 Hz, 1H), 2.49 – 2.29 (m, 3H), 2.14 (ddt, J = 13.4, 9.8, 7.7 Hz, 1H), 1.88 – 1.70 (m, 2H); **^{13}C NMR (126 MHz, $CDCl_3$)** δ (ppm) = 173.41, 166.14 (d, J = 257.3 Hz), 134.40 (d, J = 3.2 Hz), 131.65 (d, J = 9.6 Hz), 116.95 (d, J = 22.7 Hz), 77.95 (d, J = 3.7 Hz), 68.55, 67.27, 51.78 (d, J = 2.8 Hz), 30.30 (d, J = 58.1 Hz), 30.19 (d, J = 1.4 Hz), 28.77. **^{19}F NMR (471 MHz, CDCl3)** δ (ppm) = -102.6. **IR (neat, cm^{-1}):** 3108, 2956, 2875, 1721, 1588, 1495, 1354, 1290, 1231, 1142, 1078, 1032, 849, 754, 539; **HRMS** calcd. for ($C_{13}H_{17}FNaO_5S^{13}C$) $[M+Na]^+$: 340.0706 found 340.0718. **MP** = 83°C.

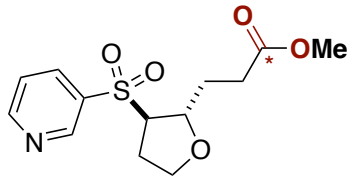

Methyl 3-((2*S,3*R**)-3-(pyridin-3-ylsulfonyl)tetrahydrofuran-2-yl)propanoate-^{13}C (23c)**. Following **GP1**, sodium pyridine-3-sulfinate **20c** (33.0 mg, 0.20 mmol) 2,3-dihydrofuran **22a** (45.4 µL, 0.60 mmol) and 2-(trimethylsilyl)ethyl acrylate (54 µL, 0.30 mmol) afforded the product after flash column chromatography on silica gel (pentane/EtOAc 2:1) as an amorphous solid. (on average: 30 mg, 49% yield). **^{1}H NMR (500 MHz, $CDCl_3$):** δ (ppm) δ 9.12 (dd, *J* = 2.4, 0.9 Hz, 1H), 8.90 (dd, *J* = 4.9, 1.6 Hz, 1H), 8.21 (ddd, *J* = 8.0, 2.4, 1.6 Hz, 1H), 7.55 (ddd, *J* = 8.0, 4.9, 0.9 Hz, 1H), 4.32 (ddd, *J* = 8.7, 5.9, 4.2 Hz, 1H), 3.97 – 3.85 (m, 1H), 3.77 (td, *J* = 8.5, 7.1 Hz, 1H), 3.66 (d, *J* = 3.9 Hz, 3H), 3.43 (ddd, *J* = 9.8, 5.9, 4.9 Hz, 1H), 2.50 – 2.27 (m, 3H), 2.17 (ddt, *J* = 13.5, 9.8, 7.7 Hz, 1H), 1.98 – 1.69 (m, 2H). **^{13}C NMR (126 MHz, $CDCl_3$)** δ 173.4, 154.7, 149.7, 136.6, 134.9, 124.1, 68.8, 67.3, 51.8 (d, J = 2.7 Hz), 30.6, 30.2(d, J = 1.5 Hz), 30.0, 28.8. (ppm) **IR (neat, cm^{-1}):** 2955, 1690, 1575, 1435, 1355, 1244, 1110, 1060, 906, 780, 711; **HRMS** calcd. for ($C_{12}H_{17}NNaO_5S^{13}C$) $[M+Na]^+$:323.0753 found 323.0760.

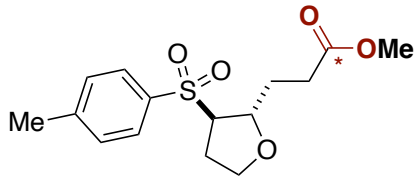

Methyl 3-((2*S,3*R**)-3-tosyltetrahydrofuran-2-yl)propanoate-1-^{13}C (23d)**. Following **GP1**, sodium benzenesulfinate **20d** (35.6 mg, 0.20 mmol) 2,3-dihydrofuran **22a** (45.4 µL, 0.60 mmol) and 2-(trimethylsilyl)ethyl acrylate (54 µL, 0.30 mmol) afforded the product after flash column chromatography on silica gel (pentane/EtOAc 2:1) as a colorless oil (on average: 37.3 mg, 60% yield). **^{1}H NMR (500 MHz, $CDCl_3$):** δ (ppm) = 7.81 – 7.74 (m, 2H), 7.40 – 7.34 (m, 2H), 4.26 (ddd, J = 8.6, 6.0, 4.1 Hz, 1H), 3.86 (ddd, J = 8.7, 7.4, 4.4 Hz, 1H), 3.73 (td, J = 8.4, 6.9 Hz, 1H), 3.65 (d, J = 3.9 Hz, 3H), 3.35 (ddd, J = 9.8, 6.0, 4.8 Hz, 1H), 2.44 (s, 3H), 2.44 – 2.30 (m, 3H), 2.12 (ddt, J = 13.4, 9.8, 7.8 Hz, 1H), 1.88 – 1.70 (m, 2H); **^{13}C NMR (126 MHz, $CDCl_3$)** δ (ppm) = 173.47, 145.28, 135.37, 130.19, 128.76, 78.01 (d, J = 3.8 Hz), 68.44, 67.32, 51.75 (d, J = 2.8 Hz), 30.42 (d, J = 58.3 Hz), 30.26 (d, J = 1.4 Hz), 28.79, 21.78. **IR (neat, cm^{-1}):** 2952, 1696, 1596, 1433, 1351, 1288, 1191, 1143, 1087, 1024, 904, 822, 750, 667, 613, 566, 540; **HRMS** calcd. for ($C_{14}H_{20}NaO_5S^{13}C$) $[M+Na]^+$: 336.0957 found 336.0962. **MP** = 77°C.

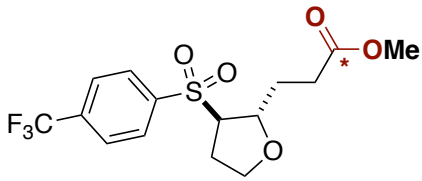

Methyl 3-((2*S,3*R**)-3-((4-(trifluoromethyl)phenyl)sulfonyl)tetrahydrofuran-2-yl)propanoate-1-^{13}C (23e)**. Following **GP1**, sodium 4-trifluoromethylbenzenesulfinate **20e** (46.4 mg, 0.20 mmol) 2,3-dihydrofuran **22a** (45.4 µL, 0.60 mmol) and 2-(trimethylsilyl)ethyl acrylate (54 µL, 0.30 mmol) afforded the product after flash column chromatography on silica gel (pentane/EtOAc 3:1) as a white solid (on average: 32.3 mg, 44% yield). **^{1}H NMR (500 MHz, $CDCl_3$):** δ (ppm) = 8.07 (d, J = 8.1 Hz, 2H), 7.87 (d, J = 8.2 Hz, 2H), 4.33 (ddd, J = 8.8, 5.9, 4.1 Hz, 1H), 3.89 (ddd, J = 8.8, 7.4, 4.4 Hz, 1H), 3.78 (td, J = 8.5, 7.1 Hz, 1H), 3.66 (d, J = 3.9 Hz, 3H), 3.43 (ddd, J = 9.7, 6.0, 4.9 Hz, 1H), 2.52 – 2.39 (m, 2H), 2.37 – 2.30 (m, 1H), 2.20 – 2.09 (m, 1H), 1.92 – 1.74 (m, 2H); **^{13}C NMR (126 MHz, $CDCl_3$)** δ (ppm) = 173.39, 141.98, 135.90 (q, J = 33.3 Hz), 129.45, 126.75 (d, J = 3.7 Hz), 123.17 (d, J = 273.1 Hz), 77.82 (d, J = 3.6 Hz), 68.40, 67.28, 51.82 (d, J = 2.7 Hz), 30.28 (d, J = 58.1 Hz), 30.24 (d, J = 1.4 Hz), 28.80. **^{19}F NMR (471 MHz, $CDCl_3$)** δ (ppm) = -63.2. **IR (neat, cm^{-1}):** 2953, 1683, 1407, 1356, 1408, 1146, 1060, 908, 855, 754, 710, 623; **HRMS**

calcd. for ($C_{14}H_{17}F_3NaO_5S^{13}C$) $[M+Na]^+$: 390.0695 found 390.0675. **MP** = 134°C.

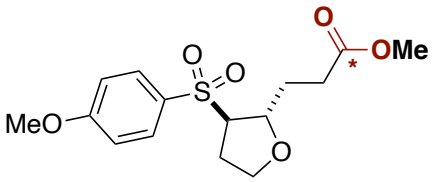

Methyl 3-((2*S,3*R**)-3-((4-methoxyphenyl)sulfonyl)tetrahydrofuran-2-yl)propanoate-^{13}C (23f)**. Following **GP1**, sodium 4-methoxybenzenesulfinate **20f** (38.8 mg, 0.20 mmol) 2,3-dihydrofuran **22a** (45.4 µL, 0.60 mmol) and 2-(trimethylsilyl)ethyl acrylate (54 µL, 0.30 mmol) afforded the product after flash column chromatography on silica gel (n-hexane/EtOAc 3:1) as a colorless oil (on average: 36.8 mg, 56% yield). **^{1}H NMR (500 MHz, $CDCl_3$):** δ (ppm) = 7.85 – 7.80 (m, 2H), 7.07 – 7.01 (m, 2H), 4.25 (ddd, J = 8.7, 6.0, 4.1 Hz, 1H), 3.89 (s, 3H), 3.88 – 3.84 (m, 1H), 3.73 (td, J = 8.4, 6.9 Hz, 1H), 3.65 (d, J = 3.8 Hz, 3H), 3.35 (ddd, J = 9.8, 6.0, 4.9 Hz, 1H), 2.50 – 2.30 (m, 3H), 2.14 (ddt, J = 13.4, 9.8, 7.7 Hz, 1H), 1.89 – 1.72 (m, 2H).; **^{13}C NMR (126 MHz, $CDCl_3$)** δ (ppm) = 173.5, 164.1, 131.0, 129.7, 114.8, 78.1, 78.1, 68.7, 67.3, 55.9, 51.8, 51.8, 30.7, 30.3, 30.3, 30.2, 28.8. **IR (neat, cm^{-1}):** 2948, 2865, 1695, 1593, 1576, 1497, 1411, 1321, 1268, 1173, 1137, 1079, 1022, 956, 936, 890, 839, 804, 669, 574, 545; **HRMS** calcd. for ($C_{14}H_{20}NaO_6S^{13}C$) $[M+Na]^+$: 352.0906 found 352.0909.

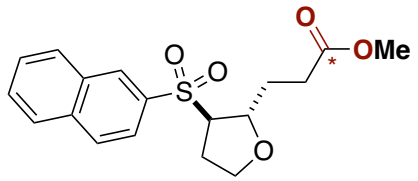

Methyl 3-((2*S,3*R**)-3-(naphthalen-2-ylsulfonyl)tetrahydrofuran-2-yl)propanoate-1-^{13}C (23g)**.

Following **GP1**, sodium naphthalene-2-sulfinate **20g** (42.8 mg, 0.20 mmol) 2,3-dihydrofuran **22a** (45.4 µL, 0.60 mmol) and 2-(trimethylsilyl)ethyl acrylate (54 µL, 0.30 mmol) afforded the product after flash column chromatography on silica gel (pentane/EtOAc 2:1) as a white solid (on average: 25.0 mg, 36% yield). **^{1}H NMR (500 MHz, $CDCl_3$):** δ (ppm) δ 8.51 (d, *J* = 1.8 Hz, 1H), 8.03 (dd, *J* = 8.3, 5.4 Hz, 2H), 7.95 (dd, *J* = 8.2, 1.4 Hz, 1H), 7.87 (dd, *J* = 8.7, 1.9 Hz, 1H), 7.73 – 7.61 (m, 2H), 4.37 (ddd, *J* = 8.6, 6.0, 4.2 Hz, 1H), 3.89 (ddd, *J* = 8.7, 7.4, 4.4 Hz, 1H), 3.79 (td, *J* = 8.4, 6.9 Hz, 1H), 3.62 (d, *J* = 3.9 Hz, 3H), 3.48 (ddd, *J* = 9.8, 6.0, 4.9 Hz, 1H), 2.52 – 2.30 (m, 3H), 2.14 (ddt, *J* = 13.4, 9.7, 7.7 Hz, 1H), 1.95 – 1.71 (m, 2H). **^{13}C NMR (126 MHz, $CDCl_3$)** 173.5, 135.6, 135.2, 132.3,

130.8, 129.9, 129.7, 129.6, 128.2, 128.0, 123.1, 68.4 , 67.4, 51.7 (d, J = 2.7 Hz), 30.7, 30.4 (d, J = 1.5 Hz), 30.1, 28.9. δ (ppm). **IR (neat, cm^{-1}):** 2945, 1680, 1435, 1300, 1225, 1131, 1107, 1065, 820, 760; **HRMS** calcd. for ($C_{17}H_{20}NaO_5S^{13}C$) $[M+Na]^+$: 372.0957 found 372.0961. **MP** = 107°C.

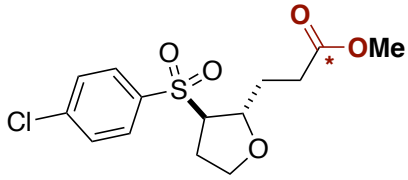

Methyl 3-((2*S,3*R**)-3-((4-chlorophenyl)sulfonyl)tetrahydrofuran-2-yl)propanoate-1-^{13}C (23h)**. Following **GP1**, sodium 4-chlorobenzenesulfinate **20h** (39.7 mg, 0.20 mmol) 2,3-dihydrofuran **22a** (45.4 µL, 0.60 mmol) and 2-(trimethylsilyl)ethyl acrylate (54 µL, 0.30 mmol) afforded the product after flash column chromatography on silica gel (pentane/EtOAc 2:1) as a white solid (on average: 33.5 mg, 50% yield). **^{1}H NMR (500 MHz, $CDCl_3$):** δ (ppm) = 7.89 – 7.81 (m, 2H), 7.61 – 7.52 (m, 2H), 4.28 (ddd, J = 8.8, 5.9, 4.1 Hz, 1H), 3.88 (ddd, J = 8.8, 7.4, 4.4 Hz, 1H), 3.75 (td, J = 8.4, 7.0 Hz, 1H), 3.66 (d, J = 3.9 Hz, 3H), 3.38 (ddd, J = 9.7, 6.0, 4.9 Hz, 1H), 2.49 – 2.37 (m, 2H), 2.37 – 2.29 (m, 1H), 2.14 (ddt, J = 13.4, 9.8, 7.7 Hz, 1H), 1.90 – 1.72 (m, 2H); **^{13}C NMR (126 MHz, $CDCl_3$)** δ (ppm) = 173.41, 141.06, 136.83, 130.24, 129.94, 77.90 (d, J = 3.6 Hz), 68.49, 67.27, 51.80 (d, J = 2.8 Hz), 30.31 (d, J = 58.1 Hz), 30.22 (d, J = 1.4 Hz), 28.78. **IR (neat, cm^{-1}):** 3093, 2951, 1687, 1581, 1354, 1302, 1281, 1202, 1145, 1078, 1029, 954, 907, 842, 762, 622, 553, 474; **HRMS** calcd. for ($C_{13}H_{17}ClNaO_5S^{13}C$) $[M+Na]^+$: 356.0411 found 356.0423. **MP** = 114°C.

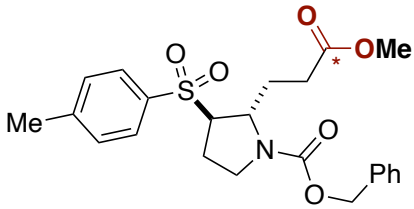

Benzyl 2-(3-methoxy-3-oxopropyl)-3-tosylpyrrolidine-1-carboxylate-^{13}C (23i). Following **GP1**, sodium benzenesulfinate **20d** (35.6 mg, 0.20 mmol) benzyl 2,3-dihydro-1*H*-pyrrole-1-carboxylate **22i** (81 µL, 0.60 mmol) and 2-(trimethylsilyl)ethyl acrylate (54 µL, 0.30 mmol) afforded the product after flash column chromatography on silica gel (pentane/EtOAc 2:1) as a colorless oil. (on average: 45 mg, 51% yield). **^{1}H NMR (500 MHz, $CDCl_3$) (253 K):** δ (ppm) δ 7.77 (d, *J* = 8.0 Hz, 2H), 7.65 (d, *J* = 7.9 Hz, 2H), 7.44 – 7.29 (m, 12H), 7.19 (d, *J* = 7.9 Hz, 2H), 5.16 (d, *J* = 12.2 Hz, 1H), 5.11 – 4.95 (m, 3H), 4.45

(dt, *J* = 7.4, 3.7 Hz, 1H), 4.40 (t, *J* = 6.9 Hz, 1H), 3.59 (d, *J* = 3.8 Hz, 3H), 3.57 (d, *J* = 3.9 Hz, 3H), 3.48 – 3.25 (m, 6H), 2.60 – 2.50 (m, 1H), 2.41 (d, *J* = 2.8 Hz, 6H), 2.36 – 2.12 (m, 5H), 1.99 – 1.65 (m, 4H).; **^{13}C NMR (126 MHz, $CDCl_3$)** δ (ppm) 173.4, 173.2, 154.7, 154.3, 145.5, 145.5, 136.2, 136.2, 133.6, 133.4, 130.2, 130.1, 128.8, 128.7, 128.6, 128.5, 128.5, 128.3, 128.2, 128.1, 127.8, 68.3, 67.3, 67.3, 67.0, 58.1, 58.0, 57.0, 57.0, 52.1, 52.0, 51.9, 44.9, 44.8, 30.5, 30.3, 30.0, 29.9, 29.8, 29.4, 24.7, 24.4, 21.9, 21.8. **IR (neat, cm^{-1}):** 2950, 1690, 1600, 1420, 1380, 1295, 1118, 10045, 906, 847, 733; **HRMS** calcd. for ($C_{22}H_{27}NO_6S^{13}C$) $[M+Na]^+$:469.1485, found 469.1491.

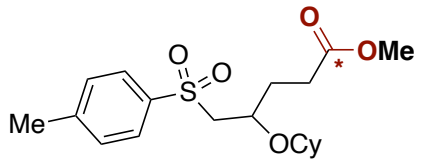

Methyl 4-(cyclohexyloxy)-5-tosylpentanoate-1-^{13}C (23j). Following **GP1**, sodium 4-methylbenzenesulfinate **20d** (35.6 mg, 0.20 mmol), (vinyloxy)cyclohexane **22j** (82 µL, 0.60 mmol) and 2-(trimethylsilyl)ethyl acrylate (54 µL, 0.30 mmol) afforded the product after flash column chromatography on silica gel (pentane/EtOAc 6:1) as a pale-yellow oil (on average: 22.8 mg, 31% yield). **^{1}H NMR (400 MHz, $CDCl_3$):** δ (ppm) = 7.8 (d, *J* = 8.1 Hz, 2H), 7.4 (d, *J* = 7.9 Hz, 2H), 4.0 – 3.9 (m, 1H), 3.7 (d, *J* = 3.8 Hz, 3H), 3.3 (dd, *J* = 14.4, 4.0 Hz, 1H), 3.2 – 3.1 (m, 2H), 2.5 (s, 3H), 2.4 – 2.4 (m, 2H), 2.1 – 2.0 (m, 1H), 1.8 (dtt, *J* = 14.5, 7.4, 3.8 Hz, 1H), 1.8 – 1.6 (m, 3H), 1.3 – 1.2 (m, 3H), 1.2 – 1.0 (m, 4H); **^{13}C NMR (101 MHz, $CDCl_3$)** δ (ppm) = 173.6, 144.9, 137.3, 130.0, 128.1, 69.8 (d, *J* = 3.7 Hz), 61.4, 51.8 (d, *J* = 2.6 Hz), 32.6 (d, *J* = 79.9 Hz), 30.8, 29.8 (d, *J* = 58.2 Hz), 25.7, 24.3 (d, *J* = 10.7 Hz), 21.8. **IR (neat, cm^{-1}):** 2929, 2856, 1693, 1597, 1449, 1302, 1142, 1071, 816, 666, 562; **HRMS** calcd. for ($C_{18}H_{28}NaO_5S^{13}C$) $[M+Na]^+$: 392.1583 found 392.1588.

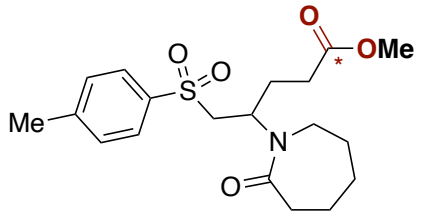

Methyl 4-(2-oxoazepan-1-yl)-5-tosylpentanoate-^{13}C (23k). Following **GP1**, sodium benzenesulfinate **20d** (35.6 mg, 0.20 mmol) 1-vinylazepan-2-one **22k** (81.2 µL, 0.60 mmol) and 2-(trimethylsilyl)ethyl acrylate (54 µL, 0.30 mmol) afforded the product after flash column chromatography on silica gel (pentane/EtOAc 2:1) as a colorless oil (on average: 37.3 mg, 60% yield). **^{1}H NMR (500 MHz, $CDCl_3$):** δ (ppm) 7.83 – 7.76 (m, 2H), 7.41 – 7.30 (m, 2H), 4.82 – 4.35 (m, 1H), 3.64 (d, *J* = 3.9 Hz, 3H), 3.34 – 3.17 (m, 2H), 3.08

(dd, *J* = 14.7, 4.0 Hz, 1H), 2.44 (s, 3H), 2.42 – 2.35 (m, 3H), 2.34 – 2.20 (m, 2H), 2.15 – 1.97 (m, 1H), 1.93 – 1.81 (m, 1H), 1.78 – 1.56 (m, 6H).**^{13}C NMR (126 MHz, $CDCl_3$)** δ (ppm) 176.7, 173.1, 144.9, 136.5, 130.0, 128.3, 57.9, 51.9 (d, *J* = 2.7 Hz), 38.0, 31.2, 30.6, 30.0, 28.8, 28.1, 23.2, 21.8. **IR (neat, cm^{-1}):** 2925, 1697, 1622, 1435, 1356, 1128, 1058; **HRMS** calcd. for ($C_{18}H_{27}NaO_5S^{13}C$) $[M+Na]^+$: 405.1536 found 405.1546.

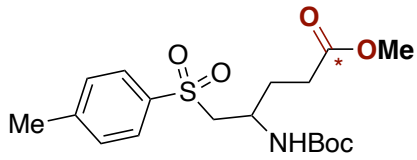

Methyl 4-((*tert*-butoxycarbonyl)amino)-5-tosylpentanoate-^{13}C (23l). Following **GP1**, sodium benzenesulfinate **20d** (35.6 mg, 0.20 mmol) *tert*-butyl vinylcarbamate **22l** (85.9 mg, 0.60 mmol) and 2-(trimethylsilyl)ethyl acrylate (54 µL, 0.30 mmol) afforded the product after flash column chromatography on silica gel (pentane/EtOAc 2:1) as a white solid (on average: 34.0 mg, 44% yield). **^{1}H NMR (500 MHz, $CDCl_3$):** δ (ppm) =δ 7.99 – 7.63 (m, 2H), 7.46 – 7.30 (m, 2H), 4.96 (s, 1H), 4.04 – 3.87 (m, 1H), 3.66 (d, *J* = 3.8 Hz, 3H), 3.49 – 3.39 (m, 1H), 3.24 (dd, *J* = 14.5, 4.7 Hz, 1H), 2.44 (s, 3H), 2.38 (q, *J* = 7.3 Hz, 2H), 2.04 (s, 2H), 1.40 (s, 9H).**^{13}C NMR (126 MHz, $CDCl_3$)** δ (ppm) 175.5, 173.5, 145.0, 137.1, 130.2, 128.0, 59.6, 51.9, 51.9, 47.01, 30.9, 30.4, 29.4, 28.4, 21. 8. **IR (neat, cm^{-1}):** 3450, 2975, 1685, 1501, 1386, 1224, 1122, 1055, 874, 760; **HRMS** calcd. for ($C_{17}H_{27}NaO_5S^{13}C$) $[M+Na]^+$: 409.1485 found 409.1482. **MP** = 131°C.

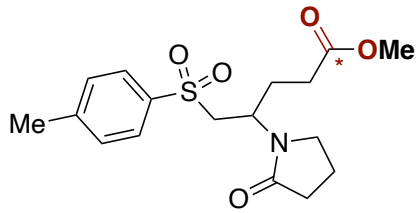

Methyl 4-(2-oxopyrrolidin-1-yl)-5-tosylpentanoate-^{13}C (23m).
Following **GP1**, sodium benzenesulfinate **20d** (35.6 mg, 0.20 mmol) 1-vinylpyrrolidin-2-one **22m** (64.1 µL, 0.60 mmol) and 2-(trimethylsilyl)ethyl acrylate (54 µL, 0.30 mmol) afforded the product after flash column chromatography on silica gel (pentane/EtOAc 2:1) a white solid (on average: 37.3 mg, 60% yield). **^{1}H NMR (500 MHz, $CDCl_3$):** δ (ppm) 7.83 – 7.70 (m, 2H), 7.40 – 7.32 (m, 2H), 4.28 (tdd, *J* = 10.4, 4.6, 3.3 Hz, 1H), 3.70 (dd, *J* = 14.7, 10.2 Hz, 1H), 3.63 (d, *J* = 3.9 Hz, 3H), 3.39 – 3.21 (m, 2H), 3.07 (dd, *J* = 14.7, 3.3 Hz, 1H), 2.43 (s, 3H), 2.35 – 2.13 (m, 4H), 2.03 (ddddd, *J* = 14.2, 10.7, 8.3, 6.0, 4.6 Hz, 1H), 1.93 – 1.75 (m, 3H). **^{13}C NMR (126 MHz, $CDCl_3$)** δ (ppm) 175.7, 172.9, 145.1, 136.2, 130.00, 128.3, 56.4, 51.9 (d, *J* = 2.8 Hz), 47.7 (d, *J* = 4.0 Hz), 44.7, 31.4, 30.8, 30.2, 27.5,

21.8, 18.3. **IR (neat, cm^{-1}):** 2935, 1675, 1433, 1383, 1256, 1146, 1108, 1095, 835, 780; **HRMS** calcd. for ($C_{16}H_{23}NaO_5S^{13}C$) $[M+Na]^+$: 377.1223 found 377.1227. **MP** = 94°C.

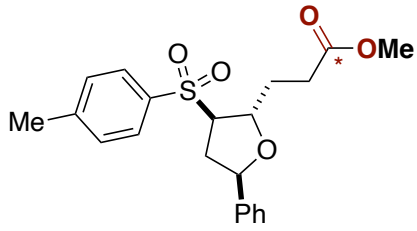

Methyl 3-((2*S,3*R**,5*R**)-5-phenyl-3-tosyltetrahydrofuran-2-yl)propanoate-^{13}C (23n)**. Following **GP1**, sodium benzenesulfinate **20d** (35.6 mg, 0.20 mmol), 2-phenyl-2,3-dihydrofuran **22n** (87.7 mg, 0.60 mmol) and 2-(trimethylsilyl)ethyl acrylate (54 µL, 0.30 mmol) afforded the product after flash column chromatography on silica gel (pentane/EtOAc 2:1) as a colorless oil (on average: 31.0 mg, 40% yield). **^{1}H NMR (500 MHz, $CDCl_3$):** δ (ppm) =δ 7.81 – 7.74 (m, 2H), 7.39 – 7.23 (m, 7H), 4.89 (dd, *J* = 10.2, 5.4 Hz, 1H), 4.66 (ddd, *J* = 9.6, 5.8, 4.0 Hz, 1H), 3.63 (d, *J* = 3.9 Hz, 3H), 3.62 – 3.57 (m, 1H), 2.59 – 2.47 (m, 2H), 2.45 (s, 3H), 2.43 – 2.38 (m, 1H), 2.30 (dt, *J* = 12.9, 9.9 Hz, 1H), 2.06 – 1.84 (m, 2H). **^{13}C NMR (126 MHz, $CDCl_3$)** δ (ppm) 173.6, 145.3, 140.0, 135.2, 130.2, 128.8, 128.6, 128.2, 126.2, 79.6, 77.9 (d, *J* = 3.8 Hz), 69.7, 51.8 (d, *J* = 2.8 Hz), 37.6, 31.0, 30.8 (d, *J* = 1.6 Hz), 21.8. **IR (neat, cm^{-1}):** 2943, 1685, 1420, 1295, 1125, 1028, 822, 702; **HRMS** calcd. for ($C_{20}H_{24}NaO_5S^{13}C$) $[M+Na]^+$: 412.1270 found 412.1274.

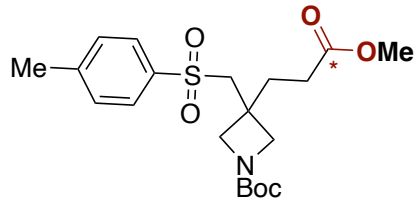

***Tert*-butyl 3-(3-methoxy-3-oxopropyl)-3-(tosylmethyl)azetidine-1-carboxylate-^{13}C (23o)**.

Following **GP1**, sodium 4-methylbenzenesulfinate **20d** (35.6 mg, 0.20 mmol), *tert*-butyl 3-methyleneazetidine-1-carboxylate **22o** (101.5 mg, 0.60 mmol) and 2-(trimethylsilyl)ethyl acrylate (54 µL, 0.30 mmol) afforded the product after flash column chromatography on silica gel (pentane/EtOAc 2:1) as a white solid (on average: 35.0 mg, 43% yield). **^{1}H NMR (500 MHz, $CDCl_3$):** δ (ppm) δ 7.80 – 7.76 (m, 2H), 7.40 – 7.33 (m, 2H), 3.77 (m, 4H), 3.67 (d, *J* = 3.9 Hz, 3H), 3.37 (s, 2H), 2.45 (s, 3H), 2.43 – 2.27 (m, 4H), 1.41 (s, 9H).**^{13}C NMR (126 MHz, $CDCl_3$)** δ (ppm) 173.2, 156.2, 145.3, 137.7, 130.3, 127.8, 80.0, 60.8, 59.1, 52.0 (d, *J* = 2.8 Hz), 35.4 (d, *J* = 4.6 Hz), 31.4 (d, *J* = 1.4 Hz), 29.7, 29.2, 28.4, 21.8. **IR (neat, cm^{-1}):** 2975, 2924, 1685, 1421, 1301, 1126, 1081, 780; **HRMS** calcd.

for ($C_{19}H_{29}NaO_5S^{13}C$) $[M+Na-CH_3]^+$: 435.1647 found 435.1648. **MP** = 124°C.

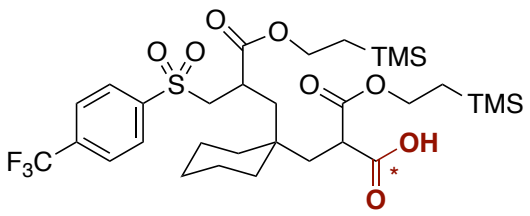

(R*)-3-oxo-2-((1-((R*)-3-oxo-2-(((4-(trifluoromethyl)phenyl)sulfonyl)methyl)-3-(2-(trimethylsilyl)ethoxy)propyl)cyclohexyl)methyl)-3-(2-(trimethylsilyl)ethoxy)propanoic acid-^{13}C (28a).

Following **GP2** but without methylation, sodium 4-(trifluoromethyl)benzenesulfinate **20e** (92.8 mg, 0.40 mmol), methylenecyclohexane **22a'** (72 µL, 0.60 mmol) and 2-(trimethylsilyl)ethyl acrylate (72 µL, 0.40 mmol) afforded the tittle compound after column chromatography on silica gel (pentane to pentane/EtOAc 8:1) as a colorless oil (on average: 60.0 mg, 42% yield, dr = 1.4:1). **^{1}H NMR (500 MHz, $CDCl_3$):** δ (ppm) δ 8.12 – 8.03 (m, 2H), 7.90 – 7.80 (m, 2H), 4.22 – 4.15 (m, 2H), 4.10 – 4.00 (m, 2H), 3.70 (t, *J* = 3.9 Hz, 3H), 3.61 (dd, *J* = 14.2, 9.9 Hz, 1H), 3.28 (dt, *J* = 8.1, 5.9 Hz, 1H), 3.15 (dt, *J* = 14.3, 3.2 Hz, 1H), 2.90 (dp, *J* = 12.4, 3.9 Hz, 1H), 2.05 – 1.94 (m, 2H), 1.88 – 1.79 (m, 1H), 1.46 – 1.29 (m, 6H), 1.18 (d, *J* = 6.0 Hz, 3H), 1.04 – 0.92 (m, 4H), 0.08 – 0.00 (m, 18H).**^{13}C NMR (126 MHz, $CDCl_3$)** δ (ppm) 174.4, 174.1, 170.9, 170.5, 142.7, 135.7(q, *J* = 33.0 Hz), 129.2, 126.5 (m), 123.3 (q, *J* = 273.0 Hz)., 64.3, 64.2, 64.1, 59.6 (d, *J* = 5.5 Hz), 52.8, 52.8, 52.7, 47.7, 47.7, 47.1, 36.3 (d, *J* = 2.0 Hz)., 35.8, 35.8, 35.3, 34.9, 25.9, 21.5, 21.4, 17.3, 17.3, 17.2, -1.4, -1.4. **IR (neat, cm^{-1}):** 2975, 1735, 1699, 1423, 1286, 1231, 1131, 1082, 831, 750; **HRMS** calcd. for ($C_{31}H_{51}F_3NaO_8SSi_2^{13}C$) $[M+Na]^+$: 732.2721 found 732.2716.

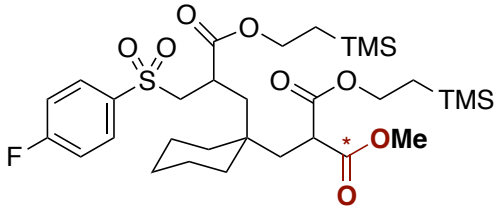

1-methyl 3-(2-(trimethylsilyl)ethyl) 2-((1-(3-oxo-2-((phenylsulfonyl)methyl)-3-(2-(trimethylsilyl)ethoxy)propyl)cyclohexyl)methyl)malonate-1-^{13}*C* (28b).

Following **GP2**, sodium 4-fluorobenzenesulfinate **20b** (72.9 mg, 0.40 mmol), methylenecyclohexane **22a'** (72 µL, 0.60 mmol) and 2-(trimethylsilyl)ethyl acrylate (72 µL, 0.40 mmol) afforded the tittle compound after column chromatophraphy on silica gel (pentane/EtOAc 9:1) as a pale-yellow oil (on average: 84.3 mg, 64% yield, dr = 4.2:1). **^{1}H NMR (400 MHz, $CDCl_3$):** δ (ppm) = 7.98 – 7.89 (m, 2H), 7.28 – 7.17 (m, 2H), 4.25 –

4.15 (m, 2H), 4.15 – 3.96 (m, 2H), 3.71 (dd, *J* = 11.7, 3.9 Hz, 3H), 3.62 – 3.44 (m, 1H), 3.33 – 3.22 (m, 1H), 3.14 – 3.05 (m, 1H), 2.86 (dh, *J* = 13.5, 3.6 Hz, 1H), 2.06 – 1.89 (m, 2H), 1.81 (ddd, *J* = 14.9, 8.2, 2.0 Hz, 1H), 1.67 (dt, *J* = 9.3, 5.7 Hz, 1H), 1.47 – 1.29 (m, 7H), 1.17 (d, *J* = 5.9 Hz, 3H), 0.97 (dtt, *J* = 11.1, 7.3, 3.0 Hz, 4H), 0.08 – -0.02 (m, 18H); **^{19}F NMR (377 MHz, $CDCl_3$):** δ (ppm) = -103.2, -103.9.; **^{13}C NMR (126 MHz, $CDCl_3$)** δ (ppm) = 170.8, 170.5, 135.3 – 135.1 (m), 131.4 (d, *J* = 9.7 Hz), 130.6 (d, *J* = 9.5 Hz), 116.6 (d, *J* = 22.6 Hz), 64.3, 64.2, 64.2, 64.0, 59.8, 59.8, 52.8, 52.7 (d, *J* = 2.8 Hz), 52.7 (d, *J* = 2.9 Hz), 48.2 (d, *J* = 57.1 Hz), 47.4 (dd, *J* = 57.1, 2.8 Hz), 36.2 (d, *J* = 2.0 Hz), 35.9, 35.8, 35.3, 34.9, 34.9, 25.9, 21.4, 17.3, 17.3, 17.2, -1.4. **IR (neat, cm^{-1}):** 2964, 2852, 1729, 1694, 1411, 1251, 1139, 1018, 906, 882, 724; **HRMS** calcd. for ($C_{30}H_{51}FNaO_8SSi_2{}^{13}C$) $[M+Na]^+$: 682.2753 found 682.2782.

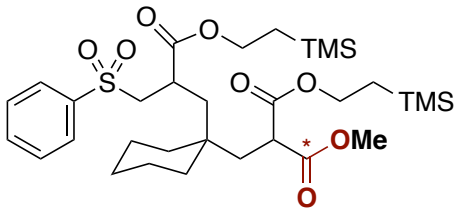

1-methyl 3-(2-(trimethylsilyl)ethyl) 2-((1-(3-oxo-2-((phenylsulfonyl)methyl)-3-(2-(trimethylsilyl)ethoxy)propyl)cyclohexyl)methyl)malonate-1-^{13}C (28c). Following **GP2**, sodium benzenesulfinate **20a** (65.7 mg, 0.40 mmol), methylenecyclohexane (72 µL, 0.60 mmol) and 2-(trimethylsilyl)ethyl acrylate (72 µL, 0.40 mmol) afforded the tittle compound after column chromatophraphy on silica gel (pentane/EtOAc 9:1) as a pale-yellow oil (on average: 70.6 mg, 55% yield, dr = 6.3:1). **^{1}H NMR (400 MHz, $CDCl_3$):** δ (ppm) = 8.0 – 7.9 (m, 2H), 7.7 – 7.6 (m, 1H), 7.6 – 7.5 (m, 2H), 4.2 (tt, *J* = 8.8, 2.1 Hz, 2H), 4.1 – 3.9 (m, 3H), 3.8 – 3.7 (m, 3H), 3.6 (ddd, *J* = 14.2, 9.7, 1.9 Hz, 1H), 3.4 – 3.2 (m, 1H), 3.1 (dt, *J* = 14.4, 2.4 Hz, 1H), 2.9 (dt, *J* = 13.3, 6.5 Hz, 1H), 2.0 – 1.9 (m, 3H), 1.8 (ddd, *J* = 14.8, 8.3, 2.3 Hz, 1H), 1.4 – 1.3 (m, 5H), 1.3 – 1.2 (m, 2H), 1.2 – 1.1 (m, 3H), 1.0 – 0.9 (m, 3H), 0.1 – 0.0 (m, 18H); **^{13}C NMR (126 MHz, $CDCl_3$)** δ (ppm) = 170.8, 170.5, 169.5, 168.9 (d, *J* = 8.8 Hz), 139.2 (d, *J* = 1.6 Hz), 133.9, 129.3, 128.4, 64.2, 64.1, 63.9, 60.5, 59.6 (d, *J* = 4.6 Hz), 52.7 (d, *J* = 2.7 Hz), 52.7 (d, *J* = 2.8 Hz), 47.7 (d, *J* = 2.9 Hz), 47.1 (d, *J* = 2.9 Hz), 36.2 (d, *J* = 2.0 Hz), 35.8, 35.8, 35.2, 34.8 (d, *J* = 2.5 Hz), 25.9, 21.4, 17.3 (d, *J* = 2.2 Hz), 17.1, 14.3, -1.4, -1.4; **IR (neat, cm^{-1}):** 2966, 2855, 1731, 1689, 1408, 1260, 1140, 1021, 910, 882, 726; **HRMS** calcd. for ($C_{30}H_{52}NaO_8SSi_2{}^{13}C$) $[M+Na]^+$: 664.2847 found 664.2761.

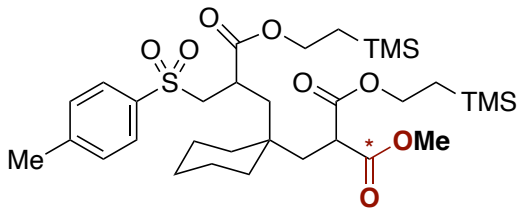

1-methyl 3-(2-(trimethylsilyl)ethyl) 2-((1-(3-oxo-2-(tosylmethyl)-3-(2-(trimethylsilyl)ethoxy)propyl)cyclohexyl)methyl)malonate-1-^{13}C (28d). Following **GP2**, sodium 4-methylbenzenesulfinate **20d** (71.2 mg, 0.40 mmol), methylenecyclohexane **22a'** (72 µL, 0.60 mmol) and 2-(trimethylsilyl)ethyl acrylate (72 µL, 0.40 mmol) afforded the tittle compound after column chromatophraphy on silica gel (pentane/EtOAc 9:1) as a pale-yellow oil (on average: 73.5 mg, 56% yield, dr = 1.6:1). **^{1}H NMR (400 MHz, $CDCl_3$):** δ (ppm) = 7.8 (dd, *J* = 8.1, 5.9 Hz, 2H), 7.4 – 7.3 (m, 2H), 4.2 – 4.2 (m, 2H), 4.1 – 4.0 (m, 2H), 3.7 – 3.7 (m, 3H), 3.6 – 3.5 (m, 1H), 3.3 (dq, *J* = 8.4, 5.8 Hz, 1H), 3.1 – 3.0 (m, 1H), 2.9 (dh, *J* = 13.1, 3.6 Hz, 1H), 2.4 (s, 3H), 2.0 – 1.9 (m, 1H), 1.4 – 1.1 (m, 12H), 1.0 – 0.9 (m, 4H), 0.9 (t, *J* = 7.0 Hz, 1H), 0.1 – 0.0 (m, 18H); **^{13}C NMR (101 MHz, $CDCl_3$)** δ (ppm) = 170.9, 170.6 (d, *J* = 1.6 Hz), 169.5, 169.0 (d, *J* = 8.7 Hz), 144.9, 136.3, 130.0, 128.4, 127.7, 64.2, 64.1, 63.8, 59.7, 59.7, 52.7 (d, *J* = 2.7 Hz), 52.7 (d, *J* = 2.8 Hz), 47.8 (d, *J* = 3.0 Hz), 47.2 (d, *J* = 3.2 Hz), 39.8, 36.3 (d, *J* = 2.0 Hz), 35.8, 35.2, 34.8 (d, *J* = 3.0 Hz), 25.9, 21.8, 21.7 – 21.2 (m), 17.3, 17.3, 17.2, 14.2, -1.4, -1.4; **IR (neat, cm^{-1}):** 2962, 1722, 1692, 1409, 1256, 1138, 1018, 932, 856, 741; **HRMS** calcd. for ($C_{31}H_{54}NaO_8SSi_2{}^{13}C$) $[M+Na]^+$: 678.3004 found 678.2942.

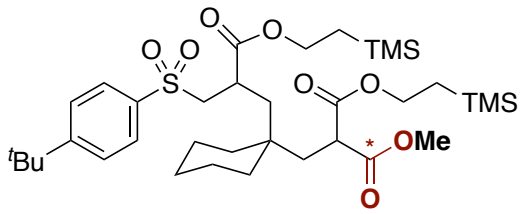

1-methyl 3-(2-(trimethylsilyl)ethyl) 2-((1-(2-(((4-(tert-butyl)phenyl)sulfonyl)methyl)-3-oxo-3-(2-(trimethylsilyl)ethoxy)propyl)cyclohexyl)methyl)malonate-1-^{13}C (28e). Following **GP3**, sodium 4-(tert-butyl)benzenesulfinate **20e'** (88.1 mg, 0.40 mmol), methylenecyclohexane **22a'** (72 µL, 0.60 mmol) and 2-(trimethylsilyl)ethyl acrylate (72 µL, 0.40 mmol) afforded the tittle compound after flash column chromatophraphy on silica gel (pentane/EtOAc 9:1) as a viscous colorless oil (on average: 49.2 mg, 35% yield, dr = 1.6:1). **^{1}H NMR (500 MHz, $CDCl_3$):** δ (ppm) = 7.85 – 7.80 (m, 2H), 7.58 – 7.53 (m, 2H), 4.23 – 4.15 (m, 2H), 4.14 – 4.02 (m, 2H), 3.70 (dd, J = 3.9, 1.5 Hz, 3H), 3.59 – 3.50 (m,

1H), 3.33 (dq, J = 8.4, 5.9 Hz, 1H), 3.07 (ddd, J = 14.2, 3.7, 2.2 Hz, 1H), 2.95 – 2.87 (m, 1H), 2.01 – 1.94 (m, J = 4.2 Hz, 2H), 1.78 (ddd, J = 14.8, 8.1, 3.3 Hz, 1H), 1.34 (s, 16H), 1.21 – 1.10 (m, 4H), 1.03 – 0.95 (m, 4H), 0.05 – 0.02 (m, 18H); **^{13}C NMR (126 MHz, $CDCl_3$)** δ (ppm) = 174.32, 170.90, 170.59, 170.54, 157.90, 136.27, 128.20, 126.36, 64.20, 64.12, 63.79, 59.67, 59.62, 52.74 (d, *J* = 2.8 Hz), 52.66 (d, *J* = 2.8 Hz), 47.47 (d, *J* = 57.1 Hz), 47.44 (d, *J* = 57.0 Hz), 36.25, 36.23, 35.70, 35.39, 35.10, 34.80, 34.78, 31.18, 25.89, 21.45 (d, *J* = 1.7 Hz), 21.42, 17.29, 17.26, 17.19, -1.37, -1.41, -1.43. **IR (neat, cm^{-1}):** 2953, 1733, 1700, 1322, 1249, 1155, 1108, 1085, 934, 835, 760; **HRMS** calcd. for ($C_{34}H_{60}NaO_8SSi_2{}^{13}C$) $[M+Na]^+$: 720.3473 found 720.3474.

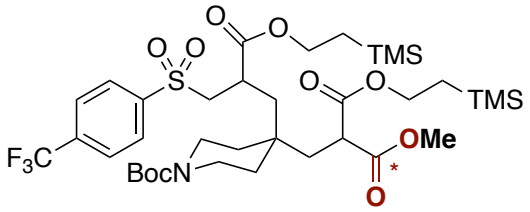

1-methyl 3-(2-(trimethylsilyl)ethyl) (R*)-2-((1-(tert-butoxycarbonyl)-4-((R*)-3-oxo-2-(((4-(trifluoromethyl)phenyl)sulfonyl)methyl)-3-(2-(trimethylsilyl)ethoxy)propyl)piperidin-4-yl)methyl)malonate-^{13}C (28f).

Following **GP2**, sodium 4-(trifluoromethyl)benzenesulfinate **20e** (93 mg, 0.40 mmol), *tert*-butyl 4-methyl enepiperidine-1-carboxylate **22f'** (118 mg, 0.60 mmol) and 2-(trimethylsilyl)ethyl acrylate (80 µL, 0.40 mmol) afforded the tittle compound after flash column chromatophraphy on silica gel (pentane to pentane/EtOAc 8:2) as a colorless oil (on average: 39.0 mg, 41% yield, dr = 1:1). **^{1}H NMR (500 MHz, $CDCl_3$):** δ (ppm) 8.07 (d, *J* = 8.0 Hz, 2H), 7.84 (d, *J* = 8.0 Hz, 2H), 4.20 (dd, *J* = 9.9, 7.4 Hz, 2H), 4.11 – 3.99 (m, 2H), 3.72 (dd, *J* = 4.0, 2.5 Hz, 3H), 3.56 (dd, *J* = 14.2, 9.1 Hz, 1H), 3.40 – 3.26 (m, 4H), 3.21 – 3.09 (m, 1H), 3.04 – 2.89 (m, 1H), 2.07 (d, *J* = 5.5 Hz, 2H), 1.94 (dd, *J* = 14.9, 8.9 Hz, 1H), 1.43 (s, 9H), 1.27 (d, *J* = 15.9 Hz, 5H), 1.02 – 0.92 (m, 4H), 0.90 – 0.81 (m, 1H), 0.04 (d, *J* = 1.6 Hz, 18H).**^{13}C NMR (126 MHz, $CDCl_3$)** δ (ppm) 170.6, 170.2, 168.8, 168.7, 154.8, 142.6, 135.8 (q, *J* = 33.1 Hz), 129.1 (q, *J* = 2.7 Hz), 126.6 (m), 123.2 (q, *J* = 273.0 Hz), 79.7, 64.6, 64.5, 64.4, 59.5, 59.4, 59.4, 53.0 (d, *J* = 2.8 Hz), 52.9 (d, *J* = 2.9 Hz), 47.5, 47.4, 47.1, 47.0, 39.1, 39.0, 35.7, 35.6, 35.0 (d, *J* = 2.2 Hz), 34.2, 34.0, 33.9, 29.8, 28.6, 17.3, 17.2, -1.4, -1.5. **IR (neat, cm^{-1}):** 2951, 1712, 1685, 1322, 11476, 1051, 835, 720; **HRMS** calcd. for ($C_{14}H_{20}NaO_5S^{13}C$) $[M+Na]^+$: 336.0957 found 336.0962.

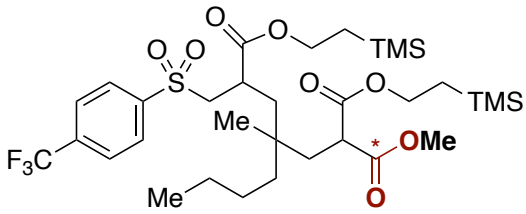

1-methyl 1,5-bis(2-(trimethylsilyl)ethyl) 3-butyl-3-methyl-6-((4-(trifluoromethyl)phenyl)sulfonyl)hexane-1,1,5-tricarboxylate-1-^{13}C (28g). Following **GP2**, sodium 4-(trifluoromethyl)benzenesulfinate **20e** (92.9 mg, 0.40 mmol), 2-methylhex-1-ene **22g'** (84.5 µL, 0.40 mmol) and 2-(trimethylsilyl)ethyl acrylate (72 µL, 0.40 mmol) afforded the tittle compound after flash column chromatophraphy on silica gel (pentane/EtOAc 10:1) as a pale yellow oil (on average: 51.0 mg, 36% yield, dr = 1:1.4:1:1.2). **^{1}H NMR (500 MHz, $CDCl_3$):** δ (ppm) = 8.06 (d, *J* = 8.1 Hz, 2H), 7.84 (d, *J* = 8.2 Hz, 2H), 4.23 – 4.14 (m, 2H), 4.10 – 3.99 (m, 2H), 3.70 (dd, *J* = 3.9, 2.1 Hz, 3H), 3.66 – 3.59 (m, 1H), 3.28 (qd, *J* = 6.2, 3.1 Hz, 1H), 3.09 (dd, *J* = 14.3, 3.3 Hz, 1H), 2.91 – 2.81 (m, 1H), 1.96 – 1.82 (m, 2H), 1.78 – 1.68 (m, 1H), 1.38 – 1.26 (m, 2H), 1.21 – 1.11 (m, 5H), 1.00 – 0.95 (m, 4H), 0.84 (q, *J* = 7.1 Hz, 3H), 0.76 (dd, *J* = 7.3, 2.6 Hz, 3H), 0.04 – 0.02 (m, 18H).; **^{19}F NMR (376 MHz, $CDCl_3$)** δ (ppm) = -63.2. **^{13}C NMR (126 MHz, $CDCl_3$)** δ (ppm) = 170.69, 170.68, 170.52, 170.49, 169.50, 169.47, 169.32, 169.31, 142.59, 135.74 (q, J = 33.1 Hz), 129.14, 126.52, 126.51 (d, J = 10.6 Hz), 126.49, 64.27, 64.23, 64.05, 59.61, 52.73, 48.04, 47.59, 42.10, 41.94, 38.63, 38.35, 37.61, 36.31, 36.25, 36.22, 29.82, 25.65, 25.56, 23.97, 23.93, 23.43, 23.41, 17.29, 17.23, 14.15, 14.13, -1.44, -1.46, -1.47. **IR (neat, cm^{-1}):** 2955, 1734, 1701, 132, 1250, 1134, 1061, 835; **HRMS** calcd. for ($C_{31}H_{53}F_3NaO_8SSi_2{}^{13}C$) $[M+Na]^+$: 734.2878 found 734.2894.

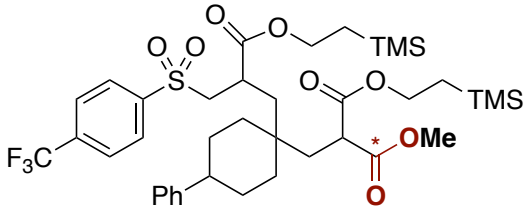

1-methyl 3-(2-(trimethylsilyl)ethyl) 2-((1-(3-oxo-2-(((4-(trifluoromethyl)phenyl)sulfonyl)methyl)-3-(2-(trimethylsilyl)ethoxy)propyl)-4-phenylcyclohexyl)methyl)malonate-1-^{13}C (28h). Following **GP2**, sodium 4-(trifluoromethyl)benzenesulfinate **20e** (92.9 mg, 0.40 mmol), (4-methylenecyclohexyl)benzene **22h'** (64.0 mg, 0.40 mmol) and 2-(trimethylsilyl)ethyl acrylate (72 µL, 0.40 mmol) afforded the tittle compound after flash column

chromatophraphy on silica gel (pentane/EtOAc 15:1) as a pale yellow oil (on average: 79.2 mg, 50% yield, dr = 6.7:5.1:1:1). **^{1}H NMR (400 MHz, $CDCl_3$):** δ (ppm) = 7.80 (d, *J* = 8.1 Hz, 2H), 7.36 (d, *J* = 7.9 Hz, 2H), 4.03 – 3.87 (m, 1H), 3.66 (d, *J* = 3.8 Hz, 3H), 3.31 (dd, *J* = 14.4, 4.0 Hz, 1H), 3.24 – 3.08 (m, 2H), 2.45 (s, 3H), 2.43 – 2.35 (m, 2H), 2.13 – 1.99 (m, 1H), 1.82 (dtt, *J* = 14.5, 7.4, 3.8 Hz, 1H), 1.76 – 1.62 (m, 3H), 1.49 (s, 1H), 1.34 – 1.21 (m, 2H), 1.19 – 1.05 (m, 4H).; **^{19}F NMR (376 MHz, $CDCl_3$)** δ (ppm) = -63.3, -63.3, -63.3. **^{13}C NMR (101 MHz, $CDCl_3$)** δ (ppm) = 170.8, 170.4, 170.4, 168.9, 168.9, 146.8, 146.7, 142.7, 135.56 (q, J = 33.4 Hz), 129.2, 129.2, 129.1, 128.5, 126.9, 126.8, 126.6, 126.5, 126.5, 126.5, 126.2, 124.6, 121.9, 64.5, 64.4, 64.3, 64.2, 64.1, 59.6, 59.5, 57.5, 52.9, 52.8, 52.8, 52.8, 52.8, 49.7, 49.1, 47.9, 47.8, 47.3, 47.3, 44.0, 43.9, 43.6, 43.5, 39.0, 38.4, 35.9, 35.9, 35.9, 35.7, 35.7, 35.6, 35.5, 35.3, 35.3, 34.9, 32.0, 31.4, 31.3, 31.0, 29.8, 29.5, 29.1, 28.9, 22.8, 17.4, 17.3, 17.3, 17.2, 14.2, -1.4, -1.5. **IR (neat, cm^{-1}):** 2954, 1732, 1699, 1404, 1322, 1250, 1135, 1061, 911, 835, 730, 699; **HRMS** calcd. for ($C_{37}H_{55}F_3NaO_8SSi_2{}^{13}C$) $[M+Na]^+$: 808.3034 found 808.3010.

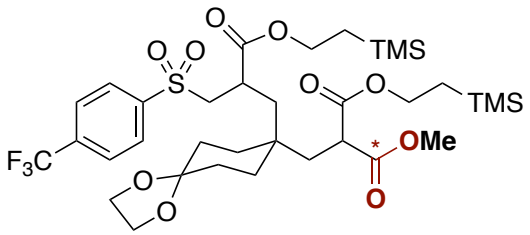

1-methyl 3-(2-(trimethylsilyl)ethyl) 2-((8-(3-oxo-2-(((4-(trifluoromethyl)phenyl)sulfonyl)methyl)-3-(2-(trimethylsilyl)ethoxy)propyl)-1,4-dioxaspiro[4.5]decan-8-yl)methyl)malonate-1-^{13}C (28i). Following **GP3** with slight modification of stoichiometry, using sodium 4-(trifluoromethyl)benzenesulfinate **20e** (92.9 mg, 0.40 mmol), 8-methylene-1,4-dioxaspiro[4.5]decane **22i'** (61.7 mg, 0.40 mmol) and 2-(trimethylsilyl)ethyl acrylate **3** (72 µL, 0.40 mmol) afforded the tittle compound after flash column chromatophraphy on silica gel (pentane/EtOAc 6:1) as a white solid (on average: 71.8 mg, 47% yield, dr = 2.3:1.6:1). **^{1}H NMR (400 MHz, $CDCl_3$):** δ (ppm) = 8.09 – 7.97 (m, 2H), 7.82 (d, J = 8.0 Hz, 2H), 4.24 – 4.14 (m, 2H), 4.13 – 3.98 (m, 2H), 3.90 (s, 1H), 3.89 – 3.85 (m, 3H), 3.74 – 3.66 (m, 3H), 3.64 – 3.47 (m, 1H), 3.29 (dtd, J = 8.4, 5.9, 4.4 Hz, 1H), 3.16 – 3.09 (m, 1H), 2.90 (td, J = 8.7, 4.8 Hz, 1H), 2.05 – 1.97 (m, 1H), 1.86 (dd, J = 14.9, 8.4 Hz, 1H), 1.76 – 1.44 (m, 4H), 1.42 – 1.31 (m, 3H), 1.27 – 1.21 (m, 2H), 1.03 – 0.91 (m, 3H), 0.90 – 0.79 (m, 2H), 0.03 – 0.01 (m, 18H); **^{19}F NMR (376 MHz, $CDCl_3$)** δ (ppm) = -63.3, -63.3, -63.3. **^{13}C NMR (101 MHz, $CDCl_3$)** δ (ppm) = 174.1, 173.8, 170.6, 170.3, 170.2, 145.0, 142.6, 135.7 (q, J = 33.2 Hz), 130.8, 129.6, 129.1, 129.1, 128.4, 128.2, 127.3, 126.6, 126.6, 126.6, 126.5, 126.5, 126.4, 126.1, 124.6, 108.2,

107.8, 107.0, 64.5, 64.4, 64.4, 64.3, 64.3, 64.2, 64.1, 64.0, 60.5, 59.5, 59.5, 52.8, 52.8, 52.8, 52.8, 52.7, 52.7, 48.7, 48.1, 47.8, 47.8, 47.3, 47.2, 39.1, 37.8, 37.8, 36.2, 36.2, 35.9, 35.9, 35.5, 35.5, 35.3, 34.8, 34.1, 33.5, 32.8, 32.3, 32.0, 31.7, 31.0, 30.5, 30.5, 30.4, 30.4, 29.8, 29.4, 29.1, 27.9, 25.4, 22.7, 22.7, 21.1, 18.8, 17.3, 17.2, 17.2, 17.2, 14.3, 14.2, 11.5, -1.4, -1.5, -1.5. **IR (neat, cm^{-1}):** 2954, 1732, 1686, 1317, 1248, 1141, 1061, 835, 763, 700; **HRMS** calcd. for ($C_{33}H_{53}F_3NaO_{10}SSi_2{}^{13}C$) $[M+Na]^+$: 790.2776 found 790.2773. **MP** = 80°C.

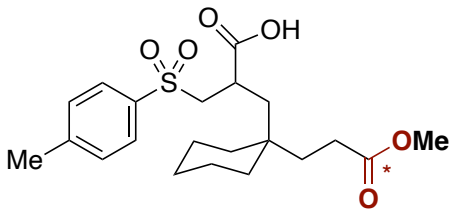

3-(1-(3-methoxy-3-oxopropyl-3-13*C*)cyclohexyl)-2-(tosylmethyl)propanoic acid (28j). Following **GP3** with some modifications, using sodium 4-(trifluoromethyl)benzenesulfinate **20d** (92.9 mg, 0.40 mmol), 8-methylene-1,4-dioxaspiro[4.5]decane **22i'** (61.7 mg, 0.40 mmol) and 2-(trimethylsilyl)ethyl acrylate **3** (72 µL, 0.40 mmol) afforded the ETMS protected crude. The crude was dissolved in 1 mL of THF to which were added 4 equiv. of TBAF (1 M, 800 µL), the reaction was then stirred at 70°C for 2h. The tittle compound was obtained after flash column chromatophraphy on silica gel (pentane/EtOAc 1:1 with 1% Et_3N; then 1:2 with 1% HCOOH) as a colorless oil (on average: 25.8 mg, 31% yield). **^{1}H NMR (400 MHz, $CDCl_3$):** δ (ppm) = 9.1 (s, 1H), 7.8 (d, *J* = 8.3 Hz, 2H), 7.4 (d, *J* = 8.1 Hz, 2H), 3.7 (d, *J* = 3.8 Hz, 3H), 3.6 (dd, *J* = 14.3, 8.8 Hz, 1H), 3.1 (dd, *J* = 14.3, 4.0 Hz, 1H), 2.9 (dp, *J* = 11.5, 4.3 Hz, 1H), 2.4 (s, 3H), 2.2 – 2.1 (m, 2H), 1.8 (dd, *J* = 14.8, 7.3 Hz, 1H), 1.7 – 1.6 (m, 2H), 1.5 (dd, *J* = 14.8, 4.5 Hz, 2H), 1.4 (p, *J* = 5.9 Hz, 5H), 1.3 – 1.1 (m, 7H), 0.9 – 0.8 (m, 1H); **^{13}C NMR (101 MHz, $CDCl_3$)** δ (ppm) = 174.6, 172.8, 145.2, 136.0, 128.4, 59.2, 51.8 (d, *J* = 2.8 Hz), 39.8, 35.7 (d, *J* = 4.3 Hz), 35.6, 35.2 (d, *J* = 21.6 Hz), 30.7, 28.5, 27.9, 26.0, 21.8, 21.4 (d, *J* = 7.1 Hz). **IR (neat, cm^{-1}):** 2925, 2854, 1692, 1597, 1436, 1302, 1139, 1086, 814, 558; **HRMS** calcd. for ($C_{20}H_{30}NaO_6S^{13}C$) $[M+Na]^+$: 434.1689 found 434.169.

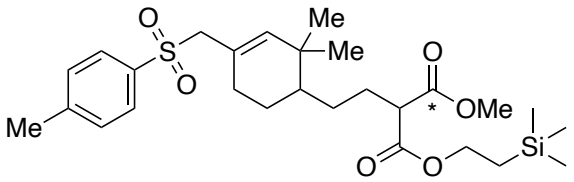

1-methyl 3-(2-(trimethylsilyl)ethyl) 2-(2-(2,2-dimethyl-4-(((4-(trifluoromethyl)phenyl)sulfonyl)methyl)cyclohex-3-en-1-yl)ethyl)malonate-1-^{13}C (32).

Following a modified **GP1**, not performing the final deprotection, sodium 4-methylbenzenesulfinate **20d** (35.6 mg, 0.40 mmol) β-Pinene (93.7 µL, 0.60 mmol) and 2-(trimethylsilyl)ethyl acrylate (54 µL, 0.30 mmol) afforded the product after flash column chromatography on silica gel (*n*-hexane/EtOAc 15:1) as a colorless oil (on average: 42.8 mg, 37% yield). **^{1}H NMR (400 MHz, $CDCl_3$):** δ (ppm) = 7.80 – 7.68 (m, 2H), 7.33 (d, *J* = 7.9 Hz, 2H), 5.40 (d, *J* = 4.7 Hz, 1H), 4.26 – 4.15 (m, 2H), 3.72 (t, *J* = 4.0 Hz, 3H), 3.65 (s, 2H), 3.34 (dt, *J* = 8.3, 6.2 Hz, 1H), 2.44 (s, 3H), 2.17 – 2.02 (m, 2H), 1.94 (t, *J* = 5.7 Hz, 2H), 1.82 – 1.69 (m, 3H), 1.30 – 1.19 (m, 1H), 1.13 (ddd, *J* = 11.5, 9.3, 5.6 Hz, 1H), 1.03 – 0.95 (m, 2H), 0.78 (s, 6H), 0.03 (d, *J* = 1.5 Hz, 9H).; **^{13}C NMR (101 MHz, $CDCl_3$)** δ (ppm) = 171.0 (d, J = 2.9 Hz), 144.6, 135.9, 132.7, 129.7, 128.6, 126.3, 64.5, 64.1, 52.7 (d, J = 4.5 Hz), 48.4, 47.9, 41.8 (d, J = 5.1 Hz), 38.1 (d, J = 2.5 Hz), 34.8 (d, J = 1.7 Hz), 30.2, 27.0, 24.0, 23.8, 21.8, 17.3, -1.4. **IR (neat, cm^{-1}):** 2954, 1736, 1698, 1249, 1146, 1087, 914, 836, 730, 570, 514; **HRMS** calcd. for ($C_{26}H_{42}NaO_6SSi^{13}C$) $[M+Na]^+$: 546.2403 found 546.2397.

2.7.2. NMR Spectra

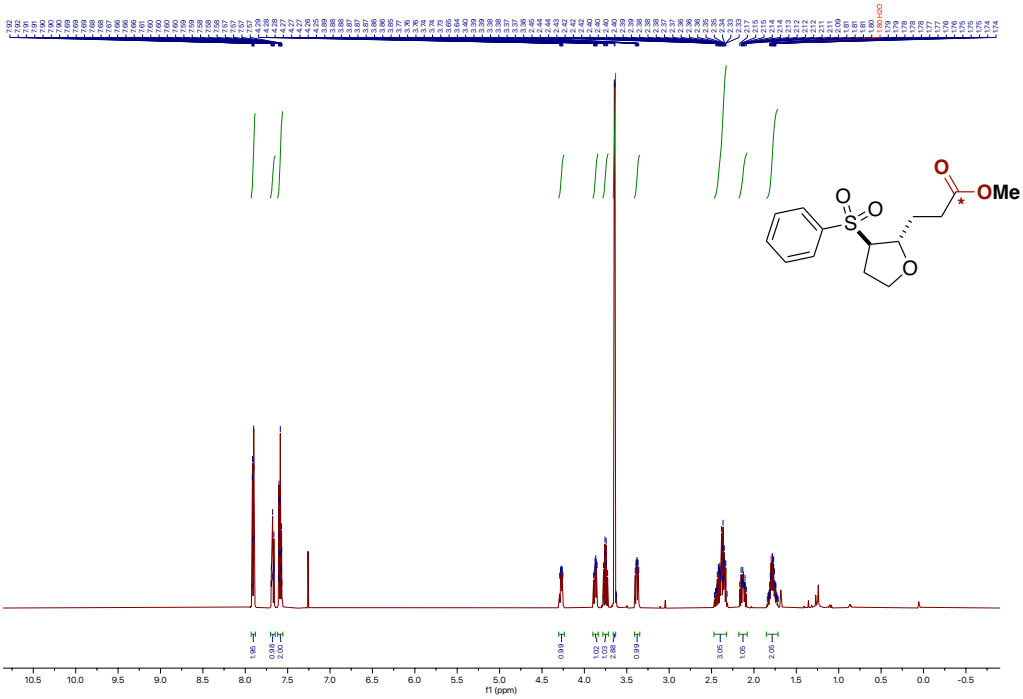

^{1}H spectrum (500 MHz, $CDCl_3$) of **23a**

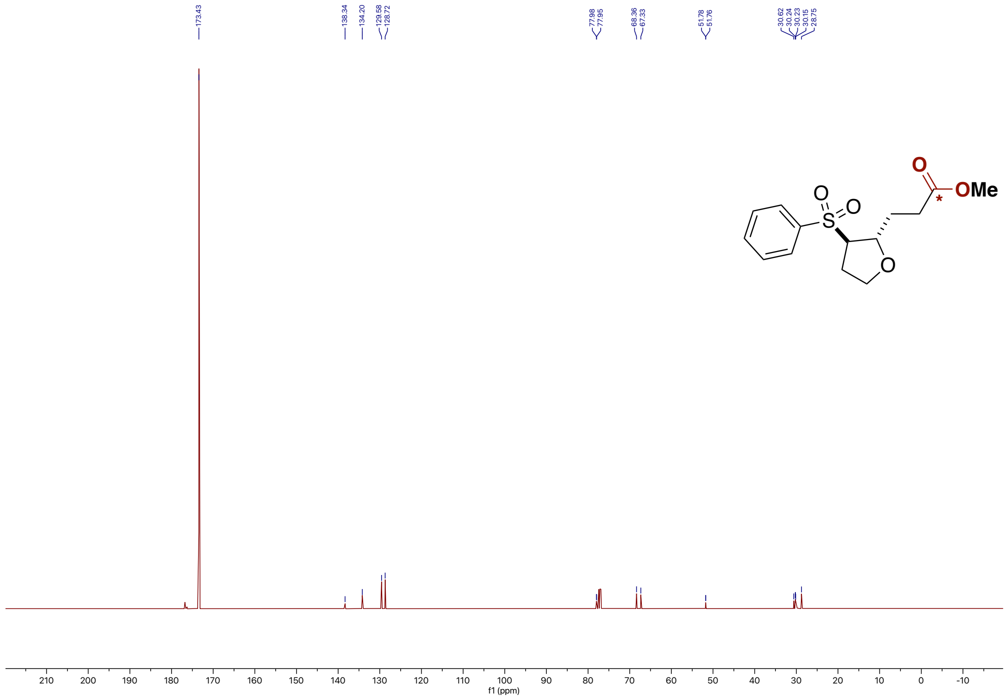

^{13}C spectrum (126 MHz, $CDCl_3$) of **23a**

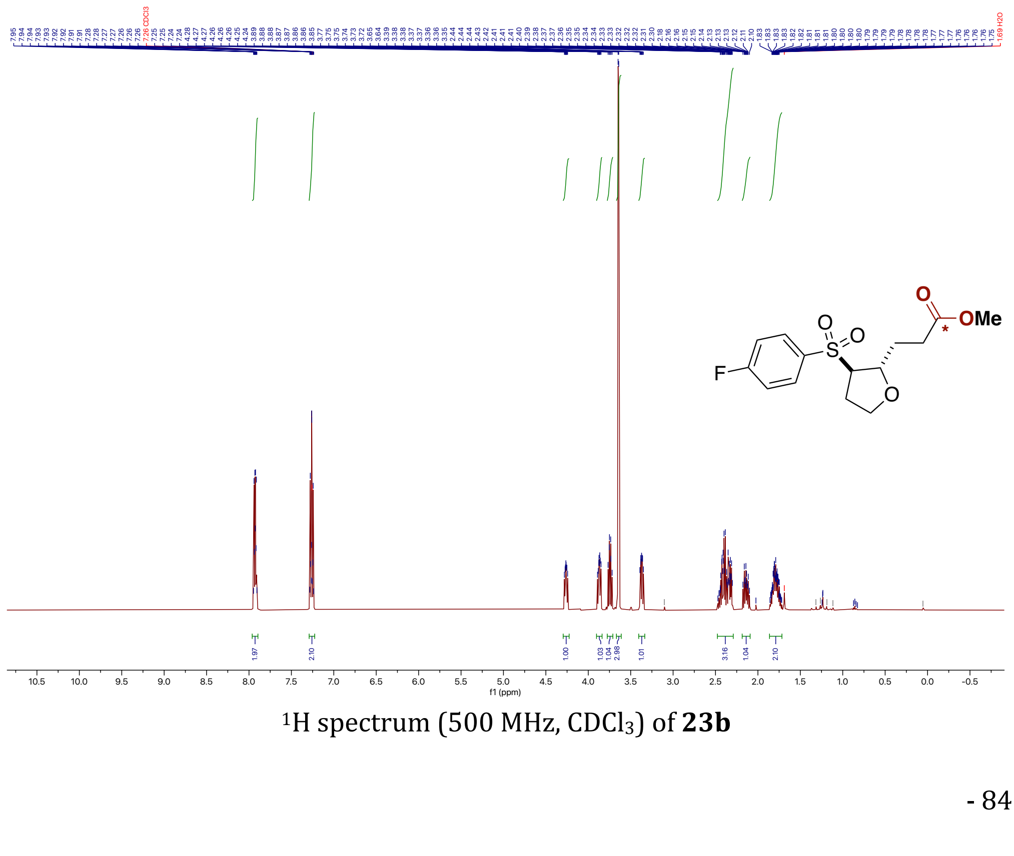

^{1}H spectrum (500 MHz, $CDCl_3$) of **23b**

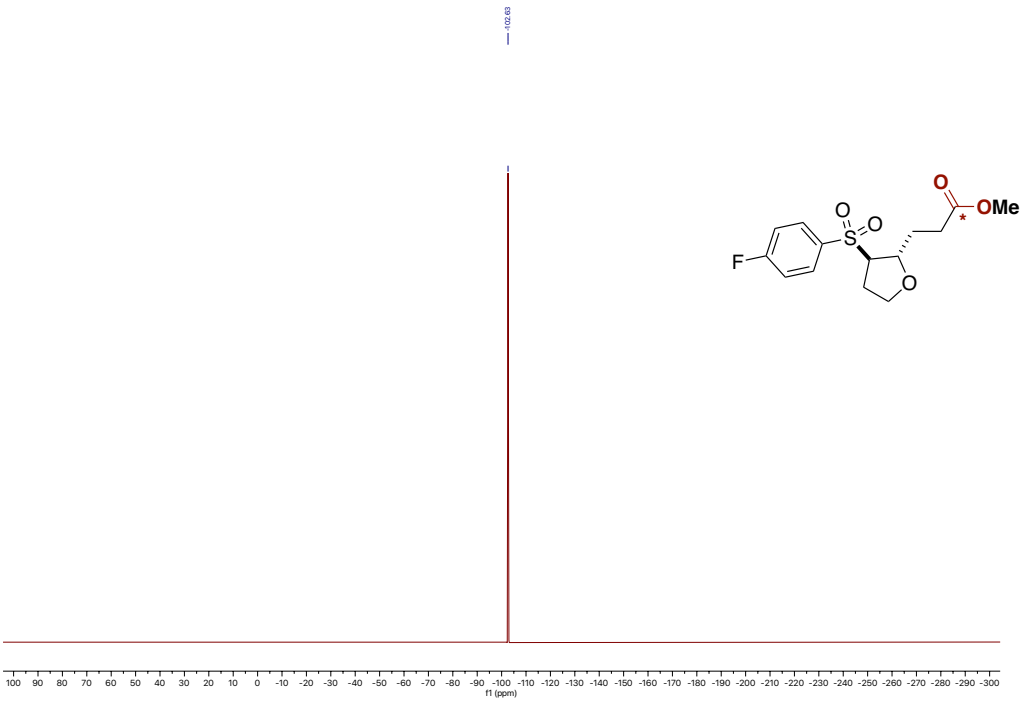

^{19}F spectrum (471 MHz, $CDCl_3$) of **23b**

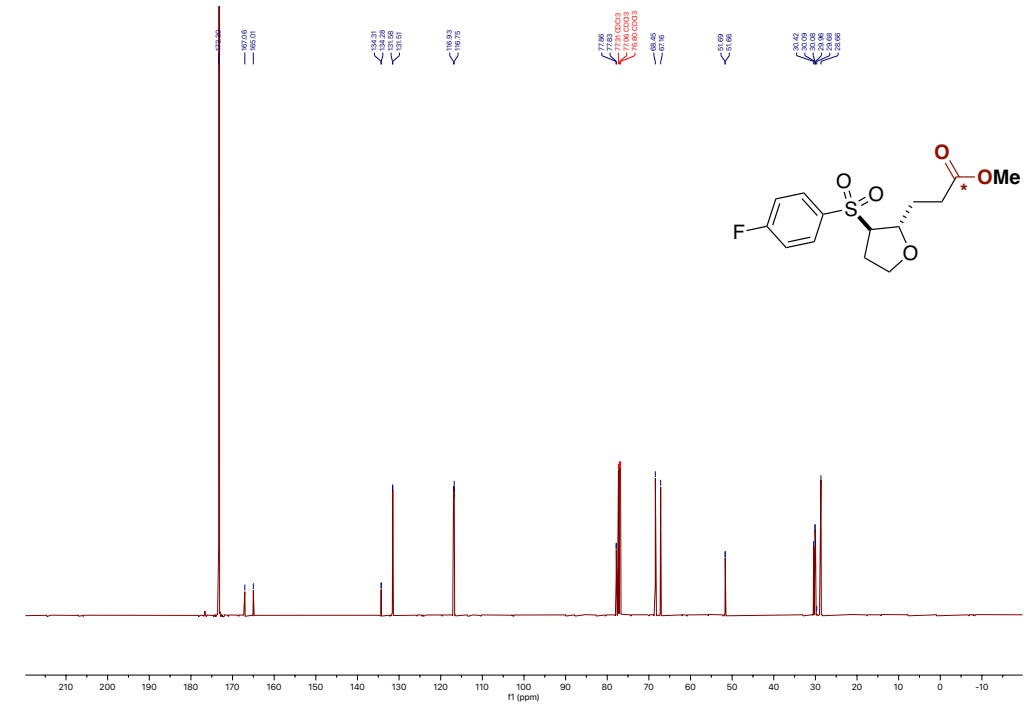

^{13}C spectrum (126 MHz, $CDCl_3$) of **23b**

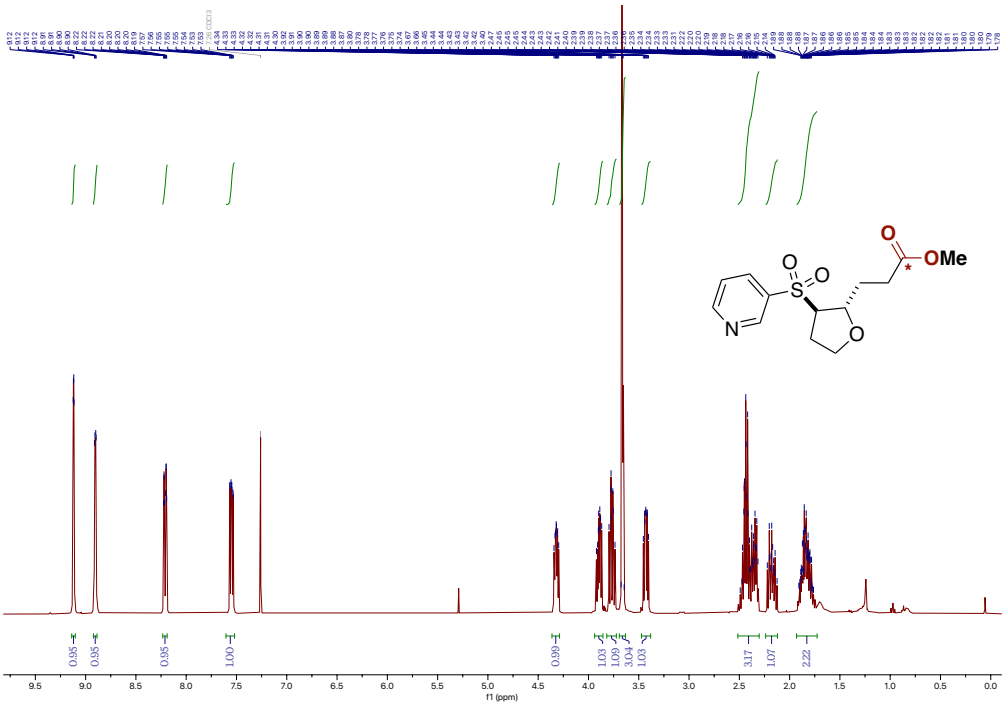

^{1}H spectrum (500 MHz, $CDCl_3$) of **23c**

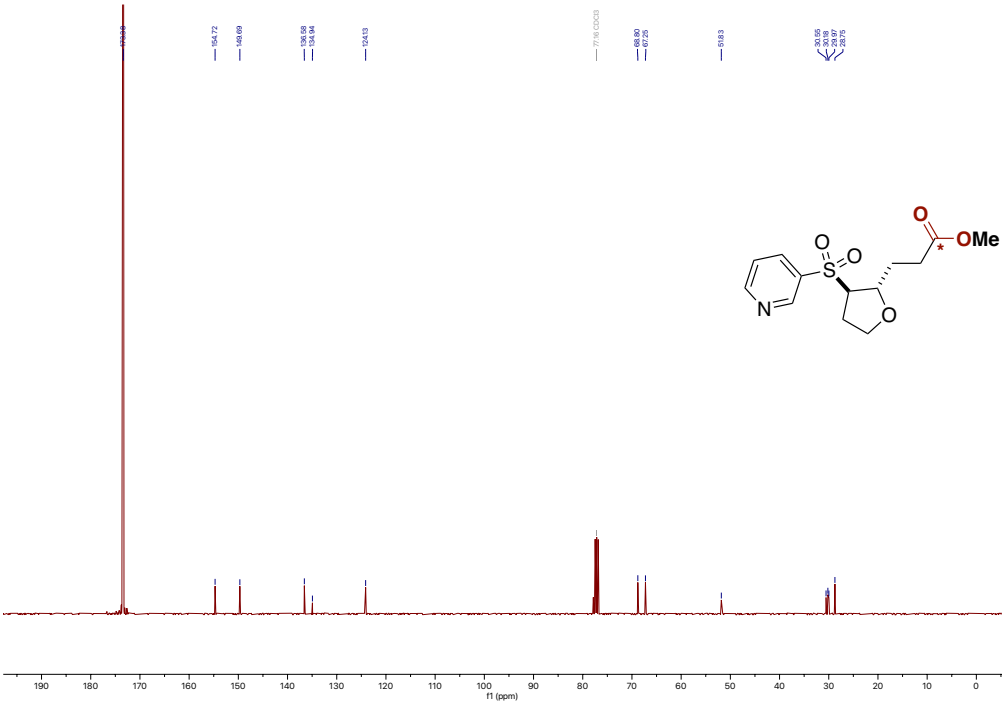

^{13}C spectrum (126 MHz, $CDCl_3$) of **23c**

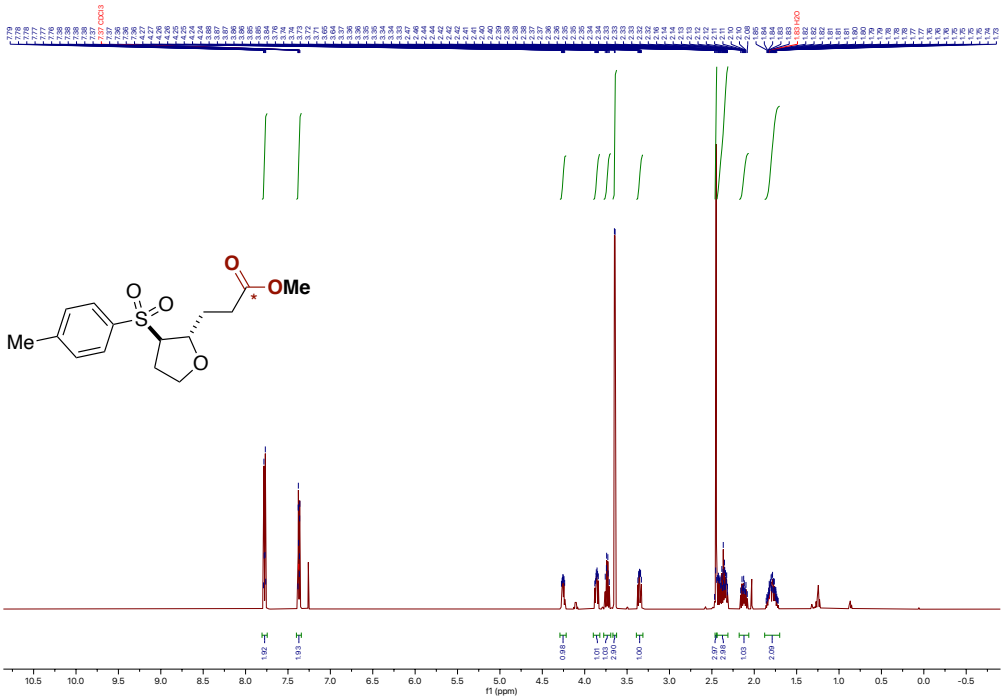

^{1}H spectrum (500 MHz, $CDCl_3$) of **23d**

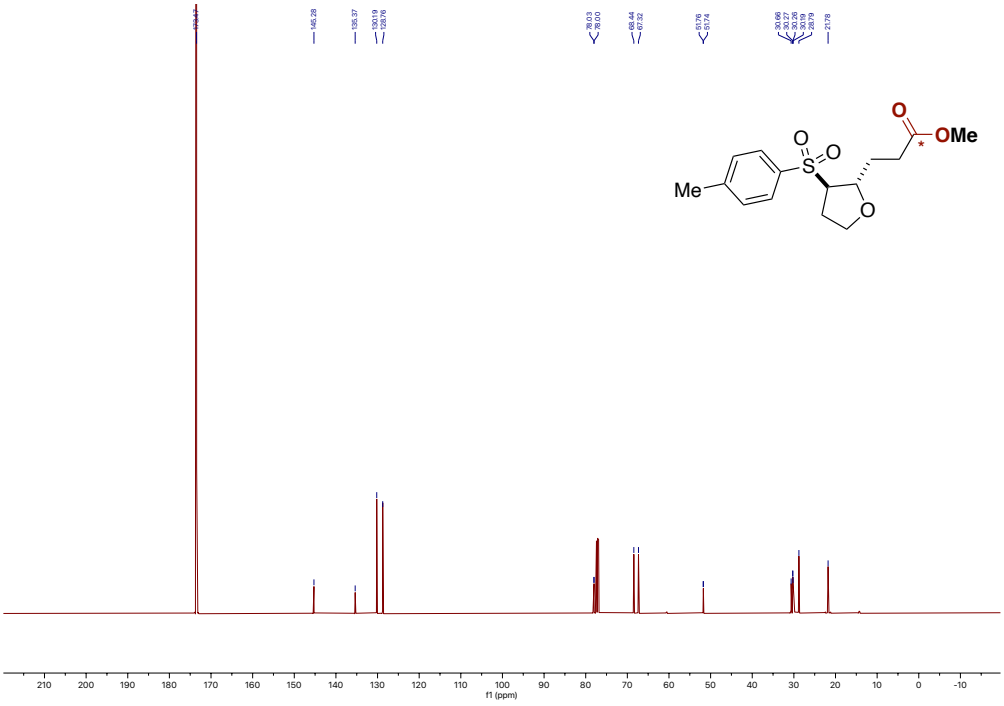

^{13}C spectrum (126 MHz, $CDCl_3$) of **23d**

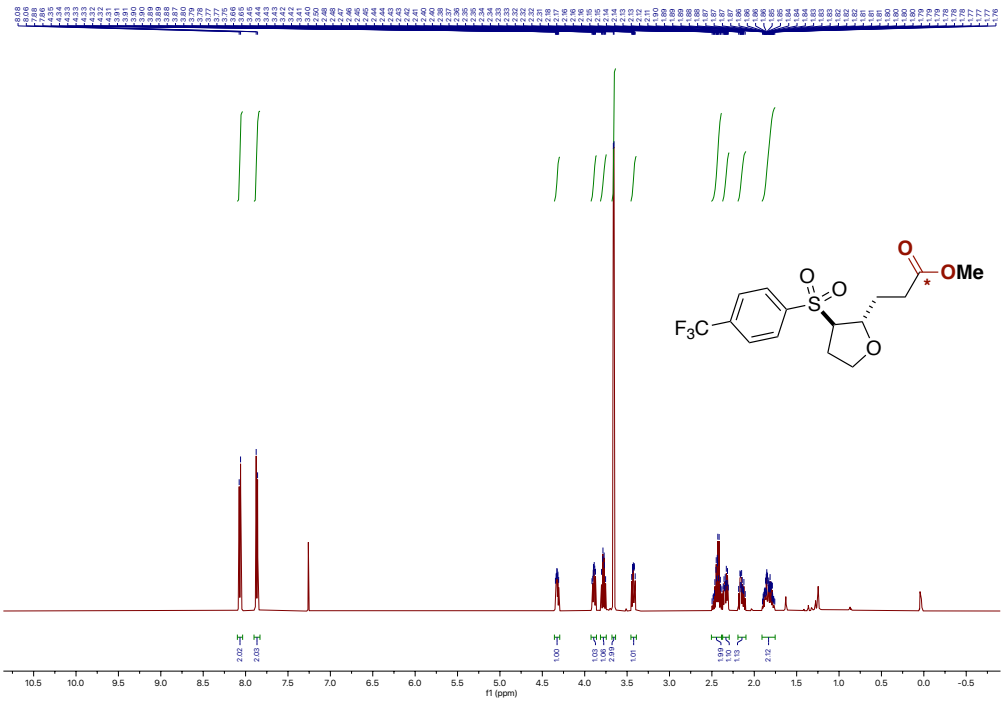

^{1}H spectrum (500 MHz, $CDCl_3$) of **23e**

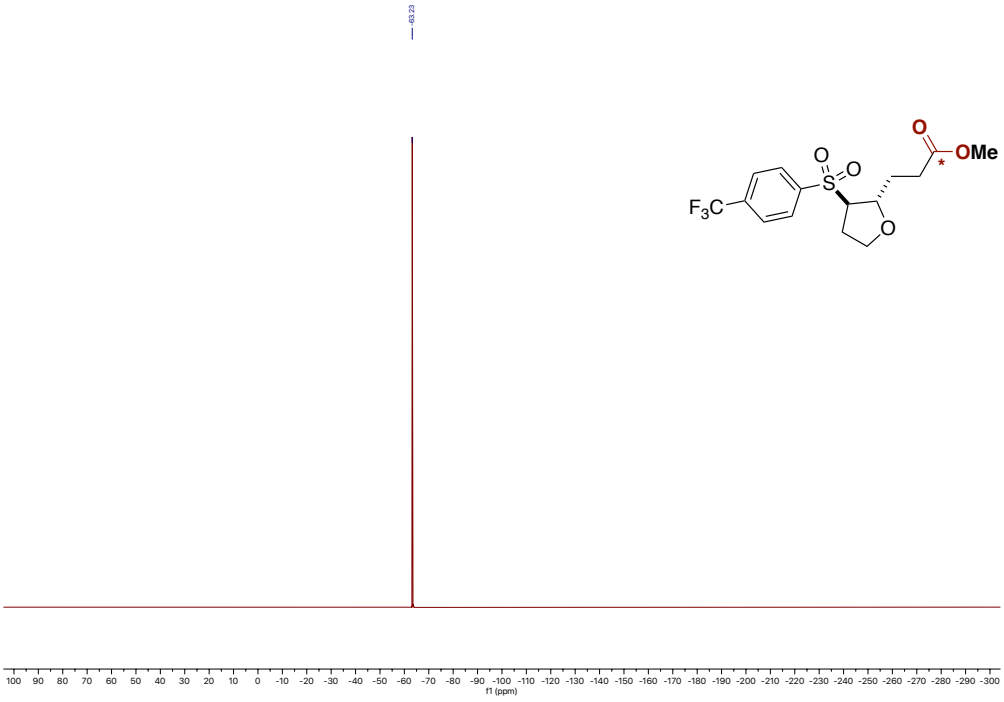

^{19}F spectrum (471 MHz, $CDCl_3$) of **23e**

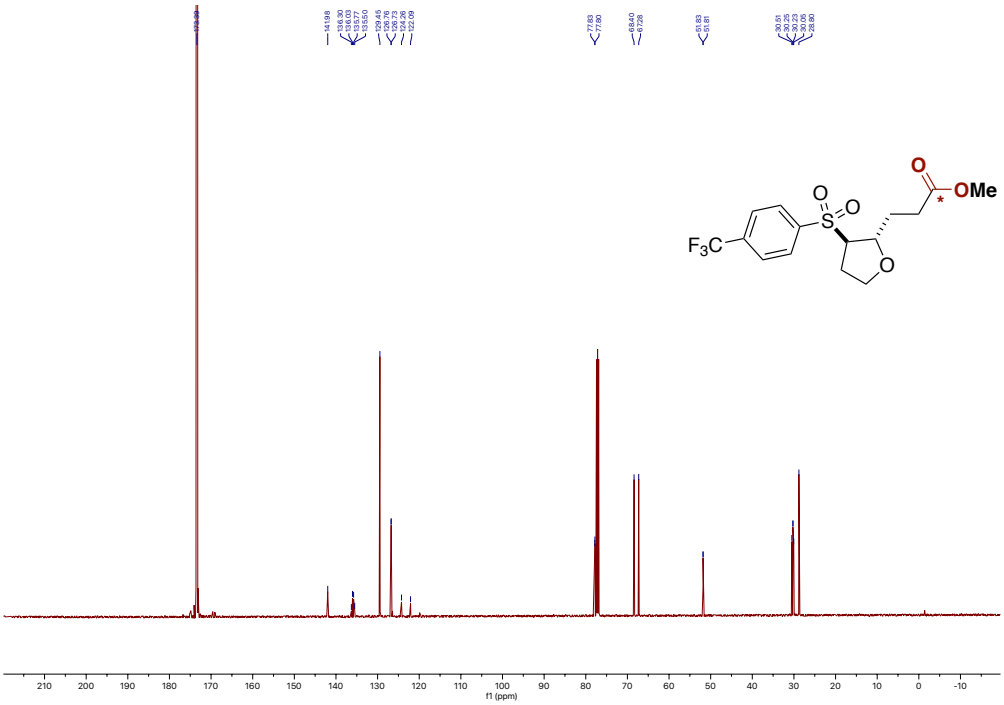

^{13}C spectrum (126 MHz, $CDCl_3$) of **23e**

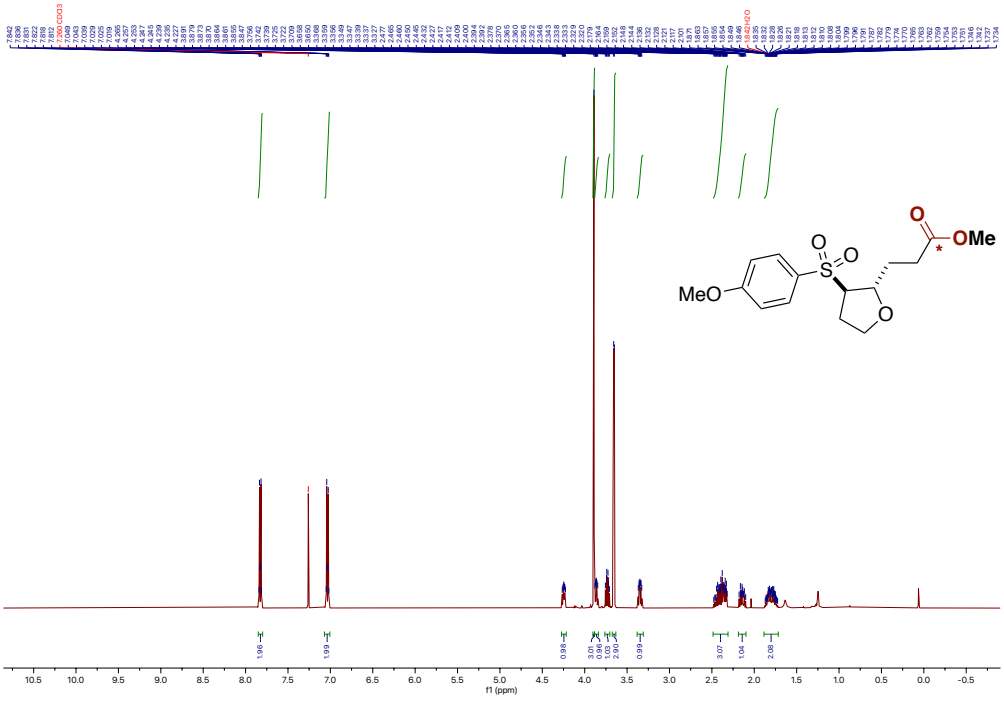

^{1}H spectrum (500 MHz, $CDCl_3$) of **23f**

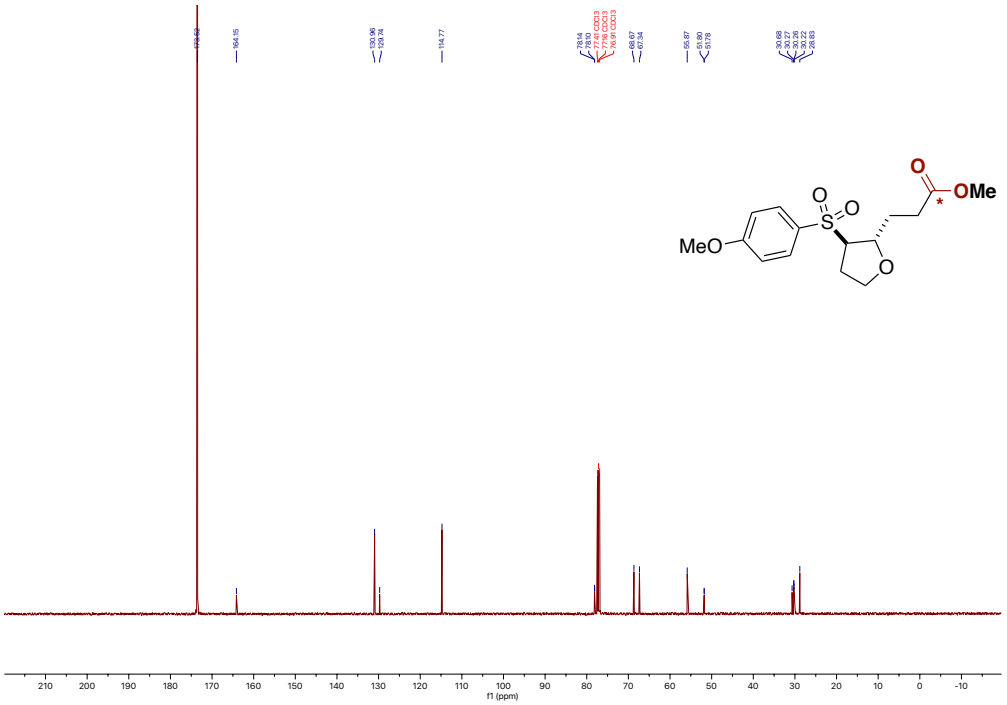

^{13}C spectrum (126 MHz, $CDCl_3$) of **23f**

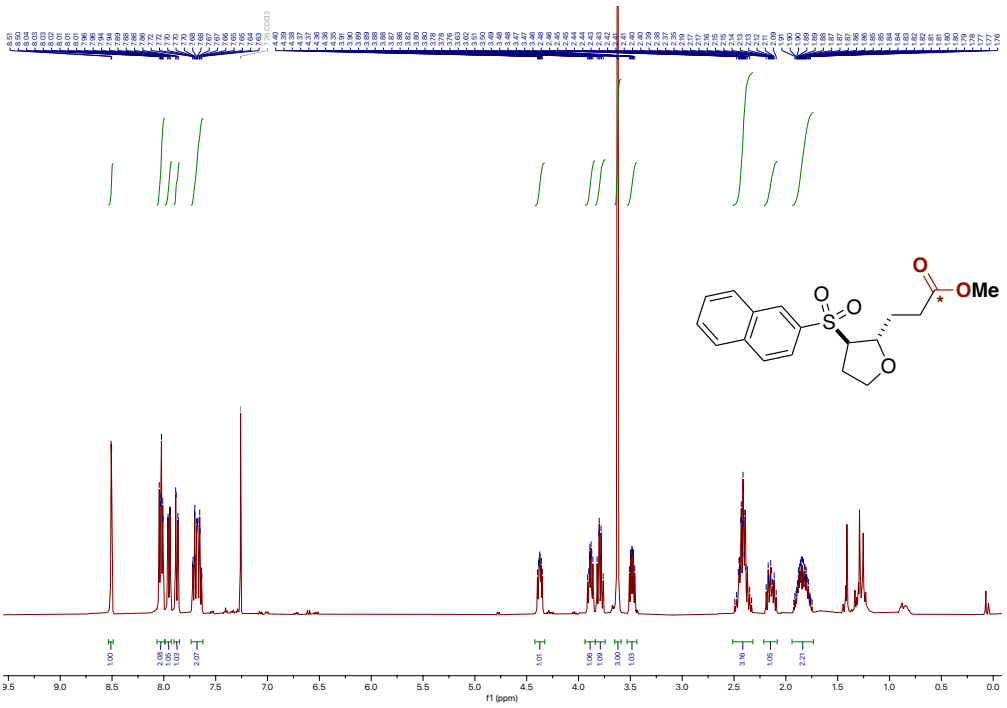

^{1}H spectrum (500 MHz, $CDCl_3$) of **23g**

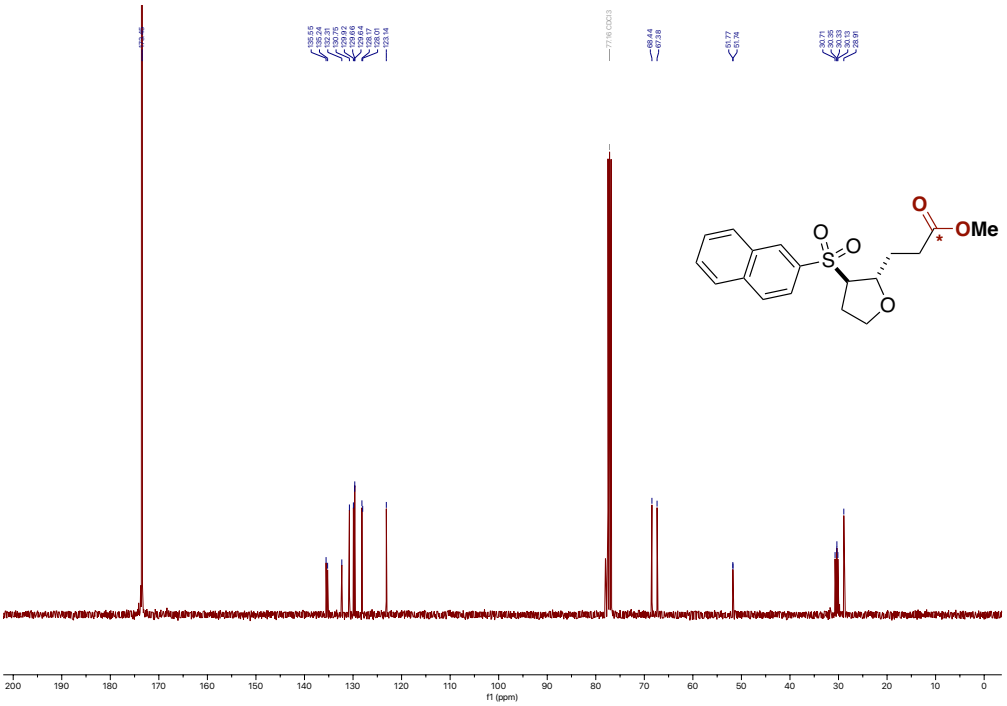

^{13}C spectrum (126 MHz, $CDCl_3$) of **23g**

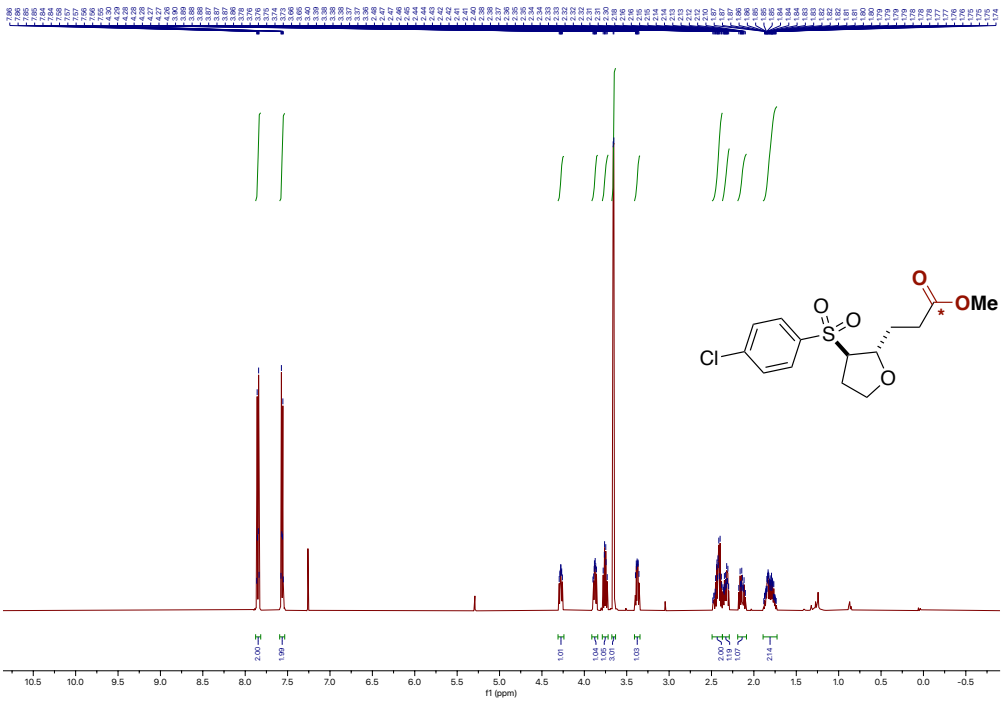

^{1}H spectrum (500 MHz, $CDCl_3$) of **23h**

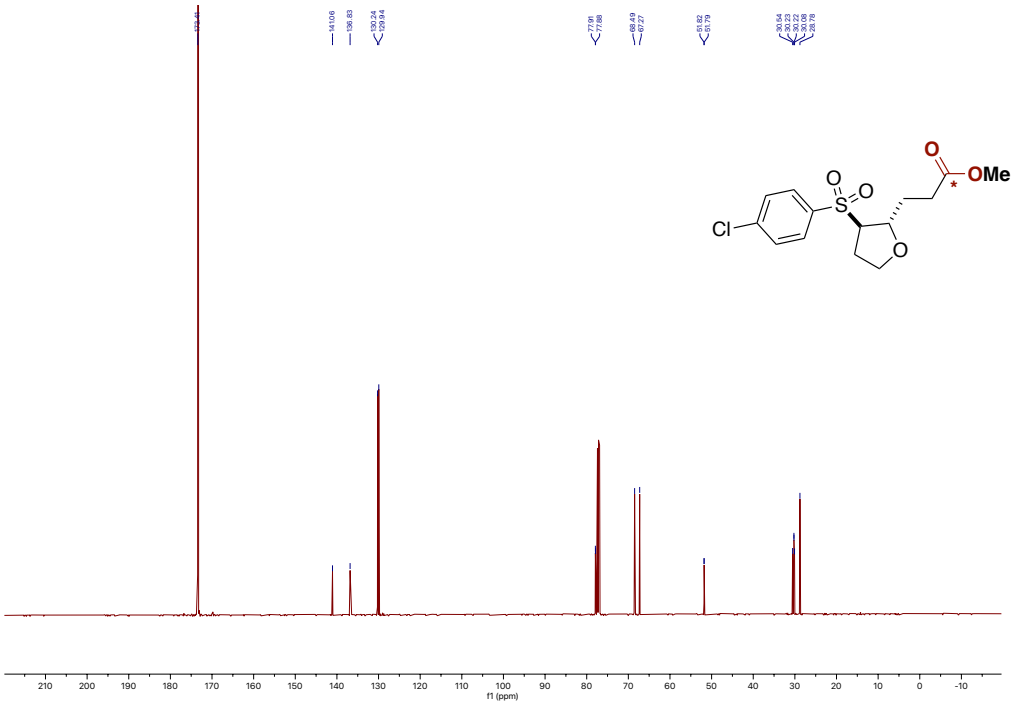

^{13}C spectrum (126 MHz, $CDCl_3$) of **23h**

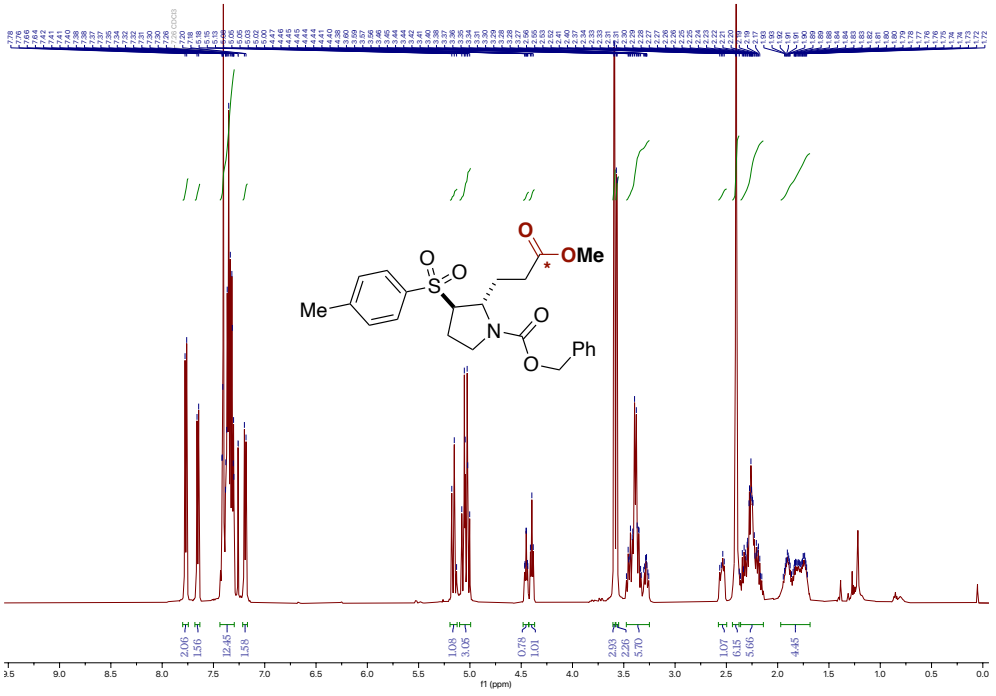

^{1}H spectrum (500 MHz, $CDCl_3$) of **23i** at 250 K

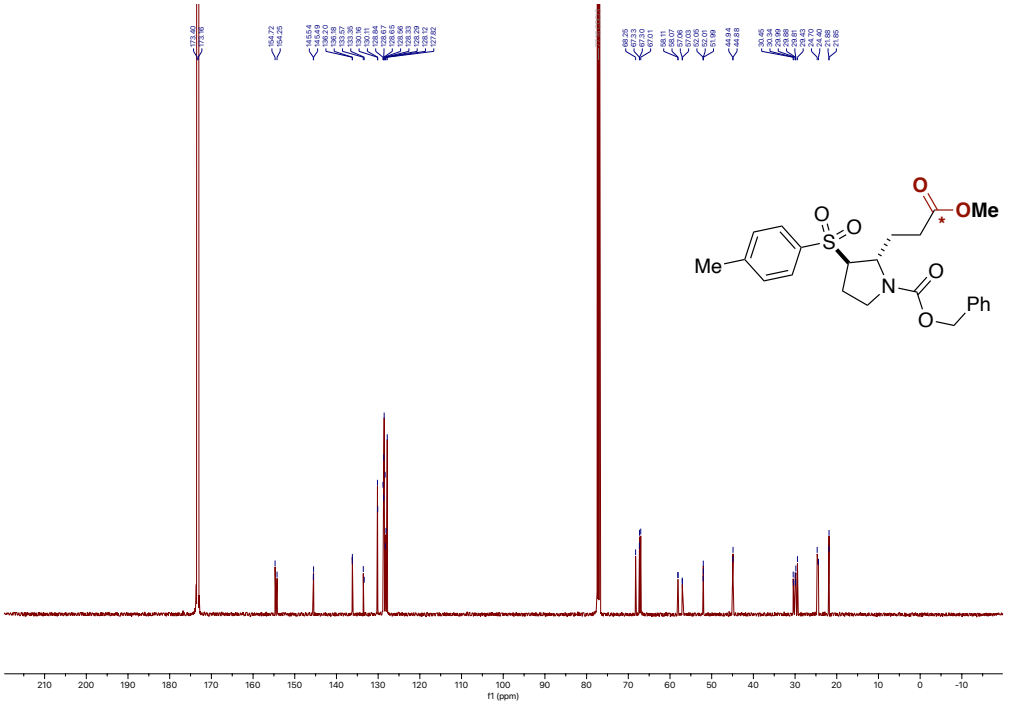

^{13}C spectrum (126 MHz, $CDCl_3$) of **23i** at 250 K

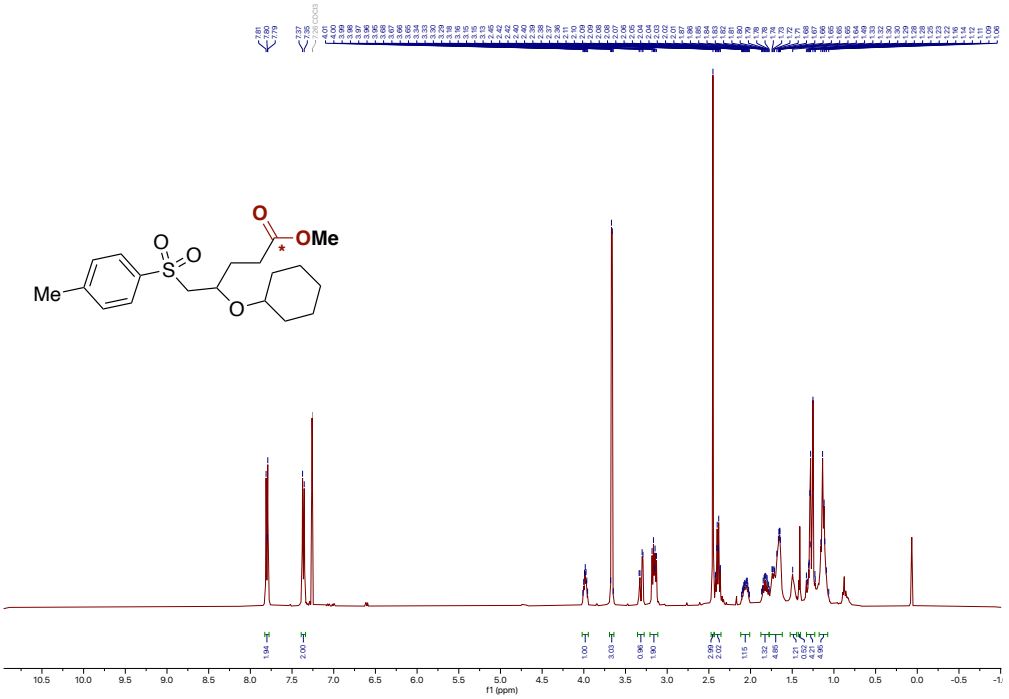

^{1}H spectrum (400 MHz, $CDCl_3$) of **23j**

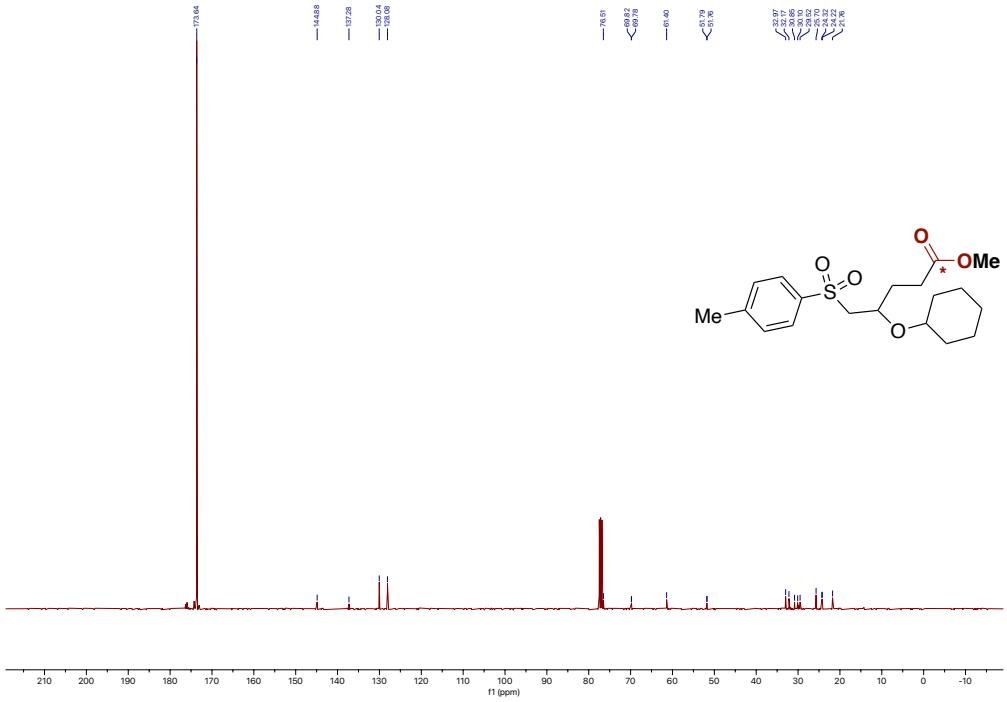

^{13}C spectrum (101 MHz, $CDCl_3$) of **23j**

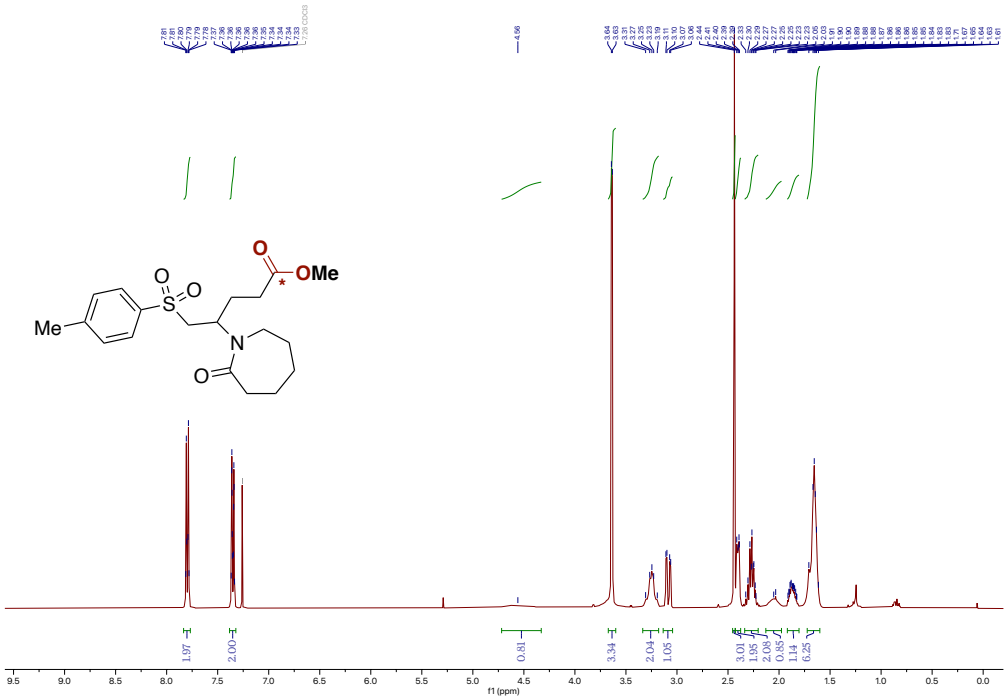

^{1}H spectrum (500 MHz, $CDCl_3$) of **23k**

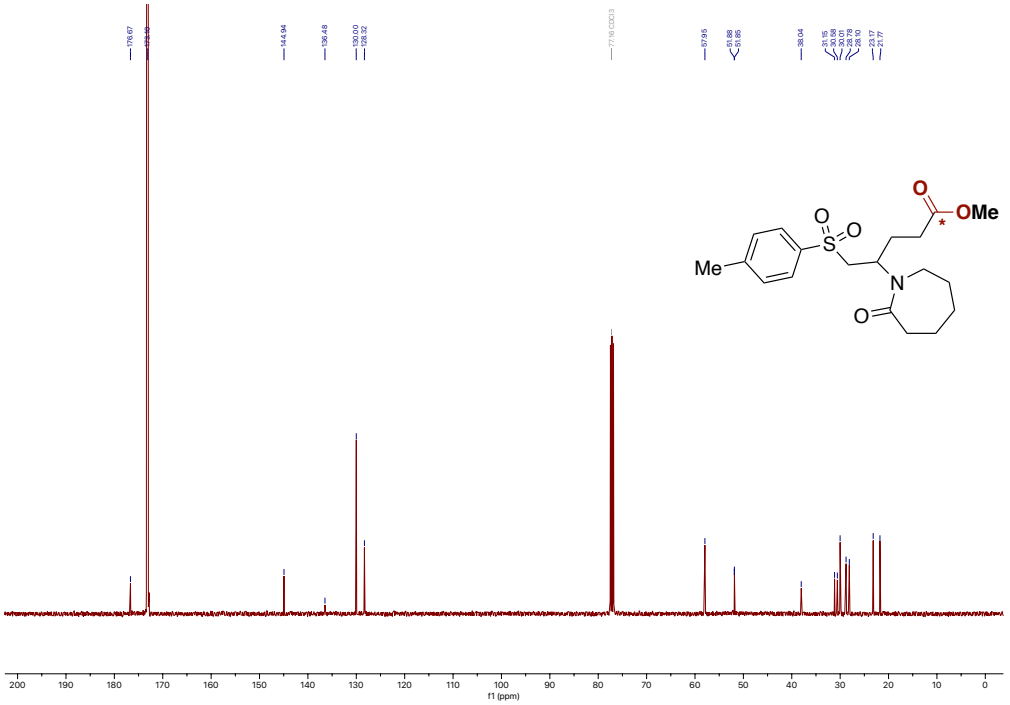

^{13}C spectrum (126 MHz, $CDCl_3$) of **23k**

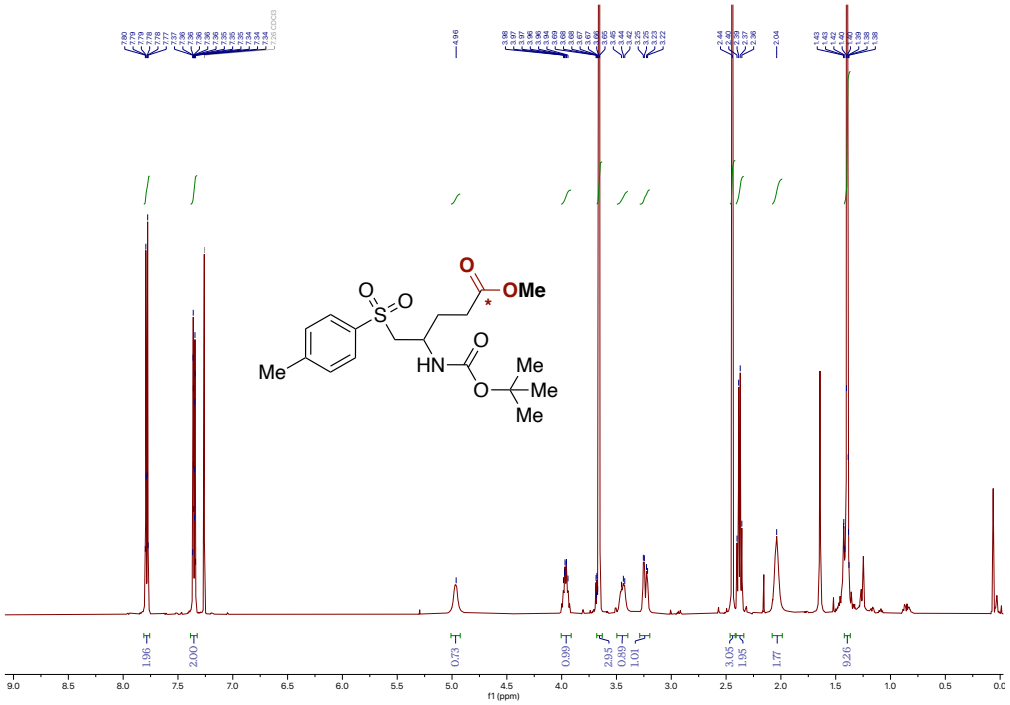

^{1}H spectrum (500 MHz, $CDCl_3$) of **23l**

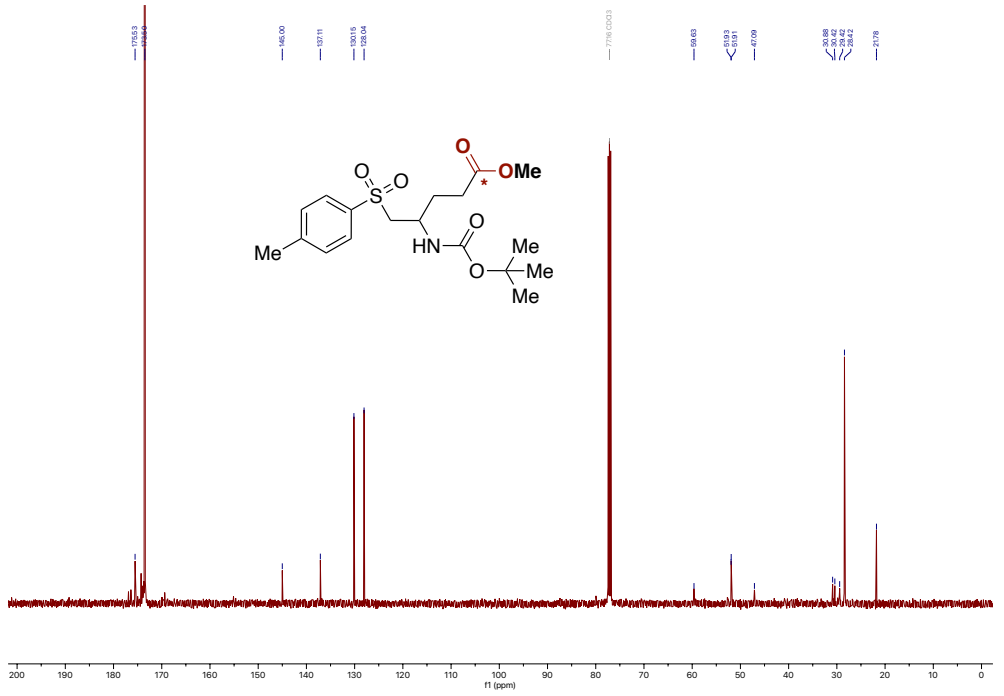

^{13}C spectrum (126 MHz, $CDCl_3$) of **23l**

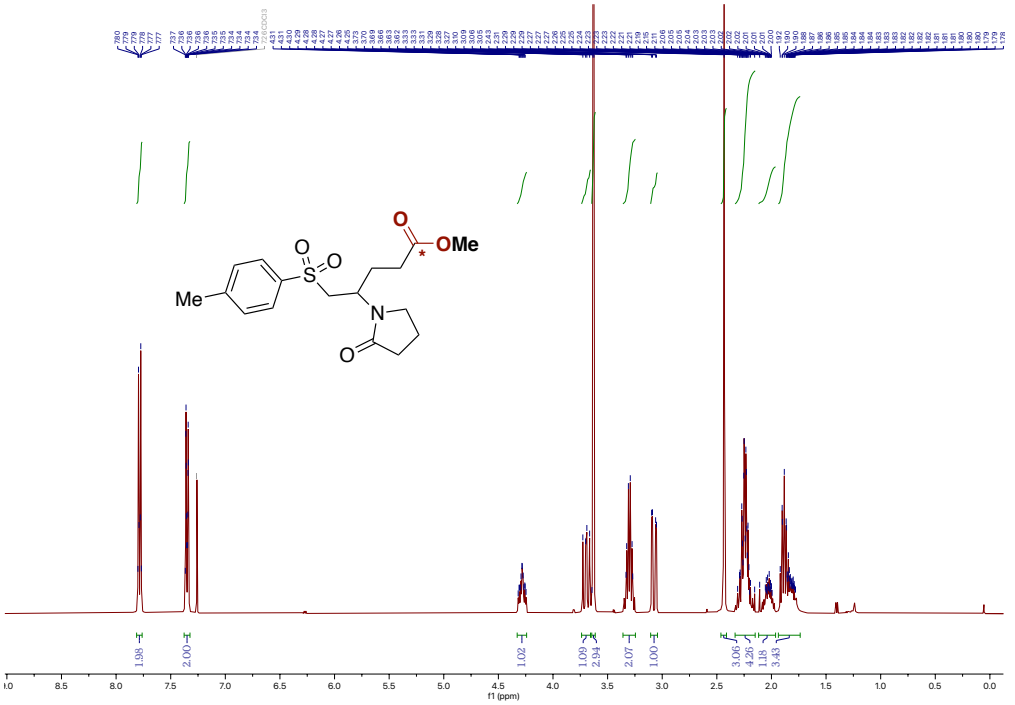

^{1}H spectrum (500 MHz, $CDCl_3$) of **23m**

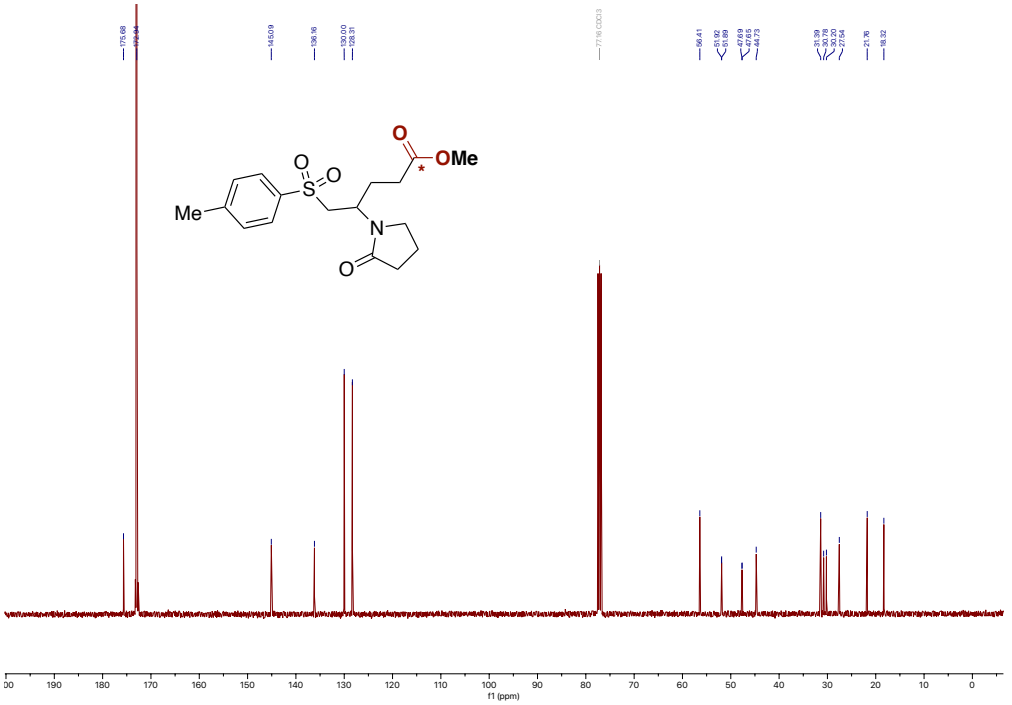

^{13}C spectrum (126 MHz, $CDCl_3$) of **23m**

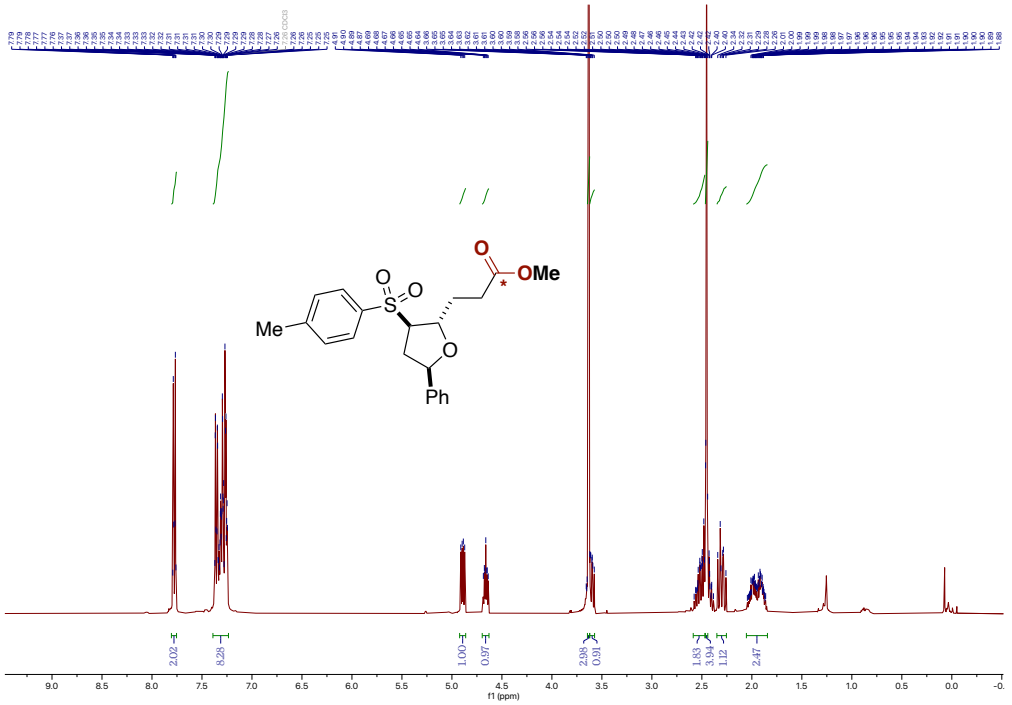

^{1}H spectrum (500 MHz, $CDCl_3$) of **23n**

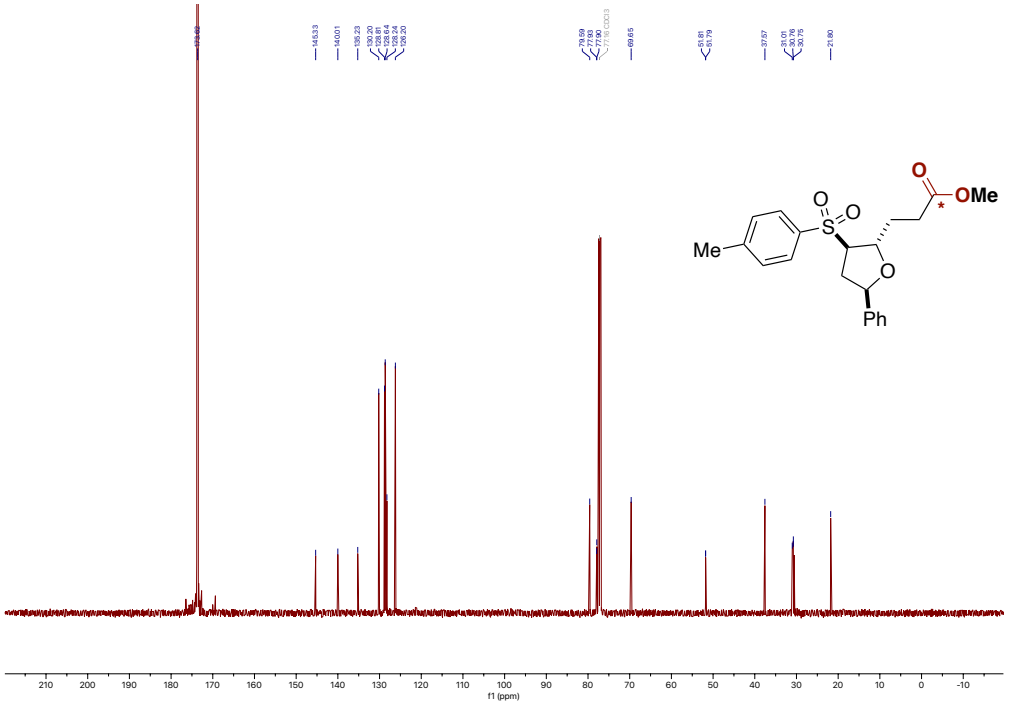

^{13}C spectrum (126 MHz, $CDCl_3$) of **23n**

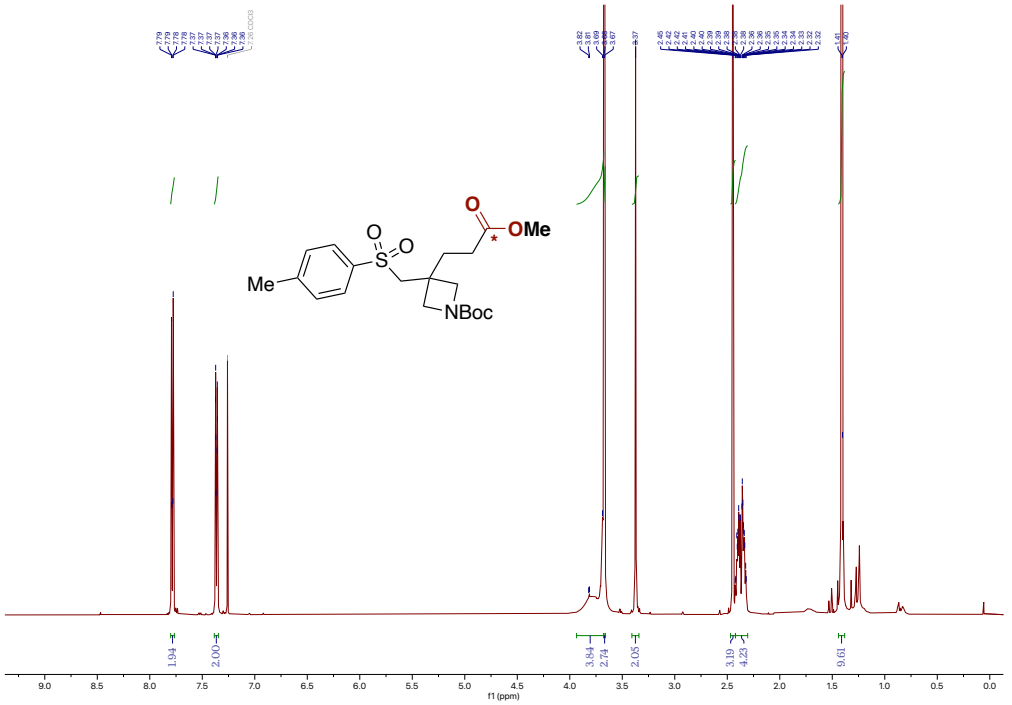

^{1}H spectrum (500 MHz, $CDCl_3$) of **23o**

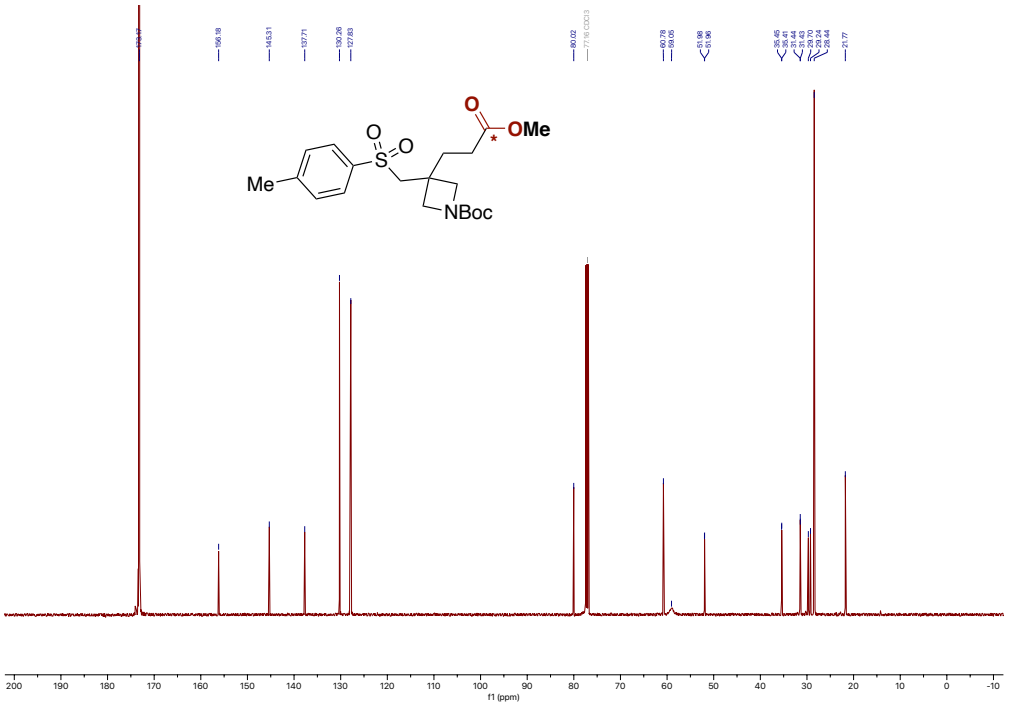

^{13}C spectrum (126 MHz, $CDCl_3$) of **23o**

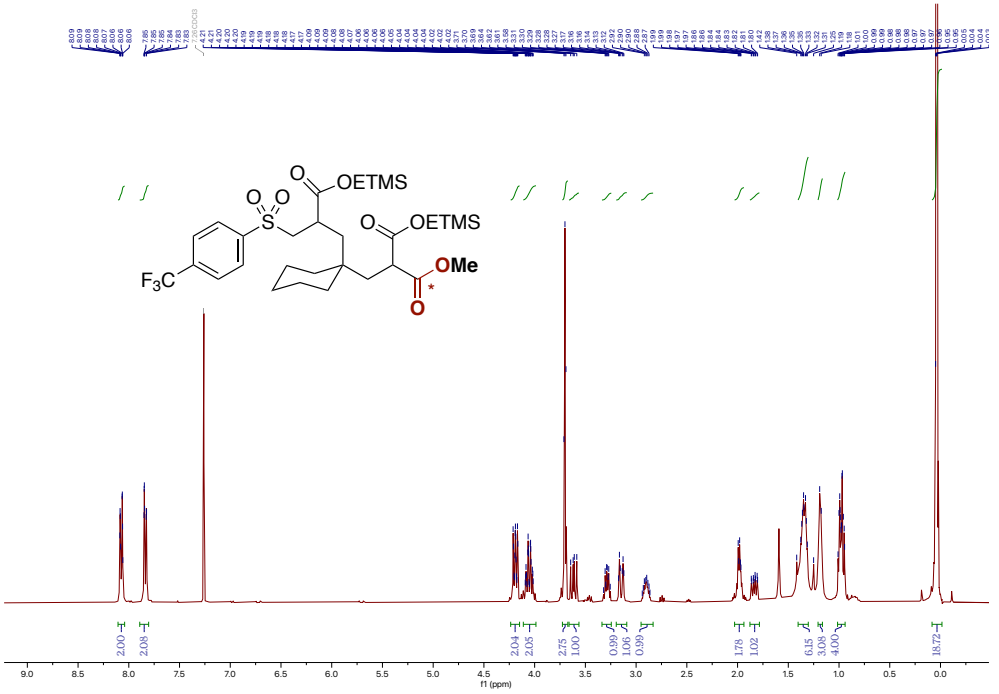

^{1}H spectrum (500 MHz, $CDCl_3$) of **28a**

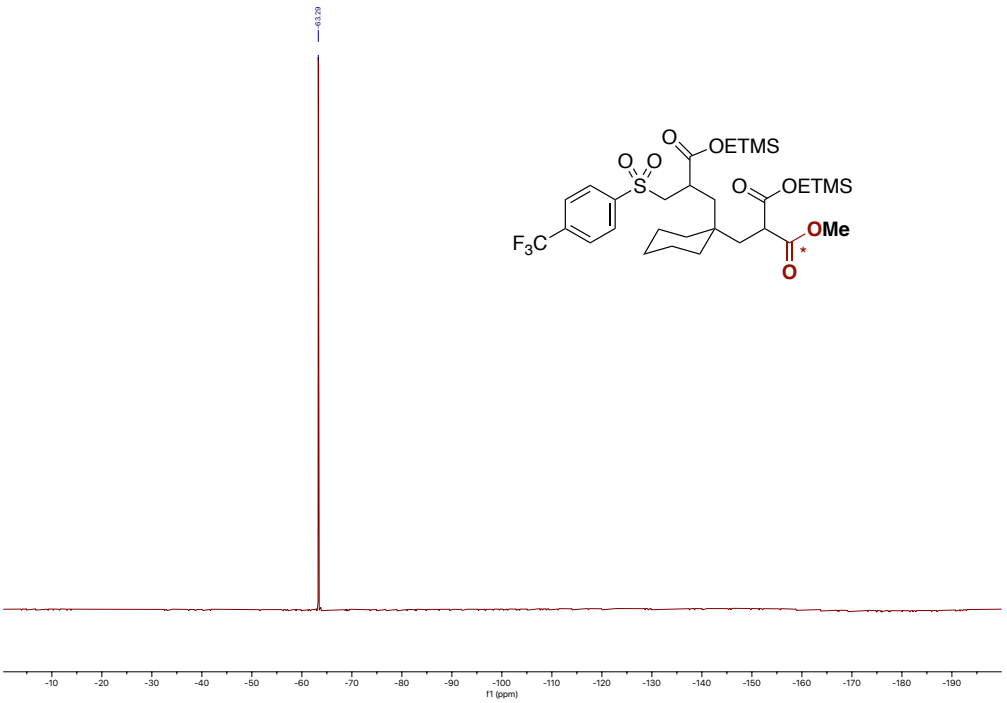

^{19}F spectrum (377 MHz, $CDCl_3$) of **28a**

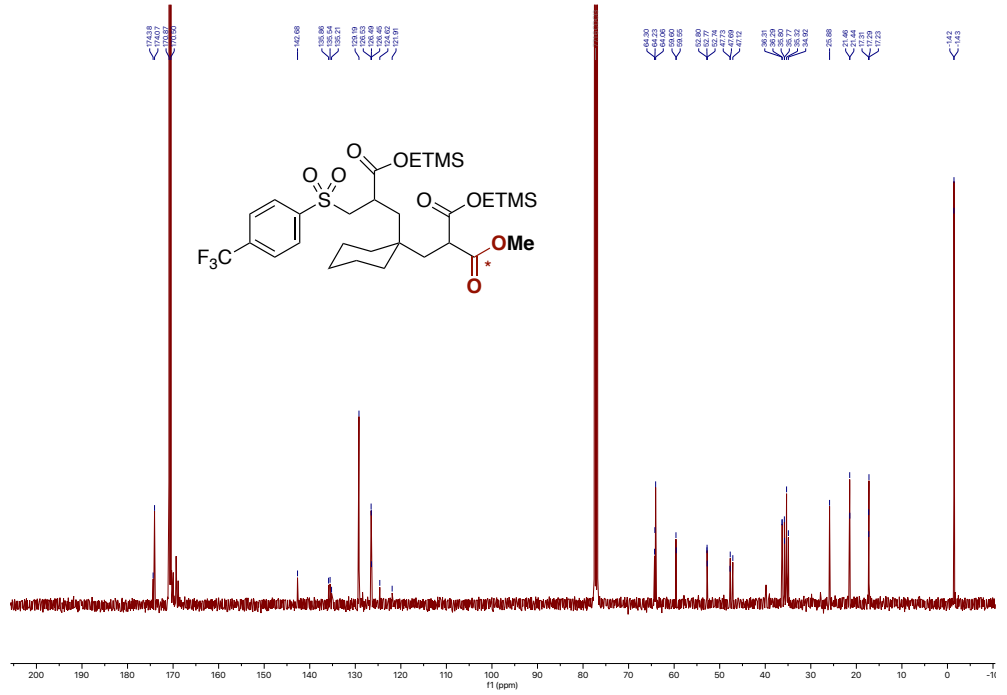

^{13}C spectrum (126 MHz, $CDCl_3$) of **28a**

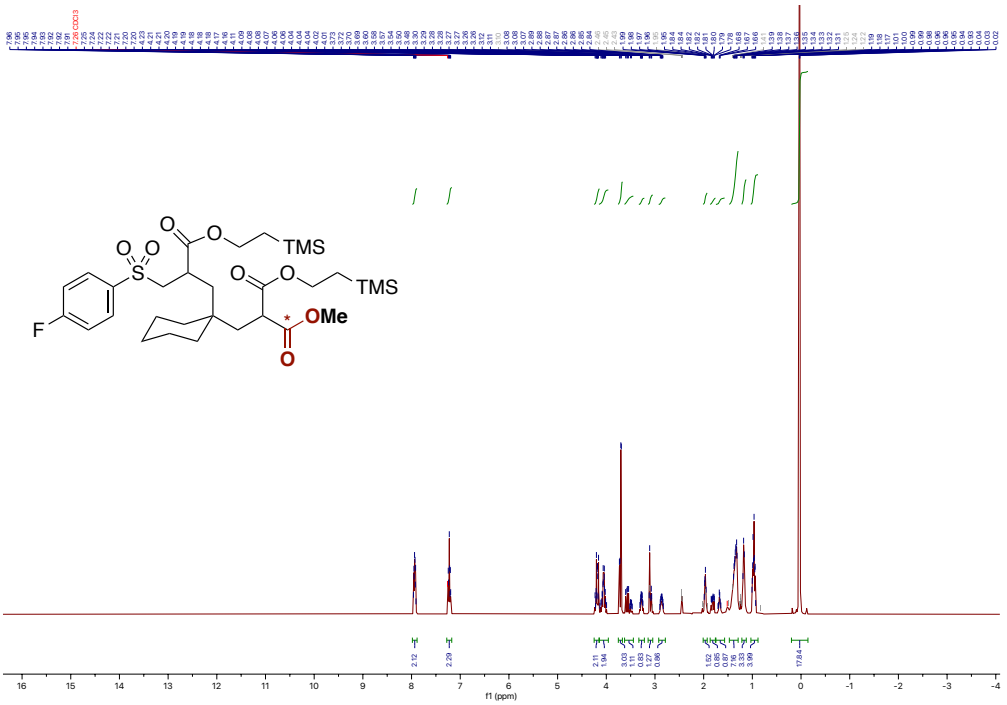

^{1}H spectrum (400 MHz, $CDCl_3$) of **28b**

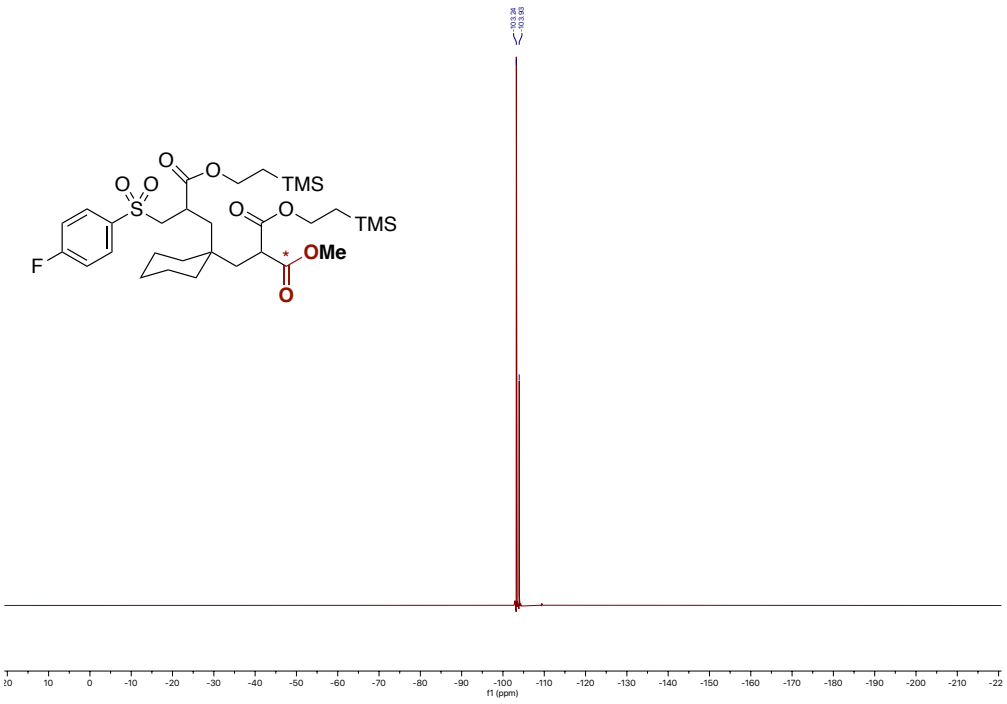

^{19}F spectrum (377 MHz, $CDCl_3$) of **28b**

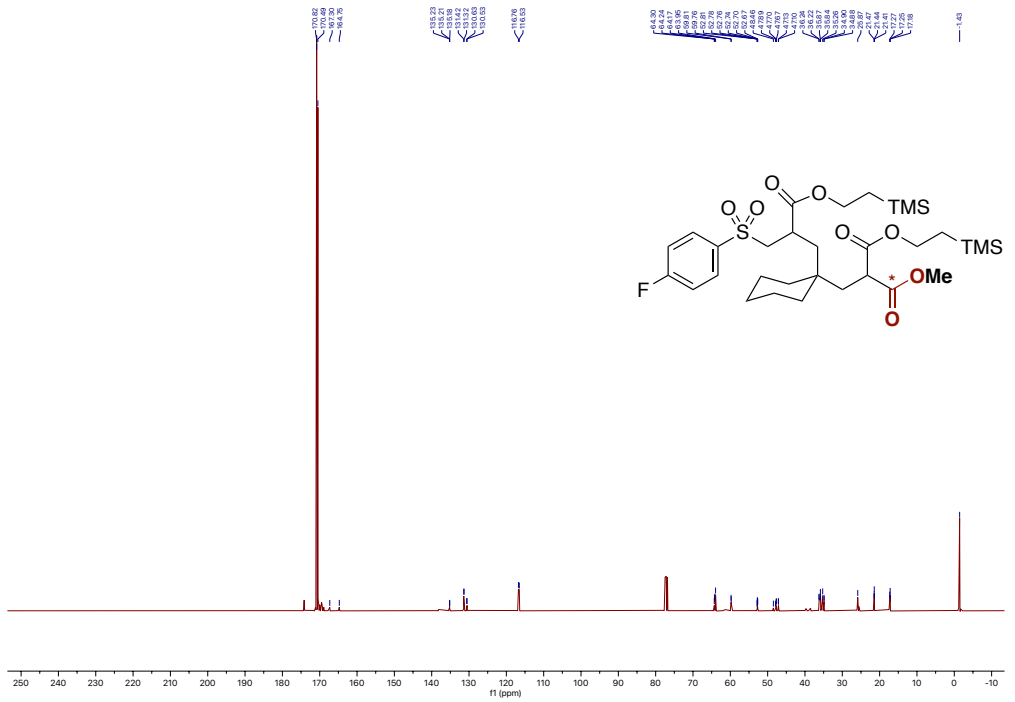

^{13}C spectrum (101 MHz, $CDCl_3$) of **28b**

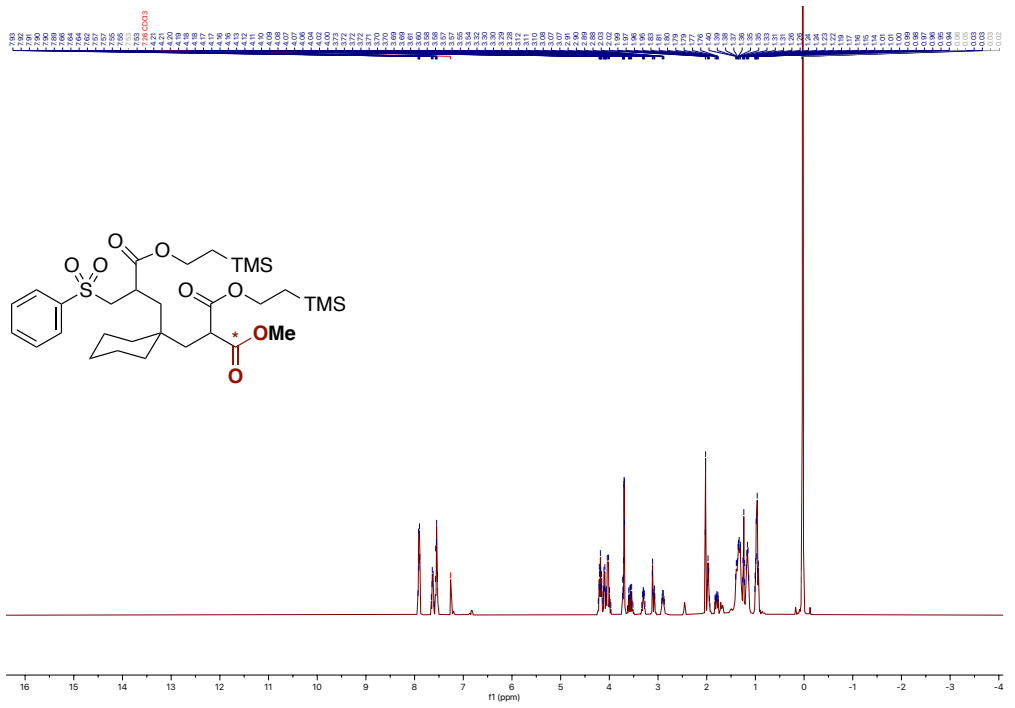

^{1}H spectrum (400 MHz, $CDCl_3$) of **28c**

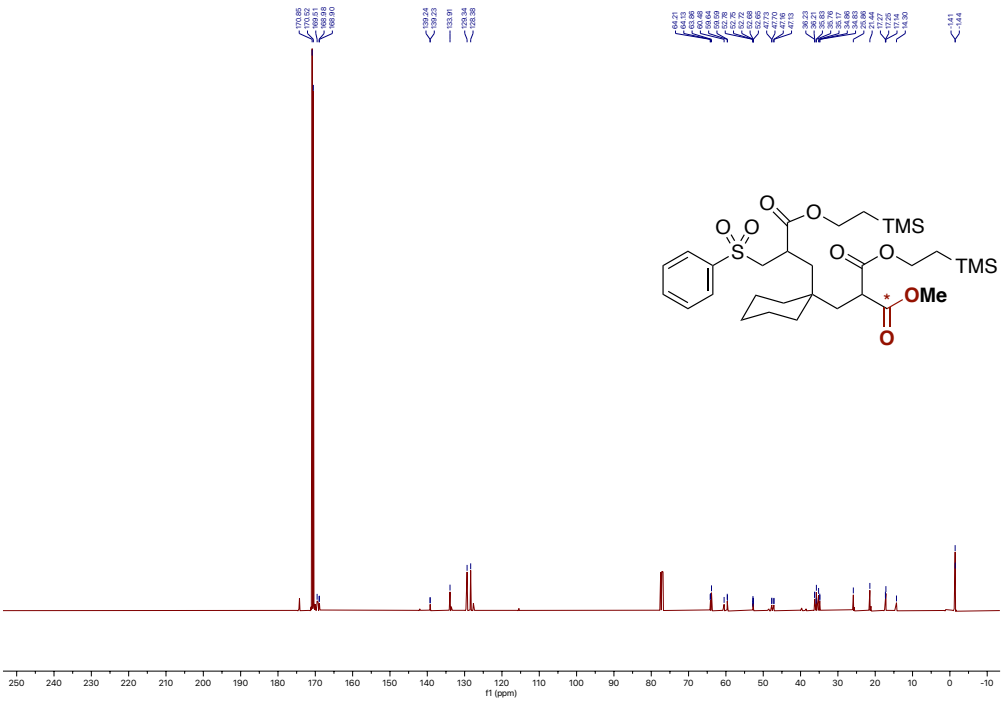

^{13}C spectrum (101 MHz, $CDCl_3$) of **28c**

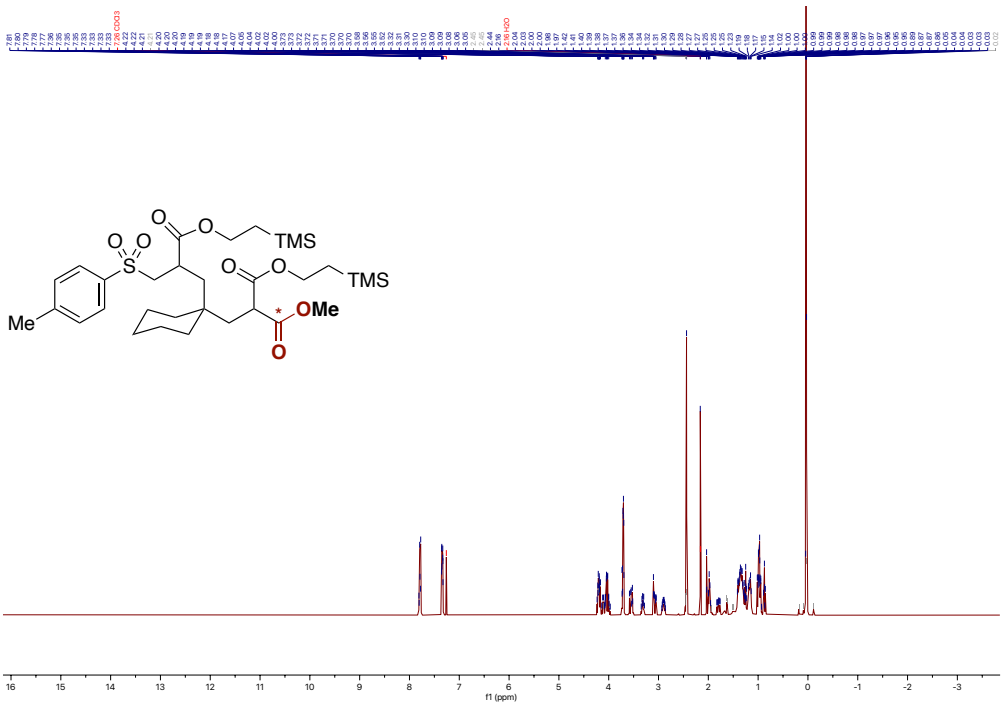

^{1}H spectrum (400 MHz, $CDCl_3$) of **28d**

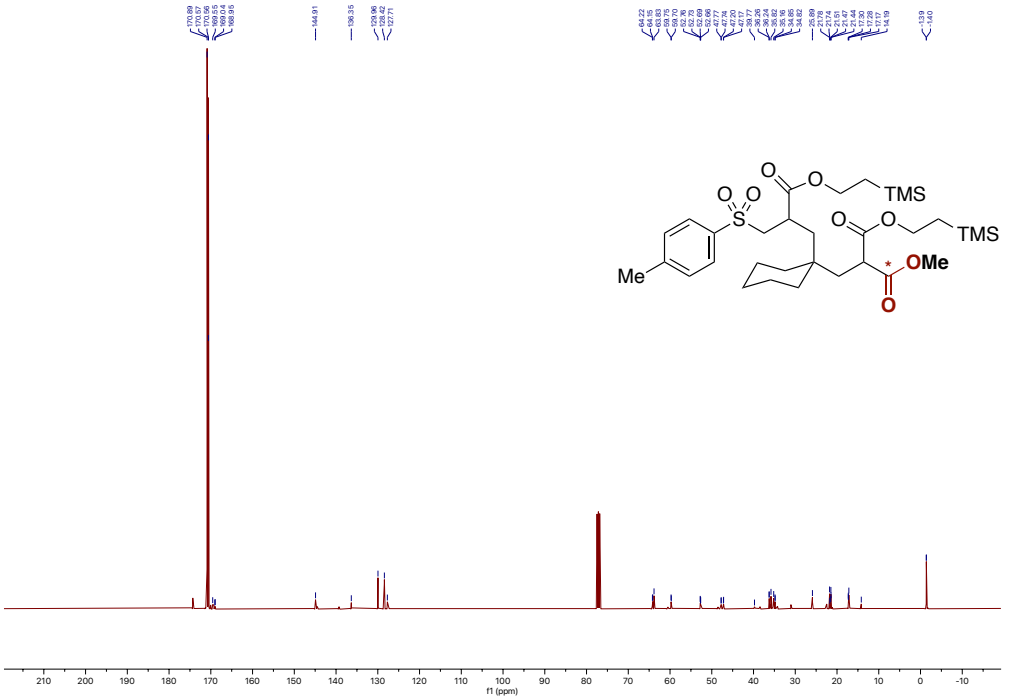

^{13}C spectrum (101 MHz, $CDCl_3$) of **28d**

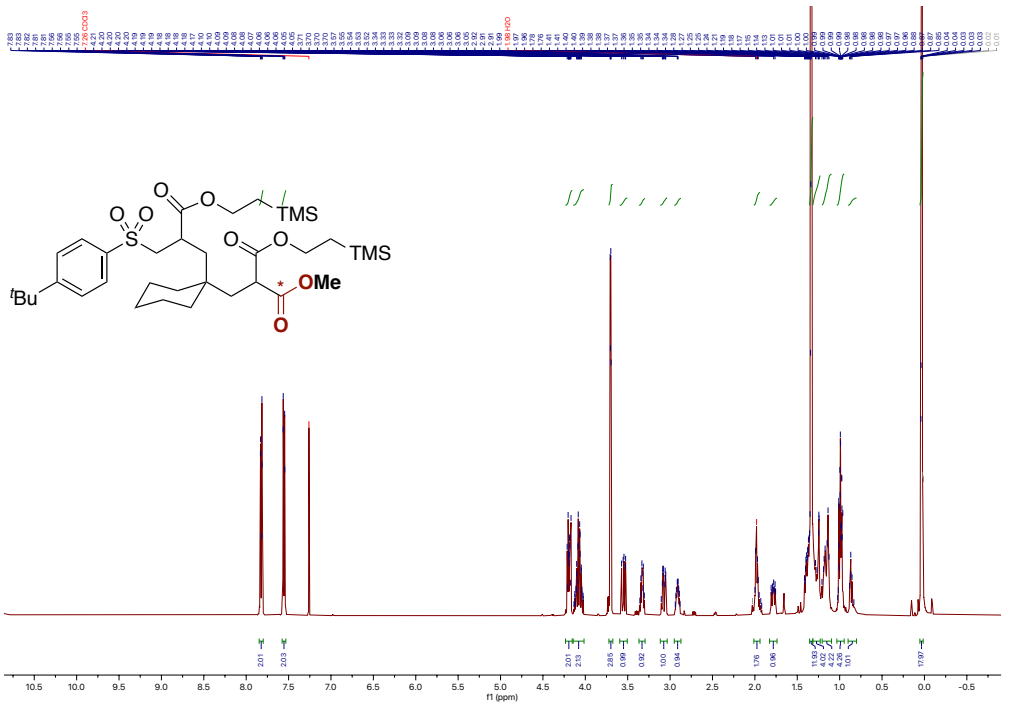

^{1}H spectrum (500 MHz, $CDCl_3$) of **28e**

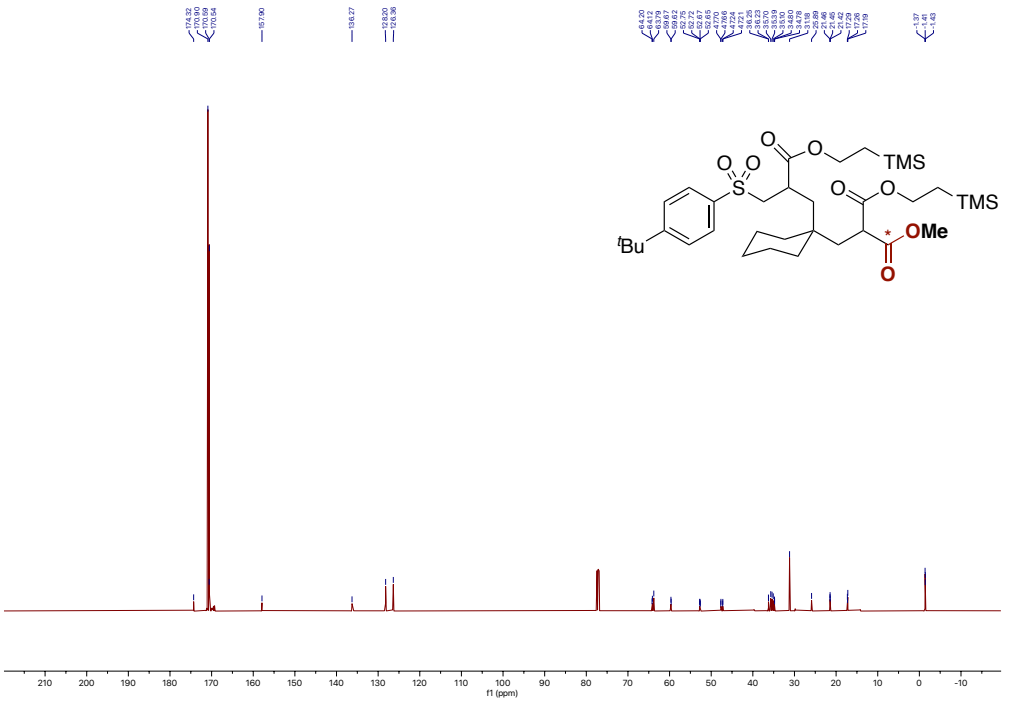

^{13}C spectrum (126 MHz, $CDCl_3$) of **28e**

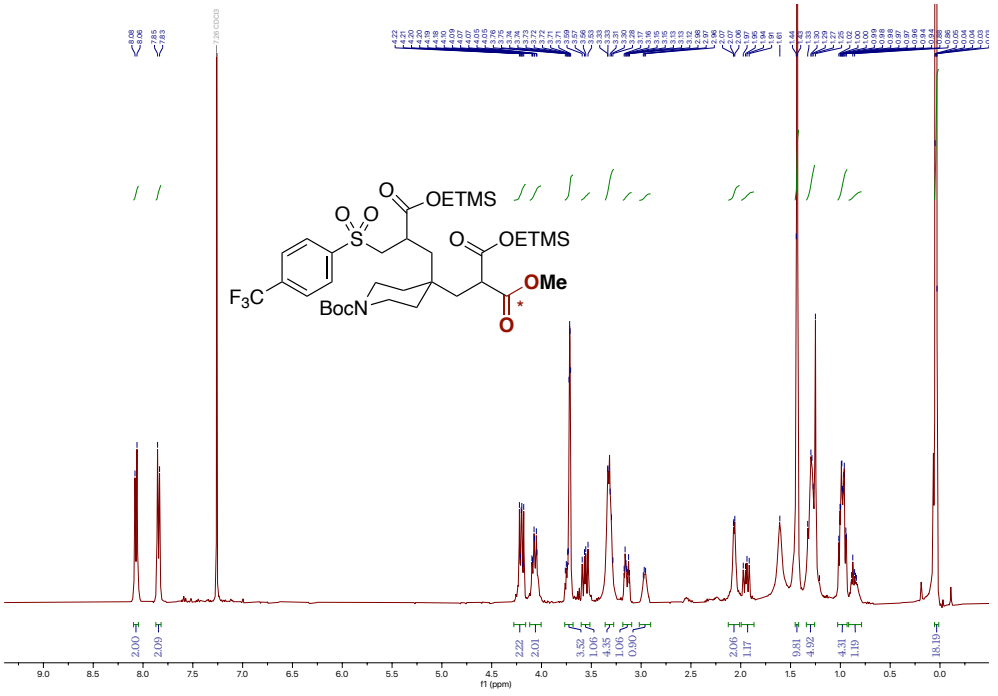

^{1}H spectrum (500 MHz, $CDCl_3$) of **28f**

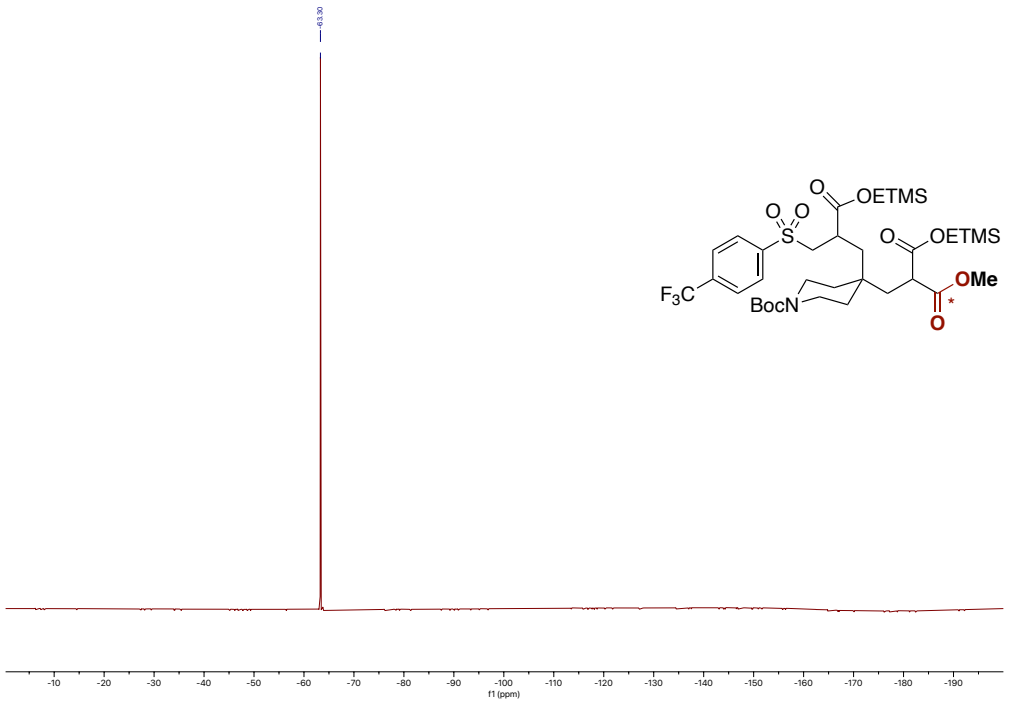

^{19}F spectrum (282 MHz, $CDCl_3$) of **28f**

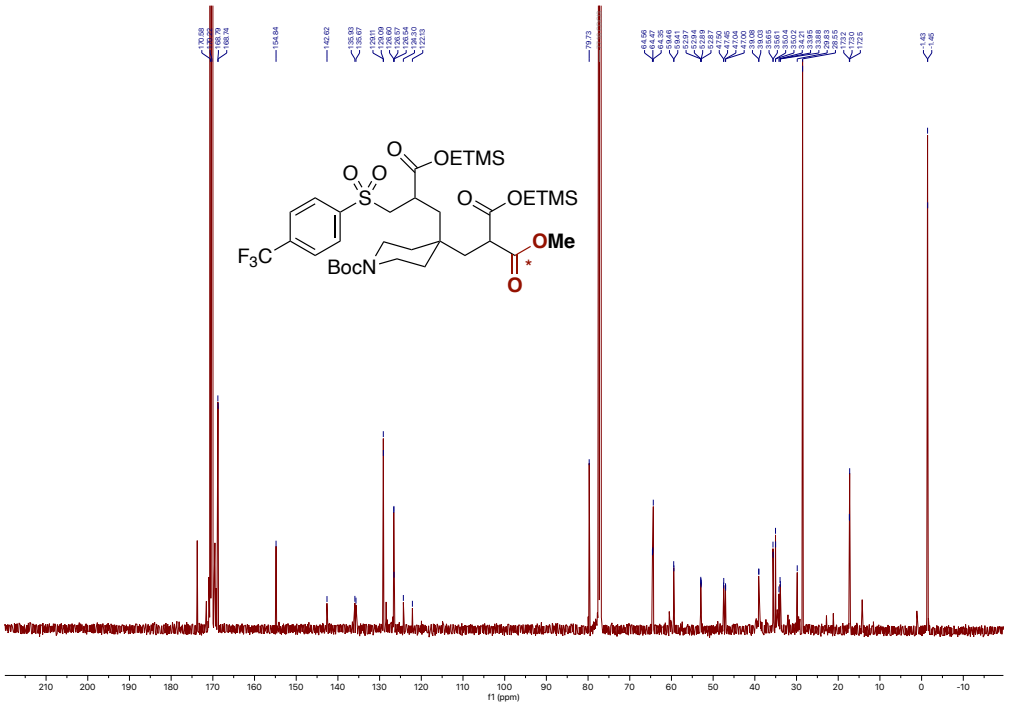

^{13}C spectrum (126 MHz, $CDCl_3$) of **28f**

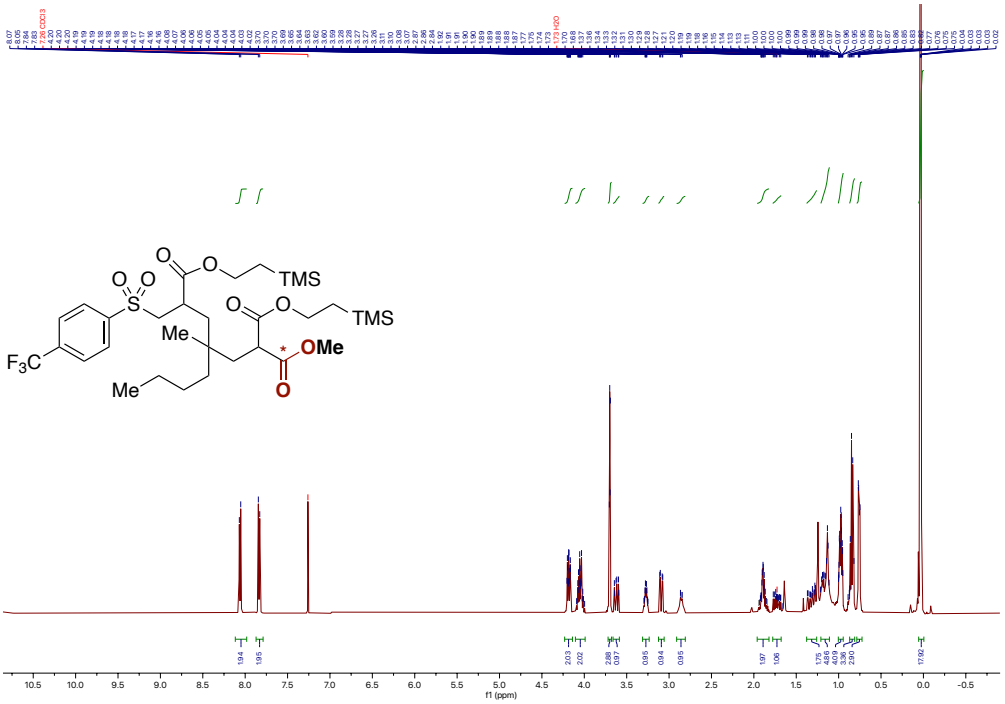

^{1}H spectrum (500 MHz, $CDCl_3$) of **28g**

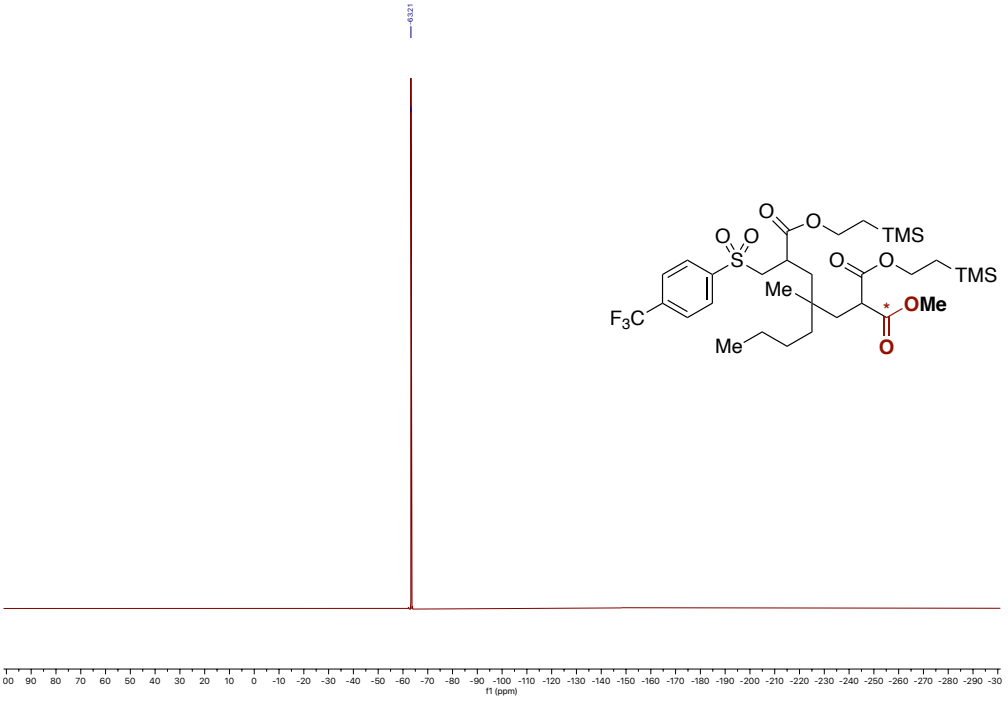

^{19}F spectrum (282 MHz, $CDCl_3$) of **28g**

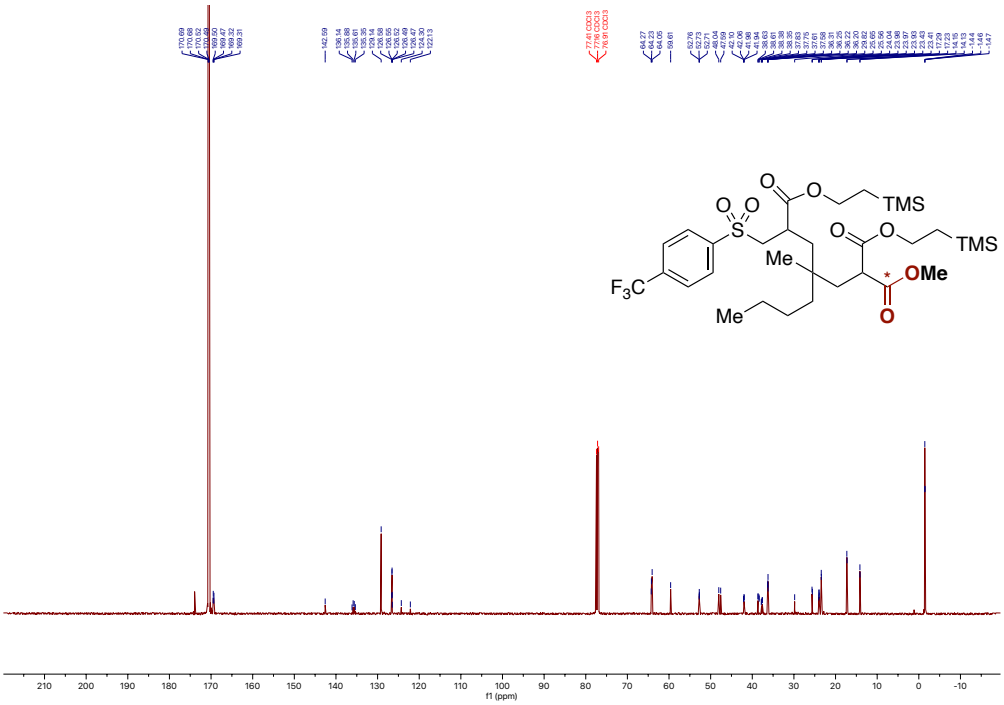

^{13}C spectrum (126 MHz, $CDCl_3$) of **28g**

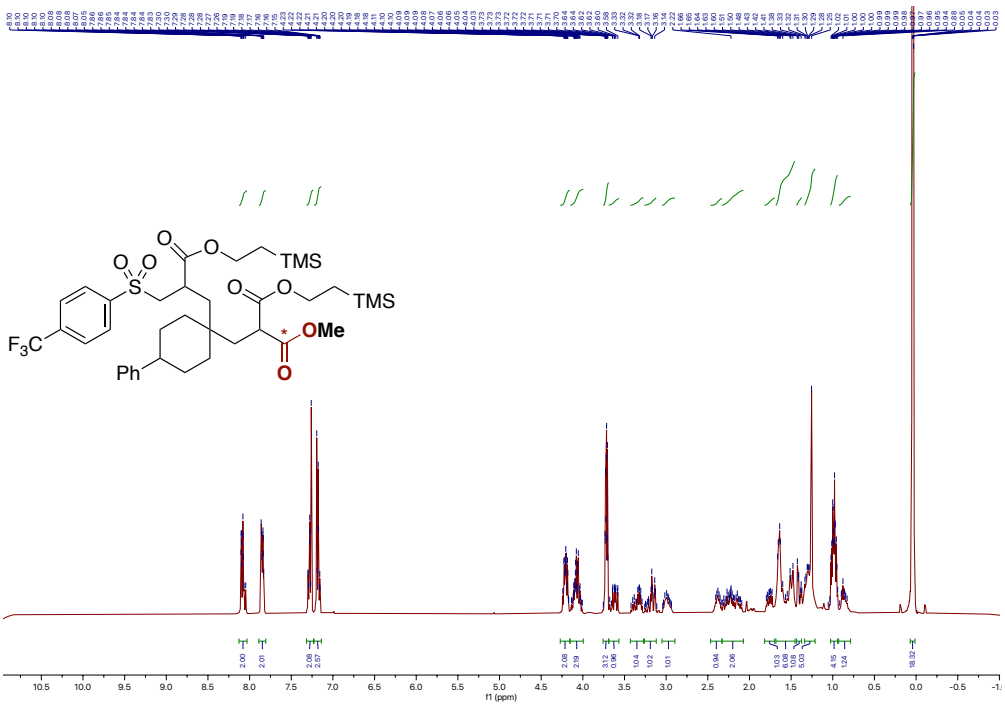

^{1}H spectrum (400 MHz, $CDCl_3$) of **28h**

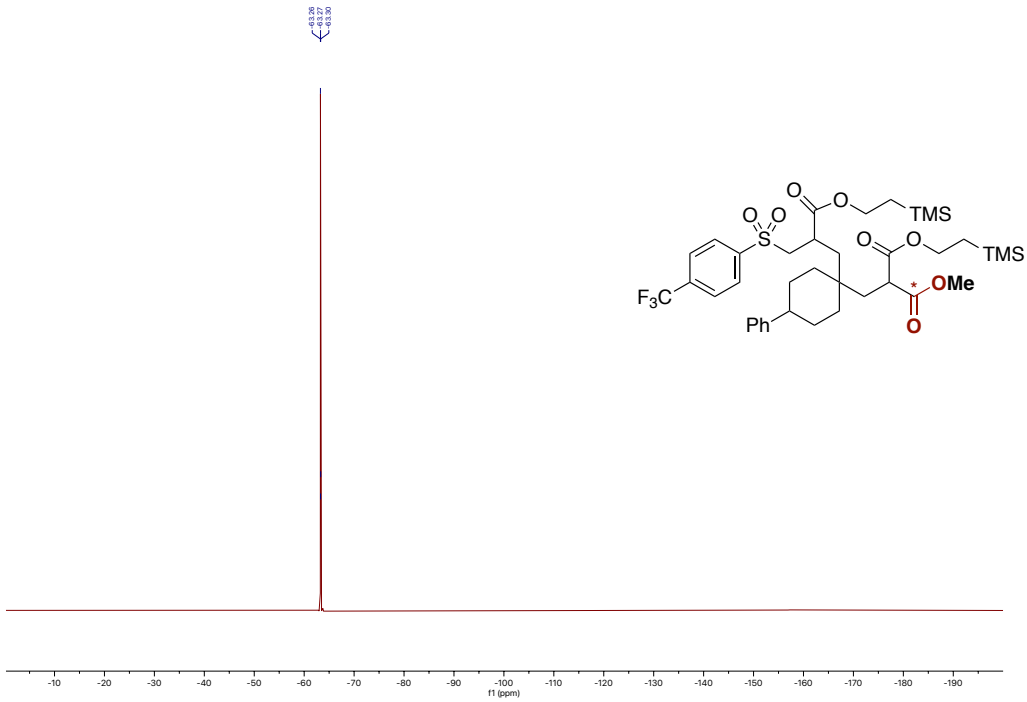

^{19}F spectrum (376 MHz, $CDCl_3$) of **28h**

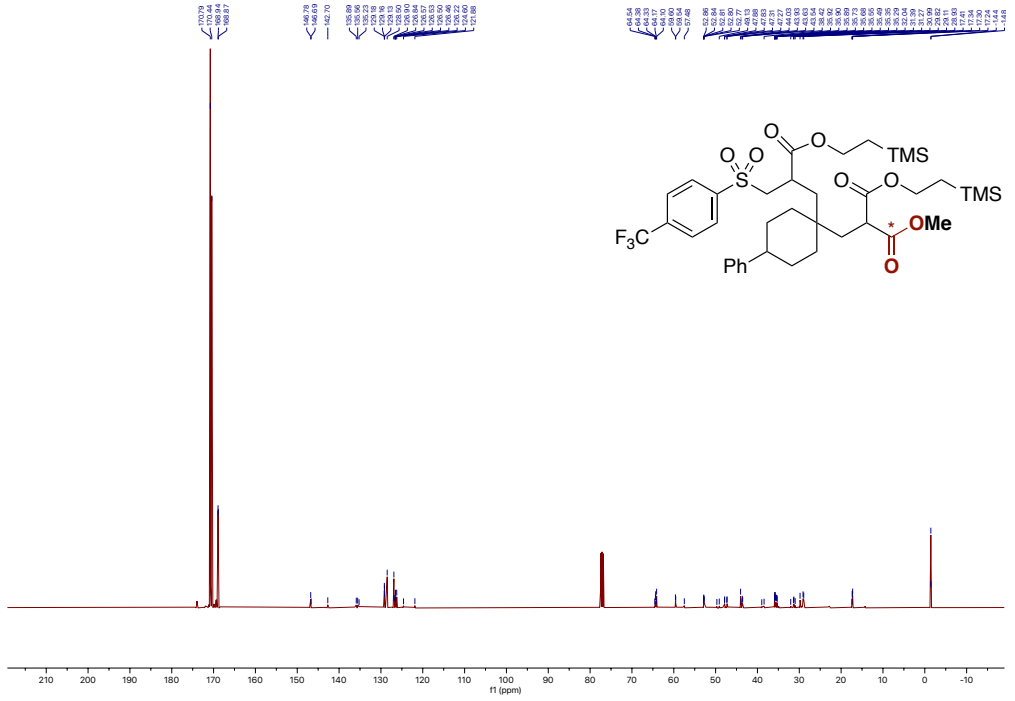

^{13}C spectrum (101 MHz, $CDCl_3$) of **28h**

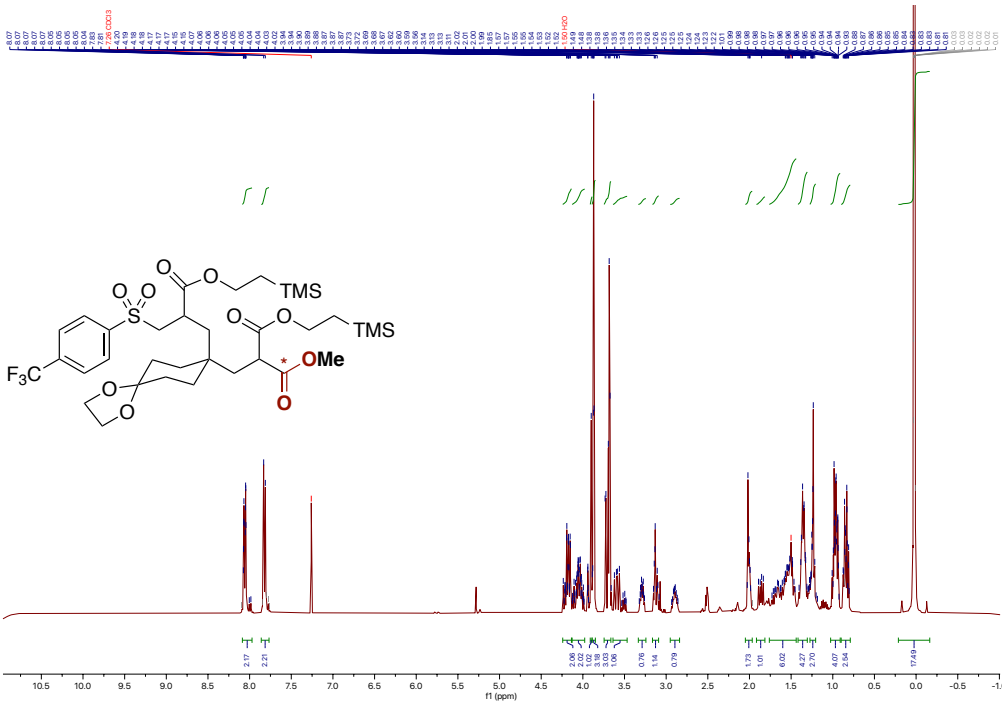

^{1}H spectrum (400 MHz, $CDCl_3$) of **28i**

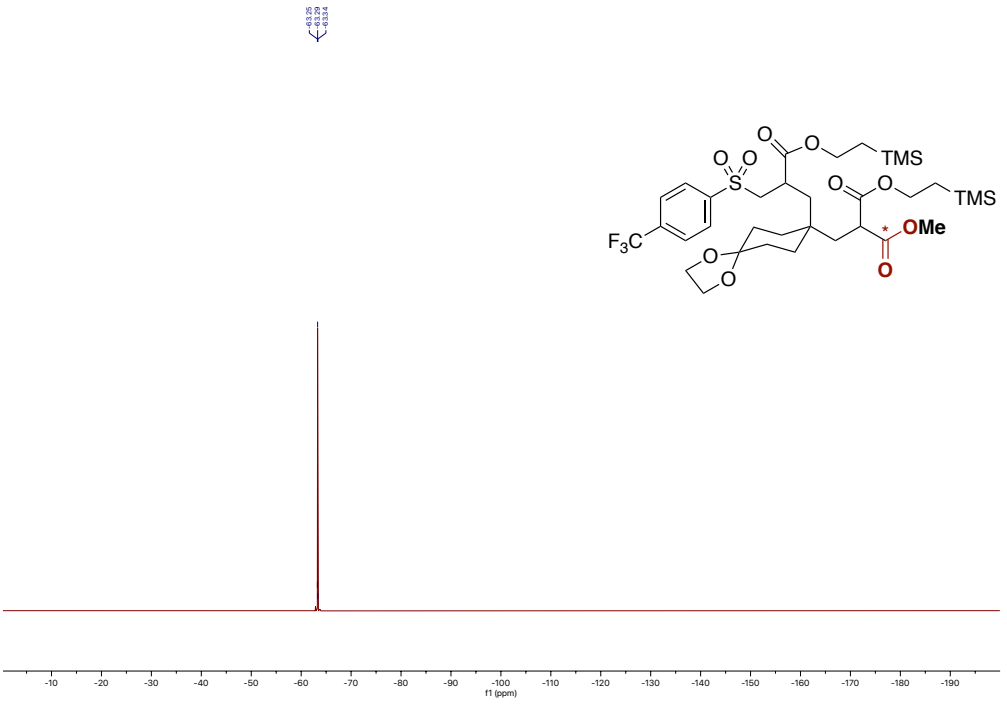

^{19}F spectrum (376 MHz, $CDCl_3$) of **28i**

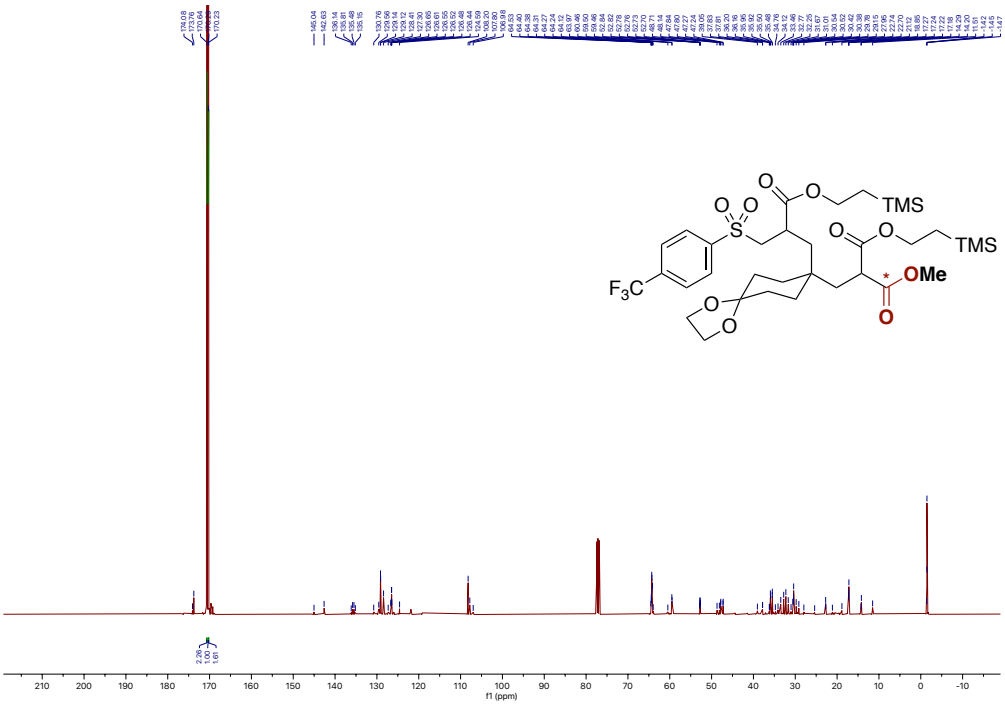

^{13}C spectrum (101 MHz, $CDCl_3$) of **28i**

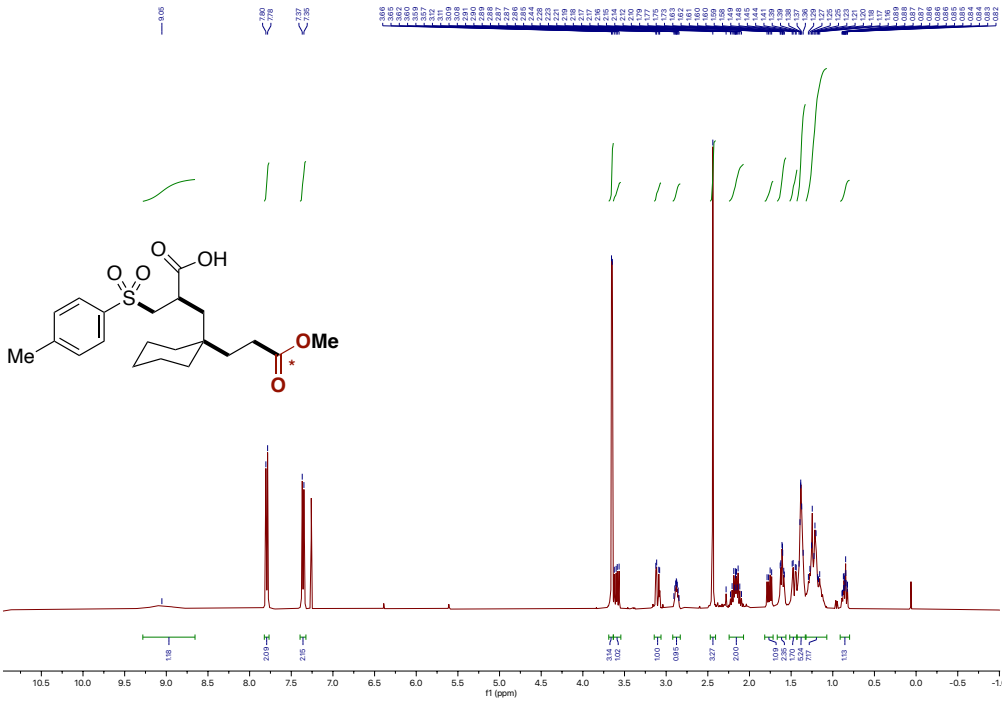

^{1}H spectrum (400 MHz, $CDCl_3$) of **28j**

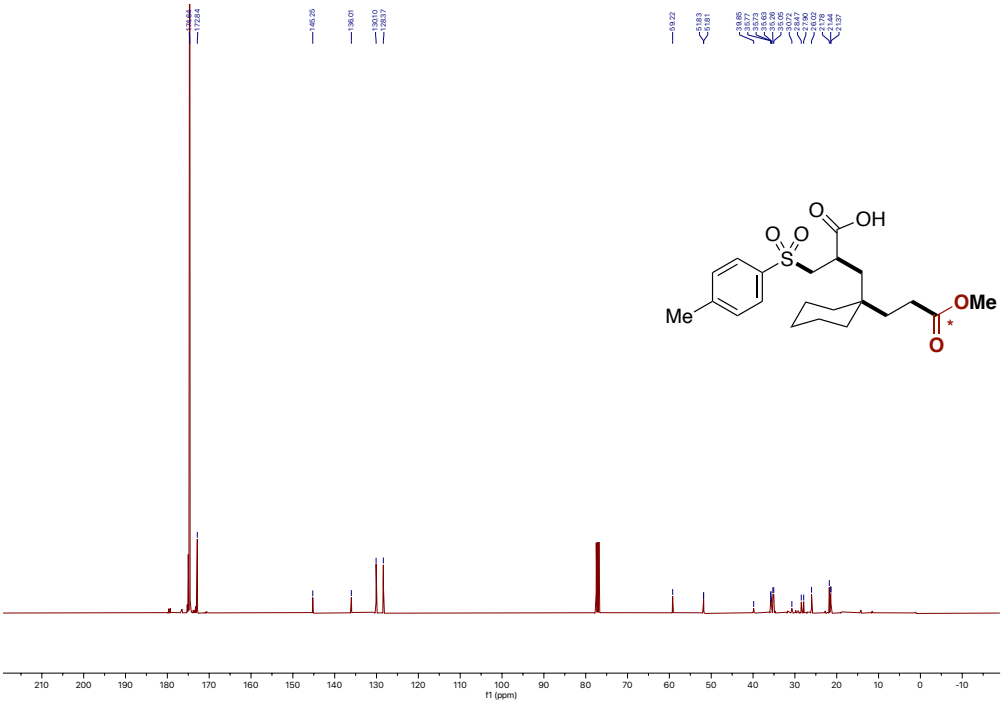

^{13}C spectrum (101 MHz, $CDCl_3$) of **28j**

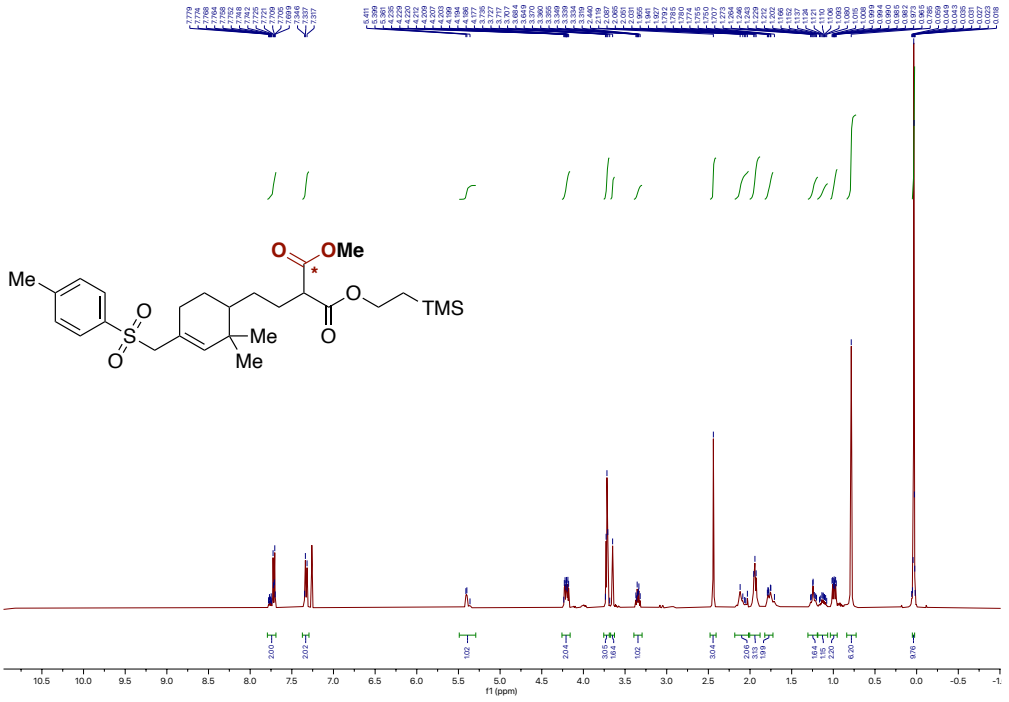

^{1}H spectrum (400 MHz, $CDCl_3$) of **32**

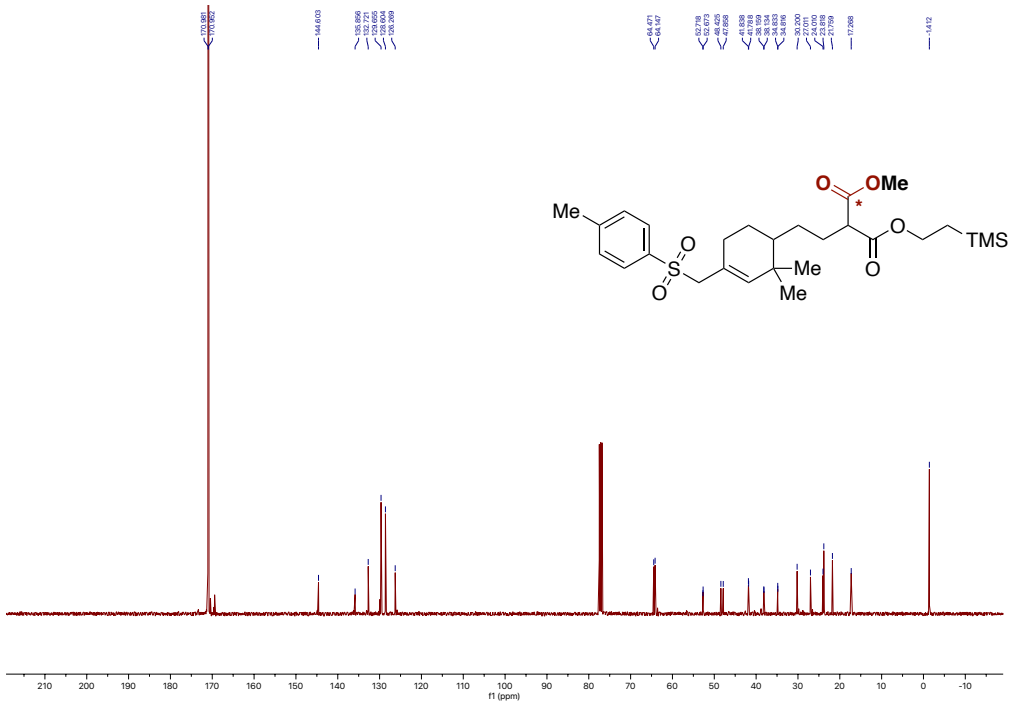

^{13}C spectrum (101 MHz, $CDCl_3$) of **32**

2.8. References

(1) Kondev, F. G.; Wang, M.; Huang, W. J.; Naimi, S.; Audi, G. The NUBASE2020 Evaluation of Nuclear Physics Properties. *Chin. Phys. C* **2021**, *45*, 030001. https://doi.org/10.1088/1674-1137/abddae.

(2) Elmore, C. S. Chapter 25 The Use of Isotopically Labeled Compounds in Drug Discovery. In *Annual Reports in Medicinal Chemistry*; Elsevier, **2009**,44, 515–534. https://doi.org/10.1016/S0065-7743(09)04425-X.

(3) Voges, R.; Heys, J. R.; Moenius, T. *Preparation of Compounds Labeled with Tritium and Carbon-14*, 1st ed.; Wiley, **2009**. https://doi.org/10.1002/9780470743447.

(4) Hanson, J. R. *The Organic Chemistry of Isotopic Labelling*; The Royal Society of Chemistry, **2011**. https://doi.org/10.1039/9781839169076.

(5) Bragg, R. A.; Sardana, M.; Artelsmair, M.; Elmore, C. S. New Trends and Applications in Carboxylation for Isotope Chemistry. *J. Label. Compd. Radiopharm.* **2018**, *61*, 934–948. https://doi.org/10.1002/jlcr.3633.

(6) Kingston, C.; Wallace, M. A.; Allentoff, A. J.; deGruyter, J. N.; Chen, J. S.; Gong, S. X.; Bonacorsi, S.; Baran, P. S. Direct Carbon Isotope Exchange through Decarboxylative Carboxylation. *J. Am. Chem. Soc.* **2019**, *141*, 774–779. https://doi.org/10.1021/jacs.8b12035.

(7) Tortajada, A.; Duan, Y.; Sahoo, B.; Cong, F.; Toupalas, G.; Sallustrau, A.; Loreau, O.; Audisio, D.; Martin, R. Catalytic Decarboxylation/Carboxylation Platform for Accessing Isotopically Labeled Carboxylic Acids. *ACS Catal.* **2019**, *9*, 5897–5901. https://doi.org/10.1021/acscatal.9b01921.

(8) Destro, G.; Loreau, O.; Marcon, E.; Taran, F.; Cantat, T.; Audisio, D. Dynamic Carbon Isotope Exchange of Pharmaceuticals with Labeled CO_2. *J. Am. Chem. Soc.* **2019**, *141*, 780–784. https://doi.org/10.1021/jacs.8b12140.

(9) Kong, D.; Munch, M.; Qiqige, Q.; Cooze, C. J. C.; Rotstein, B. H.; Lundgren, R. J. Fast Carbon Isotope Exchange of Carboxylic Acids Enabled by Organic Photoredox Catalysis. *J. Am. Chem. Soc.* **2021**, 143, 2200–2206. https://doi.org/10.1021/jacs.0c12819.

(10) Yoo, W.-J.; Zhao, L.; Li, C.-J. The A3-Coupling (Aldehyde–Alkyne–Amine) Reaction: A Versatile Method for the Preparation of Propargylamines. *Aldrichimica Acta* **2011**, *44*, 43–51.

(11) Peshkov, V. A.; Pereshivko, O. P.; Van Der Eycken, E. V. A Walk around the A3-Coupling. *Chem. Soc. Rev.* **2012**, *41*, 3790. https://doi.org/10.1039/c2cs15356d.

(12) Parsaee, F.; Senarathna, M. C.; Kannangara, P. B.; Alexander, S. N.; Arche, P. D. E.; Welin, E. R. Radical Philicity and Its Role in Selective Organic Transformations.

Nat. Rev. Chem. **2021**, *5*, 486–499. https://doi.org/10.1038/s41570-021-00284-3.

(13) Gansäuer, A.; Lauterbach, T.; Geich-Gimbel, D. Polarity Matching of Radical Trapping: High Yielding 3- *Exo* and 4- *Exo* Cyclizations. *Chem. – Eur. J.* **2004**, *10*, 4983–4990. https://doi.org/10.1002/chem.200400685.

(14) Tan, G.; Paulus, F.; Rentería-Gómez, Á.; Lalisse, R. F.; Daniliuc, C. G.; Gutierrez, O.; Glorius, F. Highly Selective Radical Relay 1,4-Oxyimination of Two Electronically Differentiated Olefins. *J. Am. Chem. Soc.* **2022**, *144*, 21664–21673. https://doi.org/10.1021/jacs.2c09244.

(15) Paulus, F.; Stein, C.; Heusel, C.; Stoffels, T. J.; Daniliuc, C. G.; Glorius, F. Three-Component Photochemical 1,2,5-Trifunctionalizations of Alkenes toward Densely Functionalized Lynchpins. *J. Am. Chem. Soc.* **2023**, *145*, 23814–23823. https://doi.org/10.1021/jacs.3c08898.

(16) Tan, G.; Paulus, F.; Petti, A.; Wiethoff, M.-A.; Lauer, A.; Daniliuc, C.; Glorius, F. Metal-Free Photosensitized Radical Relay 1,4-Carboimination across Two Distinct Olefins. *Chem. Sci.* **2023**, *14*, 2447–2454. https://doi.org/10.1039/D2SC06497A.

(17) Giese, B. Formation of CC Bonds by Addition of Free Radicals to Alkenes. *Angew. Chem. Int. Ed. Engl.* **1983**, *22*, 753–764. https://doi.org/10.1002/anie.198307531.

(18) Knobloch, E.; Brückner, R. Selective Cleavage and Decarboxylationof β-Keto Esters Derived from (Tri-methylsilyl)Ethanolin the Presence of β-Keto Esters Derived from Other Alcohols. *Synlett* **2008**, *2008*, 1865–1869. https://doi.org/10.1055/s-2008-1078568.

(19) Wagner, P. J.; Sedon, J. H.; Lindstrom, M. J. Rates of Radical Beta Cleavage in Photogenerated Diradicals. *J. Am. Chem. Soc.* **1978**, *100*, 2579–2580. https://doi.org/10.1021/ja00476a068.

CHAPTER 3. Kinetically-Controlled Ni-Catalyzed Direct Carboxylation of Unactivated Secondary Alkyl Bromides

Project done in collaboration with: Dr. Jacob Davies, Bjørn Carvalho, Dr. Basudev Sahoo, Dr. Craig S. Day, Prof. Francisco Juliá-Hernández, Dr. Yaya Duan, Dr. Alvaro Velasco-Rubio, Dr. Marc Obst, Dr. Per-Ola Norrby and Prof. Kathrin H. Hopmann. The results presented are a combination of the contribution of all the people listed above.

3.1. Introduction

As was discussed in the general introduction, carboxylation reactions have come a long way, starting from stoichiometric carboxylation with simple nucleophiles to modern catalytic methods making use of elaborated systems. The contents of this chapter focus on the field of reductive catalytic carboxylation, where the use of sacrificial reductants is required for catalyst turnover to occur. The first report of the sort was disclosed in 2009, when Martin & coworkers showed a palladium catalyzed carboxylation of aryl bromides with CO_2 (Scheme 3.1, top).[1] The work made use of $Pd(OAc)_2$, *t*BuXPhos as ligand and $ZnEt_2$ as reductant at 40°C in DMA. Additionally, 10 atm of CO_2 pressure were used for optimal reactivity. The first appearance of nickel as a catalyst, within reductive catalytic carboxylation reactions was when the group of Tsuji reported a similar method as Martin but using $NiCl_2(PPh_3)_2$ as precatalyst for the carboxylation of more challenging aryl chlorides (Scheme 3.1, middle).[2] The ease of nickel to perform oxidative addition into aryl chlorides compared to palladium was key for the improvement over Martin's report. Nickel's use, in turn, allowed for the introduction of a new sacrificial reductant in the field, powdered manganese metal.

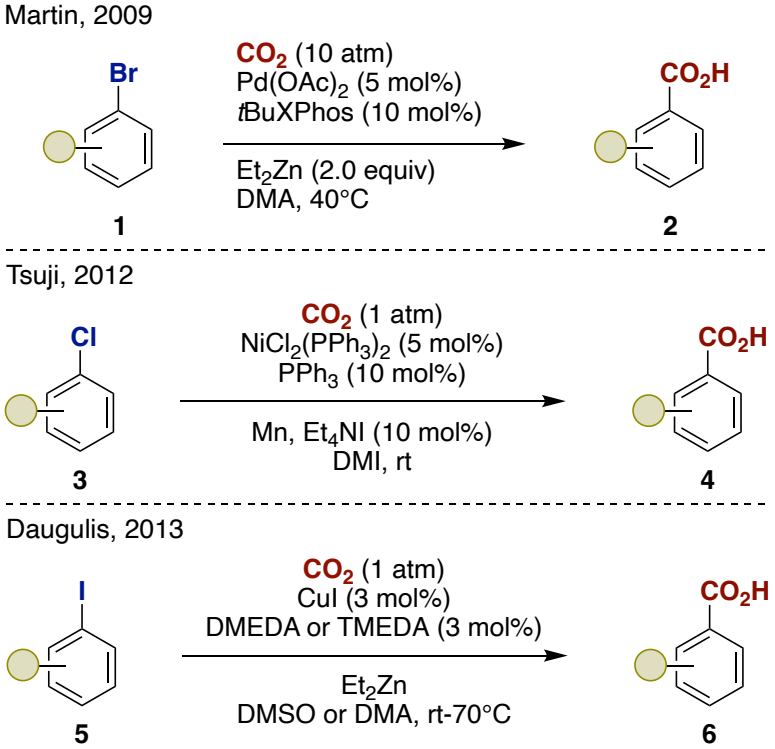

Scheme 3.1: Martin's, Tsuji's and Daugulis' reductive carboxylation reports.

The reaction developed by the group of Tsuji allowed for more available aryl chlorides to be used while operating at a decreased pressure compared to Martin's conditions, using 1 atm, which set a gold standard for future reports of the sort. Manganese is also an operationally simple reductant, although being heterogeneous which comes with its own drawbacks when scaling up a reaction. In 2013, Daugulis & coworkers reported the reductive catalytic carboxylation of aryl iodides (Scheme 3.1, bottom), which was done with a copper catalyst. Although diethyl zinc, a pyrophoric and generally reactive compound, was used as reductant, the group of Daugulis showed that the methodology was amenable to ortho substituted starting materials, which was one of the limitations of the previous reports from both Martin and Tsuji. All three of these protocols (Scheme 3.1), together, allow for the carboxylation of a broad variety of aryl halides. Nevertheless, further improvement could be made for making the carboxylation of aryl halides milder, especially given the sacrificial reductants used. The implementation of photochemistry has allowed for different other reductants to be used instead.[3] Additionally, pseudohalides, electrophiles having a similar role as an organic halide but not containing a halide atom such as triflates or sulfonates, have been investigated too.[3]

The next step in the reductive carboxylation arena was to carboxylate a sp^3 carbon. Naturally, the first report consisted of the carboxylation of benzyl halides, which was done by Martin *et al.* in 2013 (Scheme 3.2).[4] Within the same report, the group showed the carboxylation of primary, secondary and tertiary benzyl halides, individual conditions for the primary halides were identified. In all cases, the catalyst was based on $NiCl_2$ precatalysts with electron-rich phosphines. Zinc dust was used as reductant along with Lewis pairs such as HBF_4 or Bu_4NI. The group also showed that subjecting a potential Ni(II) benzyl intermediate to CO_2 did not yield any product but doing the otherwise similar reaction with addition of Zn led to a high conversion to the product, showing the innocent role of Ni(II) in the carboxylation step and involvement of a more reduced species. The Ni(II) complex **Ni-1** that was isolated showed an η^3 type coordination from the benzylic carbon along with two other carbons of the aromatic ring. This suggests that Ni as a catalyst might be kinetically stable at benzylic sites given the stabilization by extra coordination. This stabilization, in turn, might prevent the reaction to undergo unproductive pathways, notably BHE.

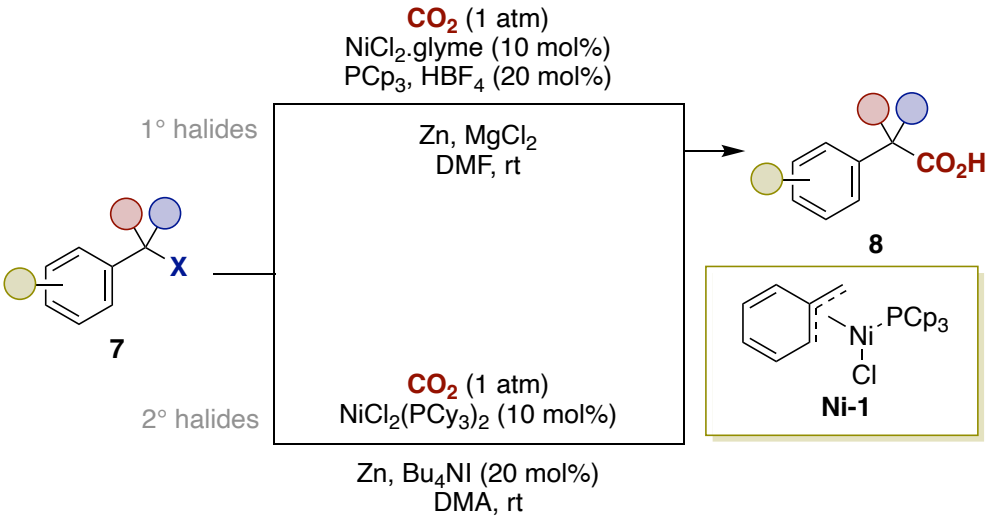

Scheme 3.2: Martin's benzyl halide carboxylation.

While the benzylic site has been suggested to be more robust against unwanted BHE processes, this would not be the same when it comes to unactivated carbon atoms bearing vicinal hydrogen atoms. The key for success in this endeavor came from Martin, in 2014, when disclosing the carboxylation of primary alkyl bromides with nickel catalysis (Scheme 3.3).[5] The ligand used in their report, being the first time such ligand class was used in the carboxylation arena, was a 1,10-phenanthroline bearing two substituents, on positions 2 and 9. The authors claimed that the substituents would in fact make the catalyst more robust with better activity and stability. The efficiency of the system is reflected by the absence of additives in the reaction. The scope of the reaction was broad, showcasing various functional groups, including some groups typically regarded as reactive within organometallic catalysis, such as aryl stannanes, phenols, aryl tosylates and aryl chlorides. The authors also showed the compatibility of primary alkyl sulfonates with the reaction after slight condition modifications. Since this work, NN ligands of the phenanthroline type, but also related bipyridines, became the state-of-the-art ligands within the field of nickel carboxylation. By substituting the ligand with electron donating methyl groups on other positions, the Martin group managed to further improve their results, carboxylating primary alkyl chlorides including a few examples of secondary and tertiary chlorides.[6] Although the substrates were somewhat biased due to their structures using C_2-symmetric secondary bromides and adamantyl bromide as tertiary bromide, this also consisted of the first report of carboxylation on all types of *unactivated* non-primary alkyl halides, namely secondary and tertiary alkyl halides.

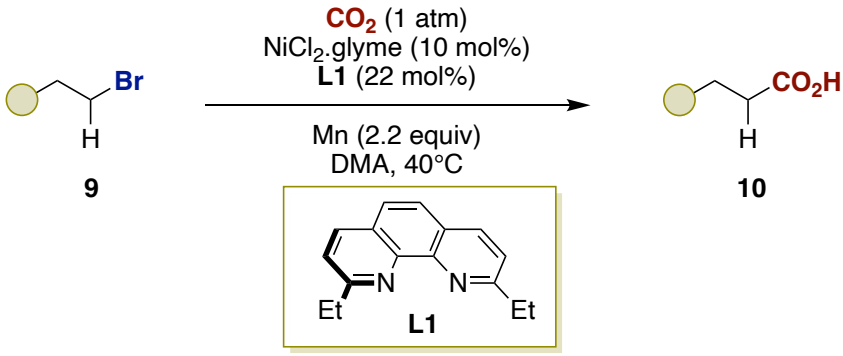

Scheme 3.3: Martin's primary alkyl bromide carboxylation.

After focusing on primary alkyl halides, the group then moved their efforts on the reactivity of *unactivated* secondary alkyl bromides specifically. In 2017, Martin & coworkers disclosed a remote C-H carboxylation from internal *unactivated* secondary bromides, leading to a carboxylation event happening at more thermodynamically favored positions for nickel.[7] The work therefore consisted of the merging of known carboxylation processes at benzylic and primary positions with what was at the time an emerging field, nickel-catalyzed chain-walking chemistry.[8] The general picture of the methodology described consists of the formation of fatty acids from internal secondary bromide precursors, regardless of the exact position of the bromide. Indeed, even isomeric mixtures of secondary alkyl bromides would lead to a sole product after reaction, as depicted in Scheme 3.4.

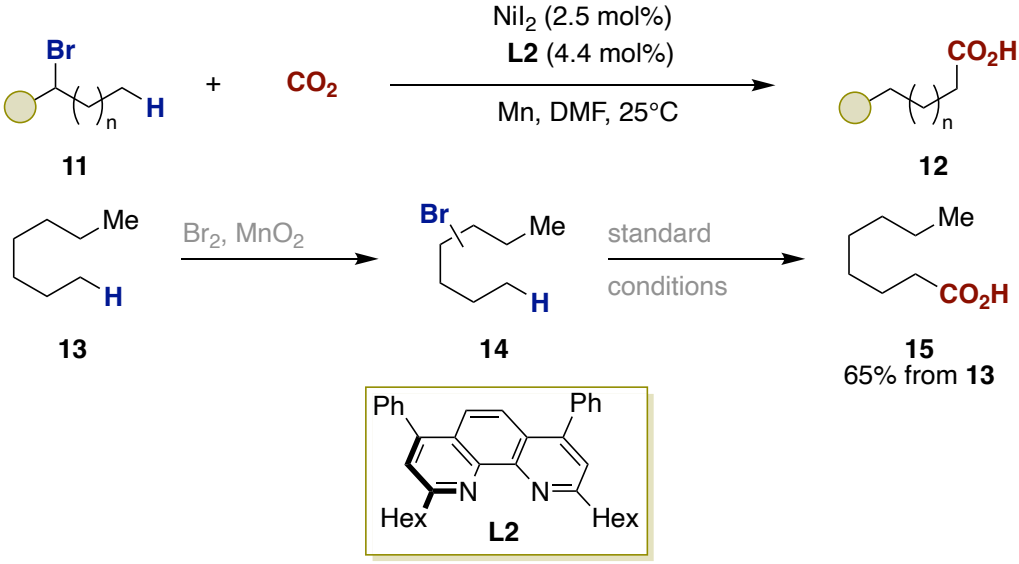

Scheme 3.4: Martin's chain-walking reductive carboxylation methodology.

For example, alkane **13** is brominated in a non-selective manner from elemental bromine and MnO_2, leading to the bromide mixture **14**, which after being submitted to the standard conditions give caprylic acid **15** as sole product in 65% yield over two steps. The conditions disclosed use NiI_2 as a nickel source in a 2.5 mol% amount, with a designed phenanthroline ligand allowing the process to reach completion. Manganese powder was used as a reductant in the reaction with DMF at 25°C. As depicted on Scheme 3.5, if both a carbonyl and terminal methyl would be present on the brominated chain **11a**, the authors demonstrated the ability to selectively carboxylate one of these positions by the sole change of reaction temperature, giving **12a** or **12b**. The observed selectivities ranged from good to excellent. This report from Martin & coworkers on the chain-walking carboxylation of secondary alkyl bromides is perhaps the work that is the most relevant for the context of the current chapter of the thesis, as a *direct* carboxylation from similar starting materials will be discussed, avoiding any BHE processes.

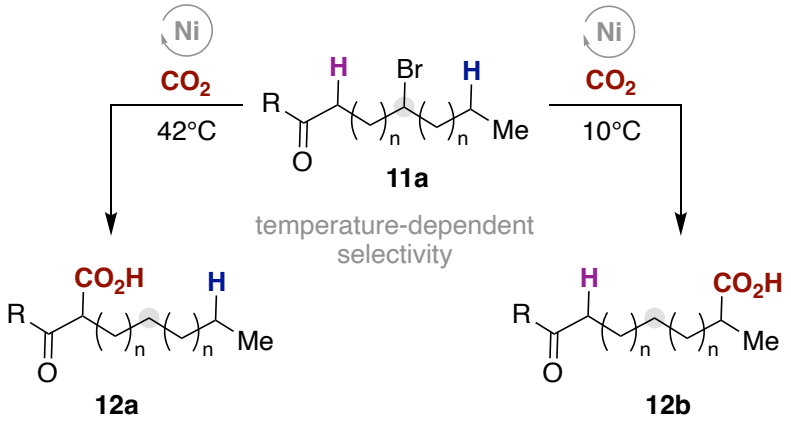

Scheme 3.5: Temperature-dependent chain-walking selectivity.

Moving on to different methodologies, a few mentions can be made in the context of photoredox chemistry when it comes to reductive carboxylation reactions. The first report of photoredox Ni carboxylation was disclosed by the König group in 2018 with a selective hydrocarboxylation of styrenes, which could be selective depending on the conditions used (Scheme 3.6).[9] The authors showed that a reductive system could efficiently be obtained when combining a nickel neocuproine (or phosphine) complex, 4-CzIPN as PC and Hantzsch ester (HEH) as a sacrificial reductant.

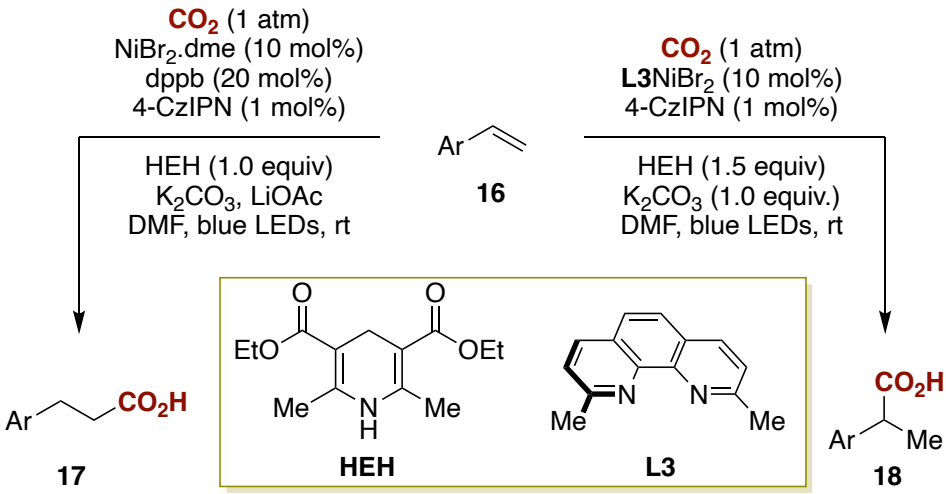

Scheme 3.6: König's reductive hydrocarboxylation of styrenes.

In comparison to the methodologies shown prior in this introduction, the Markovnikov-selective hydrocarboxylation can be compared to the last steps of the remote chain-walking carboxylation chemistry from Martin. A Ni-H species inserts into a double bond, to form a stable alkyl-Ni intermediate which, once reduced to Ni(I), is able to carboxylate the alkyl counterpart to give the desired product. It is therefore known that part of a chain-walking process can coexist with metallaphotoredox chemistry, and hence led to a second report from the König group, this time collaborating with Martin.[10] This work thus consisted in a full chain-walking carboxylation process, as envisioned by Martin in his publication from 2017, but performed under a photocatalytic manifold. The conditions reported were very close to the initial publication from König, only slight modifications were made. The ligand used for the remote carboxylation of benzylic systems was the same, being **L3**. When applying this methodology on phenyl ring-free compounds (Scheme 3.7), the conditions were slightly modified again, but this time the ligand was changed too. The best ligand was shown to be **L4**. While the carboxylation was obtained in 49%, the selectivity was not excellent, although good, giving the ratio of $\mathbf{20_l}$:$\mathbf{20_r}$ as 83 to 17, respectively. While the formation of $\mathbf{20_r}$ was to be minimized in this case, a methodology specifically and selectively generating this compound would be of great interest. Indeed, given the fact that it had never been reported and would represent the first carboxylation done on *unactivated* secondary alkyl halides in a retentive manner, such a process would also allow for the difficult avoidance of undesired BHE. While Ni cross-couplings on secondary alkyl halides are known without chain walking,[11] this is not the case within the carboxylation arena, most likely due to the fact that the CO_2 incorporation step requires prior reduction of Ni(II) to

Ni(I). Carboxylation has been shown to happen at the Ni(I) stage for Ni-alkyl complexes and it is suspected that chain-walking happens at the Ni(II) stage.[12–16] Therefore, if the SET is slow, such as when heterogeneous metals are used as reductants, chain-walking will likely happen before carboxylation. The results from König & Martin showing a selectivity of 17% retained carboxylation is a sign that incorporating a homogeneous system increases the reduction kinetics and therefore gives the opportunity to design a system prioritizing the selective, retentive carboxylation event. The homogeneous environment thereof enables the ability for a retained carboxylation, while ligand design would most likely achieve it thanks to stabilization of intermediates and prevention of BHE side processes.

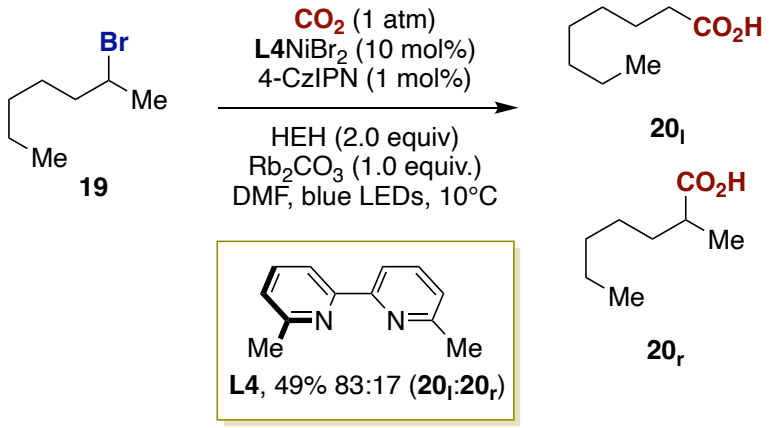

Scheme 3.7: König & Martin's photoredox remote carboxylation of secondary alkyl bromides.

3.2. General aim of the project

The reductive catalytic carboxylation of (pseudo)halides has received considerable attention over the last 15 years. Starting from aryl simple (pseudo)halides, all the way to photoredox remote C-H carboxylation techniques, . Nonetheless, the direct carboxylation of *unactivated* secondary alkyl halides has never been reported for non-biased starting materials, such as C_2-symmetric compounds, for which it cannot be distinguished whether chain-walking happened prior to carboxylation or not. The approach that was envisioned was to render the SET from Ni(II) to Ni(I) of a Ni-alkyl intermediate faster by employing controlled homogeneous conditions, such as a photoredox system. This strategy, according to our initial beliefs, should drastically increase the kinetics of the reduction and thus act to attenuate BHE which we believe to happen mostly at the Ni(II) oxidation state. Additional ligand design would likely help stabilize key intermediates, further diminishing undesired BHE.

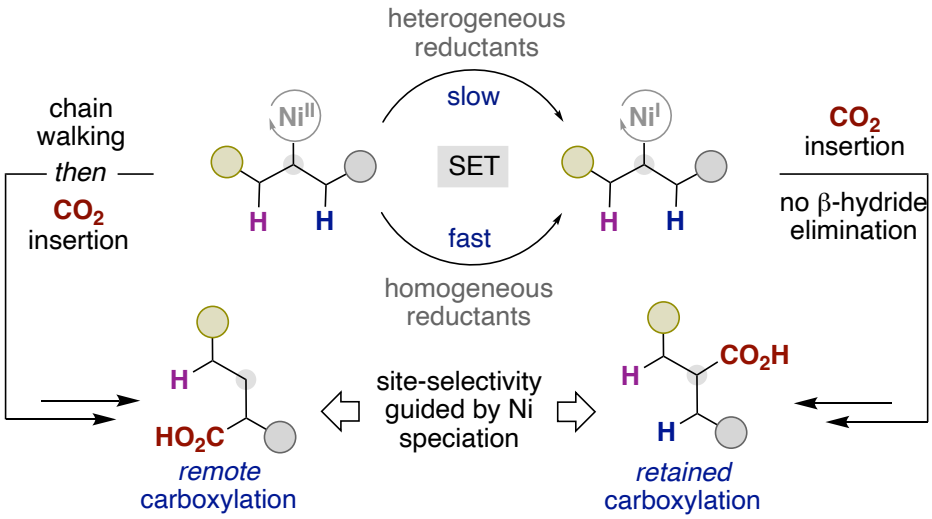

Figure 3.1: Site-selectivity guided by Ni speciation.

3.3. Optimization

The reaction discovery of this project started on the basis of the previous report from our group in collaboration with the König group.[10] We therefore started our investigation using similar conditions, with 2-bromoheptane **19** as starting material. We started with a ligand screen using $(TBA)_2[NiBr_4]$ as a Ni source, Table 3.1 shows a selection of ligands tried in the initial phase of the optimization. The precatalyst was used in 10 mol% while the ligand was used in slight excess of 15 mol% in total. The PC of choice was, as indicated, the same as in the previous report, 4-CzIPN, along with cesium carbonate as a base, in DMF at 20°C with one bar of carbon dioxide pressure. Both ligands that were used in the two previous reports of Ni photoredox carboxylation, **L3** and **L4**, gave carboxylation in 31 and 37% yield respectively, although with poor selectivity towards target product $\mathbf{20_{b(r)}}$. The reactions gave mostly linear, chain-walking product. Bulkier ligand **L5** gave the first result tending towards a retentive carboxylation with 64% selectivity, albeit with low carboxylation yield of 34%. Testing another phenanthroline with phenyl substituents (**L6**) did not improve the results obtained from **L3**, giving lower yield. Increasing further the bulkiness of the ligand, **L7** granted us gratifyingly with an excellent selectivity, showing no detectable traces of other carboxylic acids in the crude. introducing steric bulk around the nitrogen atoms of the ligand with n-hexyl groups, **L8** gave an improvedyield of 57% with good selectivity of 90% of desired product. When trying a different class of ligands, **L9** showed excellent selectivity with a low yield, when increasing the sterics, **L10** gave no carboxylation whatsoever. Finally, **L11** gave the best results with an excellent selectivity and a yield of 56%. We therefore continued our investigation with L**11** as ligand. As can be deduced with ease, the scaffold for a good ligand required bulky substituents next to the nitrogen atoms for selectivity improvements, the yield could instead beincreased with the introduction of *tert*-butyl groups on the 4,4' positions of the bipyridine. Phenanthroline did not show good compatibility with the reaction, neither did PyOx-type ligands.

Table 3.1: Initial ligand screen.

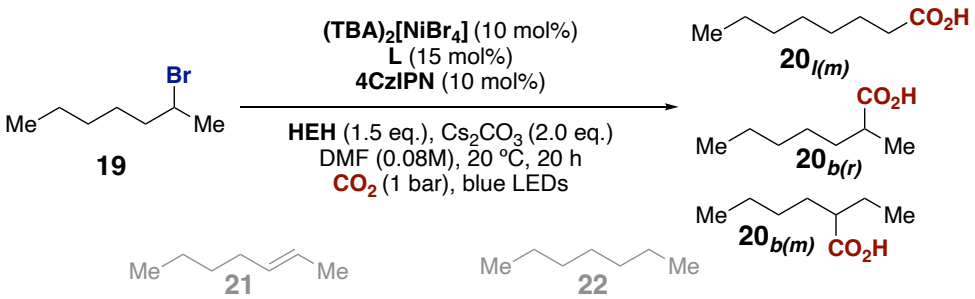

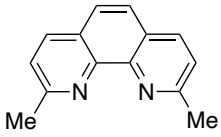

L3 Conv. >99%
20(31%), **21**(34%), **22**(3%)
l(m):b(r):b(m)=72:28:0

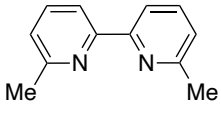

L4 Conv. >99%
20(37%), **21**(21%), **22**(4%)
l(m):b(r):b(m)=55:44:1

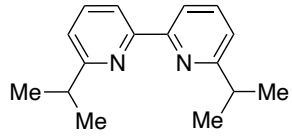

L5 Conv. 95%
20(34%), **21**(16%), **22**(10%)
l(m):b(r):b(m)=33:64:3

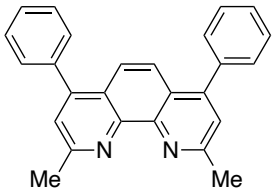

L6 Conv. >99%
20(12%), **21**(36%), **22**(9%)
l(m):b(r):b(m)=62:38:0

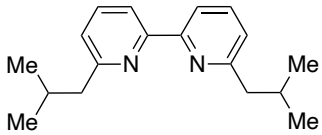

L7 Conv. 88%
20(25%), **21**(6%), **22**(7%)
l(m):b(r):b(m)=0:100:0

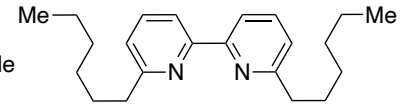

L8 Conv. 98%
20(57%), **21**(16%), **22**(10%)
l(m):b(r):b(m)=10:90:0

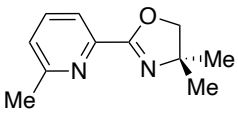

L9 Conv. 99%
20(18%), **21**(17%), **22**(21%)
l(m):b(r):b(m)=0:100:0

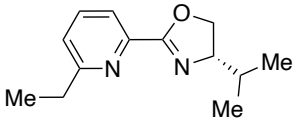

L10 Conv. 49%
20(—), **21**(5%), **22**(17%)

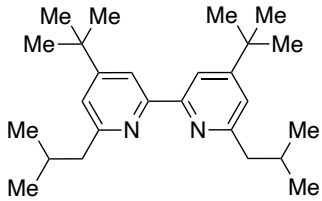

L11 Conv. 99%
20(56%), **21**(7%), **22**(3%)
l(m):b(r):b(m)=0:99:1

Next, we continued our optimization focusing on the nickel source of the mixture (Table 3.2). After screening different sources, we could see that this parameter had little effect on the selectivity of the reaction, showing the fast formation of the desired complex in solution, but rather, it affected the yield of the reaction and therefore the mass balance. The optimal Ni source proved to be $NiBr_2$.glyme, giving **20** in 64% with nearly full selectivity.

Table 3.2: Ni source screen.

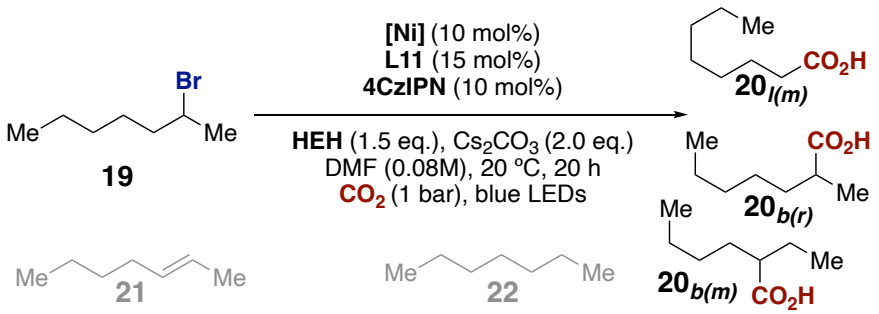

entry	Ni source	Conv. (%)	**20** (%)	l(m):b(r):b(m)	**21+22**
1	$NiCl_2$.glyme	99	61	0:99:1	7+2
2	$NiBr_2$.glyme	99	64	0:99:1	6+3
3	$NiBr_2$.diglyme	99	59	4:94:1	7+5
4	NiI_2	92	13	0:100:0	14+17
5	$(TBA)_2[NiBr_4]$	99	56	0:99:1	7+3
6	$Ni(acac)_2$	99	35	2:96:2	13+13
7	$Ni(acac\text{-}F_6)_2$	99	38	2:96:2	10+5

Then, we moved on to investigate whether a ligand-bound nickel complex would perform better than individual sources of nickel with free ligand (Table 3.3). Essentially testing an exact metal-to-ligand stoichiometry. This proved to improve our results considerably in terms of yield, keeping **L11** as optimal ligand, giving the product in 81%.

Table 3.3: Precomplex screen.

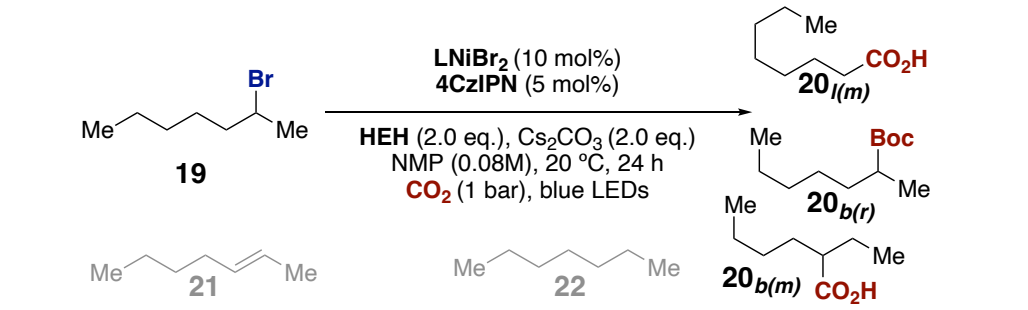

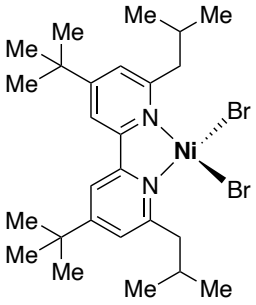

L11$NiBr_2$ Conv. >99%
2(81%), **3**(6%), **4**(2%)
l(m):b(r):b(m)=0:99:1

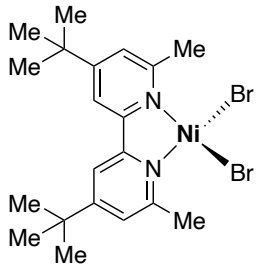

L12$NiBr_2$ Conv. >99%
2(23%), **3**(45%), **4**(5%)
l(m):b(r):b(m)=55:43:2

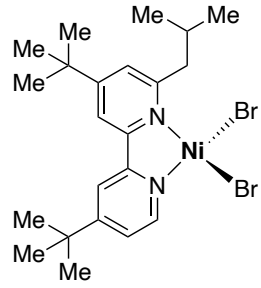

L13$NiBr_2$ Conv. >99%
2(39%), **3**(41%), **4**(15%)
l(m):b(r):b(m)=6:84:10

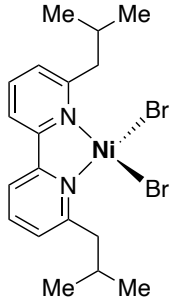

L7$NiBr_2$ Conv. 99%
2(37%), **3**(28%), **4**(24%)
l(m):b(r):b(m)=0:99:1

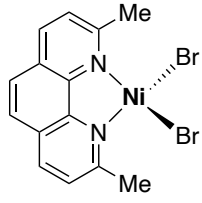

L3$NiBr_2$ Conv. >99%
2(9%), **3**(59%), **4**(3%)
l(m):b(r):b(m)=36:64:0

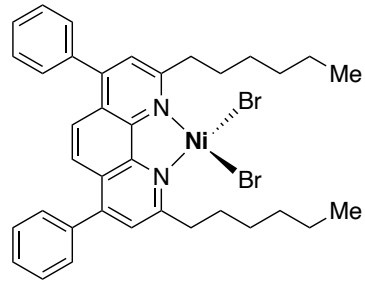

L14$NiBr_2$ Conv. 99%
2(41%), **3**(20%), **4**(3%)
l(m):b(r):b(m)=13:86:1

Once an optimal precatalyst was identified, we continued our optimization with a base screen (Table 3.4). Alkali carbonates were mainly considered given their use in the two previous reports that were known at the time.[9,10] Lighter alkali metals gave overall lower yields together with a poorer selectivity. The base used from the beginning of the optimization, Cs_2CO_3, therefore proved to be the best. When changing base class to a phosphate, the results were again poorer. We attribute the more successful use of Cs_2CO_3 to its higher solubility in organic solvent, given the bigger radius of the cesium atom compared to its smaller counterparts, allowing for more solvent molecules to coordinate it. Interestingly, using $CsHCO_3$ had negligible effect in the outcome of the reaction.

Table 3.4: Base screen.

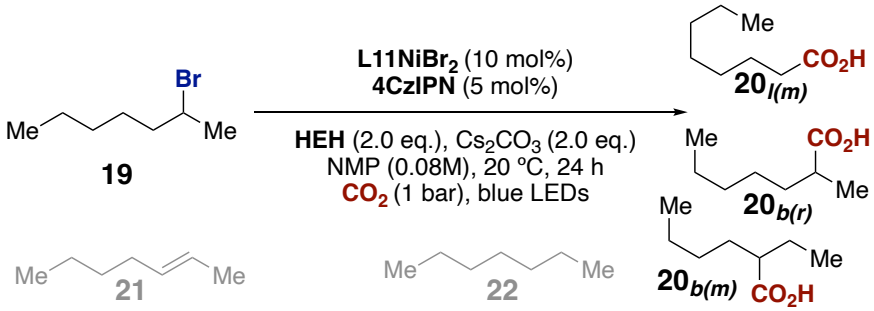

entry	Ni source	Conv. (%)	**20** (%)	l(m):b(r):b(m)	**21+22**
1	Li_2CO_3	99	8	8:88:4	26+36
2	Na_2CO_3	99	62	11:85:4	17+3
3	K_2CO_3	99	75	2:97:1	6+1
4	Rb_2CO_3	92	72	0:99:1	5+2
5	Cs_2CO_3	99	81	0:99:1	6+2
6	$CsHCO_3$	99	80	1:98:1	5+1
7	K_3PO_4	99	65	8:89:3	11+6

The PC screen shown on Table 3.5 revealed the superiority of 4CzIPN in this protocol. All other PCs tested gave lower yield and selectivity. Only 3DPAFIPN showed somewhat similar reactivity, although still inferior to 4CzIPN.

Table 3.5: Photocatalyst screen.

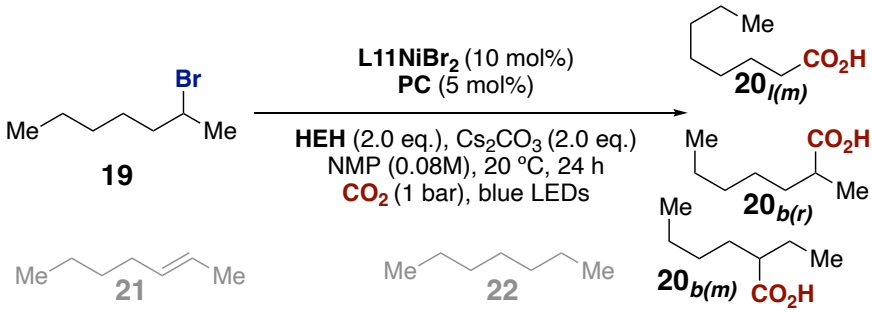

entry	Ni source	Conv. (%)	**20** (%)	l(m):b(r):b(m)	**21+22**
1	4ClCzIPN	100	29	30:64:6	31+19
2	4CzTPN	99	26	11:83:5	22+16
3	[Ir]-1	50	50	25:70:4	11+8
4	[Ir]-2	50	70	3:95:1	4+3
5	[Ir]-3	6	6	2:96:2	8+3
6	4CzIPN	99	84	2:97:1	21+5
7	3DPAFIPN	100	74	5:92:3	7+32
8	5CzBN	100	50	9:87:3	11+43
9	4DPAIPN	76	22	15:83:2	13+44

[Ir]-1 = $[Ir(dF(CF_3)ppy)dtbpy]PF_6$; [Ir]-2 = $[Ir(ppy)_2dtbpy]PF_6$; [Ir]-3 = $Ir(ppy)_3$

Control experiments were done to test whether non photoredox systems would be suitable. After trying a few conditions, only conditions similar to ones reported by Hazari *et al.* (Table 3.6, entry 3) gave product,[17] albeit in 9% yield with a 1:1 ratio of linear to branched acids.

Table 3.6: Homogeneous reductants control experiments.

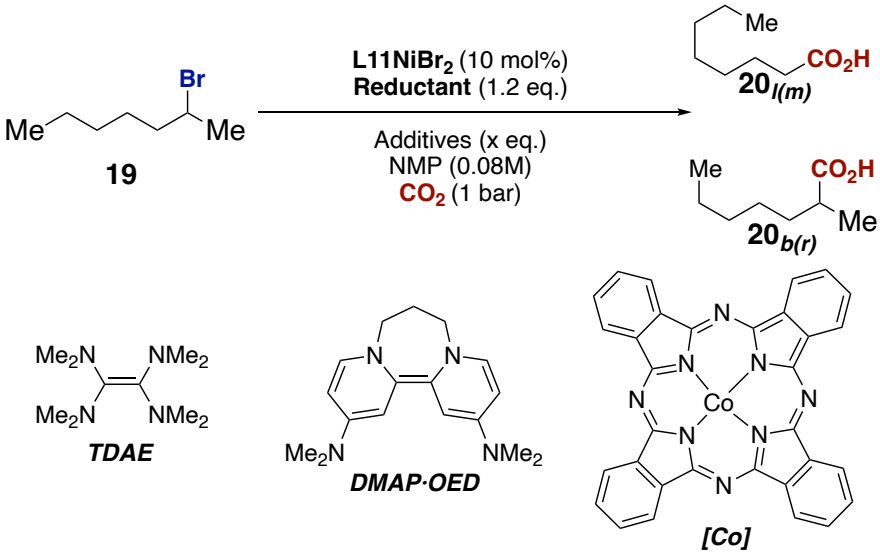

Entry	*Conditions*	Conv. (%)	*Yield(%)*	l(m):b(r)
1	TDAE, 10°C, 2h	22	0	-
2	TDAE, [Co] (2 mol%), 10°C, 2h	29	0	-
3	DMAP-OED, Cs_2CO_3 (2 eq.), LiCl (1.5 eq.), THF, 50°C, 20h	95	9	56:44
4	DMAP-OED, 25°C, 2h	87	0	-
5	DMAP-OED, [Co] (2 mol%), 25°C, 2h	63	0	-
6	DMAP-OED, CsI (1.5 eq.), 25°C, 2h	17	0	-

[a] The reactions were performed in the dark in the absence of the photocatalyst and HEH.

Finally, we have done a series of control experiments, showing that the developed conditions were the optimal ones (Table 3.7). Changing the ligand to various other ones led only to a decrease in yield and selectivity (entries 2-8). Though, ligand **L7** showed excellent selectivity despite a low yield. This shows the importance of the bulky substituents on the 6,6' positions for the selectivity of the process and the presence of the tertbutyl groups at the 4,4' positions for an optimal yield. Directly using a Ni(I) source (entry 9) did not affect the selectivity of the reaction but was detrimental for the yield. Adding more ligand to the reaction mixture (entry 10) lowers both the yield and the selectivity of the process, this supports well the need for a ligand-bound nickel precatalyst, corresponding to a precise metal-to-ligand stoichiometry. Decreasing the loading of both catalyst and PC gave poorer results (entries 11, 12). Changing base or solvent also had negative effects on the outcome (entries 13-15). All reagents were important for the success of the reaction and could not be replaced by a thermal set of conditions (entries 16-18). The secondary alkyl bromides could not be replaced by secondary alkyl iodides, tosylates or chlorides (entry 19), even when TBAB is used as a bromide source (entry 20).

Table 3.7: Final control experiments.

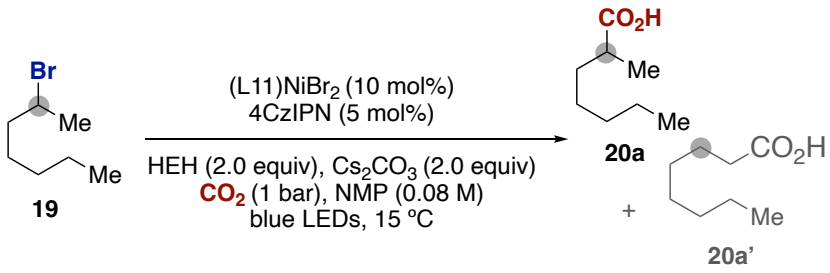

Entry	*Deviation from standard conditions*	*Yield(%)*	***2a:2a'***
1	***none***	***81 (80)***	***99:1***
2	(**L12**)$NiBr_2$ (10%) *instead of* (**L11**)$NiBr_2$	23	43:55
3	(**L7**)$NiBr_2$ (10%) *instead of* (**L11**)$NiBr_2$	37	99:0
4	(**L15**)$NiBr_2$ (10%) *instead of* (**L11**)$NiBr_2$	46	79:18
5	(**L14**)$NiBr_2$ (10%) *instead of* (**L11**)$NiBr_2$	41	86:13
6	(**L13**)$NiBr_2$ (10%) *instead of* (**L11**)$NiBr_2$	39	84:6
7	(**L4**)$NiBr_2$ (10%) *instead of* (**L11**)$NiBr_2$	14	64:36
8	(**L3**)$NiBr_2$ (10%) *instead of* (**L11**)$NiBr_2$	9	64:36
9	(**L11**)NiBr (10%) *instead of* (**L11**)$NiBr_2$	54	100:0
10	*using* additional **L1** (10 mol%)	32	82:16
11	(**L1**)$NiBr_2$ (5%) & 4CzIPN (2.5 %)	16	84:14
12	using 4CzIPN (1 %)	29	88:8
13	K_2CO_3 instead of Cs_2CO_3	75	97:2
14	K_3PO_4 instead of Cs_2CO_3	65	89:8
15	*using* DMA *instead of* NMP	52	84:12
16	*using* Mn (2.0 equiv) as reductant	0	—
17	no Cs_2CO_3	0	—
18	no (**L1**)$NiBr_2$, no 4CzIPN, no light	0	—
19	with **1**-I, **1**-OTs, **1**-Cl instead of **1**	0	—
20	with **1**-Cl and TBAB (1 eq)	traces	—

[a] Conditions: **19a** (0.25 mmol), $NiBr_2$**L11** (10 mol%), 4-CzIPN (5 mol%), HEH (0.5 mmol), Cs_2CO_3 (0.5 mmol), CO_2 (1 bar), NMP (0.08 M) at 15°C for 24h under blue LEDs irradiation. [b] Other isomers were detected in negligible amounts, GC yields using anisole as internal standard. [c] Isolated yield.

3.4. Substrate scope

3.4.1. Direct carboxylation of secondary alkyl bromides

With optimal conditions in hand, we moved on towards the study of the reaction scope. As expected, aryl group containing starting materials were well tolerated (**20b-20e**), the presence of benzylic positions was therefore not detrimental. Branched chains a carbon away from the site of reactivity did interfere with the reaction outcome (**20d**) The method was gratifyingly compatible with a range of functional groups, including indoles (**20f**), esters (**20j**, **20s**, **20w**), aryl halides (**20c**, **20l**, **20m**), alkyl (**20o**) halides, nitriles (**20p**), silanes (**20q**), unprotected alcohols (**20t**), amides (**20u**) and ketones (**20v**). The reaction was not limited to α-methyl groups, ethyl (**20g**) but also n-butyl (**20s-20x**) could be tolerated although the selectivity was generally decreased. To increase selectivity , such compounds (**20g-I**, **20s-x**, **20ac-ae**) were subjected to higher PC loading, lower temperature, and longer reaction times. Cyclic compounds were also carboxylated with success, even when bearing protecting groups on amines (**20y-20ab**). Pharmaceutically relevant valproic acid **20ad** could be obtained in 81% yield. Finally, more complex substrates containing heterocycles, or a steroid backbone were carboxylated in high yields (**20ag-20ai**).

Table 3.8: Scope of the retained carboxylation (I).

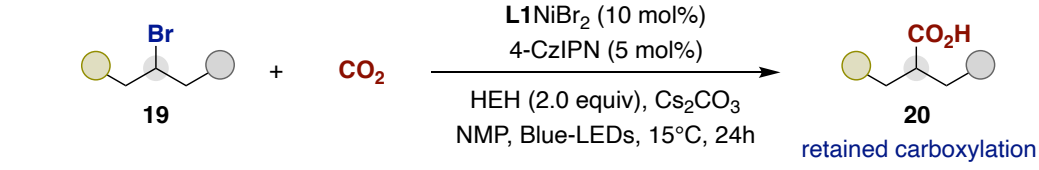

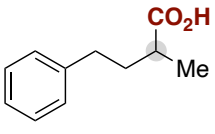

20b, 67% (R = H)

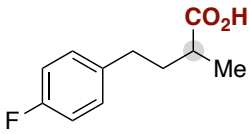

20c, 73% (R = F)

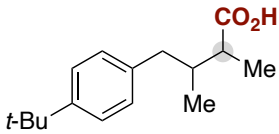

20d, 88%[c]
d:r = 1:1

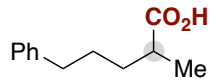

20e, 77%

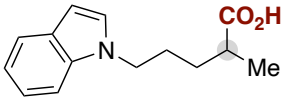

20f, 76%

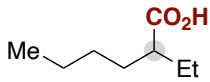

20g, 75%[c,d]

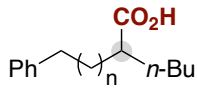

20h, 73% (n = 1)[c]
20i, 75% (n = 2)[b,d,e]

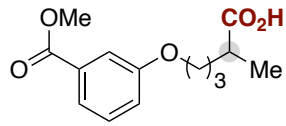

20j, 90%

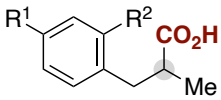

20k, 71% ($R^1 = R^2 = H$)[b]
20l, 92% ($R^1 = F$; $R^2 = H$)[c]
20m, 69% ($R^1 = Cl$; $R^2 = H$)[c]
20n, 65% ($R^1 = H$; $R^2 = OMe$)[b,d]

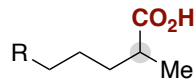

20o, 72% (R = $(CH_2)_4Cl$)
20p, 79% (R = $C(Me)_2CN$)[c]
20q, 80% (R = CH_2OTIPS)

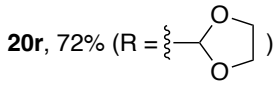

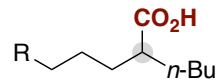

20s, 63% (R = CO_2Me)[c,e]
20t, 86% (R = CH_2OH)[c]
20u, 73% (R = CON(Ph)Me)[c]
20v, 78% (R = COMe)[c]
20w, 83% (R = CH_2OAc)[b,d,e]

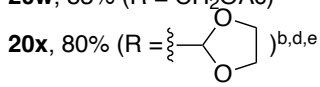

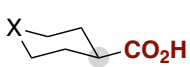

20y, 71% (X = NCbz)
20z, 70% (X = NBoc)
20aa, 65% (X = NTs)
20ab, 57% (X = O)

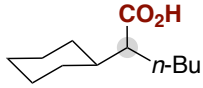

20ac, 67%[c]

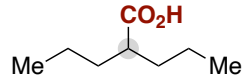

20ad, 81%[c,d]
Valproic acid

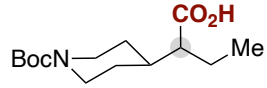

20ae, 56%[b,d,e]

[a] Conditions: As for Table 3.7. Isolated yields, average of at least two independent runs; branched:linear selectivities for **20a-20ai** rank from 8:1 to 99:1, see the experimental part for details. [b] 4-CzIPN (10 mol%). [c] 4-CzIPN (8 mol%). [d] Reaction ran at 10°C. [e] Reaction conducted for 48h. [f] HEH (3 equiv).

Table 3.9: Scope of the retained carboxylation (II).

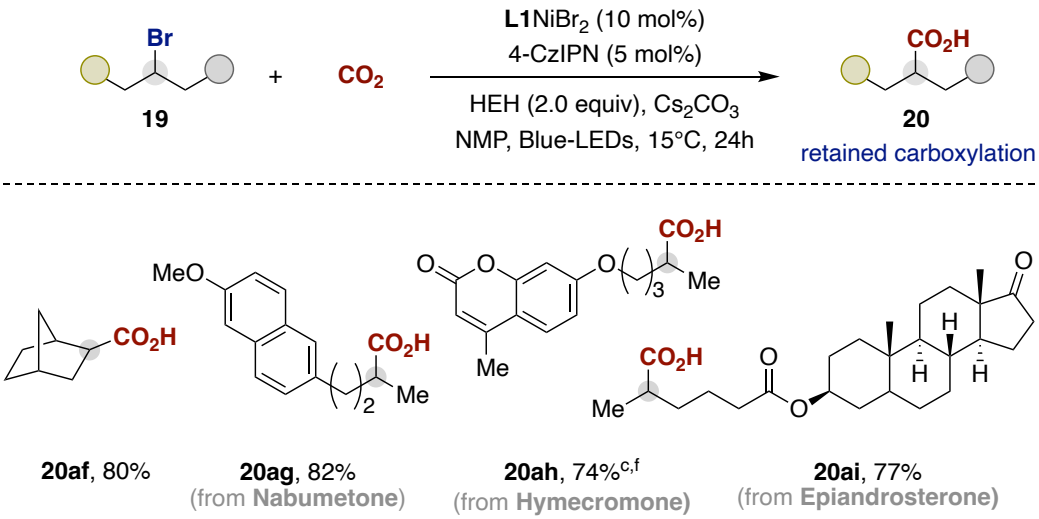

[a] Conditions: As for Table 3.7. Isolated yields, average of at least two independent runs; branched:linear selectivities for **20a-20ai** rank from 8:1 to 99:1, see the experimental part for details. [b] 4-CzIPN (10 mol%). [c] 4-CzIPN (8 mol%). [d] Reaction ran at 10°C. [e] Reaction conducted for 48h. [f] HEH (3 equiv).

3.4.2. Unsuccessful substrates

During the investigation of this positionally retentive carboxylation of alkyl bromides incompatible substrates were identified (Figure 3.2). From these starting materials, some of them did not give satisfactory results (low yield and/or low selectivity) while others decomposed or led to complex mixtures of products. To mention a few, compound **26** decomposed due to its highly electron-deficient aromatic ring, protodebromination was observed for compound **27** and C-S bond cleavage occurred when subjecting **28** to our reaction conditions. Alkynes such as **33** and **36** were very poorly supported while alkene bearing compounds such as **29** and **31** gave a mixture of products in low yield. Substrate **25** was obtained in satisfactory yield but with poor selectivity of about 70%. The phthalimide moiety is believed to do an intramolecular interaction, probably destabilizing the Ni-alkyl species involved, leading to chain-walking.

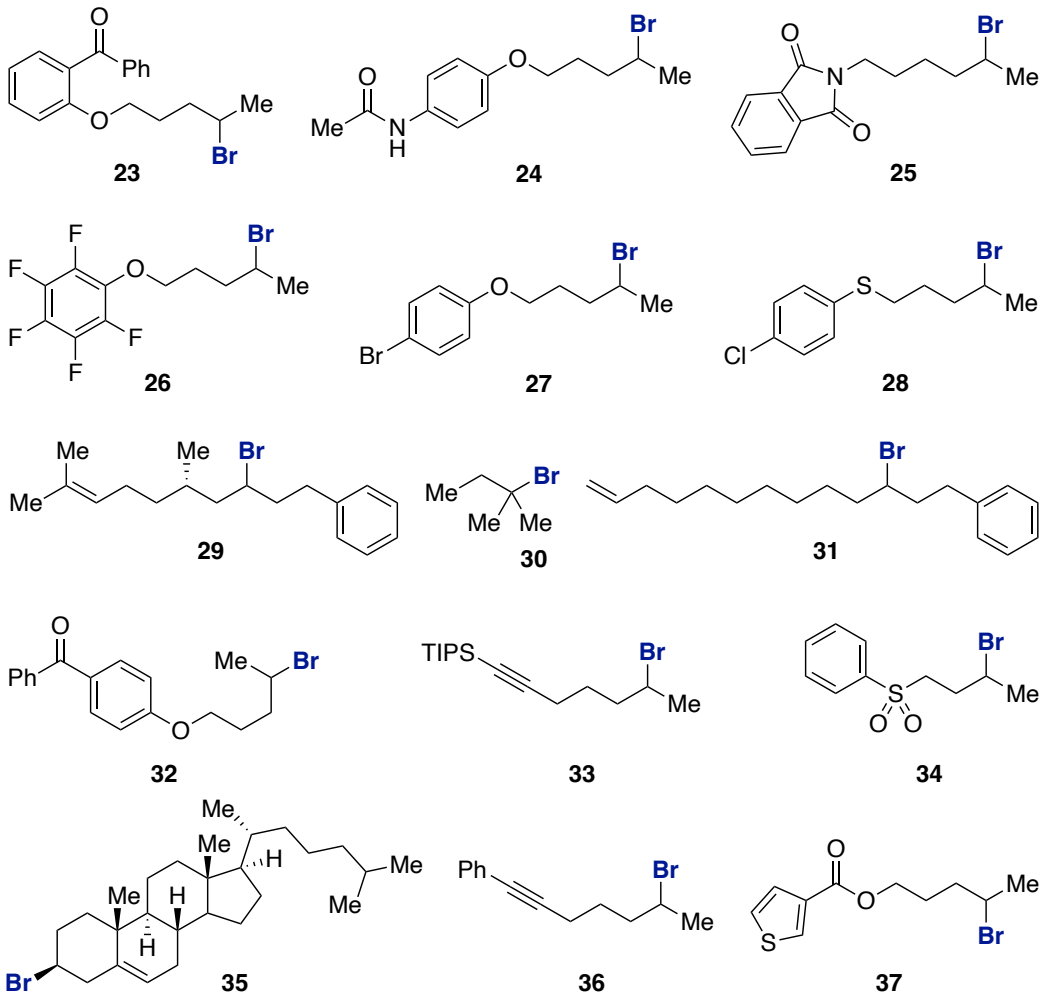

Figure 3.2: Unsuccessful substrates.

3.5. Mechanism

With the scope of the reaction explored, we sought to perform some preliminary investigations of the mechanism The first experiments that were performed consisted of stoichiometric reactions between a Ni(0) precatalyst and starting material **19a** with various conditions. Ni(0) complex Ni(**L11**)$_2$ was made by mixing the Ni(II) complex **L11**NiBr$_2$ with one equivalent of **L11** and an excess of Mg powder in THF for 5h at room temperature in a glovebox, as depicted in Scheme 3.8.

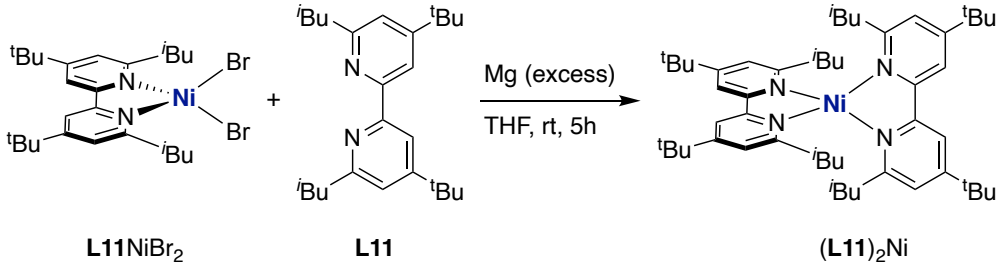

Scheme 3.8: Synthesis of the Ni(0) complex (L11)$_2$Ni.

At first, Ni(**L11**)$_2$ was mixed with **19a** under CO_2 (Scheme 3.9) to see if the oxidative addition complex would be able to undergo carboxylation , which was not the case, and no carboxylic acid product could be obtained. Then, the same experiment was repeated but this time using two equivalents of manganese powder to attempt the generation of lower valent Ni species for carboxylation of the alkyl chain. Though, no product could be observed and mostly mixtures of heptene were identified by GC. This showcases the slow kinetics of heterogeneous systems, hampering the rapid reduction of Ni(II) to a lower oxidation state prior to deleterious BHE processes. Indeed, in this case, not even the linear acid could be observed, additionally demonstrating that our ligand is not suitable for chain-walking chemistry, consistent with its design purpose. Finally, when subjecting the same two compounds to our optimized photoredox conditions, the target product could be obtained in 28% yield. This demonstrates the efficiency of photoredox homogeneous systems at delivering electrons in an efficient manner to the catalyst.

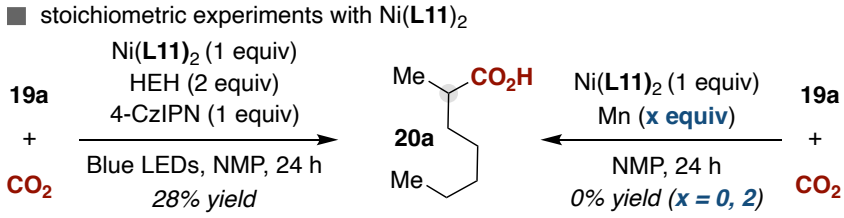

Scheme 3.9: Stoichiometric experiments with Ni(0).

A second experiment that we performed was to subject a chiral substrate, (S)-**19b**, to our reaction conditions and probe for the retention or loss of chiral information (Scheme 3.10). The obtained carboxylic acid was reduced to the corresponding alcohol with $LiAlH_4$ for the sole purpose of analysis suitability. Product **20b-OH** was received in a racemic mixture. This observation gives an indication for the formation of a free radical would escapes the solvent cage of the metal after being generated. Later recombination with a metal center to close the catalytic cycle through either face of the pro-chiral alkyl radical, giving rise to racemization. Given the literature precedents on the interaction between Ni(I) bipyridyl complexes and bromides,[18] we therefore had a hint that free radicals were involved, most likely through the oxidative addition process, in a SET fashion. We believe that loss of chirality through the formation of a carbocation is unlikely given the reductive conditions used.

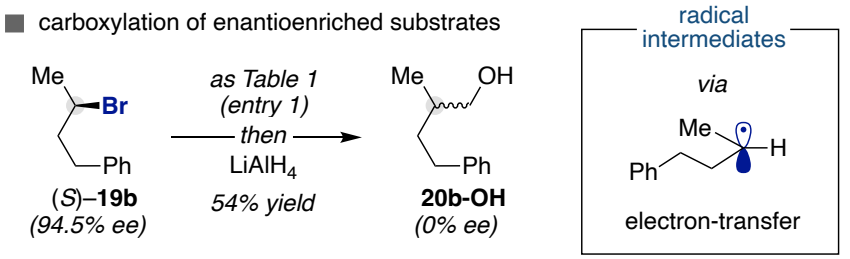

Scheme 3.10: Carboxylation of enantioenriched substrates.

After discovering that free alkyl radicals were likely generated as intermediates from our conditions, we sought to explore the reactivity of our Ni system towards unactivated secondary bromides. We knew from our first experiments, and general organometallic chemistry, that Ni(0), specifically Ni(**L11**)$_2$, would react with the secondary bromides through an oxidative addition. We therefore needed to investigate whether Ni(I) was interacting in any way with the starting materials. We performed a second stoichiometric experiment, this time mixing only starting material **19a** with a Ni(I) complex, **L11**NiBr (Scheme 3.11). The Ni(I) complex was synthesized by stirring $NiBr_2$.dme, with one equivalent of Ni(cod)$_2$ and two equivalents of ligand **L11** in THF for 24h. The experiment yielded only 2-heptene **21** as identifiable organic product and **L11**$NiBr_2$ as the inorganic part. Other products were present in small quantities on the ^{1}H NMR analysis which could not be identified. The observation proved that Ni(I) is able to react with secondary bromides, which would alleviate the need to access Ni(0). At this point, our results did nevertheless not indicate that Ni(0) was not playing a role, for which proof was beyond the scope of this project. Though, we believed that the reactivity of Ni(I) would suffice to trigger reactivity.

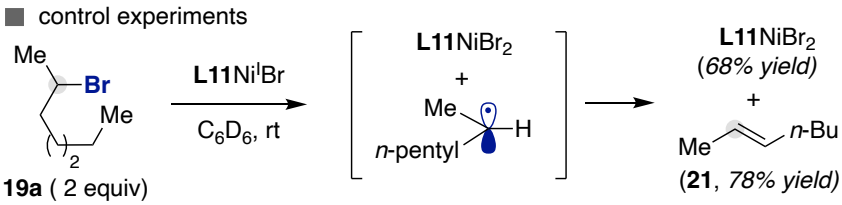

Scheme 3.11: Stoichiometric experiment with Ni(I).

A recent investigation led by Hazari *et al.*, which was not published at the time of our investigation, shows the behavior that Ni-bipyridine (bpy) systems.[19] Their report focused on bpy bearing tert-butyl groups on the 4,4' positions and bulky substituents on the 6,6' positions. Their investigation revealed that when large substituents are put on the 6,6' positions of the ligand, the redox potential of the Ni(II)/Ni(I) and NI(I)/Ni(0) couples get further separated, pushing the latter even lower than –2 V vs Fc^{+}/Fc. While we were not aware of this phenomenon, this finding reinforces the idea that Ni(0) would not be involved in our reaction conditions given the fact that it could not be generated with our mildly reducing conditions using 4-CzIPN as photocatalyst. They also showed, as could be expected, that large substituents increase the stability of Ni(I) intermediates and could therefore have helped our methodology given that we suggested the important role of such oxidation state for Ni in our catalytic cycle.

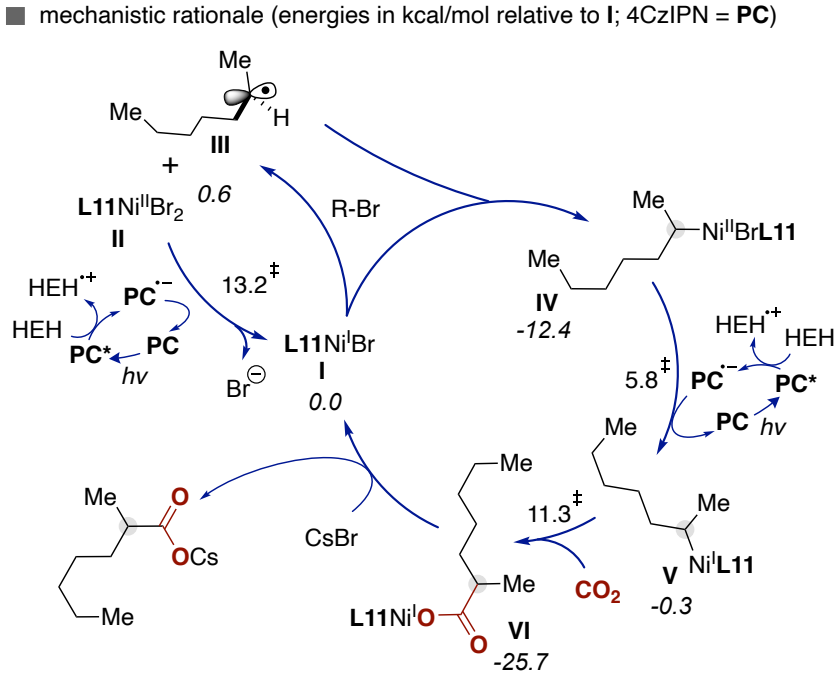

Figure 3.3: Proposed mechanistic rational for the retained carboxylation.

In order to propose and draw a full catalytic cycle, we approached experts of DFT calculations, Prof. K. Hopmann, and Dr. P.-O. Norrby. Their results, which will not be extensively discussed here, supported the major roles of Ni(I) intermediates in our protocol. A full proposed catalytic cycle is given in Figure 3.3. The cycle starts with the reduction of precatalyst **L11**$NiBr_2$ with the reduced PC to give Ni(I) **I**. Then, this intermediate reacts with the alkyl bromide giving back the Ni(II) precatalyst **II** and the free alkyl radical **III**. Another Ni(I) **I** species then recombines with the radical to give Ni(II) intermediate **IV**, believed to be the resting state of the cycle. SET reduction of **IV** with the PC leads to Ni(I) species **V**, the active carboxylation species giving rise to the Ni-carboxylate compound **VI**, which yields the product after metal exchange with a cesium cation in solution, or other cations.

A final experiment we thought about doing was a deuterium labelling experiment, aiming a seeing whether any BHE would be happening followed by rapid re-insertion of the Ni-H generated (Scheme 3.12). The methyl group next to the brominated carbon or our model substrate was therefore deuterated in order for us investigate such a phenomenon. When **19a-*d*$_3$** was subjected to our reaction conditions (Scheme 3.12, right), the desired product **20a-*d*$_3$** was obtained as sole product in 68% yield with full deuterium retention at the terminal carbon. When the same starting material was subjected to otherwise similar conditions but using **L12** instead, a 1:1 mixture of retained carboxylation and linear carboxylic acid **20a'-*d*$_3$** was obtained in 26% yield. While the retained carboxylation product was exactly the same as when using **L11**, the linear acid showed that a deuterium scrambling happened, giving rise to various ratios along the different carbons of the alkyl chain.

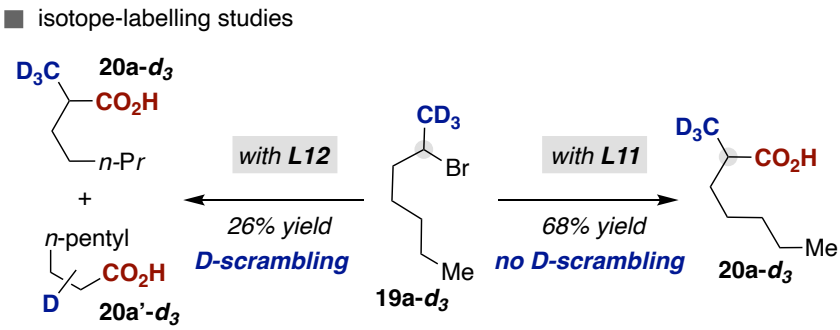

Scheme 3.12: Deuterium scrambling experiment.

.0

3.6. Conclusions

A new protocol granting access to alkyl carboxylic acids from *unactivated* secondary alkyl bromides from CO_2 is demonstrated. The reaction consists of a reductive catalytic coupling using a Ni complex as catalyst. The key parameter for achieving such products for the first time was to introduce faster kinetics when reducing the system by means of homogeneous conditions. A ligand design helped the reaction to stay selective while achieving high yields. Additionally, a preliminary mechanistic investigation revealed the intermediacy of free alkyl radicals and the importance of Ni(I) species for the reaction to occur and suggests a general Ni(II)/Ni(I) cycle. A proposed overall mechanism has been given thanks to the help of DFT studies in collaboration with other research groups.

3.7. Experimental details

Analytical methods.

^{1}H, ^{2}H, ^{19}F and ^{13}C NMR spectra were recorded on Bruker 300 MHz, Bruker 400 MHz and Bruker 500 MHz at 20 °C. All ^{1}H NMR spectra are reported in parts per million (ppm) downfield of TMS and were calibrated using the residual solvent peak of $CHCl_3$ (7.26 ppm), unless otherwise indicated. All ^{13}C NMR spectra are reported in ppm relative to TMS, were calibrated using the signal of residual $CHCl_3$ (77.16 ppm). Coupling constants, *J*, are reported in Hertz. Melting points were measured using open glass capillaries in a Büchi B540 apparatus. Gas chromatographic analyses were performed on Hewlett-Packard 6890 gas chromatography instrument with FID detector. Flash chromatography was performed with EM Science silica gel 60 (230-400 mesh) using bromocresol, potassium permanganate, or cerium molybdate as TLC stains. SFC analysis was carried out on an Agilent 1260 Infinity II SFC system.

The yields reported in Tables 3.8 and 3.9 refer to isolated yields and represent an average of at least two independent runs. The procedures described in this section are representative. Thus, the yields may differ slightly from those given in the Schemes of the manuscript.

Light source.

All reactions were performed with 451 nm LEDs (OSRAM Oslon® SSL 80 royal- blue LEDs), which were installed at the bottom of a custom-made 8 flat-bottom Schlenk tubes holder, equipped with a cooling system (the temperature was set at 15 °C, or different if stated) and a magnetic stirrer (~ 1200 rpm).

Reagents.

Commercially available materials were used as received without further purification. $NiBr_2$.glyme (97% purity), $NiBr_2$.diglyme $Ni(acac)_2$ (99.5% purity), $Ni(acac\text{-}F_6)_2$ (98% purity) were purchased from Aldrich, $NiCl_2$.glyme (97% purity), NiI_2 (99.5% purity) was purchased from Strem, Cesium carbonate (Cs_2CO_3, 99.9% purity, 20 Mesh Powder) were purchased from Alfa Aesar, Hantzsch Ester was purchased from Fluorochem, anhydrous NMP (99.5% purity) was purchased from Acros or Scharlau.

3.7.1. Optimization of the reaction conditions

General procedure.

An oven dried Schlenk tube containing a magnetic stir bar was charged with $LNiBr_2$ (0.10 equiv., 0.025 mmol), 4CzIPN (0.05 equiv., 0.0125 mmol, 10 mg), Hantzsch ester (HEH, 2.0 equiv., 0.50 mmol, 127 mg). The Schlenk tube was then taken inside a glovebox, where Cs_2CO_3 (2.0 equiv., 163 mg, 0.50 mmol,) was added. The tube was then taken out of the glovebox and connected to a vacuum line where it was evacuated and backfilled under positive CO_2 flow at least three times. The NMP (3 mL, 0.08 M) and 2-bromoheptane (1.0 equiv., 0.25 mmol, 39 μL) were added under CO_2 flow. Once all the components were added, the Schlenk tube was closed at 1 bar of CO_2 and placed in a temperature controlled photoreactor with water cooling at 15 ºC (which gives an *in situ* reaction temperature of ca. 20 ºC) and stirred for 24 h in the presence of continuous irradiation with blue light (451 nm, 2 W LED). The reaction mixture was quenched with 2 M HCl aq. solution (5 ml) to release free acid by protonation of the carboxylate salt and diluted with ethyl acetate (10 ml). Internal standard (anisole) was added to determine GC-Yield and selectivity of regioisomers.

3.7.2. Starting material and ligand synthesis

Commercially available compounds (**19g**, **19k**, **19y**, **19z**. **19aa**, **19ab**, **19ae**, **19ai**) were used as received without further purification. Compounds **19b**[20], **19c**[20], **19e**[21], **19h**[22], and **19o**[7], were known and prepared according to literature procedures.

Procedure for the Preparation of Ligand L11

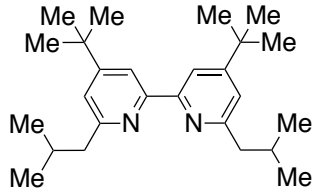

4,4'-di-tert-butyl-6,6'-diisobutyl-2,2'-bipyridine (**L11**): To a solution of 4,4'-di-tert-butyl-6,6'-bipyridine (1.34 g, 5.00 mmol, 1.00 equiv.) in THF (25 mL), isobutyllithium (1.7 M) in heptane (25 mL, 40 mmol, 8.0 equiv.) was added dropwise at 0°C. The resulting red reaction mixture was heated at 60°C overnight. The reaction was cooled to

rt and quenched with aq. NH_4Cl solution. The organic layers were extracted with DCM, washed with brine, dried with $MgSO_4$ and solvents were evaporated under reduced pressure. The crude product was solubilized in DCM (17 mL), and then activated MnO_2 (4.35 g, 50 mmol, 10 equiv.) was added. After stirring for 4h at rt, the reaction mixture was filtrated through celite and silica. The filtrate was concentrated, and the crude was purified through silica gel (pentane/Et_2O = 100/2 to 100/4) followed by recrystallization from ethanol or acetone to afford desired ligand **L11** (1.02 g, 2.68 mmol, 54%) as white solid. **^{1}H NMR** (300 MHz, $CDCl_3$): δ (ppm) = 8.19 (d, *J* = 1.8 Hz, 2H), 7.08 (d, *J* = 1.8 Hz, 2H), 2.72 (d, *J* = 7.2 Hz, 4H), 2.21 (dt, *J* = 13.5, 6.7 Hz, 2H), 1.37 (s, 18H), 0.99 (d, *J* = 6.7 Hz, 12H). **^{13}C NMR** (101 MHz, $CDCl_3$): δ (ppm) = 160.7, 160.6, 156.7, 120.3, 115.8, 47.8, 34.9, 30.8, 29.10, 22.7. **IR** (neat, cm^{-1}): 2954, 2898, 2866, 1587, 1552, 1463, 1389, 1360, 1293, 1200, 1166, 1114, 885, 723, 667. **HRMS** calcd. for ($C_{26}H_{41}N_2$) $[M+H]^+$: 381.3264, found 381.3257. **Melting Point:** 120°C

General procedure 1:

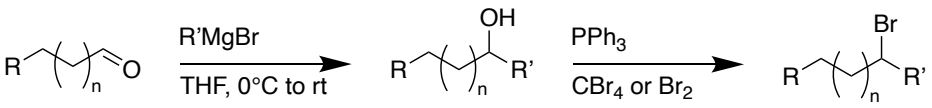

General procedure 2:

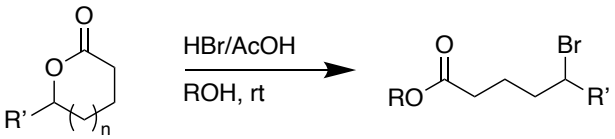

General procedure 3:

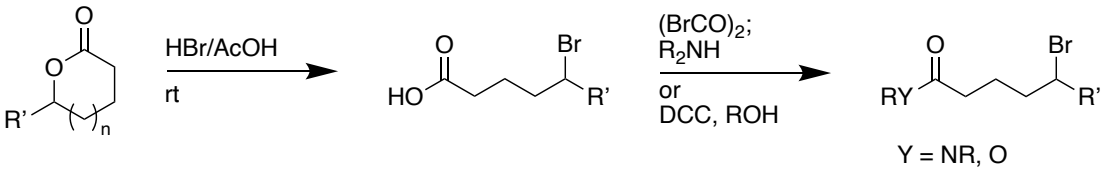

General procedure 4:

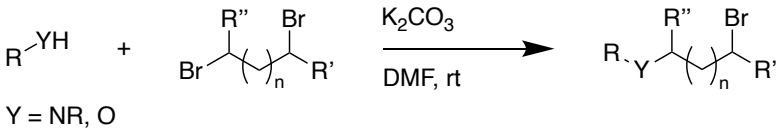

General procedure 5:

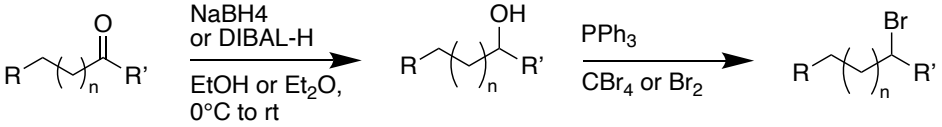

Scheme 3.13: General procedures for starting material synthesis.

General procedure 1 (Scheme 3.13). Step 1: To a solution of the corresponding aldehyde (1 equiv.) in THF (0.3 M) at 0 ºC was added a Grignard solution in THF (1.2 equiv.) and the solution was allowed to warm to rt. After 2-3 hours, saturated aqueous solution of NH_4Cl was added and the mixture extracted with EtOAc (3x). The combined organic layers were dried over $MgSO_4$ and concentrated under reduced pressure. The crude was purified by flash

column chromatography on silica if required or taken onto the next step without further purification. Step 2: To a solution of triphenylphosphine (1.2 equiv.) in dry DCM (0.2 M) at 0 ºC, bromine or CBr_4 (1.2 equiv.) was added dropwise, and the mixture stirred for 30 min. Then, a solution of the corresponding alcohol (1 equiv.) in dry DCM (0.2 M) and pyridine (1.2 equiv.) were subsequently added and the mixture was stirred for 4 h at room temperature. After completion, the mixture was partially concentrated and filtered through a plug of silica eluting with pentane. The filtrate was evaporated, and the residue purified by flash column chromatography on silica if required.

General procedure 2 (Scheme 3.13). The corresponding lactone (1 equiv.) was added to a flask containing a solution of 33% HBr in AcOH (3 M) and fitted with a reflux condenser. The reaction was heated to 75 °C for 4 hours then cooled to room temperature. Then, an excess of the appropriate alcohol was added and the solution stirred at room temperature overnight. After completion, the reaction was partially concentrated under reduced pressure, extracted with EtOAc and washed with a saturated aqueous solution $NaHCO_3$ (3x) and brine. The organic layer was then dried over anhydrous $MgSO_4$ and concentrated under reduced pressure. The residue was purified by flash column chromatography in silica gel with hexane:EtOAc (98:2).

General procedure 3 (Scheme 3.13). Step 1: The corresponding lactone (1 equiv.) was added to a flask containing a solution of 33% HBr in AcOH (3 M) and fitted with a reflux condenser. The reaction was heated to 75 °C for 4 hours then cooled to room temperature. The mixture was then partially concentrated by rotary evaporation. The residue was extracted with DCM and washed with saturated aqueous solution of NaS_2O_3. The aqueous layer was extracted with DCM (3x) and the combined organic layer were washed with brine, dried over $MgSO_4$ and concentrated. The crude carboxylic acid was used in the next step without further purification. Step 2 (Oxalyl bromide): To a cooled solution (0 ºC) of oxalyl bromide (1.4 equiv.) in anhydrous DCM (0.3 M) was added the corresponding carboxylic acid (1.0 equiv.). Then, DMF (0.2 equiv.) was added dropwise, and the reaction was stirred at 0 ºC during 2 h. After completion, the reaction was concentrated affording the corresponding crude acyl bromide that was used without further purification in the next step. Step 2 (DCC coupling): To a solution of DCC (1.2 equiv.), DMAP (10 mol%) and the alcohol (1.0 equiv.) in DCM (0.2 M) at 0°C was added dropwise a solution of the carboxylic acid in DCM (1.0 M), the solution was then stirred at the same temperature for 15 min. The reaction mixture was allowed to warm to rt and stirred overnight. Afterwards, the reaction was diluted with DCM and H_2O, the aqueous phase extracted twice with DCM, the combined organic phase dried over $MgSO_4$, filtered and solvent was removed under reduced pressure. The crude was then purified by flash column chromatography in silica gel with

pentane:EtOAc (9:1). Step 3: To a solution of the acyl bromide in anhydrous toluene (0.2 M) was added the corresponding secondary amine (1.2 equiv.) and the mixture stirred at room temperature overnight. After completion, the mixture was extracted with Et_2O and washed with brine. The organic layer was dried over anhydrous $MgSO_4$ and concentrated. The residue was purified by flash column chromatography in silica gel with hexane:EtOAc (8:1 to 2:1).

General procedure 4 (Scheme 3.13). A solution of the corresponding alcohol (1.0 equiv) and K_2CO_3 (1.2 equiv.) in DMF (0.6 M) was stirred for 1 h at room temperature. Then, the dibrominated compound (2.0 equiv) was subsequently added. The mixture was stirred at room temperature for 24-48 h. After completion, the mixture was extracted with EtOAc and washed with brine (3x). The organic layer was dried over anhydrous $MgSO_4$ and concentrated. The residue was purified by flash column chromatography in silica gel with hexane:EtOAc.

General procedure 5 (Scheme 3.13). To a solution of the corresponding ketone (1.0 equiv) in Et2O (if DIBAL-H is used, 0.4 M) or EtOH (if $NaBH_4$ is used, 0.4 M) at 0°C was added DIBAL-H (dropwise, 1.1 equiv.) or $NaBH_4$ (1.1 equiv.), the mixture was then stirred at 0°C for an hour, slowly warmed to rt and further stirred for 3h. After completion, the reaction was quenched using a sat. aq. solution of NH_4Cl. The mixture was then extracted with EtOAc and washed with water (3x). A 10% solution of sodium potassium tartrate can be used to wash if the extraction is messy due to lithium complexes. The organic layer was dried over anhydrous $MgSO_4$ and concentrated. The residue was purified by flash column chromatography in silica gel with pentane:EtOAc.

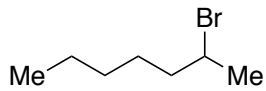

2-Bromoheptane (19a). **General Procedure 1 (GP1)**: To a stirred solution of triphenylphosphine (1.1 equiv. 20 mmol, 5.3 g) in dry DCM (0.2 M, 100 ml) at 0 ºC, bromine (1.2 equiv., 20 mmol, 1.0 ml) was added dropwise and the mixture stirred at this temperature for 30 min. Then, a solution of 2-heptanol (1.0 equiv., 17 mmol, 2.4 ml) [or other alcohol] in dry DCM (0.2 M, 50 ml) and pyridine (1.2 equiv., 20 mmol, 1.5 ml) were subsequently added drop wise and the mixture was allowed to warm to room temperature and stirred for 4 h. After completion, the mixture was partially concentrated and filtered through a plug of silica eluting with pentane to give **19a** as a colorless liquid (2.5 g, 83%) **^{1}H NMR (400 MHz, $CDCl_3$):** δ (ppm) = 4.16 (m, 1H), 1.91 – 1.75 (m, 2H), 1.73 (d, *J* = 6.6 Hz, 3H),

1.55 – 1.25 (m, 6H), 0.96 – 0.88 (d, *J* = 7.0 Hz, 3H). **^{13}C NMR (101 MHz, $CDCl_3$):** δ (ppm) = 52.16, 41.31, 31.32, 27.59, 26.61, 22.66, 14.15. Data in agreement with the literature.[23]

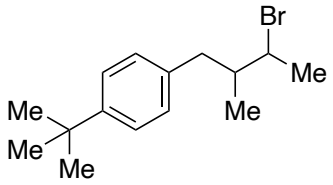

1-(3-bromo-2-methylbutyl)-4-(tert-butyl)benzene (19d). Following **GP1** from Lilial (4.1 g, 20.0 mmol), 23% over two steps. Purification by flash column chromatography (pentane) to give **19d** as a colorless oil (1.26 g, 23%, d:r = 1:1). **^{1}H NMR (500 MHz, $CDCl_3$):** δ (ppm) = 7.34 – 7.28 (m, 2H), 7.17 – 7.07 (m, 2H), 4.26 – 4.15 (m, 1H), 2.87 – 2.69 (m, 1H), 2.59 – 2.40 (m, 1H), 2.17 – 2.04 (m, 1H), 1.81 – 1.73 (m, 1H), 1.72 (d, *J* = 6.8 Hz, 3H), 1.67 (d, *J* = 6.9 Hz, 3H), 1.32 (s, 9H), 1.00 (d, *J* = 3.5 Hz, 2H), 0.99 (d, *J* = 3.6 Hz, 1H).**^{13}C NMR (75 MHz, $CDCl_3$):** δ (ppm) = 149.1, 137.2, 137.1, 129.0, 128.9, 125.4, 43.3, 42.7, 41.3, 39.6, 34.5, 31.6, 24. **IR (neat, cm^{-1}):** 2960, 2865, 1509, 1443, 1377, 1268, 1202, 1108, 1055, 1019, 837, 808, 776, 736, 679. **HRMS** calcd. for ($C_{15}H_{22}Br$) $[M-H]^+$: 281.0899 found 281.0899. The presence of additional peaks/proton count in NMR spectra are due to diastereoisomers.

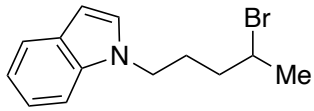

1-(4-bromopentyl)-1H-indole (19f). To a solution of Indole (1.0 equiv., 3.0 mmol, 351 mg) in dry DMF (0.4 M, 7.5 mL) under argon at rt was added by portions NaH (60% w/w, 1.1 equiv., 3.3 mmol, 132 mg). After stirring the mixture for 30 min, it was cooled to 0°C and 1,5-dibromopentane (2.0 equiv., 6.0 mmol, 1.38 g, 817 µL) was added quickly. The reaction mixture was further stirred at the same temperature for an hour and slowly brought back to rt to be stirred overnight. The reaction was quenched by addition of H_2O, and then diluted with extra portion of H_2O as well as EtOAc. The layers were separated, and the organic was further washed with three portions of H_2O. The organic layer was collected, dried over anhydrous $MgSO_4$, filtered and solvent evaporated under reduced pressure to give a crude that was purified by flash column chromatography (pentane → pentane:Et_2O 100:2), yielding **19f** as a colorless oil (733 mg, 92%) **^{1}H NMR (500 MHz, $CDCl_3$):** δ (ppm) = 7.67 (dt, J = 7.9, 1.0 Hz, 1H), 7.37 (dq, J = 8.2, 0.9 Hz, 1H), 7.28 – 7.22 (m, 1H), 7.14 (ddd, J = 8.0, 7.0, 1.0 Hz, 1H), 7.11 (d, J = 3.1 Hz, 1H), 6.53 (dd, J = 3.1, 0.9 Hz, 1H), 4.17 (td, J = 7.0, 2.8 Hz, 2H),

4.13 – 4.06 (m, 1H), 2.19 – 2.08 (m, 1H), 2.06 – 1.95 (m, 1H), 1.88 – 1.72 (m, 2H), 1.69 (d, J = 6.7 Hz, 3H).**^{13}C NMR (75 MHz, $CDCl_3$):** δ (ppm) = 136.1, 128.7, 127.7, 121.6, 121.2, 119.5, 109.4, 101.4, 50.9, 45.8, 38.3, 28.7, 26.6. **HRMS** calcd. for ($C_{13}H_{17}BrN$) $[M+H]^+$: 266.0539 found 266.0538.

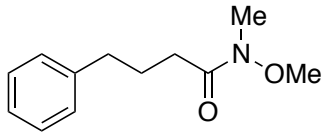

***N*-methoxy-*N*-methyl-4-phenylbutanamide (19i-a)**. To 4-phenylbutanoic acid (1.9 equiv, 20 mmol, 3.3 g,) and MeON(Me)H (1.05 equiv, 21 mmol, 2.1 g) in dry DCM (60 ml) at 0 °C was added Et_3N (2.0 equiv, 40 mmol, 5.6 ml), DMAP (0.05 equiv, 1.0 mmol, 0.12 g) and DCC (1.05 equiv, 21 mmol, 4.4 g). The reaction mixture was allowed to slowly warm to room temperature and stirred for 16 h, after which it was diluted with DCM and H_2O. The layers were separated, and the aqueous layer was extracted with DCM (x 2). The combined organic layers were dried ($MgSO_4$), filtered and reduced *in vacuo*. Purification by column chromatography on silica gel eluting with hexane:EtOAc (8:2 →7:3) gave the corresponding Weinreb amide **19i-a** (3.0 g, 72%) as colorless oil. **^{1}H NMR (500 MHz, $CDCl_3$):** δ (ppm) = 7.31 – 7.24 (m, 2H), 7.22 – 7.15 (m, 3H), 3.62 (s, 3H), 3.17 (s, 3H), 2.73 – 2.62 (m, 2H), 2.44 (t, *J* = 7.5 Hz, 2H), 2.02 – 1.92 (m, 2H). **^{13}C NMR (126 MHz, $CDCl_3$):** δ (ppm) = δ 141.9, 128.6, 128.4, 126.0, 61.3, 60.5, 35.5, 31.3, 26.2, 21.2, 14.3. Data in agreement with the literature.[24]

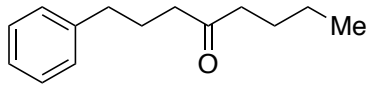

1-phenyloctan-4-one (19i-b). To **19i-a** (1.0 equiv, 5.0 mmol, 1.04 g) in dry THF (15 ml) at 0 °C was added *n*BuMgBr (1.5 equiv, 15 mmol, 2 M in THF, 3.8 ml) dropwise over 10 minutes. The mixture was allowed to warm to room temperature and then quenched with NH_4Cl (sat.) and diluted with Et_2O (15 ml). The layers were separated and then aq. layer was extracted with Et_2O (15 ml x 2). The combined organic layers were dried ($MgSO_4$), filtered and reduced *in vacuo*. Purification by column chromatography on silica gel eluting with hexane:EtOAc (9:1) gave the *n*-butyl ketone **19i-b** (0.91 g, 89%) as a colorless oil. **^{1}H NMR (400 MHz, $CDCl_3$):** δ (ppm) = 7.31 – 7.26 (m, 2H), 7.22 – 7.15 (m, 3H), 2.64 – 2.58 (m, 2H), 2.39 (dt, *J* = 15.3, 7.4 Hz, 4H), 1.98 – 1.85 (m, 2H), 1.57 – 1.49 (m, 2H), 1.35 – 1.23 (m, 2H), 0.90 (t, *J* = 7.3 Hz, 3H). **^{13}C NMR (126 MHz, $CDCl_3$):** δ (ppm) = 211.3, 141.8, 128.6, 128.5, 126.1, 42.7, 42.0, 35.3, 26.1, 25.4, 22.5, 14.0. Data in agreement with the literature.[25]

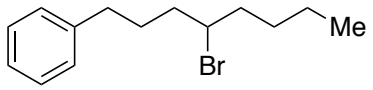

(4-bromooctyl)benzene (19i). To a stirred solution of the *n*-butyl ketone **19i-b** in dry MeOH (8 ml) at 0 °C was added $NaBH_4$ (1.1 equiv, 4.9 mmol, 0.19 g) portionwise. The reaction was stirred at this temperature for 2 h and then quenched with NH_4Cl sat. and extracted with Et_2O (30 ml x 3). The combined organic layers were dried ($MgSO_4$), filtered and reduced *in vacuo*. Purification of the crude by column chromatography on silica gel eluting with hexane:EtOAc (9:1 → 8:2) gave the targeted alcohol (0.89 g, 97%) as a colorless oil. Following **GP1** from the alcohol 4-hydroxyoctylbenzene (1.0 equiv, 4.3 mmol, 0.89 g) gave **1i** (1.0 g, 86%) as a colorless oil after purification by column chromatography on silica gel eluting with pentane. **^{1}H NMR (500 MHz, $CDCl_3$):** δ (ppm) = 7.37 – 7.24 (m, 2H), 7.23 – 7.16 (m, 3H), 4.04 (tt, J = 7.9, 5.1 Hz, 1H), 2.71 – 2.57 (m, 1H), 1.97 – 1.65 (m, 6H), 1.57 – 1.24 (m, 5H), 0.91 (t, J = 7.2 Hz, 3H); **^{13}C NMR (126 MHz, $CDCl_3$)** δ (ppm) = 142.1, 128.5, 128.5, 126.0, 58.6, 39.0, 38.8, 35.4, 29.9, 29.4, 22.3, 14.1. **IR (neat, cm^{-1}):** 3026, 2954, 2930, 2859, 1709, 1603, 1496, 1454, 1379, 1308, 1235, 1189, 1030; **HRMS** calcd. for ($C_{14}H_{21}$) $[M–Br]^+$: 189.1638 found 189.1633

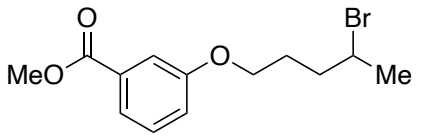

methyl 3-((4-bromopentyl)oxy)benzoate (19j). Following **GP4**, methyl 3-hydroxybenzoate (781 mg, 5.00 mmol) afforded the title compound **19j** as a colorless oil after purification by column chromatography on silica gel eluting with pentane/Et_2O (95:5). **^{1}H NMR (300 MHz, $CDCl_3$):** δ (ppm) = 7.63 (dt, *J* = 7.6, 1.3 Hz, 1H), 7.54 (dd, *J* = 2.7, 1.5 Hz, 1H), 7.34 (t, *J* = 7.9 Hz, 1H), 7.09 (ddd, *J* = 8.2, 2.6, 1.0 Hz, 1H), 4.24 – 4.16 (m, 1H), 4.08 – 4.00 (m, 2H), 3.91 (s, 3H), 2.12 – 1.87 (m, 4H), 1.76 (d, *J* = 6.7 Hz, 3H). **^{13}C NMR (101 MHz, $CDCl_3$):** δ (ppm) = 167.1, 159.0, 131.6, 129.6, 122.2, 120.0, 114.8, 67.4, 52.3, 51.3, 37.8, 27.7, 26.7; **IR (neat, cm^{-1}):** 3310, 2941, 1702, 1586, 1455, 1274, 1209, 1130, 1041, 753; **HRMS** calcd. for ($C_{13}H_{17}O_5$) $[M–H]^–$: 301.0434 found 301.0436.

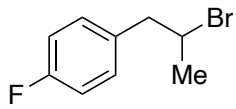

1-(2-bromopropyl)-4-fluorobenzene (19l). Following **GP5**, in an oven-dried Schlenk flask containing a magnetic stir bar under inert atmosphere, a DIBAL-H 1M solution (1.1 equiv, 5.5 mmol, 5.50 mL) was added dropwise to a solution of 1-(4-fluorophenyl)propan-2-one (1.0 equiv, 5.0 mmol, 761 mg, 667 µL) in Et_2O (8 mL) at 0 ºC. The reaction mixture was then allowed to warm up to room temperature and stirred for 5h. The reaction was quenched with a saturated aqueous NH_4Cl solution. Then, the mixture was extracted with EtOAc three times and potassium sodium tartrate solution used to solubilize the lithium salts. The organic layers were combined, dried ($MgSO_4$), filtered and concentrated in vacuo to give the crude alcohol intermediate that was purified by flash column chromatography (eluent: pentane/ethyl acetate = 3/1 – 2/1) to afford pure 1-(4-fluorophenyl)propan-2-ol (585 mg, 76%) In an oven-dried Schlenk flask containing a magnetic stir bar, CBr_4 (1.51 g, 4.55 mmol, 1.2 equiv.) was dissolved in dry DCM (0.6 M based on alcohol). After cooling the solution to 0 ºC, PPh_3 (1.49 g, 5.69 mmol, 1.5 equiv.) in DCM (1.5 M) was added dropwise and allowed to stir for 10 min to obtain a yellow solution. Then, 1-(4-fluorophenyl)propan-2-ol (585 mg, 3.79 mmol, 1.0 equiv.) in DCM (2 mL) was added dropwise to the mixture and stirred at 0°C for 15 min. The reaction mixture was allowed to warm up to rt and stirred overnight. Pentane was added to precipitate PPh_3O, which was removed by filtration and the organic filtrate was evaporated to give a crude which was purified by flash column chromatography through silica gel (eluent: pentane/diethyl ether = 100/0 - 8/1) to afford the pure product **19l** (608 mg, 2.80 mmol, 74%) as a pale-yellow oil. **^{1}H NMR (500 MHz, $CDCl_3$):** δ 7.22 – 7.15 (m, 2H), 7.07 – 6.98 (m, 2H), 4.28 (h, *J* = 6.7 Hz, 1H), 3.19 (dd, *J* = 14.2, 7.3 Hz, 1H), 3.08 (dd, *J* = 14.2, 6.8 Hz, 1H), 1.72 (d, *J* = 6.6 Hz, 3H). **^{19}F NMR (471 MHz, $CDCl_3$):** δ -116.01 (q, *J* = 4.5 Hz). **^{13}C NMR (126 MHz, $CDCl_3$):** δ 162.8, 160.9, 134.2, 134.2, 130.7, 130.7, 115.4, 115.2, 50.5, 50.5, 46.6, 25.7; **IR (neat, cm^{-1}):** 3040, 2969, 2921, 1889, 1600, 1507, 1446, 1377, 1219, 1157, 1112, 901, 819, 764; **HRMS** calcd. for ($C_9H_{10}BrF$) $[M]^+$: 215.9950 found 215.9940.

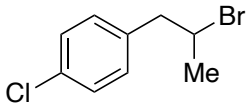

1-(2-bromopropyl)-4-chlorobenzene (19m). Following **GP5**, in an oven-dried Schlenk flask containing a magnetic stir bar under inert atmosphere, a DIBAL-H 1M solution (1.1 equiv, 5.5 mmol, 5.50 mL) was added dropwise to a solution of 1-(4-chlorophenyl)propan-

2-one (1.0 equiv, 5.0 mmol, 843 mg, 600 µL) in Et_2O (8 mL) at 0 ºC. The reaction mixture was then allowed to warm up to room temperature and stirred for 5h. The reaction was quenched with a saturated aqueous NH_4Cl solution. Then, the mixture was extracted with EtOAc three times and a potassium sodium tartrate solution used to solubilize the lithium salts. The organic layers were combined, dried ($MgSO_4$), filtered and concentrated in vacuo to give the crude alcohol intermediate that was purified by flash column chromatography (eluent: pentane/ethyl acetate = 3/1 – 2/1) to afford pure 1-(4-chlorophenyl)propan-2-ol (817 mg, 96%) In an oven-dried Schlenk flask containing a magnetic stir bar, CBr_4 (1.91 g, 5.75 mmol, 1.2 equiv.) was dissolved in dry DCM (0.6 M based on alcohol). After cooling the solution to 0 ºC, PPh_3 (1.88 g, 7.18 mmol, 1.5 equiv.) in DCM (1.5 M) was added dropwise and allowed to stir for 10 min to obtain a yellow solution. Then, 1-(4-chlorophenyl)propan-2-ol (817 mg, 4.79 mmol, 1.0 equiv.) in DCM (2 mL) was added dropwise to the mixture and stirred at 0°C for 15 min. The reaction mixture was allowed to warm up to rt and stirred overnight. Pentane was added to precipitate PPh_3O, which was removed by filtration and the organic filtrate was evaporated to give a crude which was purified by flash column chromatography through silica gel (eluent: pentane/diethyl ether = 100/0 - 9/1) to afford the pure product **19m** (916 mg, 3.92 mmol, 82%) as a pale-yellow oil. **^{1}H NMR (400 MHz, CDCl3):** δ 7.31 – 7.26 (m, 2H), 7.17 – 7.11 (m, 2H), 4.26 (dt, *J* = 7.4, 6.6 Hz, 1H), 3.16 (dd, *J* = 14.2, 7.3 Hz, 1H), 3.05 (dd, *J* = 14.2, 6.7 Hz, 1H), 1.70 (d, *J* = 6.6 Hz, 3H). **^{13}C NMR (101 MHz, CDCl3):** δ 136.9, 132.8, 130.6, 128.6, 50.1, 46.7, 25.7; **IR (neat, cm^{-1}):** 3025, 2968, 2920, 1896, 1596, 1490, 1440, 1406, 1376, 1241, 1178, 1087, 1014, 835, 798; **HRMS** calcd. for ($C_9H_{10}BrCl$) $[M]^+$: 231.9649 found 231.9644.

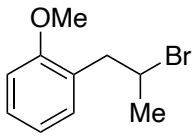

1-(2-bromopropyl)-2-methoxybenzene (19n). In an oven-dried Schlenk flask containing a magnetic stir bar under inert atmosphere, $NaBH_4$ (1.4 equiv, 2.30 mmol, 86 mg) was added portion wise to a solution of 1-(2-methoxyphenyl)propan-2-one (1.0 equiv, 1.60 mmol, 264 mg, 250 µL) in Et_2O (4 mL) at 0 ºC. The reaction mixture was then allowed to warm up to room temperature and stirred for 3h. The reaction was quenched with a 1M HCl solution. Then, the mixture was extracted with EtOAc three times. The organic layers were combined, dried ($MgSO_4$), filtered and concentrated in vacuo to give the crude alcohol intermediate that was used in the next step without further purification. In an oven dried Schlenk flask containing a magnetic stir bar, CBr_4 (584 mg, 1.76 mmol, 1.1 equiv.) was dissolved in dry DCM (0.6 M based on alcohol). After cooling the solution to 0 ºC, PPh_3 (462 mg, 1.76 mmol,

1.1 equiv.) in DCM (1.5 M) was added dropwise and allowed to stir for 10 min to obtain a yellow solution. Then, 1-(2-methoxyphenyl)propan-2-ol (266 mg, 1.60 mmol, 1.0 equiv.) in DCM (1 mL) was added dropwise to the mixture and stirred at 0°C for 15 min. The reaction mixture was allowed to warm up to rt and stirred overnight. Pentane was added to precipitate PPh_3O, which was removed by filtration and the organic filtrate was evaporated to give a crude which was purified by flash column chromatography through silica gel (eluent: pentane) to afford the pure product **19n** (233 mg, 1.02 mmol, 64%) as a pale-yellow oil. **^{1}H NMR (500 MHz, $CDCl_3$):** δ (ppm) = 7.22 (ddd, J = 8.2, 7.4, 1.8 Hz, 1H), 7.14 (dd, J = 7.4, 1.8 Hz, 1H), 6.92 – 6.82 (m, 2H), 3.81 (s, 3H), 3.07 (dd, J = 13.3, 6.8 Hz, 1H), 2.91 – 2.83 (m, 1H), 2.72 (dd, J = 13.3, 7.6 Hz, 1H), 1.17 (d, J = 7.0 Hz, 3H);**^{13}C NMR (126 MHz, $CDCl_3$):** δ (ppm) = 157.5, 131.5, 128.2, 127.0, 120.3, 110.3, 55.2, 50.0, 42.6, 25.9; **IR (neat, cm^{-1}):** 2956, 2920, 2833, 1599, 1490, 1462, 1375, 1287, 1240, 1175, 11233, 1047, 1027, 998, 748; **HRMS** calcd. for ($C_{10}H_{13}O$) $[M\text{-}Br]^+$: 149.0961 found 149.0960.

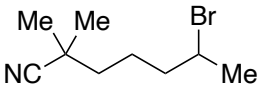

6-Bromo-2,2-dimethylheptanenitrile (19p). Diisopropylamine (2 equiv, 20 mmol, 2.0 g) was dissolved in dry THF (35 ml) and cooled to 0 ºC. *n*-BuLi (14 mmol, 2.5 M, 5.6 ml) was added drop wise and then the solution was cooled to -78ºC. Isobutyronitrile (1.0 equiv., 10.0 mmol, 0.69 g) was added dropwise and the reaction mixture was stirred for 1 h. This solution was then transferred dropwise to a solution of 1,4-dibromopentane (2 equiv, 20 mmol, 4.6 g) in dry THF (5 ml) at -78 ºC and stirred at this temperature for 2 h. The reaction mixture was allowed to warm to room temperature and stirred overnight. The reaction was quenched with H_2O and extracted with DCM (3 x 50 ml). The combined organic layers were dried ($MgSO_4$), filtered and concentrated *in vacuo*. The crude mixture was purified by column chromatography on silica gel eluting with hexane:ethyl acetate (9:1) to afford the pure product **19p** (1.62 g, 74%) as a pale-yellow oil. **^{1}H NMR (300 MHz, $CDCl_3$):** δ (ppm) = 4.18 – 4.07 (m, 1H), 1.88 – 1.49 (m, 6H), 1.72 (d, *J* = 6.7 Hz, 3H), 1.35 (s, 6H); **^{13}C NMR (75 MHz, $CDCl_3$):** δ (ppm) = 125.1, 50.9, 40.9, 40.4, 32.4, 26.8, 26.7, 26.6. Data in agreement with the literature.[10]

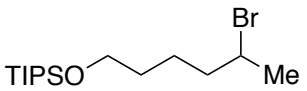

((5-bromohexyl)oxy)triisopropylsilane (19q). To alcohol 5-bromohexan-1-ol (1.0 equiv., 3.0 mmol, 0.54 g) in dry DCM (0.3 M, 5 ml) was added imidazole (2.5 equiv., 4.0 mmol, 0.27

g) followed by TIPSCl (1.25 equiv., 2.0 mmol, 0.39 g). The reaction mixture was allowed to warm to room temperature and stirred overnight. The reaction was quenched with $NaHCO_3$ (sat.) and extracted with DCM (x3). The combined organic layers were washed with brine, dried ($MgSO_4$), filtered and reduced *in vacuo*. Column chromatography on silica gel eluting with hexane:EtOAc (95:5) gave **19q** (0.63 g, 62%) as a colorless oil. **^{1}H NMR (400 MHz, $CDCl_3$):** δ (ppm) = 3.70 – 3.61 (m, 2H), 2.51 – 2.40 (m, 1H), 1.77 – 1.66 (m, 1H), 1.63 – 1.51 (m, 2H), 1.51 – 1.36 (m, 3H), 1.18 (dd, J = 7.0, 4.4 Hz, 3H), 1.10 – 1.02 (m, 21H); **^{13}C NMR (101 MHz, $CDCl_3$)**: δ (ppm) = 63.3, 51.9, 41.2, 32.5, 26.5, 24.4, 18.2, 12.2. **IR (neat, cm^{-1}):** 2941, 2865, 1463, 1100, 996, 881, 678, 657. **HRMS** calcd. for ($C_{15}H_{34}BrOSi$) $[M+H]^+$: 337.1557, found 337.1558.

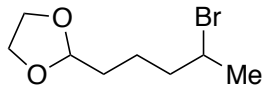

2-(4-bromopentyl)-1,3-dioxolane (19r). To the corresponding ester[26] (4.0 mmol, 0.84 g) in DCM (0.2 M, 10 ml) was added DIBAL-H (1 M in hexanes, 1.1 equiv, 4.4 mmol, 4.4 ml) dropwise. The mixture was stirred at this temperature for 1 h before being poured onto crushed ice and 1.5 ml of conc. HCl. The mixture was stirred until it reached room temperature and then the organic phase was separated, dried ($MgSO_4$), filtered and reduced *in vacuo*. The crude was purified by flash column chromatography on silica gel eluting with pentane: Et_2O (9:1) to give 5-bromohexanal (0.46 g, 64%) as a colorless oil. **^{1}H NMR (400 MHz, $CDCl_3$):** δ (ppm) = 9.78 (t, *J* = 1.5 Hz, 1H), 4.20 – 4.06 (m, 1H), 2.48 (tt, *J* = 6.7, 1.5 Hz, 2H), 1.93 – 1.74 (m, 4H), 1.72 (d, *J* = 6.6 Hz, 1H) 2H missing. **^{13}C NMR (126 MHz, $CDCl_3$)** δ (ppm) = 202.0, 50.9, 43.2, 40.4, 26.5, 20.5. **IR (neat, cm^{-1}**): 2951, 2922, 2878, 1739, 1455, 1410, 1379, 1279, 1211, 1140, 1122. To 5-bromohexanal (1.0 equiv, 3.0 mmol, 0.54 g) in dry toluene (0.5 M, 6 ml) was added dry ethylene glycol (1.1 equiv, 3.3 mmol, 185 µl) and $TsOH.H_2O$ (0.1 equiv, 0.2 mmol, 57 mg) and heated to reflux with Dean-Stark condenser for 2 days. After this time, the crude was concentrated and purified by column chromatography on silica gel eluting with hexane:EtOAc (9:1) to give **19r** (0.33 g, 49%) as a colorless oil. **^{1}H NMR (400 MHz, $CDCl_3$):** δ (ppm) = 4.86 (t, *J* = 4.4 Hz, 1H), 4.21 – 4.07 (m, 1H), 4.01 – 3.92 (m, 2H), 3.90 – 3.80 (m, 2H), 1.94 – 1.76 (m, 2H), 1.71 (d, *J* = 6.7 Hz, 3H), 1.70 – 1.60 (m, 3H), 1.56 – 1.50 (m, 1H); **^{13}C NMR (101 MHz, $CDCl_3$):** δ (ppm) = 104.5, 65.1, 65.0, 51.5, 41.1, 33.3, 26.5, 22.5; **IR (neat, cm^{-1}**): 2951, 2922, 2878, 1739, 1455, 1410, 1379, 1279, 1211, 1140, 1122; **HRMS** calcd. for ($C_8H_{16}BrO_2$) $[M+H]^+$: 223.0328, found 223.0319.

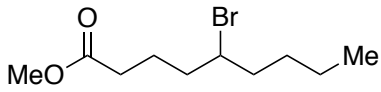

Methyl 5-bromononanoate (19s). Following **GP2**, δ-Nonalactone (1.0 equiv., 20 mmol, 3.5 ml) was added to a flask containing a solution of 33% HBr in AcOH (3.5 M, 5.7 ml) and fitted with a reflux condenser. The reaction was stirred at 75 °C for 4 hours and then cooled to room temperature. MeOH (10 ml) was added, and the reaction was stirred overnight at room temperature. After completion, the reaction was partially concentrated under reduced pressure, extracted with EtOAc, and washed with a saturated aqueous solution $NaHCO_3$ (x3) and brine. The organic layer was then dried ($MgSO_4$), filtered and concentrated *in vacuo*. The crude was purified by flash column chromatography on silica gel eluting with hexane:EtOAc (9:1) to give **19s** (4.3 g, 85%) as a colorless oil. **^{1}H NMR (400 MHz, $CDCl_3$):** δ (ppm) = 4.07 – 3.96 (m, 1H), 3.68 (s, 3H), 2.41 – 2.30 (m, 2H), 1.98 – 1.68 (m, 6H), 1.59 – 1.37 (m, 2H), 1.37 – 1.21 (m, 2H), 0.91 (t, J = 7.2 Hz, 3H). **^{13}C NMR (101 MHz, $CDCl_3$):** δ (ppm) = 173.78, 57.8, 51.7, 38.9, 38.4 33.4, 29.78, 23.1, 22.2, 14.1. **IR (neat, cm^{-1}):** 2995, 2933, 2872, 1736, 1435, 1364, 1195, 1173, 1113, 1001; **HRMS** calcd. for ($C_{10}H_{19}BrNaO_2$) $[M+Na]^+$: 273.0461, found 273.0457.

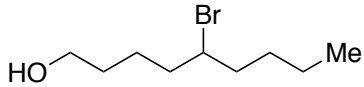

5-bromononan-1-ol (19t). To a solution of ester **19s** (1.0 equiv, 3.0 mmol, 0.75 g) in dry Et_2O (12 mL) at 0°C was added dropwise a solution of LiAlH4 in Et2O (1 M, 1.5 equiv., 2.2 mL). The reaction was allowed to warm to rt and stirred until completion. The reaction was quenched by slow addition of a 2 M aqueous NaOH solution. The salts were removed by filtration and the aqueous phase extracted with Et_2O three times. The alcohol **19t** (0.65 g, 97%) was obtained as a colorless oil after purification by column chromatography on silica gel eluting with hexane:EtOAc (4:1→2:1). **^{1}H NMR (500 MHz, $CDCl_3$):** δ (ppm) = δ 4.03 (tt, *J* = 7.7, 5.3 Hz, 1H), 3.67 (t, *J* = 6.1 Hz, 2H), 1.90 – 1.76 (m, 4H), 1.69 – 1.47 (m, 5H), 1.46 – 1.26 (m, 4H), 0.91 (t, *J* = 7.3 Hz, 3H).**^{13}C NMR (101 MHz, $CDCl_3$):** δ (ppm) = 62.9, 58.7, 39.0, 32.3, 29.9, 24.0, 22.3, 14.1; Data in agreement with the literature.[27]

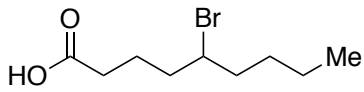

5-bromononanoic acid: δ-Nonalactone (1.0 equiv., 20 mmol, 3.5 ml) [or other lactone] was added to a flask containing a solution of 33% HBr in AcOH (3.5 M, 5.7 ml) and fitted with a reflux condenser. The reaction was heated to 75 °C for 4 hours and then cooled to room temperature. The residue was diluted with DCM and washed with saturated aqueous solution of NaS_2O_3 (x3). The aqueous layer was extracted with DCM (x3) and the combined organic layers were washed with brine, dried ($MgSO_4$) and concentrated *in vacuo* to give 5-bromononanoic acid (4.7 g, 99%) was used in the next step without further purification. **^{1}H NMR (400 MHz, $CDCl_3$):** δ (ppm) = 4.01 (tt, *J* = 7.7, 5.1 Hz, 1H), 2.46 – 2.32 (m, 2H), 1.99 – 1.69 (m, 6H), 1.57 – 1.46 (m, 1H), 1.45 – 1.24 (m, 3H), 0.91 (t, *J* = 7.2 Hz, 3H). **^{13}C NMR (101 MHz, $CDCl_3$):** δ (ppm) = 179.8, 57.7, 39.0, 38.3, 33.5, 29.8, 22.9, 22.3, 14.1; **IR (neat, cm^{-1}):** 2956, 2931, 2872, 1704, 1457, 1413, 1282, 1231, 1114.

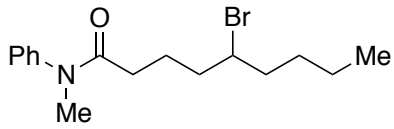

5-bromo-N-methyl-N-phenylnonanamide (19u): To a cooled solution (0 ºC) of oxalyl bromide (1.4 equiv., 2.8 mmol, 0.4 ml) in anhydrous DCM (0.3 M, 6.7 ml) was added the carboxylic acid from the previous step (1.0 equiv., 2 mmol, 0.47 g). Then, DMF (0.2 equiv., 0.4 mmol, 31 µl) was added dropwise and the reaction was stirred at 0 ºC during 2 h. After completion, the reaction was concentrated affording the corresponding crude acyl bromide that was used without further purification in the next step. To a solution of the acyl bromide in dry toluene (0.2 M, 10 ml) was added the *N*-methyl aniline (1.2 equiv., 2.4 mmol, 260 µl) and the mixture stirred at room temperature overnight. After completion, the mixture was extracted with Et_2O and washed with brine. The organic layer was dried over anhydrous $MgSO_4$ and concentrated. The residue was purified by flash column chromatography in silica gel with hexane/EtOAc (8:1 to 2:1) to give **19u** (0.27 g, 41%) as a pale orange oil. **^{1}H NMR (400 MHz, $CDCl_3$):** δ (ppm) = 7.46 – 7.38 (m, 2H), 7.34 (t, *J* = 7.4 Hz, 1H), 7.21 – 7.12 (m, 2H), 3.93 (m, 1H), 3.26 (s, 3H), 2.08 (t, *J* = 6.1 Hz, 2H), 1.85 – 1.66 (m, 6H), 1.56 – 1.38 (m, 1H), 1.40 – 1.23 (m, 3H), 0.89 (t, *J* = 7.2 Hz, 3H). **^{13}C NMR (126 MHz, $CDCl_3$):** δ (ppm) = 172.7, 144.2, 130.0, 128.0, 127.5, 58.3, 38.8, 38.7, 37.5, 33.5, 29.8, 23.7, 22.3, 14.1. **IR (neat, cm^{-1}):** 2955, 2931, 1733, 1655, 1595, 1495, 1454, 1419, 1385, 1290, 1238, 1117, 1027; **HRMS** calcd. for ($C_{16}H_{25}BrNO$) $[M+H]^+$: 326.1114 found 326.1115.

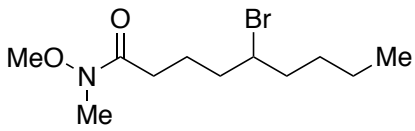

5-bromo-N-methoxy-N-methylnonanamide. To the carboxylic acid from the previous step (1.0 equiv, 5 mmol, 1.19 g) in dry DCM (0.33 M, 15 ml) at 0 °C was added CDI (1.2 equiv, 6.0 mmol, 0.97 g). The reaction mixture was stirred for 30 mins at this temperature before adding MeON(Me)H (2.4 equiv, 12 mmol, 1.17 g) was added. The mixture was allowed to warm to room temperature and stirred overnight. After this time, the suspension was filtered and the filter cake washed with DCM. The filtrate was then washed with H_2O and brine, dried ($MgSO_4$), filtered and reduced *in vacuo*. Purification by column chromatography on silica gel eluting with hexane:EtOAc (9:1 →8:2) gave the targeted Weinreb amide (1.39 g, 99%) as a pale yellow oil. **^{1}H NMR (400 MHz, $CDCl_3$):** δ (ppm) = 4.00 - 4.09 (m, 1H), 3.68 (s, 3H), 3.18 (s, 3H), 2.51 – 2.36 (m, 2H), 1.95 – 1.70 (m, 6H), 1.59 – 1.47 (m, 1H), 1.43 – 1.24 (m, 3H), 0.91 (t, *J* = 7.2 Hz, 3H); **^{13}C NMR (101 MHz, $CDCl_3$):** δ (ppm) = 172.2, 61.34, 58.3, 38.9, 38.8, 32.3, 31.3, 29.8, 22.8, 22.3, 14.1.

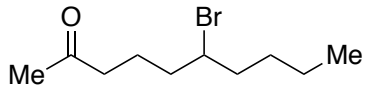

6-bromodecan-2-one (19v): To the previous Weinreb amide (1.0 equiv, 5.0 mmol, 1.39 g) in dry THF (15 ml) at 0 °C was added MeMgBr (1.1 equiv, 5.5 mmol, 3 M in Et_2O, 1.8 ml) dropwise over 10 minutes. The mixture was allowed to slowly warm to room temperature and then quenched with NH_4Cl sat. and diluted with Et_2O (15 ml). The layers were separated and then aq. layer was extracted with Et_2O (15 ml x 2). The combined organic layers were dried ($MgSO_4$), filtered and reduced *in vacuo*. Purification by column chromatography on silica gel eluting with pentane:Et_2O (9:1) gave the methyl ketone **19v** (1.14 g, 97%) as a colorless oil. **^{1}H NMR (400 MHz, $CDCl_3$):** δ (ppm) = 4.05 – 3.94 (m, 1H), 2.46 (td, *J* = 6.6, 2.3 Hz, 2H), 2.14 (s, 3H), 1.89 – 1.77 (m, 5H), 1.76 – 1.66 (m, 1H), 1.55 – 1.45 (m, 1H), 1.43 – 1.24 (m, 3H), 0.91 (t, *J* = 7.2 Hz, 3H); **^{13}C NMR (126 MHz, $CDCl_3$):** δ (ppm) = 208.6, 58.1, 43.0, 38.9, 38.5, 30.0, 29.8, 22.3, 22.0, 14.1. **IR (neat, cm^{-1}):** 2956, 2932, 2862, 1715, 1456, 1431, 1411, 1361, 1259, 1235, 1162, 1116; **HRMS** calcd. for ($C_{10}H_{19}BrNaO$) $[M+Na]^+$: 257.0511, found 257.0509.

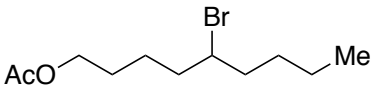

5-bromononyl acetate (19w). To a solution of alcohol **19t** (1.0 equiv, 2.0 mmol, 0.42 g) in dry DCM (0.2 M) at 0°C was added DMAP (10 mol%, 0.2 mmol, 24 mg), followed by acetic anhydride (2.0 equiv., 4.0 mmol, 0.38 mL) and Et_3N (2.0 equiv., 4.0 mmol, 0.56 mL). The reaction was allowed to warm to rt and stirred overnight. The mixture was quenched with H_2O and extracted using DCM three times. The organic phase was dried over anhydrous $MgSO_4$, filtered and solvent removed under reduced pressure. **19w** (0.32 g, 60%) was obtained as a colorless oil after purification by column chromatography on silica gel eluting with hexane:EtOAc (9:1→8:2). **^{1}H NMR (400 MHz, $CDCl_3$):** δ (ppm) = 4.07 (t, J = 6.4 Hz, 2H), 4.01 (tt, J = 7.5, 5.4 Hz, 1H), 2.05 (s, 3H), 1.90 – 1.73 (m, 4H), 1.73 – 1.59 (m, 3H), 1.59 – 1.45 (m, 2H), 1.44 – 1.22 (m, 3H), 0.91 (t, J = 7.2 Hz, 3H).**^{13}C NMR (101 MHz, $CDCl_3$):** δ (ppm) = 171.3, 64.4, 58.34 39.1, 38.8, 29.9, 28.2, 24.2, 22.3, 21.1, 14.1. **IR (neat, cm^{-1}):** 2955, 2934, 2862, 1737, 1458, 1434, 1365, 1232, 1040; **HRMS** calcd. for ($C_{11}H_{21}BrNaO_2$) $[M+Na]^+$: 287.0617 found 287.0614.

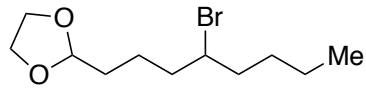

2-(4-bromooctyl)-1,3-dioxolane (19x). To a solution of ester **19s** (1 equiv, 2.0 mmol, 0.50 g) in DCM (0.2 M, 10 ml) at -78°C was added DIBAL-H (1 M in hexanes, 1.1 equiv., 2.2 mmol, 2.2 mL) dropwise. The reaction was stirred at -78°C for an hour and then poured onto crushed ice and aq. HCl (36%, 1.5 mL). The mixture was stirred until it reached rt, the layers were separated, and the organic phase was dried over anhydrous $MgSO_4$, filtered and solvent evaporated under reduced pressure to give the intermediate aldehyde (0.44 g, quant.) that was utilized without further purification. **^{1}H NMR (400 MHz, $CDCl_3$):** δ (ppm) = 9.80 (t, *J* = 1.6 Hz, 1H), 4.04 (ddt, *J* = 12.3, 10.5, 3.9 Hz, 1H), 2.59 – 2.33 (m, 2H), 2.01 – 1.74 (m, 6H), 1.60 – 1.49 (m, 1H), 1.47 – 1.27 (m, 3H), 0.94 (t, J = 7.2 Hz, 3H). To a solution of the previous aldehyde (1.0 equiv, 1.4 mmol, 0.44 g) in toluene (0.5 M, 4.0 mL) was added ethylene glycol (1.1 equiv., 2.2 mmol, 136.6 mg) and TsOH.H2O (0.1 equiv., 0.2 mmol, 38 mg) and set on a Dean-Stark apparatus. The reaction was stirred at reflux for 2 days. After this time, the crude was concentrated and purified by column chromatography on silica gel eluting with hexane:EtOAc (9:1) to give **19x** (0.3 g, 57%) as a colorless. **^{1}H NMR (400 MHz, $CDCl_3$):** δ (ppm) = 4.86 (t, *J* = 4.3 Hz, 1H), 4.02 (ddd, *J* = 12.9, 7.5, 5.5 Hz, 1H), 3.99 – 3.93 (m, 2H), 3.89 – 3.81 (m, 2H), 1.90 – 1.78 (m, 4H), 1.75 – 1.62 (m, 3H), 1.56 – 1.47 (m, 2H), 1.44 – 1.25 (m, 3H), 0.91 (t, J = 7.2 Hz, 3H); **^{13}C NMR (101 MHz, $CDCl_3$):** δ (ppm) = 104.5, 65.1, 65.0, 58.5,

39.1, 39.0, 33.4, 29.9, 22.3, 14.1. **IR (neat, cm^{-1}):** 2954, 2931, 2872, 1737, 1458, 1434, 1410, 1380, 1235, 1140, 1034; **HRMS** calcd. for ($C_{11}H_{20}BrO_2$) [M-H]$^+$: 263.0641 found 263.0638.

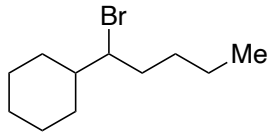

(1-bromopentyl)cyclohexane (19ac). To a stirred solution of cyclohexanecarbaldehyde (1.00 equiv, 15.0 mmol, 1.8 mL) under argon in dry THF (43 ml, 0.35 M) at 0 ºC, ^{n}BuMgCl (1.2 equiv, 18 mmol, 2 M, 9 mL) was added dropwise. Then the reaction was allowed to warm up to rt and stirred until starting material disappeared, monitored by TLC (ca. 3 h). Afterwards, the reaction was quenched with a saturated aqueous solution of NH_4Cl and extracted with Et_2O (3 x 20 mL). The organic phases were collected and dried over $MgSO_4$, the volatiles were removed in vacuo and the crude of the reaction was purified by flash column chromatography (gradient Hexanes/AcOEt 5% to 20%) to afford 1-cyclohexylpentan-1-ol (2.25g, 13.2 mmol, 88%) as colorless oil. 1H NMR (400 MHz, CDCl3) δ 3.34 (dt, J = 8.6, 4.0 Hz, 1H), 1.85 – 1.71 (m, 3H), 1.65 (m, 2H), 1.55 – 0.95 (m, 13H), 0.91 (t, J = 7.0 Hz, 3H). 13C NMR (101 MHz, CDCl3) δ 76.4, 43.7, 34.0, 29.4, 28.3, 27.8, 26.7, 26.5, 26.4, 23.0, 14.2.

To a stirred solution of 1-cyclohexylpentan-1-ol (1.00 equiv, 13.2 mmol, 2.25 g) in DCM (0.5 M, 27 mL) at 0 ºC under argon atmosphere, Et_3N (2 equiv, 26.5 mmol, 3.7 mL) was added. The reaction was stirred for 5 min and then MsCl (1.2 equiv, 1.2 mL, 15.9 mmol) was added dropwise. Afterwards, the reaction was allowed to warm up to rt and stirred for an additional 2h. The reaction was quenched with water. The organic phase was washed with 1M solution of HCl (2x), a saturated solution of $NaHCO_3$ (2x) and brine (2x), dried over $MgSO_4$ and the solvent was removed in vacuo to yield the desired product that was used in the next step without further purification.

To a stirred solution of the previously synthesized 1-cyclohexylpentyl methanesulfonate in acetone (0.5 M, 27 mL) was added LiBr (4.0 equiv, 4.6 g, 53 mmol) and the reaction was stirred for 16 h at 45 ºC. Then, the reaction was quenched with water and extracted with Et_2O (2x). The combined organic layers were washed with brine, dried over $MgSO_4$ and the solvent was removed carefully in the rotavapor (30 ºC, 500 mbar). The crude of the reaction was dissolved in pentane (20 mL) and filtered through a plug of silica, to yield the desired product with some impurities (alkene elimination product) of around 30%, judged by NMR crude.

To a solution of the desired impure product (1.3 g) in Et_2O (20 mL) at 0 ºC under argon atmosphere was added a solution of OsO_4 (1 g, 4 mmol) in Et_2O (20 mL). After 30 min the

reaction was warmed up to rt and stirred for 90 min. Once the reaction reached completion, according to TLC (alkene rf: 0.98, bromide rf: 0.95 in pure hexane) the solvent was removed in the rotavapor (30 ºC, 500 mbar) and pentane (20 mL) was added to the crude. The crude was filtered through a silica/celite/flurosil (1:1:1) plug and washed with pentane to yield the target product **19ac** (800 mg, 3.22 mmol, 25% (3 steps)) as a colorless oil. **^{1}H NMR (400 MHz, $CDCl_3$):** δ (ppm) = 3.97 (dt, J = 8.8, 4.3 Hz, 1H), 2.15 – 1.45 (m, 7H), 1.44 – 1.11 (m, 8H), 0.90 (dt, J = 12.2, 7.2 Hz, 5H); **^{13}C NMR (101 MHz, $CDCl_3$)** δ (ppm) = 66.3, 44.6, 36.0, 31.2, 30.4, 29.3, 26.5, 26.4, 26.3, 22.3, 14.1; **IR (neat, cm^{-1}):** 2924, 2853, 2666, 1699, 1448, 1417, 1289, 1236, 1202; **HRMS** calcd. for ($C_{11}H_{21}$) $[M\text{-}Br]^+$: 153.1638 found 153.1632.

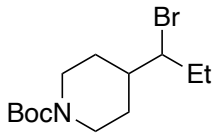

tert-butyl 4-(1-bromopropyl)piperidine-1-carboxylate (19ae). In an oven-dried round bottom flask containing a magnetic stir bar under inert atmosphere, EtMgBr (1.05 equiv, 8.40 mmol, 3 M, 2.80 mL) was added dropwise to a solution of *tert*-butyl 4-formylpiperidine-1-carboxylate (1.0 equiv, 8.0 mmol, 1.71 g) in THF (23 mL) at 0 ºC. The reaction mixture was stirred for 1h and then allowed to warm up to room temperature and further stirred for 3 h. The reaction was quenched using 1M HCl. DCM was added and the mixture transferred to a separatory funnel. The organic phase was collected, and the aqueous phase extracted twice more with DCM. The combined organic phase was dried over $MgSO_4$, filtered, and evaporated under reduced pressure. Purification by flash column chromatography (pentane:EtOAc 2:1) gave the alcohol intermediate (1.01 g, 52%). In an oven-dried Schlenk flask containing a magnetic stir bar, triphenylphosphine (1.31 g, 4.98 mmol, 1.2 equiv.) and CBr_4 (1.65 g, 4.98 mmol, 1.2 equiv.) were dissolved in dry DCM (0.6 M based on alcohol). After cooling the solution to 0 ºC, the alcohol intermediate (1.01 g, 4.15 mmol, 1 equiv.) diluted in DCM (0.5 M) was added dropwise and the reaction stirred for 10 min. The reaction mixture was allowed to warm up to rt and stirred overnight. Then, the solution was concentrated *in vacuo* to ca. 10 mL, followed by addition of pentane to precipitate the triphenylphosphine oxide side product which was filtered off. The collected organic phase was concentrated under reduced pressure. The crude mixture was purified by flash column chromatography through silica gel (eluent: pentane:EtOAc 95:5-9:1) to afford the pure product **19ae** (470.2 mg, 1.54 mmol, 37%) as a colorless viscous oil. **^{1}H NMR (500 MHz, $CDCl_3$):** δ (ppm) = 4.19 (d, *J* = 13.2 Hz, 2H), 3.92 (dt, *J* = 9.0, 4.7 Hz, 1H), 2.70 (t, *J* = 12.9 Hz, 2H), 1.94 – 1.79 (m, 3H), 1.78 – 1.67 (m, 2H), 1.48 (s, 9H), 1.46 – 1.32 (m, 2H), 1.09 (t, *J* = 7.2 Hz, 3H).**^{13}C NMR (126 MHz, $CDCl_3$):** δ (ppm) = 154.9, 79.6, 65.7, 43.8, 42.9, 30.1, 29.2, 28.6,

12.6.; **IR (neat, cm^{-1}):** 2968, 2934, 2851, 1685, 1418, 1363, 1277, 1231, 1159, 1098, 967, 865; **HRMS** calcd. for ($C_{13}H_{24}BrNNaO_2$) $[M+Na]^+$: 328.0883 found 328.0884.

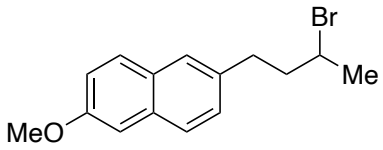

2-(3-bromobutyl)-6-methoxynaphthalene (19ag). Following **GP5**, sodium tetrahydroborate (0.240 g, 6.35 mmol) was added in small portions to the solution of Nabumetone (1.00 g, 4.38 mmol) in absolute ethanol (12 mL) at -10°C under an N_2 atmosphere. The reaction mixture was stirred for 1 h at -10°C and 3 h at rt. The solvent was evaporated under reduced pressure and the residue was dissolved in dichloromethane (50 ml), washed carefully with cold H_2O (2x30 ml), dried through a phase separator and concentrated in vacuo to provide 4-(6-methoxynaphthalen-2-yl)butan-2-ol (964 mg, 96 %) as a white solid. To a solution of 4-(6-methoxynaphthalen-2-yl)butan-2-ol (964 mg, 4.19 mmol) in dry DCM (8 ml) at 0°C, perbromomethane (1.67 g, 5.02 mmol) was added. After 10 min, a solution of triphenylphosphine (3.35 ml, 5.02 mmol) in DCM (1.5 M) was added dropwise at 0°C. Then, the reaction mixture was allowed to warm to rt and was stirred for 3h. After reaction was completed, the solvent was evaporated under vacuum and the product was purified by column chromatography (heptane:EtOAc gradient 0% -> 40%) to yield 2-(3-bromobutyl)-6-methoxynaphthalene **19ag** (1.14 g, 93 %) as a white solid. **^{1}H NMR (500 MHz, $CDCl_3$):** δ (ppm) = 7.72 – 7.64 (m, 2H), 7.61 – 7.56 (m, 1H), 7.31 (dd, J = 8.3, 1.8 Hz, 1H), 7.17 – 7.08 (m, 2H), 4.15 – 4.05 (m, 1H), 3.92 (s, 3H), 2.99 (ddd, J = 14.0, 8.8, 5.2 Hz, 1H), 2.88 (ddd, J = 13.8, 8.7, 7.2 Hz, 1H), 2.21 (dtd, J = 14.2, 8.8, 5.3 Hz, 1H), 2.12 (dddd, J = 14.4, 8.7, 7.2, 4.4 Hz, 1H), 1.75 (d, J = 6.7 Hz, 3H).**^{13}C NMR (126 MHz, $CDCl_3$)** δ (ppm) = 157.4, 136.2, 133.3, 129.2, 129.1, 127.9, 127.1, 126.7, 119.0, 105.8, 55.5, 51.1, 42.8, 34.0, 26.7. **Melting Point:** 60°C. Data in agreement with the literature.[10]

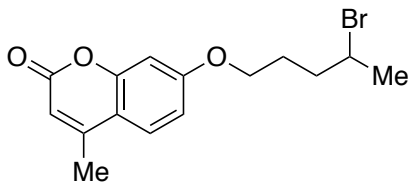

7-((4-bromopentyl)oxy)-4-methyl-2*H*-chromen-2-one (19ah). 4-Methylumbelliferone (1.0 equiv, 8.0 mmol, 1.41 g) and K_2CO_3 (1.2 equiv., 9.6 mmol, 1.33 g) were stirred at room temperature in dry DMF (13 mL) for an hour. Then, 1.5-dibromopentane (2.0 equiv., 16.0

mmol, 3.68 g, 2.2 mL) was subsequently added. The mixture was stirred at room temperature for 24h. After completion, water was added, and the mixture was extracted twice with EtOAc and combined organic layers combined and washed with brine. The organic layer was then dried over $MgSO_4$, filtered, and concentrated *in vacuo*. The residue was purified by flash chromatography (Pentane:EtOAc 3:1) to afford 7-((4-bromopentyl)oxy)-4-methyl-2H-chromen-2-one **19ah** (1.45 g, 97%) as a white solid. **^{1}H NMR (400 MHz, $CDCl_3$):** δ (ppm) = 7.49 (d, *J* = 8.8 Hz, 1H), 6.85 (dd, *J* = 8.8, 2.5 Hz, 1H), 6.80 (d, *J* = 2.5 Hz, 1H), 6.13 (q, *J* = 1.2 Hz, 1H), 4.25 – 4.14 (m, 1H), 4.10 – 4.01 (m, 2H), 2.40 (d, *J* = 1.3 Hz, 3H), 2.13 – 1.91 (m, 4H), 1.76 (d, *J* = 6.7 Hz, 3H).; **^{13}C NMR (126 MHz, $CDCl_3$):** δ (ppm) = 13C NMR (101 MHz, CDCl3) δ 162.1, 161.4, 155.4, 152.7, 125.7, 113.7, 112.7, 112.1, 101.5, 67.8, 51.0, 37.7, 27.6, 26.7, 18.8; **IR (neat, cm^{-1}):** 3074, 2955, 2920, 1709, 1609, 1562, 1511, 1470, 1445, 1425, 1389, 1372, 1347, 1283, 1262, 1239, 1204, 1169, 1152, 1134, 1071, 1042, 1017; **HRMS** calcd. for ($C_{15}H_{18}BrO_3$) $[M+H]^+$: 325.0434 found 325.0437. **Melting Point:** 75°C

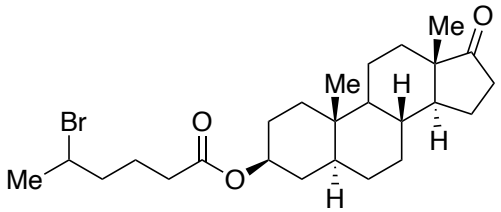

(3*S*,5*S*,10*S*,13*S*,14*S*)-10,13-dimethyl-17-oxohexadecahydro-1*H*-cyclopenta[*a*]- 166 -henanthrene-3-yl 5-bromohexanoate (19ai). Following **GP3**. Δ-Hexanolactone (1.0 equiv., 20 mmol, 2.2 ml) was added to a flask containing a solution of 33% HBr in AcOH (3.5 M, 5.7 ml) and fitted with a reflux condenser. The reaction was heated to 75 °C for 4 hours and then cooled to room temperature. The residue was diluted with DCM and washed with saturated aqueous solution of NaS_2O_3 and H_2O twice. The organic layer was dried ($MgSO_4$) and concentrated *in vacuo* to give 5-bromohexanoic acid (3.6 g, 89%) which was used in the next step without further purification. To a solution of Epiandrosterone (1.0 equiv., 3.0 mmol, 871 mg), DCC (1.2 equiv., 3.6 mmol, 743 mg) and DMAP (0.1 equiv., 0.3 mmol, 37 mg) in DCM (0.2 M) at 0°C was added a solution of 5-bromohexanoic acid (2 M, 1 equiv., 3.0 mmol, 585 mg, 1.5 mL) dropwise. The reaction was then allowed to warm to rt and stirred overnight. Water was added and the mixture transferred to a separatory funnel. The organic phase was collected, and the aqueous phase further washed with two portions of DCM. The combined organic layers were dried over anhydrous $MgSO_4$, filtered and solvent evaporated under reduced pressure. The crude was purified trough flash column

chromatography (Pentane:EtOAc 9:1) to yield **19ai** (1.16 g, 83%) as a white solid. **^{1}H NMR (400 MHz, $CDCl_3$):** δ (ppm) = 4.70 (tt, J = 11.3, 4.9 Hz, 1H), 4.18 – 4.06 (m, 1H), 2.49 – 2.37 (m, 1H), 2.36 – 2.25 (m, 2H), 2.13 – 1.99 (m, 1H), 1.98 – 1.86 (m, 1H), 1.85 – 1.74 (m, 7H), 1.71 (d, J = 6.7 Hz, 4H), 1.69 – 1.57 (m, 2H), 1.57 – 1.42 (m, 3H), 1.42 – 1.15 (m, 7H), 1.10 – 0.90 (m, 2H), 0.87 – 0.82 (m, 6H), 0.71 (ddd, J = 11.9, 10.2, 4.1 Hz, 1H); **^{13}C NMR (101 MHz, $CDCl_3$):** δ (ppm) = 173.1, 73.6, 54.4, 51.5, 47.9, 44.8, 36.8, 36.0, 35.8, 35.2, 34.6, 34.1, 33.0, 31.7, 30.9, 28.4, 27.6, 25.0, 22.8, 21.9, 20.6, 17.8, 17.1, 13.9, 12.3; **IR (neat, cm^{-1}):** 2944, 2914, 2847, 1732, 1718, 1449, 1419, 1377, 1357, 1322, 1295, 1273, 1249, 1232, 1188, 1152, 1132, 1116, 1101, 1059, 1014; **HRMS** calcd. For ($C_{25}H_{40}BrO_3$) $[M+H]^+$: 467.2155 found 467.2159. **Melting Point:** 109°C

Preparation of the Ni precatalysts

The synthesis of Ni precatalyst was based on a the modification of a known procedure reported in the literature.[28]

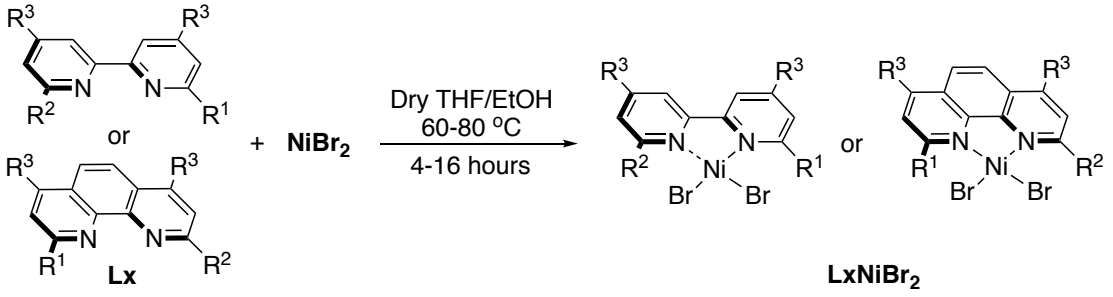

General procedure: To an oven-dried reaction vial or sealed tube was added $NiBr_2$.glyme (1 equiv) and the corresponding ligand (1.1-1.2 equiv). The tube was then connected to a vacuum line where it was evacuated and backfilled under Argon flow at least three times. Then, dry ethanol or dry THF was added as solvent. The mixture was stirred for 4-16 hours upon heating (60-80 °C). The mixture was allowed to cool to rt and the solid was collected by filtration, washed with cold EtOH followed by cold pentane to yield pure complex of the type $LniBr_2$.

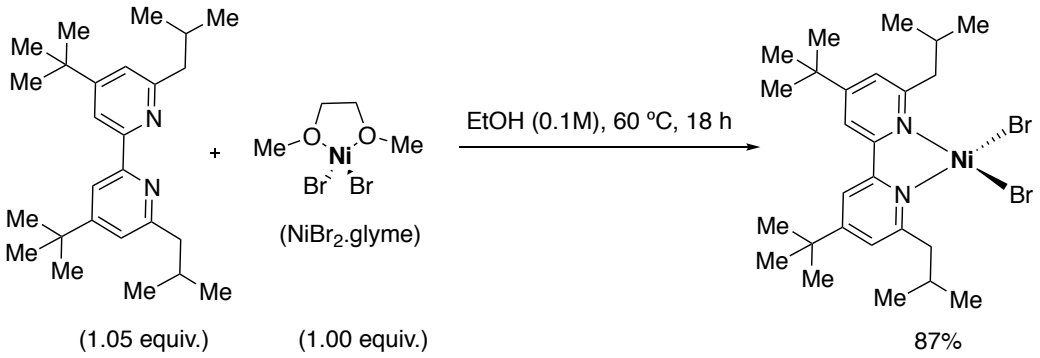

Synthesis of L11NiBr$_2$. A two-neck round-bottom flask equipped with reflux condenser and magnetic stir bar was charged with $NiBr_2$.glyme (154 mg, 0.500 mmol, 1.0 equiv.), ligand **L11** (200 mg, 0.525 mmol, 1.05 equiv.) and ethanol (5 mL). The resulting reaction mixture was heated at 60 ºC for 18 h. After cooling to rt, the solid precipitate was filtered, washed with ethanol followed by pentane and dried under reduced pressure to deliver desired complex as purple solid (262 mg, 0.44 mmol, 87%). The complex was recrystallized from dichloromethane/pentane (6/1) to afford the paramagnetic purple crystals that were analyzed by X-ray diffraction.

^{1}H NMR (400 MHz, THF-d_8) δ 72.72 (s, 4H), 58.66 (s, 4H), 24.63 (s, 5H), 20.33 (s, 3H).
^{13}C omitted due to line broadening of paramagnetic (**L11**)$NiBr_2$.

3.7.3. Retained Carboxylation of Secondary Alkyl bromides

General Procedure 6 (GP6): An oven-dried Schlenk tube containing a magnetic stir bar was charged with L11NiBr$_2$ (0.10 equiv), 4CzIPN (0.05 equiv.), Hantzsch ester (HEH, 2.0 equiv) and the alkyl bromide (1.0 equiv, if it is solid). The Schlenk tube was then taken inside a glovebox, where Cs_2CO_3 (2.0 equiv.) was added. The tube was then taken out of the glovebox and connected to a vacuum line where it was evacuated and back-filled under CO_2 flow at least three times. The alkyl bromide (1.0 equiv., if it is liquid) and NMP (0.08 M) were added under CO_2 flow. Once all the components were added, the Schlenk tube was closed at the atmospheric pressure of CO_2 (1 bar) and placed in a temperature controlled photoreactor with cooling set at 15ºC (which gives an *in situ* reaction temperature of ca 20ºC) and stirred for 24 h in the presence of continuous irradiation with blue light (451 nm, 1 W LED).

Work-up 1 (W1): The reaction mixture was carefully quenched with 2 M HCl aq. solution and diluted with EtOAc (10 ml). The layers were separated, and the aqueous layer was extracted with EtOAc (10 ml). The combined organic layers were then washed with 2 M HCl solution (10 ml x 3), dried ($MgSO_4$) and concentrated *in vacuo*. Then the crude mixture was dissolved in Et_2O (10 ml) and the organic phase was extracted with 1 M NaOH aq. solution (5 ml x 3). The combined aqueous phases were acidified to < pH = 2 using 2 M HCl aq. solution (8 ml). Finally, the acidic aqueous phase was extracted with EtOAc or Et_2O (10 ml x 2) depending on how soluble the compound is in the solvent used. The combined organic layers were washed with 2 M HCl solution (10 ml x 3), dried ($MgSO_4$), filtered and reduced *in vacuo* to give the pure carboxylic acid.
Work-up 2 (W2): The reaction mixture was carefully quenched with H_2O (10 ml) and diluted with EtOAc (10 ml). The layers were separated, and the mildly basic aq. layer was extracted with EtOAc (10 ml). The combined organic layers were then back extracted with mildly basic NaOH (0.2 M) to avoid loss of any product to the organic layer. The combined aqueous layer was then carefully acidified with 2 M HCl solution (~20 drops) until pH = 3–4 and then extracted with EtOAc (10 ml x 2). The combined organic layers were then washed with 2 M HCl solution (10 ml x 5) to remove NMP, dried ($MgSO_4$), filtered and reduced *in vacuo* to give the pure carboxylic acid.
Work-up 3 (W3): The reaction mixture was carefully quenched with H_2O (10 ml) and diluted with EtOAc (10 ml). The layers were separated, and the mildly basic aq. layer was extracted with EtOAc (10 ml). The combined organic layers were then back extracted with mildly basic NaOH (0.2 M) to avoid loss of any product to the organic layer. The combined aqueous layers were then carefully acidified with 2 M HCl solution (~25 drops) until pH = 3–4 and then extracted with EtOAc (10 ml x 2). The combined

organic layers were then washed with H_2O (10 ml), dried ($MgSO_4$), filtered and reduced *in vacuo* to ~5 ml. The residue was then further washed with H_2O/ brine (10 ml x 3), dried ($MgSO_4$), filtered and reduced *in vacuo* to give the pure carboxylic acid.

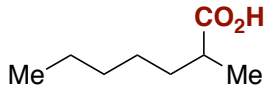

2-methylheptanoic acid (20a). Following **GP6**, 2-bromo-heptane **19a** (44.8 mg, 0.25 mmol, 40 µL) afforded the title compound as colorless liquid after **W1** (On average: 29 mg, 81%, 99:1 selectivity by GC-fid). **^{1}H NMR (500 MHz, $CDCl_3$):** δ (ppm) = δ 2.52 – 2.39 (m, 1H), 1.75 – 1.62 (m, 1H), 1.50 – 1.38 (m, 1H), 1.38 – 1.22 (m, 6H), 1.18 (d, J = 7.0 Hz, 3H), 0.92 – 0.84 (m, 3H); **^{13}C NMR (101 MHz, $CDCl_3$)** δ (ppm) = 183.4, 39.5, 33.6, 31.84, 267.0, 22.6, 17.0, 14.6. Spectroscopic data for **200a** match those previously reported in literature.

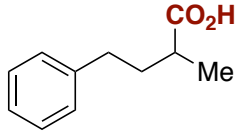

2-Methyl-4-phenylbutanoic acid (20b). Following **GP6**, (3-bromobutyl)benzene (**19b**) (0.25 mmol, 53 mg) afforded the title compound **20b** as colorless liquid after **W1** (On average: 30 mg, 0.17 mmol, 67%, >20:1 selectivity determined by ^{1}H NMR). **^{1}H NMR (300 MHz, $CDCl_3$):** δ (ppm) = 7.27 – 7.32 (m, 2H), 7.17 – 7.22 (m, 3H), 2.68 (t, *J* = 7.9 Hz, 2H), 2.47 – 2.58 (m, 1H), 2.00 – 2.12 (m, 1H), 1.70 – 1.82 (m, 1H), 1.25 (d, *J* = 7.0 Hz, 3H); **^{13}C NMR (75 MHz, $CDCl_3$)** δ (ppm) = 183.2, 141.6, 128.6, 128.6, 126.1, 39.0, 35.3, 33.5, 17.1. Spectroscopic data match those previously reported in literature.[29]

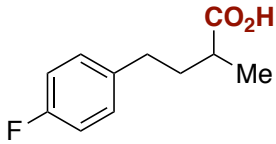

4-(4-Fluorophenyl)-2-methylbutanoic acid (20c). Following **GP6**, 1-(3-bromobutyl)-4-fluorobenzene (**19c**) (0.25 mmol, 58 mg) afforded the title compound **20c** as pale-yellow liquid after **W1** (In average, 36 mg, 0.18 mmol, 73%, >20:1 selectivity determined by ^{1}H NMR). **^{1}H NMR (400 MHz, $CDCl_3$):** δ (ppm) = 7.13 – 7.16 (m, 2H), 6.94 – 6.99 (m, 2H), 2.65 (t, *J* = 7.9 Hz, 2H), 2.46 – 2.54 (m, 1H), 1.98 – 2.07 (m, 1H), 1.68 – 1.77 (m, 1H), 1.24 (d, *J* = 7.0 Hz, 3H);**^{13}C NMR (101 MHz, $CDCl_3$)** δ (ppm) = 183.2, 161.5 (d, *J* = 243.6 Hz), 137.2 (d, *J* = 3.3

Hz), 129.9 (d, *J* = 7.9 Hz), 115.3 (d, *J* = 21.2 Hz), 38.9, 35.4, 32.7, 17.1; **^{19}F NMR (376 MHz, $CDCl_3$)** δ (ppm) = -117.59; **IR (neat, cm^{-1}):** 3030, 3001, 2983, 1701, 1598, 1560, 1539, 1431, 1219, 1180, 813; **HRMS** calcd. for ($C_{11}H_{12}FO_2$) $[M-H]^-$: 195.0827 found 195.0826.

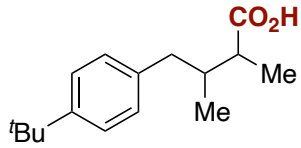

4-(4-(*tert*-Butyl)phenyl)-2,3-dimethylbutanoic acid (20d). Following **GP6** with 8 mol% of 4-CzIPN, 1-(3-bromo-2-methylbutyl)-4-(*tert*-butyl)benzene (**19d**) (70.8 mg, 0.25 mmol) afforded the title compound **20d** as colorless liquid after **W1** (On average: 55.1 mg, 0.22 mmol, 88%, >95:5 selectivity, dr = 1:1). **^{1}H NMR (400 MHz, $CDCl_3$):** δ (ppm) = 7.31 (d, *J* = 7.6 Hz, 2H), 7.12 (d, *J* = 7.6 Hz, 2H), 2.83 (dd, *J* = 13.5, 5.3 Hz, 1H), 2.67 (dd, *J* = 13.5, 6.4 Hz, 1H), 2.53 – 2.34 (m, 2H), 2.32 – 2.04 (m, 1H), 1.32 (s, 9H), 1.20 (dd, *J* = 23.3, 7.1 Hz, 3H), 0.91 (dd, *J* = 13.2, 6.8 Hz, 3H). **^{13}C NMR (101 MHz, $CDCl_3$)** δ (ppm) = 182.7 (d, *J* = 58.7 Hz), 148.9 (d, *J* = 10.3 Hz), 137.5 (d, *J* = 24.6 Hz), 128.9 (d, *J* = 16.5 Hz), 125.3 (d, *J* = 8.4 Hz), 43.7 (d, *J* = 71.5 Hz), 40.10 (d, *J* = 110.4 Hz), 37.7 (d, *J* = 126.5 Hz), 34.5 (tertiary C of ^{t}Bu), 31.6 (Methyl C signal of ^{t}Bu), 16.2 (d, *J* = 127.3 Hz), 12.9 (d, *J* = 248.3 Hz); **IR (neat, cm^{-1}):** 2960, 1700, 1457, 1411, 1266, 1231, 1108, 1018, 906, 808, 729; **HRMS** calcd. for ($C_{16}H_{23}O_2$) $[M-H]^-$: 247.1704 found 247.1707.

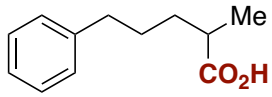

2-Methyl-5-phenylpentanoic acid (20e). Following **GP6** with 10 mol% of 4-CzIPN at 10°C for 48h, (4-bromopentyl)benzene **19e** (57 mg, 0.25 mmol) afforded the title compound **20e** as colorless liquid after **W2** (on average: 37 mg, 77%, >20:1 selectivity determined by ^{1}H NMR). **^{1}H NMR (500 MHz, $CDCl_3$):** δ (ppm) = 7.30 (dd, J = 8.7, 6.7 Hz, 2H), 7.21 (dd, J = 8.3, 6.7 Hz, 3H), 2.65 (t, J = 7.5 Hz, 2H), 2.51 (h, J = 6.9 Hz, 1H), 1.82 – 1.64 (m, 3H), 1.57 – 1.46 (m, 1H), 1.21 (d, J = 7.0 Hz, 3H); **^{13}C NMR (101 MHz, $CDCl_3$)** δ (ppm) = 183.5, 142.2, 128.5, 128.4, 125.9, 39.4, 35.9, 33.2, 29.1, 17.0; **HRMS** calcd. for ($C_{12}H_{15}O_2$) $[M-H]^-$: 191.1078 found 191.1079. Data in agreement with the literature.[30]

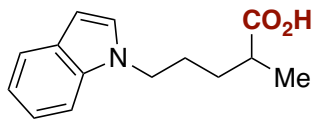

5-(1*H*-Indol-1-yl)-2-methylpentanoic acid (20f). Following **GP6**, 1-(4-bromopentyl)-1*H*-indole (**19f**, 67 mg, 0.25 mmol) afforded the title compound **20f** as brown liquid after **W1** (On average: 44 mg, 0.19 mmol, 76%, >20:1 selectivity determined by ^{1}H NMR). **^{1}H NMR (300 MHz, $CDCl_3$):** δ (ppm) = 7.65 (d, *J* = 7.8 Hz, 1H), 7.35 (dd, *J* = 8.2, 1.0 Hz, 1H), 7.22 (ddd, *J* = 8.3, 6.9, 1.3 Hz, 1H), 7.10 – 7.14 (m, 2H), 6.51 (d, *J* = 3.2 Hz, 1H), 4.14 (td, *J* = 7.0, 1.5 Hz, 2H), 2.42 – 2.54 (m, 1H), 1.86 – 1.96 (m, 2H), 1.67 – 1.79 (m, 1H), 1.41 – 1.53 (m, 1H), 1.18 (d, *J* = 7.0 Hz, 3H); **^{13}C NMR (75 MHz, $CDCl_3$)** δ (ppm) = 182.8, 136.0, 128.7, 127.8, 121.6, 121.1, 119.4, 109.4, 101.3, 46.2, 39.2, 30.8, 28.0, 17.1; **IR (neat, cm^{-1}):** 3126, 2935, 1702, 1601, 1465, 1321, 1198, 1120, 781; **HRMS** calcd. for ($C_{14}H_{16}NO_2$) [M–H]$^-$: 230.1187, found 230.1187.

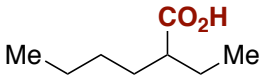

2-ethylhexanoic acid (20g). Following **GP6** but with 8 mol% 4-CzIPN and a reaction temperature of 10°C (ca. 15°C *in situ*), 3-bromo-heptane **19g** (0.25 mmol, 39 µL) afforded the title compound **20g** as colorless liquid after **W1** (On average: 27 mg, 0.19 mmol, 75%, 16:1 selectivity determined by ^{1}H NMR). **^{1}H NMR (400 MHz, $CDCl_3$):** δ (ppm) = δ 2.38 (tt, *J* = 8.5, 5.5 Hz, 1H), 1.81 – 1.54 (m, 4H), 1.48 – 1.33 (m, 4H), 1.03 (t, *J* = 7.4 Hz, 3H), 0.98 (t, *J* = 7.2 Hz, 3H).**^{13}C NMR (126 MHz, $CDCl_3$)** δ (ppm) = 183.1, 47.3, 31.6, 29.7, 25.3, 22.8, 14.0, 11.9. Spectroscopic data match those previously reported in literature.[31]

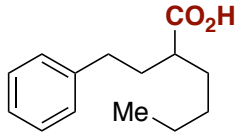

2-Phenethylhexanoic acid (20h). Following **GP6** but with 8 mol% 4-CzIPN, (3-bromoheptyl)benzene (**19h**, 64 mg, 0.25 mmol) afforded the title compound **20h** as colorless liquid after **W1** (On average: 40 mg, 0.18 mmol, 73%, 20:1 selectivity determined by ^{1}H NMR). **^{1}H NMR (400 MHz, $CDCl_3$):** δ (ppm) = 7.30 (dd, J = 8.0, 6.9 Hz, 2H), 7.25 – 7.16 (m, 3H), 2.77 – 2.58 (m, 2H), 2.43 (tt, J = 8.7, 5.3 Hz, 1H), 2.08 – 1.95 (m, 1H), 1.88 – 1.77 (m, 1H), 1.74 – 1.66 (m, 1H), 1.61 – 1.50 (m, 1H), 1.40 – 1.29 (m, 4H), 0.94 – 0.87 (m, 3H); **^{13}C NMR (101 MHz, $CDCl_3$)** δ (ppm) = 183.0, 141.7, 129.0, 128.5, 126.1, 45.1, 33.9, 33.7, 32.0, 29.5, 22.7, 14.0. Data in agreement with the literature.[32]

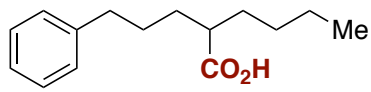

2-(3-phenylpropyl)hexanoic acid (20i). Following **GP6** but with 10 mol% 4-CzIPN (20 mg), a reaction temperature of 10°C (ca. 15°C *in situ*) and irradiated for 48 h, **19i** (67 mg, 0.25 mmol) afforded the title compound **20i** as colorless liquid after **W2** (On average: 44 mg, 75%, >20:1 selectivity determined by quantitative ^{13}C NMR). **^{1}H NMR (400 MHz, $CDCl_3$):** δ (ppm) = 10.03 (s, 1H), 7.32 – 7.24 (m, 2H), 7.22 – 7.15 (m, 3H), 2.63 (t, *J* = 7.3 Hz, 2H), 2.46 – 2.33 (m, 1H), 1.79 – 1.59 (m, 4H), 1.59 – 1.43 (m, 2H), 1.38 – 1.25 (m, 4H), 0.90 (t, *J* = 6.2 Hz, 3H); **^{13}C NMR (101 MHz, $CDCl_3$)** δ (ppm) = 183.0, 142.2, 128.5, 128.5, 125.9, 45.5, 35.9, 32.0, 31.9, 29.6, 29.3, 22.7, 14.0; **IR (neat, cm^{-1}):** 3026, 2929, 2858, 1702, 1649, 1496, 1454, 1408, 1288, 1235, 1113, 1030; **HRMS** calcd. for ($C_{15}H_{21}O_2$) [M-H]$^-$: 233.1547 found 233.1548.

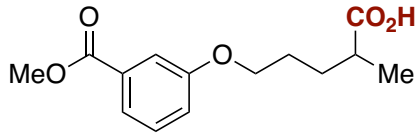

5-(3-(Methoxycarbonyl)phenoxy)-2-methylpentanoic acid (20j). Following **GP6**, methyl 3-((4-bromopentyl)oxy)benzoate (**19j**, 75 mg, 0.25 mmol) afforded the title compound **20j** as pale-yellow liquid after **W1** (On average: 60 mg, 0.23 mmol, 90%, 16:1 selectivity determined by ^{1}H NMR). **^{1}H NMR (300 MHz, $CDCl_3$):** δ (ppm) = 7.63 (dt, *J* = 7.7, 1.3 Hz, 1H), 7.56 (dd, *J* = 2.7, 1.5 Hz, 1H), 7.34 (t, *J* = 7.9 Hz, 1H), 7.08 – 7.12 (m, 1H), 4.32 (t, *J* = 6.2 Hz, 2H), 3.85 (s, 3H), 2.50 – 2.61 (m, 1H), 1.78 – 1.89 (m, 3H), 1.56 – 1.66 (m, 1H), 1.23 (d, *J* = 7.0 Hz, 3H); **^{13}C NMR (75 MHz, $CDCl_3$)** δ (ppm) = 182.8, 166.6, 159.7, 131.7, 129.5, 122.1, 119.6, 114.2, 64.9, 55.6, 39.1, 30.0, 26.5, 17.1; **IR (neat, cm^{-1}):** 3310, 2941, 1702, 1586, 1455, 1274, 1209, 1130, 1041, 753; **HRMS** calcd. for ($C_{14}H_{17}O_5$) [M–H]$^-$: 265.1081 found 265.1078.

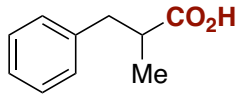

2-methyl-3-phenylpropanoic acid (20k). Following **GP6** with 10% of 4-CzIPN (19.7 mg), (2-bromopropyl)benzene (49.8 mg, 0.25 mmol) afforded the title compound **20k** as colorless liquid after **W1** (On average: 29 mg, 71%, ≥ 95% selectivity determined by ^{1}H NMR). **^{1}H NMR (400 MHz, $CDCl_3$):** δ (ppm) = 7.29 (tt, *J* = 6.8, 1.1 Hz, 2H), 7.25 – 7.16 (m, 3H), 3.08 (dd, *J* = 13.4, 6.4 Hz, 1H), 2.78 (h, *J* = 6.7 Hz, 1H), 2.68 (dd, *J* = 13.4, 8.0 Hz, 1H), 1.19 (d, *J* = 6.9 Hz, 3H).; **^{13}C NMR (101 MHz, $CDCl_3$)** δ (ppm) = 181.1, 139.2, 129.2, 128.6, 126.6,

41.2, 39.5, 16.7. Data in agreement with the literature.[33]

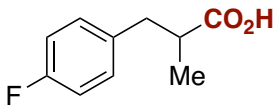

3-(4-fluorophenyl)-2-methylpropanoic acid (20l). Following **GP6** with 8% of 4-CzIPN (15.8 mg), (1-(2-bromopropyl)-4-fluorobenzene **19l** (54.3 mg, 0.25 mmol) afforded the title compound **20l** as a pale-yellow oil after **W1** (On average: 42 mg, 92%, 93% selectivity determined by ^{19}F NMR). **^{1}H NMR (400 MHz, $CDCl_3$):** δ (ppm) = 7.20 – 7.13 (m, 2H), 7.03 – 6.96 (m, 2H), 3.05 (dd, *J* = 13.2, 6.4 Hz, 1H), 2.76 (dq, *J* = 12.6, 6.5 Hz, 1H), 2.69 (dd, *J* = 13.2, 7.6 Hz, 1H), 1.21 (d, *J* = 6.7 Hz, 3H).; **^{19}F NMR (471 MHz, $CDCl_3$):** δ (ppm) = 116.67 – -116.79 (m).; **^{13}C NMR (101 MHz, $CDCl_3$):** δ (ppm) = 182.4, 162.7, 160.8, 134.8, 134.7, 130.6, 130.5, 115.5, 115.3, 41.5, 38.6, 16.6; **HRMS** calcd. for ($C_{10}H_{10}FO_2$) [M-H]$^-$: 181.0670 found 181.0665. Data in agreement with the literature.[34]

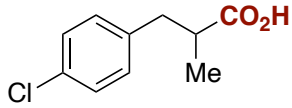

3-(4-chlorophenyl)-2-methylpropanoic acid (20m). Following **GP6** with 8% of 4-CzIPN (15.8 mg), (1-(2-bromopropyl)-4-chlorobenzene **19m** (58.4 mg, 0.25 mmol) afforded the title compound **20m** as a pale-yellow oil after **W1** (On average: 34.0 mg, 69%, ≥ 95% selectivity determined by ^{1}H NMR). **^{1}H NMR (500 MHz, $CDCl_3$):** δ (ppm) = 7.30 – 7.26 (m, 2H), 7.19 – 7.10 (m, 2H), 3.05 (dd, *J* = 13.5, 6.7 Hz, 1H), 2.82 – 2.72 (m, 1H), 2.68 (dd, *J* = 13.5, 7.7 Hz, 1H), 1.21 (d, *J* = 6.9 Hz, 3H).; **^{13}C NMR (126 MHz, $CDCl_3$):** δ (ppm) 182.2, 137.5, 132.3, 130.4, 128.6, 41.19, 38.6, 16.6; **HRMS** calcd. for ($C_{10}H_{10}ClO_2$) [M-H]$^-$: 197.0375 found 197.0381. Data in agreement with the literature.[34]

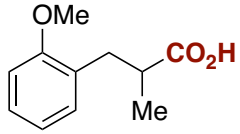

3-(2-methoxyphenyl)-2-methylpropanoic acid (20n). Following **GP6** with 10% of 4-CzIPN (19.7 mg) at 10°C, 1-(2-bromopropyl)-2-methoxybenzene **19n** (57.3 mg, 0.25 mmol) afforded the title compound **20n** as a pale-yellow oil after **W1** (On average: 31.3 mg, 65%, ≥ 95% selectivity determined by ^{1}H NMR). **^{1}H NMR (500 MHz, $CDCl_3$):** δ (ppm) = 7.22 (ddd, *J* = 8.1, 7.4, 1.8 Hz, 1H), 7.14 (dd, *J* = 7.4, 1.8 Hz, 1H), 6.88 (td, *J* = 7.4, 1.1 Hz, 1H), 6.85 (dd, *J* = 8.2, 1.1 Hz, 1H), 3.81 (s, 3H), 3.07 (dd, *J* = 13.3, 6.8 Hz, 1H), 2.87 (h, 1H), 2.72 (dd, J = 13.3, 7.7 Hz, 1H), 1.17 (d, *J* = 7.0 Hz, 3H).; **^{13}C NMR (126 MHz, $CDCl_3$)** δ (ppm) = 183.1, 157.6, 130.9,

127.8, 127.5, 120.3, 110.2, 55.1, 39.4, 34.3, 16.8; **HRMS** calcd. for ($C_{11}H_{13}O_3$) [M-H]$^-$: 193.0870 found 193.0870. Data in agreement with the literature.[35]

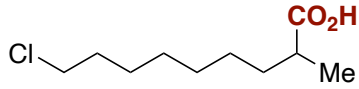

9-Chloro-2-methylnonanoic acid (20o). Following **GP6**, 8-bromo-1-chlorononane (**19o**, 60.4 mg, 0.25 mmol) afforded the title compound **20o** as pale-yellow liquid after **W1** (On average: 37 mg, 0.18 mmol, 72%, >20:1 selectivity determined by ^{1}H NMR). **^{1}H NMR (400 MHz, $CDCl_3$):** δ (ppm) = 3.52 (t, *J* = 6.7 Hz, 2H), 2.50 – 2.39 (m, 1H), 1.80 – 1.71 (m, 2H), 1.67 (dt, *J* = 14.9, 7.5 Hz, 1H), 1.47 – 1.37 (m, 3H), 1.37 – 1.28 (m, 6H), 1.17 (d, *J* = 7.0 Hz, 3H); **^{13}C NMR (101 MHz, $CDCl_3$)** δ (ppm) = 183.6, 45.2, 39.5, 33.6, 32.7, 29.4, 28.8, 27.1, 26.9, 17.0; **IR (neat, cm^{-1}):** 3104, 2930, 2856, 1702, 1483, 1319, 1236, 970, 643, 507; **HRMS** calcd. for ($C_{10}H_{18}ClO_2$) [M–H]$^-$: 205.1001 found 205.0996.

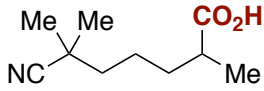

6-Cyano-2,6-dimethylheptanoic acid (20p). Following **GP6** but with 8 mol% 4-CzIPN, 6-bromo-2,2-dimethylheptanenitrile (**19p**, 55 mg, 0.25 mmol) afforded the title compound **20p** as colorless oil after **W1** (On average: 36 mg, 0.20 mmol, 79%, >20:1 selectivity determined by ^{1}H NMR). **^{1}H NMR (400 MHz, $CDCl_3$):** δ (ppm) 2.55 – 2.43 (m, 1H), 1.77 – 1.67 (m, 1H), 1.55 – 1.43 (m, 5H), 1.33 (s, 6H), 1.20 (d, *J* = 7.0 Hz, 3H); **^{13}C NMR (101 MHz, $CDCl_3$)** δ (ppm) = 182.8, 125.1, 40.9, 39.3, 33.3, 32.4, 26.8 (d, *J* = 3.7 Hz, two methyl group split), 23.1, 17.0; **IR (neat, cm^{-1}):** 3035, 2987, 2640, 2240, 1703, 1453, 1361, 1260, 1245, 983, 824; **HRMS** calcd. for ($C_{10}H_{16}NO_2$) [M-H]$^-$: 182.1187 found 182.1187.

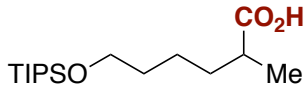

2-methyl-6-((triisopropylsilyl)oxy)hexanoic acid (20q). Following **GP6**, **19q** (0.25 mmol, 84 mg) afforded the title compound **20q** as colorless oil (On average: 60 mg, 80%, >20:1 selectivity determined by ^{1}H NMR) after purification by column chromatography (in this case the product was too apolar and unstable to be successfully purified by **W1-3**). **^{1}H NMR (500 MHz, $CDCl_3$):** δ (ppm) 8.86 (s, 1H), 3.67 (t, *J* = 6.4 Hz, 2H), 2.50 – 2.40 (m, 1H), 1.75 – 1.66 (m, 1H), 1.59 – 1.51 (m, 2H), 1.50 – 1.35 (m, 3H), 1.20 – 1.14 (m, 3H), 1.10 – 0.99 (m, 21H). **^{13}C NMR (101 MHz, $CDCl_3$)** δ (ppm) = 183.3, 63.3, 39.5, 33.5, 33.0, 23.6, 18.2, 16.9, 12.2. **IR (neat, cm^{-1}):** 2940, 2865, 1706, 1463, 1416, 1382, 1284, 1239, 1103, 1071, 1013;

HRMS calcd. for ($C_{16}H_{33}O_3Si$) [M-H]$^-$: 301.2204 found 301.2215.

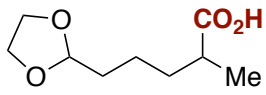

5-(1,3-dioxolan-2-yl)-2-methylpentanoic acid (20r). Following **GP6**, **19r** (0.25 mmol, 56 mg) afforded the title compound **20r** as colorless oil after **W3** (On average: 34 mg, 72%, >20:1 selectivity determined by ^{1}H NMR). **^{1}H NMR (500 MHz, $CDCl_3$):** δ (ppm) = 4.84 (t, *J* = 4.7 Hz, 1H), 4.02 – 3.88 (m, 2H), 3.89 – 3.77 (m, 2H), 2.51 – 2.37 (m, 1H), 1.77 – 1.69 (m, 1H), 1.69 – 1.62 (m, 2H), 1.53 – 1.40 (m, 3H), 1.17 (d, *J* = 7.0 Hz, 3H).**^{13}C NMR (101 MHz, $CDCl_3$)** δ (ppm) = 183.0, 104.6, 104.4, 65.0, 39.4, 33.8, 33.4, 21.8, 16.9.; **IR (neat, cm^{-1}):** 2944, 2880, 1703, 1463, 1410, 1212, 1140, 1124, 1055, 1028; **HRMS** calcd. for ($C_9H_{15}O_4$) [M-H]$^-$: 187.0976 found 187.0977.

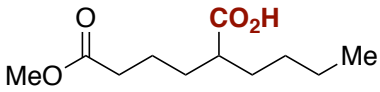

2-butyl-6-methoxy-6-oxohexanoic acid (20s). Following **GP6** but with 8 mol% 4-CzIPN and irradiated for 48h, **19s** (0.25 mmol, 63 mg) afforded the title compound **20s** as colorless oil after **W3** (On average: 34 mg, 0.20 mmol, 63%, >20:1 selectivity determined by quantitative ^{13}C NMR). **^{1}H NMR (500 MHz, $CDCl_3$):** δ (ppm) = 3.66 (s, 3H), 2.38 – 2.28 (m, 2H), 1.70 – 1.58 (m, 4H), 1.57 – 1.43 (m, 2H), 1.36 – 1.24 (m, 4H), 0.88 (t, *J* = 7.0 Hz, 3H). **^{13}C NMR (126 MHz, $CDCl_3$)** δ (ppm) = 182.5, 174.0, 51.7, 45.3, 34.0, 31.9, 31.5, 29.5, 22.8, 22.7, 14.0; **IR (neat, cm^{-1}):** 2932, 2862, 1703, 1646, 1508, 1458, 1408, 1302, 1194, 1115; **HRMS** calcd. for ($C_{10}H_{19}O_4$) [M-H]$^-$: 215.1289 found 215.1297.

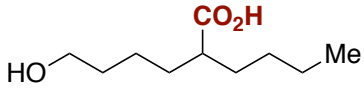

2-butyl-6-hydroxyhexanoic acid (20t). Following **GP6** but with 8 mol% 4-CzIPN, **19t** (0.25 mmol, 56 mg) afforded the title compound **20t** as colorless oil after **W2** (On average: 32 mg, 86%, 20:1 selectivity determined by quantitative ^{13}C NMR). **^{1}H NMR (500 MHz, $CDCl_3$):** δ (ppm) = 6.72 (s, 1H), 3.62 (t, *J* = 6.4 Hz, 2H), 2.32 (tt, *J* = 9.1, 5.2 Hz, 1H), 1.71 – 1.17 (m, 13H), 0.87 (t, *J* = 6.8 Hz, 3H); **^{13}C NMR (126 MHz, $CDCl_3$)** δ (ppm) = 181.8, 62.5, 45.7, 32.4, 32.1, 32.0, 29.6, 23.7, 22.7, 14.0. **IR (neat, cm^{-1}):** 3334, 2932, 2860, 1702, 1459, 1408, 1379, 1229, 1193, 1049; **HRMS** calcd. for ($C_{10}H_{19}O_3$) [M-H]$^-$: 187.1340 found 187.1341.

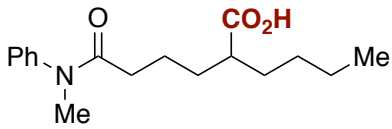

2-butyl-6-(methyl(phenyl)amino)-6-oxohexanoic acid (20u). Following **GP6** but with 8 mol% 4-CzIPN, **19u** (0.25 mmol, 82 mg) afforded the title compound **20u** as a colorless oil after **W2** (On average: 53 mg, 73%, 16:1 selectivity determined by quantitative ^{13}C NMR). **^{1}H NMR (400 MHz, $CDCl_3$):** δ (ppm) = 9.16 (s, 1H), 7.40 (t, *J* = 7.4 Hz, 2H), 7.32 (t, *J* = 7.3 Hz, 1H), 7.15 (d, *J* = 7.6 Hz, 2H), 3.24 (s, 3H), 2.32 – 2.17 (m, 1H), 2.07 (t, *J* = 7.3 Hz, 2H), 1.68 – 1.45 (m, 4H), 1.45 – 1.32 (m, 2H), 1.32 – 1.12 (m, 4H), 0.85 (t, *J* = 6.7 Hz, 3H). **^{13}C NMR (101 MHz, $CDCl_3$)** δ (ppm) = 181.3, 173.3, 144.1, 129.9, 128.0, 127.3, 45.3, 37.5, 34.1, 31.8, 31.8, 29.5, 23.4, 22.7, 14.0; **IR (neat, cm^{-1}):** 3061, 2931, 2860, 1725, 1704, 1655, 1622, 1592, 1496, 1457, 1391, 1274, 1187, 1159, 1117, 1027; **HRMS** calcd. for ($C_{17}H_{24}NO_3$) [M-H]$^-$: 290.1762 found 290.1760.

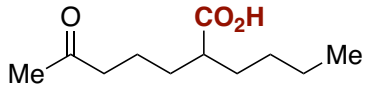

2-butyl-6-oxoheptanoic acid (20v) Following **GP6** but with 8 mol% 4-CzIPN, **19v** (0.25 mmol, 56 mg) afforded the title compound **20v** as colorless oil after **W2** (On average: 39 mg, 78%, 12:1 selectivity determined by quantitative ^{13}C NMR). **^{1}H NMR (400 MHz, $CDCl_3$):** δ (ppm) = δ 2.43 (t, 2H), 2.40 – 2.27 (m, 1H), 2.11 (s, 3H), 1.68 – 1.54 (m, 4H), 1.52 – 1.41 (m, 2H), 1.34 – 1.24 (m, 4H), 0.90 – 0.81 (m, 3H); **^{13}C NMR (101 MHz, $CDCl_3$)** δ (ppm) = δ 209.0, 182.5, 45.4, 43.5, 31.9, 31.5, 30.0, 29.5, 22.7, 21.6, 14.0; **IR (neat, cm^{-1}):** 2933, 2861, 1702, 1458, 1411, 1360, 1288, 1230, 1179, 1160, 1112; **HRMS** calcd. for ($C_{11}H_{19}O_3$) [M-H]$^-$: 199.1340 found 199.1343.

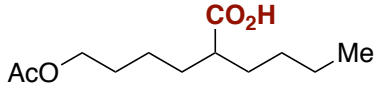

6-acetoxy-2-butylhexanoic acid (20w). Following **GP6** but with 10 mol% 4-CzIPN, a reaction temperature of 10 °C (ca. 15°C *in situ*) and irradiated for 48 h, **19w** (0.25 mmol, 66 mg) afforded the title compound **20w** as colorless oil after **W3** (On average: 42 mg, 83%, ≥20:1 selectivity determined by quantitative ^{13}C NMR). **^{1}H NMR (400 MHz, $CDCl_3$):** δ (ppm) = 2.32 (tt, J = 8.7, 5.3 Hz, 1H), 2.01 (s, 3H), 1.74 – 1.54 (m, 4H), 1.57 – 1.15 (m, 10H), 0.86 (td, J = 6.2, 2.4 Hz, 3H); **^{13}C NMR (101 MHz, $CDCl_3$):** δ (ppm) = 182.5, 171.4, 64.4, 45.5, 32.0, 31.8, 29.6, 28.6, 23.9, 22.7, 21.1, 14.0; **IR (neat, cm^{-1}):** 2932, 2860, 1728, 1708, 1650, 1459, 1405, 1336, 1302, 1237, 1169, 1115, 1043; **HRMS** calcd. for ($C_{12}H_{21}O_4$) [M-H]$^-$: 229.1445 found 229.1443.

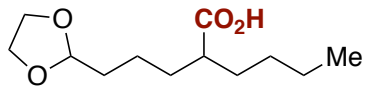

2-(3-(1,3-dioxolan-2-yl)propyl)hexanoic acid (20x). Following **GP6** but with 10 mol% 4-CzIPN and a reaction temperature of 10 °C (ca. 15°C *in situ*) for 48 h, **19x** (0.25 mmol, 66 mg) afforded the title compound **20x** as colorless oil after **W3** (On average: 46 mg, 80%, 7:1 selectivity determined by ^{1}H NMR). **^{1}H NMR (400 MHz, $CDCl_3$):** δ (ppm) = 4.84 (t, *J* = 4.6 Hz, 1H), 4.00 – 3.88 (m, 2H), 3.88 – 3.78 (m, 2H), 2.38 – 2.26 (m, 1H), 1.75 – 1.57 (m, 4H), 1.56 – 1.39 (m, 4H), 1.38 – 1.18 (m, 4H), 0.92 – 0.84 (m, 3H); **^{13}C NMR (126 MHz, $CDCl_3$, major isomer)** δ (ppm) = 182.6, 104.5, 65.0, 45.6, 33.9, 32.1, 31.9, 29.6, 22.7, 22.0, 14.0; **IR (neat, cm^{-1}):** 2930, 2862, 1734, 1703, 1459, 1441, 1286, 1233, 1141, 1033, 943; **HRMS** calcd. for ($C_{12}H_{21}O_4$) [M-H]$^-$: 229.1445 found 229.1438.

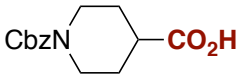

1-((Benzyloxy)carbonyl)piperidine-4-carboxylic acid (20y). Following **GP6**, *N*-Cbz-4-bromo-piperidine **19y** (75 mg, 0.25 mmol) afforded the title compound **20y** as a yellow oil after **W2** (On average: 47 mg, 71%, single regioisomer). **^{1}H NMR (400 MHz, $CDCl_3$):** δ (ppm) = 10.14 (s, 1H), 7.42 – 7.28 (m, 5H), 5.14 (s, 2H), 4.10 (d, *J* = 15.0 Hz, 2H), 2.96 (t, *J* = 12.4 Hz, 2H), 2.51 (tt, *J* = 10.8, 3.9 Hz, 1H), 1.93 (d, *J* = 12.8 Hz, 2H), 1.76 – 1.57 (m, 2H); **^{13}C NMR (101 MHz, $CDCl_3$)** δ (ppm) = 180.2, 155.4, 136.7, 128.6, 128.2, 128., 67.4, 43.3, 40.7, 27.7. Data in agreement with the literature.[36]

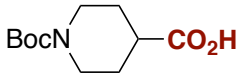

1-(Tert-butoxycarbonyl)piperidine-4-carboxylic acid (20z). Following **GP6**, *N*-Boc-4-bromo-piperidine **19z** (66 mg, 0.25 mmol) afforded the title compound **20z** as a white solid after **W2** (On average: 40 mg, 70%, single regioisomer). **^{1}H NMR (400 MHz, $CDCl_3$):** δ (ppm) = 4.00 (d, *J* = 13.3 Hz, 2H), 2.85 (t, *J* = 12.2 Hz, 2H), 2.47 (tt, *J* = 11.0, 3.8 Hz, 1H), 1.90 (d, *J* = 11.8 Hz, 2H), 1.63 (qd, *J* = 11.3, 4.1 Hz, 2H), 1.44 (s, 9H).**^{13}C NMR (101 MHz, $CDCl_3$)** δ (ppm) = 180.4, 154.9, 79.9, 43.1 (br), 41.0, 28.6, 27.9. **Melting Point:** 114°C. Data in agreement with the literature.[36]

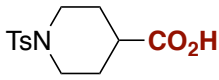

1-Tosylpiperidine-4-carboxylic acid (20aa). Following **GP6**, *N*-Ts-4-bromo-piperidine **19aa** (80 mg, 0.25 mmol) afforded the title compound **20aa** as a white solid after **W2** (On

average: 46 mg, 65%, single regioisomer). **^{1}H NMR (400 MHz, $CDCl_3$):** δ (ppm) = 10.48 (s, 1H), 7.61 (d, *J* = 7.9 Hz, 2H), 7.31 (d, *J* = 7.9 Hz, 2H), 3.64 (dt, *J* = 12.2, 4.1 Hz, 2H), 2.54 – 2.36 (m, 5H), 2.27 (tt, *J* = 10.8, 4.0 Hz, 1H), 2.11 – 1.91 (m, 2H), 1.79 (dtd, *J* = 14.5, 11.7, 3.9 Hz, 3H). **^{13}C NMR (101 MHz, $CDCl_3$)** δ (ppm) = 180.2, 143.8, 133.1, 129.8, 127.7, 45.4, 39.9, 27.3, 21.6. **Melting Point:** 167°C. Data in agreement with the literature.[36]

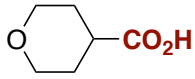

Tetrahydro-2H-pyran-4-carboxylic acid (20ab). Following **GP6**, 4-bromo-morpholine **19ab** (41 mg, 0.25 mmol) afforded the title compound **20ab** as a white solid after **W2** (On average: 19 mg, 57%, single regioisomer). **^{1}H NMR (500 MHz, $CDCl_3$):** δ (ppm) = 9.52 (s, 1H), 3.95 (dt, *J* = 11.6, 3.7 Hz, 1H), 3.43 (td, *J* = 10.7, 2.0 Hz, 1H), 2.41 (t, *J* = 8.1 Hz, 2H), 2.05 – 1.99 (m, 2H), 1.88 – 1.73 (m, 2H). **^{13}C NMR (126 MHz, $CDCl_3$)** δ (ppm) = 180.48, 67.11, 39.93, 28.50. **Melting Point:** 84°C Data in agreement with the literature.[36]

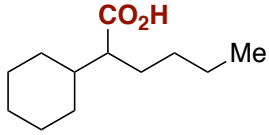

2-cyclohexylhexanoic acid (20ac). Following **GP6** with 8 mol% of 4-CzIPN, **19ac** (58 mg, 0.25 mmol) afforded the title compound **20ac** as colorless liquid after **W1** (On average: 33 mg, 67%, 20:1 selectivity determined by quantitative ^{13}C NMR). **^{1}H NMR (500 MHz, $CDCl_3$):** δ (ppm) = 2.14 (ddd, J = 9.6, 7.5, 4.8 Hz, 1H), 1.85 – 1.77 (m, 1H), 1.77 – 1.61 (m, 4H), 1.60 – 1.48 (m, 3H), 1.39 – 1.21 (m, 6H), 1.21 – 1.14 (m, 1H), 1.12 – 1.06 (m, 1H), 1.05 – 0.92 (m, 1H), 0.89 (t, J = 7.0 Hz, 3H); **^{13}C NMR (126 MHz, $CDCl_3$)** δ (ppm) = 182.5, 52.1, 40.2, 31.1, 30.6, 30.1, 29.0, 26.5, 26.5, 26.4, 22.8, 14.1.**IR (neat, cm^{-1}):** 2924, 2853, 2666, 1699, 1448, 1417, 1289, 1236, 1202; **HRMS** calcd. for ($C_{12}H_{21}O_2$) [M-H]$^-$: 197.1547 found 197.1547.

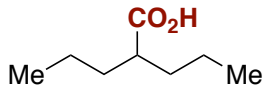

2-propylpentanoic acid (20ad). Following **GP6** but with 8 mol% 4CzIPN and a reaction temperature of 10°C (*in situ* temperature ca. 15°C), 4-bromo-heptane **19ad** (0.25 mmol, 39 µL) afforded the title compound **20ad** as colorless liquid after **W1** (On average: 29.5 mg, 81%, 20:1 selectivity determined by ^{1}H NMR integration). **^{1}H NMR (500 MHz, $CDCl_3$):** δ (ppm) = δ 2.38 (tt, *J* = 8.8, 5.3 Hz, 1H), 1.67 – 1.56 (m, 2H), 1.50 – 1.38 (m, 2H), 1.35 (dddd, *J* = 14.1, 9.3, 7.1, 4.1 Hz, 4H), 0.91 (t, *J* = 7.3 Hz, 6H). **^{13}C NMR (126 MHz, $CDCl_3$)** δ (ppm)

= 183.3, 45.3, 34.5, 20.7, 14.1. Spectroscopic data for match those previously reported in literature.[37]

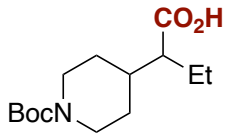

2-(1-(tert-butoxycarbonyl)piperidin-4-yl)butanoic acid (20ae). Following **GP6** with 10% of 4-CzIPN (19.7 mg) at 10°C for 48h, tert-butyl 4-(1-bromopropyl)piperidine-1-carboxylate **19ae** (76.6 mg, 0.25 mmol) afforded the title compound **20ae** as a colorless viscous oil after **W3** (On average: 37.8 mg, 56%, ≥ 95% selectivity determined by ^{1}H NMR). **^{1}H NMR (500 MHz, $CDCl_3$):** δ (ppm) = 4.11 (s, 2H), 2.66 (s, 2H), 2.16 – 2.07 (m, 1H), 1.78 – 1.55 (m, 5H), 1.44 (s, 9H), 1.33 – 1.11 (m, 2H), 0.93 (t, J = 7.4 Hz, 3H);**^{13}C NMR (126 MHz, $CDCl_3$)** δ (ppm) = 181.0, 155.0, 79.7, 52.8, 38.1, 30.1, 29.6, 28.6, 22.3, 12.1; **IR (neat, cm^{-1}):** 2966, 2935, 1717, 1621, 1474, 1443, 1365, 1288, 1252, 1223, 1146, 1071, 972, 861, 780; **HRMS** calcd. for ($C_{14}H_{24}NO_4$) [M-H]$^-$: 270.1711 found 270.1718. Boc rotamers lead to extra ^{13}C peaks and broaden peaks.

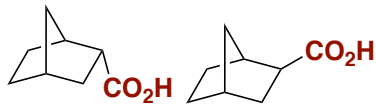

(1*S*,2*S*,4*R*)-bicyclo[2.2.1]heptane-2-carboxylic acid (20af). Following **GP6**, *exo*-2-bromonorbornane **19af** (44 mg, 0.25 mmol) afforded the title compound **20af** as a white solid after **W2** (On average, 28 mg, 80%, *endo:exo* 20:1). **^{1}H NMR (400 MHz, $CDCl_3$):** δ (ppm) = 2.80 (dt, *J* = 9.7, 4.5 Hz, 1H), 2.56 – 2.53 (m, 1H), 2.36 (dd, *J* = 9.2, 5.3 Hz, 1H), 2.30 (d, *J* = 4.4 Hz, 1H), 1.90 – 1.78 (m, 1H), 1.61 – 1.43 (m, 4H), 1.31 – 1.12 (m, 3H).**^{13}C NMR (101 MHz, $CDCl_3$)** δ (ppm) = 182.6, 46.5, 41.1, 36.7, 36.2, 34.2, 29.6, 28.7. **Melting Point:** 50°C. Data in agreement with the literature.[38]

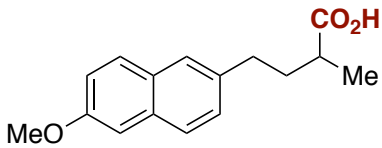

4-(6-Methoxynaphthalen-2-yl)-2-methylbutanoic acid (20ag). Following **GP6**, 2-(3-bromobutyl)-6-methoxynaphthalene **19ag** (73 mg, 0.25 mmol) afforded the title compound **20ag** as white solid after **W1** (On average: 53 mg, 0.21 mmol, 82%, >20:1 selectivity determined by ^{1}H NMR). **^{1}H NMR (500 MHz, $CDCl_3$):** δ (ppm) = 7.68 (d, *J* = 8.3 Hz, 2H), 7.56 (s, 1H), 7.31 (dd, *J* = 8.4, 1.8 Hz, 1H), 7.11 – 7.14 (m, 2H), 3.91 (s, 3H), 2.81 (t, *J* = 7.2 Hz, 2H), 2.52 – 2.59 (m, 1H), 2.10 – 2.17 (m, 1H), 1.79 – 1.86 (m, 1H), 1.26 (d, *J* = 7.0 Hz, 3H); **^{13}C NMR**

(126 MHz, $CDCl_3$) δ (ppm) = 183.0, 157.4, 136.8, 133.2, 129.2, 129.1, 127.9, 127.0, 126.5, 118.9, 105.8, 55.4, 39.0, 35.3, 33.5, 17.1; **IR (neat, cm^{-1}):** 3055, 2972, 2937, 1703, 1634, 1606, 1483, 1391, 1265, 1229, 1031, 850; **HRMS** calcd. for ($C_{16}H_{18}NaO_3$ $[M+Na]^+$: 281.1148. found 281.1150; **Melting Point:** 113ºC.

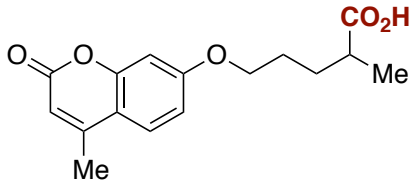

2-methyl-5-((4-methyl-2-oxo-2*H*-chromen-7-yl)oxy)pentanoic acid (20ah). Following **GP6** but with 8 mol% 4-CzIPN, 7-((4-bromopentyl)oxy)-4-methyl-2*H*-chromen-2-one **19ah**, 81.3 mg, 0.25 mmol) afforded the title compound **20ah** as beige solid after **W3** (On average: 54 mg, 74%, 20:1 selectivity). **^{1}H NMR (400 MHz, $CDCl_3$):** δ (ppm) = 7.46 (d, *J* = 8.8 Hz, 1H), 6.83 (dd, *J* = 8.8, 2.5 Hz, 1H), 6.76 (d, *J* = 2.5 Hz, 1H), 6.11 (q, *J* = 1.2 Hz, 1H), 4.04 – 3.96 (m, 2H), 2.53 (dt, *J* = 11.3, 6.8 Hz, 1H), 2.37 (d, *J* = 1.2 Hz, 3H), 1.91 – 1.79 (m, 3H), 1.72 – 1.60 (m, 1H), 1.23 (d, *J* = 7.0 Hz, 3H); **^{13}C NMR (126 MHz, $CDCl_3$):** δ (ppm) = δ 182.3, 162.1, 161.7, 155.2, 152.9, 125.6, 113.5, 112.7, 111.8, 101.4, 68.2, 39.1, 29.9, 26.7, 18.7, 17.1. **IR (neat, cm^{-1}):** 3059, 2961, 2935, 2875, 1719, 1678, 1603, 1555, 1509, 1460, 1389, 1370, 1347, 1270, 1227, 1205, 1162, 1136, 1071, 1011; **HRMS** calcd. For ($C_{16}H_{17}O_5$) $[M-H]^-$: 289.1081 found 289.1085; **Melting Point:** 103ºC.

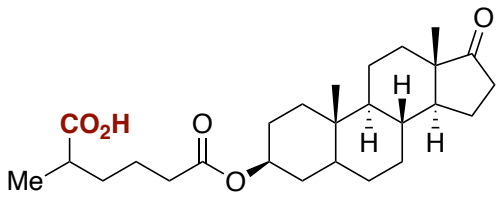

6-(((3S,10S,13S)-10,13-dimethyl-17-oxohexadecahydro-1H-cyclopenta[a]- 181 -henanthrene-3-yl)oxy)-2-methyl-6-oxohexanoic acid (20ai). Following **GP6**, (3S,10S,13S)-10,13-dimethyl-17-oxohexadecahydro-1H-cyclopenta[a]- 181 -henanthrene-3-yl 5-bromohexanoate **19ai** (117 mg, 0.25 mmol) afforded the title compound **20ai** as white solid after **W2** (On average: 84 mg, 77%, single isomer). **^{1}H NMR (400 MHz, $CDCl_3$):** δ (ppm) = 4.69 (tt, *J* = 10.8, 4.8 Hz, 1H), 2.43 (dd, *J* = 19.4, 8.7 Hz, 1H), 2.27 (t, *J* = 6.9 Hz, 2H), 2.06 (dt, *J* = 19.0, 8.7 Hz, 1H), 1.92 (ddd, *J* = 12.0, 8.5, 5.8 Hz, 1H), 1.85 – 1.13 (m, 24H), 1.08 – 0.93 (m, 2H), 0.85 (d, *J* = 3.4 Hz, 6H), 0.71 (td, *J* = 11.3, 4.0 Hz, 1H); **^{13}C NMR (101 MHz, $CDCl_3$)** δ (ppm) = 221.6, 182.3, 173.0, 73.6, 54.4, 51.4, 47.9, 44.7, 39.2, 36.8, 35.9, 35.7, 35.1, 34.5, 34.0, 32.9, 31.6, 30.9, 28.3, 27.5, 22.7, 21.9, 20.5, 16.9, 13.9, 12.3; **IR (neat, cm^{-1}):** 2933, 2858, 1728, 1452, 1407,

1373, 1248, 1173, 1151, 1129, 1103, 1060, 1013; **HRMS** calcd. For ($C_{26}H_{39}O_5$) [M-H]$^-$: 431.2803 2 found 431.2799; **Melting Point:** 123ºC.

3.7.4. Mechanistic investigation

(1) Deuterium Labeling Experiment:

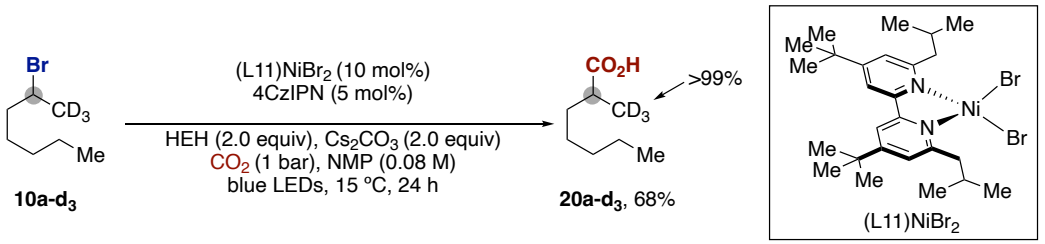

The photocarboxylation of deuterated 2-bromoheptane (**19a**-*d*$_3$, 0.25 mmol) was performed under standard conditions. The desired product **20a**-*d*$_3$ (25 mg, 0.17 mmol, 68%) was obtained as colorless oil. The ^{2}H NMR spectra revealed no scrambling of deuterium isotope throughout the hydrocarbon chain via β-hydride elimination/migratory insertion.

^{2}H NMR (77 MHz, $CHCl_3$): δ (ppm) = 1.15 (s, 3D).

^{2}H NMR of **20a**-d_3

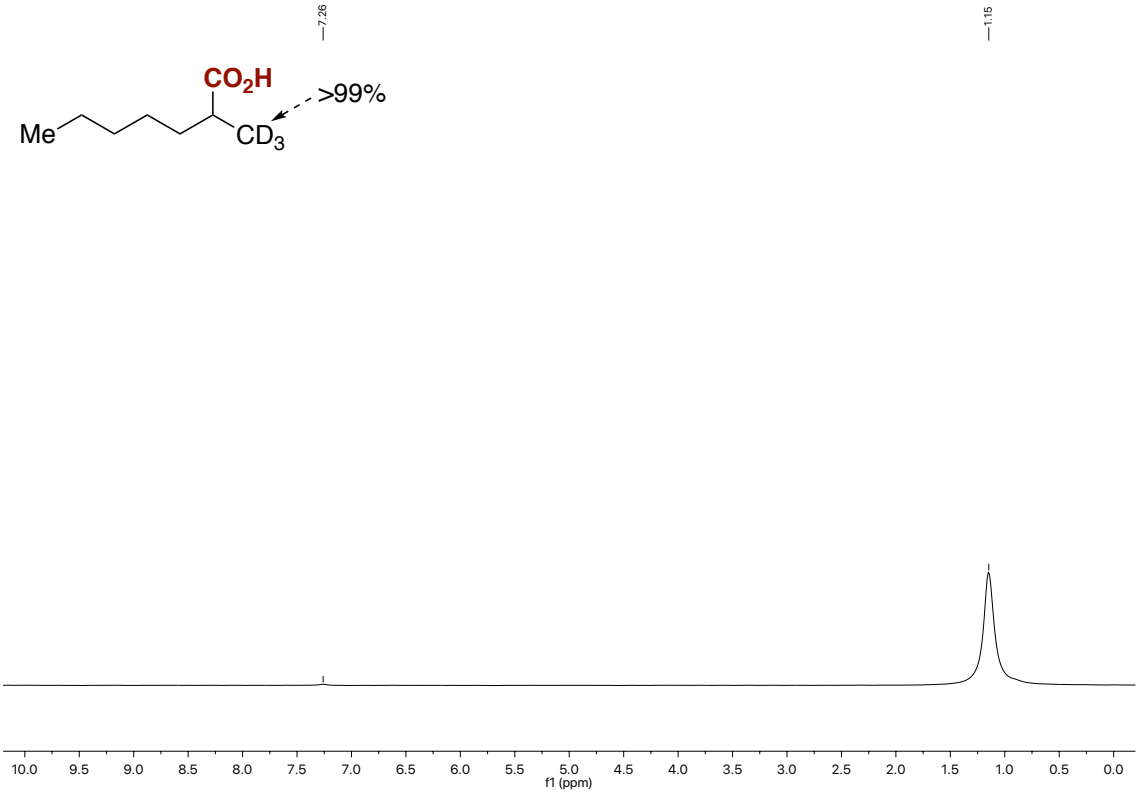

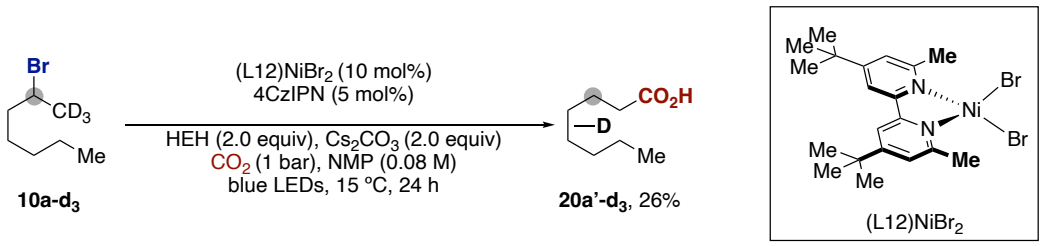

The photocarboxylation of deuterated 2-bromoheptane (**19a**-d_3, 0.25 mmol) was performed under standard conditions but using (**L12**)$NiBr_2$ (10%) instead as a catalyst. A mixture of products **20a**-d_3 and **20a'**-d_3 (9.6 mg, 0.06 mmol, 26%) was obtained as colorless oil. The ^{2}H NMR spectra revealed no scrambling of deuterium for **20a**-d_3 while scrambling is observed for the chain-walking product **20a'**-d_3. The following peak integration is performed only on the peaks corresponding to **20a'**-d_3 for calculation of deuterium scrambling. The internal deuterium counts are marked as unknown since

their integration falls under the peak of compound **20a**-d_3. Therefore, the other values are given as qualitative measurements. **^{2}H NMR (77 MHz, $CHCl_3$)**: δ (ppm) = 2.23 (s, 1.20D), 1.55 (s, 0.69D), 0.79 (s, 1.11D).

^{2}H NMR of **20a**-d_3 and **20a'**-d_3

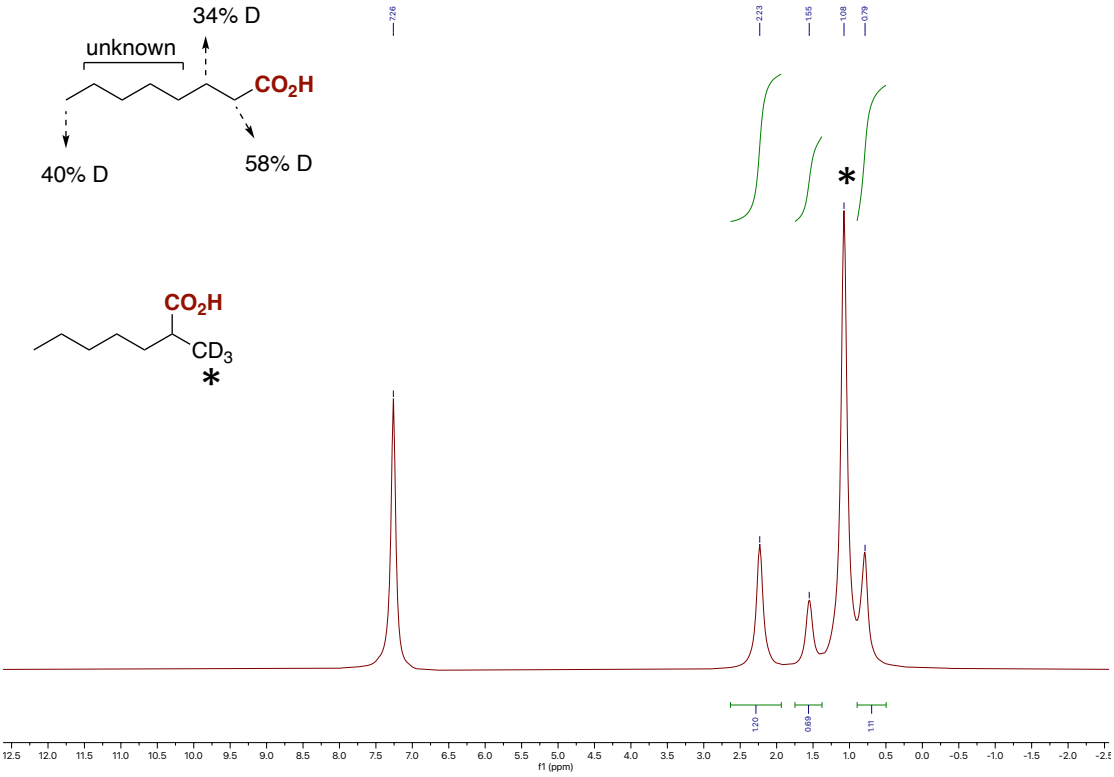

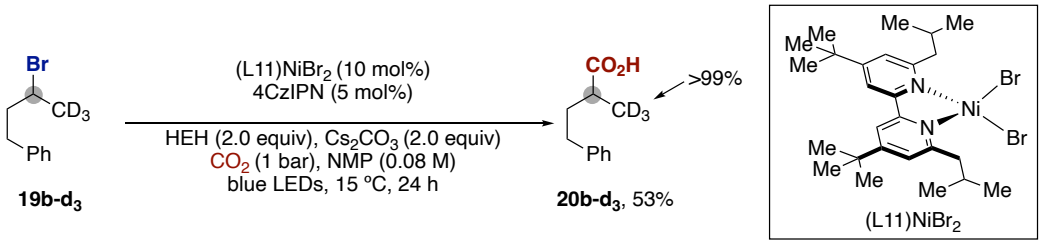

The photocarboxylation of deuterated **19b** (**19b**-d_3, 0.25 mmol) was performed under standard conditions. The desired product **20b**-d_3 (24 mg, 0.13 mmol, 53%, 97% selectivity by ^{1}H NMR) was obtained as a pale yellow oil. The ^{2}H NMR spectra revealed

little scrambling of deuterium isotope throughout the hydrocarbon chain via β-hydride elimination/migratory insertion, corresponding to the benzylic carboxlic acid side product **20b'**-d_3. Although the selectivity is lower with 97%, the target product **20b**-d_3 shows no scrambling itself, the other peaks only come from the side product.
^{2}H NMR (77 MHz, $CHCl_3$): δ (ppm) = 1.21 (s, 3D).

^{2}H NMR of **20b**-d_3

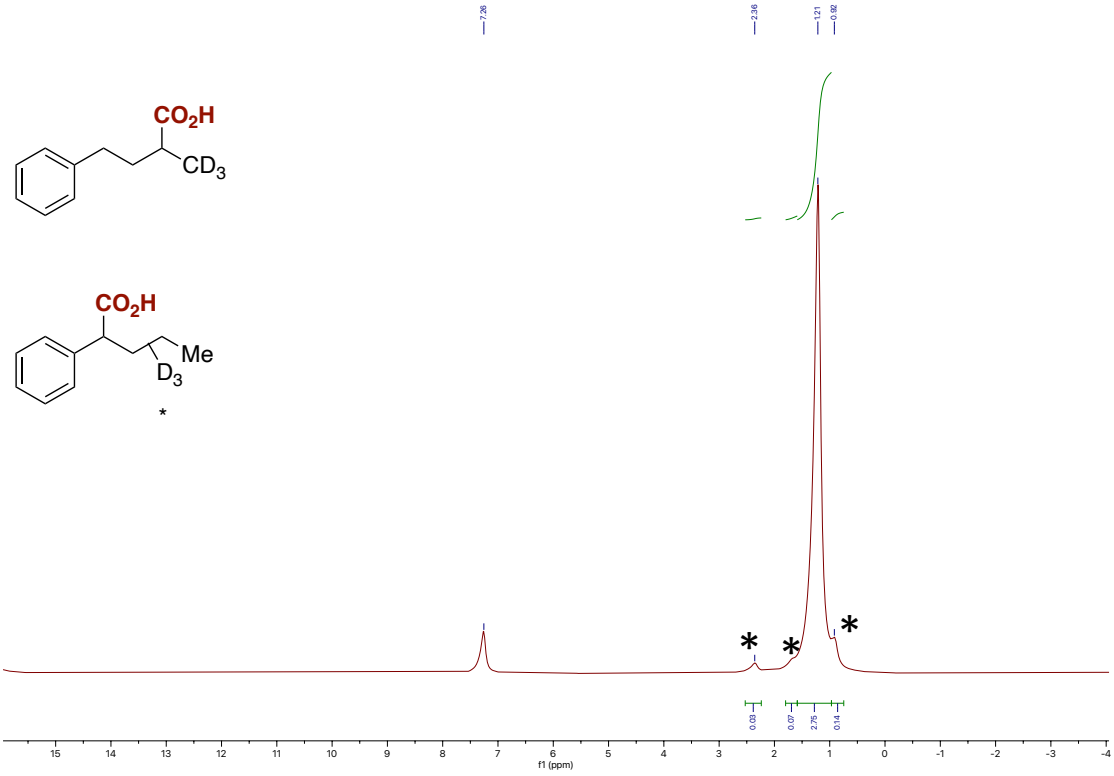

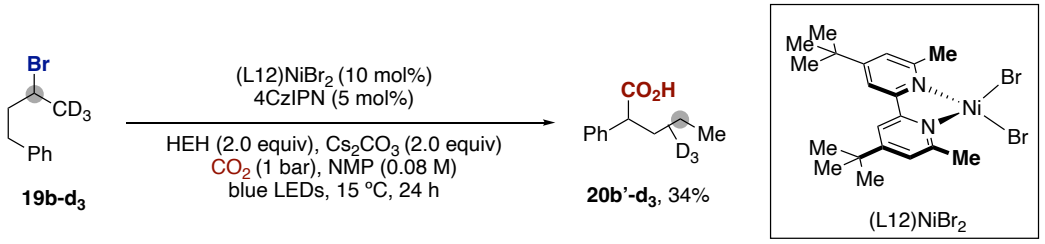

The photocarboxylation of deuterated **19b** (**19b**-d_3, 0.25 mmol) was performed under standard conditions but using (**L12**)$NiBr_2$ (10%) instead as a catalyst. A mixture of products **20b**-d_3 and **20b'**-d_3 (15,4 mg, 0.09 mmol, 34%) was obtained as a pale-yellow

oil. The selectivity is 1.6 : 1 (**20b**-d_3 : **20b'**-d_3), determined by ^{1}H NMR. The ^{2}H NMR spectra revealed no scrambling of deuterium for **20b**-d_3 while scrambling is observed for the chain-walking product **20b'**-d_3. No peak integration has been done for this compound as the peak from **20b**-d_3 covers one peak out of four. The results of the integration would be too off to be meaningful. Though, the peak distribution is qualitatively similar than for **20a'**-d_3.**^{2}H NMR (77 MHz, $CHCl_3$)**: δ (ppm) = 2.32 (s), 1.66 (s), 0.88 (s).

^{2}H NMR of **20b**-d_3 and **20b'**-d_3

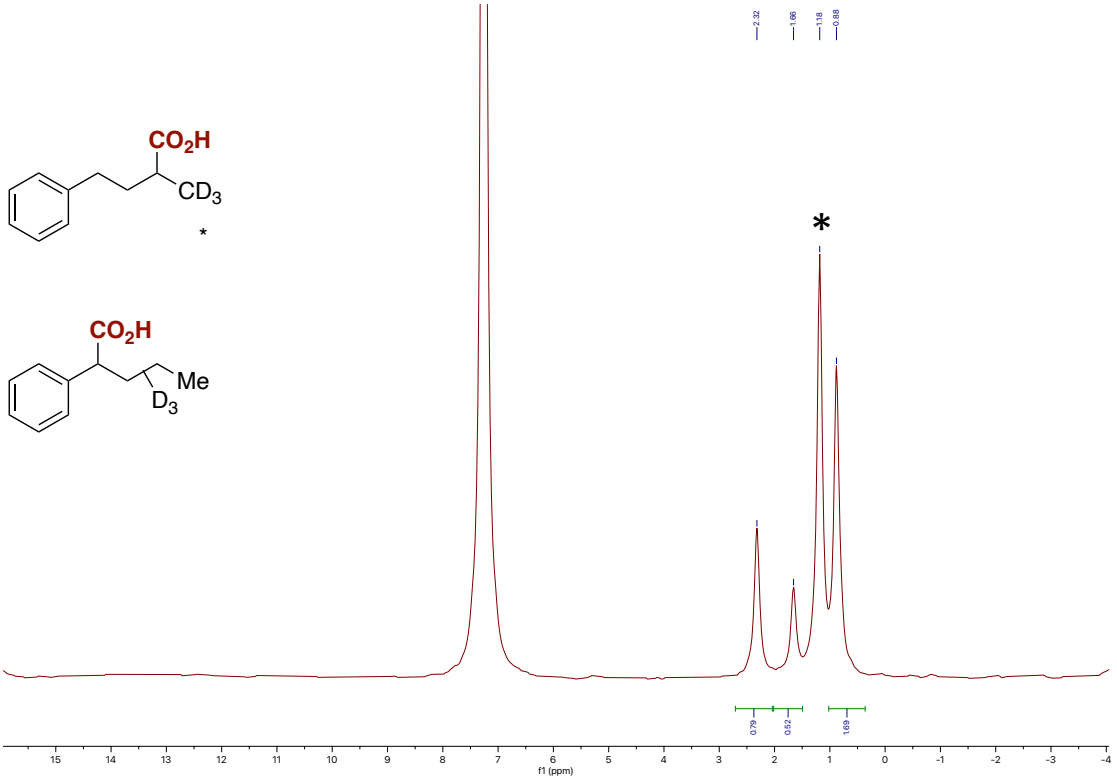

(2) Reaction with *enantiopure* Alkyl bromide

The photocarboxylation of (*S*)-**19b** (53.3 mg, 0.25 mmol, 94.5% ee) furnished desired carboxylic acid **20b** (30 mg, 0.17 mmol, 67%, branched:linear ratio of >99:1), which was reduced to the corresponding alcohol **20b-OH** to determine the corresponding ee value. The formation of racemic product **20b-OH** indicated that the reaction likely proceeds through alkyl radical intermediate.

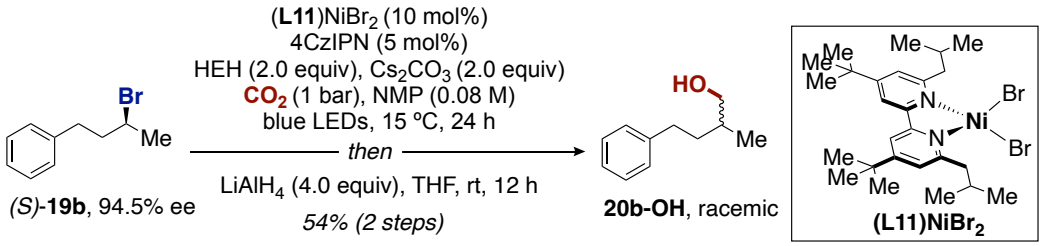

The enantiopure alkyl bromide (*S*)-**19b** (94.5% ee) was synthesized following the modified literature reported by Denmark et al.[39] Colorless liquid: **^{1}H NMR (300 MHz, $CHCl_3$):** δ (ppm) = 7.26 – 7.31 (m, 2H), 7.15 – 7.21 (m, 3H), 3.44 – 3.52 (m, 2H), 2.55 – 2.56 (m, 2H), 1.64 – 1.83 (m, 2H), 1.41 – 1.49 (m, 2H), 0.99 (d, *J* = 6.6 Hz, 3H); **^{13}C NMR (75 MHz, $CHCl_3$):** δ (ppm) = 142.60, 128.34, 125.72, 68.21, 35.37, 34.97, 33.30, 16.51. Spectroscopic data for **20b-OH** match those previously reported in literature.[40]

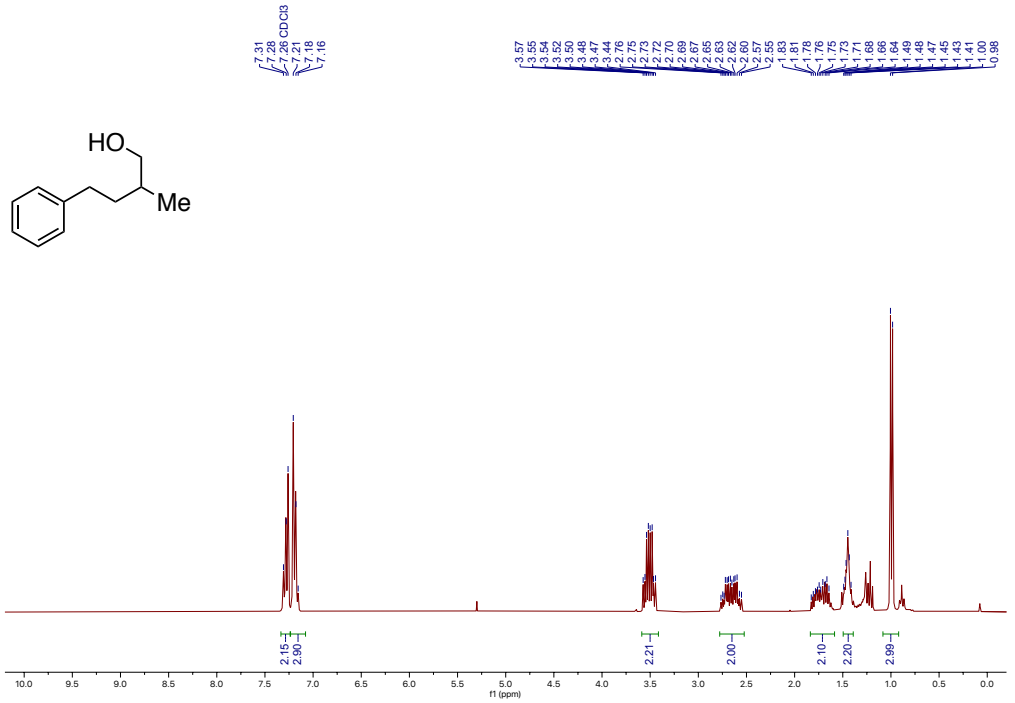

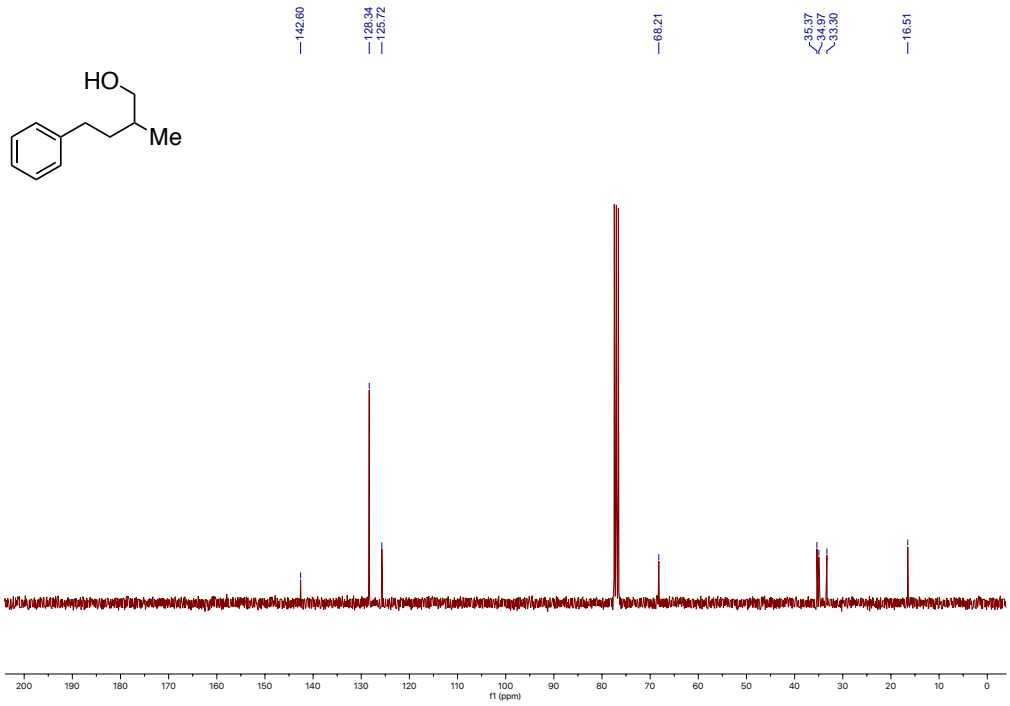
142.60
128.34
125.72
68.21
35.37
34.97
33.30
16.51
HO
Me
200
190
180
170
160
150
140
130
120
110
100
90
80
70
60
50
40
30
20
10
0
f1 (ppm)

(3-bromobutyl)benzene

Racemic Sample

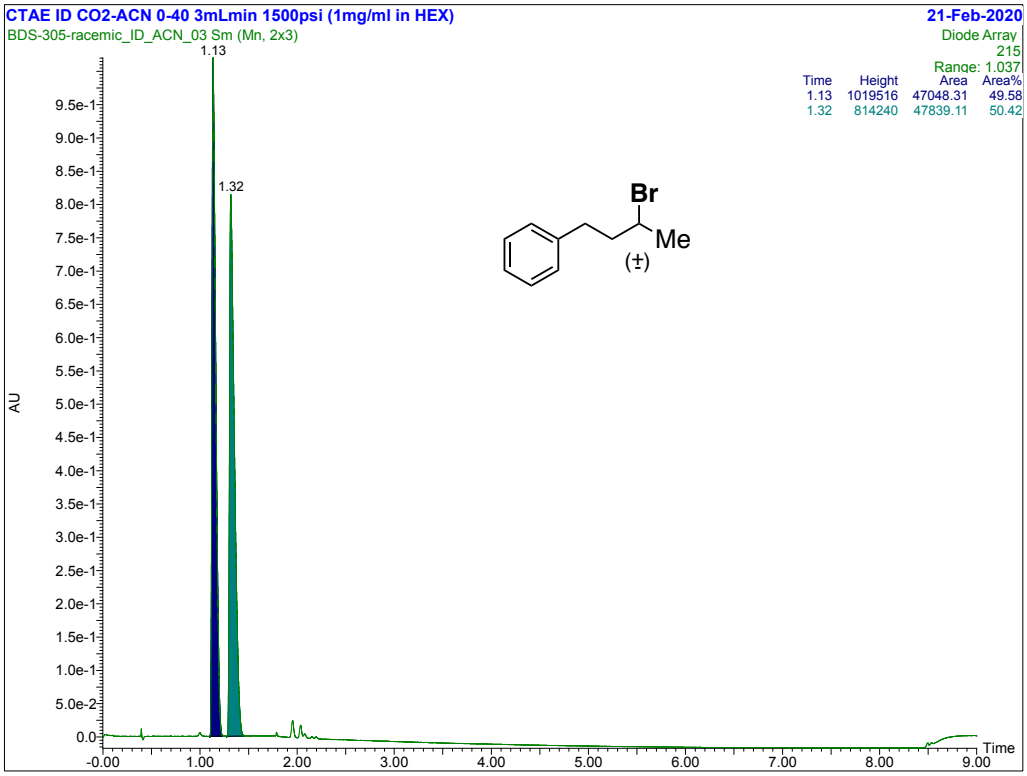

Enantioenriched Sample

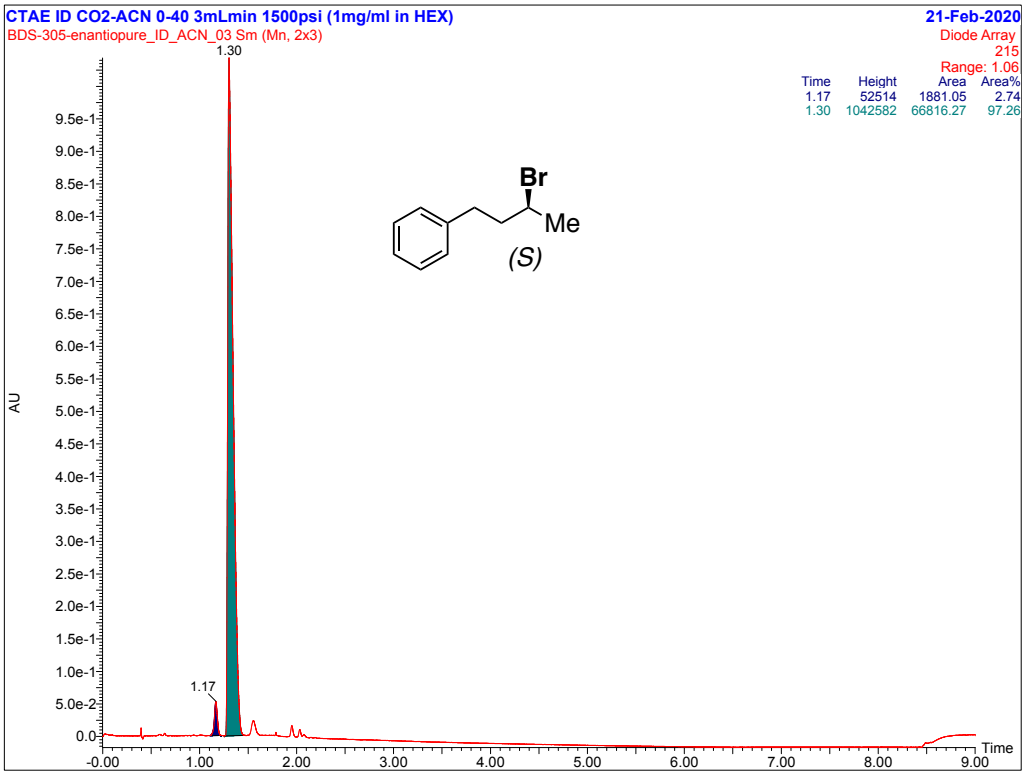

2-methyl-4-phenylbutan-1-ol

Racemic Sample

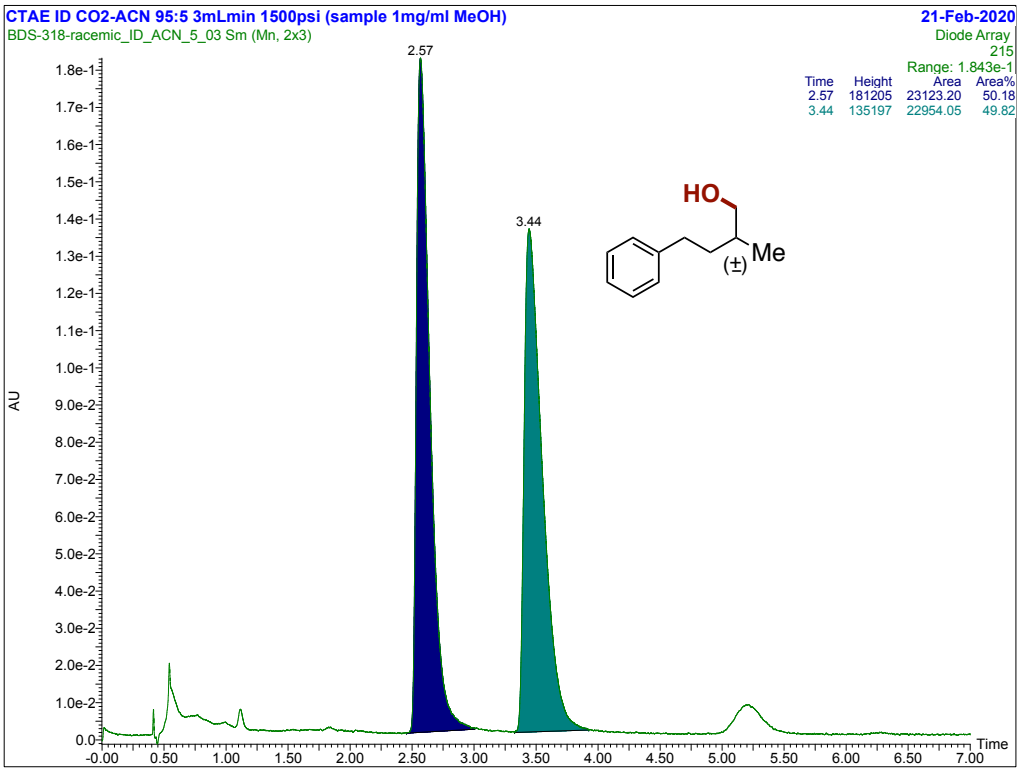

Enantioenriched Sample

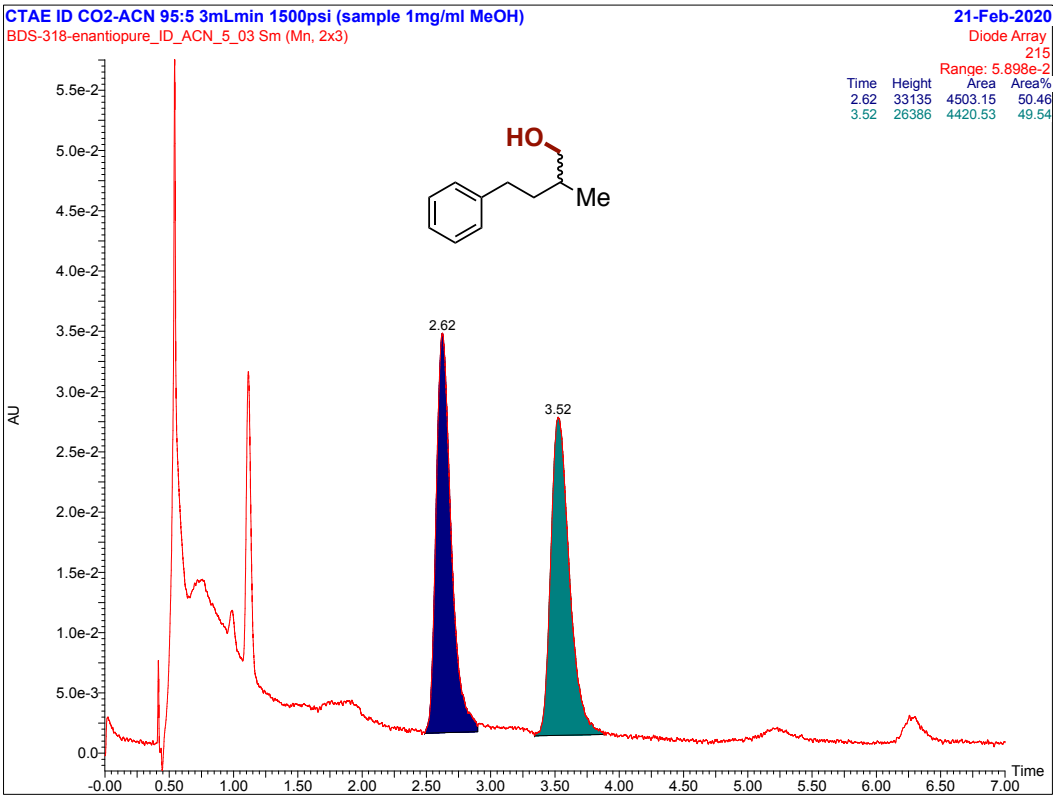

(3) Radical trapping experiment:

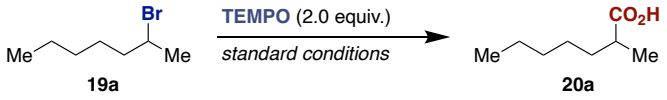

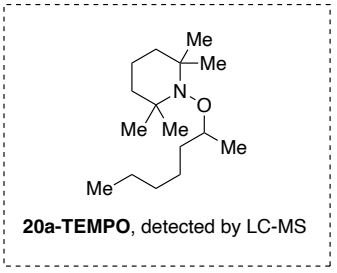

20a-TEMPO, detected by LC-MS

An oven-dried Schlenk tube containing a magnetic stir bar was charged with L11NiBr$_2$ (15 mg, 10 mol%, 25 µmol), 4CzIPN (10 mg, 5 mol%, 12.5 µmol), Hantzsch ester (HEH, 127 mg, 2.0 equiv, 0.50 mmol) and TEMPO (78 mg, 2.0 equiv., 0.50 mmol). The Schlenk tube was then taken inside a nitrogen-filled glovebox, where Cs_2CO_3 (163 mg, 2.0 equiv., 0.50 mmol) was added. The tube was then sealed, taken out of the glovebox and connected to a vacuum line where it was evacuated and back-filled under CO_2 flow at

least three times. The alkyl bromide **19a** (45 mg, 40 µL, 1.0 equiv, 0.25 mmol) and NMP (3.0 mL, 0.08 M) were added under CO_2 flow. Once all the components were added, the Schlenk tube was closed at the CO_2 pressure of 1 bar and placed in a temperature controlled photoreactor with cooling set at 15ºC (which gives an *in situ* reaction temperature of ca. 20ºC) and stirred for 24 h in the presence of continuous irradiation with blue light (451 nm, 1 W LED). The reaction was then quenched with dropwise addition of a saturated aqueous NH_4Cl solution and extracted twice using EtOAc. The combined organic layers were dried over $MgSO_4$ and used directly for sampling with LC-MS and GC-FID. The solvent was then removed *in vacuo* to perform a proton NMR of the crude, revealing not even traces of **20a** but with 57% conversion of **19a**. The corresponding **20a-TEMPO** was detected by LC-MS as an acetonitrile adduct in ESI positive mode. The fragmentations' m/z values support the structure of the adduct.

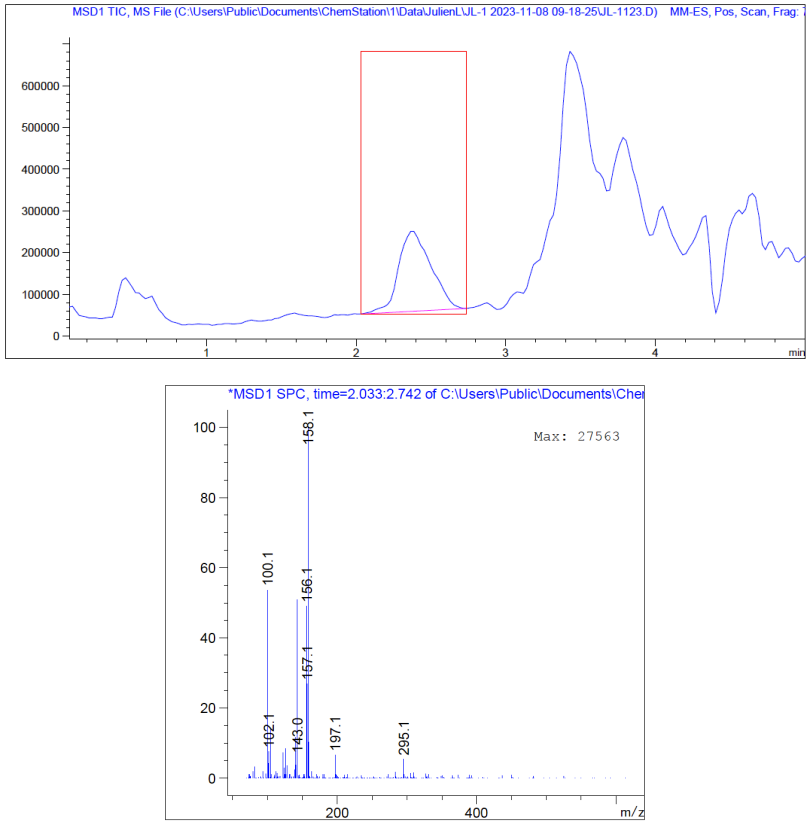

Scheme 1: TEMPO trapping experiment.

(4) Stoichiometric Studies:

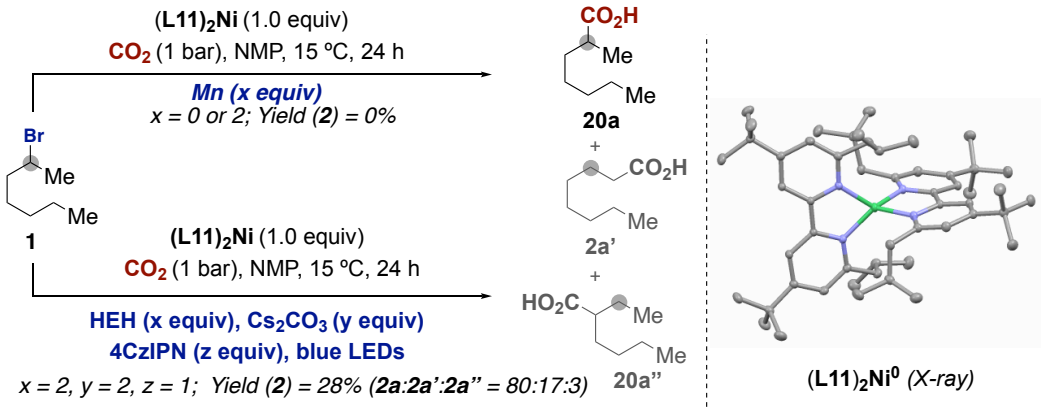

Scheme 2: Stoichiometric studies.

Several stoichiometric experiments were carried out with preformed 1.0 equiv of (**L11**)Ni(0) complex. While 2-bromoheptane (**19a**) was treated with (**L11**)Ni(0) complex (1.0 equiv) in CO_2 atmosphere in the absence of sacrificial reductant, no desired carboxylic acids were obtained, rather 2-heptene (70%) and n-heptane (7%) obtained as byproducts. Performing the same reaction in the presence of Mn (2.0 equiv) furnished no acids as well, with significant amounts of n-heptane (95%) and traces of 2-heptene (<5%). However, the catalytic activity for carboxylation can be recovered in the presence of 4CzIPN (1.0 equiv), HEH (2.0 equiv) and Cs_2CO_3 (2.0 equiv), delivering desired acids **20a** (28%, **2a:2a':2a"** = 80:17:3).

Synthesis of (L11)$_2$Ni

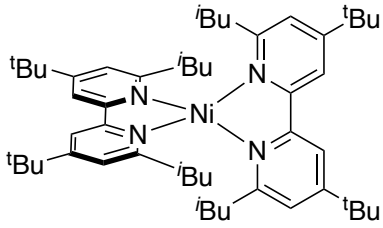

In the glovebox, (**L11**)NiBr$_2$ (201 mg, 0.34 mmol) was added to a 10 mL vial with **L11** (140 mg, 0.37mmol) and Mg powder (204 mg, 8.39 mmol). A stir bar was added, then the vial was charged with 6 mL of THF turning the pink powder to a pink suspension. After 5 hours the solvent was removed and dissolved in minimal amount of toluene to give a blue solution. This solution was filtered through a pipette plug of celite and a blue solution collected. The solvent was again removed to give an (**L11**)$_2$Ni (286 mg, 98 % yield) as a blue powder.

^{1}H NMR (400 MHz, Toluene-d_8) δ 7.75 (s, 1H), 7.65 (s, 1H), 3.23 (d, *J* = 7.0 Hz, 2H), 2.74 – 2.42 (m, 1H), 1.28 (s, 9H), 0.64 (d, *J* = 6.6 Hz, 6H). **^{13}C NMR (126 MHz, Toluene-d_8)** δ 162.1, 140.56, 137.8, 119.4, 118.5, 52.0, 37.0, 30.7, 28.5, 27.5, 22.7, 22.3.

Synthesis of (L11)NiBr

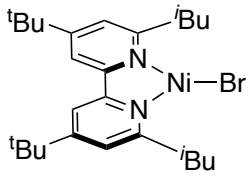

In the glovebox, (**L11**)$NiBr_2$ (40.1 mg, 0.07 mmol) was added to a 10 mL vial with **L11** (25.6 mg, 0.07 mmol) and $Ni(COD)_2$ (18.8 mg, 0.07 mmol). A stir bar was added, then the vial was charged with 3 mL of THF turning the pink powder to a pink suspension. After 18 hours the solvent was removed to afford a deep green solid. The solid was washed with cold (-36 °C) pentane (1 mL x 3) to give (**L11**)NiBr (47.1 mg, 68 % yield) as a green powder.
^{1}H NMR (400 MHz, Toluene-d_8): δ 35.00 (s, 1H), 20.83 (s, 1H). **^{13}C** omitted due to line broadening of paramagnetic (**L11**)$NiBr_2$.

Stoichiometric experiment of (L11)NiBr and 2-bromoheptane

In the glovebox, 2-bromoheptane **19a** (7.3 mg, 0.04 mmol) and 1,3,5-trimethoxybenzene (TMB) (2.0 mg, 0.01 mmol) were added to a 4 mL vial and dissolved in 1 mL C_6D_6. This solution was then transferred to a J. Young NMR tube, and the initial integration ratio of 2-bromoheptane and TMB was measured. This solution was then brought back into the glovebox and added to a stirred solution of (**L11**)NiBr (11.0 mg, 0.02 mmol) in 1 mL C_6D_6. After 10 min of stirring, this solution was then transferred back into the J. Young NMR tube and measured by ^{1}H and paramagnetic ^{1}H NMR showing full conversion to (**L11**)$NiBr_2$ and 76% yield of 2-hexene to (**L11**)NiBr. This solution was then brought back into the glovebox and transferred to a 10 mL vial. Pentane (4 mL) was then added to precipitate a pink solid, where the light pink filtrate was decanted. The remaining solid was dried to afford (**L11**)$NiBr_2$ (8.3 mg, 68 % yield) as a pink powder.

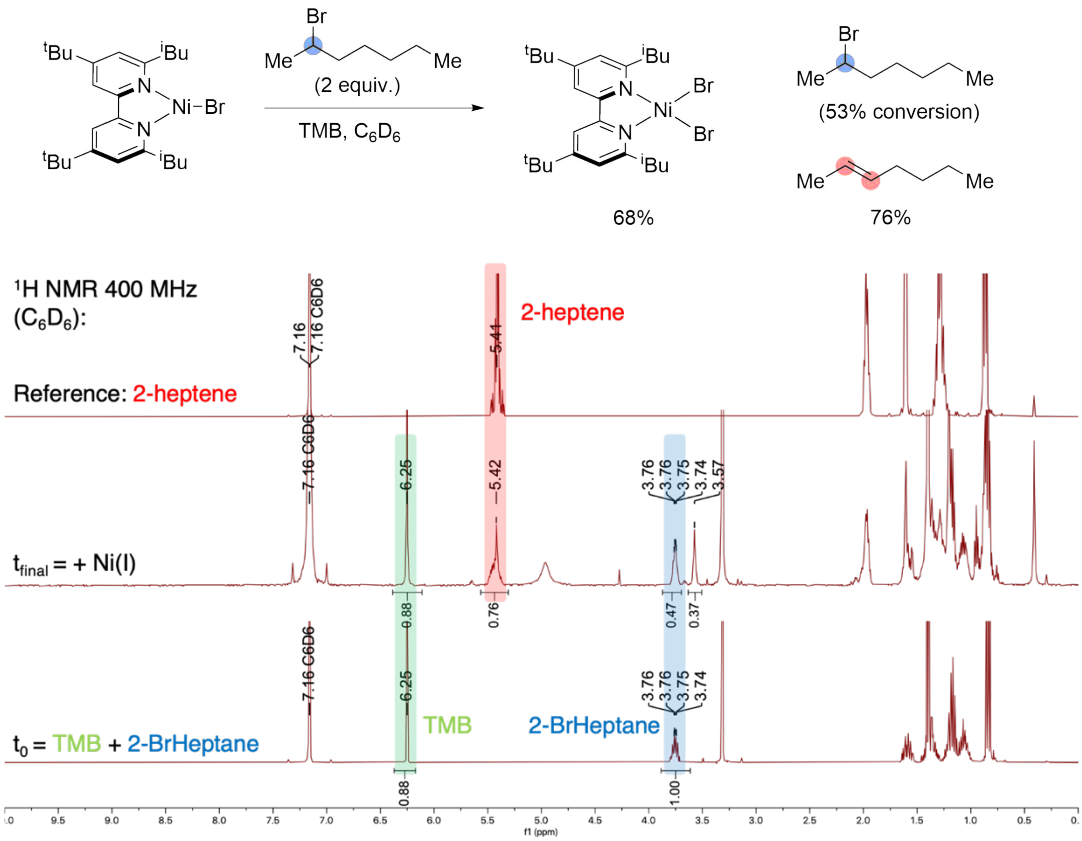

Figure 0.1: 1H spectra (C6D6, 400 MHz) of the reaction between (L11)NiBr and 2-bromoheptane (blue) forming 2-heptene (red) (internal standard = TMB (1,3,5-trimethoxybenzene, green)).

(5) Effect of Photocatalyst-to-Ni Catalyst ratio on Selectivity:

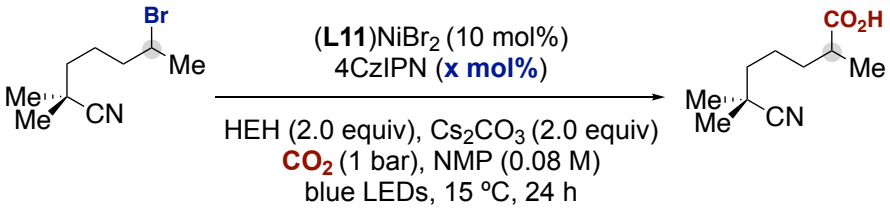

x = 2, Yield = 87%, r:m = 92:8
x = 4, Yield = 89%, r:m = 95:5
x = 6, Yield = 87%, r:m = 97:3
x = 8, Yield = 89%, r:m = over 99:1

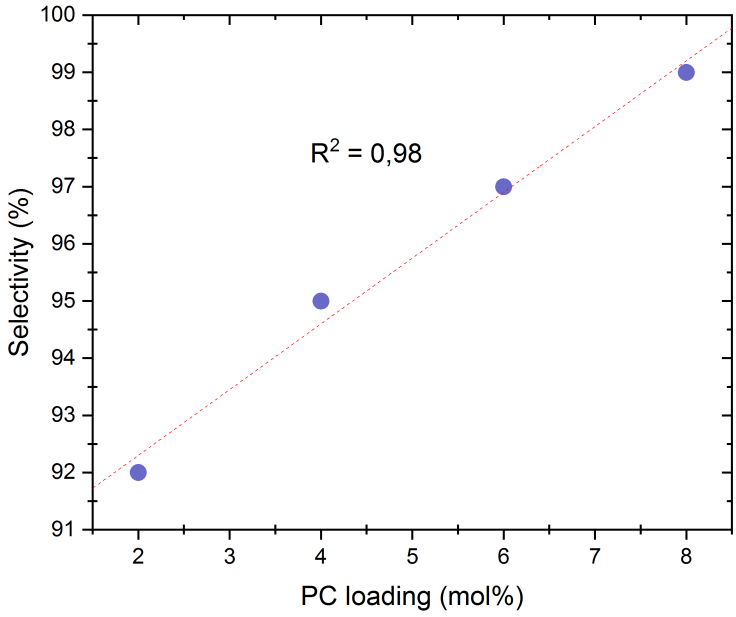

Figure 0.2: Influence of photocatalyst loading on the selectivity outcome.

As shown in the above scheme and graph, an improved *branched to linear* selectivity can be observed with the increasing loading of photocatalyst. This indicates that the rate of SET reduction of Ni(II) to Ni(I) by the Photocatalytic cycle is crucial to ensure a good retained selective carboxylation.

3.7.5. NMR spectra

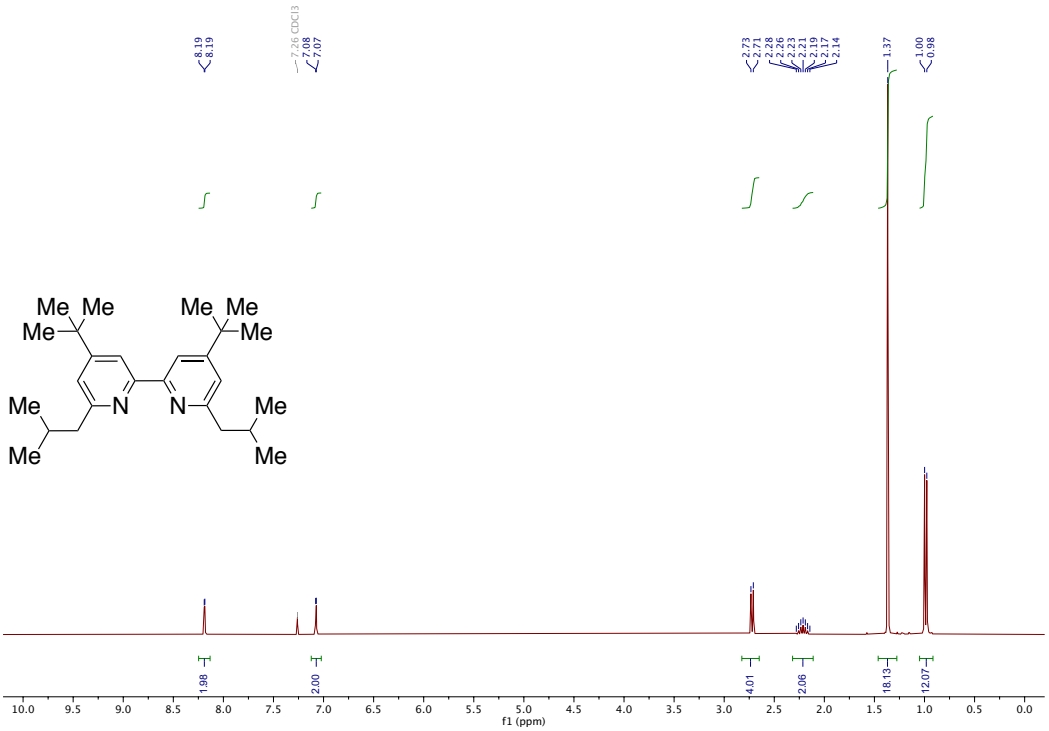

^{1}H spectrum (400 MHz, $CDCl_3$) of **L11**

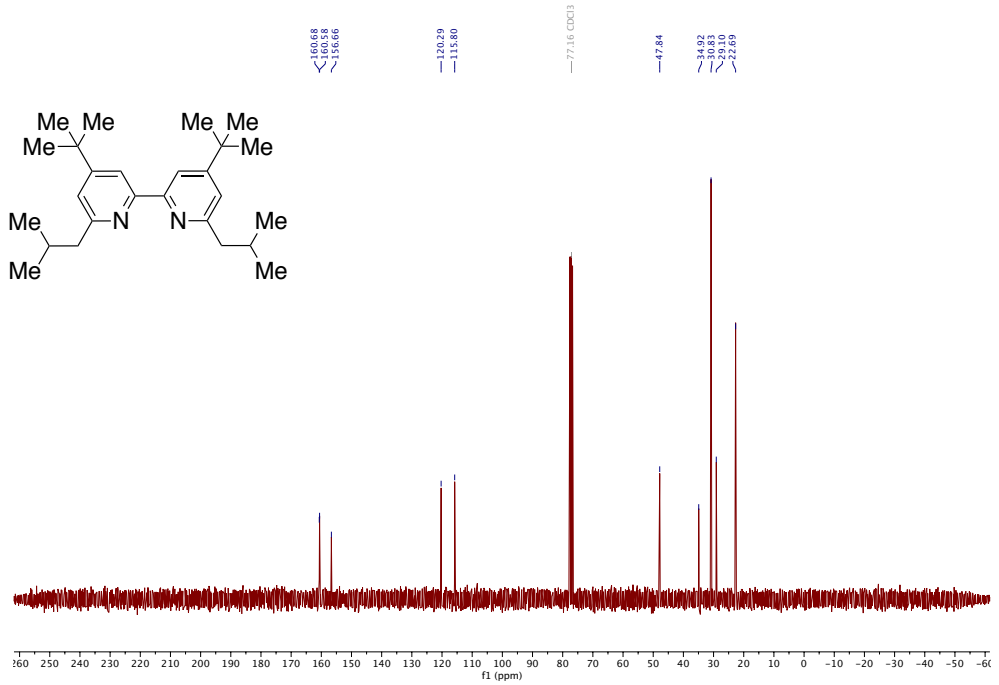

^{13}C spectrum (101 MHz, $CDCl_3$) of **L11**

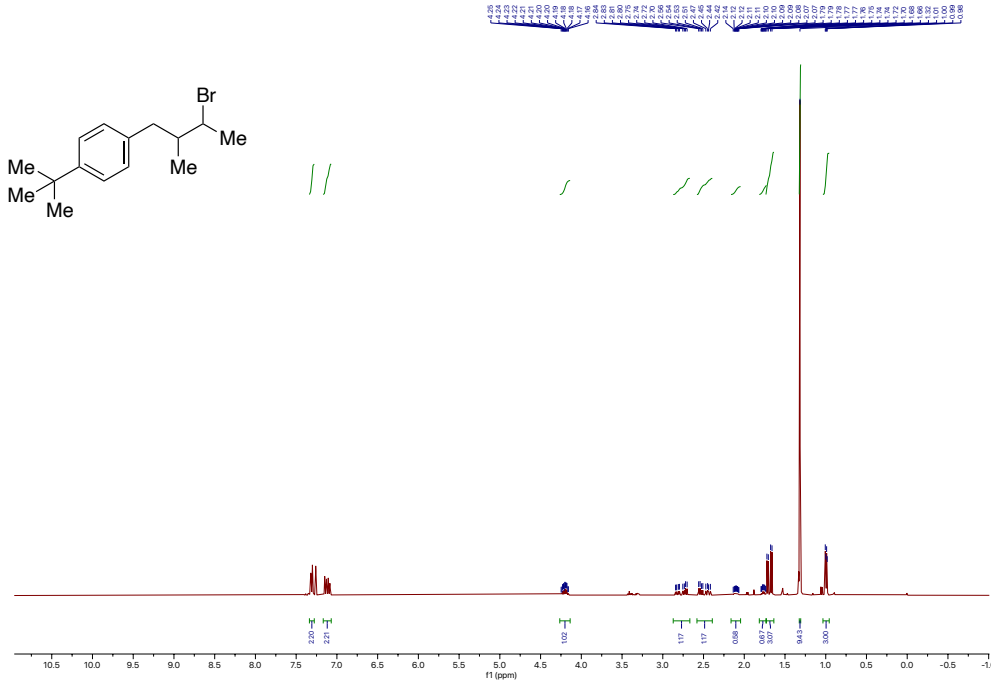

^{1}H spectrum (500 MHz, $CDCl_3$) of **19d**

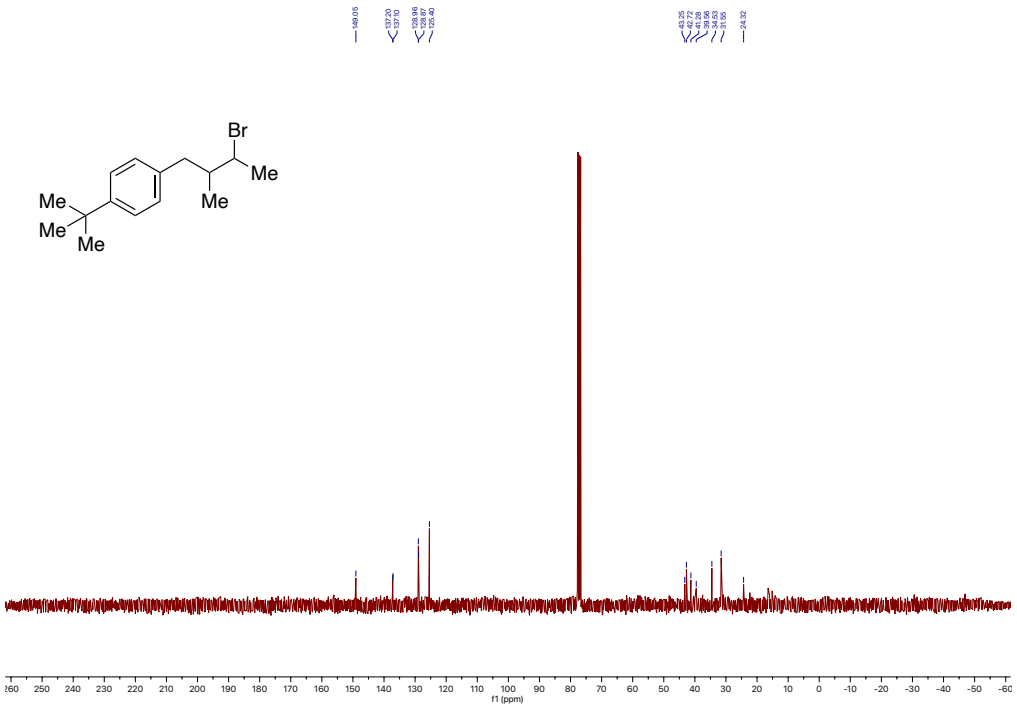

^{13}C spectrum (75 MHz, $CDCl_3$) of **19d**

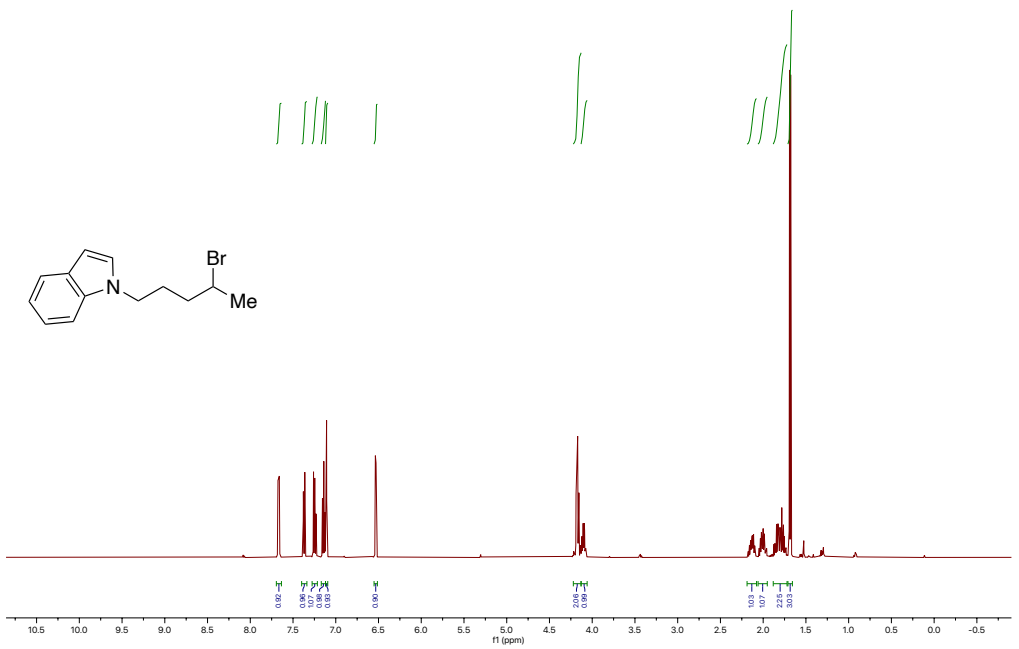

^{1}H spectrum (500 MHz, $CDCl_3$) of **19f**

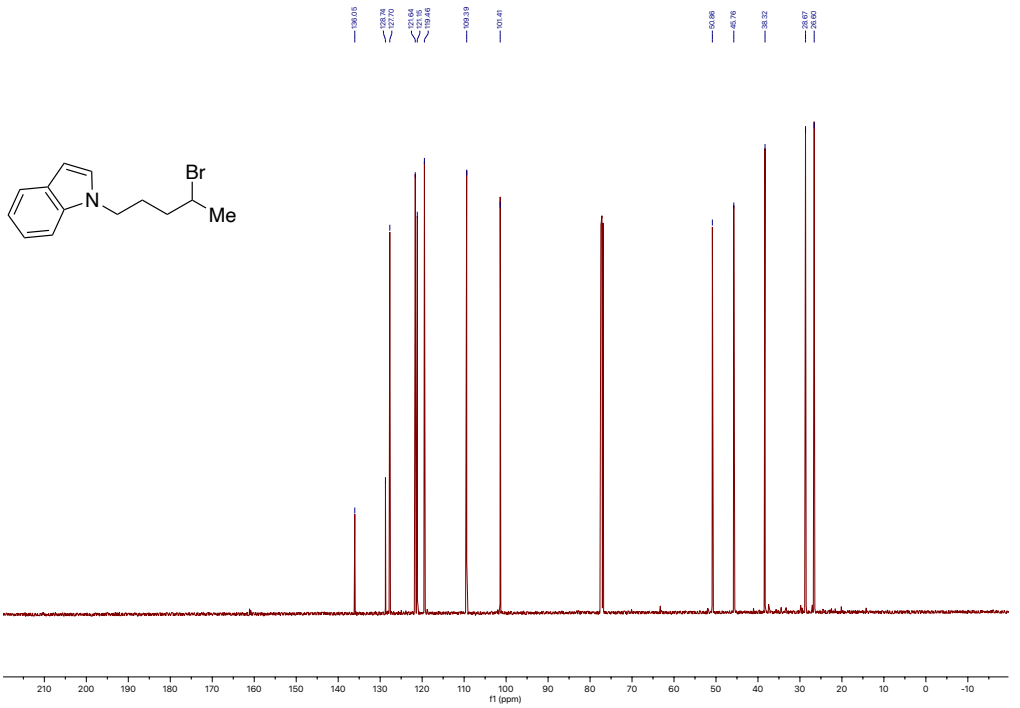

^{13}C spectrum (126 MHz, $CDCl_3$) of **19f**

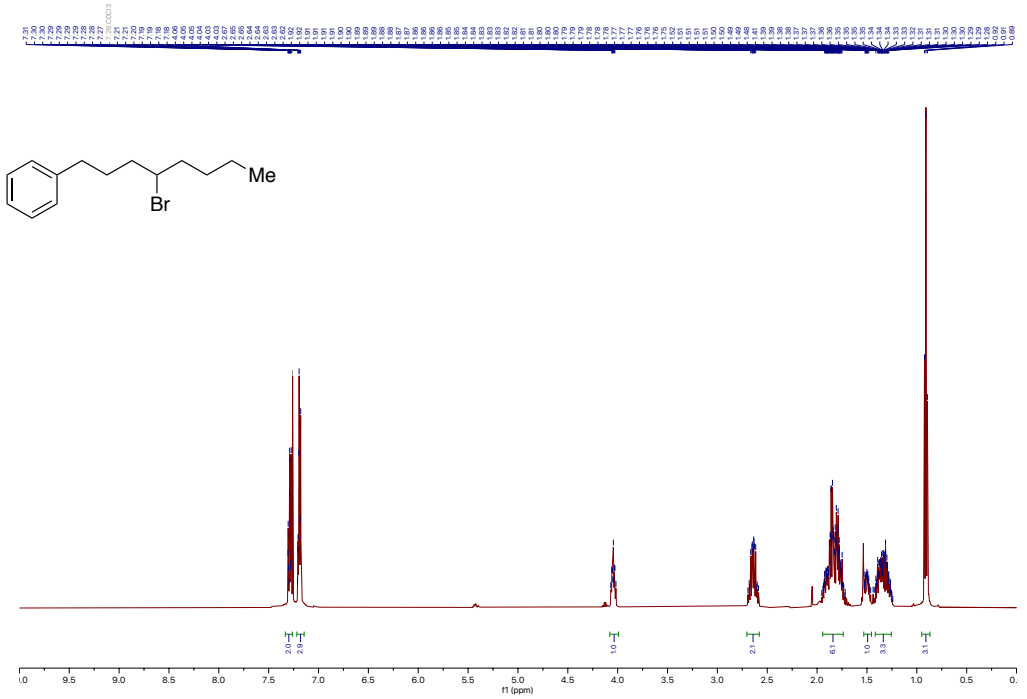

^{1}H spectrum (400 MHz, $CDCl_3$) of **19i**

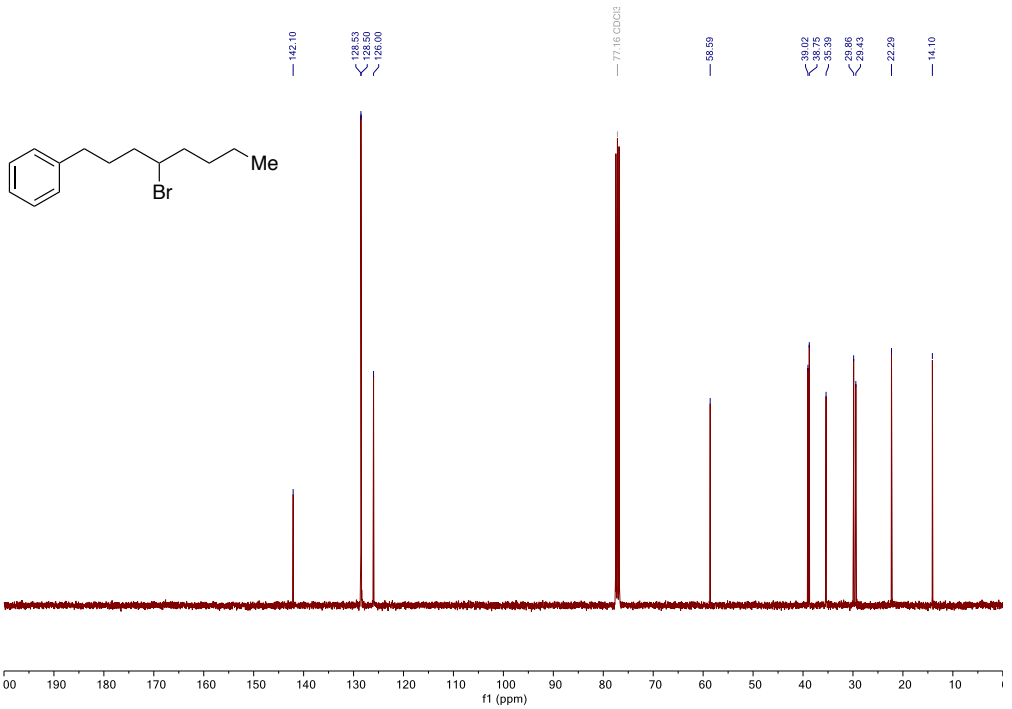

^{13}C spectrum (101 MHz, $CDCl_3$) of **19i**

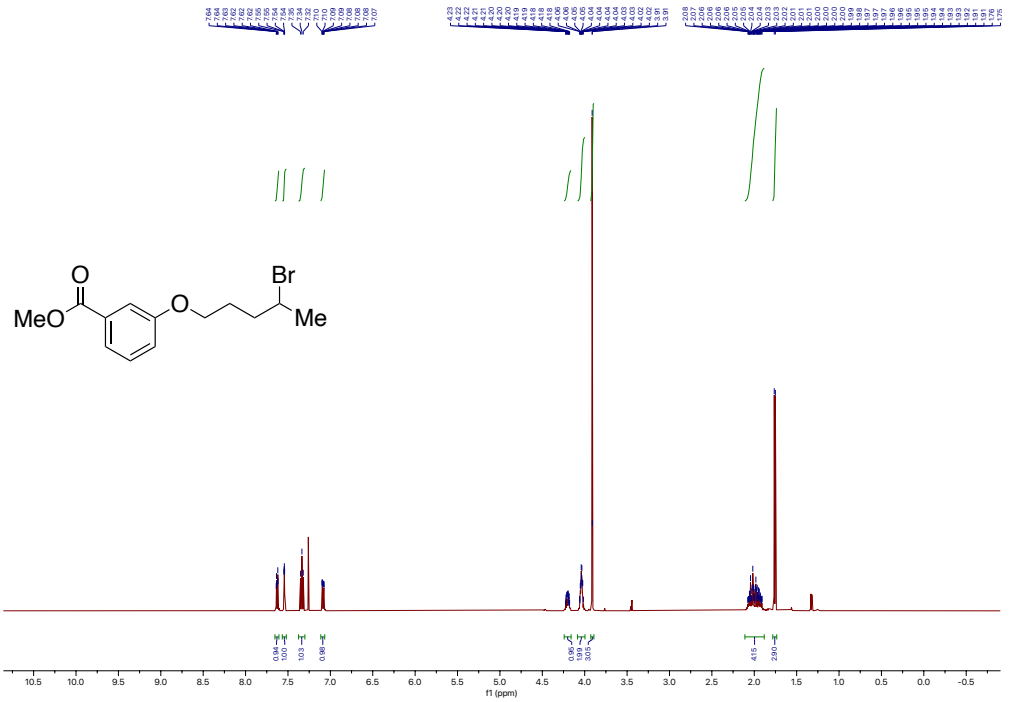

^{1}H spectrum (300 MHz, $CDCl_3$) of **19j**

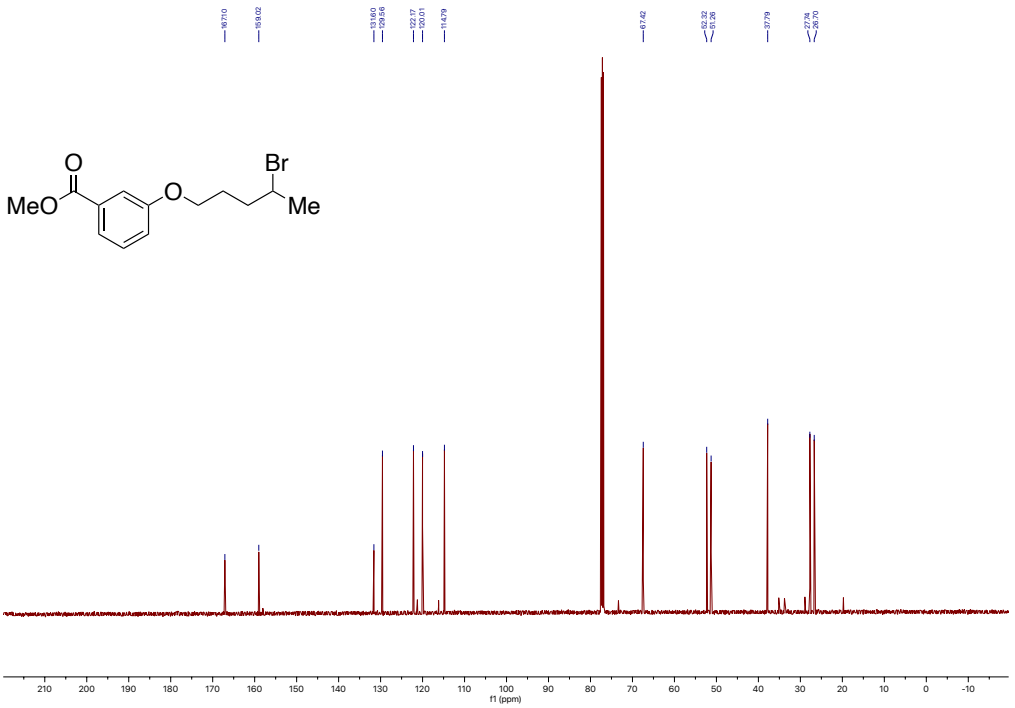

^{13}C spectrum (101 MHz, $CDCl_3$) of **19j**

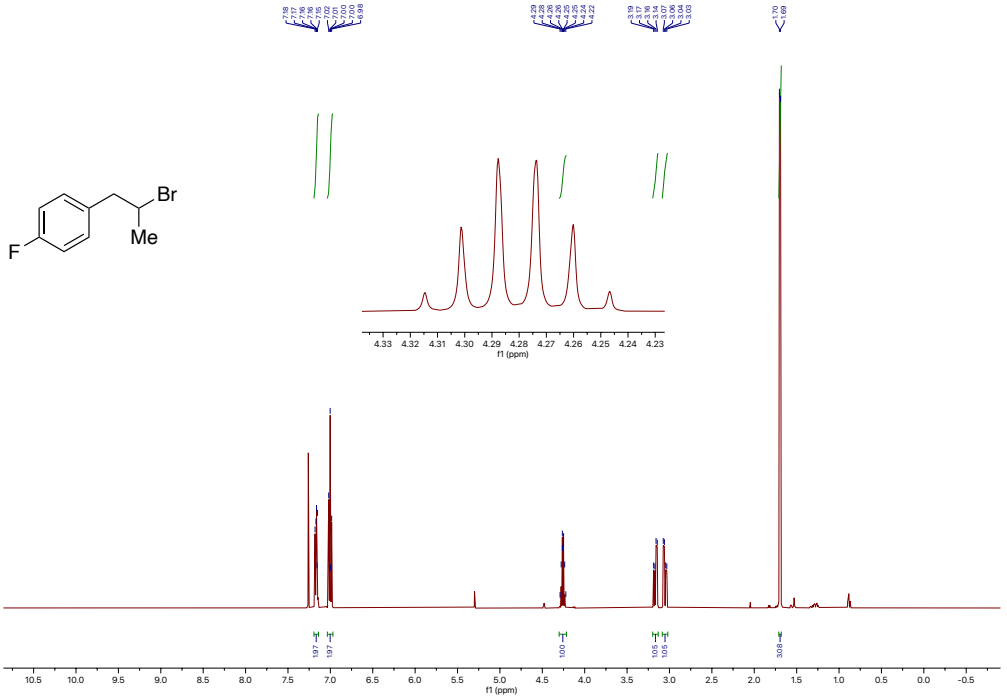

^{1}H spectrum (500 MHz, $CDCl_3$) of **19l**

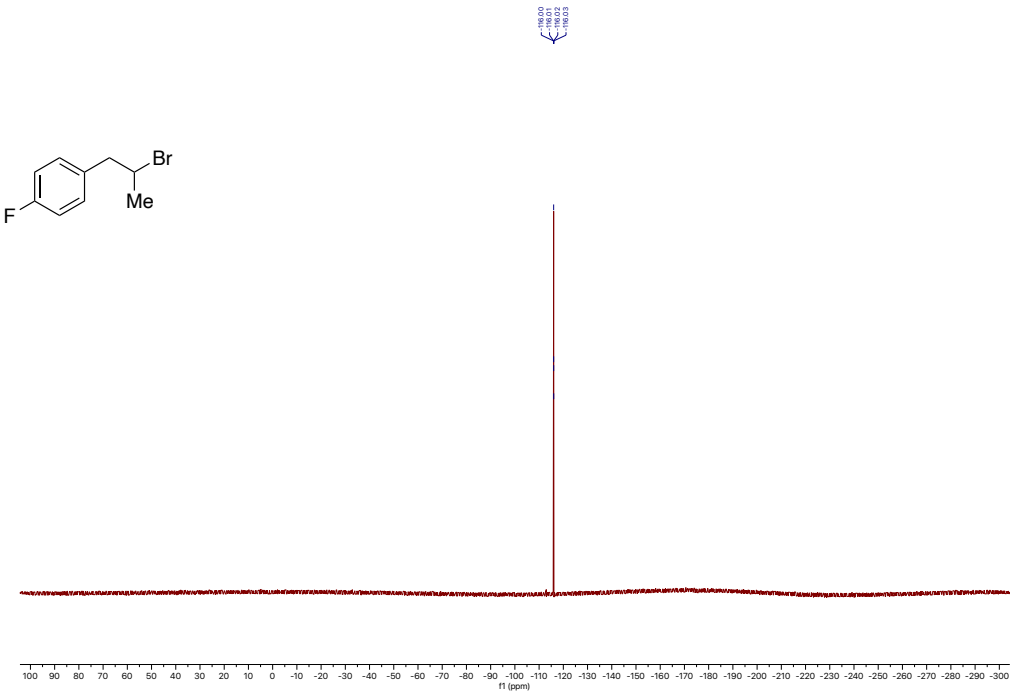

^{19}F spectrum (471 MHz, $CDCl_3$) of **19l**

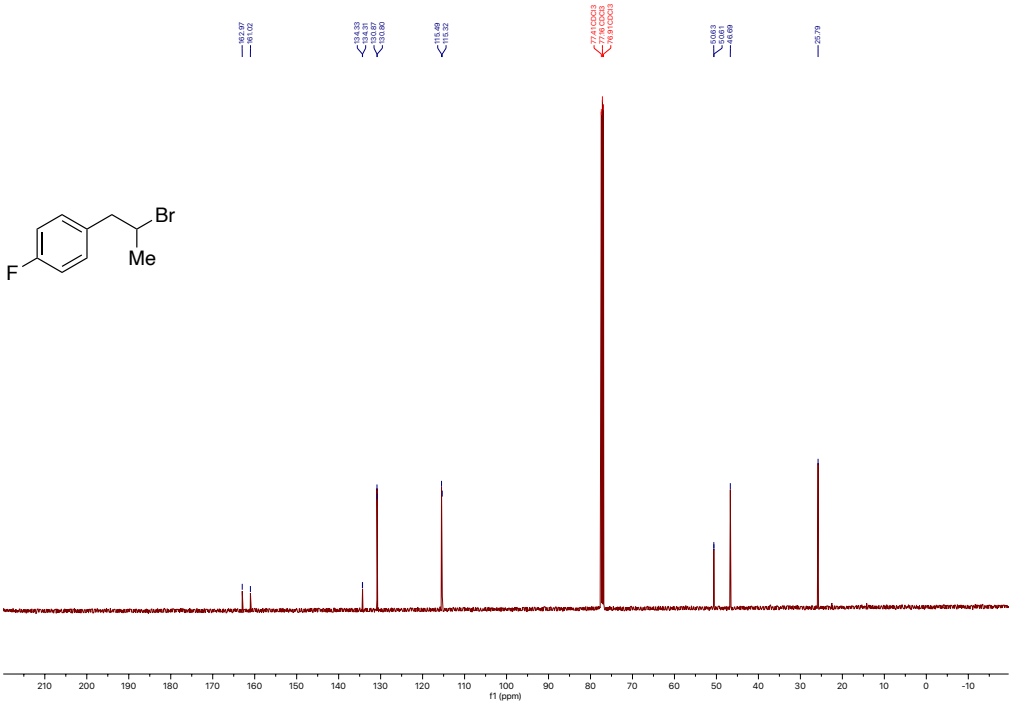

^{13}C spectrum (126 MHz, $CDCl_3$) of **19l**

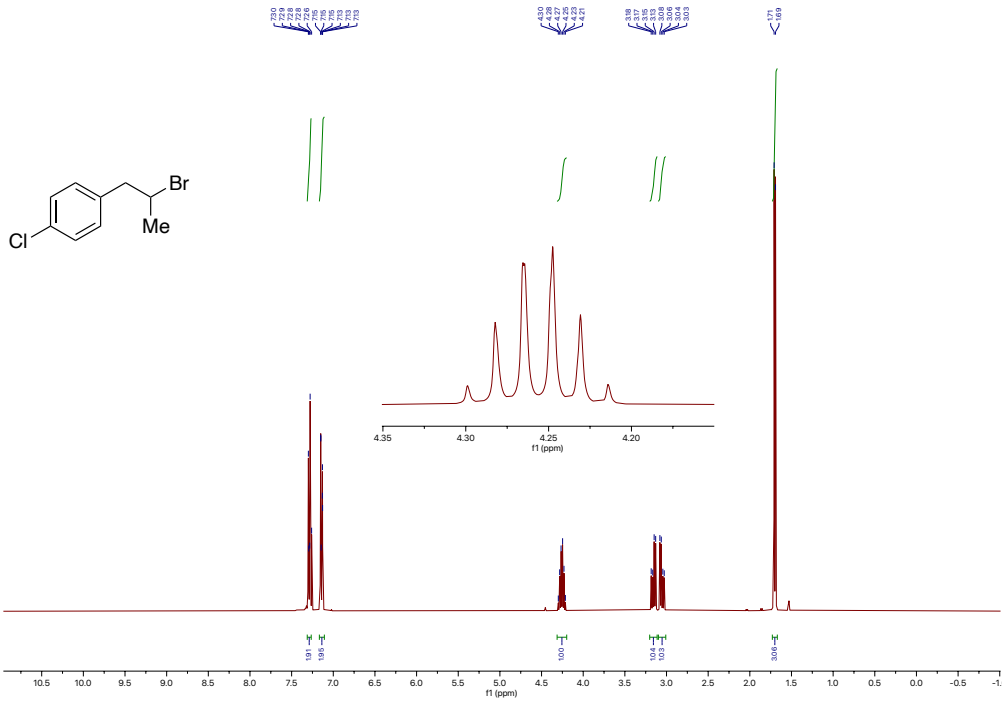

^{1}H spectrum (400 MHz, $CDCl_3$) of **19m**

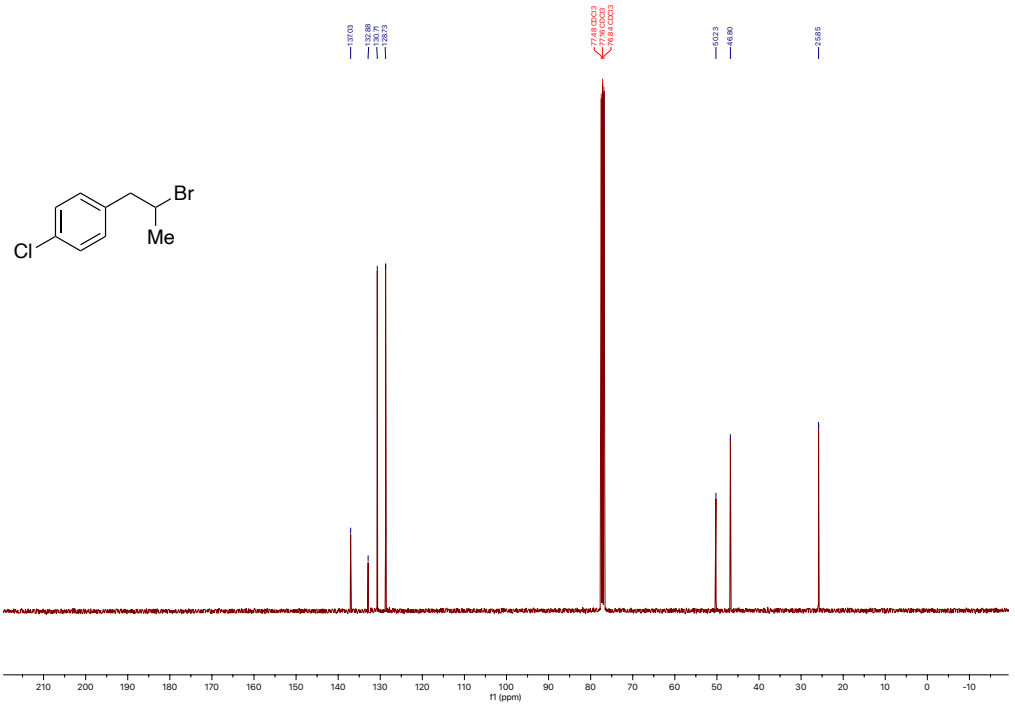

^{13}C spectrum (101 MHz, $CDCl_3$) of **19m**

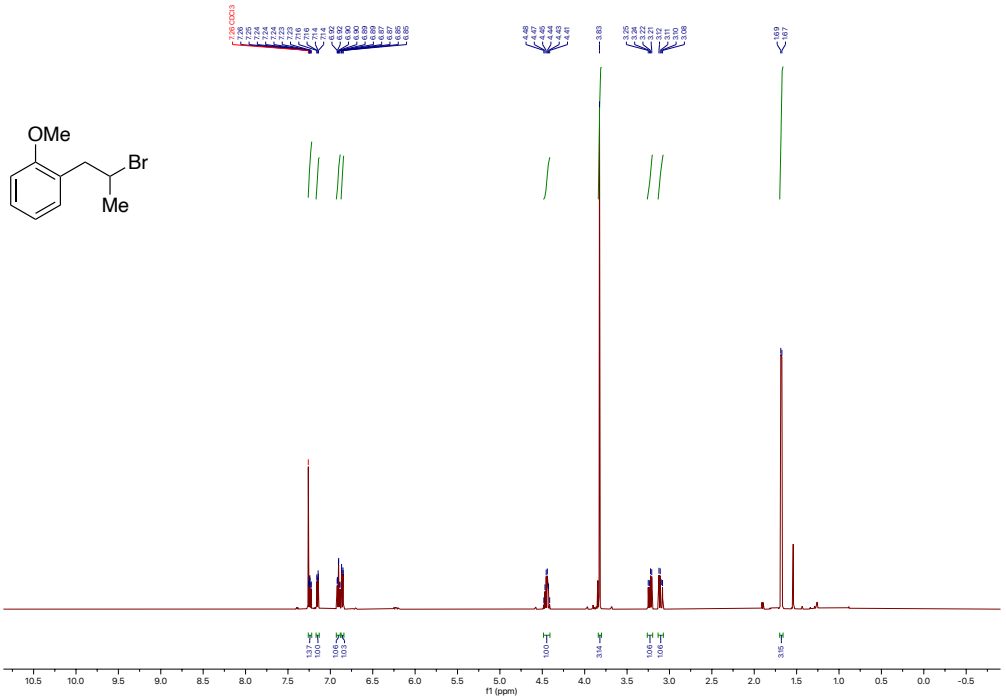

^{1}H spectrum (500 MHz, $CDCl_3$) of **19n**

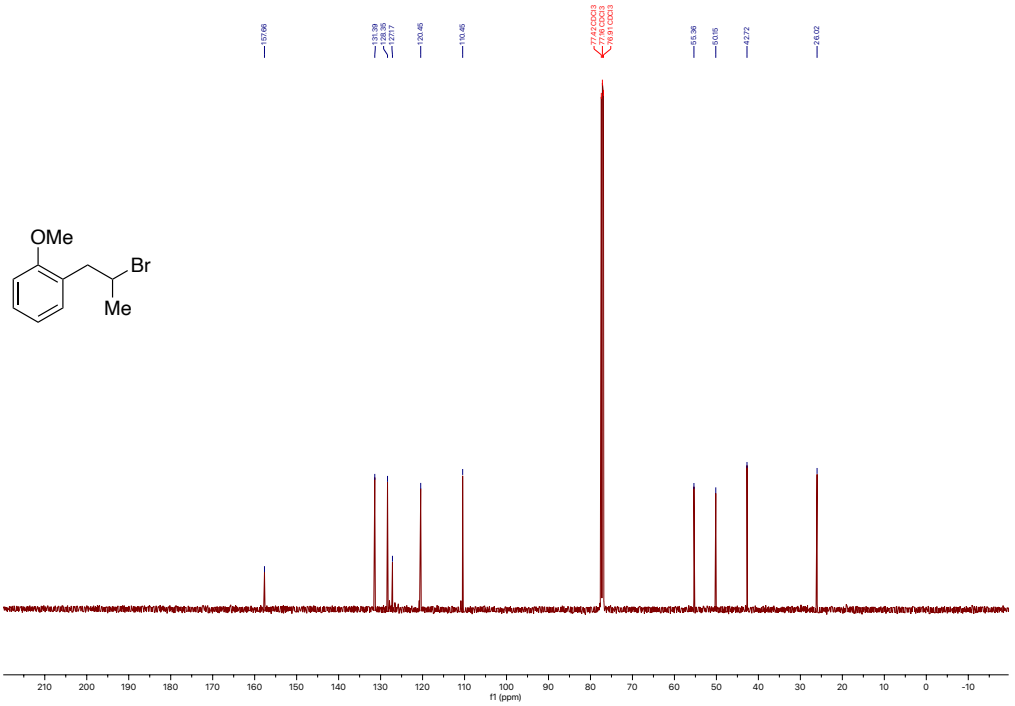

^{13}C spectrum (126 MHz, $CDCl_3$) of **19n**

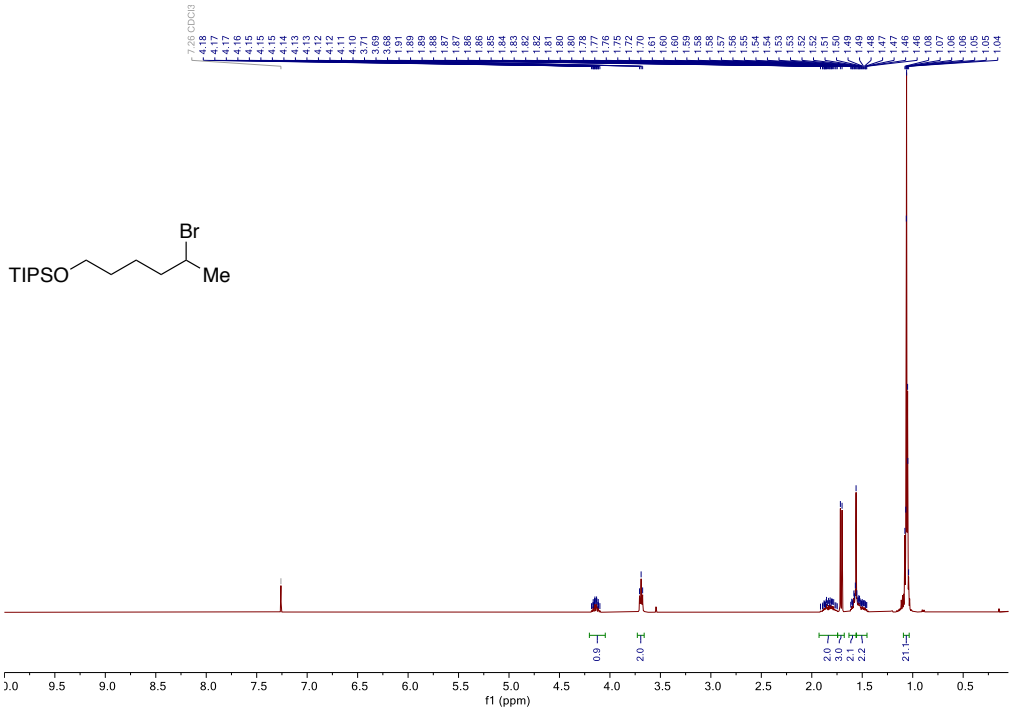

^{1}H spectrum (400 MHz, $CDCl_3$) of **19q**

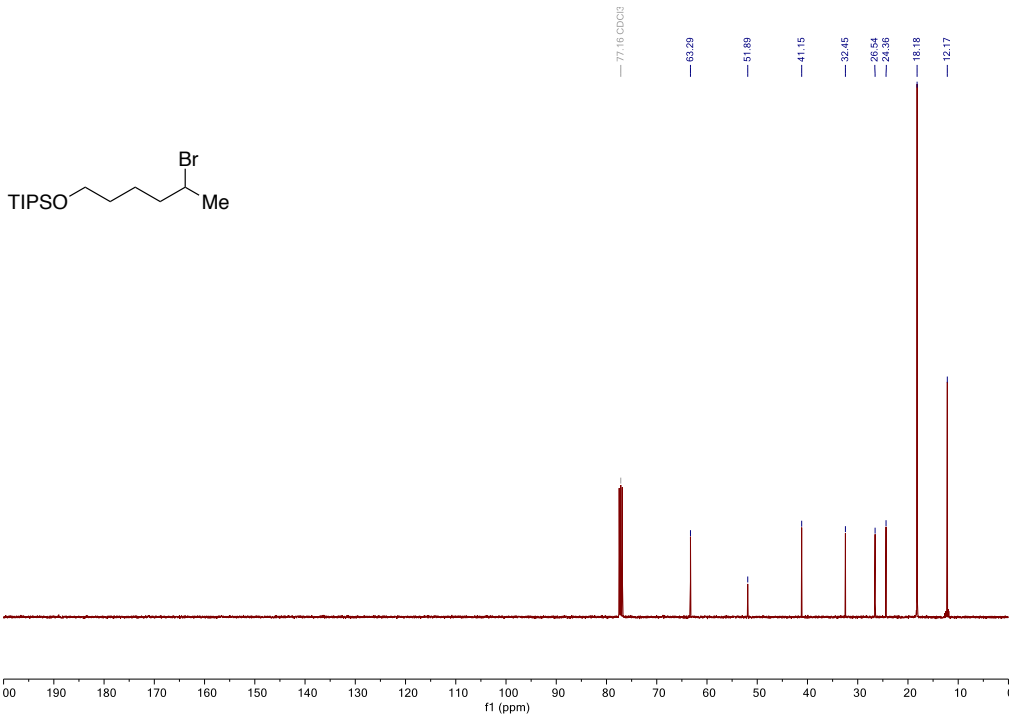

^{13}C spectrum (101 MHz, $CDCl_3$) of **19q**

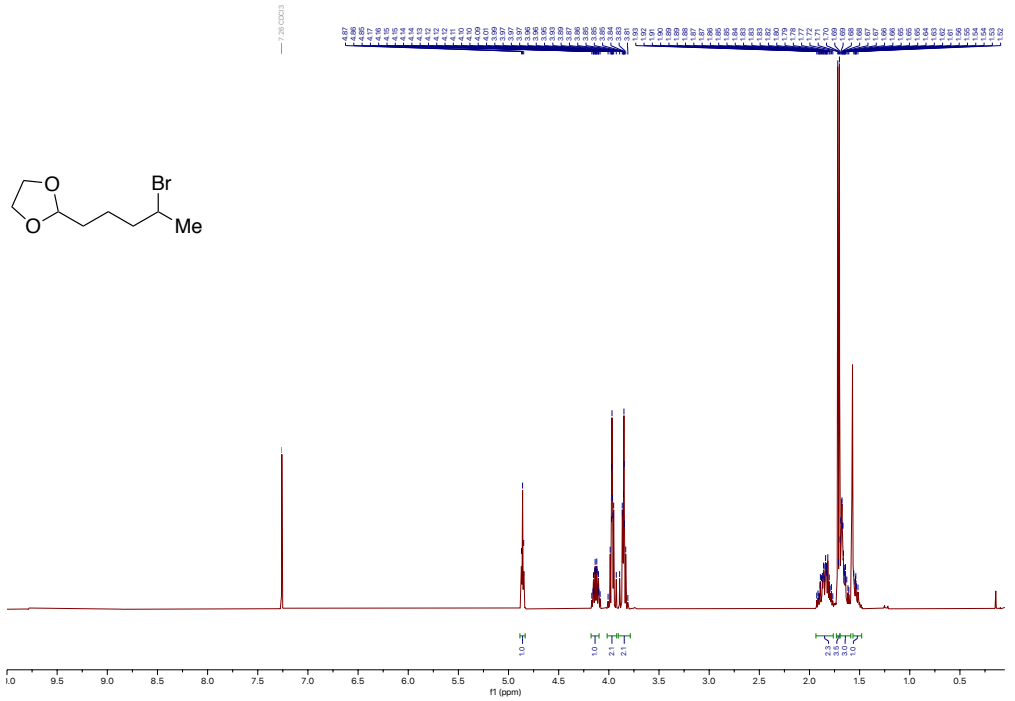

^{1}H spectrum (400 MHz, $CDCl_3$) of **19r**

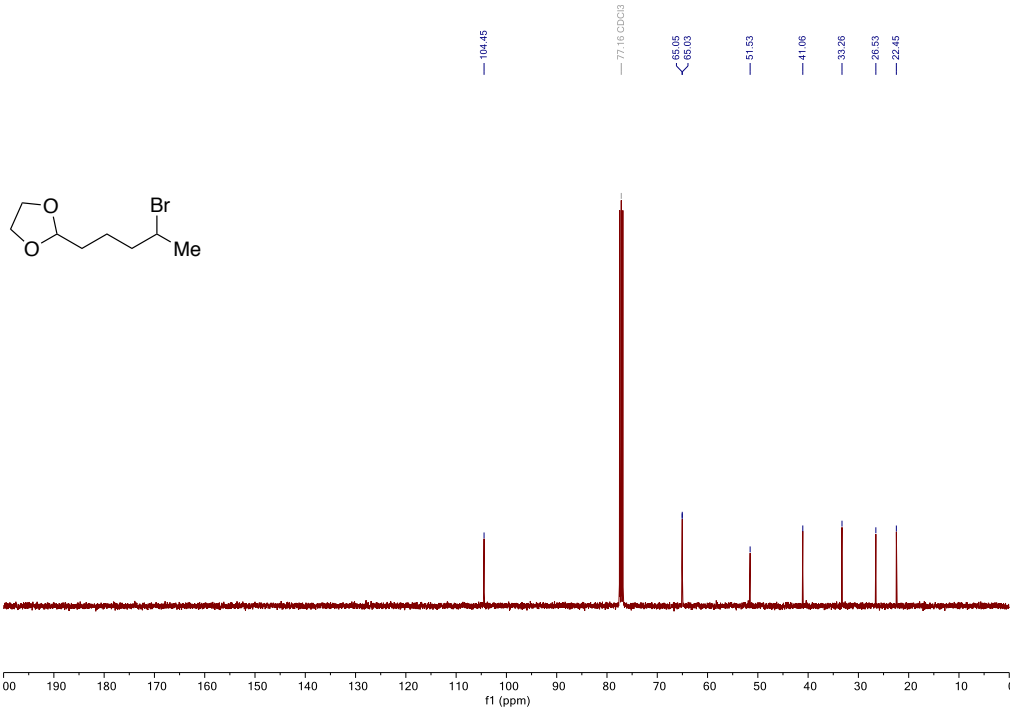

^{13}C spectrum (101 MHz, $CDCl_3$) of **19r**

^{1}H spectrum (400 MHz, $CDCl_3$) of **19s**

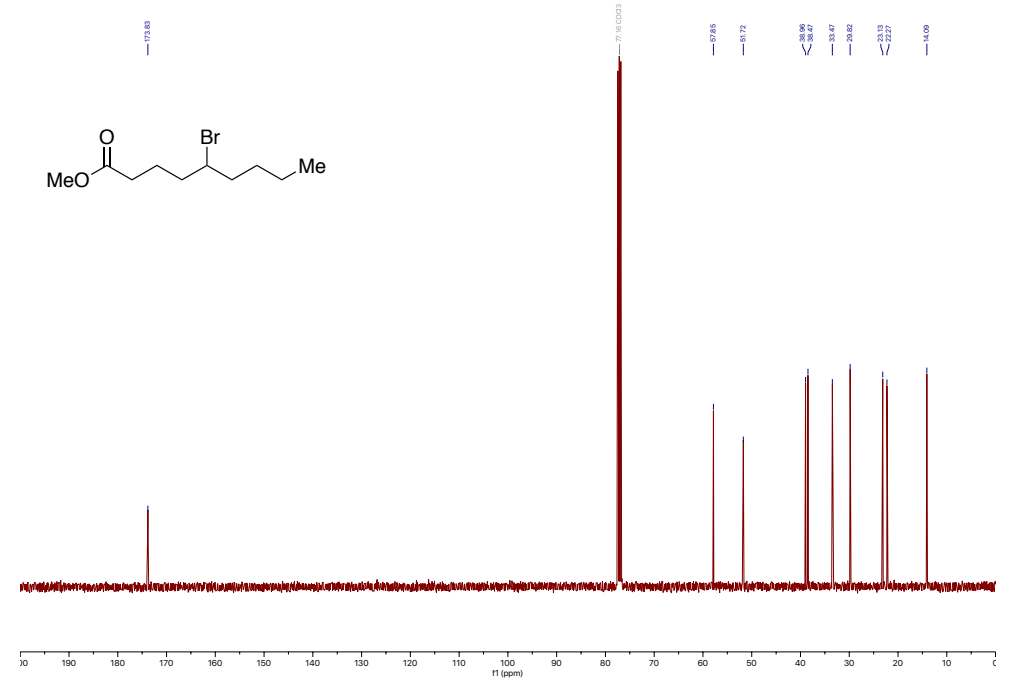

^{13}C spectrum (101 MHz, $CDCl_3$) of **19s**

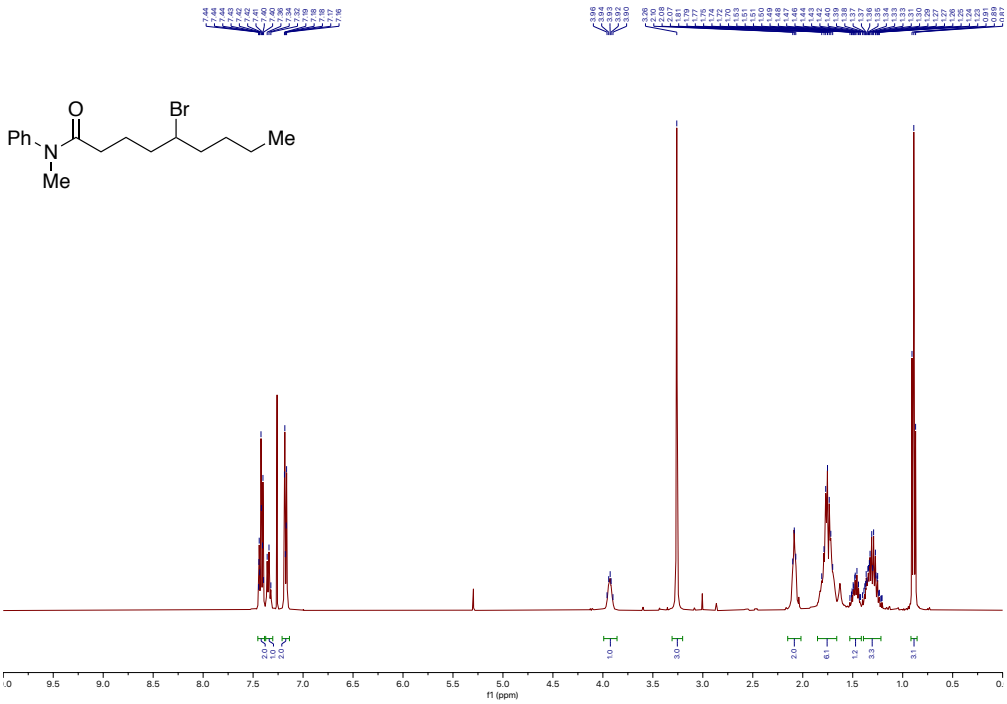

^{1}H spectrum (400 MHz, $CDCl_3$) of **19u**

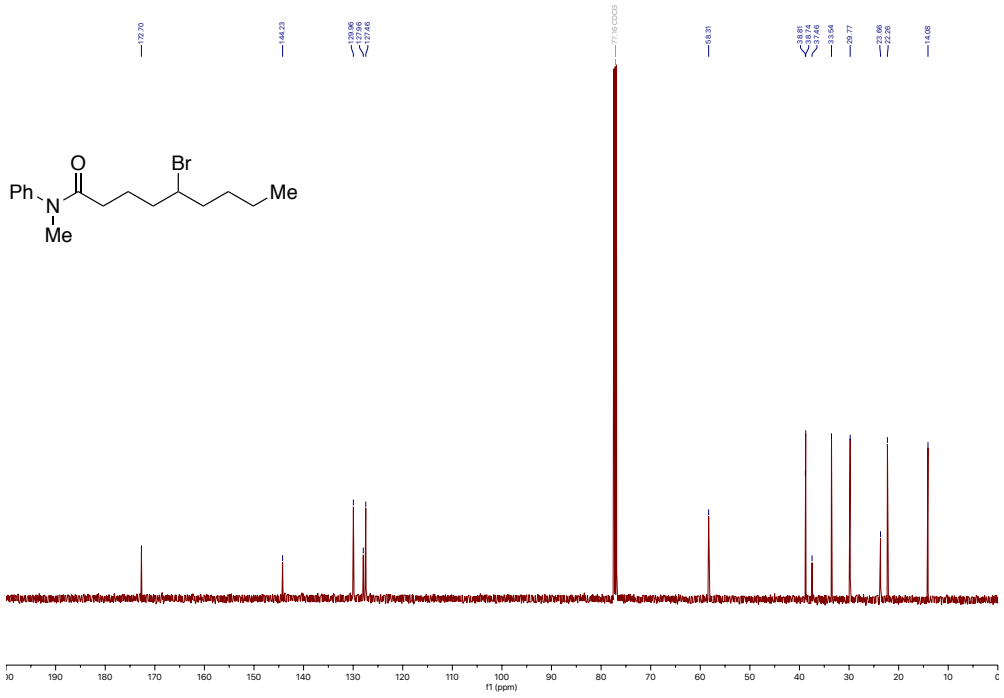

^{13}C spectrum (126 MHz, $CDCl_3$) of **19u**

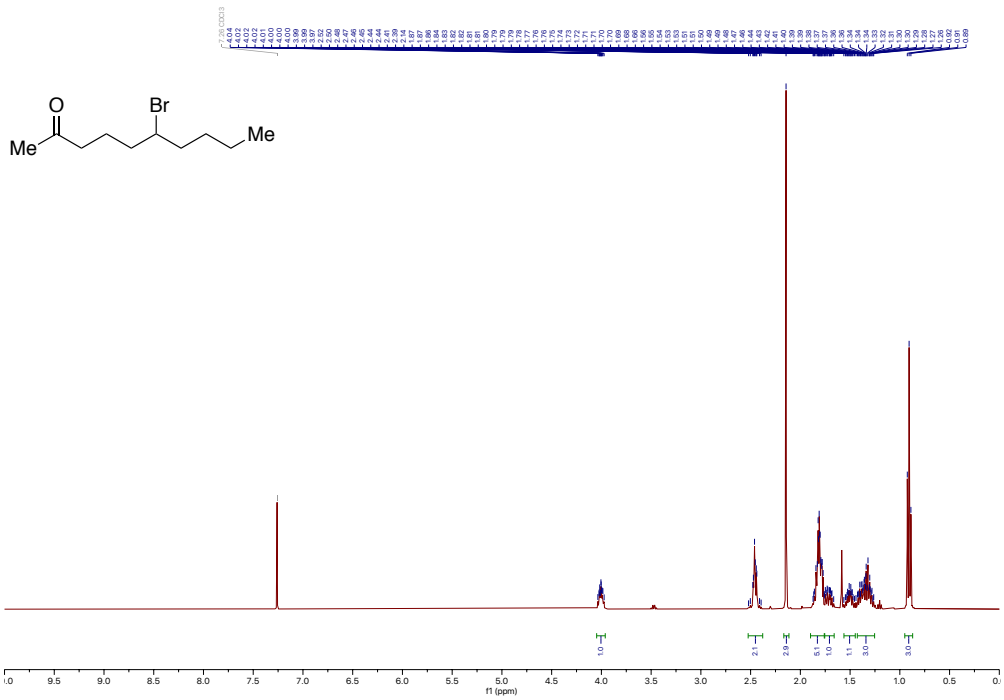

^{1}H spectrum (400 MHz, $CDCl_3$) of **19v**

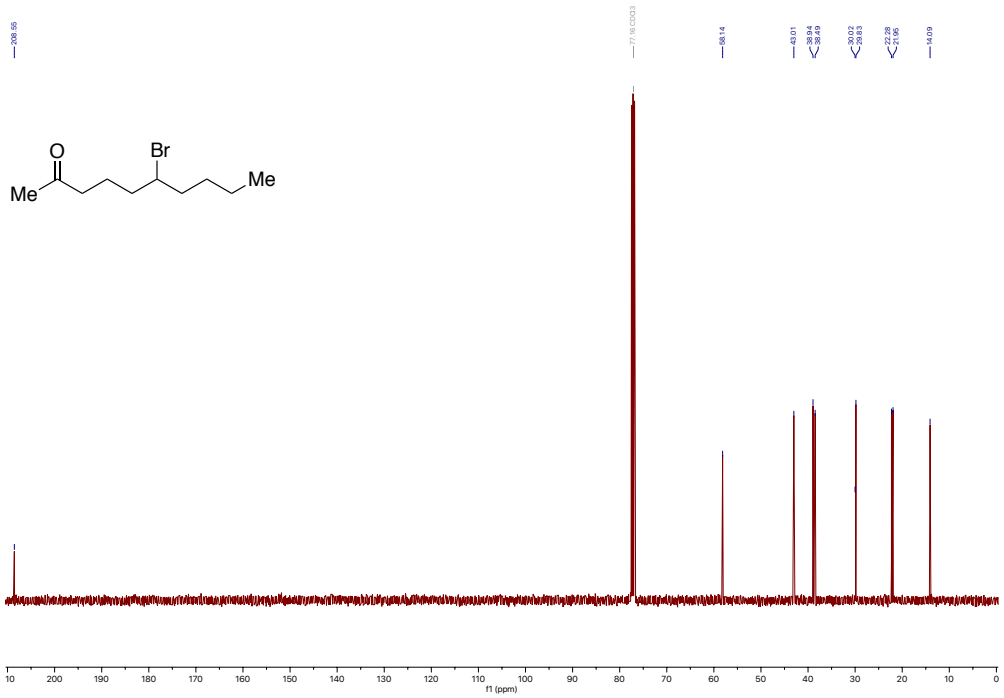

^{13}C spectrum (126 MHz, $CDCl_3$) of **19v**

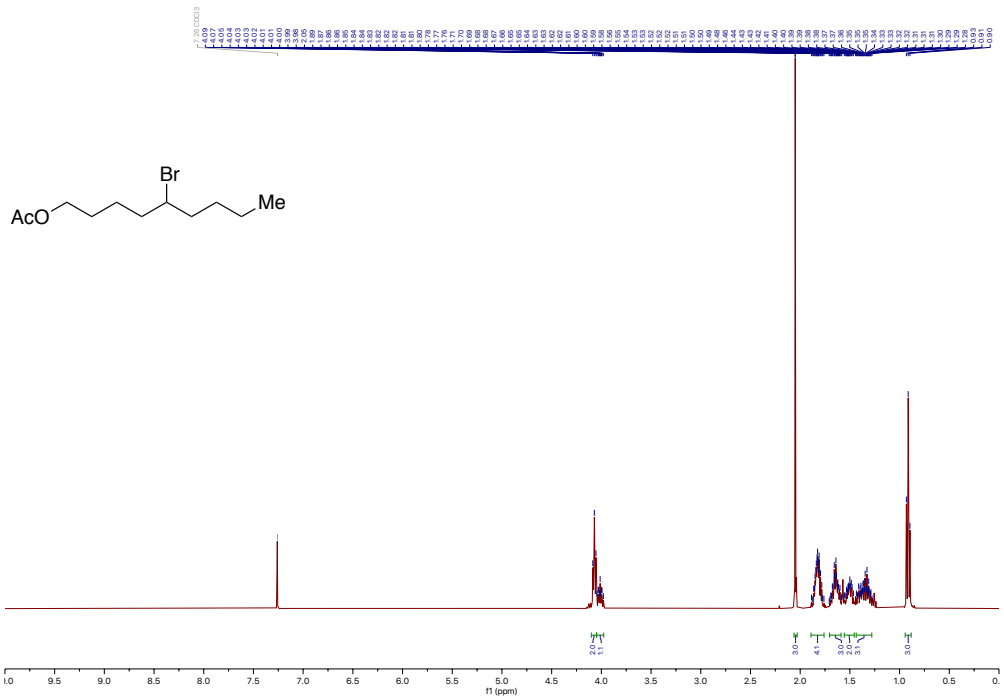

^{1}H spectrum (500 MHz, $CDCl_3$) of **19w**

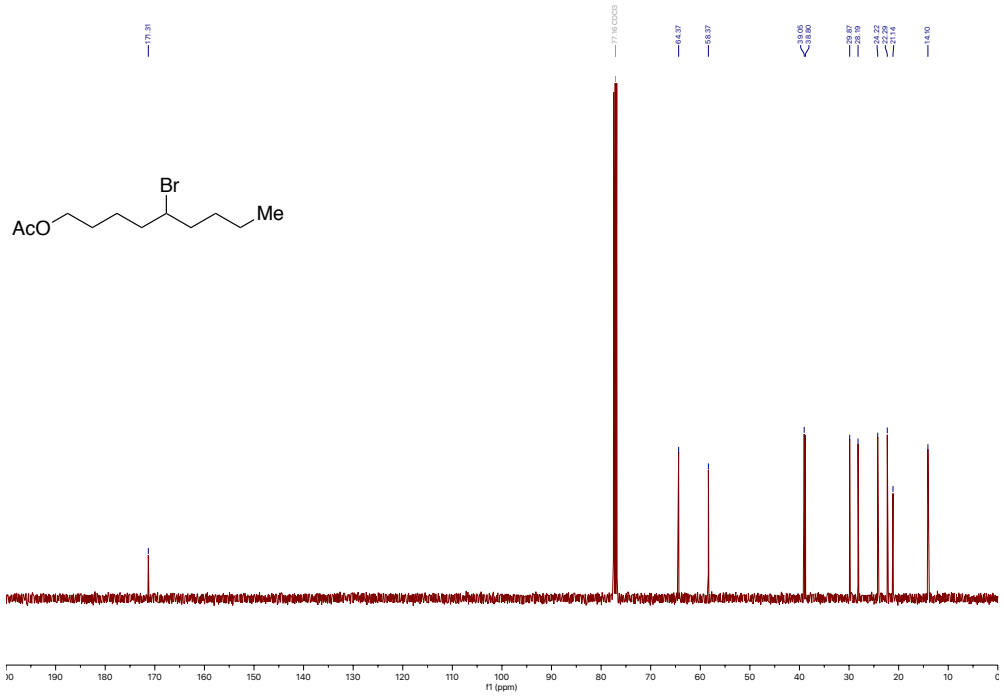

^{13}C spectrum (101 MHz, $CDCl_3$) of **19w**

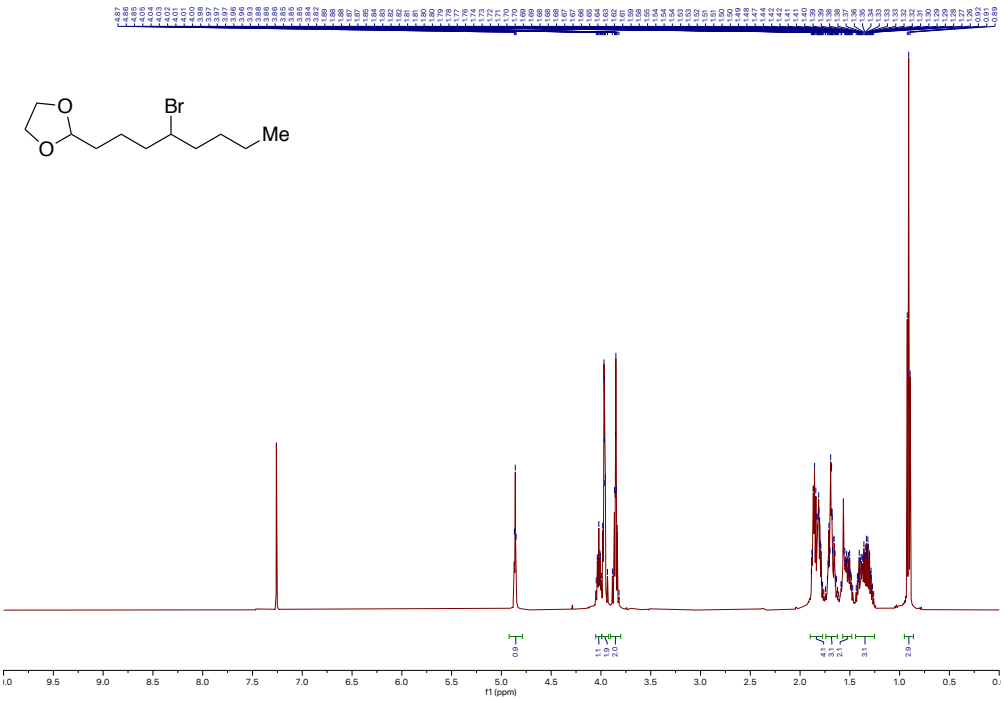

^{1}H spectrum (400 MHz, $CDCl_3$) of **19x**

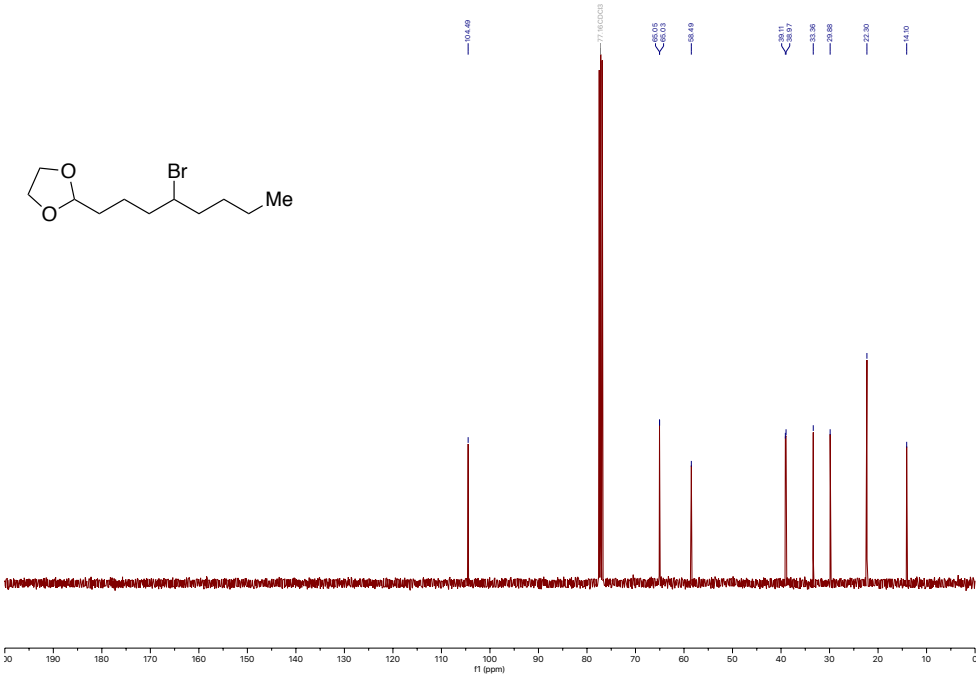

^{13}C spectrum (101 MHz, $CDCl_3$) of **19x**

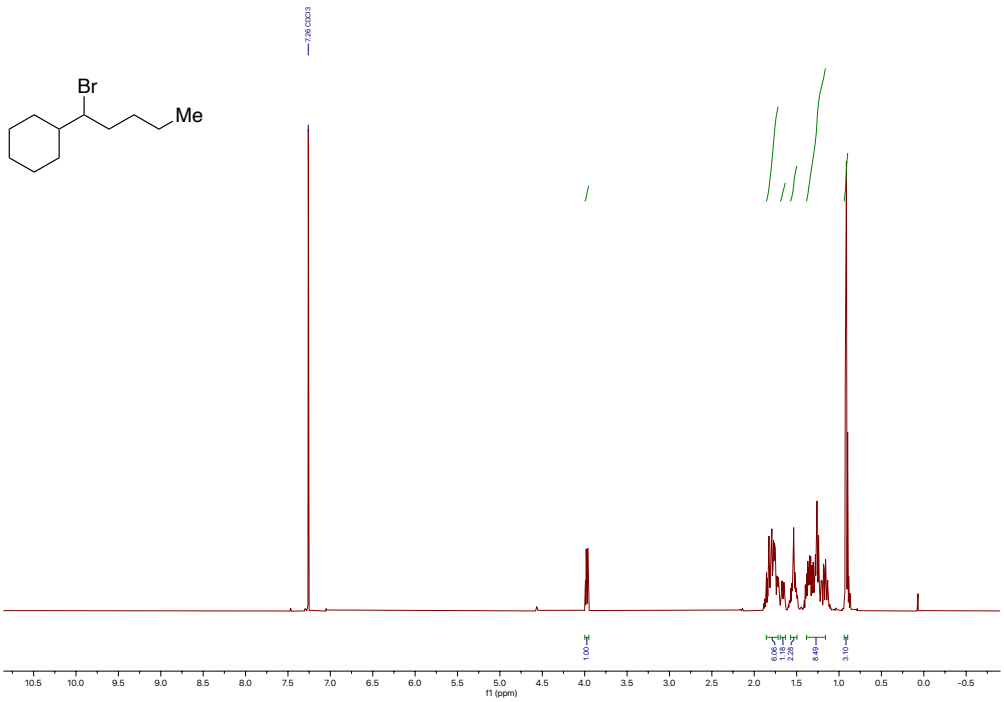

^{1}H spectrum (500 MHz, $CDCl_3$) of **19ac**

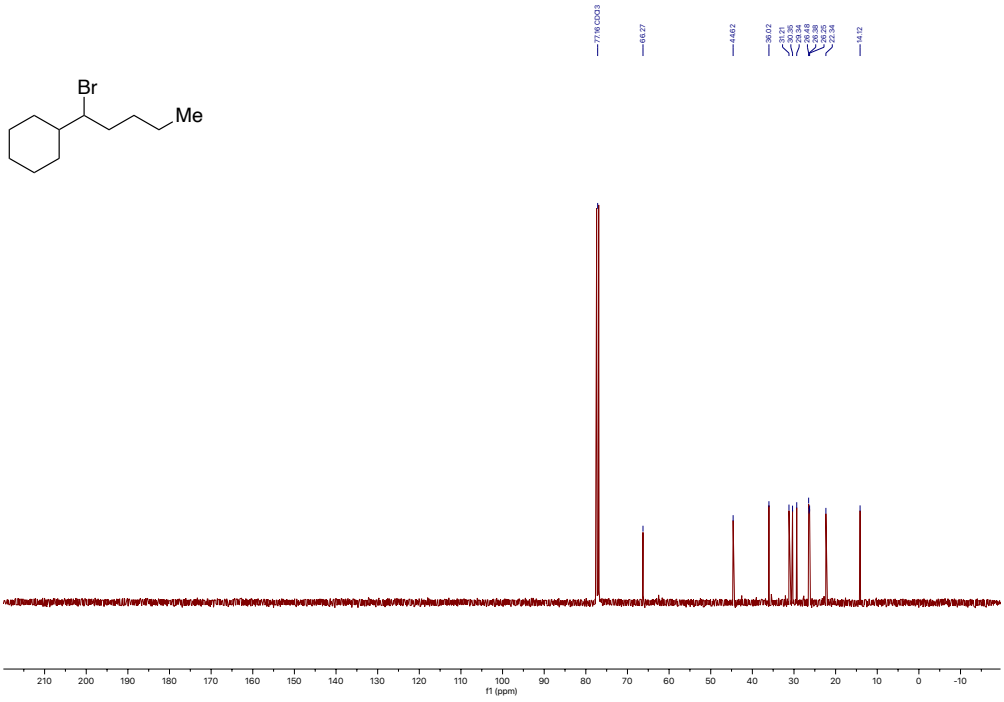

^{13}C spectrum (126 MHz, $CDCl_3$) of **19ac**

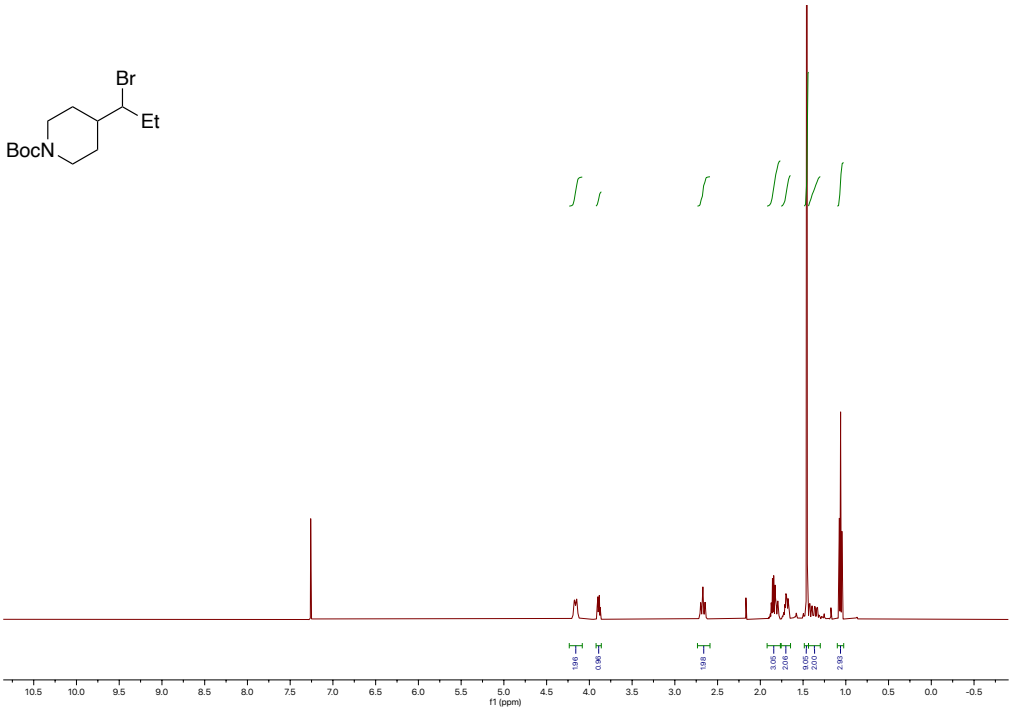

^{1}H spectrum (500 MHz, $CDCl_3$) of **19ae**

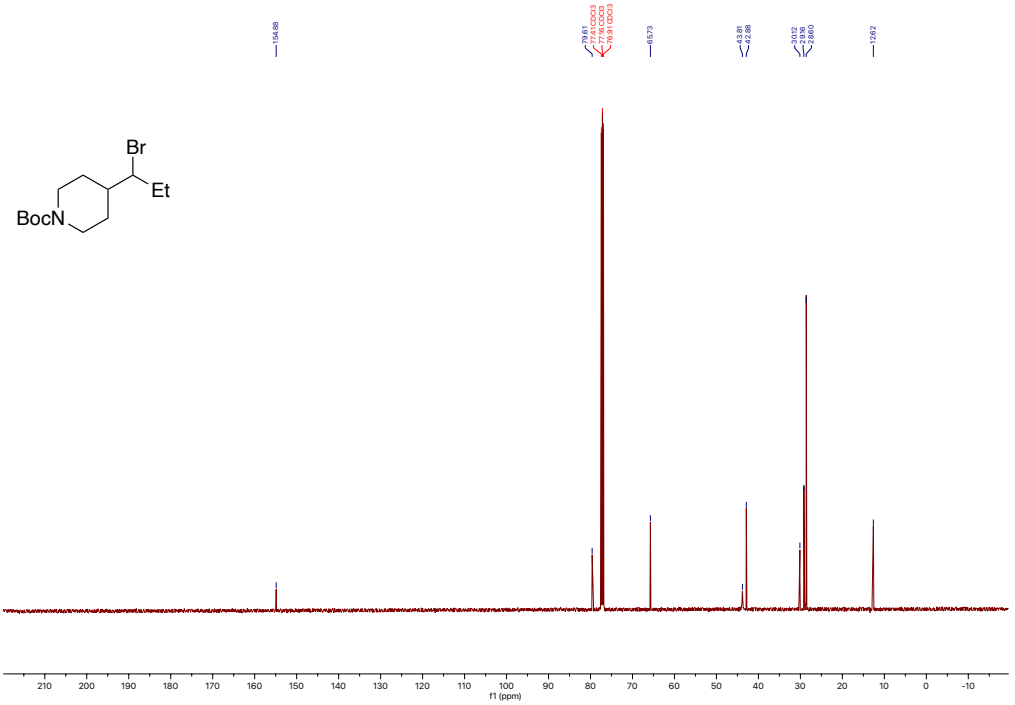

^{13}C spectrum (126 MHz, $CDCl_3$) of **19ae**

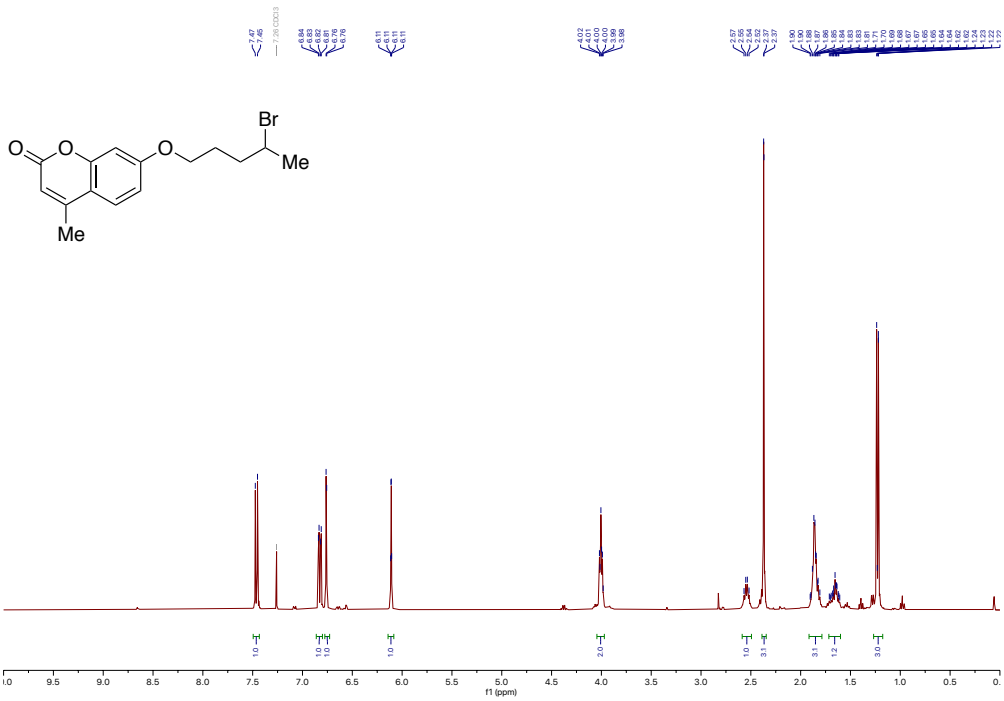

^{1}H spectrum (400 MHz, $CDCl_3$) of **19ah**

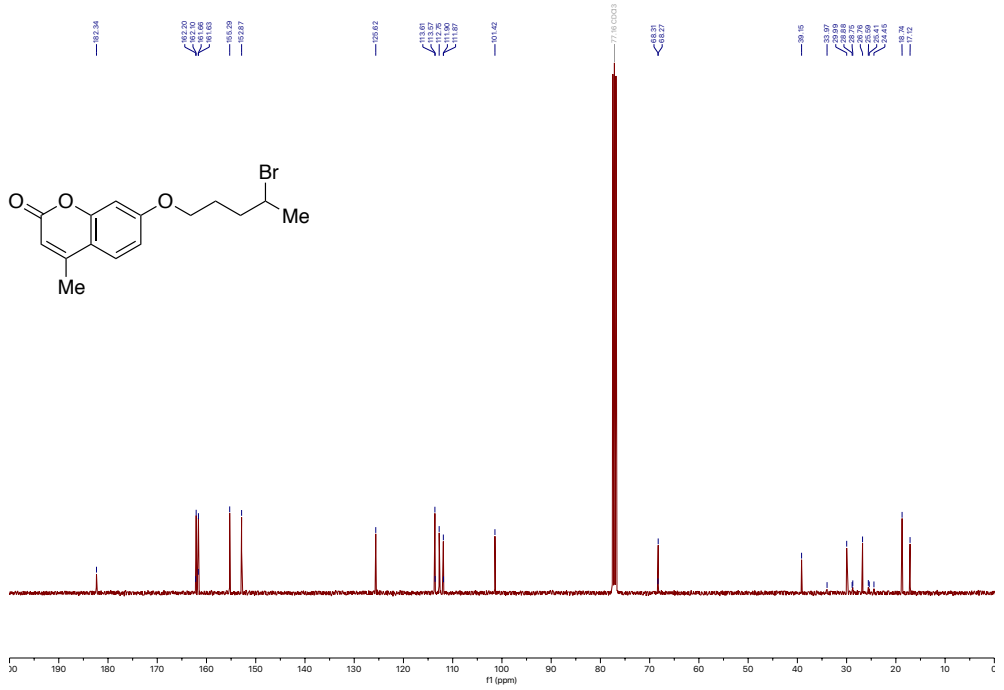

^{13}C spectrum (126 MHz, $CDCl_3$) of **19ah**

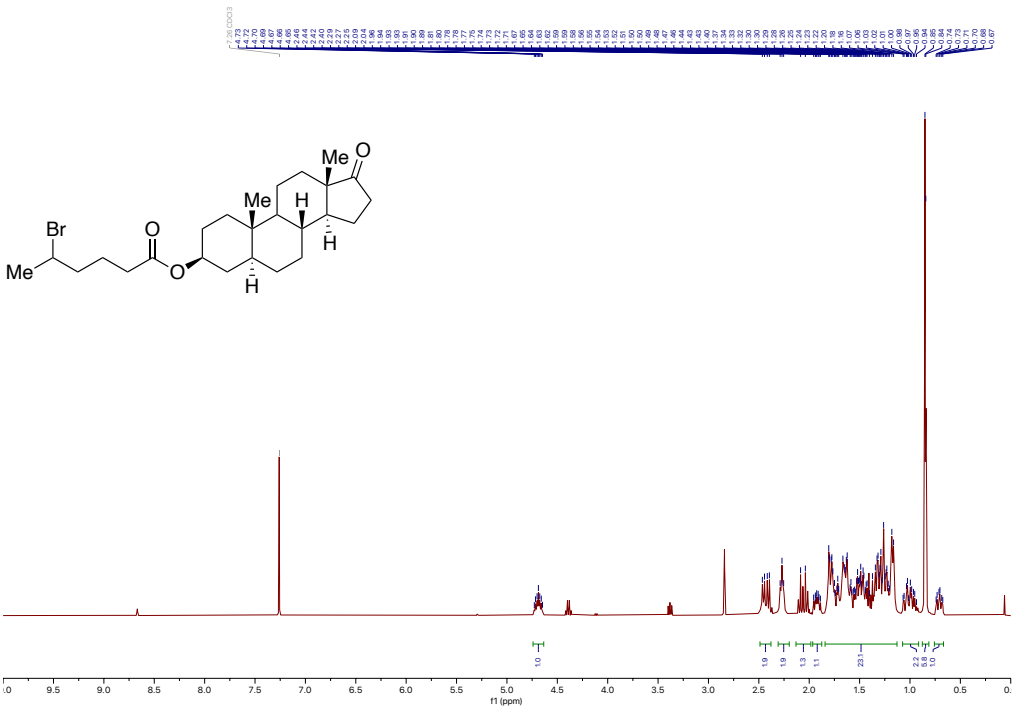

^{1}H spectrum (400 MHz, $CDCl_3$) of **19ai**

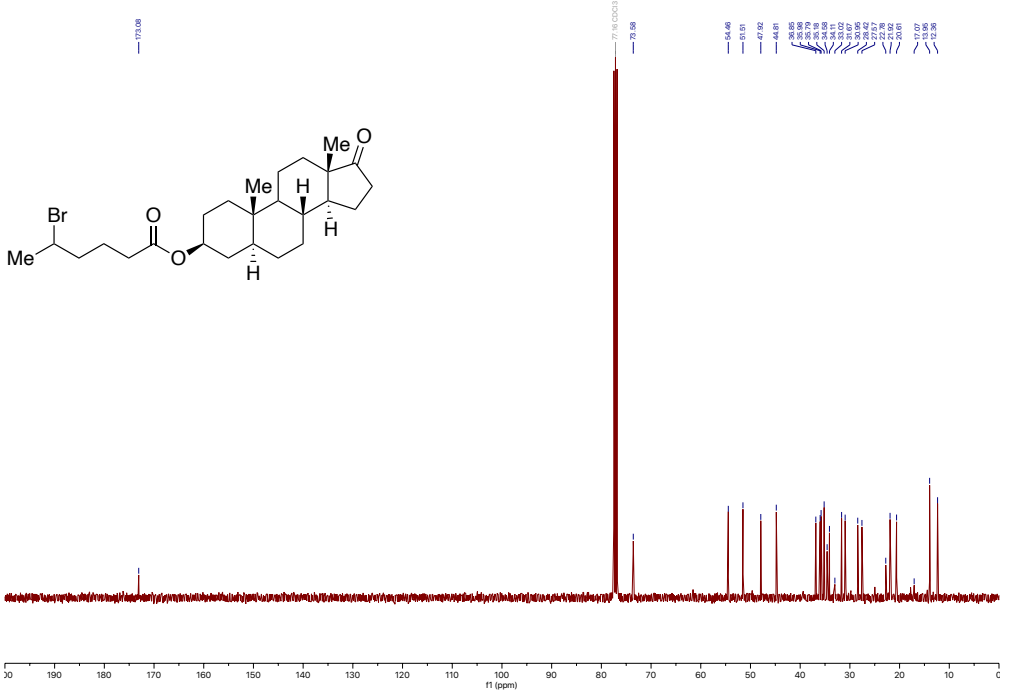

^{13}C spectrum (101 MHz, $CDCl_3$) of **19ai**

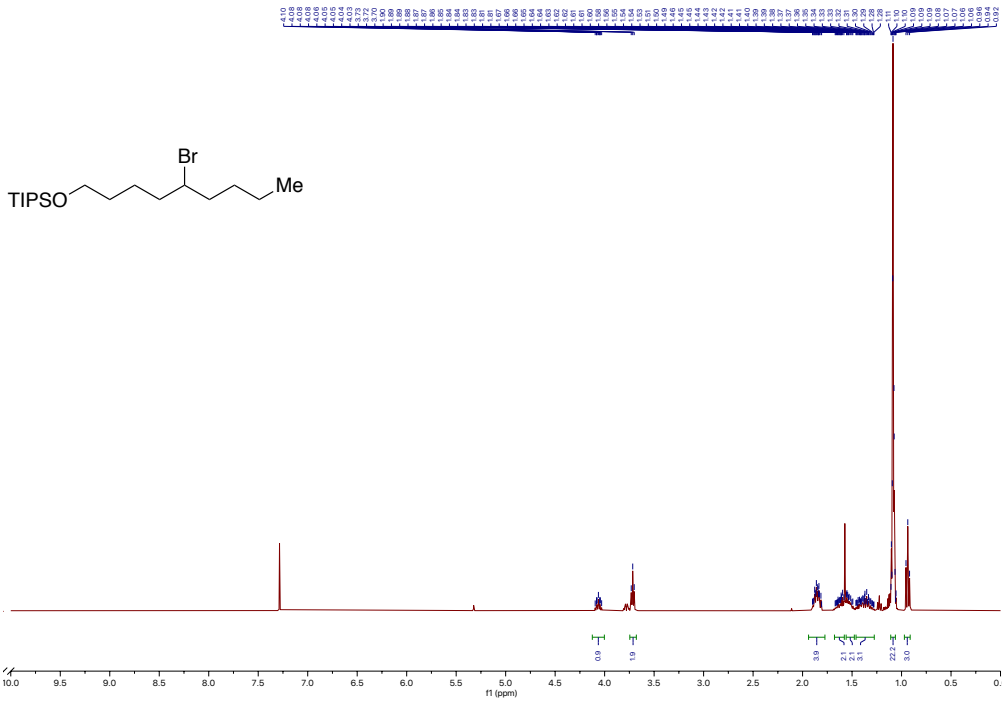

^{1}H spectrum (400 MHz, $CDCl_3$) of **19aj**

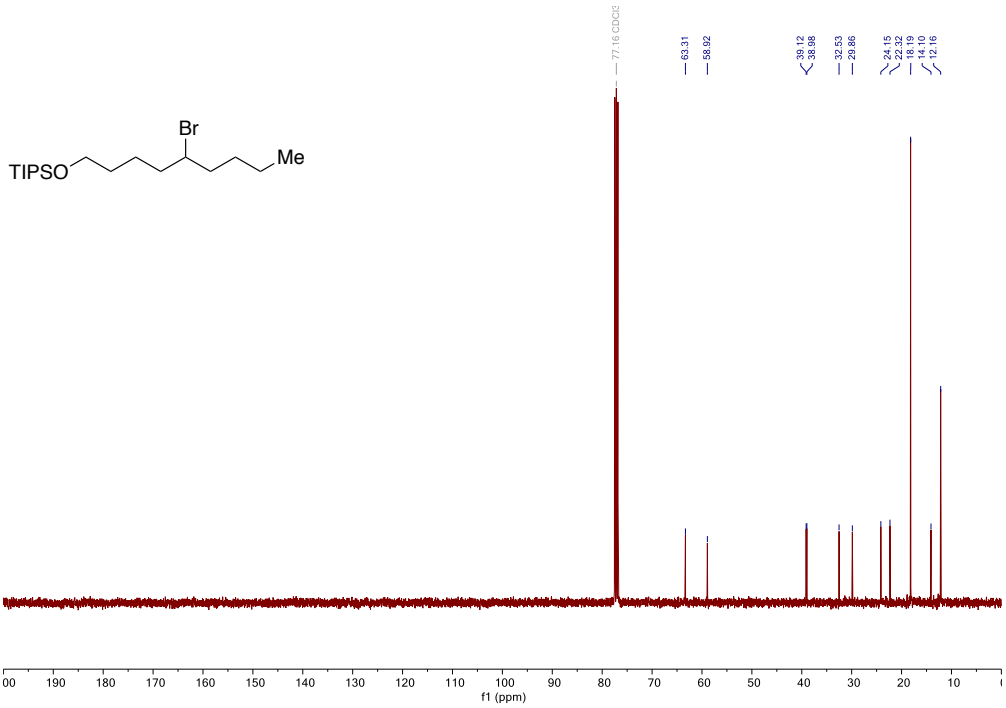

^{13}C spectrum (101 MHz, $CDCl_3$) of **19aj**

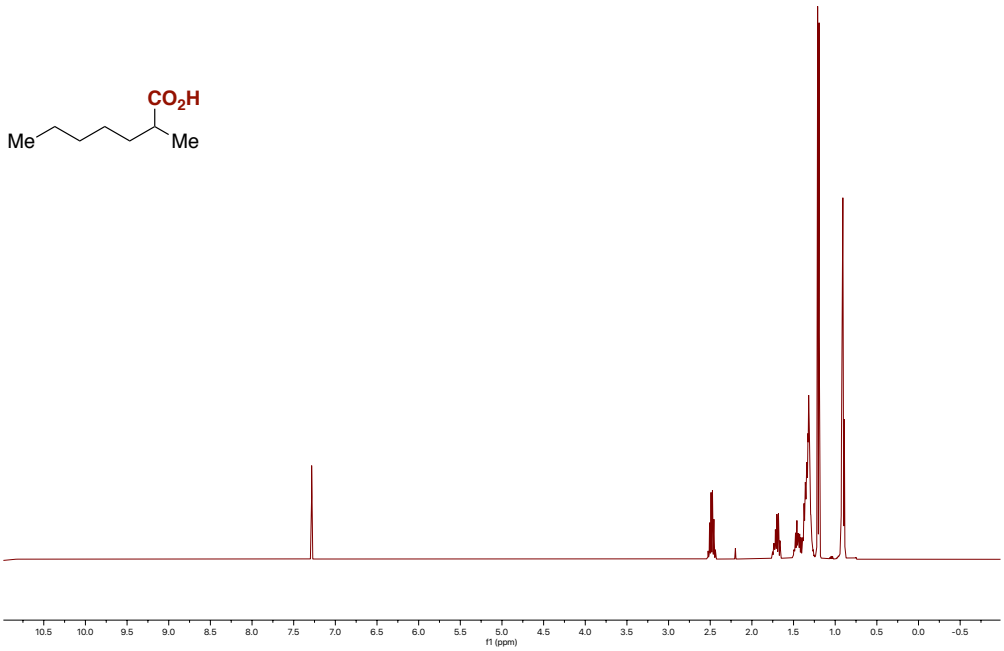

^{1}H spectrum (400 MHz, $CDCl_3$) of **20a**

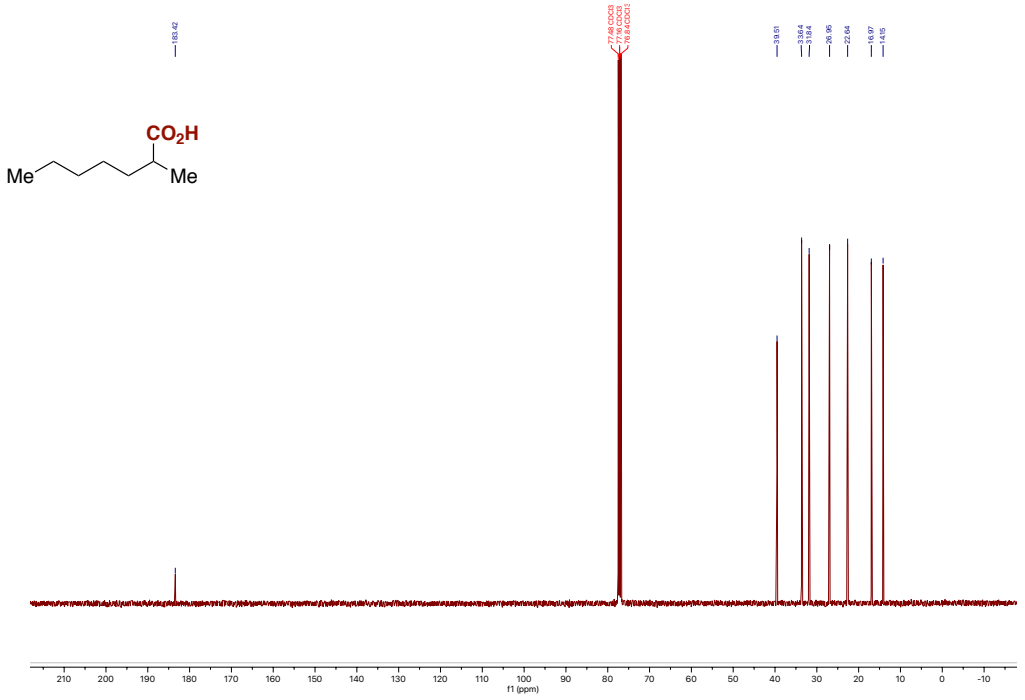

^{13}C spectrum (101 MHz, $CDCl_3$) of **20a**

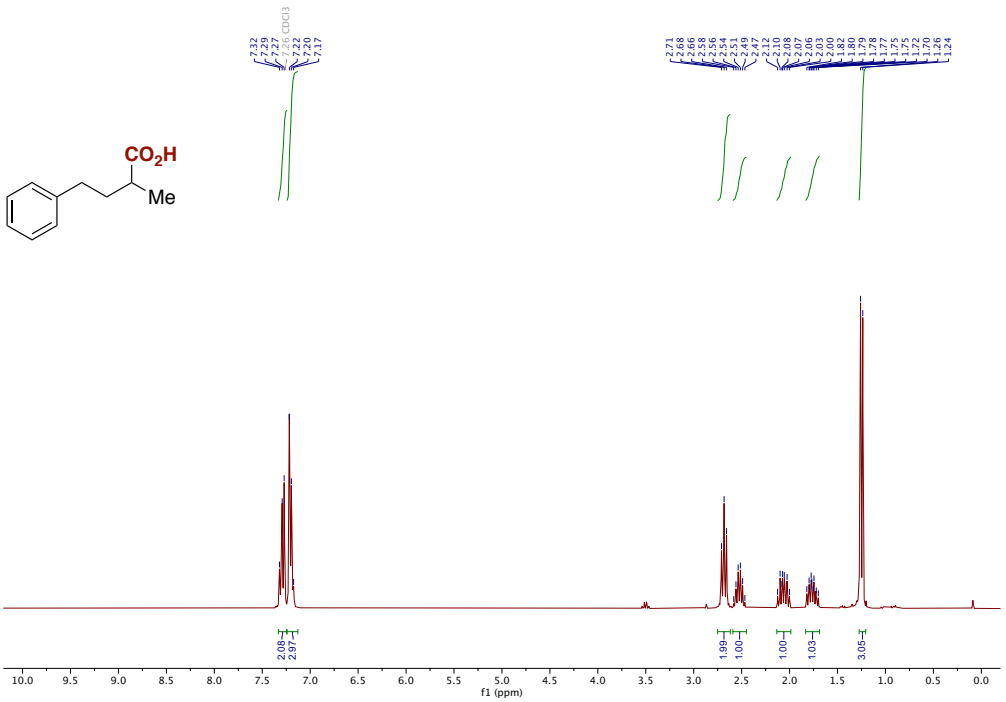

^{1}H spectrum (300 MHz, $CDCl_3$) of **20b**

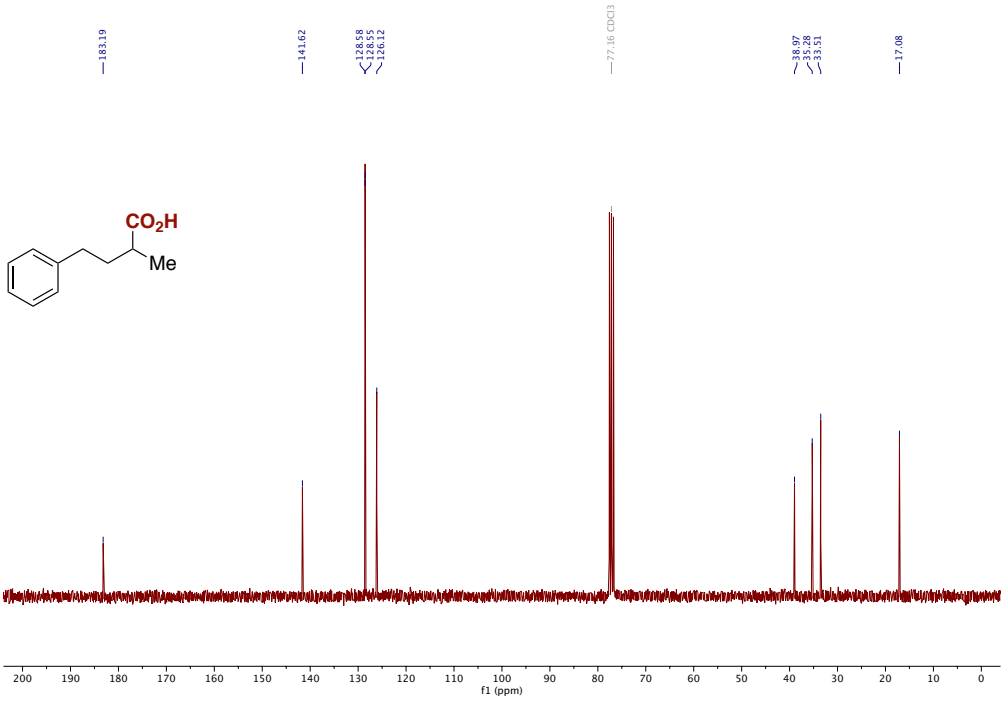

^{13}C spectrum (75 MHz, $CDCl_3$) of **20b**

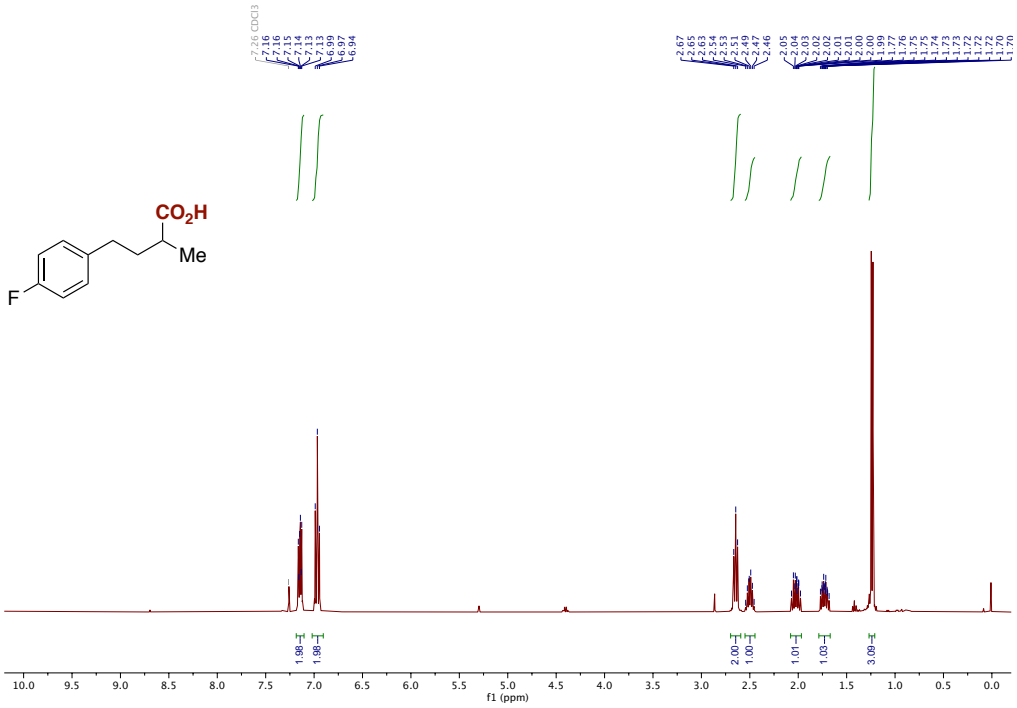

^{1}H spectrum (400 MHz, $CDCl_3$) of **20c**

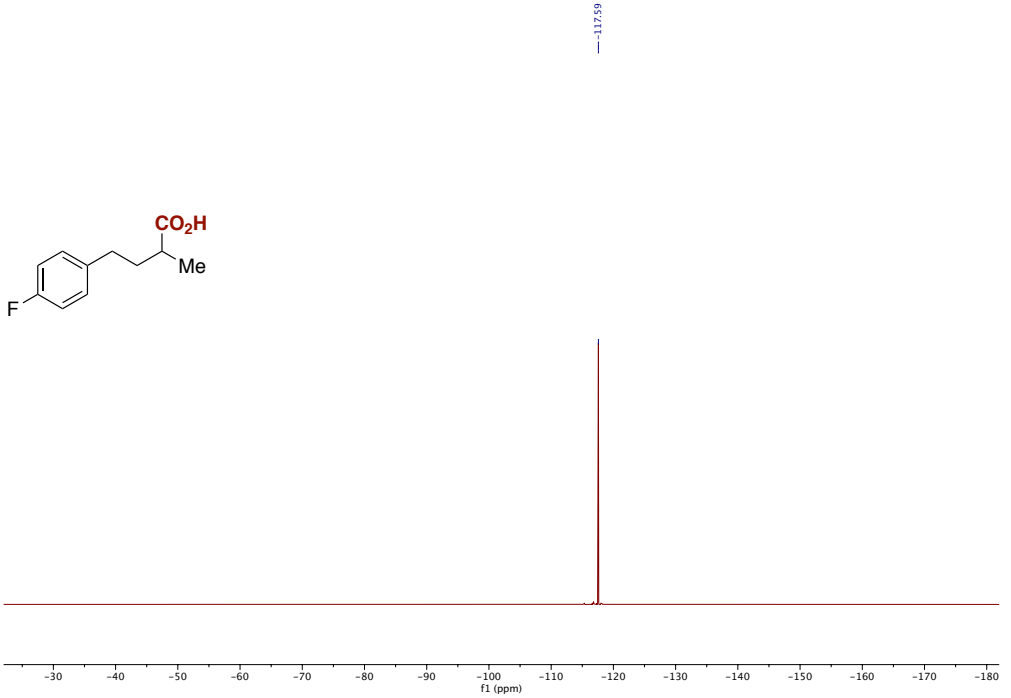

^{19}F spectrum (376 MHz, $CDCl_3$) of **20c**

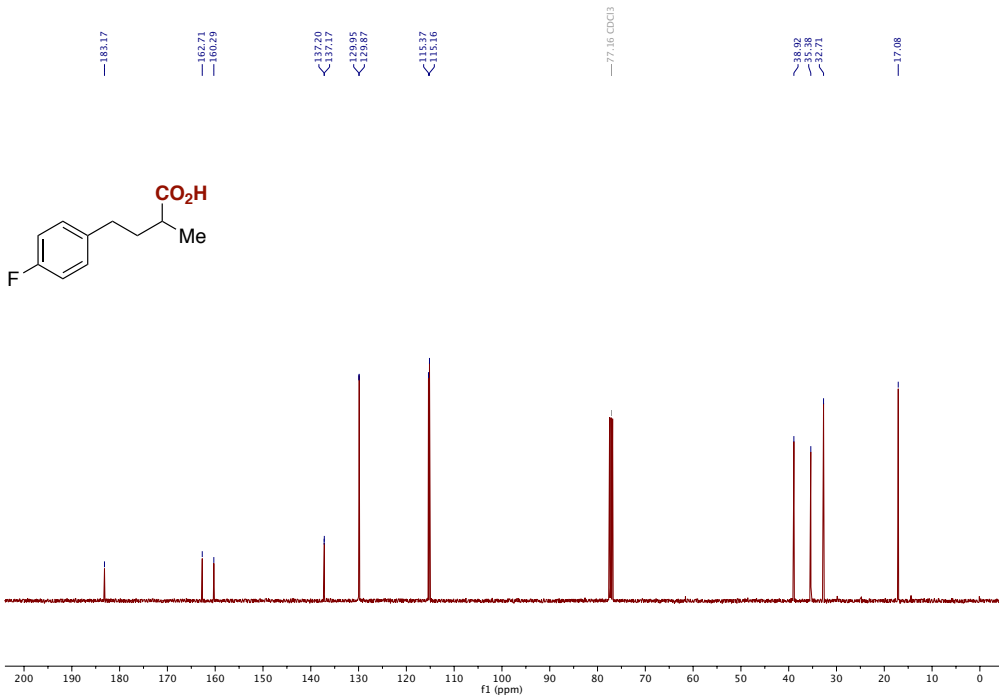

^{13}C spectrum (101 MHz, $CDCl_3$) of **20c**

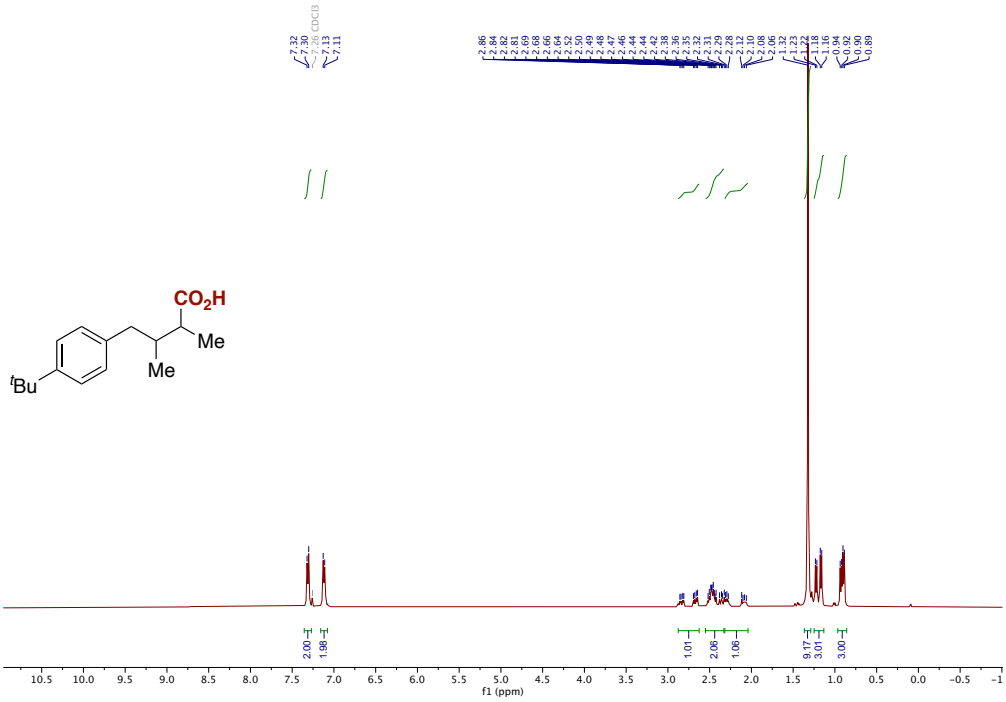

^{1}H spectrum (400 MHz, $CDCl_3$) of **20d**

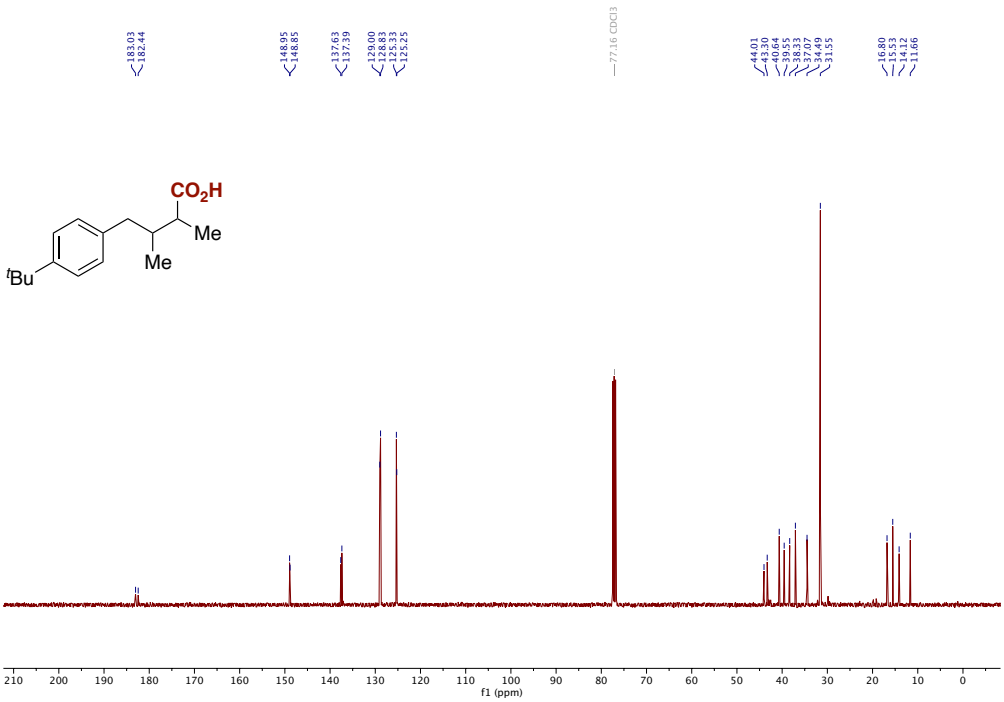

^{13}C spectrum (101 MHz, $CDCl_3$) of **20d**

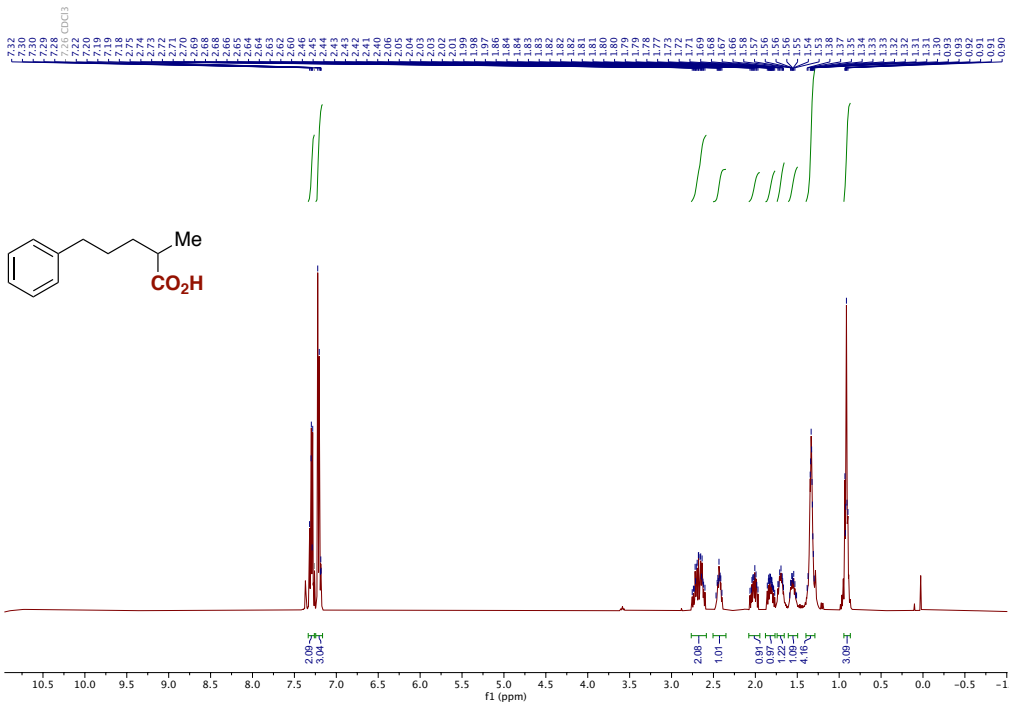

^{1}H spectrum (400 MHz, $CDCl_3$) of **20e**

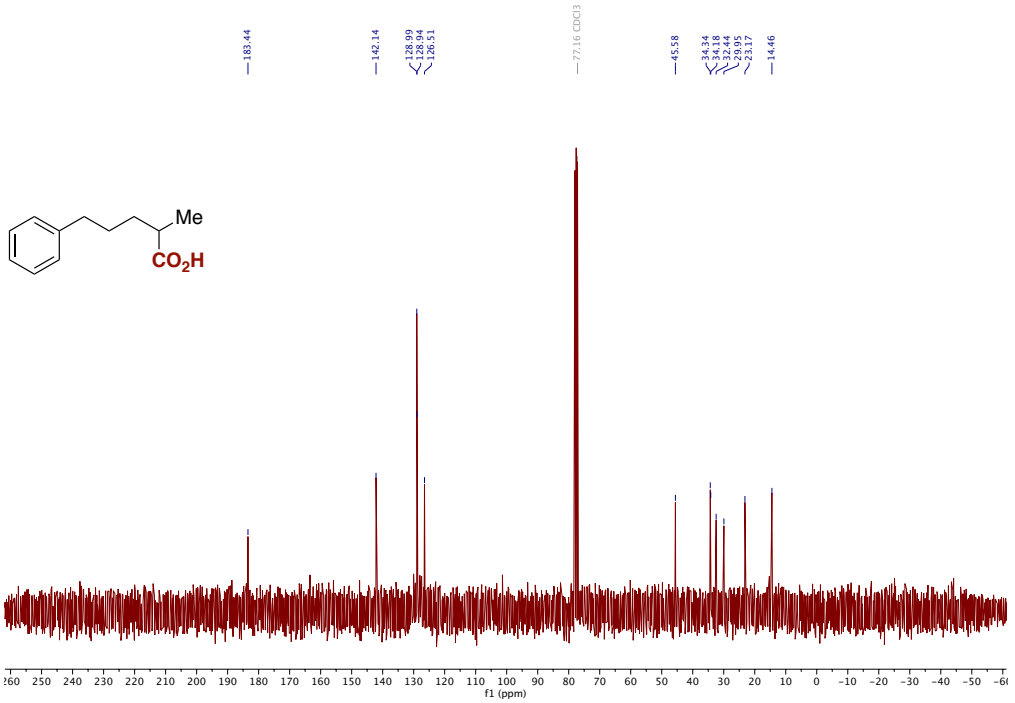

^{13}C spectrum (101 MHz, $CDCl_3$) of **20e**

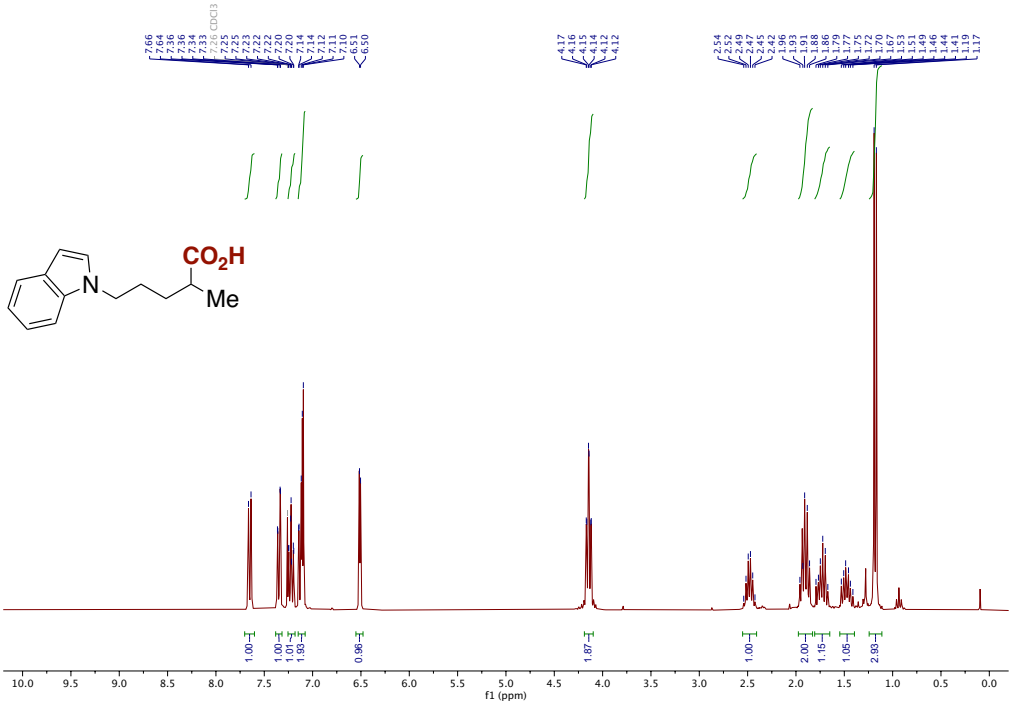

^{1}H spectrum (300 MHz, $CDCl_3$) of **20f**

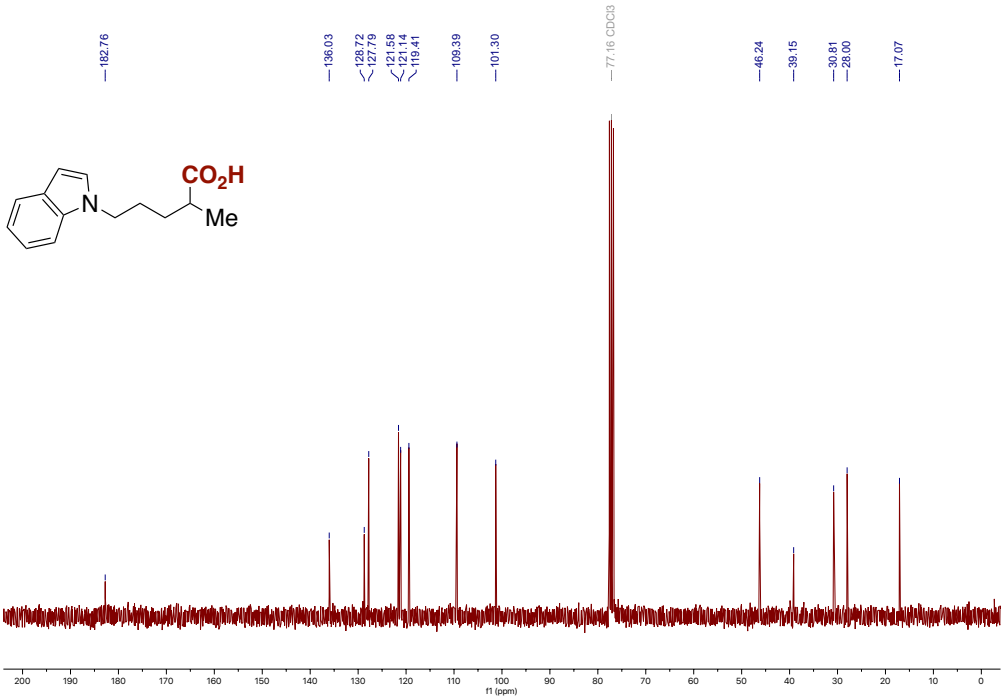

^{13}C spectrum (75 MHz, $CDCl_3$) of **20f**

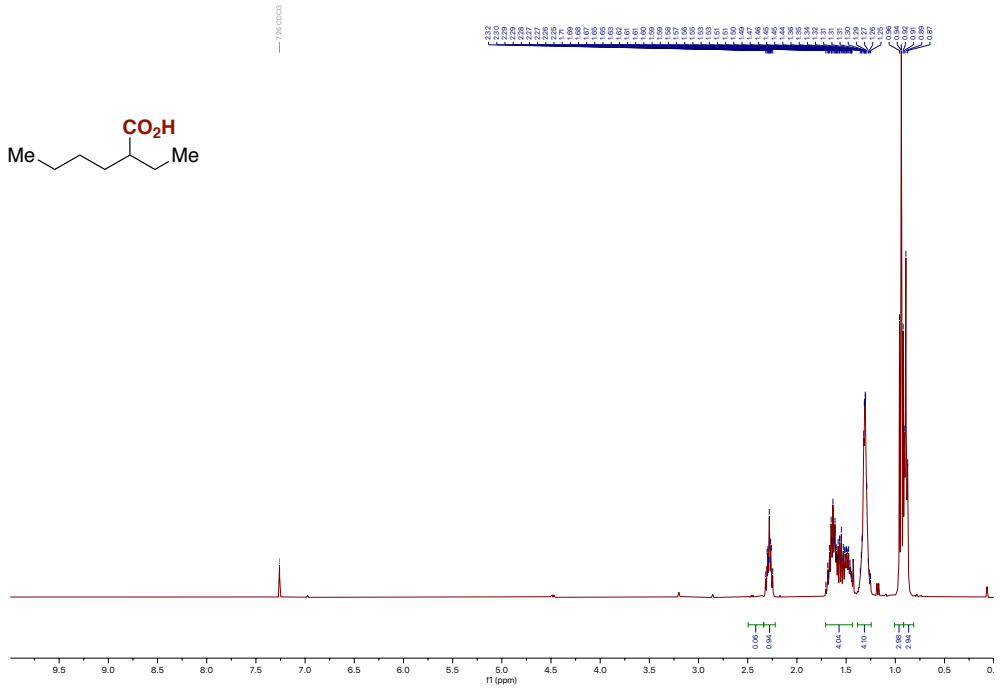

^{1}H spectrum (400 MHz, $CDCl_3$) of **20g**

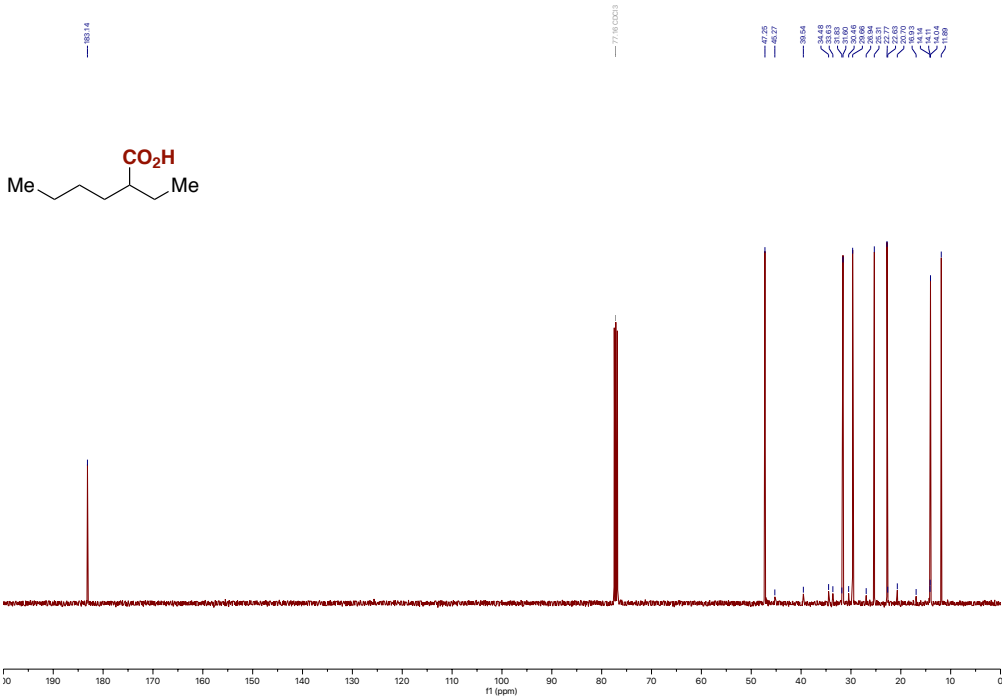

^{13}C spectrum (101 MHz, $CDCl_3$) of **20g**

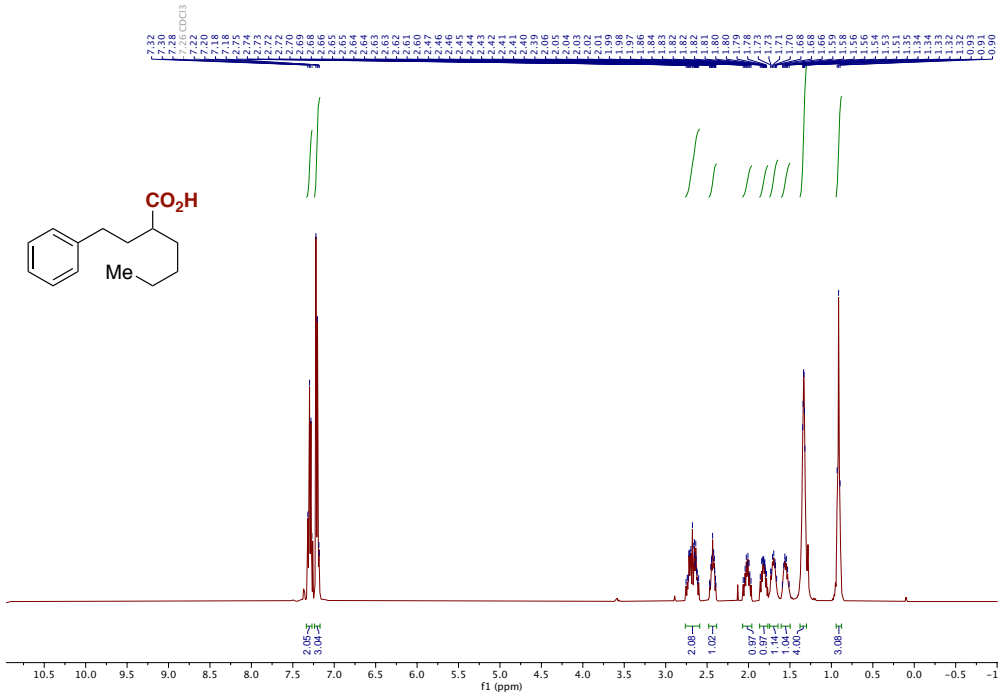

^{1}H spectrum (400 MHz, $CDCl_3$) of **20h**

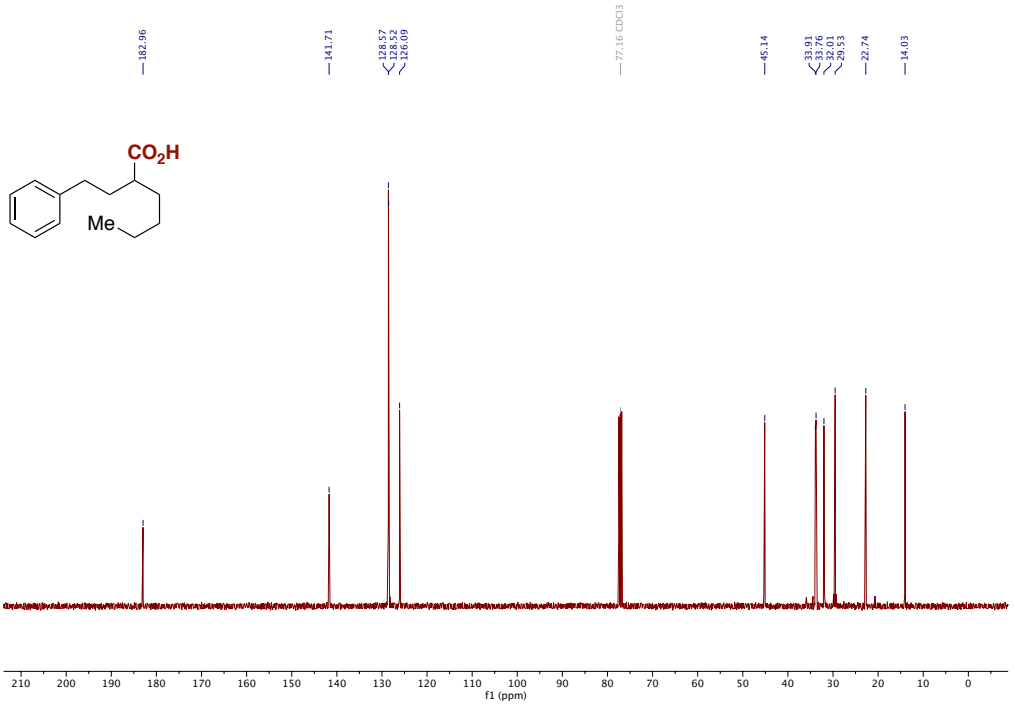

^{13}C spectrum (101 MHz, $CDCl_3$) of **20h**

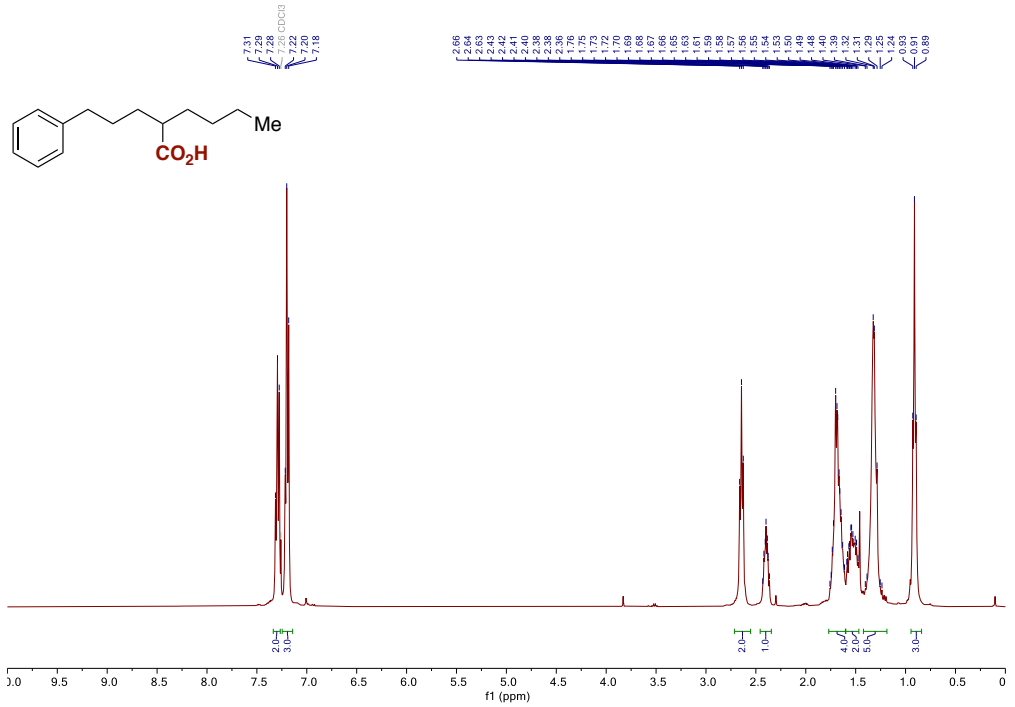

^{1}H spectrum (400 MHz, $CDCl_3$) of **20i**

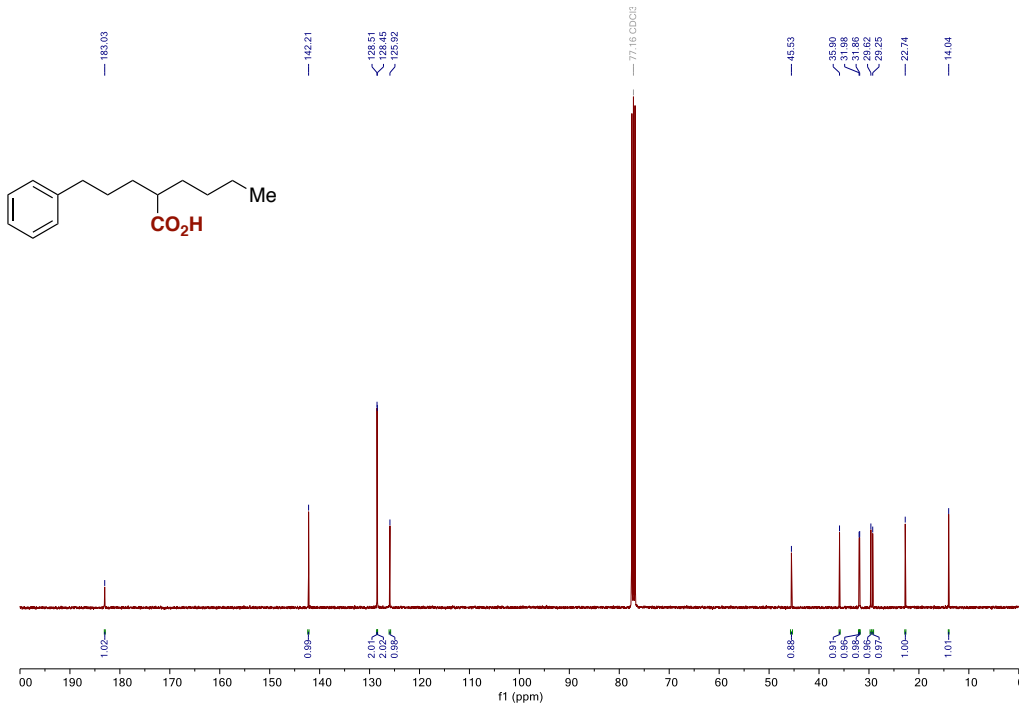

^{13}C spectrum (101 MHz, $CDCl_3$) of **20i**

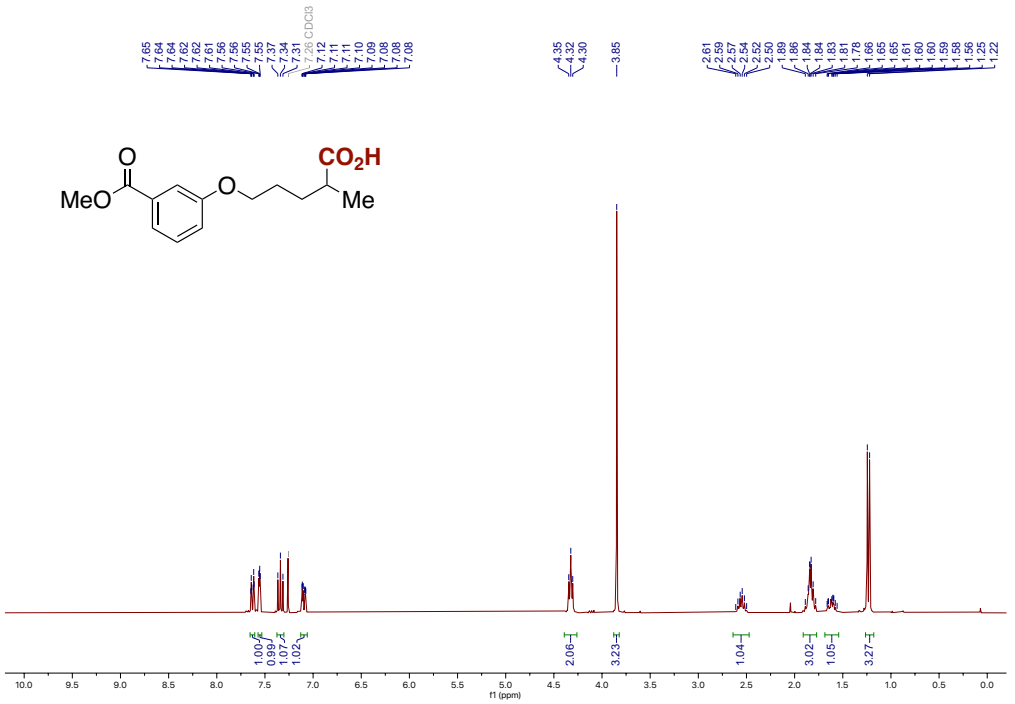

^{1}H spectrum (300 MHz, $CDCl_3$) of **20j**

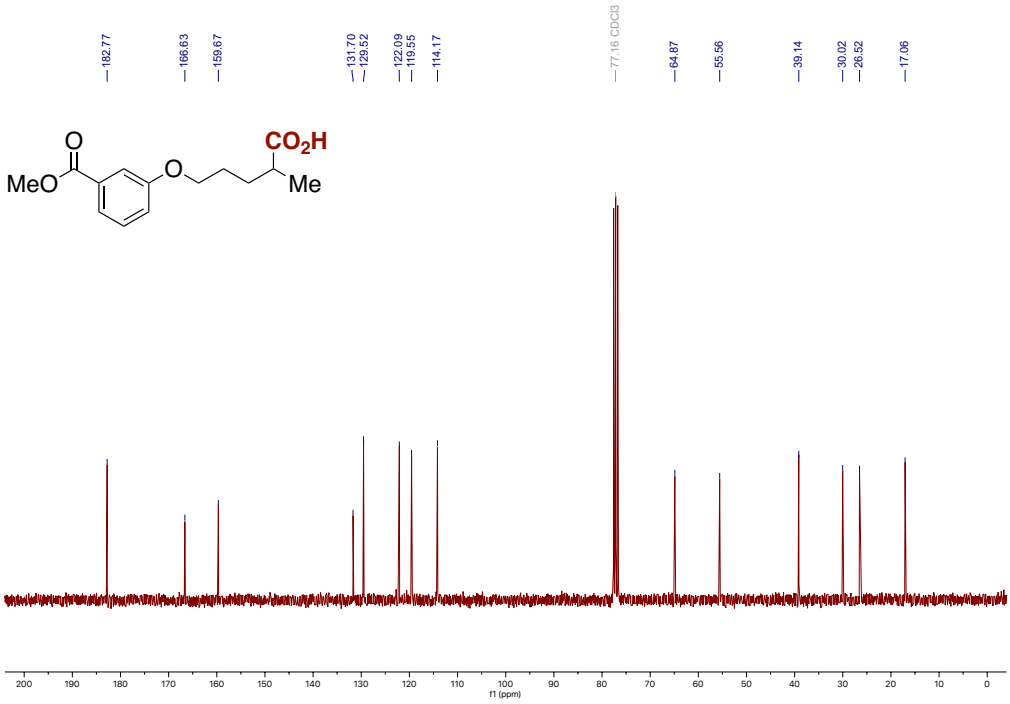

^{13}C spectrum (75 MHz, $CDCl_3$) of **20j**

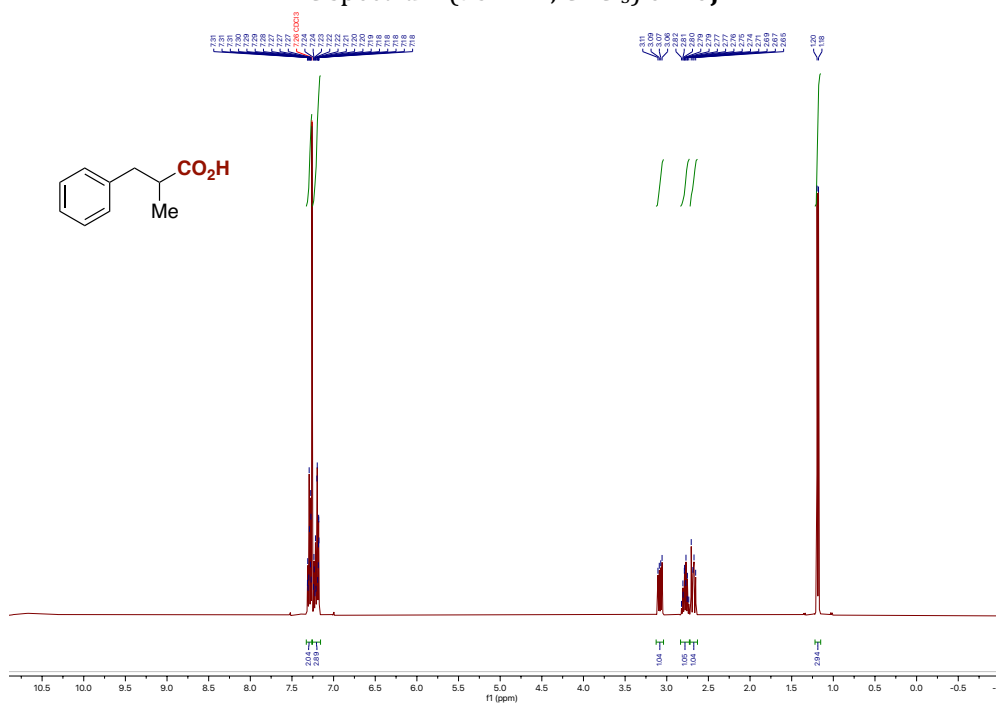

^{1}H spectrum (400 MHz, $CDCl_3$) of **20k**

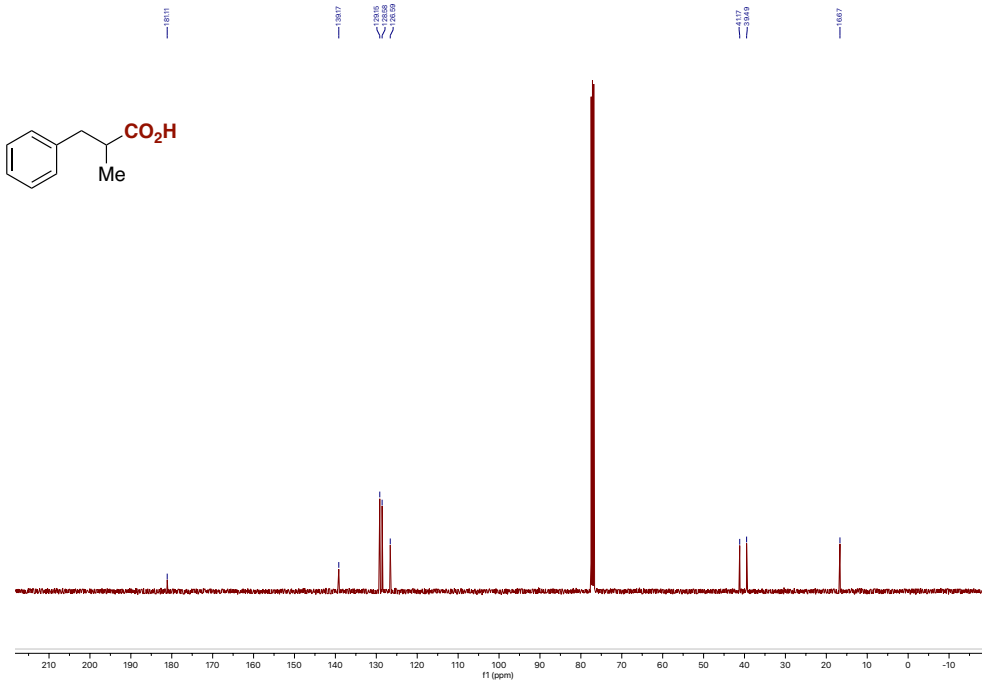

^{13}C spectrum (101 MHz, $CDCl_3$) of **20k**

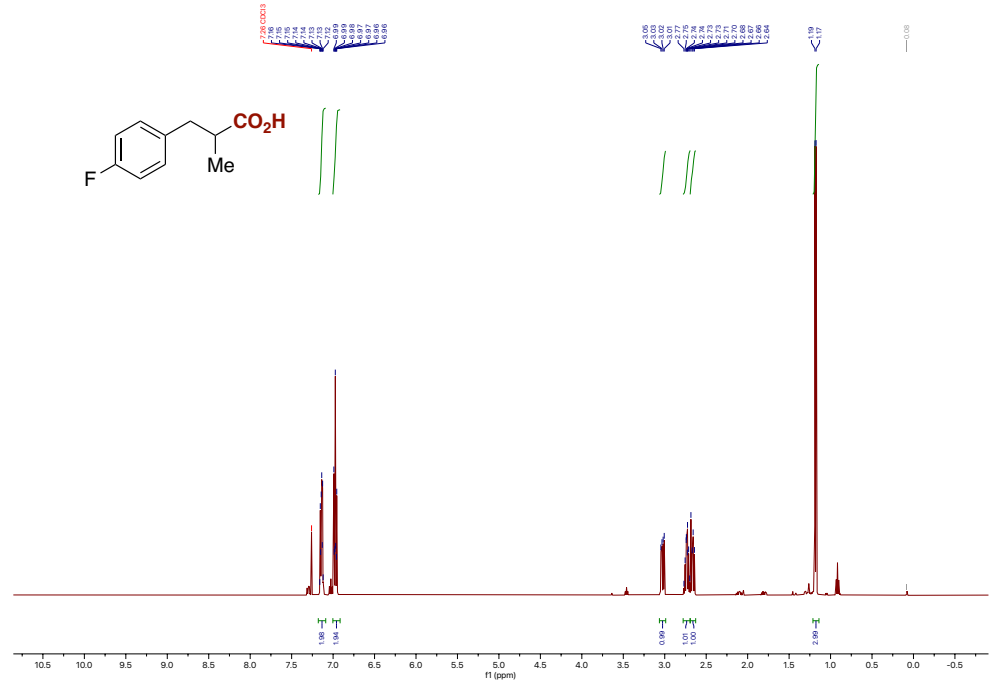

^{1}H spectrum (400 MHz, $CDCl_3$) of **20l**

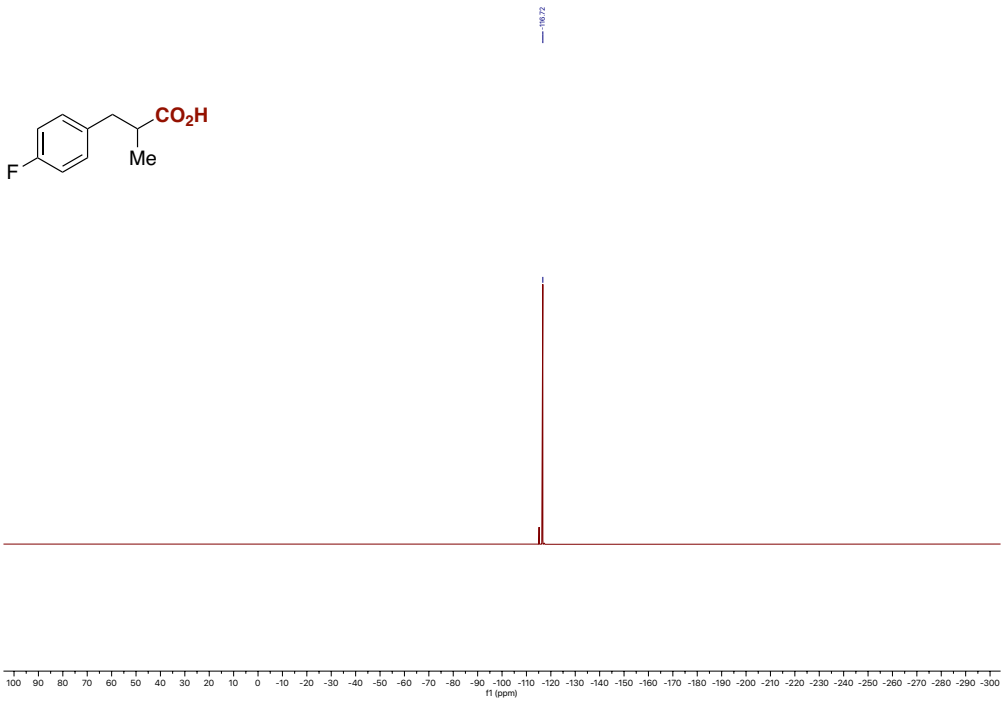

^{19}F spectrum (471 MHz, $CDCl_3$) of **20l**

The background impurity peaks for this compound **20l** correspond to the chain-walking side product, with carboxylation at the benzylic position.

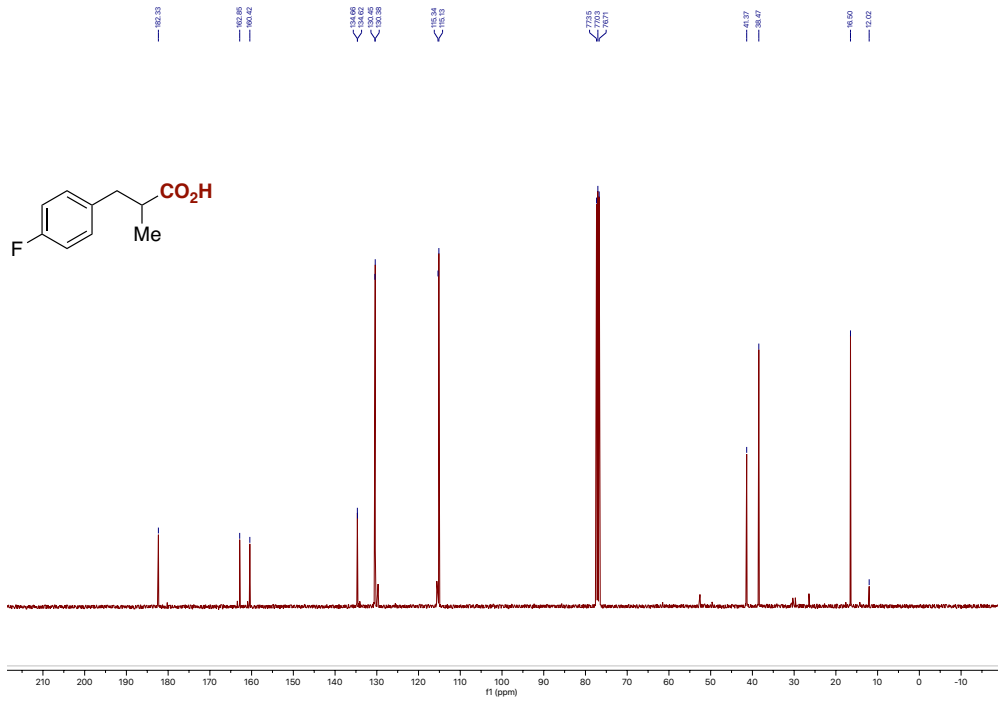

^{13}C spectrum (101 MHz, $CDCl_3$) of **20l**

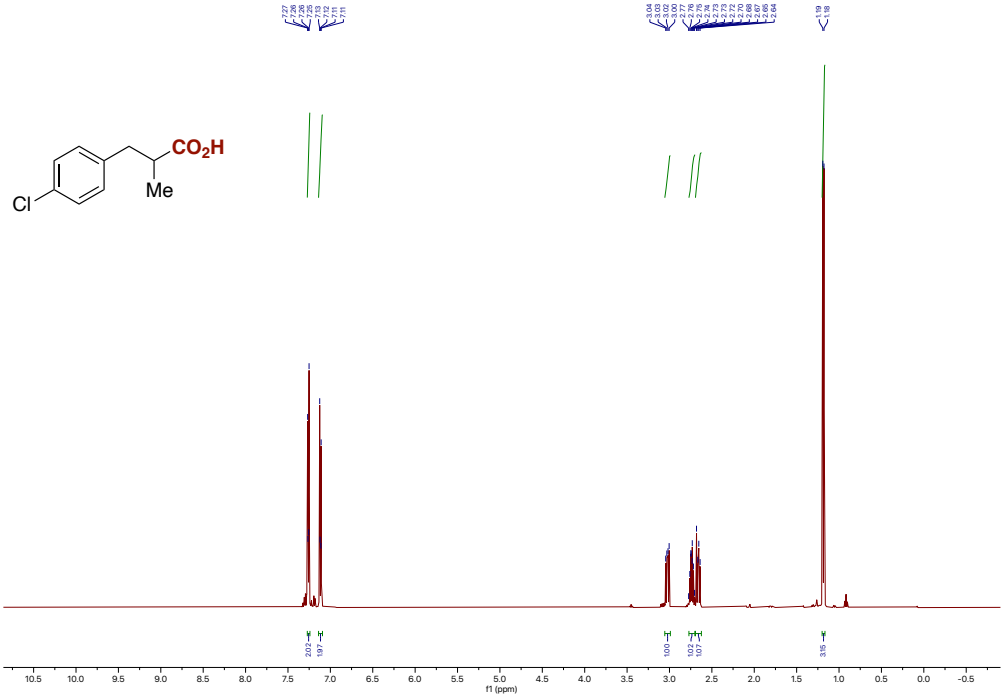

^{1}H spectrum (500 MHz, $CDCl_3$) of **20m**

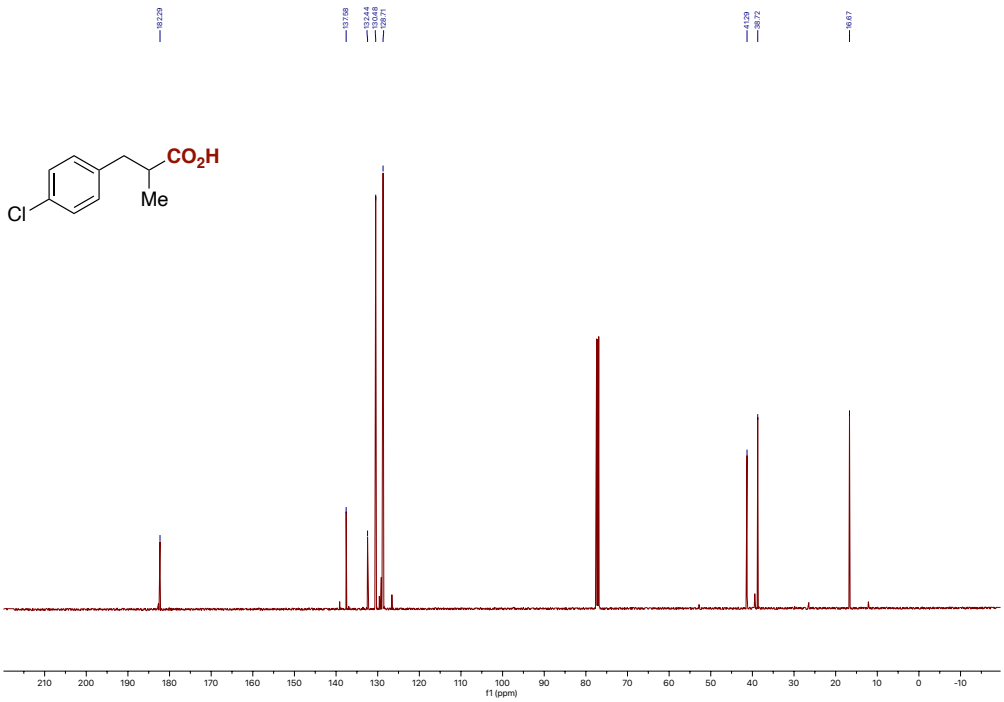

^{13}C spectrum (126 MHz, $CDCl_3$) of **20m**

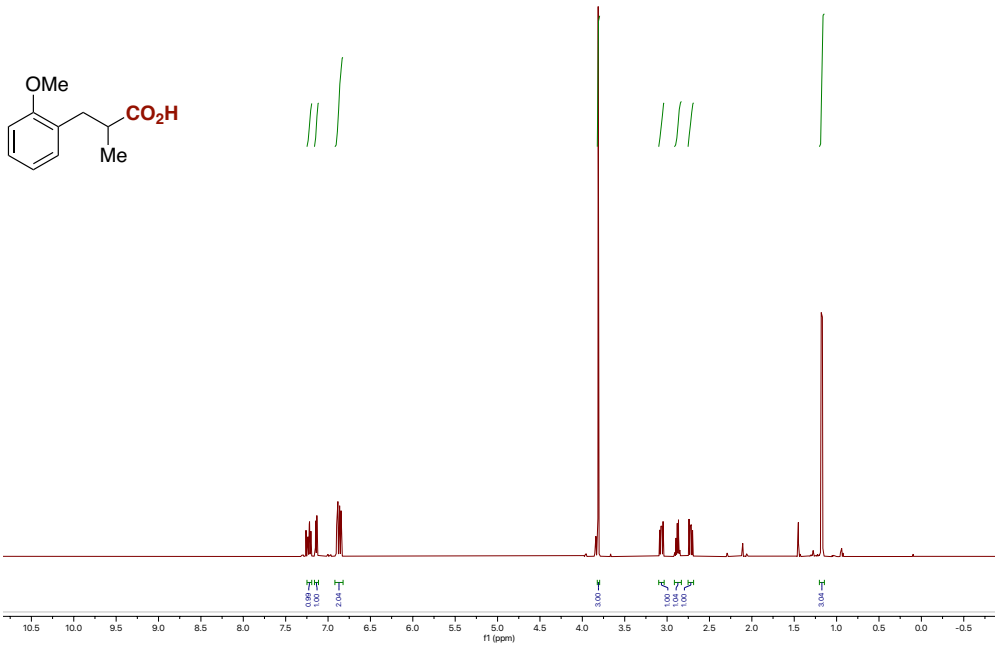

^{1}H spectrum (500 MHz, $CDCl_3$) of **20n**

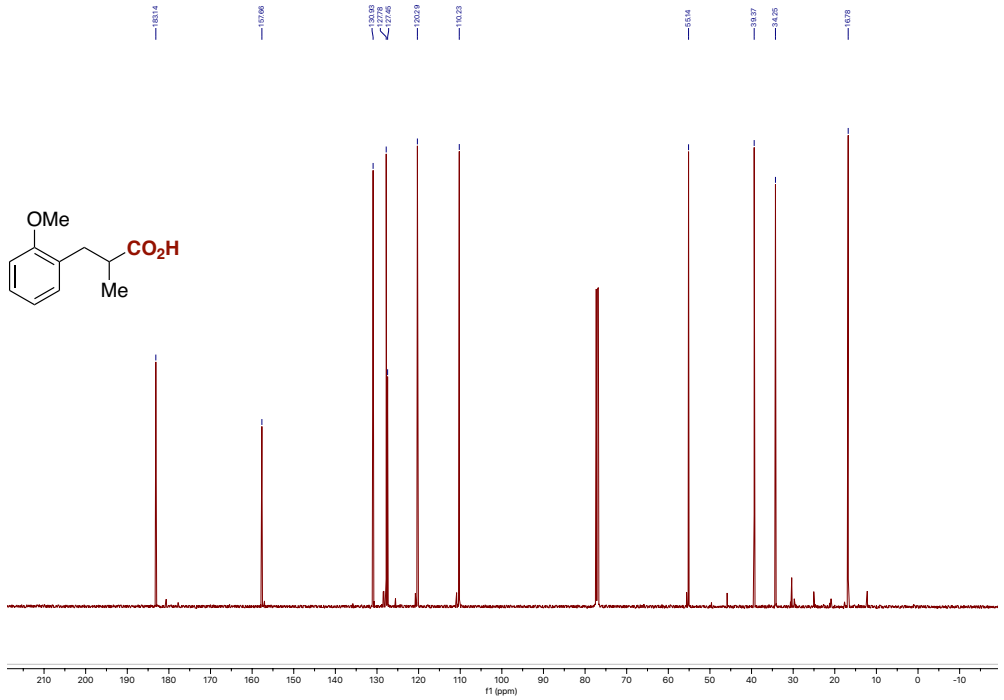

^{13}C spectrum (126 MHz, $CDCl_3$) of **20n**

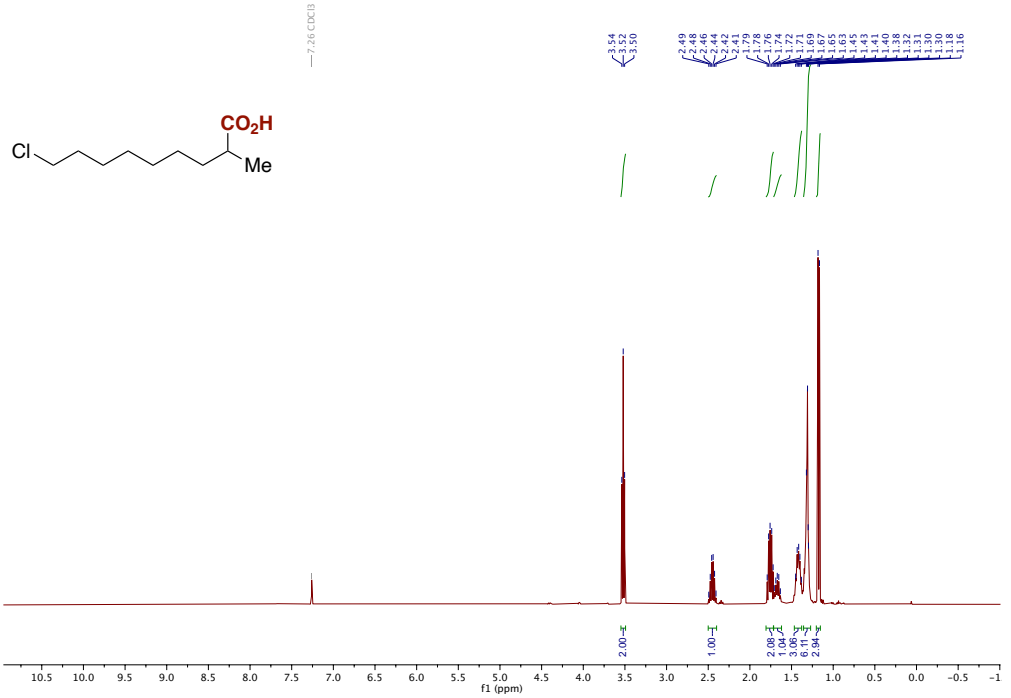

^{1}H spectrum (400 MHz, $CDCl_3$) of **20o**

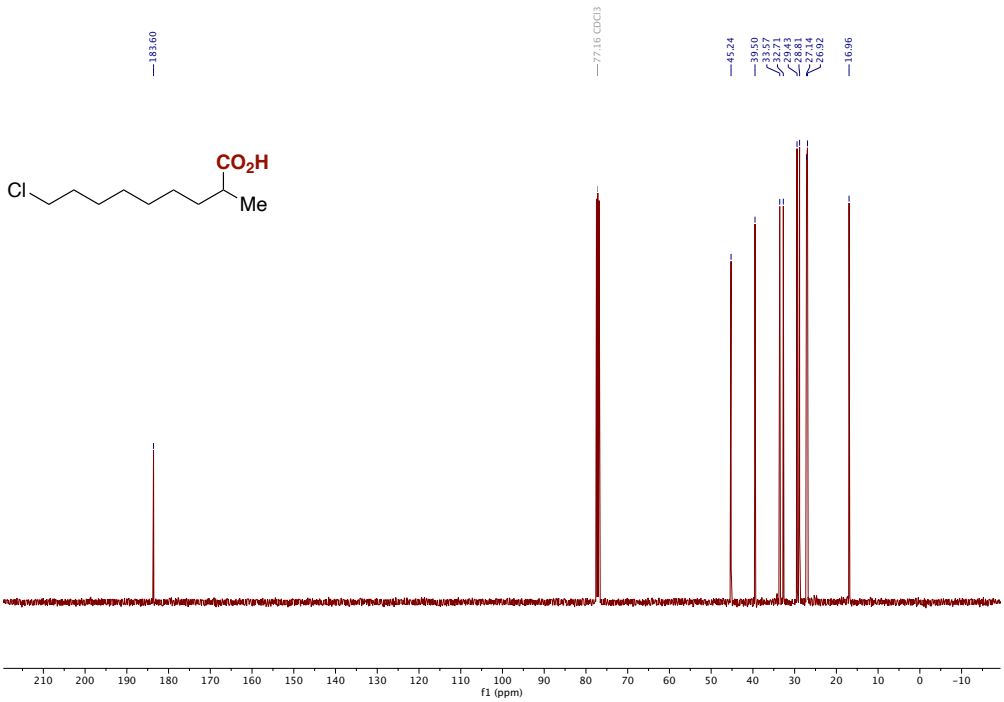

^{13}C spectrum (101 MHz, $CDCl_3$) of **20o**

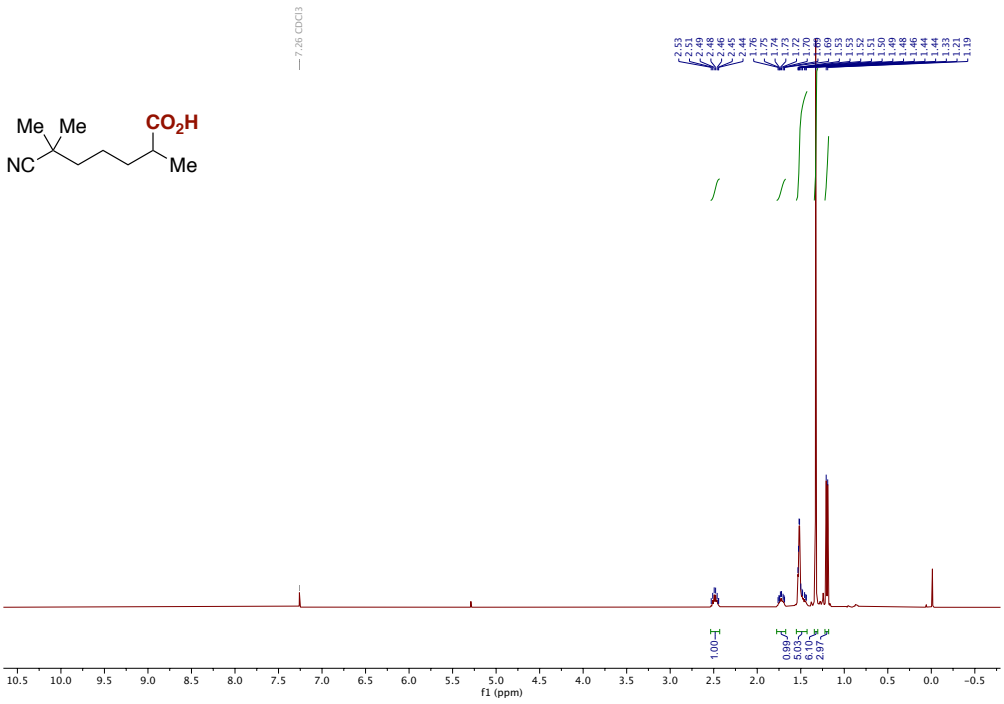

^{1}H spectrum (400 MHz, $CDCl_3$) of **20p**

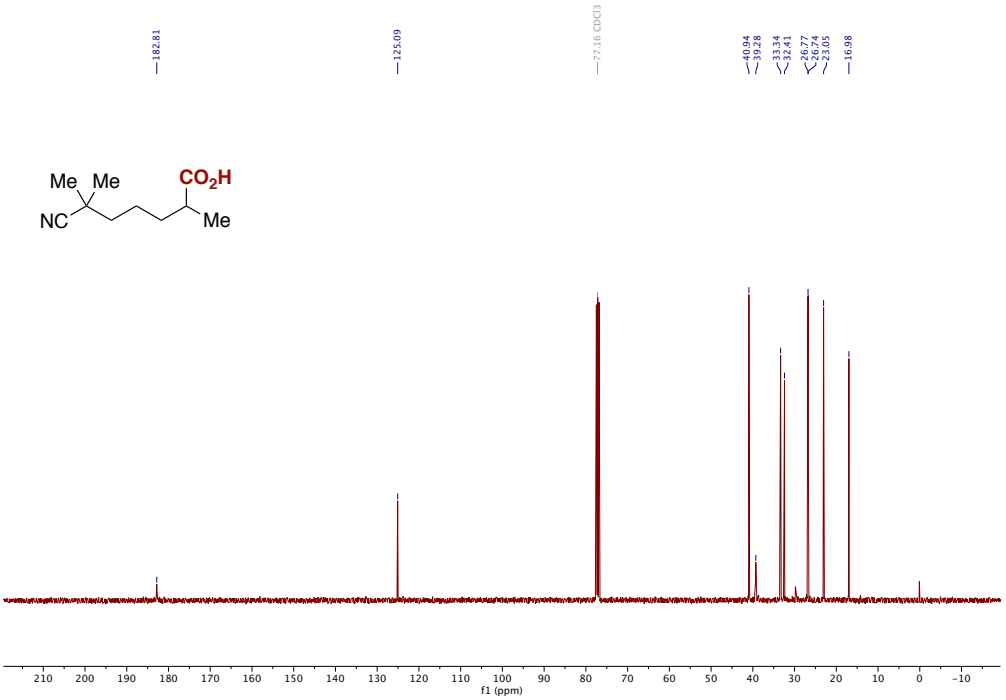

^{13}C spectrum (101 MHz, $CDCl_3$) of **20p**

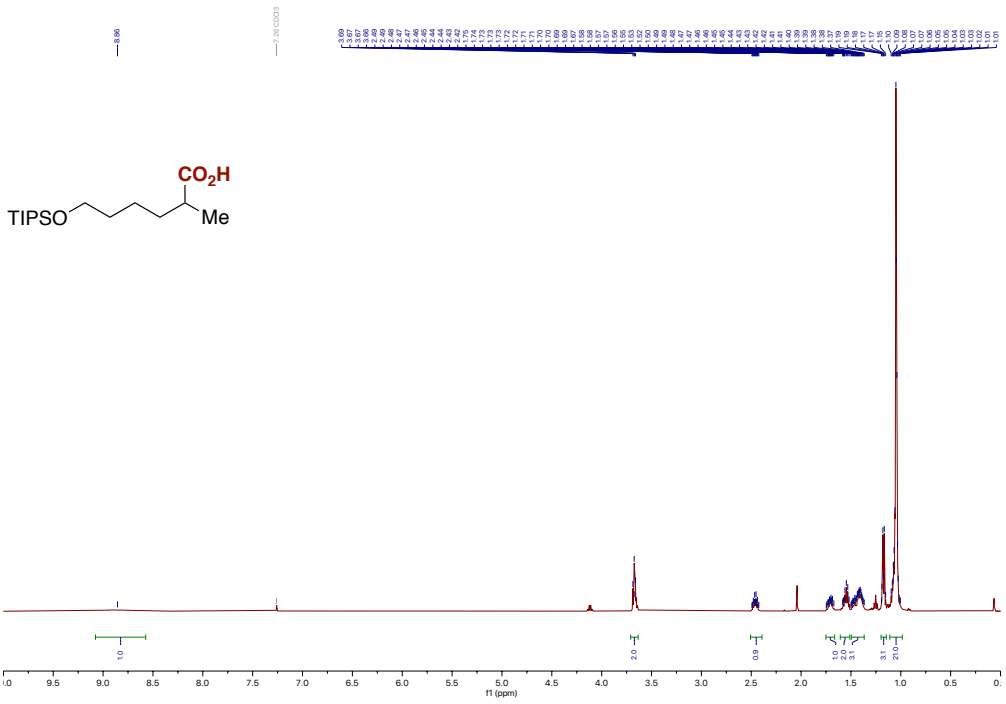

^{1}H spectrum (500 MHz, $CDCl_3$) of **20q**

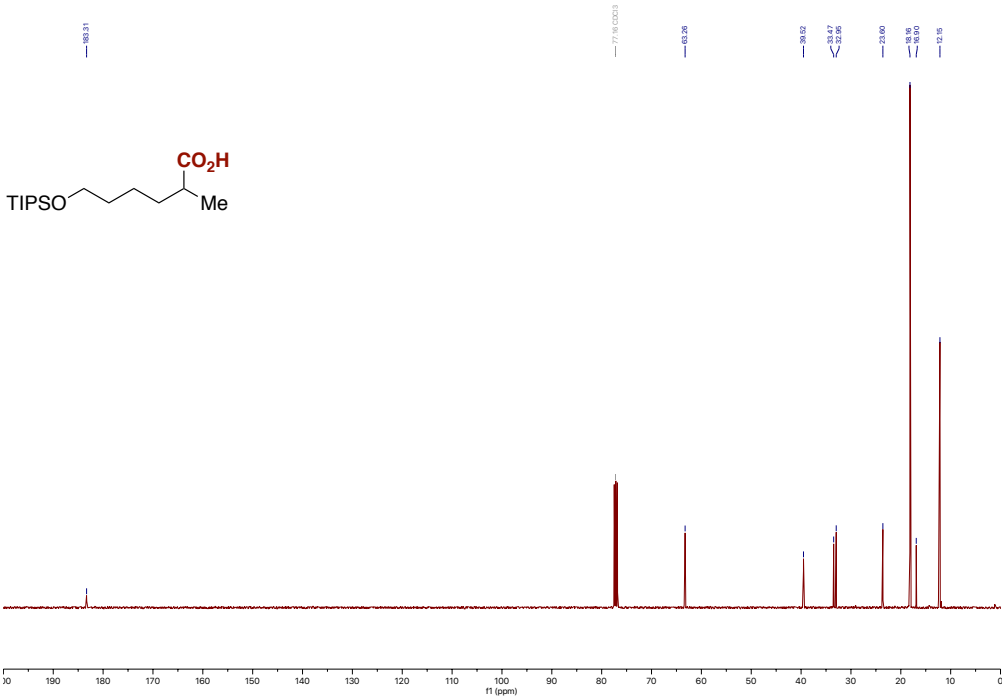

^{13}C spectrum (101 MHz, $CDCl_3$) of **20q**

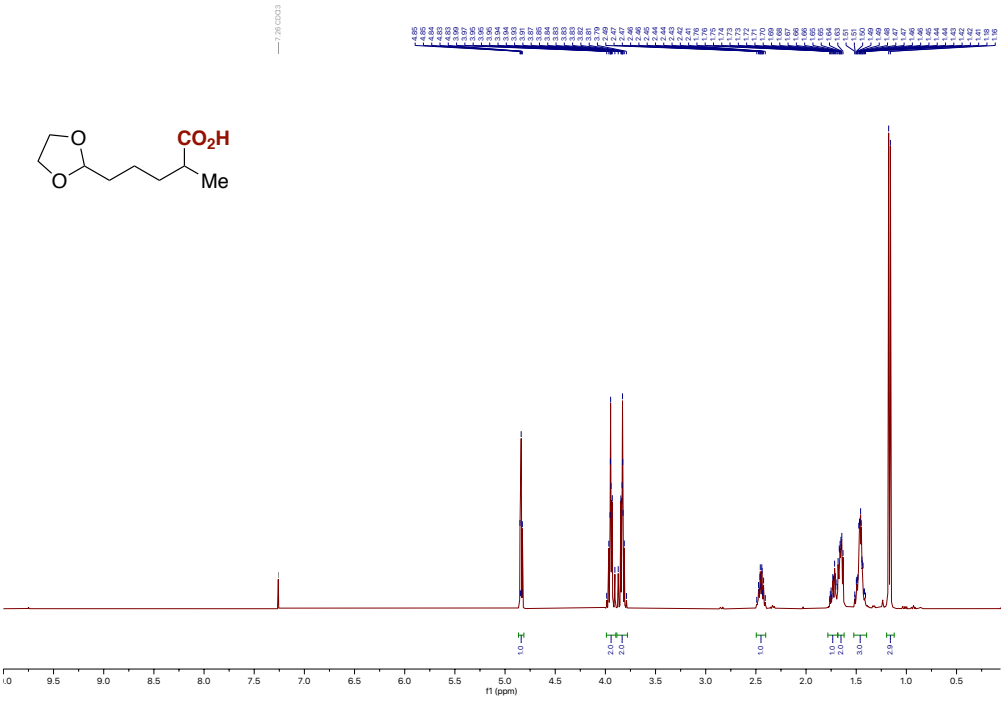

^{1}H spectrum (500 MHz, $CDCl_3$) of **20r**

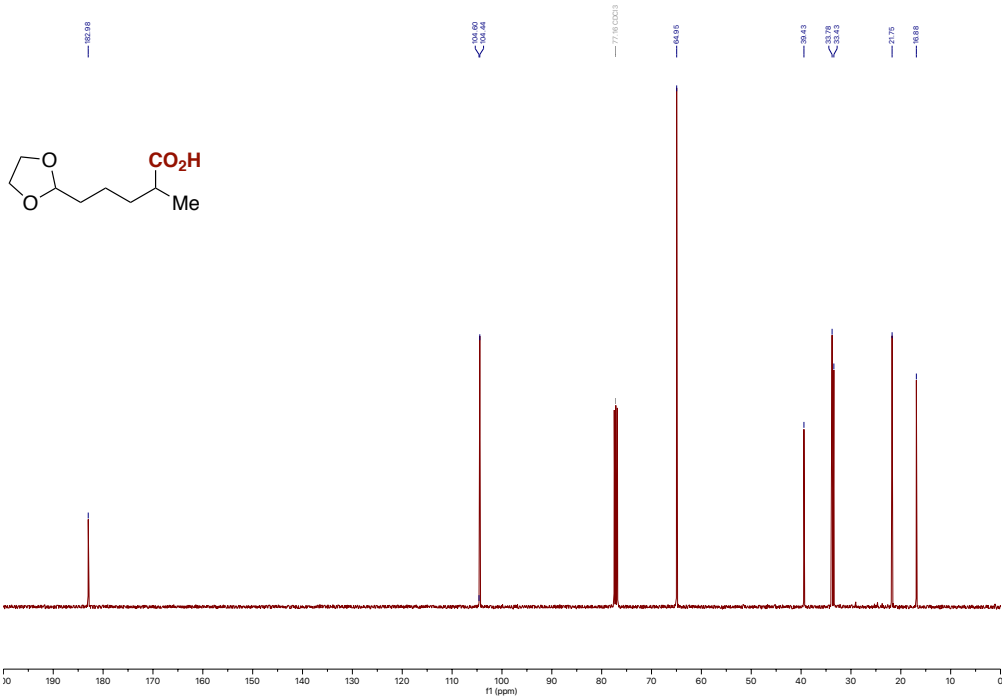

^{13}C spectrum (101 MHz, $CDCl_3$) of **20r**

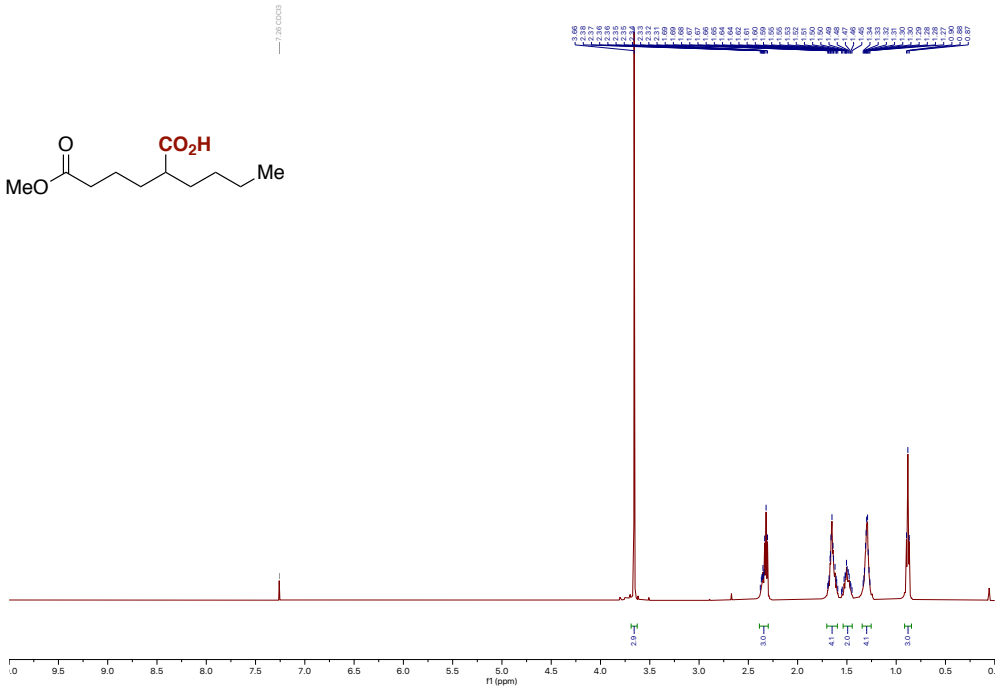

^{1}H spectrum (500 MHz, $CDCl_3$) of **20s**

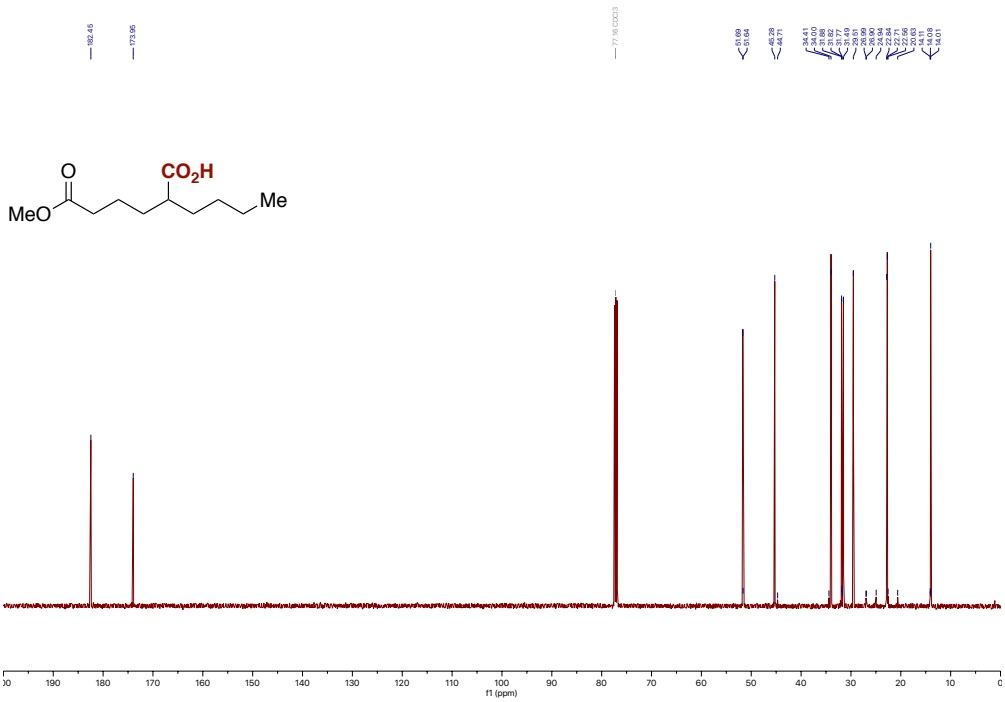

^{13}C spectrum (126 MHz, $CDCl_3$) of **20s**

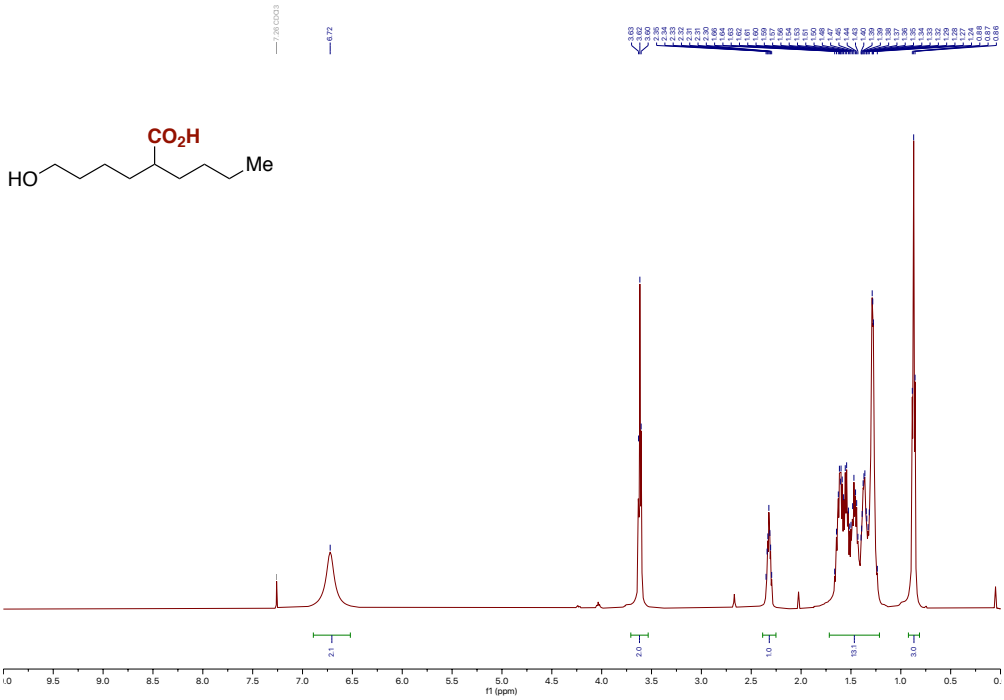

^{1}H spectrum (500 MHz, $CDCl_3$) of **20t**

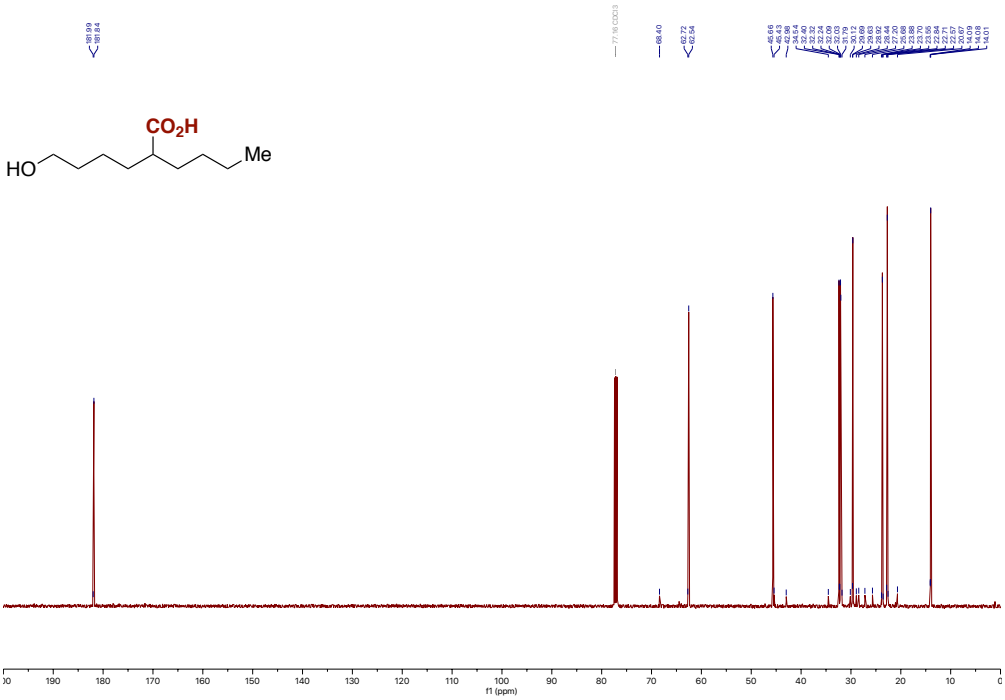

^{13}C spectrum (126 MHz, $CDCl_3$) of **20t**

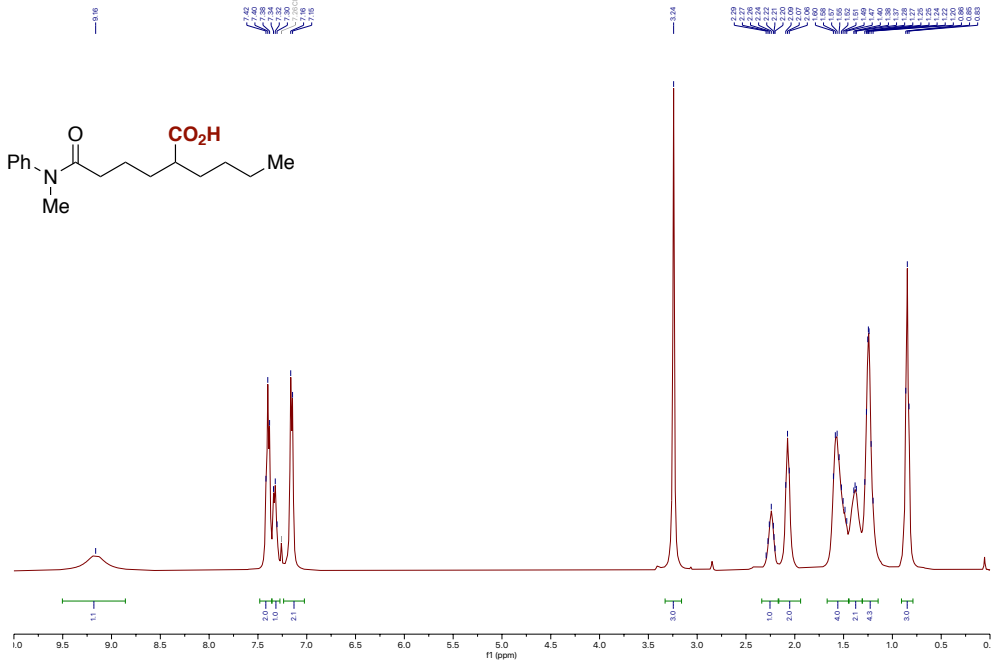

^{1}H spectrum (400 MHz, $CDCl_3$) of **20u**

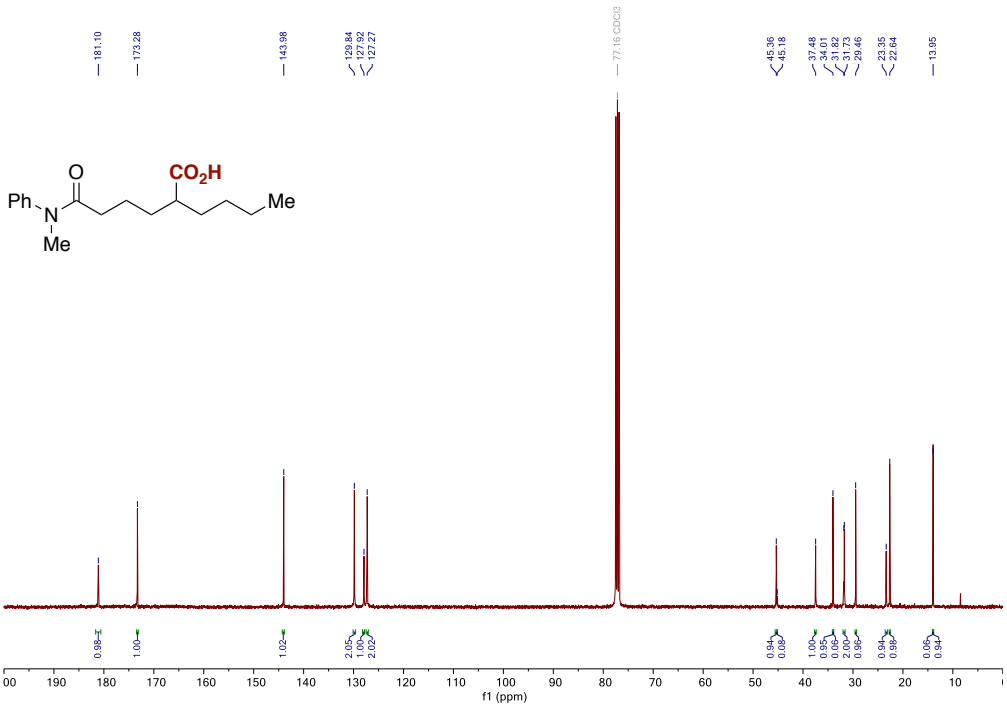

^{13}C spectrum (101 MHz, $CDCl_3$) of **20u**

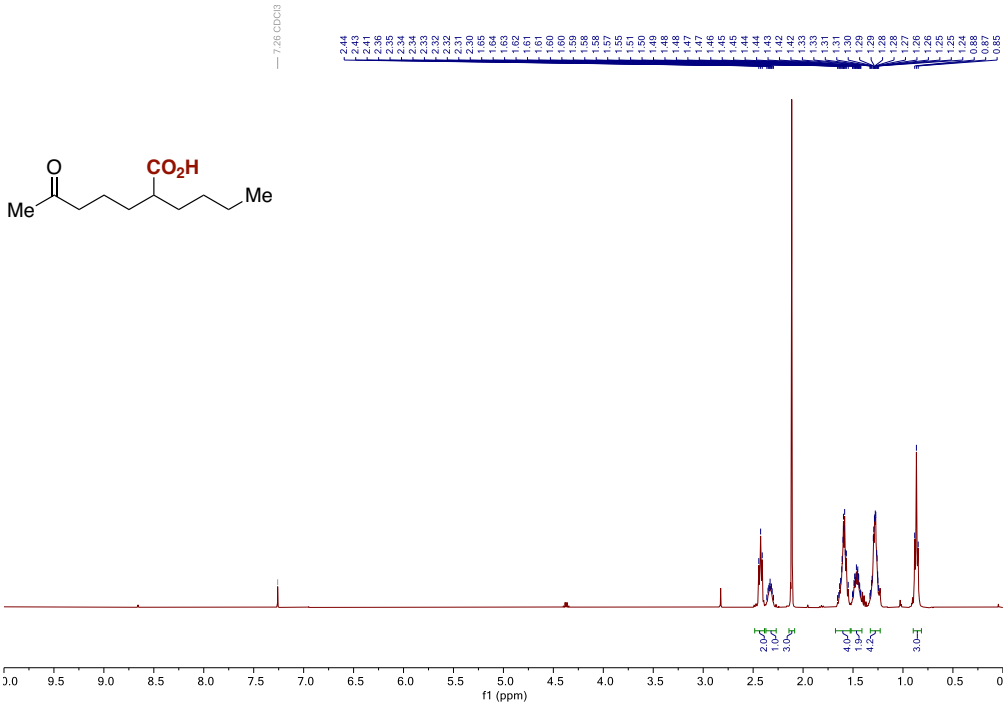

^{1}H spectrum (400 MHz, $CDCl_3$) of **20v**

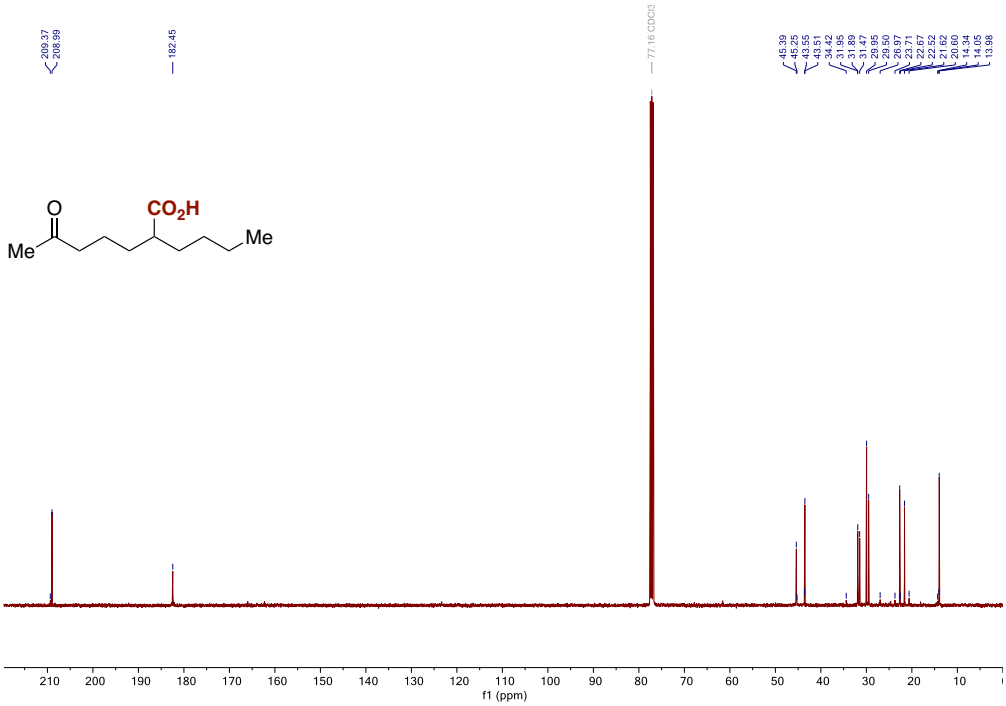

^{13}C spectrum (101 MHz, $CDCl_3$) of **20v**

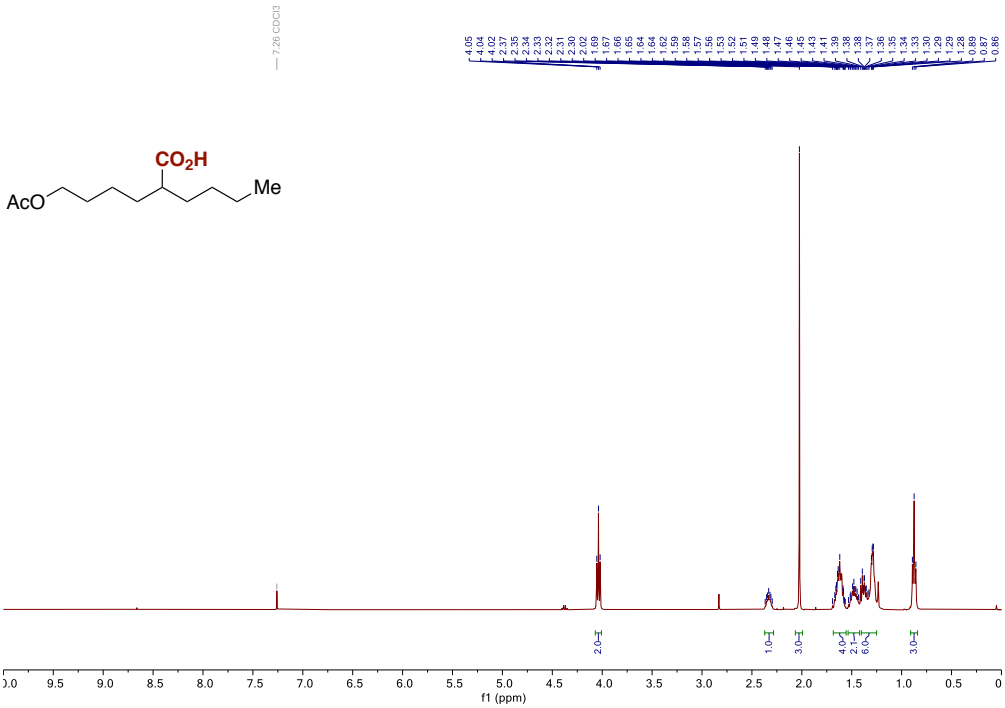

^{1}H spectrum (400 MHz, $CDCl_3$) of **20w**

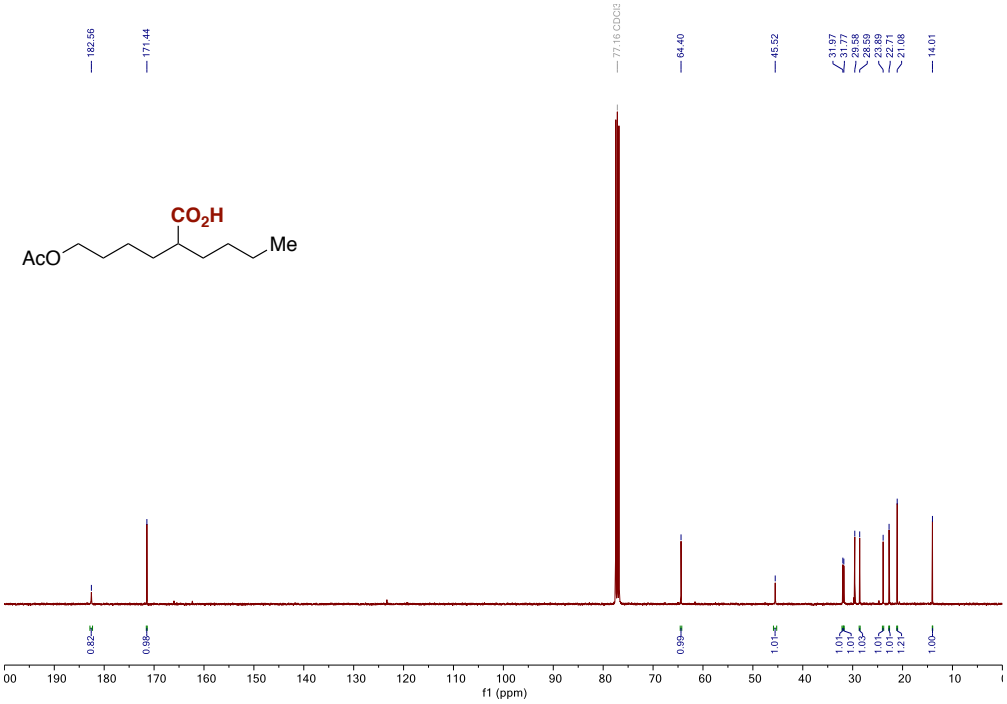

^{13}C spectrum (101 MHz, $CDCl_3$) of **20w**

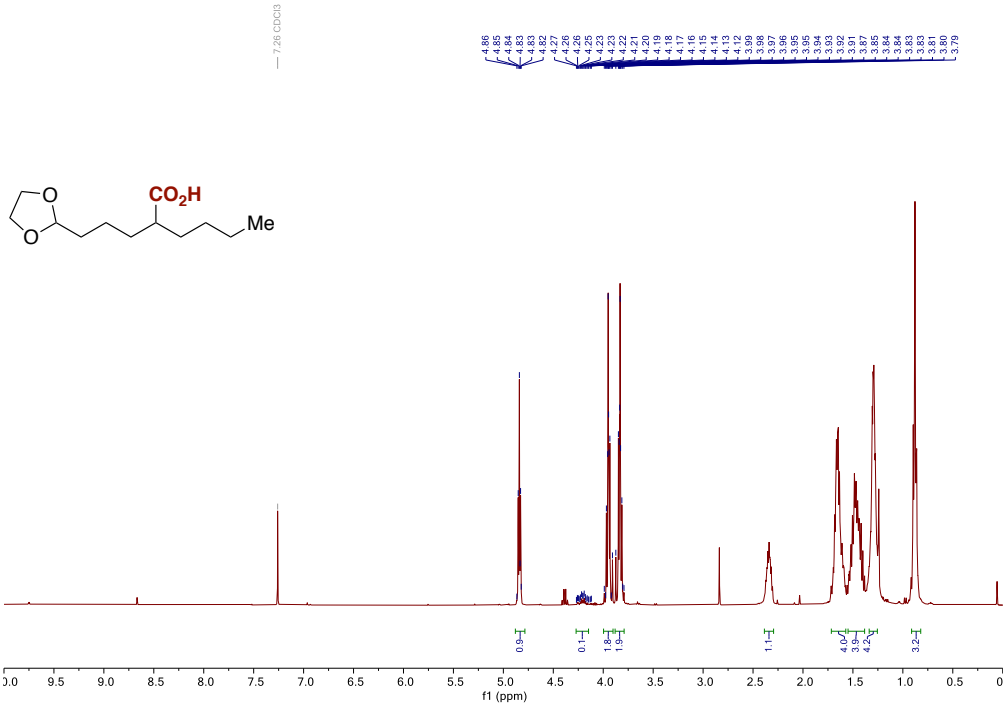

^{1}H spectrum (400 MHz, $CDCl_3$) of **20x**

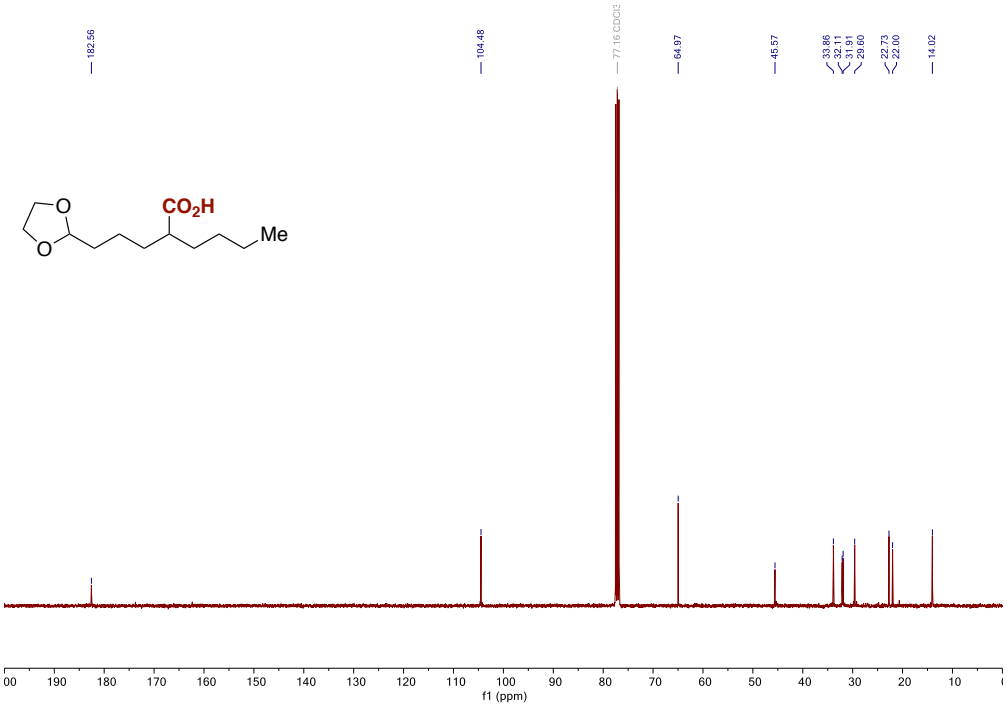

^{13}C spectrum (126 MHz, $CDCl_3$) of **20x**

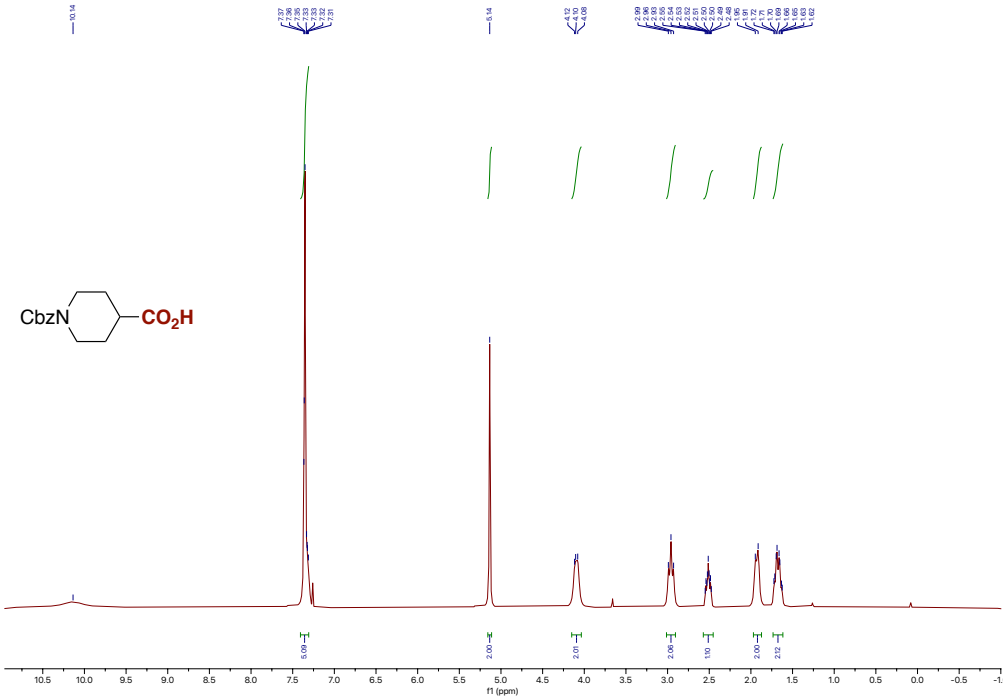

^{1}H spectrum (400 MHz, $CDCl_3$) of **20y**

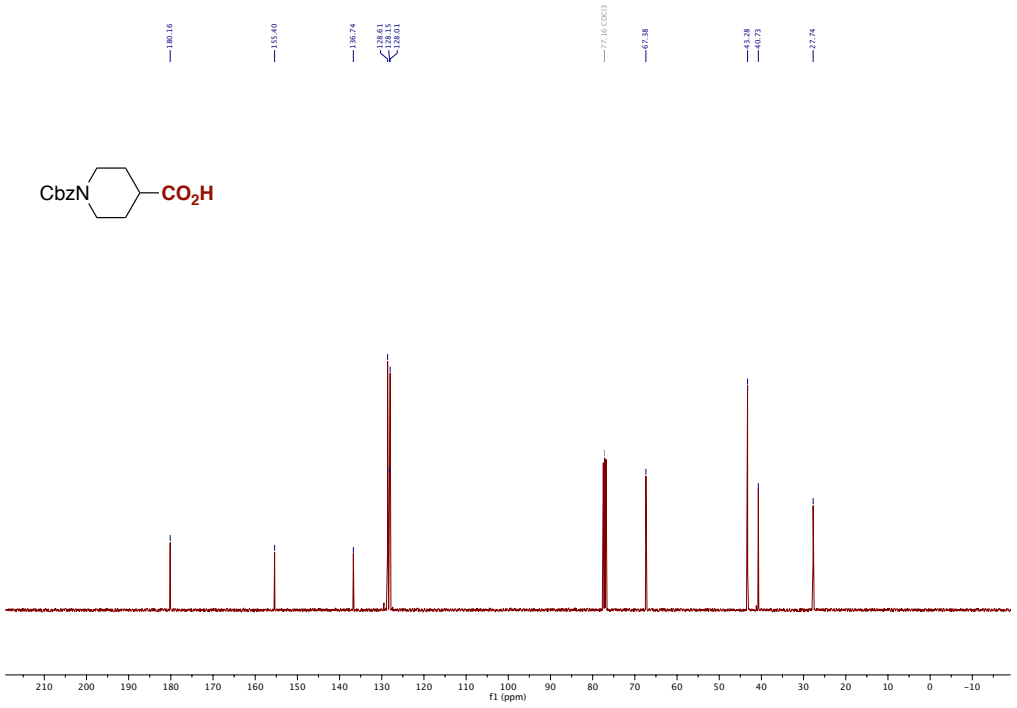

^{13}C spectrum (101 MHz, $CDCl_3$) of **20y**

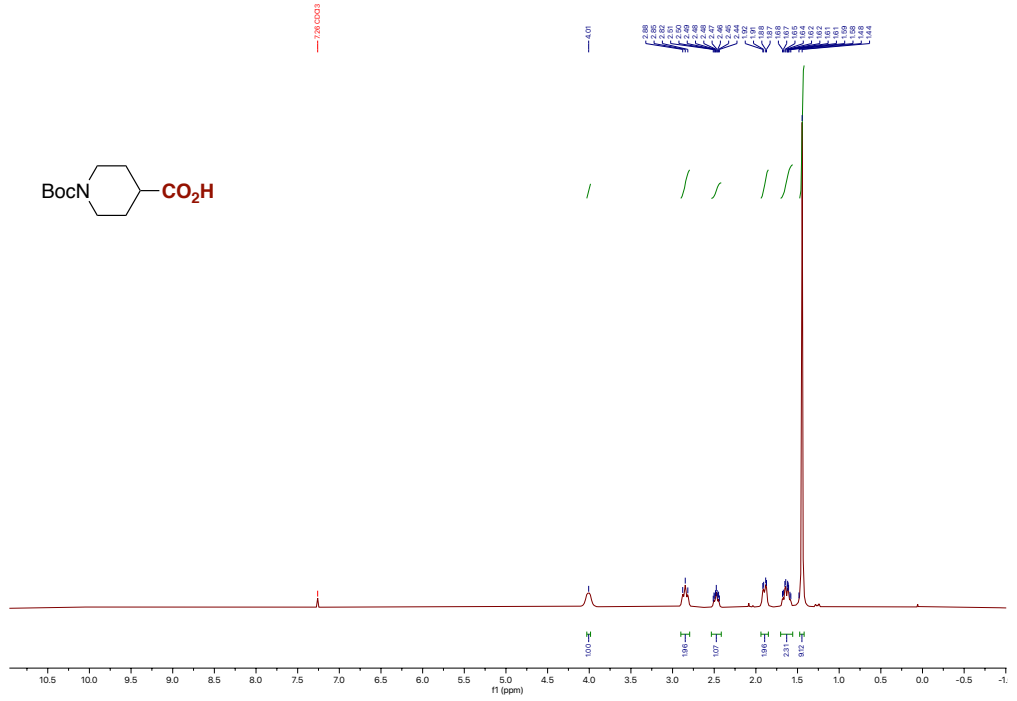

^{1}H spectrum (400 MHz, $CDCl_3$) of **20z**

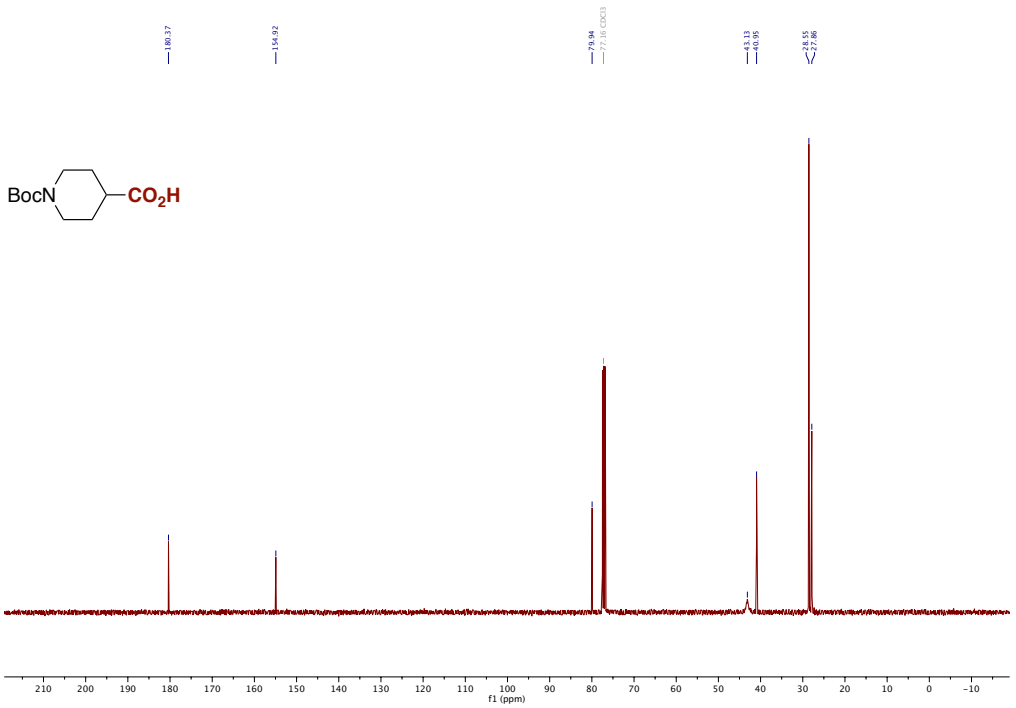

^{13}C spectrum (101 MHz, $CDCl_3$) of **20z**

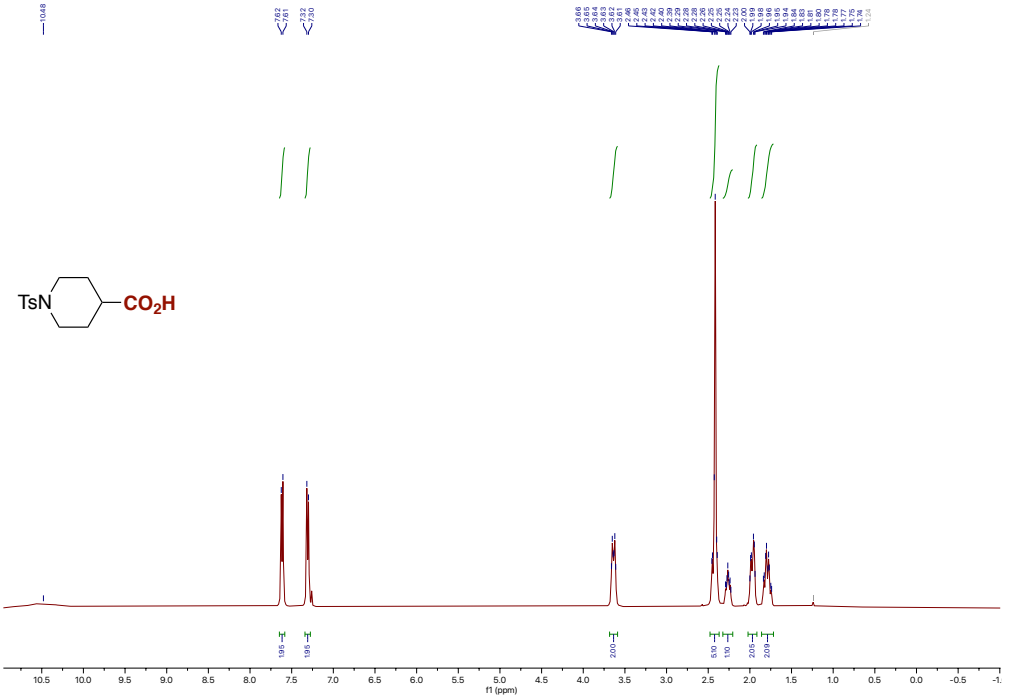

^{1}H spectrum (400 MHz, $CDCl_3$) of **20aa**

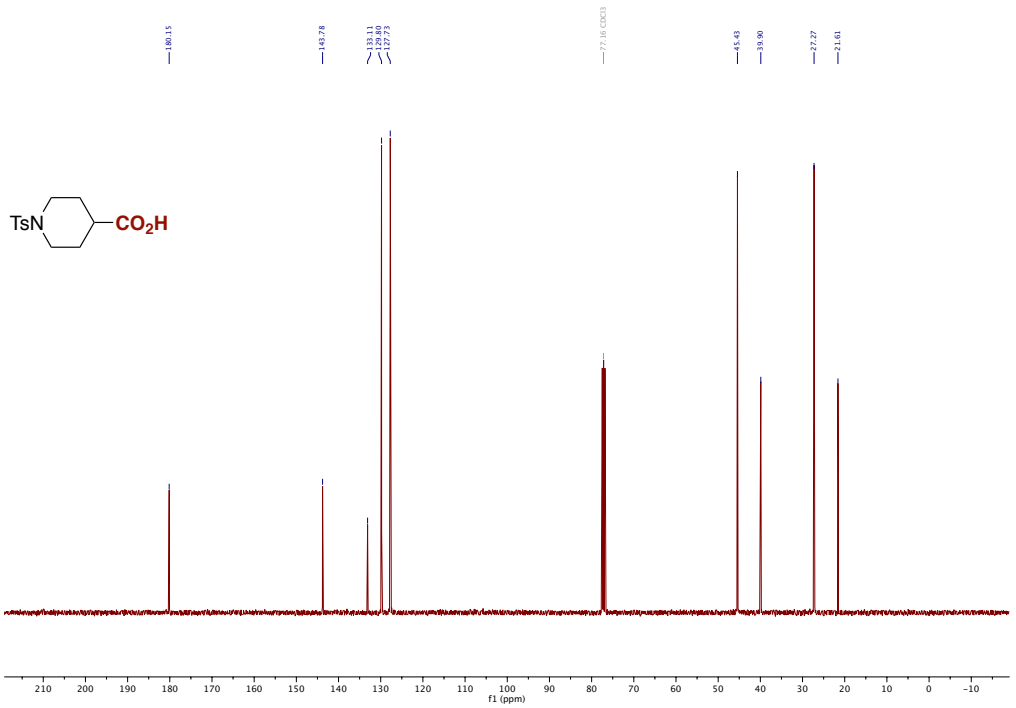

^{13}C spectrum (101 MHz, $CDCl_3$) of **20aa**

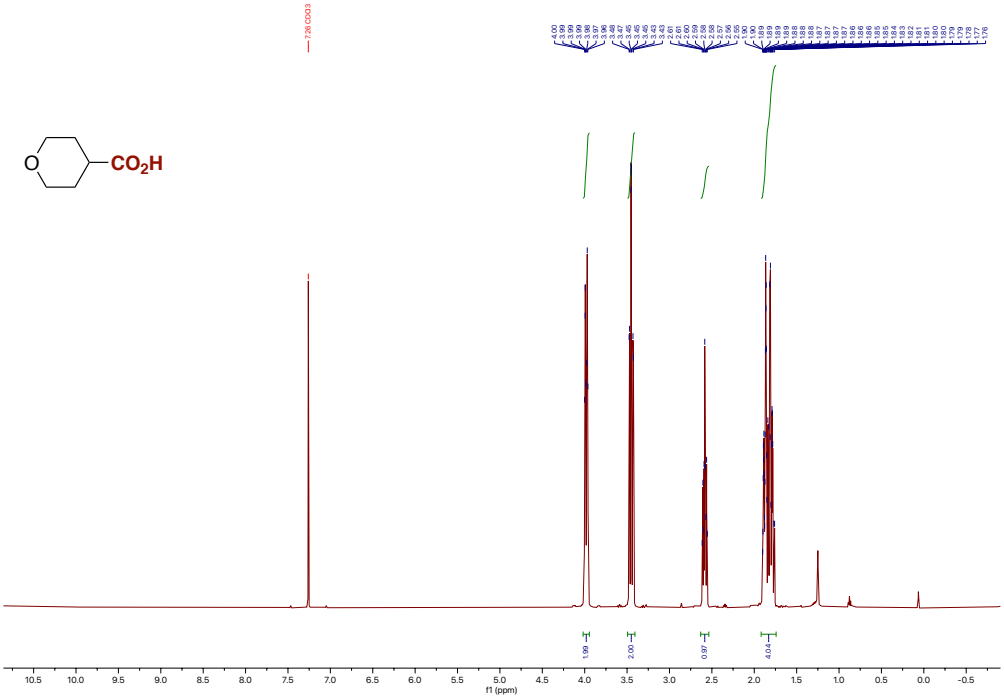

^{1}H spectrum (500 MHz, $CDCl_3$) of **20ab**

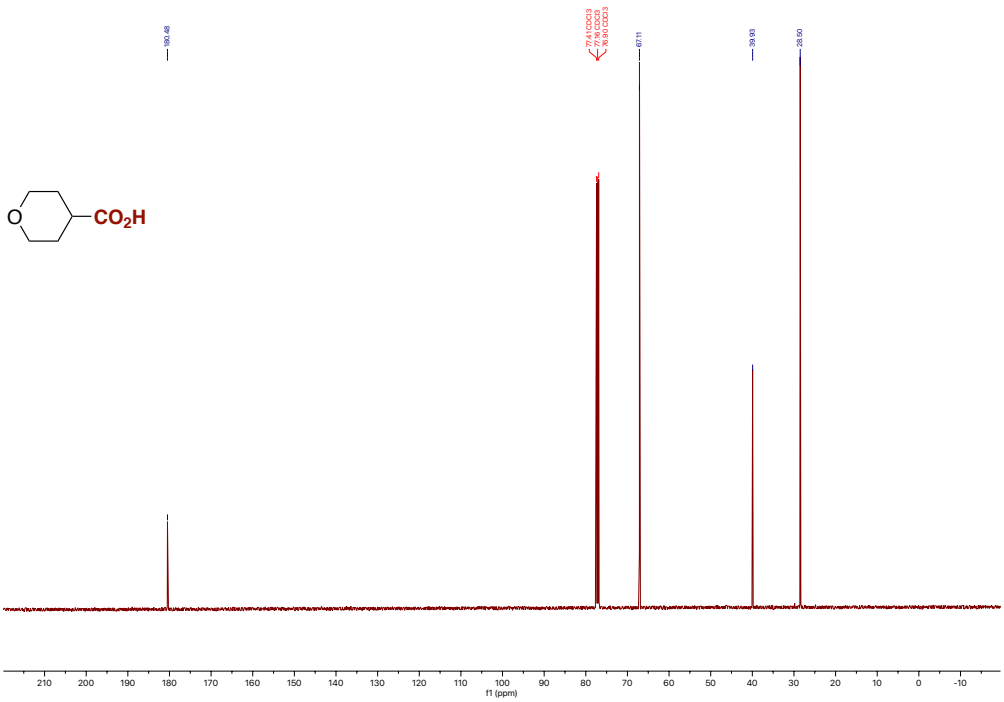

^{13}C spectrum (126 MHz, $CDCl_3$) of **20ab**

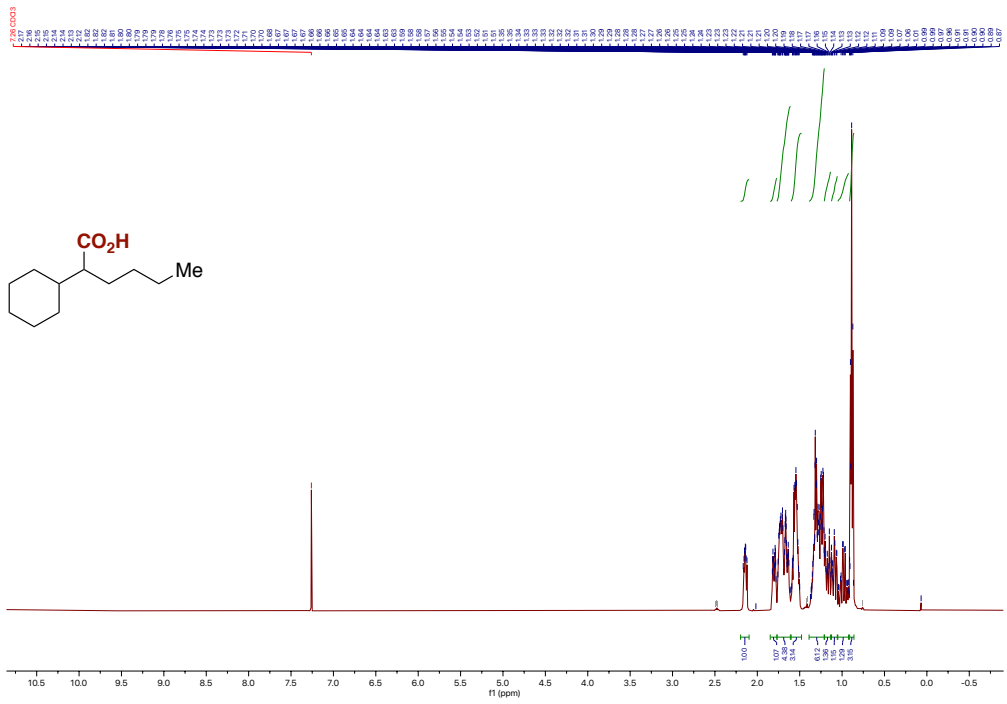

^{1}H spectrum (500 MHz, $CDCl_3$) of **20ac**

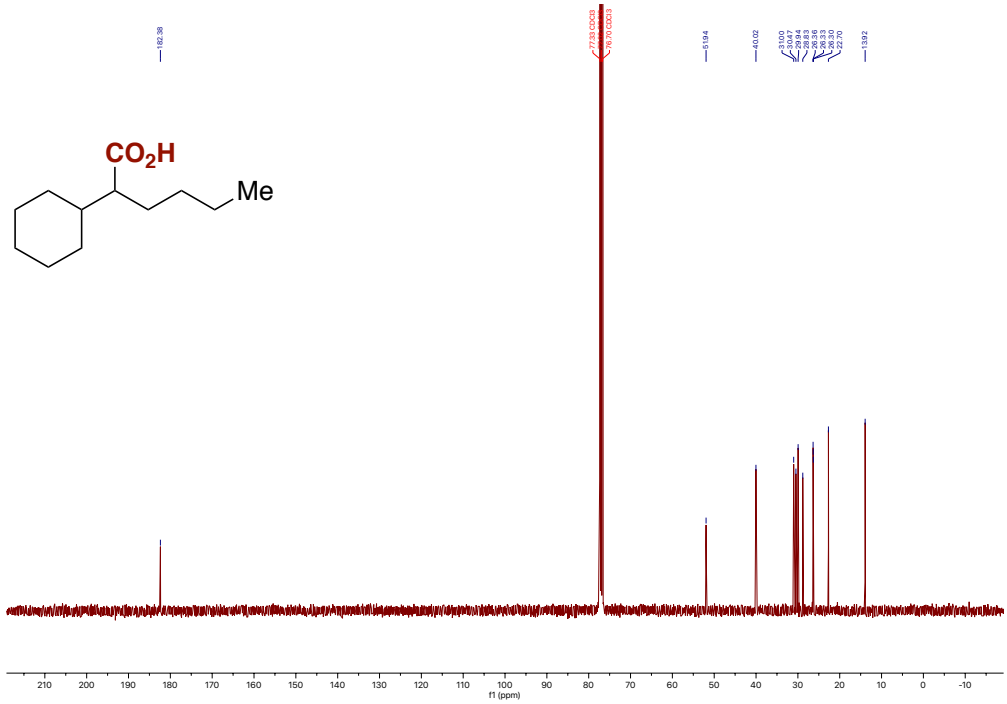

^{13}C spectrum (101 MHz, $CDCl_3$) of **20ac**

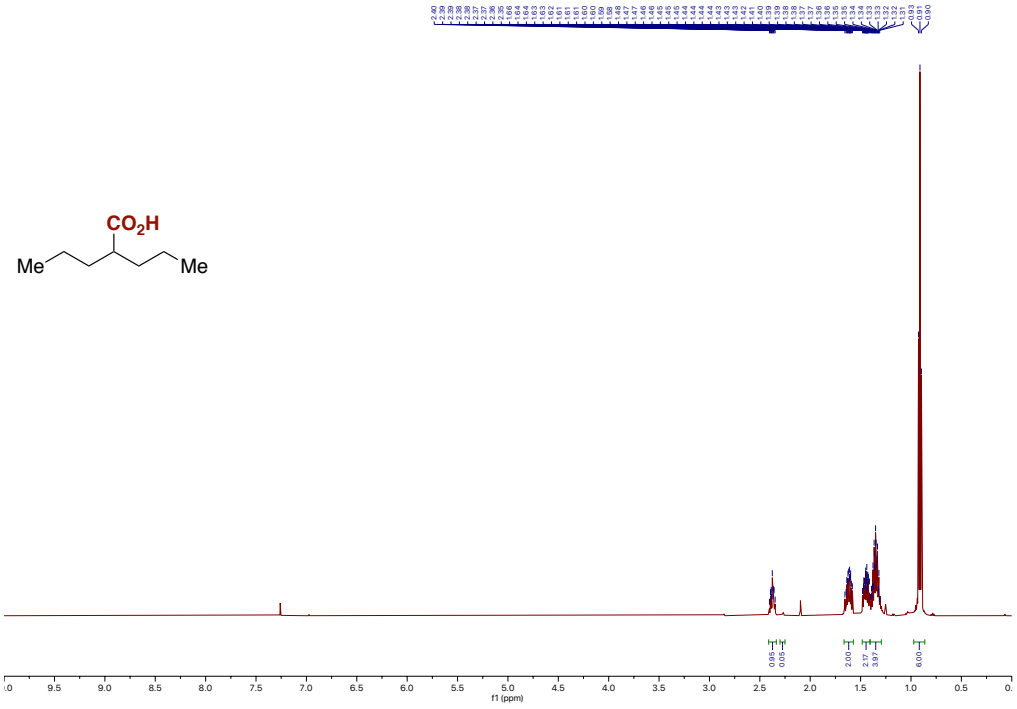

^{1}H spectrum (500 MHz, $CDCl_3$) of **20ad**

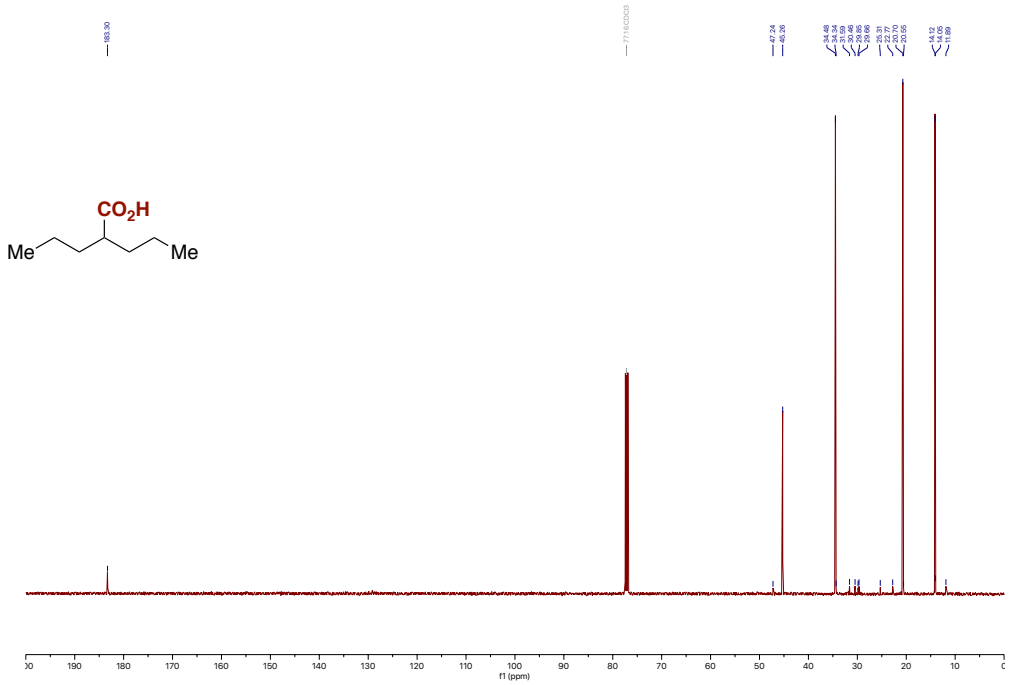

^{13}C spectrum (126 MHz, $CDCl_3$) of **20ad**

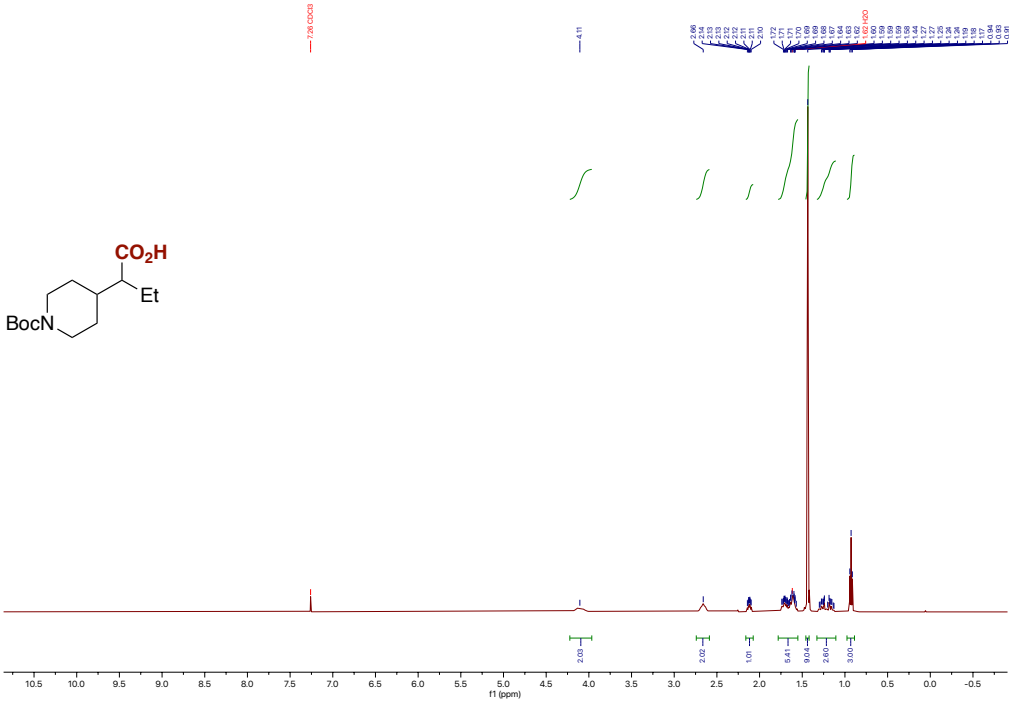

^{1}H spectrum (500 MHz, $CDCl_3$) of **20ae**

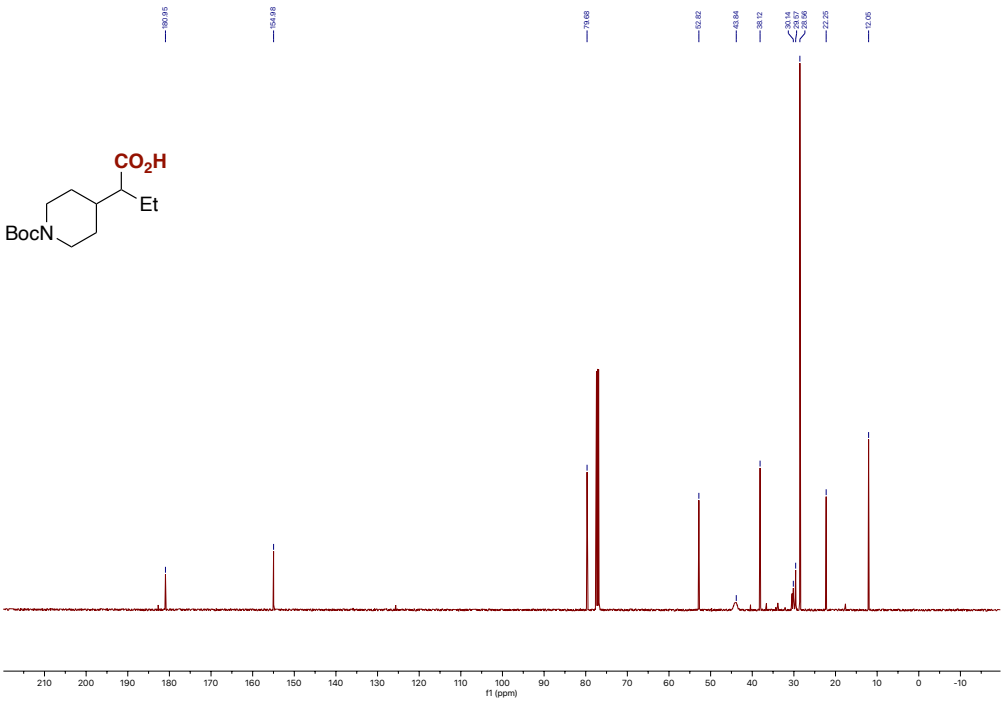

^{13}C spectrum (126 MHz, $CDCl_3$) of **20ae**

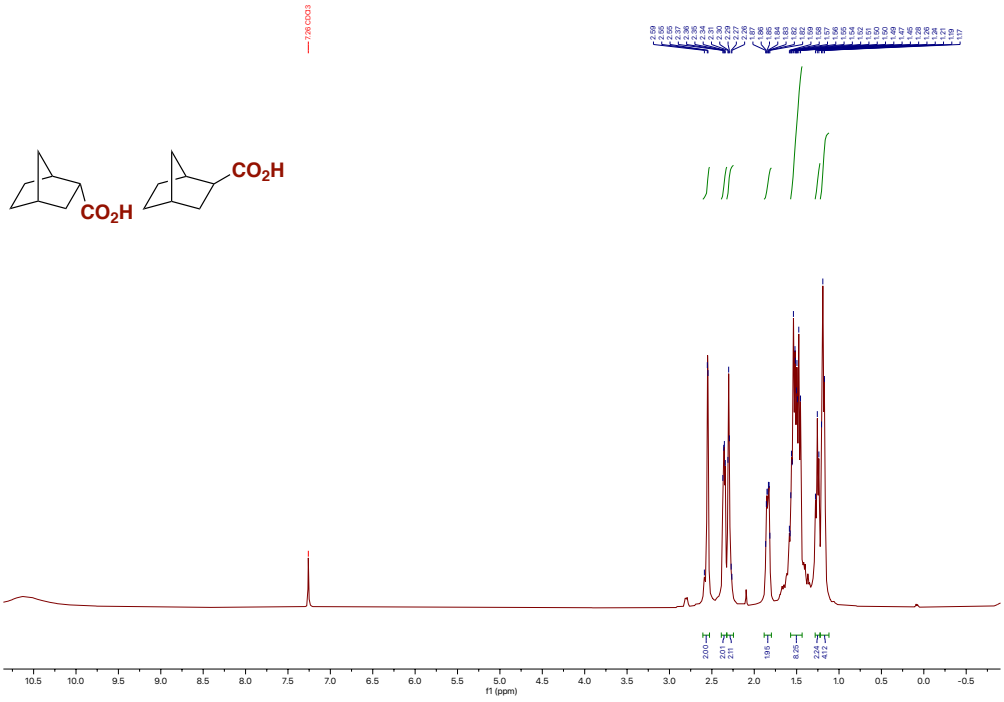

^{1}H spectrum (400 MHz, $CDCl_3$) of **20af**

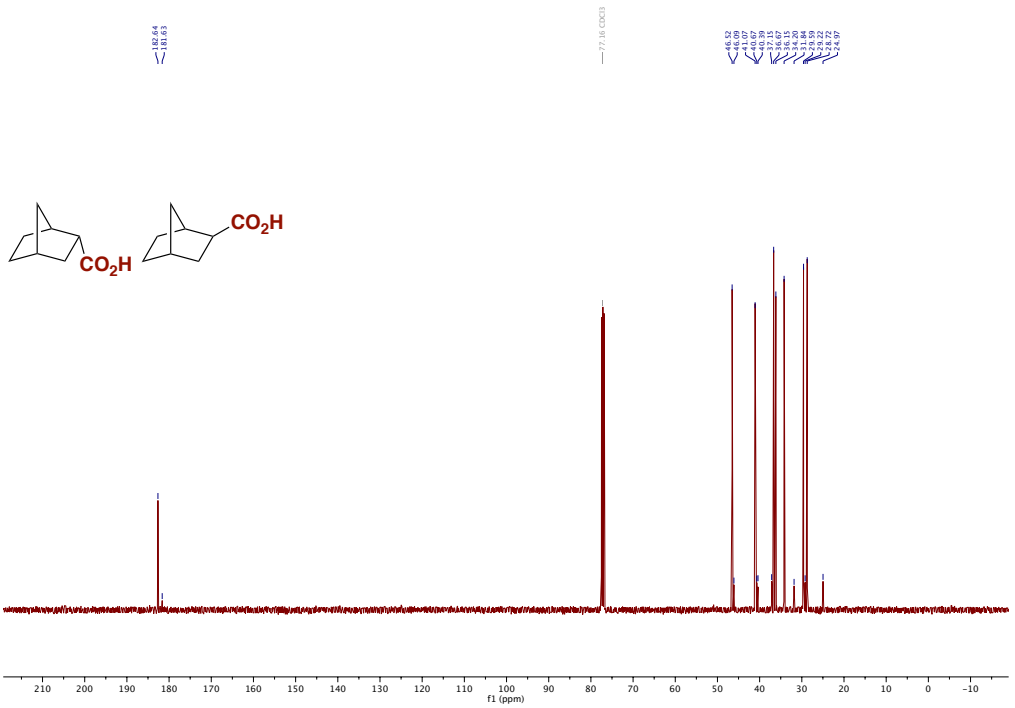

^{13}C spectrum (101 MHz, $CDCl_3$) of **20af**

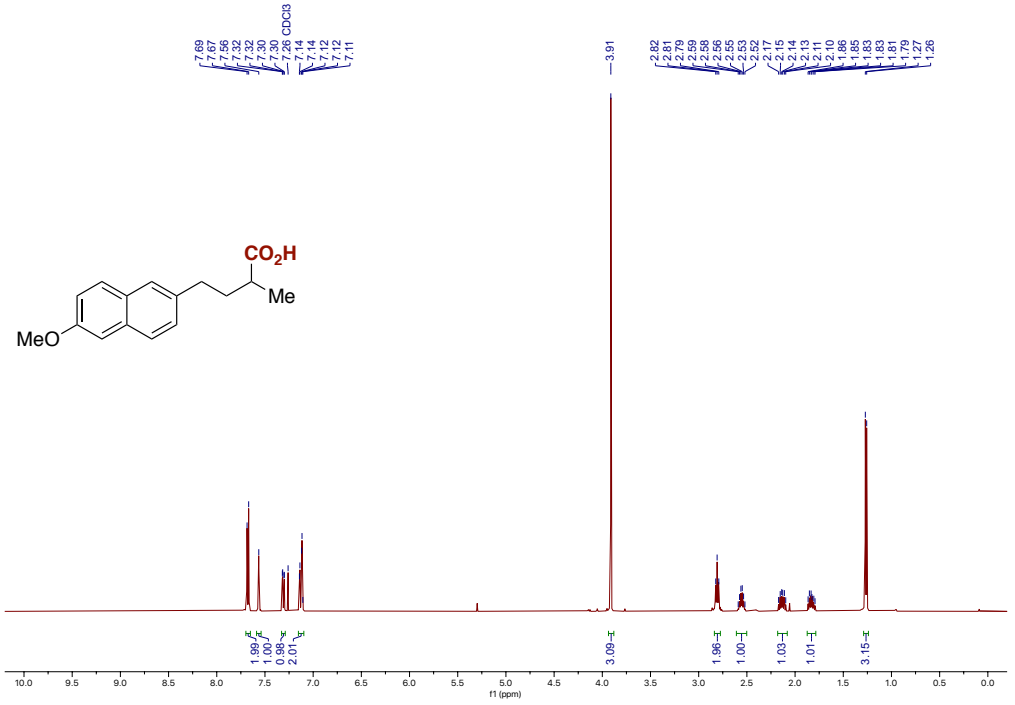

^{1}H spectrum (500 MHz, $CDCl_3$) of **20ag**

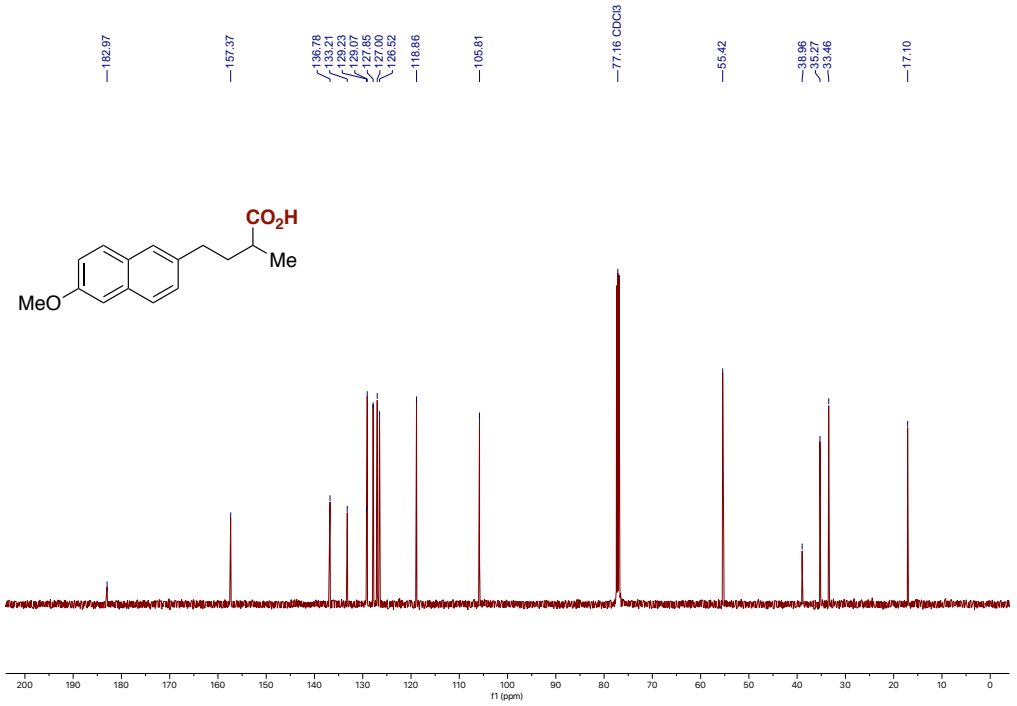

^{13}C spectrum (126 MHz, $CDCl_3$) of **20ag**

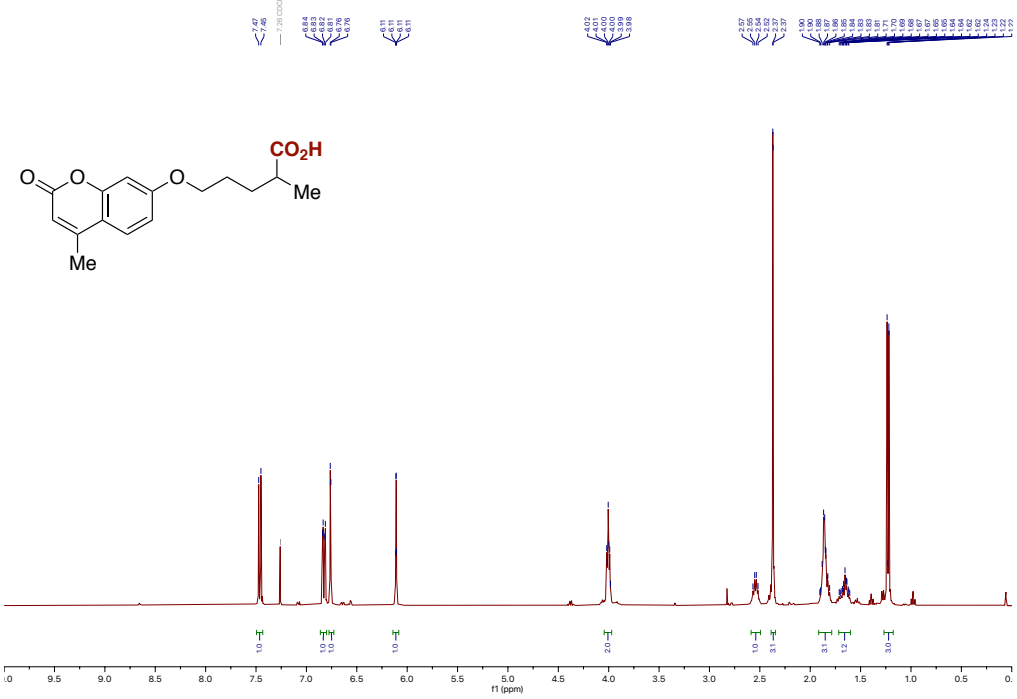

^{1}H spectrum (400 MHz, $CDCl_3$) of **20ah**

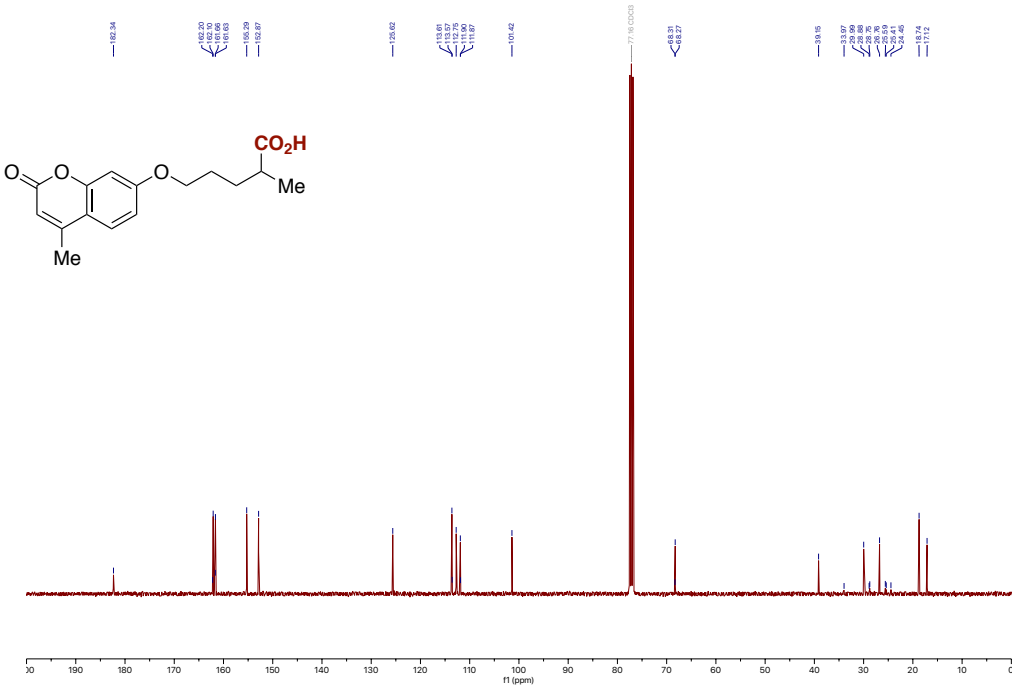

^{13}C spectrum (101 MHz, $CDCl_3$) of **20ah**

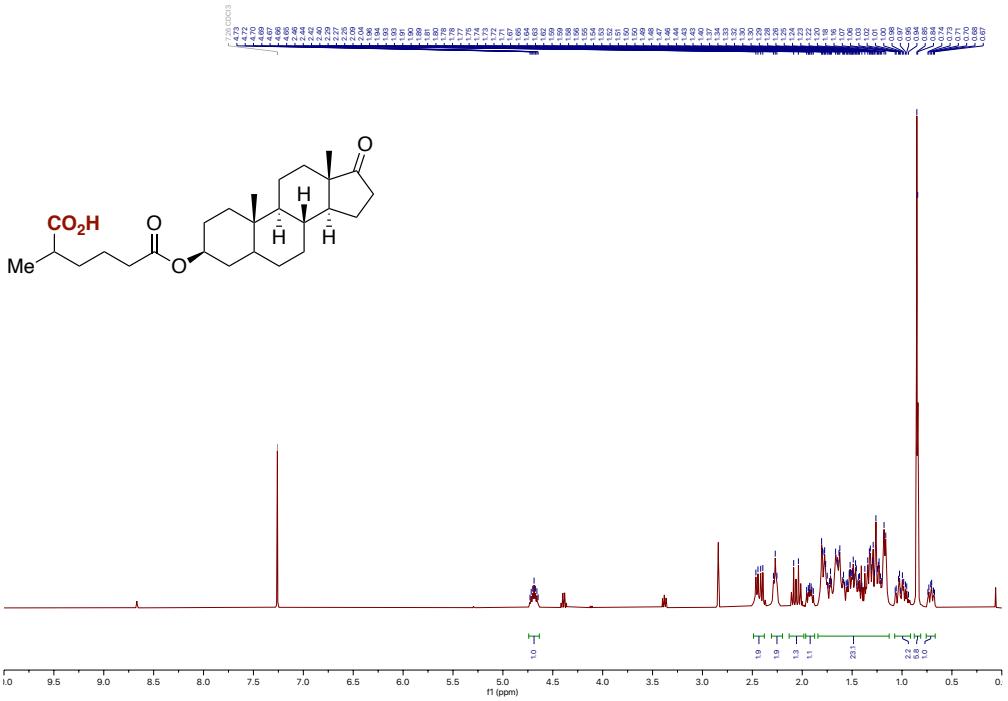

^{1}H spectrum (400 MHz, $CDCl_3$) of **20ai**

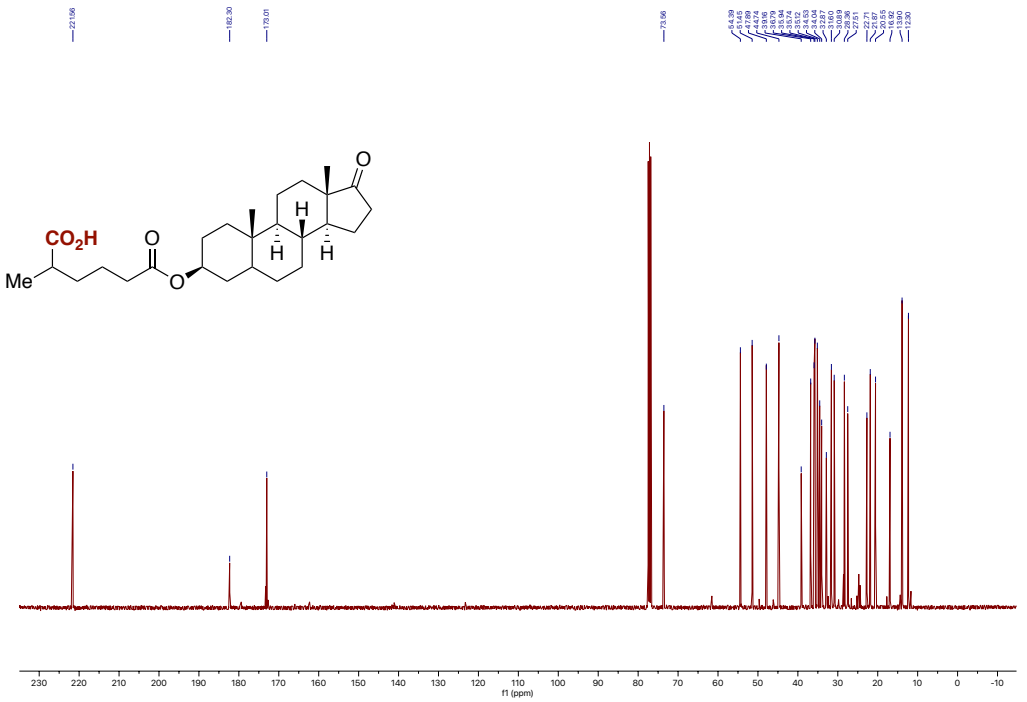

^{13}C spectrum (101 MHz, $CDCl_3$) of **20ai**

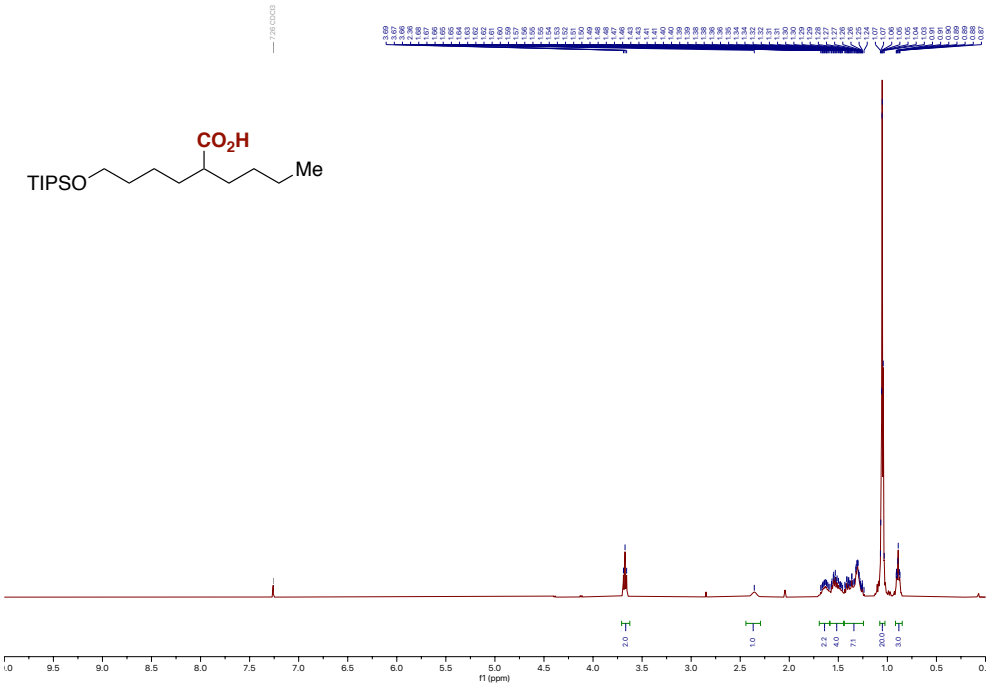

^{1}H spectrum (400 MHz, $CDCl_3$) of **20aj**

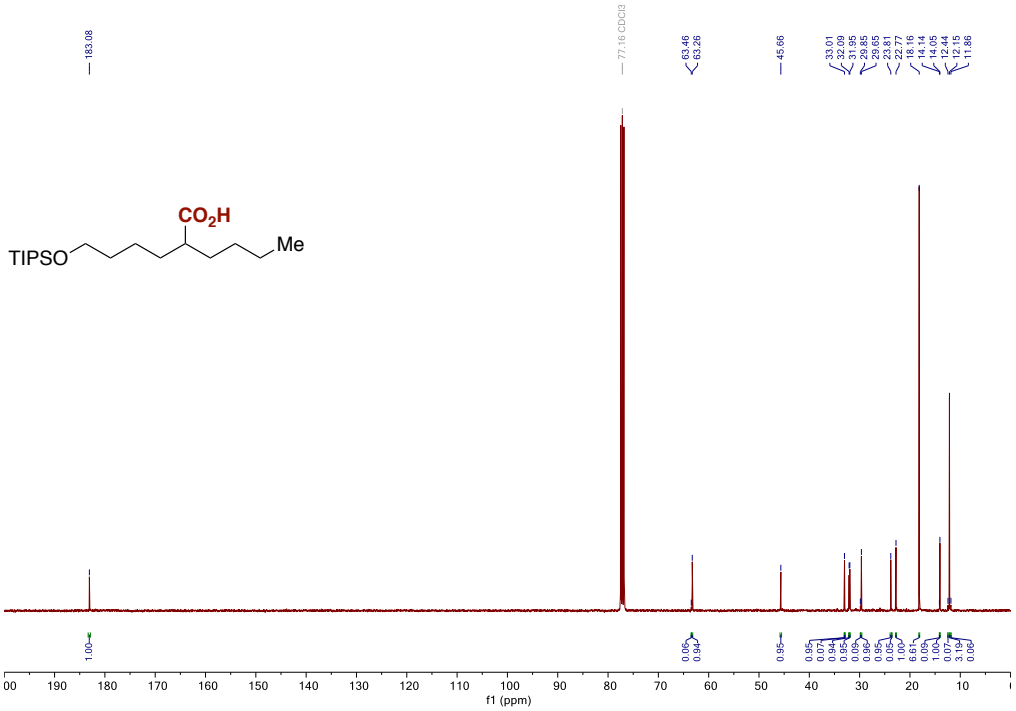

^{13}C spectrum (101 MHz, $CDCl_3$) of **20aj**

3.8. References

(1) Correa, A.; Martín, R. Palladium-Catalyzed Direct Carboxylation of Aryl Bromides with Carbon Dioxide. *J. Am. Chem. Soc.* **2009**, *131*, 15974–15975. https://doi.org/10.1021/ja905264a.

(2) Fujihara, T.; Nogi, K.; Xu, T.; Terao, J.; Tsuji, Y. Nickel-Catalyzed Carboxylation of Aryl and Vinyl Chlorides Employing Carbon Dioxide. *J. Am. Chem. Soc.* **2012**, *134*, 9106–9109. https://doi.org/10.1021/ja303514b.

(3) Tortajada, A.; Juliá-Hernández, F.; Börjesson, M.; Moragas, T.; Martin, R. Transition-Metal-Catalyzed Carboxylation Reactions with Carbon Dioxide. *Angew. Chem. Int. Ed.* **2018**, *57*, 15948–15982. https://doi.org/10.1002/anie.201803186.

(4) León, T.; Correa, A.; Martin, R. Ni-Catalyzed Direct Carboxylation of Benzyl Halides with CO_2. *J. Am. Chem. Soc.* **2013**, *135*, 1221–1224. https://doi.org/10.1021/ja311045f.

(5) Liu, Y.; Cornella, J.; Martin, R. Ni-Catalyzed Carboxylation of Unactivated Primary Alkyl Bromides and Sulfonates with CO_2. *J. Am. Chem. Soc.* **2014**, *136*, 11212–11215. https://doi.org/10.1021/ja5064586.

(6) Börjesson, M.; Moragas, T.; Martin, R. Ni-Catalyzed Carboxylation of Unactivated Alkyl Chlorides with CO_2. *J. Am. Chem. Soc.* **2016**, *138*, 7504–7507. https://doi.org/10.1021/jacs.6b04088.

(7) Juliá-Hernández, F.; Moragas, T.; Cornella, J.; Martin, R. Remote Carboxylation of Halogenated Aliphatic Hydrocarbons with Carbon Dioxide. *Nature* **2017**, *545*, 84–88. https://doi.org/10.1038/nature22316.

(8) Wang, Y.; He, Y.; Zhu, S. NiH-Catalyzed Functionalization of Remote and Proximal Olefins: New Reactions and Innovative Strategies. *Acc. Chem. Res.* **2022**, *55*, 3519–3536. https://doi.org/10.1021/acs.accounts.2c00628.

(9) Meng, Q.-Y.; Wang, S.; Huff, G. S.; König, B. Ligand-Controlled Regioselective Hydrocarboxylation of Styrenes with CO_2 by Combining Visible Light and Nickel Catalysis. *J. Am. Chem. Soc.* **2018**, *140*, 3198–3201. https://doi.org/10.1021/jacs.7b13448.

(10) Sahoo, B.; Bellotti, P.; Juliá-Hernández, F.; Meng, Q.; Crespi, S.; König, B.; Martin, R. Site-Selective, Remote Sp^3 C–H Carboxylation Enabled by the Merger of Photoredox and Nickel Catalysis. *Chem. – Eur. J.* **2019**, *25*, 9001–9005. https://doi.org/10.1002/chem.201902095.

(11) Lu, Z.; Fu, G. C. Alkyl–Alkyl Suzuki Cross-Coupling of Unactivated Secondary Alkyl Chlorides. *Angew. Chem. Int. Ed.* **2010**, *49*, 6676–6678. https://doi.org/10.1002/anie.201003272.

(12) Sayyed, F. B.; Tsuji, Y.; Sakaki, S. The Crucial Role of a Ni(I) Intermediate in Ni-Catalyzed Carboxylation of Aryl Chloride with CO_2: A Theoretical Study. *Chem. Commun.* **2013**, *49* (91), 10715. https://doi.org/10.1039/c3cc45836a.

(13) Sayyed, F. B.; Sakaki, S. The Crucial Roles of $MgCl_2$ as a Non-Innocent Additive in the Ni-Catalyzed Carboxylation of Benzyl Halide with CO_2. *Chem Commun* **2014**, *50*, 13026–13029. https://doi.org/10.1039/C4CC04962D.

(14) Diccianni, J. B.; Hu, C. T.; Diao, T. Insertion of CO_2 Mediated by a (Xantphos)Ni^{I} – Alkyl Species. *Angew. Chem. Int. Ed.* **2019**, *58*, 13865–13868. https://doi.org/10.1002/anie.201906005.

(15) Somerville, R. J.; Odena, C.; Obst, M. F.; Hazari, N.; Hopmann, K. H.; Martin, R. Ni(I)–Alkyl Complexes Bearing Phenanthroline Ligands: Experimental Evidence for CO_2 Insertion at Ni(I) Centers. *J. Am. Chem. Soc.* **2020**, *142*, 10936–10941. https://doi.org/10.1021/jacs.0c04695.

(16) Zhang, B.; Yang, S.; Li, D.; Hao, M.; Chen, B.-Z.; Li, Z. Insights into the Regioselective Hydrocarboxylation of Styrenes with CO_2 Controlled by the Ligand of Nickel Catalysts. *ACS Sustain. Chem. Eng.* **2021**, *9*, 4091–4101. https://doi.org/10.1021/acssuschemeng.0c08845.

(17) Charboneau, D. J.; Brudvig, G. W.; Hazari, N.; Lant, H. M. C.; Saydjari, A. K. Development of an Improved System for the Carboxylation of Aryl Halides through Mechanistic Studies. *ACS Catal.* **2019**, *9*, 3228–3241. https://doi.org/10.1021/acscatal.9b00566.

(18) Lin, Q.; Fu, Y.; Liu, P.; Diao, T. Monovalent Nickel-Mediated Radical Formation: A Concerted Halogen-Atom Dissociation Pathway Determined by Electroanalytical Studies. *J. Am. Chem. Soc.* **2021**, *143*, 14196–14206. https://doi.org/10.1021/jacs.1c05255.

(19) Huang, H.; Alvarez-Hernandez, J. L.; Hazari, N.; Mercado, B. Q.; Uehling, M. R. Effect of 6,6′-Substituents on Bipyridine-Ligated Ni Catalysts for Cross-Electrophile Coupling. *ACS Catal.* **2024**, *14*, 6897–6914. https://doi.org/10.1021/acscatal.4c00827.

(20) Sargent, B. T.; Alexanian, E. J. Palladium-Catalyzed Alkoxycarbonylation of Unactivated Secondary Alkyl Bromides at Low Pressure. *J. Am. Chem. Soc.* **2016**, *138*, 7520–7523. https://doi.org/10.1021/jacs.6b04610.

(21) Ito, H.; Kubota, K. Copper(I)-Catalyzed Boryl Substitution of Unactivated Alkyl Halides. *Org. Lett.* **2012**, *14*, 890–893. https://doi.org/10.1021/ol203413w.

(22) Vasil'eva, T. T.; Gapusenko, S. I.; Vitt, S. V.; Terent'ev, A. B. Homolytic Addition of Benzyl Bromide to Unsaturated Compounds in Conditions of Metal-Complex Initiation. *Bull. Russ. Acad. Sci. Div. Chem. Sci.* **1992**, *41*, 1841–1845. https://doi.org/10.1007/BF00863820.

(23) Montoro, R.; Wirth, T. Direct Bromination and Iodination of Non-Activated Alkanes by Hypohalite Reagents. *Synthesis* **2005**, 9, 1473–1478. https://doi.org/10.1055/s-2005-865322.

(24) Zygalski, L.; Middel, C.; Harms, K.; Koert, U. Enolizable β-Fluoroenones: Synthesis and Asymmetric 1,2-Reduction. *Org. Lett.* **2018**, *20*, 5071–5074. https://doi.org/10.1021/acs.orglett.8b02435.

(25) Gilbert, J. C.; Giamalva, D. H.; Weerasooriya, U. Intramolecular Carbon-Hydrogen Insertions of Alkylidenecarbenes. I. Selectivity. *J. Org. Chem.* **1983**, *48*, 5251–5256. https://doi.org/10.1021/jo00174a019.

(26) Schmidt, V. A.; Quinn, R. K.; Brusoe, A. T.; Alexanian, E. J. Site-Selective Aliphatic C–H Bromination Using *N* -Bromoamides and Visible Light. *J. Am. Chem. Soc.* **2014**, *136*, 14389–14392. https://doi.org/10.1021/ja508469u.

(27) Gruhle, K.; Müller, S.; Meister, A.; Drescher, S. Synthesis and Aggregation Behaviour of Single-Chain, 1,32-Alkyl Branched Bis(Phosphocholines): Effect of Lateral Chain Length. *Org. Biomol. Chem.* **2018**, *16*, 2711–2724. https://doi.org/10.1039/C8OB00424B.

(28) Yakhvarov, D.; Trofimova, E.; Sinyashin, O.; Kataeva, O.; Budnikova, Y.; Lönnecke, P.; Hey-Hawkins, E.; Petr, A.; Krupskaya, Y.; Kataev, V.; Klingeler, R.; Büchner, B. New Dinuclear Nickel(II) Complexes: Synthesis, Structure, Electrochemical, and Magnetic Properties. *Inorg. Chem.* **2011**, *50*, 4553–4558. https://doi.org/10.1021/ic2002546.

(29) Gaydou, M.; Moragas, T.; Juliá-Hernández, F.; Martin, R. Site-Selective Catalytic Carboxylation of Unsaturated Hydrocarbons with CO_2 and Water. *J. Am. Chem. Soc.* **2017**, *139*, 12161–12164. https://doi.org/10.1021/jacs.7b07637.

(30) Lin, T.; Gu, Y.; Qian, P.; Guan, H.; Walsh, P. J.; Mao, J. Nickel-Catalyzed Reductive Coupling of Homoenolates and Their Higher Homologues with Unactivated Alkyl Bromides. *Nat. Commun.* **2020**, *11*, 5638. https://doi.org/10.1038/s41467-020-19194-x.

(31) Doni, E.; O'Sullivan, S.; Murphy, J. A. Metal-Free Reductive Cleavage of Benzylic Esters and Ethers: Fragmentations Result from Single and Double Electron Transfers. *Angew. Chem. Int. Ed.* **2013**, *52*, 2239–2242. https://doi.org/10.1002/anie.201208066.

(32) Fujita, T.; Watanabe, S.; Suga, K.; Nakayama, H. The Reaction of Carboxylic Acids with Conjugated Olefins Using Sodium Naphthalenide in the Presence of *N*, *N*, *N′*,

N′- Tetramethylethylenediamine. *Synthesis* **1979**, *1979*, 310–311. https://doi.org/10.1055/s-1979-28664.

(33) Seo, H.; Liu, A.; Jamison, T. F. Direct β-Selective Hydrocarboxylation of Styrenes with CO_2 Enabled by Continuous Flow Photoredox Catalysis. *J. Am. Chem. Soc.* **2017**, *139*, 13969–13972. https://doi.org/10.1021/jacs.7b05942.

(34) Cai, Z.; Li, S.; Gao, Y.; Fu, L.; Li, G. Weak, Bidentate Chelating Group Assisted Cross-Coupling of C(Sp^3)–H Bonds in Aliphatic Acid Derivatives with Aryltrifluoroborates. *Chem. Commun.* **2018**, *54*, 12766–12769. https://doi.org/10.1039/C8CC07481J.

(35) Ren, W.; Wang, M.; Guo, J.; Zhou, J.; Chu, J.; Shi, Y.; Shi, Y. Pd-Catalyzed Regioselective Branched Hydrocarboxylation of Terminal Olefins with Formic Acid. *Org. Lett.* **2022**, *24*, 886–891. https://doi.org/10.1021/acs.orglett.1c04231.

(36) Winkler, M.; Meischler, D.; Klempier, N. Nitrilase-Catalyzed Enantioselective Synthesis of Pyrrolidine- and Piperidinecarboxylic Acids. *Adv. Synth. Catal.* **2007**, *349*, 1475–1480. https://doi.org/10.1002/adsc.200700040.

(37) Palmieri, A.; Gabrielli, S.; Ballini, R. Michael Reaction of Nitroalkanes with β-Nitroacrylates under a Solid Promoter: Advanced Regio- and Diastereoselective Synthesis of Nitro-Functionalized α,β-Unsaturated Esters and 1,3-Butadiene-2-Carboxylates. *Adv. Synth. Catal.* **2010**, *352*, 1485–1492. https://doi.org/10.1002/adsc.201000142.

(38) Juhl, M.; Laursen, S. L. R.; Huang, Y.; Nielsen, D. U.; Daasbjerg, K.; Skrydstrup, T. Copper-Catalyzed Carboxylation of Hydroborated Disubstituted Alkenes and Terminal Alkynes with Cesium Fluoride. *ACS Catal.* **2017**, *7*, 1392–1396. https://doi.org/10.1021/acscatal.6b03571.

(39) Denmark, S. E.; Cresswell, A. J. Iron-Catalyzed Cross-Coupling of Unactivated Secondary Alkyl Thio Ethers and Sulfones with Aryl Grignard Reagents. *J. Org. Chem.* **2013**, *78*, 12593–12628. https://doi.org/10.1021/jo402246h.

(40) Shenouda, H.; Alexanian, E. J. Manganese-Catalyzed Stereospecific Hydroxymethylation of Alkyl Tosylates. *Org. Lett.* **2019**, *21*, 9268–9271. https://doi.org/10.1021/acs.orglett.9b03706.

CHAPTER 4. Redox Neutral Ni-Catalyzed Direct Carboxylation of Unactivated Secondary Alkyl Bromides

Project done in collaboration with: Dr. Jacob Davies and Dr. Ha Phan. The results presented are a combination of the contribution of all the people listed above.

4.1. Introduction

The birth of photoredox catalysis has opened new avenues for methodology development. Particularly, as has been discussed in the previous chapters of the present thesis, photoredox catalysis has unearthed previously unattainable one-electron reactivity, generating open-shell intermediates under mild reaction conditions, enabling a plethora of diverse transformations.[1,2] Among other fields, photoredox catalysis has been employed within the context of carboxylation chemistry for the generation of carboxylic acids. A notable example in such context is the photochemical hydrocarboxylation of *unactivated* alkenes with CO_2 through the corresponding CO_2 radical anion (CRA) (Scheme 4.1).[3] In this scenario, the excited photocatalyst undergoes oxidative quenching with DIPEA, generating a reduced PC^{-1} intermediates which can be photoexcited under the light irradiation employed. Such highly reducing $*PC^{-1}$ species is able to reduce CO_2 to the CRA, which inserts into an *unactivated* olefin. The newly formed alkyl radical **3** engages in a HAT process with DIPEA to yield the desired carboxylate product.

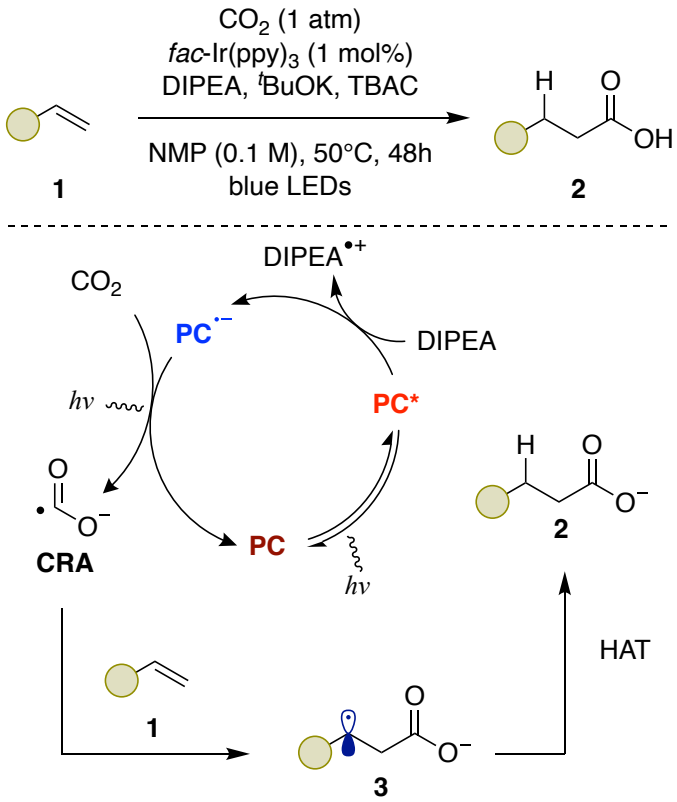

Scheme 4.1: Yu's hydrocarboxylation of unactivated olefins.

This approach allowed for an efficient carboxylation of alkenes using CO_2 as C1 source, bypassing the need for transition metal catalysts. Although representing an elegant solution to a previously unmet challenge, the use of sacrificial reductants and a gas system - typically in the carboxylation arena[4] - limits the uptake at an industrial level when compared to a potential redox-neutral process that would make use of a safer and more user-friendly solid C1 synthon.[5] A cheap chemical, which can also be made in bulk from CO_2, is formic acid. The exploitation of its salts as potential CRA precursors makes it a chemical of high interest in this endeavor.

4.1.1. CO_2 radical anion

The one electron reduction of CO_2 gives rise to the CRA, a highly reducing species with a redox potential of -2.2 V vs SCE, as shown in 1984 by Vianello *et al.* in their seminal study on the electroreduction of styrene and benzonitrile with CO_2.[6] In their work, the authors report the first carboxylation of an activated olefin, styrene, using CO_2 in a

reducing environment by generation of the CRA (Scheme 4.2). Despite the apparent serendipity of the discovery, it was observed that benzonitrile (**BN**) was a good catalyst to generate the CRA in solution, yielding oxalate as sole product by CO2 dimerization. While attempting to translate this chemistry to styrene **4**, a harder to reduce substrate, the authors observed formation of 3-phenylpropiolic acid **6** along with doubly carboxylated phenylsuccinic acid **7**. This shows the direct addition of CO_2 into the double bond. After investigating the process with electrochemical methods, they suggested the formation of the CRA from CO_2, which could then add directly into the double bond of styrene, constituting the very first example of carboxylation with the CRA. Although the carboxylation of styrene with CO_2 happened at a very low potential (ca. -2.5 V vs SCE), mixing benzonitrile and styrene together in the presence of CO_2 decreased the potential needed for the carboxylation to -2.2 V vs SCE instead. This result ruled out the possibility of preliminary styrene reduction followed by addition to CO2, suggesting that benzonitrile acts as catalyst to generate the CRA, instead. The CRA is proposed to react with neutral styrene **4** by a radical addition mechanism. The authors suggested that the radical intermediate **5** can either be reduced further and then getting protonated by residual water (5 to 6) or react with another CRA to yield doubly carboxylated compound **7**. Nowadays, a more accepted mechanism for the formation of 7 would be radical-polar crossover of **5** to its corresponding benzylic anion followed by a nucleophilic carboxylation with CO_2.

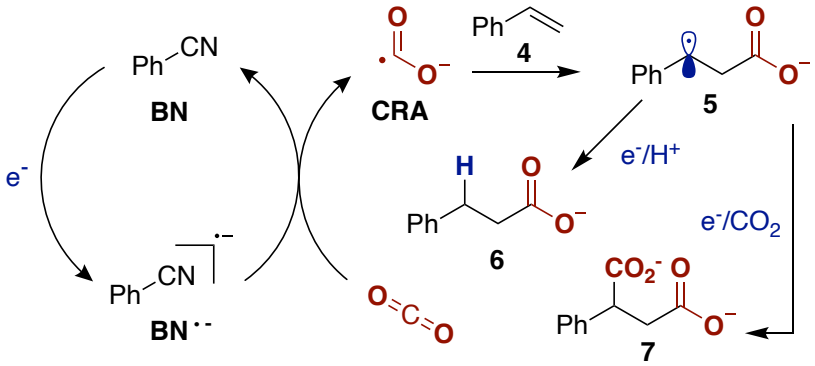

Scheme 4.2: Investigation of the CRA-mediated carboxylation of styrene by Vianello et al.

In 1993, Kubiak showed that the CRA could be photochemically generated by the photoexcitation of a tri-nickel cluster.[7] The CRA was trapped using cyclohexene, leading to the 1,2- dicarboxylated products as a cis/trans mixture. The Ni cluster used in this study required a very short wavelength (~300 nm) for productive photoinduced electron transfer (PET) with CO_2 in a non-catalytic manner. After these two reports, the field became somewhat dormant until Jamison's report in 2017 on the synthesis of amino acids from amines in flow chemistry (Scheme 4.3).[8] The use of highly reducing p-

terphenyl as PC in a flow-chemistry setting allowed the direct single electron reduction of CO_2 and radical-radical coupling between the CRA and the *in situ* generated alpha amino radical. Although the scope was limited to alpha aryl amine, this protocol represented the first example of CRA generation through a photocatalytic manifold and paved the way to further developments.

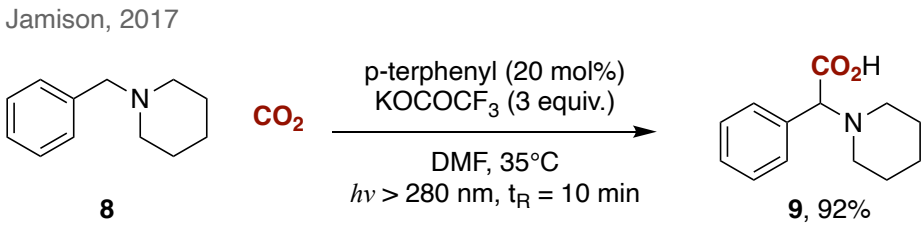

Scheme 4.3: Jamison's photocatalytic amino acid synthesis.

4.1.2. Hydrogen-Atom Transfer

Hydrogen-atom transfer (HAT) processes have been known for a long time and consist of the single-step transfer of a hydrogen atom from a neutral molecule to a radical species (Figure 4.1). When the HAT event takes place from a C-H bond, a C-centered radical is generated. While HAT processes have been known to happen through thermal processes with metals,[9] or, more commonly, using azobisisobutyronitrile (AIBN) , the emergence of photochemistry led to a renaissance in HAT-based synthetic methods.[10,11]

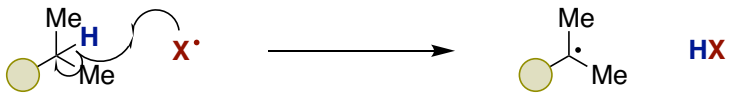

Figure 4.1: Hydrogen atom transfer process.

HAT can be utilized as a tool to generate CRA without using highly reducing conditions. Specifically, the relatively low bond dissociation energy (BDE) of the C-H bond in formate salts make them viable substrates for HAT events, liberating the sought-after CRA.[12]

4.1.3. Formate salts as reducing agents

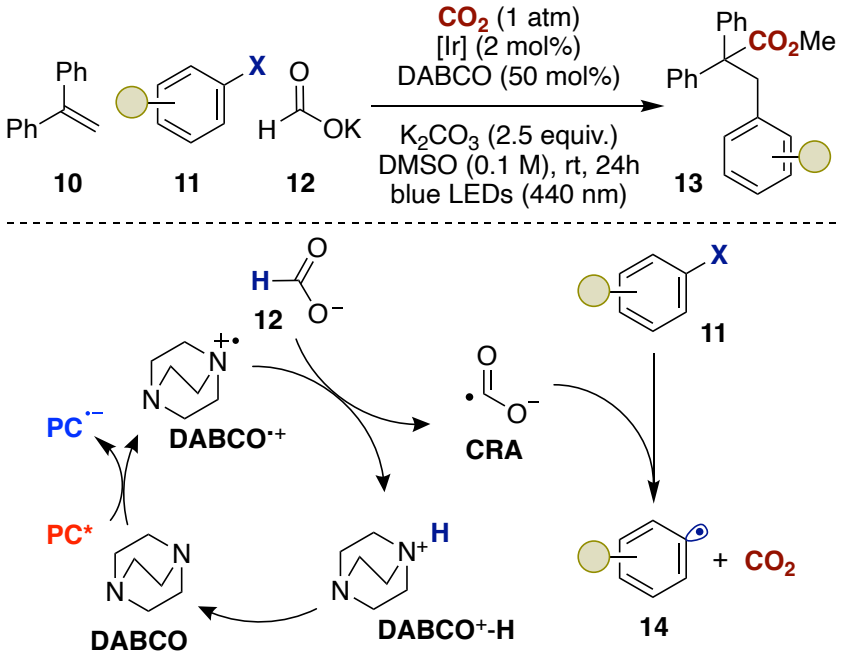

Scheme 4.4: Li's arycarboxylation of alkenes.

The first example of the use of formate salts in a carboxylation context was reported in 2020 by the group of Li (Scheme 4.4).[13] In this reaction, the CRA was not involved in the carboxylation step but rather enabled the reduction of aryl chlorides to their corresponding radicals. The odd-electron intermediates react with alkenes and *in fine*, give carboxylic acids from CO_2. As previously mentioned, the authors introduced a new way of generating the CRA using HAT. In this case, DABCO was used as a catalytic mediator between the PC and formate. The oxidation of DABCO to its radical cation by *PC leads to the generation of a good HAT reagent, able to abstract the hydrogen atom of formate. The newly formed CRA could reduce the aryl halides **11** to the corresponding radical **14**, which engages in further steps. The protonated DABCO, obtained after the HAT step, regenerates the free base by simple introduction of a stoichiometric inorganic base.

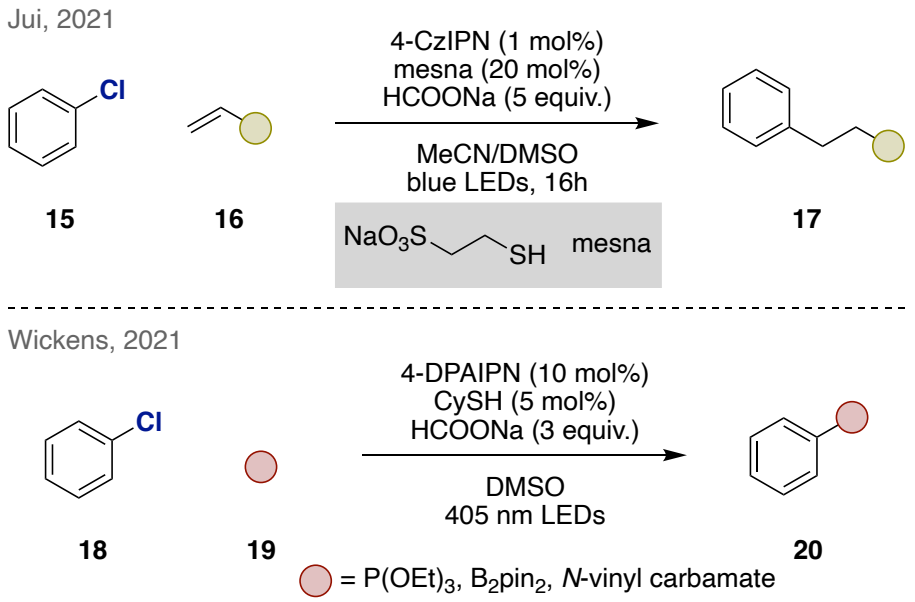

Scheme 4.5: Jui's and Wickens' methodologies based on the reduction of aryl chlorides with formate.

The following year, the Jui group reported a similar reaction employing more challenging aryl chlorides as aryl radical precursors to react with *unactivated* alkenes in a hydroarylation protocol (Scheme 4.5, top).[14] Thiols were used as HAT catalysts instead of DABCO. Shortly after, Wickens & coworkers independently reported a similar protocol consisting of a dechlorofunctionalization of aryl chlorides (Scheme 4.5, bottom).[15] This photocatalytic methodology was also based on the generation of the CRA by HAT, using a thiol as HAT catalyst.

4.1.4. Formate salts as carboxylation reagents

In 2021, the Wickens group disclosed the first example of hydrocarboxylation of activated alkenes by HAT-generated CRA as the carboxylation reagent using a thiol as HAT-catalyst.[16] Here, the protocol followed an earlier observation by Jui on the ability of CRA to reduce alkenes with more positive redox potential but adding to those with more negative potentials. In fact, Wickens demonstrated the systematic addition of formate salts derived CRA into activated alkenes, giving rise to homobenzylic carboxylic acids (Scheme 4.6). By deuterium-labeling experiment, the authors convincingly proved that the hydrogen atom added on the benzylic position does come mostly from formate, giving credit to the role of the thiol as hydrogen shuttle. The PC of choice, 4-DPAIPN was added in 0.1 mol%, effectively acting as a radical initiator for the thiol catalyst to

function. Adventitious water present in the solvent could also, after proton exchange with the thiol catalyst, act as a hydrogen source for the benzylic position when present. The group showcased a wide substrate scope, though, no reaction with *unactivated* olefins was observed. The following year, Yu & coworkers disclosed a hydrocarboxylation protocol based on conPET generated CRA, which targeted *unactivated* olefins. While it comes as a surprise that such strikingly different results were achieved by the two groups utilizing very similar conditions. As mentioned by the authors, a possible explanation might come from the fact that the CRA was generated less efficiently under Yu's conditions, reducing the concentration of such reactive species in solution, thus preventing their parasitic dimerization. Indeed, given that both the CRA and *unactivated* alkenes are considered electron-rich, their coupling is electronically mismatched, raising the activation barrier, thus leading to slow addition step.

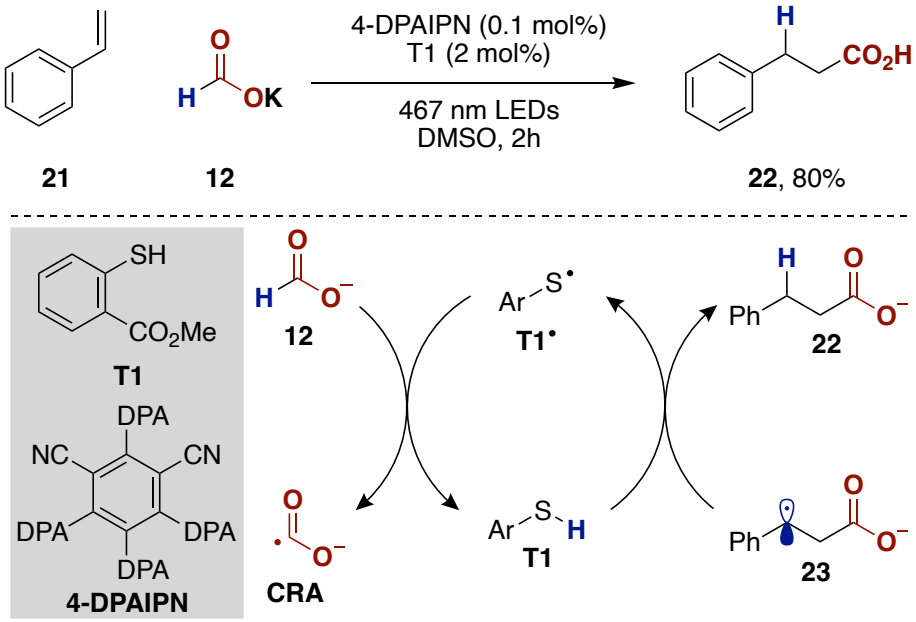

Scheme 4.6: Wickens' hydrocarboxylation of activated alkenes.

In 2023, the Wickens' group extended their hydrocarboxylation protocol to unactivated olefins, a HAT-mediated formation of CRA.[17] This methodology proves more attractive to industrial application, due to the use of solids reagents and milder reducing conditions. Mechanistic investigation showed that 4-DPAIPN was not required, as the thiol could be activated by sole irradiation of the reaction mixture system, providing even simpler reaction conditions.

4.1.5. Radiolabeling

As was discussed in the second chapter of this thesis, labeling of organic molecules is of utmost importance when it comes to studying the pharmacokinetic properties of a drug candidate. Specifically, pharmaceutical companies are able to perform ADME studies thanks to heavier isotope incorporation, which differentiates the masses of the starting compound and its metabolites within a complex mixture of non-labeled compounds. In turn, this allows for the quantitative measurement of metabolite formation and rates of excretion of the drug. Alternatively, radioactive isotopes rather than heavier but stable isotopes can be incorporate into a drug candidate. Among other radioactive isotopes, ^{14}C instead of ^{13}C, because it is particularly well-suited to ADME studies because of its β-decay mode and a half-life of 5700 years. The use of radioisotopes makes compounds more easily detected and quantified, thus representing an unvaluable tool for tracing the fate of a drug candidate within the body. As for ^{13}C incorporation, many methods have been developed, although special attention is placed to safety concerns, given the health hazards associated with radioactivity. Hence, radiochemists tend to favor more classical carboxylation methods, such as the carboxylation of Grignard reagents or cross-couplings of aryl halides, to the installation of labeled cyanide anions, followed by nitrile hydrolysis (Scheme 4.7).

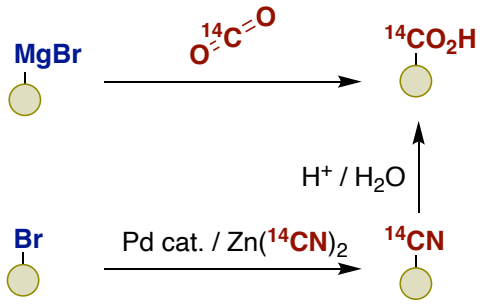

Scheme 4.7: Typical procedures used to access ^{14}C-labeled compounds.

Besides reaction yield and selectivity, additional metrics need to be considered, when performing a radiolabeling reaction: the radiochemical yield (RCY) and specific activity (SA). The RCY corresponds to the amount of radioactivity present in the product compared to the amount introduced with starting materials. This can be compared to a normal yield, being the amount of moles of product collected compared to the amount of moles of the limiting starting reagent used. The RCY is given in percent, with the related radioactivities measured in Becquerel (Bq) or Curie (Ci) (1 MBq = 27.03 μCi). It is important to note that the RCY is an *independent* value to the yield in moles. A reaction could have a low yield but high RCY, the opposite or any other combination. The RCY,

therefore, generally is a measure of how efficiently the radioisotope has successfully been incorporated in the product and not a report of how well the reaction itself worked, although in some cases, the RCY can be equal to the yield if the mechanism allows for the incorporation of precisely one equivalent of radioactive isotope and none of the so-called *cold* isotopes. The SA is the amount of radioactivity of a compound given per unit of moles, typically given in TBq/mol, KBq/nmol or Ci/mmol. It is measured by quantitatively comparing the mass spectra of a labelled compound to the spectra of its non-labeled counterpart, typically using the total ion count values. It is also possible to give the gravimetric specific activity (GSA), given in MBq/mg. The GSA is more easily measured, using the total activity of a sample and dividing it by its mass, and is therefore a measure of the activity per unit of mass rather than of unit per mole.

4.2. General aim of the project

In 2024, Martin and co-workers disclosed the first protocol for the carboxylation of *unactivated* secondary alkyl bromides.[18] While this methodology represents the first report in this context, some aspects could be improved – as previously described for with the work of Yu and Wickens. The reaction proceeds under reducing conditions and using gaseous CO_2 as a C1 source. Despite the very good results described in Martin's work, we wondered whether it would be feasible to further improve the system, combining our knowledge in Ni-based carboxylation chemistry with the recently described use of formate salts as carboxylation agents in a redox neutral process.

Figure 4.2: Redox-neutral Ni-photocatalyzed carboxylation.

4.3. Optimization

Our investigation started with combining the conditions previously reported by Martin for alkyl halide retained carboxylation and known procedures using formate salts as carboxylating reagents (Table 4.1).[13,18] A few PC were tried in both NMP and DMSO, using DABCO with inorganic bases at 40°C, targeting a HAT-based strategy. To our delight, product was found in 27% yield with 96% selectivity when the ligand (15 mol%) and metal source (10 mol%) were mixed in situ at 20°C.

Table 4.1: Initial screens.

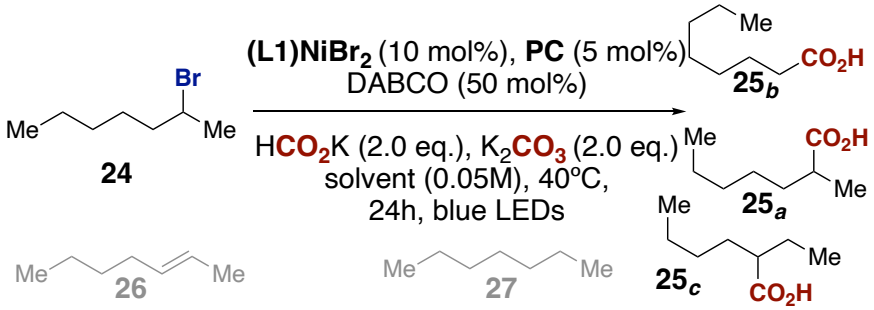

entry	PC	Solvent	Conv. / %	**20** / % (20_a)	**26+27**
1	4CzIPN	NMP	91	0	64+19
2[b]	4CzIPN	NMP	85	0	43+25
3	4CzIPN	DMSO	99	0	11+12
4	4CzIPN	NMP:DMSO	94	0	8+17
5	4DPAIPN	NMP	69	0	35+26
6	4DPAIPN	DMSO	99	0	28+16
7	$[Ir(ppy)_2dtbpy]PF_6$	NMP	100	0	50+32
8	$[Ir(ppy)_2dtbpy]PF_6$	DMSO	100	0	n.d.
9[c]	4DPAIPN	DMSO	100	27 (96)	28+16

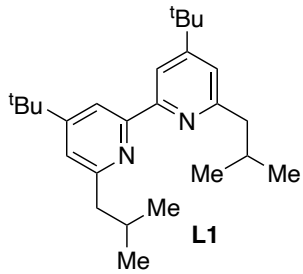

[a] determined by GC-FID after workup [b] no DABCO was used [c] reaction performed with $NiBr_2$·glyme (10 mol%) and L1 (15 mol%) at 20 ºC

Next, we screened different HAT catalysts, including S-or N-based compounds. The stoichiometry of DABCO was tested as well and control experiments were performed. DABCO proved to be the best catalyst when used in 50 mol%, resulting in 31% yield of the desired retained carboxylation product in 97% selectivity. The control experiments showed that both the HAT catalyst (Table 4.2, entry 3) and the formate salt (entry 8) are necessary for the reaction to occur. Removal of the inorganic base (entry 9) led to a decrease in yield and selectivity, showing the importance of its presence in the reaction mixture. Looking through this series of results, it is quite striking that only DABCO gave promising results, whilst no other catalyst was able to yield any product. Nonetheless, it is important to keep in mind that the HAT catalyst and the PC work as a binary system since their respective redox potentials need to match for productive SET. This fundamental aspects hints to the fact that only a dearth of HAT-catalysts is optimal for a given PC, and vice versa. In retrospect, this suggests that high throughput experiment (HTE) techniques would have been the perfect platform to find the best PC/HAT-catalyst combination.

Table 4.2: HAT catalyst screen.

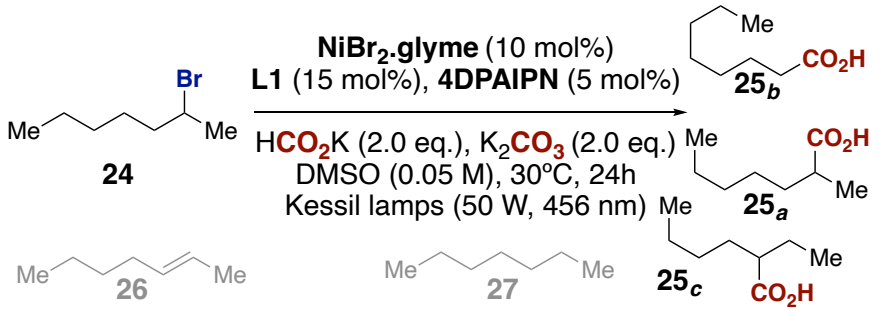

entry	HAT reagent (eq.)	Conv. / %	**20** / % (20_a)	**26+27**
1	DABCO (0.5)	100	31 (97)	14+10
2	DABCO (0.25)	100	13	9+10
3	-	99	0	15+9
4	*i*Bu_3N (0.25)	100	8	16+4
5	PhSH (0.25)	100	0	4+12
6	Methyl thioglycolate (0.25)	100	0	4+10
7	Quinuclidine (0.5)	94	0	6+10
8[b]	DABCO (0.5)	53	0	7+4
9[c]	DABCO (0.5)	100	22 (88)	28+16
10[d]	DABCO (0.5)	100	0	3+32

[a] determined by GC-FID after workup [b] no HCO_2K [c] no K_2CO_3 [d] no Ni/L. A Kessil lamp system was used here instead of a blue LED photoreactor.

We continued our investigation with the screening of photocatalysts. While the use of 3DPAFIPN proved promising (Table 4.3, entry 2), the results were unfortunately not reproducible. Given that no other result was satisfactory in terms of selectivity over yield, 4DPAIPN was selected as the optimal photocatalyst for further studies.

Table 4.3: Photocatalyst screen.

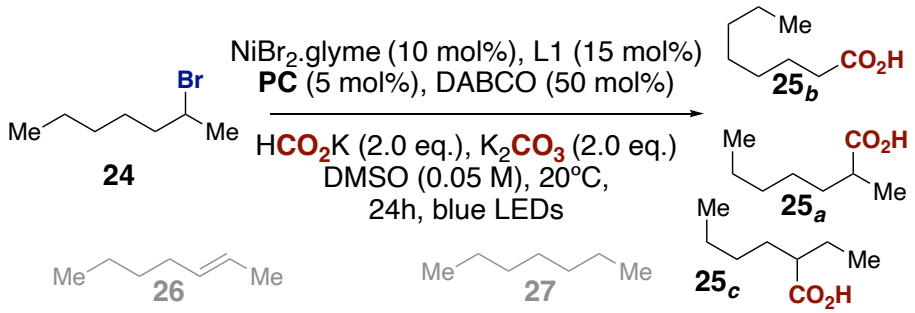

entry	PC	Conv. / %	**20** / % (20_a)	**26+27**
1	5CzBN	75	0	5+3
2	3DPAFIPN	100	48 (100)[c,d]	12+7
3	3DPA2FIPN	92	18 (96)	8+2
4	3DPAClIPN	91	17 (85)	6+2
5	3ClCzIPN	79	6 (n.d.)	5+3
6	4CzIPN[e]	23	0	2+3
7	3DPAFIPN[e]	98	49 (82)	7+6
8	3DPA2FIPN[e]	99	42 (59)	12+10
9[b]	TBADT	55	0	4+0
10[b]	$(p\text{-}F\text{-}C_6H_4)_2CO$	55	0	3+2

[a] determined by GC-FID after workup [b] no DABCO was added [c] 46% isolated but unable to reproduce this result. [d] only **2a** was detected. [e] performed in DMF.

The effect of the nature of the cation on the reaction performance was targeted next (Table 4.4). We reasoned that different cations might have an impact on the solubility of the salts or other species in solution - therefore on reaction kinetics indirectly - but also act as potential Lewis acids. The results indicated that the cations of choice had little effect on the selectivity but more pronounced effect on the yield. The best combinations were found with potassium formate while the carbonate could bear potassium, cesium or be changed to potassium phosphate without negatively impacting the outcome of the reaction. The addition of a crown-ether (entry 7) had a slight detrimental effect and was therefore deemed unnecessary.

Table 4.4: Salts screen.

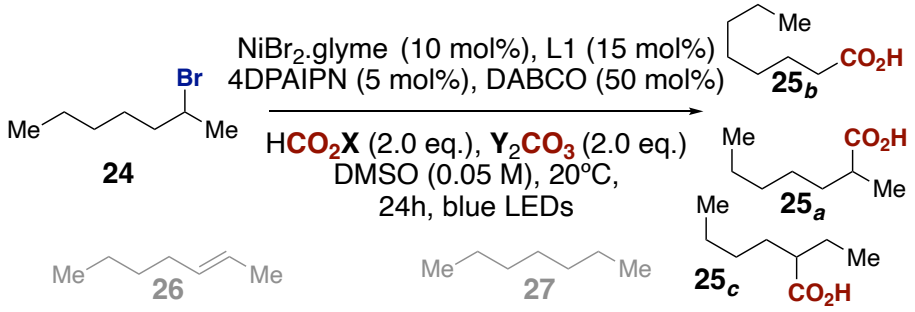

entry	X= Y=	Conv. / %	**20** / % (20_a)	**26+27**
1	K, K	100	32 (99)	12+7
2	Na, K	94	12 (100)[b]	8+13
3	Cs, K	99	7 (100)[b]	11+10
4	NH_4, K	73	4 (100)[b]	4+21
5	K, Cs	100	31 (98)	15+5
6	K, K_3PO_4	100	31 (98)	14+9
7[c]	K, K	100	29 (97)	6+1

[a] determined by GC-FID after workup [b] only **2a** was detected. [c] 18-crown-6 (2 eq.) was added.

A few solvents gave higher yields than DMSO, but the selectivity was consistently lower (Table 4.5). Nonetheless, we chose DMF to conduct further studies, due to a better balance between yields and selectivity (entry 3).

Table 4.5: Solvent screen.

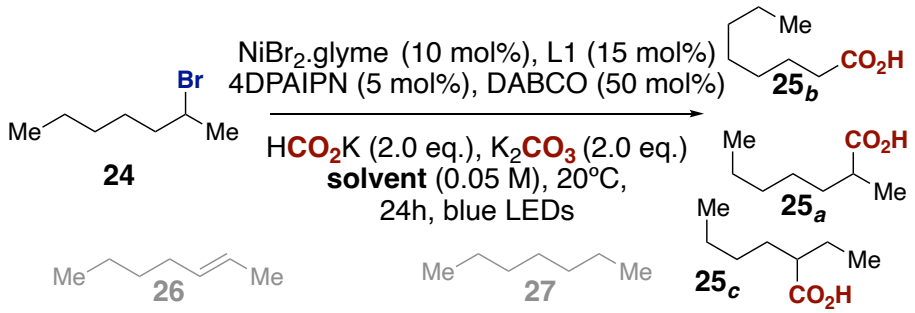

entry	**Solvent**	Conv. / %	**20** / % (20_a)	**26+27**
1	MeCN	76	6 (94)	16+10
2	THF	13	0	2+4
3	DMF	100	50 (83)	9+9
4	DMA	90	37 (76)	8+11
5	NMP	90	35 (67)	10+8
6	Acetone	98	0	15+30
7	DCM	100	11 (82)	5+21
8	DMSO	100	32 (99)	12+7
9	DMSO (0.08 M)	100	38 (98)	11+2
10	DMSO (0.1 M)	100	29 (98)	10+3

[a] determined by GC-FID after workup

Using DMF as solvent, we embarked in a second round of screening of salts, bases, and temperature (Table 4.6). We found that superior results were obtained conducting the reactions at 10°C rather than at 20°C. Moreover, using cesium cation for both formate and carbonate salts or a combination of potassium formate with cesium pivalate at 10°C, afforded 25a in 55% or 45% yield, respectively, and in almost perfect selectivity in both cases (entries 7 and 9). We therefore continued our investigation based on these results.

Table 4.6: Salt, base and temperature screen.

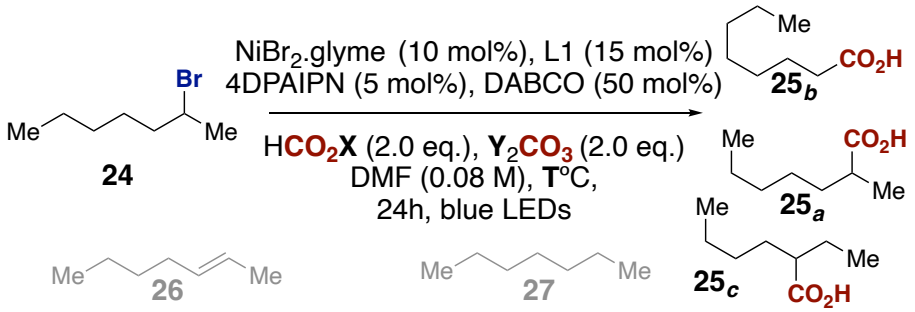

entry	X= Y=	T / °C	Conv. / %	**20** / % (20_a)	**26+27**
1	K, K	20	100	50 (83)	9+9
2	K, K	10	91	61 (88)	6+8
3	Cs, K	10	100	59 (97)	5+8
4	Cs, K	20	100	34 (96)	7+10
5	K, Cs	10	99	54 (93)	7+6
6	K, Cs	20	99	50 (92)	8+7
7	Cs, Cs	10	100	55 (98)	5+8
8	K, CsOAc	10	100	49 (95)	7+10
9	K, CsOPiv	10	100	45 (98)	8+10
10	K, CsF	10	48	5 (n.d.)	3+14
11	K, $CsHCO_3$	10	99	60 (95)	8+8
12	K, Rb	10	100	48 (89)	9+9
13[b]	K, K	10	100	50 (82)	10+3
14[b]	K, K	10	97	45 (90)	10+9

[a] determined by GC-FID after workup [b] 18-crown-6 (2 eq.) was added. [c] 4 eq. of HCO_2K was added.

4.4. ^{14}C labeling

Based on a collaboration with AstraZeneca, we decided to use this methodology for the incorporation of radioactive ^{14}C into organic molecules using labeled formate salt as carboxylating agent. The state-of-the-art strategy of making carbon-labeled carboxylic acids relies either on gaseous systems (CO_2 or CO), on solids CO_2 precursors (Ba_2CO_3), or through a two-step synthesis protocol using labeled cyanide salts first, then hydrolyzing the corresponding nitrile group.[19-22] However, unactivated secondary alkyl carboxylic acids, with only one report, can only be accessed with Martin & coworker's protocol,[18] employing gaseous CO_2 with an overpressure of 1 bar, constituting a hazardous method in the context of radiolabeling chemistry. Therefore, the use of formate, a non-volatile compound would prove useful. At the time of the collaboration, the conditions of the reaction were not fully optimized and corresponded to what is shown in Table 4.6. For commercial availability reasons, we could not get labeled cesium formate, thus preventing the application of the conditions shown in entry 7. Instead, we decided to pursue the conditions using cesium pivalate as a base along with potassium formate as carboxylating agent (entry 9). After a few attempts to reproduce our results with naturally abundant ^{12}C potassium formate in the AstraZeneca laboratories in Göteborg in Sweden, we managed to obtain the desired product in 39% isolated yield with excellent selectivity (Scheme 4.8).

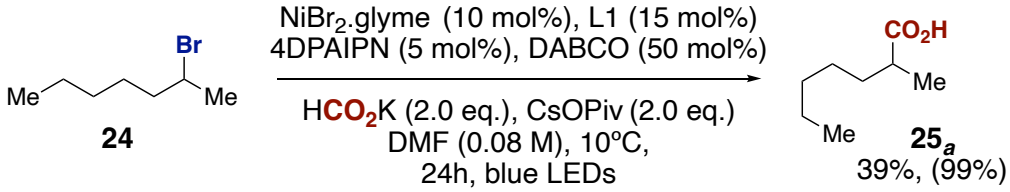

Scheme 4.8: Reproducing our initial results at AstraZeneca, Göteborg. Isolated yield.

Before being able to try the same reaction using ^{14}C-labeled formate salt, the experimental protocol had to be modified for incorporation of the radioactive compound. Indeed, while the *cold* reaction is performed in a classical fashion, adding all solids in the flask followed by all liquids, the radioactive ^{14}C potassium formate was purchased as a 2 M aqueous solution, which would not be compatible with our reaction conditions. Therefore, different procedures were tried before continuing with our studies. At this stage, it was considered not necessary to achieve full isotope labelling in the carboxylation reaction, therefore, and to limit the doses of radioactivity to handle, both *hot* and *cold* formate salts were used in the reactions, thus "diluting" the ^{14}C content

The final experimental protocol (Figure 4.3) consisted in pre-mixing the nickel precursor, the ligand, the PC, and DABCO in a Schlenk tube, followed by exchange of atmosphere to nitrogen and addition of dry DMF. In a second Schlenk flask, the desired amount of *hot* aqueous formate solution was dried - by heating under a nitrogen flow, first, and vacuum, then - the *cold* formate and the appropriate base were then added. At this stage, the Ni-containing stock solution was added into the second Schlenk flask under nitrogen atmosphere, followed by the starting material, 2-bromoheptane **19**. The sealed tube was then placed in a water-cooled photoreactor and irradiated for 24h before work up and purification.

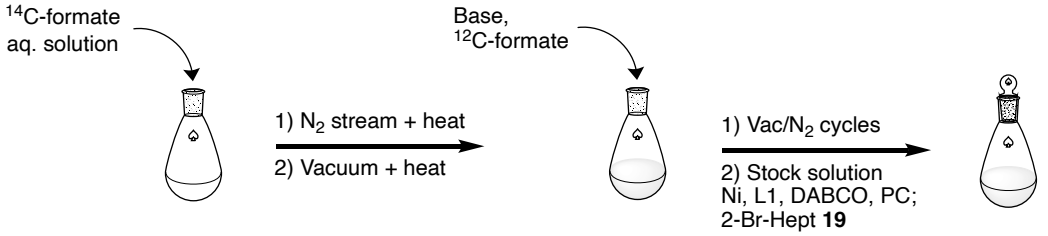

Figure 4.3: Visual representation of the protocol used for radiolabeling.

The procedure was standardized employing *cold* formate only, in order to minimize radioactive handling. With a good procedure in hand, we tested the reaction with *hot* formate, and we were delighted to find that very similar yields and selectivity were obtained with respect to the *cold* version (Scheme 4.9). The obtained RCY was 34%, along with a selectivity of 94%, determined by radio-HPLC. The measured SA was of 0.31 TBq/mol.

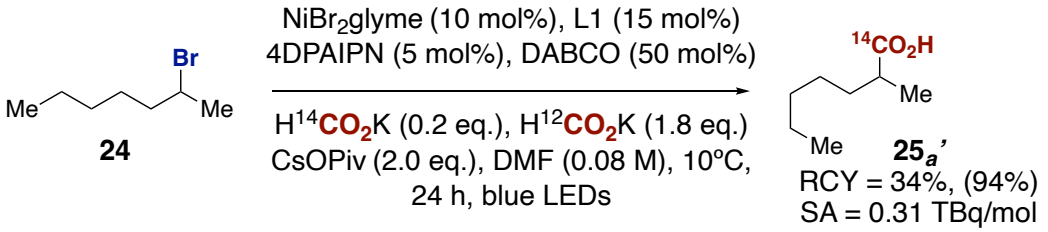

Scheme 4.9: Radiocarboxylation of a secondary alkyl bromide.

In order to demonstrate the generality of this radiolabeling method, two more alkyl bromides were tried, using 100 MBq of *hot* formate (Figure 4.4). Nabumetone-derived compound **21** was obtained in a RCY of 35% with a SA of 0.24 TBq/mol and >99% regioselectivity. Unfortunately, we were not able to obtain the Troglitazone-derived compound **22** in an analytically sufficient quantity to carry out all the required measurements. Considering the relative structural complexity of this molecule, the presence of an acidic proton, and of a S-containing moiety, it is conceivable that the

reaction did not work at all. The endocyclic sulfur atom could also be susceptible to SET processes with the photocatalyst, potentially leading to a decomposition of the starting material along with premature ending of the reaction. Additionally, three benzylic methyl groups are present, which are notoriously reactive under HAT conditions.

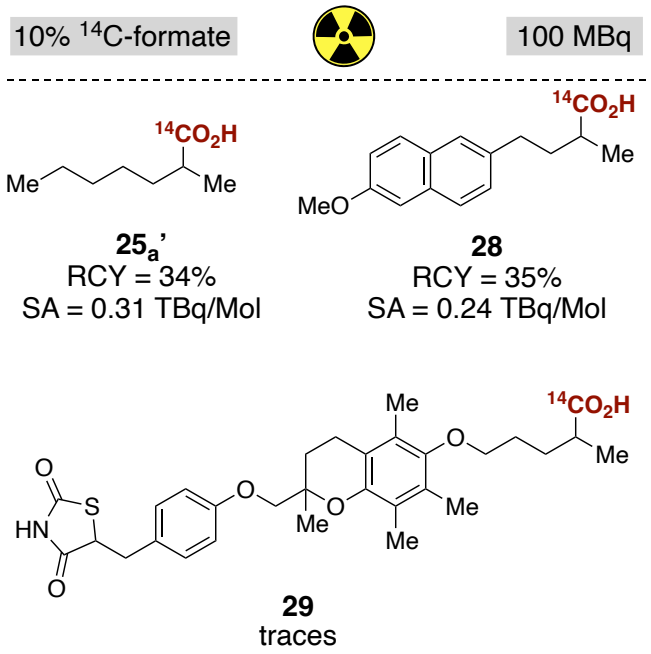

Figure 4.4: Summary of the radiolabeling scope.

4.5. Reproducibility issues

During the development of a protocol for the radiolabeling of secondary alkyl bromides with formate, the *cold* reaction was still being optimized in parallel (*vide infra*). Although the optimization campaign highlighted some excellent results, these could not be reproduced.

Salt combinations were investigated again, including a broader temperature range going down to 0°C (Table 4.7). The results showed that cesium formate seems to be giving better selectivity along with slightly higher yields, with low temperatures also being beneficial (entries 8-11). Although the reactions were set up in the glovebox, we reasoned that the solvent and salts employed are known to be particularly hygroscopic, so we investigated to understand if traces of water could have a detrimental effect on the reaction (entries 5-7). The experimental finding clearly pointed towards the negative

effect of water on the system. Simply setting the reaction on the bench, under air, before transferring to the glovebox for solvent addition already decreased the reaction regioselectivity (entry 5), while conducting the reaction completely under air (entry 6) or with intentionally added water (entry 7) were even worse in both yields and selectivity.

Table 4.7: Second screen of salt combinations with temperature.

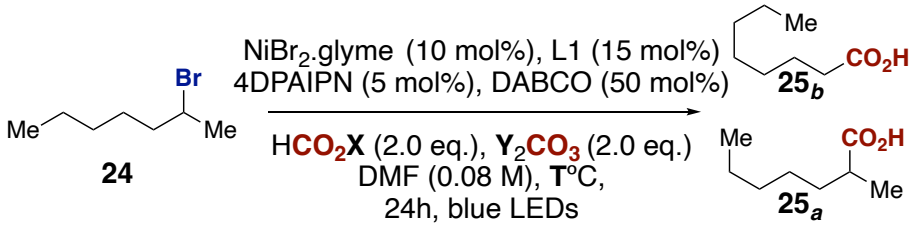

entry	X= Y=	T / °C	Conv. / %	20 / % (20_a)
1	K, K	20	100	50 (83)
2	K, K	10	91	61 (88)
3	K, K	5	80	48 (85)
4	K, K	0	67	36 (83)
5[b]	K, K	5	98	50 (85)
6[b,c]	K, K	5	97	37 (89)
7[b,d]	K, K	5	97	33 (95)
8	Cs, K	20	100	34 (96)
9	Cs, K	10	100	59 (97)
10	Cs, K	5	99	69 (97)
11	Cs, K	0	95	75 (99)
12	Cs, Cs	10	100	55 (98)
13	K, Cs	20	99	50 (92)
14	K, Cs	10	99	54 (93)

[a] determined by GC-FID after workup. [b] all reaction components added on the bench. [c] under air. [d] with 2 eq. H_2O added.

We therefore pursued further optimization aiming at improving the selectivity with potassium formate (Table 4.8). The first observation was that using this salt in combination with cesium pivalate gave excellent selectivity (entries 1-4), in accordance to previous results (table X, entry X). The yield could be raised to 63% when temperature decreased to 0°C. When setting the reaction at 5°C but weighing solids on the bench, the yield was negatively impacted, decreasing from 55% to 35%. If the same reaction was performed under air with additional water added, no product was obtained. Other bases were tried but did not give satisfactory selectivity and were therefore not considered for

further studies. However, at this point we faced significant reproducibility issues, with the last reproducible results being the ones shown in Table X, entry 2, which are the same used during the radiolabelling studies.

Table 4.8: Screening of other reaction parameters, using potassium formate, to improve the regioselectivity of the transformation.

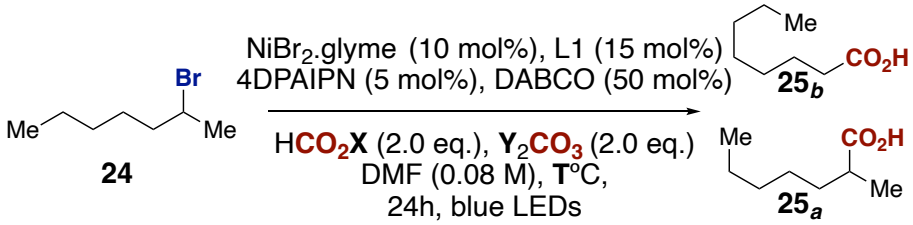

entry	X= Y=	T / °C	Conv. / %	20 / % (20_a)
1	K, CsOAc	10	100	49 (95)
2	K, CsOPiv	10	100	45 (98)
3	K, CsOPiv	5	99	55 (98)
4	K, CsOPiv	0	95	63 (98)
5[b]	K, CsOPiv	5	100	35 (98)
6[b,c]	K, CsOPiv	5	98	24 (97)
7	K, CsF	10	98	5 (-)
8	K, $CsHCO_3$	15	48	60 (95)
9	K, $CsHCO_3$	5	99	61 (93)
10	K, $CsHCO_3$	0	89 / 81	55 (90) / 46 (83)
11[b]	K, $CsHCO_3$	5	99	57 (93)
12[b,c]	K, $CsHCO_3$	5	44	1 (-)
13	K, Rb	10	100	48 (89)
14	Na, CsOPiv	10	78	35 (76)

[a] determined by GC-FID after workup. [b] all reaction components added on the bench. [c] under air with H_2O (2 equiv.) added.

The results shown on Table 4.9 are part of the reproducibility issues, and were obtained within a short timeframe, which were not reliable on the long term. In this series of results, the selectivity was always excellent (>96%) along with high yields. Due to the surprisingly positive results, when compared to previous findings, and their unreproducible nature, we decided to investigate the effect external factors, such as the presence of impurities or the potential use of wrong/mislabelled reagents.

Table 4.9: Final optimization attempts.

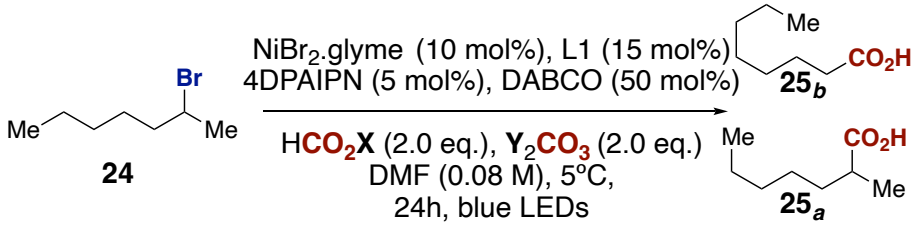

entry	X= Y= (eq.)	Deviation	Conv. / %	**20** / % (20_a)
1	Cs (2), K (2)	-	99	97 (99)
2	Cs (1), K (2)	-	89	71 (98)
3	Cs (2), K (1)	-	99	92 (99)
4	Cs (1), K (1)	-	87	72 (96)
5	Cs (1.5), K (1.5)	-	90	72 (97)
6	Cs (2), K (2)	(L1)$NiBr_2$	90	83 (99)
7	Cs (2), K (2)	(L1)$NiBr_2$, 0.13 M	89	79 (98)
8	Cs (2), K (2)	(L1)$NiBr_2$, 0.2 M	81	69 (98)
9	Cs (2), K (2)	(L1)$NiBr_2$, 0.05 M	94	89 (99)

[a] determined by GC-FID after workup

Our initial rationalization for the loss of reactivity was the presence of water traces but the high yields observed in Table 4.9 could not be reproduced even after careful drying solvents – monitored by Karl-Fisher analysis - and monitoring all the reagents used. Given that 2-bromoheptane **24** was homemade by an Appel reaction from the corresponding alcohol, we wondered whether traces of triphenylphosphine or triphenylphosphine oxide in the compound would be helping the reaction, acting as potential ligand for the metal center. We therefore performed control experiments using various amounts of added phosphine (Table 4.10). However, the addition of triphenylphosphine from 1 to 20% (entries 2-4) delivered no product, as well as using triphenylphosphine oxide (entry 5). When trying the reaction using a phosphine additive, without any bipyridine ligand – to avoid competition for binding to the metal center - (entry 6), again no product was formed.

We then tested whether using the more soluble ammonium formate could improve the reactivity, but, despite the excellent regioselectivity, only 12% yield was attained (entry 7). Although this was not nearly as good as we expected, the reaction proved to work to some extent.

Table 4.10: Effect of triphenylphosphine and triphenylphosphine oxide on the reaction outcome.

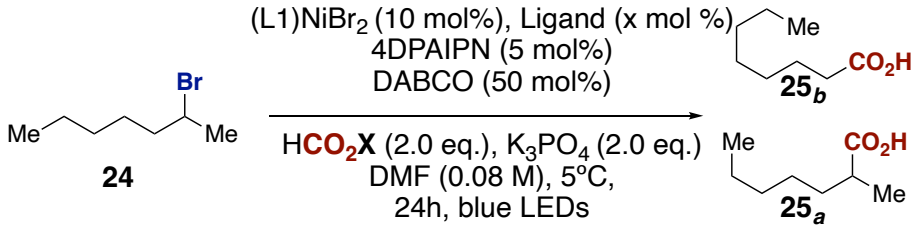

entry	Ligand	Formate	Conv. / %	**20** / % (20_a)
1	No ligand	HCOOCs	-	-
2	PPh_3 1%	HCOOCs	-	-
3	PPh_3 5%	HCOOCs	-	-
4	PPh_3 20%	HCOOK	-	-
5	$P(O)Ph_3$ 1-5%	HCOOCs	-	-
6[b]	PPh_3 20%	$HCOONH_4$	-	-
7	PPh_3 20%	$HCOONH_4$	-	12 (95)

[a] determined by GC-FID after workup. [b] $NiBr_2$.dme was used as nickel source.

At this point, we decided to pause the project and focus on other methodologies ongoing in the group.

Soon after this decision, Fu and co-workers published the metallaphotoredox Ni-catalyzed carboxylation of aryl halides with formate salts, demonstrating the feasibility of a closely related transformation using the same approach we have attempted.[23] Intriguingly, the authors showcased the essential role of the bipyridine/phosphine binary system for the successful realization of the desired transformation.

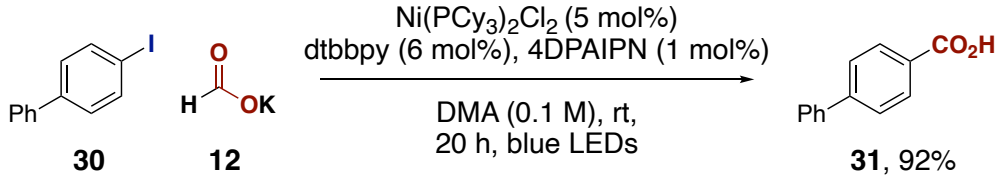

Scheme 4.10: Fu's metallaphotoredox Ni-catalyzed carboxylation of aryl halides with potassium formate.

This report suggests that residual P-containing impurities might play a key role in our system, too, auguring well for a future successful implementation of our target reaction.

4.6. Conclusions

An extension to our previous protocol, aiming at synthesizing secondary alkyl carboxylic acids from secondary alkyl bromides is described. The reaction is redox neutral and based on nickel metallaphotoredox chemistry, wherein a highly reactive CO_2 radical anion is employed as both carboxylating agent and reductant. The protocol has been modified in order to be used within the context of radiolabeling, giving incorporation of ^{14}C in target products. The radiolabeling proved to be working as well as the normal reaction using *cold* formate. Therefore, by improving the general outcome of the methodology, higher amounts of labeling products could likely be obtained. The methodology was not fully optimized since reproducibility issues arose, resulting in pausing further development. Early investigation aiming at solving this issue and the precedent furnished by a recently published work by the Fu group suggests that the incorporation of both a bipyridine and phosphine ligand might be key for future improvements of the reaction.

4.7. Experimental details

Analytical methods.

^{1}H, ^{2}H, ^{19}F and ^{13}C NMR spectra were recorded on Bruker 300 MHz, Bruker 400 MHz and Bruker 500 MHz at 20 °C. All ^{1}H NMR spectra are reported in parts per million (ppm) downfield of TMS and were calibrated using the residual solvent peak of $CHCl_3$ (7.26 ppm), unless otherwise indicated. All ^{13}C NMR spectra are reported in ppm relative to TMS, were calibrated using the signal of residual $CHCl_3$ (77.16 ppm). Coupling constants, *J*, are reported in Hertz. Melting points were measured using open glass capillaries in a Büchi B540 apparatus. Gas chromatographic analyses were performed on Hewlett-Packard 6890 gas chromatography instrument with FID detector. Flash chromatography was performed with EM Science silica gel 60 (230-400 mesh) using bromocresol, potassium permanganate, or cerium molybdate as TLC stains. SFC analysis was carried out on an Agilent 1260 Infinity II SFC system.
The procedures described in this section are representative. Thus, the yields may differ slightly from those given in the Schemes of the manuscript.

Light source.

All reactions were performed with 451 nm LEDs (OSRAM Oslon® SSL 80 royal- blue LEDs), which were installed at the bottom of a custom-made 8 flat-bottom Schlenk tubes holder, equipped with a cooling system (the temperature was set at 10 °C, or different if stated) and a magnetic stirrer (~ 1000 rpm).

Reagents.

Commercially available materials were used as received without further purification. $NiBr_2$.glyme (97% purity) was purchased from Aldrich, anhydrous DMA and DMSO (99.5% purity) were purchased from Acros or Scharlau and dried additionally when needed.

4.7.1. Optimization of the reaction conditions

General procedure.

An oven dried crimp vial containing a magnetic stir bar was brought into a glovebox. The vial was charged with $NiBr_2$.dme (0.10 equiv., 0.025 mmol), the formate salt (1.0 equiv., 0.25 mmol), 4DPAIPN (0.05 equiv., 0.0125 mmol, 10 mg), DABCO (0.5 equiv., 0.125 mmol, 14 mg), the base (2.0 equiv., 0.5 mmol) and the solvent. The vial was then sealed with a crimped cap and taken out of the glovebox to be placed in a temperature controlled photoreactor with water cooling at a set temperature (which gives an internal reaction temperature of ca. 5 °C superior to the set one) and stirred for 24 h in the presence of continuous irradiation with blue light (451 nm, 2 W LED). The reaction mixture was quenched with 2 M HCl aq. solution (5 ml) to release free acid by protonation of the carboxylate salt, diluted with ethyl acetate (10 ml), and washed three times with an aqueous 1 M HCl solution. The organic phase was collected, dried over $MgSO_4$, and filtered. Internal standard (anisole) was added to determine GC-Yield and selectivity of regioisomers.

4.7.2. Starting materials' preparation

Compounds **24** and **28-Br** were known and prepared according to literature procedures.[18]

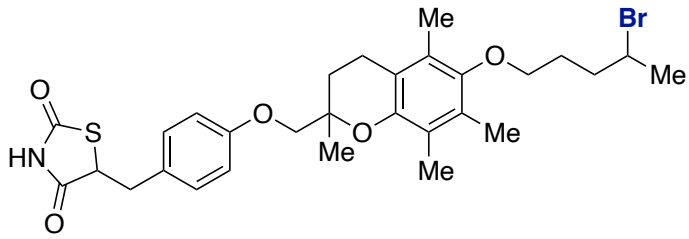

5-(4-((6-((4-bromopentyl)oxy)-2,5,7,8-tetramethylchroman-2-yl)methoxy)benzyl)thiazolidine-2,4-dione (29-Br). A solution of troglitazone (73.2 mg, 0.17 mmol) and potassium carbonate (27.5 mg, 0.20 mmol) in DMF (1 ml) was stirred for 1h at room temperature. Then, 1,4-dibromopentane (0.027 ml, 0.20 mmol) was subsequently added. The mixture was stirred at room temperature for 24h. After completion, the mixture was extracted with EtOAc and washed with brine. The organic layer was dried and concentrated. The residue was purified by flash chromatography (Heptane:EtOAc 30%) to afford 5-(4-((6-((4-bromopentyl)oxy)-2,5,7,8-tetramethylchroman-2-

yl)methoxy)benzyl)thiazolidine-2,4-dione **29-Br** (97 mg, 99 %) as an off white gum. **^{1}H NMR (500 MHz, $CDCl_3$):** δ (ppm) = 7.2 – 7.1 (m, 2H), 6.9 – 6.8 (m, 2H), 4.4 (ddd, *J* = 8.7, 3.9, 2.2 Hz, 1H), 4.1 – 4.0 (m, 1H), 4.0 (d, *J* = 9.0 Hz, 1H), 3.9 (d, *J* = 1.5 Hz, 1H), 3.6 – 3.5 (m, 2H), 3.4 (dtd, *J* = 14.2, 3.8, 1.5 Hz, 1H), 3.1 (dddd, *J* = 14.1, 8.6, 3.9, 1.6 Hz, 1H), 2.7 – 2.6 (m, 2H), 2.2 (s, 3H), 2.1 (d, *J* = 6.4 Hz, 7H), 1.9 (dt, *J* = 13.5, 6.7 Hz, 1H), 1.8 – 1.5 (m, 7H), 1.4 (s, 3H); **^{13}C NMR (126 MHz, $CDCl_3$):** δ (ppm) = 174.0 (d, *J* = 3.0 Hz), 171.2 (d, *J* = 2.5 Hz), 158.7, 145.1 (d, *J* = 5.7 Hz), 130.6 (d, *J* = 6.2 Hz), 127.6, 122.7, 121.4, 118.7, 117.4, 115.0 (d, *J* = 4.0 Hz), 74.1, 72.7 (d, *J* = 3.9 Hz), 51.7 – 51.4 (m), 50.5, 50.4, 41.1 (d, *J* = 12.5 Hz), 37.7, 38.1 – 37.4 (m), 28.8, 26.5 (d, *J* = 6.3 Hz), 26.1, 25.9, 22.8, 20.4, 12.3, 11.9, 11.4; **MS** calcd. for ($C_{29}H_{37}BrNO_5S$) $[M+H]^+$: 590.16 found 590.20.

4.7.3. Radiolabeling

General Procedure 1 (GP1):

In a Schlenk flask were introduced 4,4'-di-tert-butyl-6,6'-diisobutyl-2,2'-bipyridine (L1) (14 mg, 0.04 mmol), $NiBr_2$.glyme (7.7 mg, 0.03 mmol), 4-DPAIPN (10.0 mg, 0.01 mmol), the alkyl bromide - if solid - (0.25 mmol) and DABCO (14.3 mg, 0.13 mmol). An inert atmosphere was set in the flask by performing three cycles of vacuum/N_2 backfilling. Then, DMF (3 mL) was added, and the solution was stirred at rt for 15 min. In a second Schlenk flask was added an aqueous solution of ^{14}C potassium formate (4.16 mg, 0.05 mmol, 100 MBq). Water was evaporated by heating gently the flask while flushing N_2 gas inside and then kept heating while putting the flask under vacuum for 15 min. Cesium pivalate (117 mg, 0.50 mmol) was added, followed by ^{12}C potassium formate- (38 mg, 0.45 mmol). An inert atmosphere was introduced in the flask through 3 cycles of vacuum/N_2 backfilling. Under a N_2 flow, 3 mL of stock solution from the first Schlenk flask was added, followed by the alkyl bromide - if liquid - (0.25 mmol). The Schlenk tube was then sealed and put on a water-cooled photoreactor (450 nm) for 24h. The reaction mixture was then quenched with an aqueous 3M HCl solution. Water (5 mL) was added, and the mixture extracted with Et_2O 3 times. The combined organic layer was washed twice with an aqueous 1M HCl solution and then extracted twice with an aqueous 2M NaOH solution. The layers were separated, and the aqueous phase was acidified using an aqueous HCl solution to obtain a slightly cloudy aqueous phase. This layer was finally extracted twice with Et_2O or EtOAc, from which the solvent evaporated *in vacuo* to give the pure product.

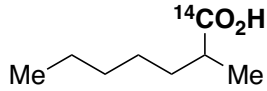

2-methylheptanoic-1-14*C* acid (25$_a$'). Following **GP1**, 2-bromoheptane **24** (45.0 mg, 39 µL, 0.25 mmol) afforded the title compound **20$_a$'** as a pale-yellow oil (17.01 MBq, RCY = 34%, 8.0 mg, 22%, 94% branched product, determined by radio-HPLC, SA = 0.31 TBq/mol). **^{1}H NMR (500 MHz, $CDCl_3$):** δ (ppm) = 2.5 (h, *J* = 6.9 Hz, 1H), 1.7 – 1.6 (m, 1H), 1.5 – 1.4 (m, 1H), 1.4 – 1.3 (m, 6H), 1.2 (dd, *J* = 7.1, 1.4 Hz, 3H), 0.9 – 0.8 (m, 3H); **^{13}C NMR (126 MHz, $CDCl_3$):** δ (ppm) = 183.4, 39.5, 33.6, 31.8, 27.1, 26.9, 22.6, 17.0, 14.2; **MS** calcd. for ($C_7{}^{14}CH_{15}O_2$) [M-H]$^-$: 145.11 found 145.05.

The additional peaks in the carbon NMR are attributed to the linear carboxylic acid side product.

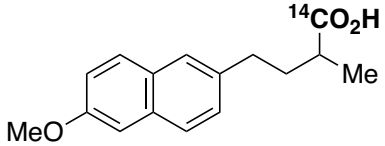

4-(6-methoxynaphthalen-2-yl)-2-methylbutanoic-1-^{14}*C* acid (28). Following **GP1**, 2-(3-bromobutyl)-6-methoxynaphthalene (54.3 mg, 0.25 mmol) afforded the title compound **28** as a white solid (17.32 MBq, RCY = 35%, 22.5 mg, 35%, >99% selectivity determined by radio-HPLC, SA = 0.24 TBq/mol). **^{1}H NMR (500 MHz, $CDCl_3$):** δ (ppm) = 7.7 – 7.7 (m, 2H), 7.6 (s, 1H), 7.3 – 7.3 (m, 1H), 7.2 – 7.1 (m, 2H), 3.9 (s, 3H), 2.9 – 2.8 (m, 2H), 2.6 (h, *J* = 7.0 Hz, 1H), 2.2 – 2.1 (m, 1H), 1.9 – 1.8 (m, 1H), 1.3 (d, *J* = 1.6 Hz, 3H); **^{13}C NMR (126 MHz, $CDCl_3$):** δ (ppm) = 183.3, 157.3, 136.7, 133.2, 129.2, 129.1, 127.8, 127.0, 126.5, 118.8, 105.8, 55.4, 39.0, 35.2, 33.4, 17.1; **MS** calcd. for ($C_{15}{}^{14}CH_{17}O_3$) [M-H]$^-$: 259.12 found 259.12.

4.7.4. NMR Spectra

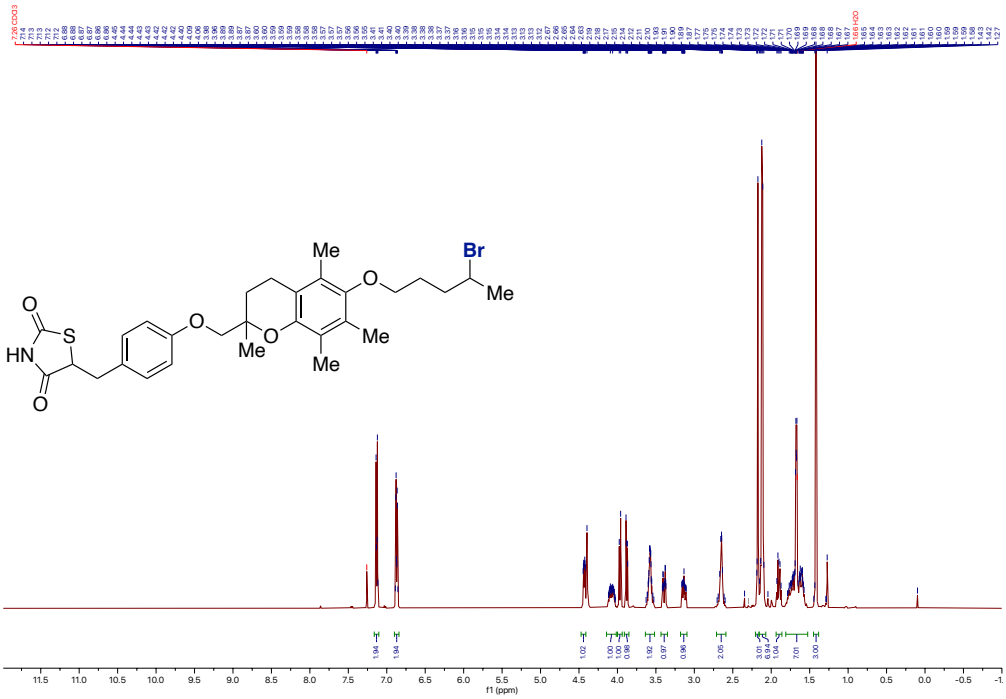

^{1}H spectrum (500 MHz, $CDCl_3$) of **29-Br**

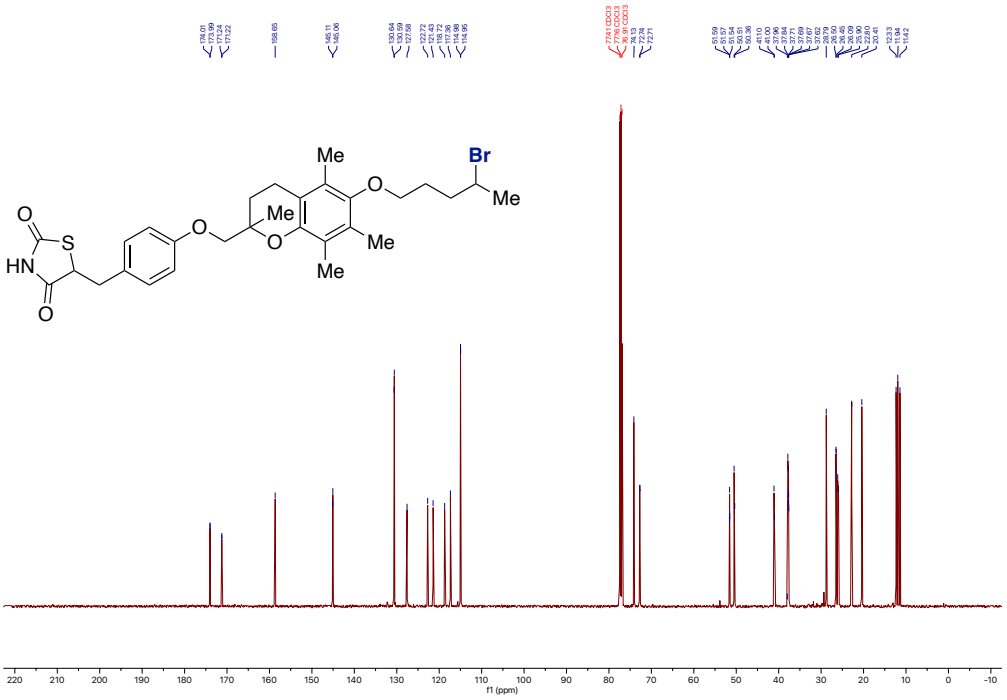

^{13}C spectrum (126 MHz, $CDCl_3$) of **29-Br**

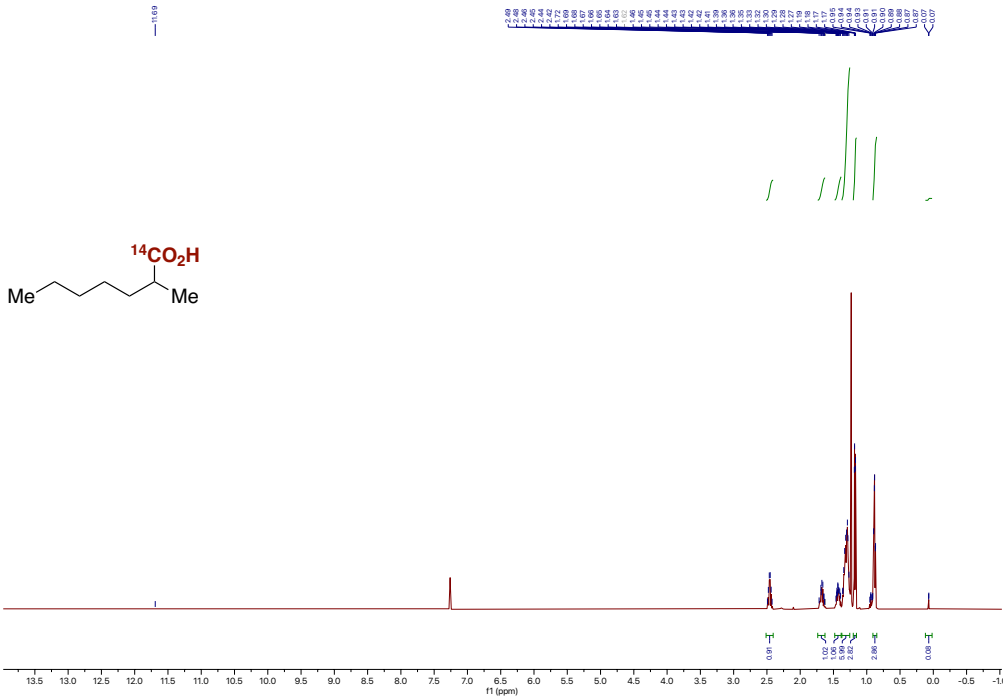

^{1}H spectrum (500 MHz, $CDCl_3$) of **25$_a$'**

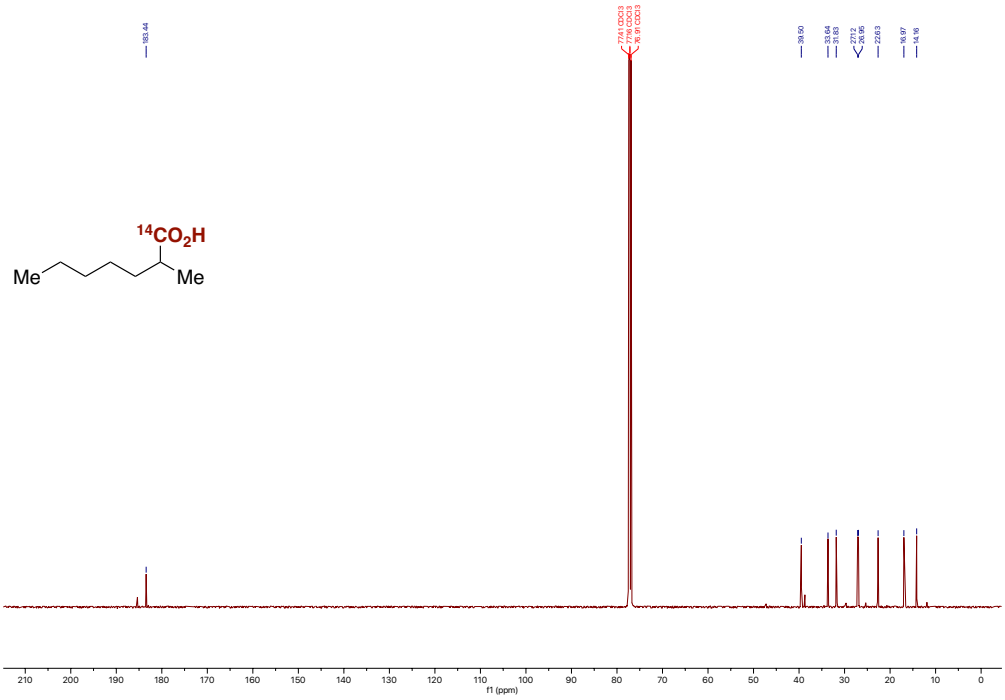

^{13}C spectrum (126 MHz, $CDCl_3$) of **25$_a$'**

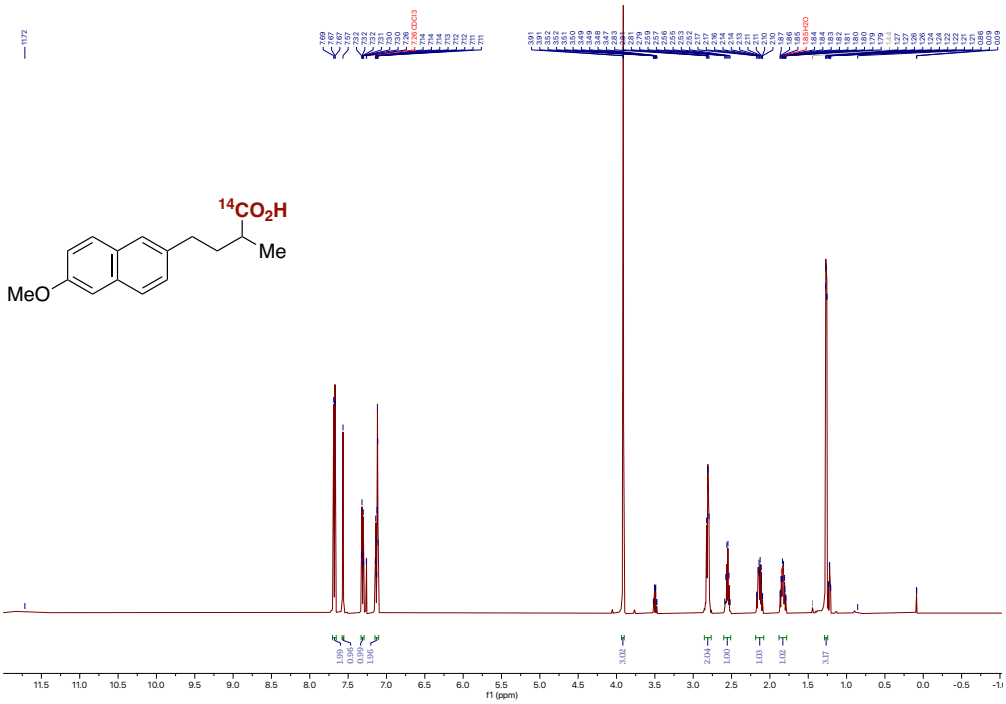

^{1}H spectrum (500 MHz, $CDCl_3$) of **28**

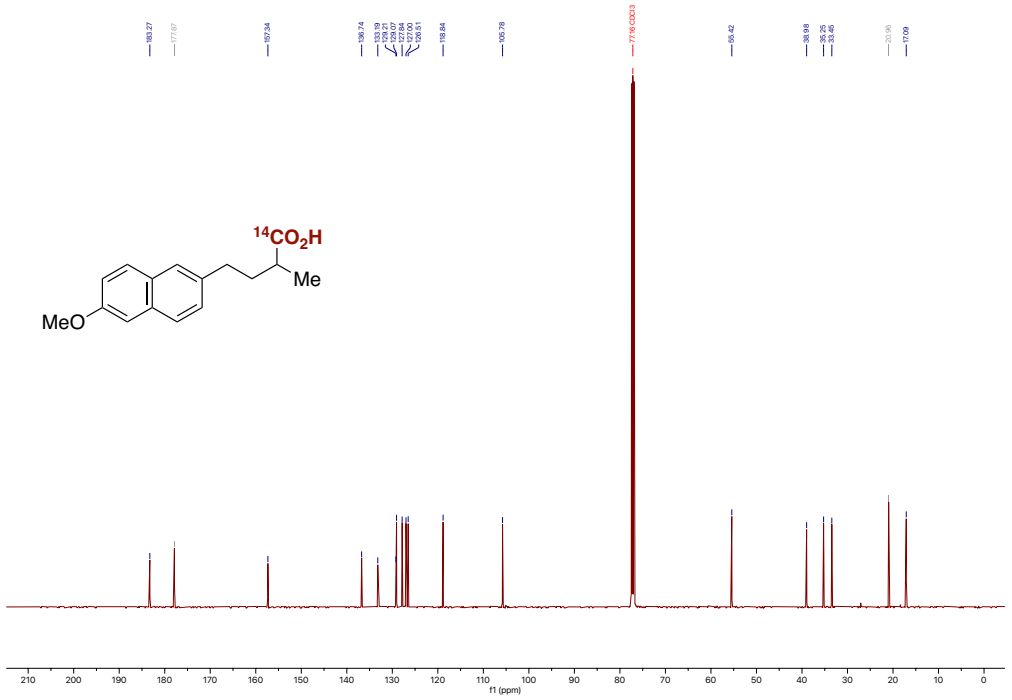

^{13}C spectrum (126 MHz, $CDCl_3$) of **28**

The peaks at 177 and 21 ppm correspond to acetic acid, arising from hydrolysis of EtOAc during the purification procedure, which was not removed to avoid further handling of radioactive material.

4.8. References

(1) Tay, N. E. S.; Lehnherr, D.; Rovis, T. Photons or Electrons? A Critical Comparison of Electrochemistry and Photoredox Catalysis for Organic Synthesis. *Chem. Rev.* **2021**, acs.chemrev.1c00384. https://doi.org/10.1021/acs.chemrev.1c00384.

(2) Chan, A. Y.; Perry, I. B.; Bissonnette, N. B.; Buksh, B. F.; Edwards, G. A.; Frye, L. I.; Garry, O. L.; Lavagnino, M. N.; Li, B. X.; Liang, Y.; Mao, E.; Millet, A.; Oakley, J. V.; Reed, N. L.; Sakai, H. A.; Seath, C. P.; MacMillan, D. W. C. Metallaphotoredox: The Merger of Photoredox and Transition Metal Catalysis. *Chem. Rev.* **2022**, *122* (2), 1485–1542. https://doi.org/10.1021/acs.chemrev.1c00383.

(3) Song, L.; Wang, W.; Yue, J.-P.; Jiang, Y.-X.; Wei, M.-K.; Zhang, H.-P.; Yan, S.-S.; Liao, L.-L.; Yu, D.-G. Visible-Light Photocatalytic Di- and Hydro-Carboxylation of Unactivated Alkenes with CO2. *Nat. Catal.* **2022**, *5* (9), 832–838. https://doi.org/10.1038/s41929-022-00841-z.

(4) Tortajada, A.; Juliá-Hernández, F.; Börjesson, M.; Moragas, T.; Martin, R. Transition-Metal-Catalyzed Carboxylation Reactions with Carbon Dioxide. *Angew. Chem. Int. Ed.* **2018**, *57* (49), 15948–15982. https://doi.org/10.1002/anie.201803186.

(5) Davies, J.; Lyonnet, J. R.; Zimin, D. P.; Martin, R. The Road to Industrialization of Fine Chemical Carboxylation Reactions. *Chem* **2021**, *7* (11), 2927–2942. https://doi.org/10.1016/j.chempr.2021.10.016.

(6) Filardo, G.; Gambino, S.; Silvestri, G.; Gennaro, A.; Vianello, E. Electrocarboxylation of Styrene through Homogeneous Redox Catalysis. *J. Electroanal. Chem. Interfacial Electrochem.* **1984**, *177* (1–2), 303–309. https://doi.org/10.1016/0022-0728(84)80232-6.

(7) Morgenstern, D. A.; Wittrig, R. E.; Fanwick, P. E.; Kubiak, C. P. Photoreduction of Carbon Dioxide to Its Radical Anion by Nickel Cluster [Ni3(.Mu.3-I)2(Dppm)3]: Formation of Two Carbon-Carbon Bonds via Addition of Carbon Dioxide Radical Anion to Cyclohexene. *J. Am. Chem. Soc.* **1993**, *115* (14), 6470–6471. https://doi.org/10.1021/ja00067a096.

(8) Seo, H.; Katcher, M. H.; Jamison, T. F. Photoredox Activation of Carbon Dioxide for Amino Acid Synthesis in Continuous Flow. *Nat. Chem.* **2017**, *9* (5), 453–456. https://doi.org/10.1038/nchem.2690.

(9) Mayer, J. M. Understanding Hydrogen Atom Transfer: From Bond Strengths to Marcus Theory. *Acc. Chem. Res.* **2011**, *44* (1), 36–46. https://doi.org/10.1021/ar100093z.

(10) Capaldo, L.; Ravelli, D. Hydrogen Atom Transfer (HAT): A Versatile Strategy for Substrate Activation in Photocatalyzed Organic Synthesis. *Eur. J. Org. Chem.* **2017**, *2017* (15), 2056–2071. https://doi.org/10.1002/ejoc.201601485.

(11) Capaldo, L.; Ravelli, D.; Fagnoni, M. Direct Photocatalyzed Hydrogen Atom Transfer (HAT) for Aliphatic C–H Bonds Elaboration. *Chem. Rev.* **2022**, *122* (2), 1875–1924. https://doi.org/10.1021/acs.chemrev.1c00263.

(12) Majhi, J.; Molander, G. A. Recent Discovery, Development, and Synthetic Applications of Formic Acid Salts in Photochemistry. *Angew. Chem. Int. Ed.* **2023**, e202311853. https://doi.org/10.1002/anie.202311853.

(13) Wang, H.; Gao, Y.; Zhou, C.; Li, G. Visible-Light-Driven Reductive Carboarylation of Styrenes with CO_2 and Aryl Halides. *J. Am. Chem. Soc.* **2020**, *142* (18), 8122–8129. https://doi.org/10.1021/jacs.0c03144.

(14) Hendy, C. M.; Smith, G. C.; Xu, Z.; Lian, T.; Jui, N. T. Radical Chain Reduction via Carbon Dioxide Radical Anion ($CO_2^{\bullet-}$). *J. Am. Chem. Soc.* **2021**, *143* (24), 8987–8992. https://doi.org/10.1021/jacs.1c04427.

(15) Chmiel, A. F.; Williams, O. P.; Chernowsky, C. P.; Yeung, C. S.; Wickens, Z. K. Non-Innocent Radical Ion Intermediates in Photoredox Catalysis: Parallel Reduction Modes Enable Coupling of Diverse Aryl Chlorides. *J. Am. Chem. Soc.* **2021**, jacs.1c05988. https://doi.org/10.1021/jacs.1c05988.

(16) Alektiar, S. N.; Wickens, Z. K. Photoinduced Hydrocarboxylation via Thiol-Catalyzed Delivery of Formate Across Activated Alkenes. *J. Am. Chem. Soc.* **2021**, jacs.1c07562. https://doi.org/10.1021/jacs.1c07562.

(17) Alektiar, S. N.; Han, J.; Dang, Y.; Rubel, C. Z.; Wickens, Z. K. Radical Hydrocarboxylation of Unactivated Alkenes via Photocatalytic Formate Activation. *J. Am. Chem. Soc.* **2023**, *145* (20), 10991–10997. https://doi.org/10.1021/jacs.3c03671.

(18) Davies, J.; Lyonnet, J. R.; Carvalho, B.; Sahoo, B.; Day, C. S.; Juliá-Hernández, F.; Duan, Y.; Álvaro Velasco-Rubio; Obst, M.; Norrby, P.-O.; Hopmann, K. H.; Martin, R. Kinetically-Controlled Ni-Catalyzed Direct Carboxylation of Unactivated Secondary Alkyl Bromides without Chain Walking. *J. Am. Chem. Soc.* **2024**, *146* (3), 1753–1759. https://doi.org/10.1021/jacs.3c11205.

(19) Elmore, C. S. Chapter 25 The Use of Isotopically Labeled Compounds in Drug Discovery. In *Annual Reports in Medicinal Chemistry*; Elsevier, **2009**,44, 515–534. https://doi.org/10.1016/S0065-7743(09)04425-X.

(20) Voges, R.; Heys, J. R.; Moenius, T. *Preparation of Compounds Labeled with Tritium and Carbon-14*, 1st ed.; Wiley, **2009**. https://doi.org/10.1002/9780470743447.

(21) Hanson, J. R. *The Organic Chemistry of Isotopic Labelling*; The Royal Society of Chemistry, **2011**. https://doi.org/10.1039/9781839169076.

(22) Bragg, R. A.; Sardana, M.; Artelsmair, M.; Elmore, C. S. New Trends and Applications in Carboxylation for Isotope Chemistry. *J. Label. Compd. Radiopharm.* **2018**, *61*, 934–948. https://doi.org/10.1002/jlcr.3633.

(23) Fu, M.-C.; Wang, J.-X.; Du, F.-M.; Fu, Y.; Ge, W. Dual Nickel/Photoredox Catalyzed Carboxylation of C(Sp2)-Halides with Formate. *Org. Chem. Front.* **2022**, 10.1039.D2QO01361D. https://doi.org/10.1039/D2QO01361D.

CHAPTER 5. General Conclusion

5.1. Conclusions

In order to summarize the present thesis, the main points of all chapters involving experimental work will be highlighted. All the protocols showcased in this thesis fall within the context of photoredox catalysis for the purpose of making carboxylic acids from C1 molecules. These methods proved to be mild and selective.

5.1.1. Chapter 2

- The development of a multicomponent coupling reaction has been disclosed, involving cheap and available starting materials to build larger scaffolds.
- The use of isotopically enriched CO_2 allowed for the incorporation of 100% ^{13}C in the final carboxylic acid.
- The mechanism involves a series of radical coupling, terminating with a radical polar crossover for the nucleophilic addition to CO_2.
- The selectivity can be modified depending on the class of starting material used.

5.1.2. Chapter 3

- A selective carboxylation of *unactivated* secondary alkyl bromides have been described with mild metallaphotoredox conditions.
- The method makes use of easily accessible alkyl bromides to directly gain access to valuable carboxylic acids with excellent selectivity.
- Preliminary mechanistic investigation demonstrates the important intermediacy of Ni(I) complexes along with the formation of free alkyl radicals.

5.1.3. Chapter 4

- A redox neutral approach to the generation of alkyl carboxylic acids from *unactivated* secondary alkyl bromides using formate salts has been shown.
- The protocol shows excellent selectivity ,although not fully optimized in terms of yield.
- The incorporation of ^{14}C in organic molecules could be performed using this method, showing the potential implementation in a radiochemistry context.

UNIVERSITAT ROVIRA I VIRGILI
CARBOXYLATIVE METHODOLOGIES VIA PHOTOREDOX CATALYSIS
Julien Lyonnet